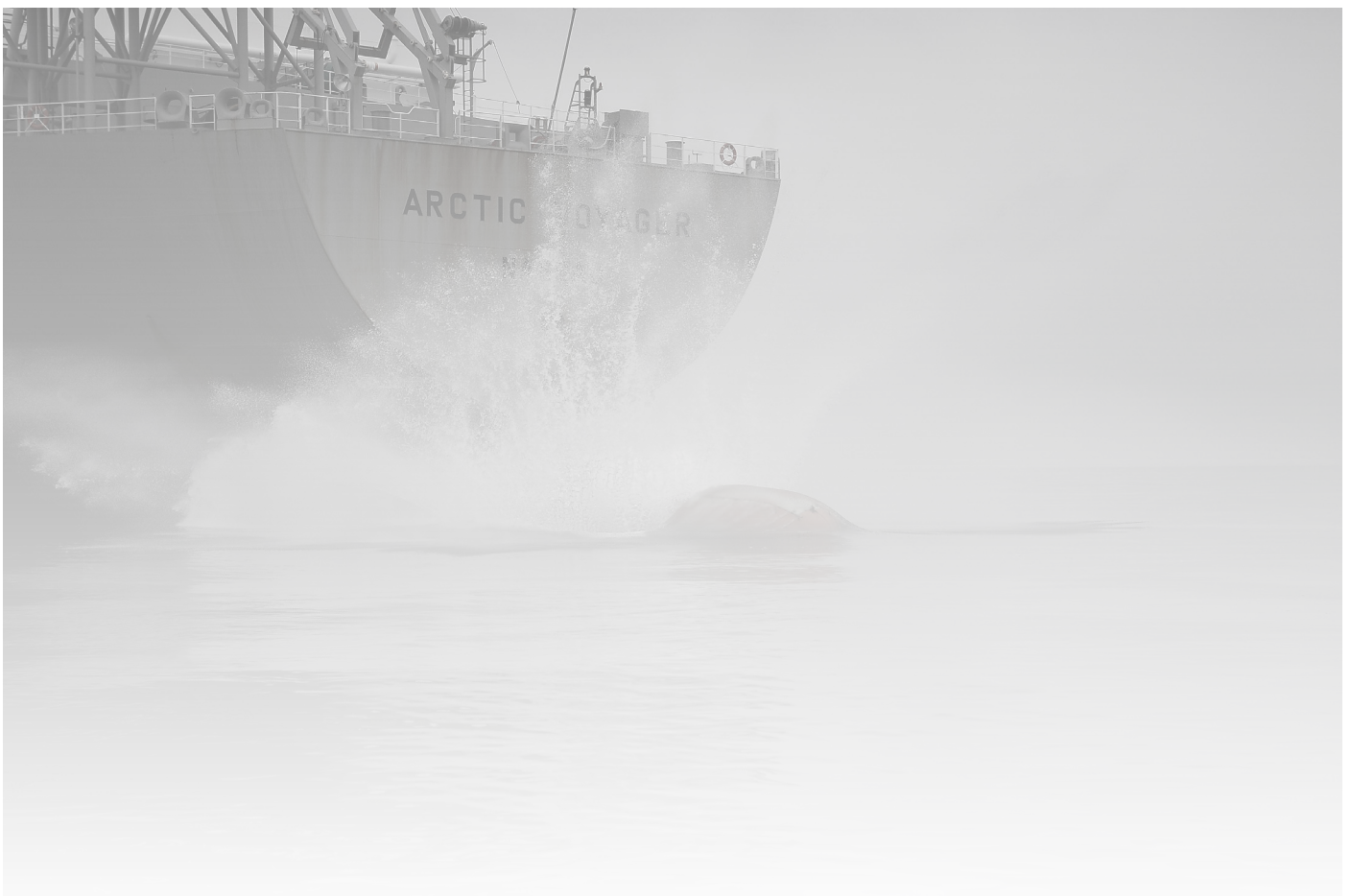




15th
International
Ship Stability Workshop
June 13-15, 2016, Stockholm, Sweden



Proceedings
Anders Rosén & Martin Schreuder (editors)



15th
International
Ship Stability Workshop
June 13-15, 2016, Stockholm, Sweden

Arranged and hosted by Chalmers University of Technology and KTH Royal Institute of Technology



Co-arranged with Lighthouse Swedish Maritime Competence Centre



Supported by



Proceedings of the 15th International Ship Stability Workshop (ISSW 2016)

Anders Rosén & Martin Schreuder (editors)

ISBN 978-91-7729-038-4

Stockholm, Sweden, June 2016

ISSW is part of a longstanding series of international technical meetings in the field of ship stability, dynamics and safety consisting of the STAB conferences, which are held every third year, and the ISSW workshops, which are held in the years between the conferences. These conferences and workshops are initiated and supervised by the STAB International Standing Committee and arranged and hosted by a Local Organizing Committee, each time in different corners of the world. Other important contributors are Session Organizers, Authors/Presenters, and Sponsors. All these contributors to ISSW 2016, as listed in the following pages, and are gratefully acknowledged. Also Katarina Wignell and Hiba Fawaz (Chalmers) and Emil Andersson, Egil Gustafsson, Sarah Hagman, Rickard Holmgren, and Anders Sjule (KTH Students) are gratefully acknowledged for contributing to the preparation of these proceedings and for various efforts during the workshop. More information about ISSW and STAB, proceedings from past events, and other information concerning ship stability, safety and dynamics, can be found at www.shipstab.org.

The opinions expressed in the here included papers are those of the authors and not necessarily those of any organization with which the authors have been associated.

ISSW 2016 Local Organizing Committee:

Anders Rosén, KTH Royal Institute of Technology
Martin Schreuder, Chalmers University of Technology

ISSW 2016 Co-Organizer:

Lighthouse Swedish Maritime Competence Centre

ISSW 2016 Session Organizers:

Vadim Belenky, David Taylor Model Basin
Hendrik Bruhns, Herbert-ABS Software Solutions LLC
Gabriele Bulian, University of Trieste
Alexander Degtyarev, St.Petersburg State University
Jan De Kat, American Bureau of Shipping
Alberto Francescutto, University of Trieste
Jean-François Leguen, DGA Techniques Hydrodynamiques
Marcelo Neves, COPPE UFRJ
Luis Pérez Rojas, Technical University of Madrid
Anders Rosén, KTH Royal Institute of Technology
Pekka Ruponen, NAPA Ltd
Martin Schreuder, Chalmers University of Technology
Kostas Spyrou, National Technical University of Athens
Naoya Umeda, Osaka University
Frans Walree, MARIN
Kenneth Weems, David Taylor Model Basin

ISSW 2016 Authors/Presenters: See the table of contents on the following pages

ISSW 2016 Sponsors:

DNV-GL	SSPA
Office of Naval Research Global (ONRG)	Stiftelsen Sveriges Sjömanshus
Sjöfartsverket	Svensk Sjöfart
Stena Teknik	Wallenius Lines

STAB International Standing Committee:

Kostas Spyrou, National Technical University of Athens, Chairman
Vadim Belenky, David Taylor Model Basin
Hendrik Bruhns, Herbert Software Solutions
Gabriele Bulian, University of Trieste
Alexander Degtyarev, St.Petersburg State University
Alberto Francescutto, University of Trieste
Jan Otto de Kat, American Bureau of Shipping
Toru Katayama, Osaka Prefecture University
Luis Perez-Rojas, Universidad Politécnica de Madrid
William Peters, U.S. Coast Guard
Marcelo Santos Neves, Universidade Federal do Rio de Janeiro
Naoya Umeda, Osaka University
Dracos Vassalos, University of Strathclyde
Frans van Walree, Maritime Research Institute Netherlands

Contents

Session 1: Second generation intact stability criteria

<i>"Current state of the second generation intact stability criteria - achievements and remaining issues"</i> by Naoya Umeda and Alberto Francescutto	3
<i>"Model experiment of an offshore supply vessel running in astern waves"</i> by Naoya Umeda, Aqmil Alway, Satoshi Usada, Akihiko Matsuda and Daisuke Terada	11
<i>"Probabilistic direct stability assessment"</i> by Vladimir Shigunov	17
<i>"Regulatory aspects of implementation of second generation IMO intact stability criteria"</i> by William Peters and Vadim Belenky	27
<i>"Different computations of parametric roll level 2 criterion"</i> by François Grinnaert, Jean-Yves Billard, and Jean-Marc Laurens	33
<i>"Validation of one numerical method for parametric roll criteria with experiments"</i> by Jiang Lu and Min Gu	41

Session 2: Validation of numerical methods

<i>"Towards accurate computations of active stabiliser fins, focusing on dynamic stall"</i> by Gerson Fernandes, Geert Kapsenberg, Maarten Kerkvliet, and Frans van Walree	51
<i>"Fast time domain calculations with non-linear Anti-Roll Tank coupling using retardation functions"</i> by Nicolas F.A.J. Carette	59
<i>"Specific intended uses: Establishing verification, validation and accreditation objectives"</i> by Arthur Reed	67

Session 3: Novel approaches to ship stability

<i>"Towards a theory of surf-riding in two-frequency and multi-frequency waves"</i> by Kostas Spyrou, Ioannis Kontolefas and Nikolaos Themelis	75
<i>"Split-time algorithm implementation in advanced hydrodynamic codes"</i> by Kenneth Weems and Vadim Belenky	83
<i>"Motion Perturbation Metric for Broaching-to"</i> by Vadim Belenky, Kostas Spyrou and Kenneth Weems	89

Session 4: Computational and stochastic methods

<i>"New models of irregular waves - way forward"</i> by Arthur Reed, Alexander Degtyarev, Ivan Gankevich and Kenneth Weems	95
<i>"Validation of split-time method with volume-based numerical simulation"</i> by Kenneth Weems, Vadim Belenky and Bradley Campbell	103
<i>"On the tail of nonlinear roll motions"</i> by Vadim Belenky, Dylan Glotzer and Themistoklis Sapsis	109
<i>"Numerical Simulation KPI Equation"</i> by Alexander Bogdanov and Vladimir Mareev	115

(cont.)

Session 5: Damage stability of passenger ships

- "Holistic perspective on damage stability standards for RoPax ships"* 121
by Jan Bergholtz, Tryggve Ahlman, Martin Schreuder, Ronnie Hanzén, Per Wimby, and Sten Rosenqvist
- "An alternative system for damage stability enhancement"* 129
by Dracos Vassalos, Evangelos Boulougouris and Donald Paterson
- "On damaged ship survivability assessment in design and operation of passenger ships"* 135
by Jakub Cichowicz and Alistair Murphy
- "Application of vessel TRIAGE for a damaged passenger ship"* 141
by Petri Pennanen, Pekka Ruponen, Jori Nordström, and Floris Goerlandt
- "Numerical flooding simulations - a useful tool for marine casualty investigations"* 147
by Stefan Krüger

Session 6: Roll damping

- "Estimation of force coefficients for normal forces on bilge keels and skin friction roll damping of ships by CFD"* 157
by Sven Wassermann, Gregor Krambs, and Moustafa Abdel-Maksoua
- "Validation of CFD simulation for ship roll damping using one pure car carrier and one standard model"* 165
by Min Gu, Shuxia Bu, Gengyao Qiu, Ke Zeng, Chengsheng Wu, and Jiang Lu
- "Effect of vortex shedding and free surface interaction on roll damping due to large amplitude roll motion"* 173
by Burak Yıldız, Ahmet Yurtseven and Toru Katayama
- "A framework for holistic roll damping prediction"* 183
by Carl-Johan Söder and Anders Rosén

Session 7: Operational aspects of ship stability

- "Operational stability beyond rule compliance"* 193
by Mikael Huss
- "Real-time stability assessment in mid-sized fishing vessels"* 201
by Marcos Míguez González, Vicente Díaz Casás, and Lucía Santiago Caamaño
- "Estimation of the metacentric height by using onboard monitoring roll data based on time series analysis"* 209
by Daisuke Terada, Masahiro Tamashima, Ikuo Nakao, and Akihiko Matsuda
- "Maneuverability in adverse conditions: assessment framework and examples"* 217
by Vladimir Shigunov, Apostolos Papanikolaou, and Dionysia Chroni

Session 8: Stability of naval vessels

- "Correlations of GZ curve parameters"* 229
by Doug Perrault
- "Application of 2nd generation intact stability criteria on naval ships"* 239
by François Grinnaert, Paola Gualeni, Jean-Yves Billard, Jean-Marc Laurens, and Nicola Petaccc
- "Conduction of a wind tunnel experiment to investigate the ship stability weather criterion"* 245
by Arman Ariffin, Shuhaimi Mansor, and Jean-Marc Laurens
- "USN's standard practice for the construction of a composite allowable KG curve using the load shift method"* 253
by Vytenis Senuta and Lauren Moraski

Current state of the second generation intact stability criteria - achievements and remaining issues

Naoya Umeda, *Osaka University*, umeda@naoe.eng.osaka-u.ac.jp

Alberto Francescutto, *University of Trieste*, francesc@units.it

ABSTRACT

The paper summarises background and current status of the development of the second generation intact stability criteria at the International Maritime Organization (IMO) by January 2016. The decisions at the IMO so far together with the remaining issues, such as the required safety levels for vulnerability criteria, and operational limitation and the guidelines are presented.

Keywords: *IMO, intact stability, pure loss of stability, parametric roll, broaching, dead ship stability, excessive acceleration*

1. INTRODUCTION

The second generation intact stability criteria development launched in 2001 was a part of the revision of the Intact Stability Code at the IMO (Francescutto, 2015). The existing intact stability code known as IS Code 2008 (IMO, 2009) consists of the purely empirical criteria based on Rahola's work, which was adopted at the IMO in 1968, and the semi-empirical criterion using energy balance of simplified ship roll model in irregular beam wind and waves, which was adopted at the IMO in 1985. In the empirical criteria casualty data of ships having their length of 100 metres or less were used for obtaining the relationship between GZ curve parameters and ship stability safety. In the semi-empirical criterion casualty data of ships by 1950's were used to determine the critical value of average wind velocity, i.e. 26 m/s. Since they are directly or indirectly based on casualty data of ships existing before their developments, these two criteria could be regarded as the first generation criteria. As a result, applicability of these existing criteria to current ships cannot be straightforwardly guaranteed. The current major ship types, such as containerships, car carriers, RoPax ships, were not so easily found in 1950's and the sizes of these ships, particularly containerships and cruise ships, are drastically increasing year by year. For properly guarantee the stability safety for contemporary ships, new criteria are required, which can be named as the second generation intact stability criteria.

The adopted approach for the second generation intact stability criteria is physics-based, and multi-layered. Since progress of ship design is faster than accumulating accident data, empirical approaches are not practical. If criteria are based on physics, limitation of their applicability can be significantly removed. Current ship dynamics together with ship hydrodynamics seem to be sufficient for assessing safety of intact ships by using numerical simulation in time domain and scaled model experiments. However, the use of such advanced tools for practical purpose cannot be mandated because these tools require experts, qualified experimental facilities and time. Since the IS Code shall be applied to all passenger and cargo ships of 24 metres or larger, the number of experts and experimental facilities are definitely insufficient. Since intact stability could be related to both details of hull form and basic specifications of contract, the use of advanced tools could be impractical for early design stage. Therefore, it was agreed that, if a ship complies with simplified criteria, the application of advanced tools can be exempted. Here the simplified criteria as lower level ones should be still physics-based but with larger margin. As a result, the framework of the whole criteria can avoid inconsistent judgement in which a ship complying with the lower level criterion could fail to comply with the higher level criterion. During the discussion, the lower level criteria were made to consist of two levels: level 1 only requires a pocket calculator while level 2 requires a spread sheet-type calculation. These are named as "vulnerability criteria". On the contrary, the assessment using an

advanced tool, named “direct stability assessment”, requires a computer and, occasionally experimental facilities.

This set of intact stability criteria deals with five major failure modes, i.e. pure loss of stability, parametric roll, broaching, dead ship stability and excessive acceleration.

In case that a ship fails to comply with these criteria, the ship could be allowed to navigate with operational guidelines based on the direct stability assessment procedures or operational limitations based on the level 2 vulnerability criteria.

By the 3rd session of the Sub-Committee on Ship Design and Construction (SDC) in February 2016, all vulnerability criteria with a limited number of remaining issues were agreed (IMO, 2015a and 2016). Major remaining issues are the standards, which specify the required safety levels. For supplementing the descriptions of calculation procedures in vulnerability criteria for each failure mode, explanatory notes were also developed again with a limited number of remaining issues. This paper summarises these remaining issues in the vulnerability criteria and their explanatory notes. Furthermore, discussion points for direct stability assessment, operational limitation and guidelines are also highlighted.

2. PURE LOSS OF STABILITY

When a wave is positioned with the crest amidships, the roll restoring moment could be reduced. This is due to the effect of transom stern and/or bow flare. If the ship runs with high speed in following seas, this reduction continues longer than in head waves. If the ship speed is slightly smaller than the surf-riding threshold, the ship speed increases at a wave crest so that the duration of reduced restoring moment could be extremely long. If the ship with high speed significantly heels because of reduction of restoring moment, asymmetry of the underwater submerged volume could induce a hydrodynamic yaw moment, which could act as external heel moment on a wave crest amidship.

Therefore, in a numerical simulation model for this failure mode, not only reduction of GZ curve but also the effect of surge motion and roll-yaw coupling should be taken into account.

Based on this understanding, the level 2 vulnerability criterion for this mode has a requirement of the ship forward speed. If the Froude number defined with calm-water velocity exceeds 0.24, the ship can be vulnerable to this failure mode. This is because it is already established that the surf-riding threshold with the wave steepness of 1/10 can be defined as the nominal Froude number of 0.3. Then the level 2 criterion requires the GZ calculation for a ship in longitudinal waves in which the wavelength is equal to the ship length as a conservative assumption. Since an actual wavelength can be different, the steepness used here is adjusted with this equivalent wave and ocean wave spectrum with the specified significant wave height and the mean wave period by using the least square method in space. This procedure is well known as Grim’s effective wave concept.

Once the GZ curve of the equivalent wave is obtained, it will be compared with an external heeling moment due to forward velocity. If the equilibrium between the restoring moment and the external moment occurs at a heel angle larger than 15 degrees for a passenger ship and 25 degrees for a cargo ship, the ship is judged to be vulnerable to this failure mode. In addition, if the angle of vanishing stability without external moment is larger than 30 degrees, the ship is also judged to be vulnerable. This procedure is repeated for all combinations of significant wave height and mean wave period, which appear in the wave scatter tables normally in the North Atlantic. Then their weighted average, which means the probability of dangerous sea states for this failure mode in the specified water area, is used for the final judgement in the level 2. If the attained value is larger than the required value, which is tentatively set to 0.06, the ship is judged to be vulnerable to this failure mode.

The critical Froude number and heel angles are determined with the recent accidents of RoPax and RoRo ships, which can be presumed to be relevant to this failure mode. The required value was determined with many sample calculation results for existing and coming passenger and cargo ships. At this moment this required value has not yet been finalised but it should be done by 2018.

The level 1 criterion was obtained by simplifying the level 2. While the speed requirement is the same as the level 2, the GZ

calculation in waves is replaced with the GM calculation in waves. Furthermore, a method for a fast approximate calculation of GM is provided other than direct hydrostatic calculation. Here GM in waves can be calculated only with a conventional hydrostatic table and pocket calculator so that workload of ship designers is very small. Regarding the relationship with actual ocean waves, the representative wave steepness is determined using the wave scatter diagram, which is 0.0334 for the North Atlantic. The required value for the GM in waves is not yet determined but tentatively set to 0.05 m. This means that the effect of ship speed is ignored. Generally speaking, GM well represents GZ at least at smaller angle, with the exception of ships having a large beam to depth ratio.

During the development stage of these criteria, most sample calculations were executed with the approximate method for GM in waves, which appeared to be reasonably conservative with respect to the direct hydrostatic calculation. As a result, the outcomes of the level 1 are more conservative than those of the level 2. However, it was experienced that, using the direct hydrostatic calculation, the level 1 occasionally occurs to be less conservative than the level 2 so that some “false negative” cases appear for ships having large beam to depth ratio. Typical examples are offshore supply vessels. Finding a way to resolve this issue is an urgent matter. This may suggest that the required value for the level 1 could depend on the GM calculation methods because the current required value was set mainly with the approximate GM calculation. The current draft indicates that this criterion may not be applied to “a vessel with extended low weather deck due to increased likelihood of water on deck or deck-in-water”.

3. PARAMETRIC ROLL

A ship in waves may experience the restoring variation with time. Under certain conditions, this restoring variation could induce violent roll motion, with maximum amplitude which can be much larger than beam-sea resonance. This phenomenon can be categorised as parametric resonance. Using a coupled heave-roll-pitch model in time domain, it is possible to accurately predict parametric roll resonance in irregular longitudinal waves. Such numerical simulation can be used as a tool for direct stability assessment.

For vulnerability level 2 criteria, an uncoupled roll model is used so that time-domain simulation can be avoided. Ignoring dynamic coupling effect with vertical motion normally could result in over-estimation of restoring variation in head waves so that we may provide conservative predictions in the level 2. It is noteworthy here that roll damping moment including bilge keel effect should be estimated by using simplified Ikeda’s semi-empirical method or alternatives to it.

In case of the uncoupled roll model, the occurrence zone of parametric roll can be analytically evaluated. These estimations for typical 16 regular waves constitute the first check of the level 2.

However, since the zone for parametric roll occurrence is very wide for slender ships such as container ships, we have to evaluate amplitude of parametric roll for our final judgement even in the level 2, which is named as the second check. If we apply an averaging method or equivalent to the uncoupled roll model, the amplitudes of parametric roll can be estimated almost immediately including stability of the coexisting solutions. Here GM is assumed to vary with time but nonlinear characters of GZ curve are kept as that in calm water. For accurately modelling a hydrostatically calculated GZ curve, numerical simulations of the uncoupled roll model in time domain can be recommended. Thus, the SDC agreed to use the numerical simulation as a standard method and to keep the averaging method as an alternative. In this case, calculated results could depend on initial conditions so that use-friendly guidelines should be developed as soon as possible.

This procedure for estimating the roll amplitude is repeated for all combinations of the significant wave height and the mean wave period, which appear in the wave scattering tables normally in the North Atlantic and then their weighted average, which means the probability of dangerous sea states for this failure mode in the specified water area, is used for the final judgement in the level 2. If the attained value is larger than the required value, which is tentatively set to 0.06, the ship is judged to be vulnerable to this failure mode.

For the level 1, the procedure used in the level 2 is further simplified. If we ignore nonlinearity in both GZ and roll damping as well as the mean of

GM variation, the formula of the averaging method can be restricted to a simple estimation formula as a function of GM variation amplitude and roll damping. Regarding the relationship with actual ocean waves, the representative wave steepness is determined using the wave scatter diagram, which is 0.0167 for the North Atlantic. Further simplifying Ikeda's method and hydrostatic GM estimation, we can calculate the attained value in the level 1 only with a hydrostatic table, bilge keel area ratio and a pocket calculator.

For this failure mode, major remaining issues are the required value of the second check of the level 2 criterion, development of the guidelines for numerical simulation in time domain. In addition, estimation of the roll natural roll period should be discussed further.

4. BROACHING

Even a directionally stable ship in calm water can be directionally unstable at wave downslope. If surf-riding occurs, a ship can be captured at wave downslope so that the ship could fail to keep its straight course in stern quartering waves even with its maximum steering effort. This is known as broaching. Because of surf-riding, the ship forward speed is high. As a result, yaw angular velocity due to directional instability could result in violent centrifugal force, which could induce extremely large heel.

Probability of stability failure due to broaching can be predicted by combining a probabilistic wave theory and a coupled surge-sway-yaw-roll numerical model with accurately estimated manoeuvring coefficients. This could be utilised as a tool for direct stability assessment. Obviously accurate estimation of manoeuvring coefficients cannot be mandated for all SOLAS ships.

Thus, the SDC already agreed for the vulnerability criteria to deal with surf-riding in place of broaching. If we avoid surf-riding, possibility of stability failure due to broaching is small enough. It should be underlined that typical surf-riding can be dealt even with an uncoupled surge model in following waves so that we do not have to estimate manoeuvring coefficients.

In the level 2 criterion, critical nominal speeds for surf-riding of a self-propelled ship in regular following waves are estimated for various

wavelengths and wave heights by a perturbation method starting with its solution without surge damping. Then the occurrence probability of waves that the ship can be surf-ridden is calculated with a stochastic wave theory and the North Atlantic wave statistics. Finally the probability of surf-riding occurrence when a ship meets one local wave is calculated and compared with the acceptable safety level. Based on sample calculation results for relevant ships, the acceptable safety level is tentatively set to be 0.005. It is noteworthy here that accurate prediction of calm-water resistance up to wave celerity is required and the acceptable safety level depends on prediction accuracy of wave-induced surge force.

For avoiding such difficulties and designers' workloads, the level 1 criterion was developed with sample calculation results for various ships under the wave steepness of 1/10 with measured wave-induced surge force and calm-water resistance. As a result, we concluded that, if nominal Froude number is smaller than 0.3, surf-riding is not likely to be met. This criterion and standard is the same as those in the ship-independent operational guidance in the MSC. 1/Circ. 1228. In addition, with calculated results based on the level 2, it was also concluded that, if the ship length is larger than 200 metres, the ship is out of scope of this failure mode. This is because ocean waves are too short for such longer ship to be surf-ridden.

For this failure mode, major remaining issues are curve fitting method for calm-water resistance, empirical estimations of self-propulsion factors and thrust estimation for unconventional propulsive systems.

5. DEAD SHIP STABILITY

If a ship loses all propulsion power or a ship master decides to stop engine power for avoiding other dangerous phenomena, the ship would be under beam wind and wave conditions for longer duration as a worst situation. This is known as dead ship condition, and the weather criterion was originally developed for this condition but with a simplified energy balance analysis. However, the weather criterion is believed to excessively limit the freedom of designing contemporary ships such as large cruise ships. Thus, new criteria for this failure mode were developed.

Probability of stability failure under this condition can be estimated with the Monte Carlo numerical simulation in irregular beam wind and waves by using a sway-heave-roll-pitch model. This could be utilised as a tool for direct stability assessment but small probability could require so many realisations for accurately obtaining the probability for a practical ship.

The use of an analytical solution of uncoupled roll model is a way to significantly reduce computation time. In the level 2 criterion, the SDC agreed to use linear GZ curve up to the critical heel angle. Above the critical angle, the GZ is assumed to be zero. Here the critical heel angle is determined to keep the area of original GZ curve up to the angle of vanishing stability, which is responsible for dynamic ship stability, as the same as the approximate GZ. Thanks to linear GZ, we have no difficulty for calculating the probability of stability failure in irregular beam wind and waves with a wave scattering diagram. Here the roll damping and the roll exciting moment can be estimated with simplified Ikeda's method and the Froude-Krylov approach assuming rectangular hull sections, respectively. If the calculated probability for the relevant water area is larger than the acceptable safety level, the ship is judged to be vulnerable to this failure mode. The value of acceptable safety level is tentatively set to 0.06 or 0.04, based on the sample calculations using existing and actually designed ships.

Regarding the level 1 criterion, the SDC also agreed to use the current weather criterion but with the extended wave table that was already adopted in the MSC.1/Circ. 1200 for the experiment-supported weather criterion. This is because the current weather criterion can be regarded as a simplified version of the level 2 methodology with several assumptions for wind gustiness, wave irregularity and so on.

For this failure mode, major remaining issues are the required value of the level 2 criterion, development of guidelines for alternative roll damping estimation using CFD (computational fluid dynamics) and the applicability of simplified wave excitation prediction to trimmed conditions.

The use of new vulnerability criteria could change the safety level guaranteed by the current weather criterion. For this purpose, some sample

calculations using many existing ships having wider loading conditions were executed by one of the authors (IMO, 2015b). Firstly, the calculated attained values, i.e. C values, are plotted as a function of the metacentric height, GM , as shown in Figure 1. It does not show any distinct correlation between GM and C , which corresponds to a capsizing probability index for a ship in beam wind and waves. Although larger GM is expected to provide better stability, the existence of roll resonance, which occurs at the ship-dependent natural roll period, results in no distinct correlation. Secondly, the calculated C values are plotted as a function of the ratio of the heeling energy and residual restoring energy, b/a , in the level 1 as shown in Figure 2. In this figure, broadly speaking, the values of C decrease with the increasing value of b/a . This is because both methods deal with stability failure mode in beam wind and waves. Looking into detail, some scatters can be found in the b/a region between 1.1 and 5.5. This is probably due to the difference in estimation accuracy of roll motions between the two different modelling. Almost vertical trend of C can be found when b/a is zero. This is because the level 1 assumes only one stationary sea state for determining loss of static balance between GZ and wind heeling lever and the level 2 uses many different sea states and their occurrence probability included in the wave scattering diagram for the same purpose. If we use 0.04 or 0.06 as the required value, no "false negative" case exists at least in these sample ships. In other words, some ships failing to comply with the current weather criterion can be regarded as non-vulnerable for dead ship stability failure keeping the safety level that the current weather criterion requires. More data are required for finalising this issue.

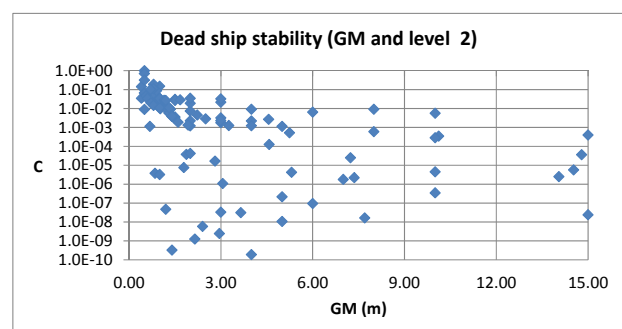


Figure 1: Relationship between the metacentric height and the C value in the level 2 criterion (IMO, 2015b).

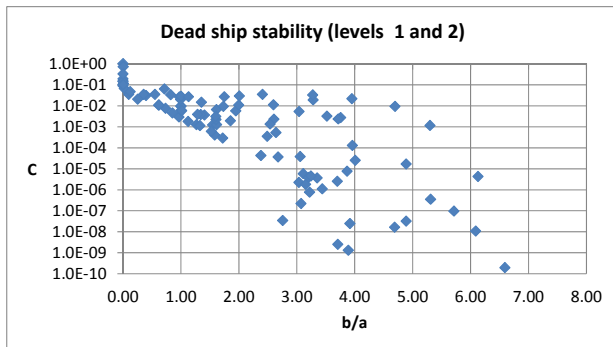


Figure 2: Relationship between the b/a in the level 1 criterion and the C value in the level 2 (IMO, 2015b).

6. EXCESSIVE ACCELERATION

If GM is excessively large, the natural roll period can be too small so that large acceleration under synchronous resonance could act on crew or cargoes. Since actual fatal accidents for modern containerships under ballast conditions were reported, this situation was also included as a stability failure. However, the problem to be solved is almost linear so that a standard seakeeping tool can be used with acceptable acceleration value. This could be a tool for direct stability assessment. However there is a different-type difficulty. A conservative estimation here could require too small GM , which can be smaller than GM required by other stability criteria.

Therefore, the vulnerability criteria should be more conservative than the direct stability assessment but its margin should be smallest. In the level 2 criterion, the uncoupled roll model in long-crested irregular waves without forward velocity is used because beam seas can be regarded as a worst situation. By using the linear response operator, wave spectrum, the Froude-Krylov wave exciting moment and the equivalent linearization of roll damping, the variance of lateral acceleration can be calculated. Then, assuming the Rayleigh distribution of roll amplitude, critical acceleration value and the wave scattering diagram, the long-term probability of lateral acceleration exceeding its critical value can be obtained. If it is larger than the acceptable level, the ship is judged as vulnerable to this failure mode. Here the critical acceleration value is tentatively set as 9.81 m/s^2 and the proposed acceptable values ranges from 1.1×10^{-4} to 0.043.

For the level 1 criterion, the level 2 procedure is simplified by approximating the wave frequency in the numerator with the natural roll frequency. As

a result, we can obtain a simple formula without integral, which depends on the wave steepness from the weather criterion and roll damping coefficient. Here the roll damping and wave excitation are estimated by simplified methods. The proposed critical acceleration values here range from 5.3 m/s^2 to 8.59 m/s^2 .

For this failure mode, major remaining issues are the critical acceleration values of both the level 1 and 2, the acceptable safety level of the level 2, an example application of level 2 criterion to be included in the explanatory notes.

7. OPERATIONAL LIMITATION & GUIDANCE

It can be easily presumed that a safety level estimated with a perfect direct stability assessment, if available, could be smaller than the actual accident rate. This is because operators might avoid existing dangers by avoiding some dangerous wave and operational conditions. Thus ignoring operational aspects cannot be justified. On the other hand, the outcomes from the level 2 criterion and the direct stability assessment can be useful to improve operator's actions to avoid dangers. Therefore, the SDC agreed to allow the ship operation if the ship are judged as vulnerable to a failure in the level 2 but the operational limitation based on the level 2 application outcomes is provided. Similarly, operational guidance based on the direct stability assessment can be used for a ship failed to pass the direct stability assessment.

The operational limitation agreed at the working group of the SDC can be provided with the use of alternative wave scattering diagram specifying water area and season for each loading condition. However, it is still discussed whether the operational limitation can include effects of operational elements, i.e. propeller revolution and heading angle, as well as the wave period or not. Some delegations say that estimation accuracies of the level 2 methods on these elements are not sufficient: the others say that, if we ignore these elements, most of current containerships may not be allowed to operate any more. Further discussion is needed with sample calculation results. For the operational guidelines, all wave and operational elements can be used but developing such guidelines for each ship requires tremendous

computational time with a well validated numerical code.

8. CONCLUSIONS

Major remaining issues for vulnerability criteria are finalising the standards, in other words required safety levels. To do so, the relevant organisations are requested to execute sample calculations using existing and coming SOLAS and LL ships for their various GMs, draughts and trims. For direct stability assessment, more submissions of comparisons between the simulations and experiments are indispensable. We would appreciate it very much if you would contribute to these matters based on your own research projects.

9. ACKNOWLEDGEMENTS

This work was supported by a Grant-in Aid for Scientific Research from the Japan Society for Promotion of Science (JSPS KAKENHI Grant Number 15H02327). It was partly carried out as a research activity of Goal-based Stability Criteria

Project of Japan Ship Technology Research Association in the fiscal years of 2015 funded by the Nippon Foundation. The authors appreciate Miss Naho Yamashita for her effective assistance in the sample calculation.

10. REFERENCES

Francescutto, A., 2015, "Intact Stability Criteria of Ships –Past, Present and Future", Proceedings of the 12th International Conference on Stability of Ships and Ocean Vehicles, Glasgow, pp. 1199-1209.

IMO, 2009, International Code on Intact Stability, 2008.

IMO, 2015a, Report of the Working Group (Part 1), SDC 2/WP.4.

IMO, 2015b, Information Collected by the Correspondence Group on Intact Stability Regarding Second Generation Intact Stability Criteria, SDC 3/INF.10.

IMO, 2016, Report of the Working Group (Part 1), SDC 3/WP.5.

Model Experiment of an Offshore Supply Vessel Running in Astern Waves

Naoya Umeda, *Osaka University*, umeda@naoe.eng.osaka-u.ac.jp

Aqmil Alway, *NAPA Japan*, Aqmil.Alway@napa.fi

Satoshi Usada, *Osaka University*, usada.satoshi@gmail.com

Akihiko Matsuda, *National Research Institute of Fisheries Engineering*, amatsuda@fra.affrc.go.jp

Daisuke Terada, *National Research Institute of Fisheries Engineering*, dterada@fra.affrc.go.jp

ABSTRACT

At the IMO (International Maritime Organization), the second generation intact stability criteria for pure loss of stability are now under development. In its latest draft, vessels with extended low weather deck such as offshore supply vessels (OSVs) are exempted from this application but its backgrounds have not yet been explained other than sample calculation reports of inconsistencies between different levelled criteria. To solve this problem, we executed model experiments for a typical OSV in astern waves and then identified that the OSV is not relevant to the phenomenon that the pure loss of stability criteria assume but is relevant to the phenomenon due to trapped water on deck. Further, effect of low weather deck length is investigated by systematically modifying hull forms with help of a CAD software.

Keywords: *IMO, Second generation intact stability criteria, pure loss of stability, water on deck, OSV*

1. INTRODUCTION

The second generation intact stability criteria to be developed by the IMO are requested to cover stability failure due to pure loss of stability in following and stern quartering waves (Umeda & Francescutto, 2016). For this failure mode, the direct stability assessment and two-layered vulnerability criteria should be developed. As a possible tool for the direct stability assessment, a coupled surge-sway-yaw-roll numerical model in irregular waves was developed and validated with model experiments using a containership (Kubo et al., 2012).

Based on the knowledge obtained from this numerical model, the level 1 and 2 vulnerability criteria were developed. Here the level 1 and 2 criteria utilize GM and GZ in longitudinal waves, respectively. The standards of these criteria were tentatively determined to avoid the “false negative” problem between the two levels in many sample calculation results except for offshore supply vessels (IMO, 2015). The sample calculations executed by two delegations indicate that offshore supply vessels easily comply with the level 1 but do

not so with the level 2. This is a so-called “false negative” problem, which should be avoided in regulatory applications. Thus, the current vulnerability criteria are allowed not to be applied to “a vessel with extended low weather deck due to increased likelihood of water on deck or deck-in-water”.

However, its definition of the extended low weather deck, based on a model experiment or equivalent, was not yet established by 2015. In fact, even a published free-running model experiment of an offshore supply vessel in astern waves had not been available so far. Therefore, the authors newly executed a model experiment using a scaled model of typical offshore supply vessel in stern quartering waves and compared the obtained results with the second generation criteria. As a result, the reasons why OSVs should be exempted from the application of the pure loss of stability criteria are revealed. Furthermore, for investigating the effect of weather deck length, calculations of the vulnerability criteria were also conducted by systematically modifying above-water hull forms of the offshore supply vessel using a CAD software, i.e. the NAPA software.

2. SUBJECT SHIP AND MODEL EXPERIMENT

Free-running model experiments of the 60 m long offshore supply vessel (OSV), as shown in Fig. 1-2, in stern quartering waves were conducted at a seakeeping and manoeuvring basin of the National Research Institute of Fisheries Engineering of Japan. The vessel has a deck house in its fore part and a low weather deck situated from its midship to its stern with bulwarks and freeing ports. The length of the low weather deck is 35 m in full scale. Its service Froude number is 0.3 with twin propellers and twin rudders. Its principal particulars and righting arm curve are shown in Table 1 and Fig. 3, respectively. The metacentric height is set to marginally comply with level 2 criteria for pure loss of stability, which is lower than the designed one. The vessel under the experimental condition is judged not vulnerable to pure loss of stability with the level 1 criterion because the GM with the wave steepness of 0.334 is 1.32 m, which is much larger than 0.05m. However, it critically complies with the level 2 criterion with CR value of 0.06. Thus an inconsistency between the two levels could appear if the calm-water GM is smaller than 1.45m.

The vessel model ran with a constant propeller revolution and attempted to keep its specified course with a PD autopilot in stern quartering waves. The translational and rotary motions of the vessel model were measured by an optical tracking system, consisting of two theodolites and two prisms, an optical-fibre gyroscope, respectively. The model was rereleased when water waves were sufficiently propagated in the water area of the basin. These experimental procedures are based on the ITTC (International Towing Tank Conference) recommended procedures for intact stability model test (ITTC, 2008).

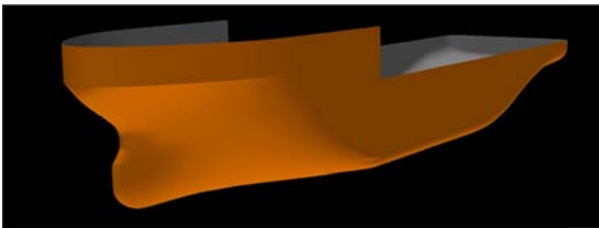


Fig.1 3D view of the hull form of the used OSV



Fig.2 Free-running model experiment of the OSV in stern quartering waves

Table 1 Principal particulars of the OSV

Items	Ship	Model
L_{bp}	60.00m	2.00m
Moulded Breadth	16.40m	0.546m
Moulded Depth	7.20m	0.24m
Moulded draught	6.00m	0.20m
Metacentric height (GM)	1.45m	0.0482m
Natural roll period	11.50s	2.10 s

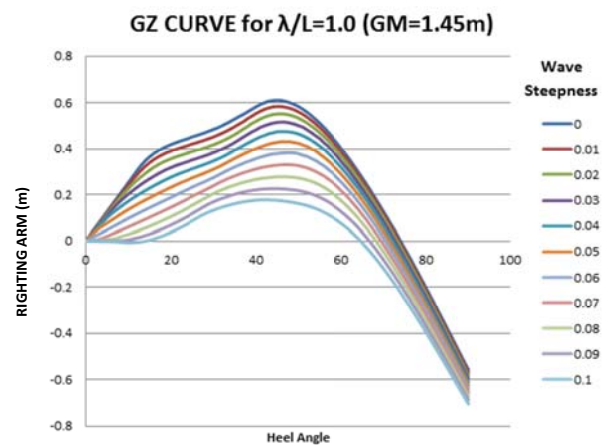


Fig. 3 GZ curve of the OSV at a wave crest amidship in longitudinal waves. Here the wavelength is equal to the ship length and the wave steepness ranges from 0 to 0.1

3. EXPERIMENTAL RESULTS AND DISCUSSION

The maximum roll angles measured during each model run in stern waves are shown in Fig. 4. Here the wavelength is equal to the ship length, as the worst case assumed in the criteria for pure loss of stability and the nominal Froude number ranges from 0.24 to 0.37 as also specified by the criteria. The used wave steepness H/λ , are 0.03, 0.05 and

0.1. The results indicate that roll angles under these wave and operational conditions are smaller than 15 degrees so that no real danger can be expected.

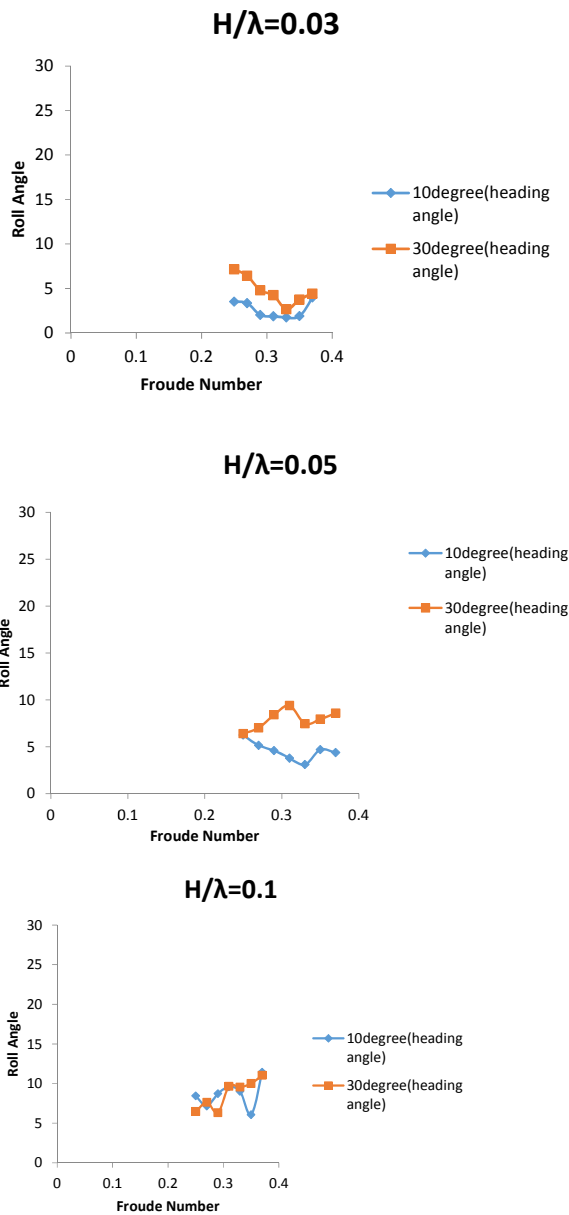


Fig. 4 Maximum roll angles (degrees) recorded in the experiment for the wavelength to ship length ratio of 1.0 and the wave steepness of 0.03, 0.05 and 0.1 with the auto pilot courses of 10 and 30 degrees from the wave direction.

This would be because the trapped water-on-deck acted as a kind of anti-rolling tank. This is because that the estimated natural period of possible trapped water on deck, which ranges between 1.8 s and 2.4s in model scale as shown in Fig. 5, is comparable to the natural roll period of 2.1s. The roll decay test of this model in calm water with large instantaneous initial roll angle was

rapidly damped as shown in Fig.6. Thus, we can presume that this large roll damping is due to resonance of ship roll motion and the trapped water on deck. This is similar to a mechanism of an anti-rolling tank.

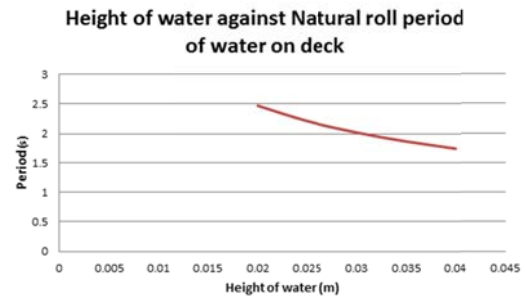


Fig. 5 Estimated natural period of trapped water on deck as a function of water depth.

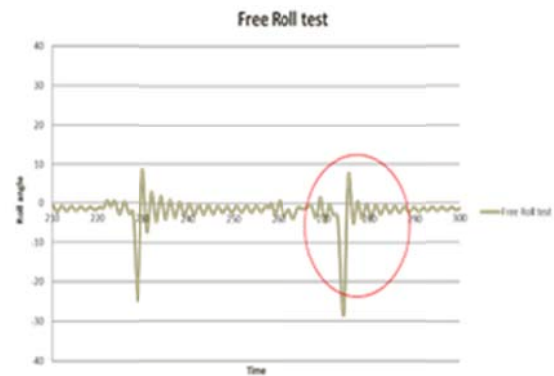


Fig. 6 Time series of roll decay test with the large instantaneous initial roll angle in degrees.

As a next step, model runs were conducted under longer waves. Here the ratio of wavelength to ship length, λ/L , was 1.5 and the wave steepness is 0.1. In this case larger water volume was trapped on deck because water ingress across the bulwarks exceeds egress through the freeing ports. The results shown in Fig. 7 indicate that larger roll angles such as about 50 degrees were recorded. When the speed decreases, the roll angle increases. This tendency is completely different from pure loss of stability.

The reason of the larger roll could be the heeling moment of trapped water-on-deck, which could depend on the height of bulwarks. In the case of this OSV, if the roll angle exceeds about 21 degrees, the relative water level exceeds the bulwark. As shown in the GZ curve for this wavelength as shown in Fig. 8, the loll angle is larger than 20 degrees and the angle of vanishing

stability is slightly larger than 50 degrees. Thus, the bulwark submergence cannot be avoided at a wave crest amidship and then the maximum roll angle could be 50 degrees. This suggests that the reason of large roll seems to be hydrostatic heel moment due to water on deck.

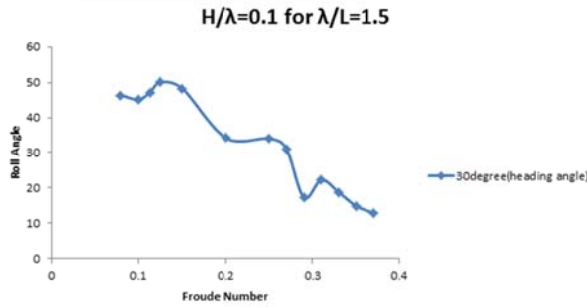


Fig. 7 Maximum roll angles (degrees) recorded each free running test for the wavelength to ship length of 1.5 with the wave steepness of 0.1.

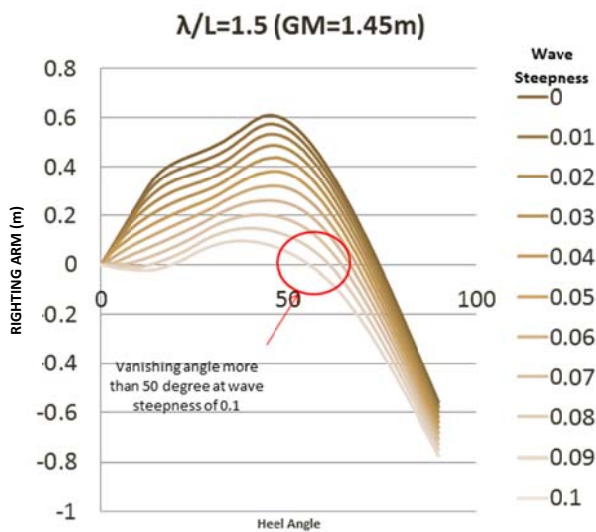


Fig. 8 GZ curve of the OSV at a wave crest amidship in longitudinal waves for the wavelength to ship length of 1.5 and the wave steepness ranges from 0 to 0.1.

For investigating mechanism of this dangerous phenomenon further, the coupled surge-sway-yaw-roll numerical model proposed by Kubo et al. (2012) was used for simulating the dynamic ship behaviour under the wave conditions used in the experiment. This is a manoeuvring-type model with linear wave exciting forces and restoring variation focusing on low frequency phenomena but the effect of trapped water on deck is not taken into account. All propulsion and manoeuvring

coefficients as the input for the simulation model are estimated with conventional captive model experiments. The linear wave exciting forces and restoring variation were calculated by a slender body theory with low encounter frequency assumption and a direct pressure integral of incident wave pressure up to instantaneous water level, respectively.

The comparisons between the experiments and the simulations are shown in Figs. 9-10. For the higher speed case shown in Fig. 9, both the measured and calculated roll periods are twice the encounter wave period and different from the natural roll period. The maximum roll angle occurs whenever the ship centre meets a wave crest. Thus this could be a period doubling phenomenon due to restoring variation experimentally identified for containerships by Kan et al. (1990). The measured roll amplitude is much smaller than the calculated one so that the trapped water that is not included in the numerical model has a role to damp the roll motion as a kind of anti-rolling tank.

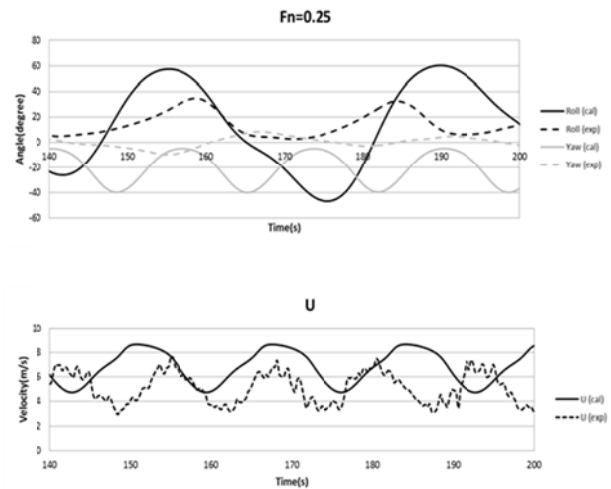


Fig. 9 Comparison between the simulation and the experiment for the wave steepness of 1/10, the wavelength to ship length of 1.5, the nominal Froude number is 0.25, the specific heading angle from the wave direction of 30 degrees and the rudder gain of 3.0. Here the positive roll means starboard side down and the positive yaw does starboard turn.

For the lower speed case shown in Fig. 10, the period doubling phenomenon were again found in both the experiment and the simulation. The measured roll amplitude is much larger than the simulated one. Furthermore, the mean of the measured roll angle is also larger than that of the

calculated roll angle. This suggests that hydrostatic heel moment due to trapped water on deck, which is not included in the numerical model, has a crucial role for inducing the extremely large roll angle in the experiment.

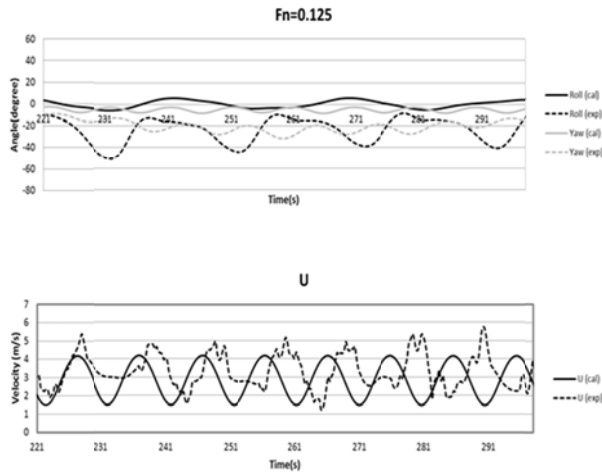


Fig. 10 Comparison between the simulation and the experiment for the wave steepness of 1/10, the wavelength to ship length of 1.5, the nominal Froude number is 0.125, the specific heading angle from the wave direction of 30 degrees and the rudder gain of 3.0.

4. EFFECT OF WEATHER DECK LENGTH

To create a proper definition for a vessel with extended low weather deck, the NAPA system was used to make systematically modified hulls of our offshore supply vessel (OSV) model.

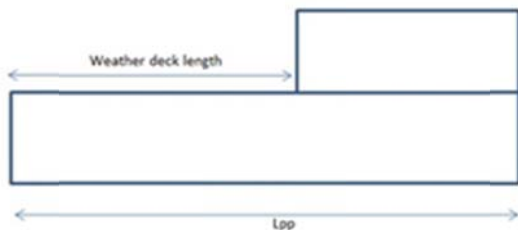


Fig.11 Simplified OSV with weather deck length definition.

The weather deck length, as defined in Fig. 11, was systematically modified with keeping other dimensions constant. Then the level 1 and 2 criteria were applied to the generated hulls. All modified hulls comply with the level 1 with directly calculated GM in waves because the required value

is 0.05m. The level 2 criteria consist of two requirements: CR1 is based on the angle of vanishing stability and CR2 is based on the angle of heel under action of the speed-dependent heeling lever. The standard for these values are 0.06. Here the Froude number is set to be 0.25. The results are shown in Fig. 12. Thus, when the weather deck length is larger than half the ship length between perpendiculars, the CR2 value rapidly increases so that the vessel is judged as vulnerable to pure loss of stability. To avoid such “false negative” case, it can be recommended to include the low weather deck length in the definition of a vessel with extended low weather deck.

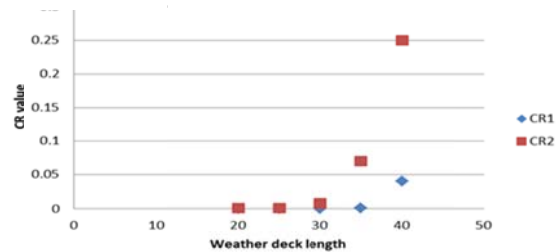


Fig.12 Weather deck length and CR values from Level 2 program results.

5. CONCLUSIONS

From this study, it can be concluded that pure loss of stability at higher speed in astern waves is not relevant to this OSV. However, large heel could occur due to trapped water on deck at very slow speed.

Based on the systematic hull modification survey, it also can be conclude here that, if the length of low weather deck is less than 0.5Lpp, it is not appropriate to apply the level 2 pure loss criterion to this type of ships.

6. ACKNOWLEDGEMENTS

This work was supported by a Grant-in Aid for Scientific Research from the Japan Society for Promotion of Science (JSPS KAKENHI Grant Number 15H02327). It was partly carried out as a research activity of Goal-based Stability Criteria Project of Japan Ship Technology Research Association in the fiscal years of 2015 funded by the Nippon Foundation. It was also a part of the collaborative research on intact stability between NAPA Japan and Osaka University. The authors sincerely thank these organizations.

7. REFERENCES

- Umeda, N. and Francescutto, A., 2016, "Current state of the second generation intact stability criteria - achievements and remaining issues", Proceedings of the 15th International Ship Stability Workshop, Stockholm.
- ITTC, 2008, Recommended Procedures, Model Tests on Intact Stability, 7.5-02-07-04.
- IMO, 2015, Report of the Working Group (Part 1), SDC 2/WP.4.
- Kan, M., Saruta, Taguchi, H., Yasuno, M. and Takaishi, Y., 1990, "Model Tests on Capsizing of a Ship in Quartering Waves", Proceedings of the 4th International Conference on Stability of Ships and Ocean Vehicles, Naples, pp.109-116.
- Kubo, H., Umeda, N., Yamane, K. and Matsuda, A., 2012, "Pure Loss of Stability in Astern Seas -Is It Really Pure?-", Proceedings of the 6th Asia-Pacific Workshop on Marine Hydrodynamics, Johor, pp.307-312.

Probabilistic Direct Stability Assessment

Vladimir Shigunov, *DNVGL Maritime, Hamburg, Germany*, vladimir.shigunov@dnvgl.com

ABSTRACT

According to the Second Generation Intact Stability Criteria (SGISC), developed by IMO, assessment of dynamic intact stability of ships can be done using either of three “levels” of assessment: Levels 1 and 2 involve significant simplifications, whereas Level 3 is based on advanced numerical simulation methods and allows, in principle, using probabilistic measures directly as safety criteria. Because the number of stability failures per design life is very low (problem of rarity), and because reliable estimation of probabilistic measures requires multiple realisations, direct use of probabilistic measures requires very long simulation time. Two possible solutions for this problem are studied in the paper: one uses extrapolation of the mean time to stability failure over wave height, and the other the reduction of the total space of conditions encountered during the design life (sea states, wave directions and ship speeds) to a small number of selected situations (“design sea state approach”), which are supposed to adequately reflect the ship’s dynamic stability in all conditions. Accuracy and adequacy of these two approaches is checked in numerical simulations.

Keywords: *Intact Stability, Probabilistic Methods, Design Sea States*

1. INTRODUCTION

According to the framework of the Second Generation Intact Stability Criteria (SGISC), the ship design should fulfill (in each condition of loading) requirements of any of three assessment Levels (1, 2 or 3), Fig. 1. Alternatively, Operational Limitations (OL) or Operational Guidance (OG) can be developed, based on results of Level 2 or Level 3 assessment, respectively.



Figure 1: Second Generation Intact Stability Criteria.

Level 3, including Direct Stability Assessment (DSA) and Operational Guidance (OG), is based on direct numerical simulation of ship motions in waves and allows, in principle, using direct probabilistic measures of the likelihood of failure as safety criteria: probability of failure in given time or time to failure. Although direct numerical simulations have been already used by designers

and Classification Societies (e.g. for the definition of structural loads, dimensioning of cargo securing and lashing, passenger comfort assessment and accident investigation), and although SOLAS allows, in principle, their use as alternative design assessment methods for the evaluation of ship dynamic stability, practical approval by the Administrations requires definition of clear and uniform procedures, as well as availability of suitable tools.

What is the sense of going for Level 3 assessment when a ship (in a particular loading condition) fails to fulfill Level 1 and Level 2? Simplifications involved in Level 1 and Level 2 procedures lead to scatter of assessment results compared to the true performance, which has to be compensated by safety margins. The safety margins are adjusted in such a way that all vessels, passing Levels 1 and 2, are sufficiently safe (which means that vessels, not passing these assessment levels, are not necessarily unsafe). Better accuracy of DSA allows reducing safety margins, thus loading conditions, not fulfilling Level 1 and 2 assessments, may be evaluated as sufficiently safe by DSA. Moreover, loading conditions failing DSA may still be allowed as seagoing loading conditions if Operational Guidance is provided. This means increased payload and better operability.

Level 1 and Level 2 criteria are close to finalization [1]; work on DSA and OG is planned to be finished by SDC4 (February 2017). Therefore, DSA and OG should be discussed in detail until then; this paper provides input for such discussion.

2. PROBABILISTIC MEASURES

Either non-probabilistic (mean roll amplitude, maximum roll amplitude per specified exposure time, root-mean-square of roll angle etc.) or probabilistic measures can be used as safety criteria. When a probabilistic approach is used for DSA or OG, one possibility is to directly use the *probability of stability failure during a given exposure time* as a criterion. This probability can be found by direct counting, e.g. as (weighted over all sea states) number of stochastic realisations of each sea state in which stability failure occurred to the entire number of realisations.

Alternatively to directly using probability of stability failure during a given time, another probabilistic measure is frequently used, the *average time to stability failure*. It is convenient and common to assume stability failure events to be described as a stationary Poisson process (which can be done if stability failure events are independent of each other). One way to achieve the independence of stability failure events in simulations is by performing them only until the first stability failure event. For a Poisson process, the *time interval until stability failure* is a random variable, satisfying exponential distribution with a constant rate parameter r and

- probability density function

$$f(x;r) = re^{-rx} \text{ for } x \geq 0 \text{ and } 0 \text{ otherwise} \quad (1)$$

- cumulative distribution function

$$F(x;r) = 1 - e^{-rx} \text{ for } x \geq 0; 0 \text{ otherwise} \quad (2)$$

- average time until stability failure

$$E\{X\} \equiv \bar{T} = 1/r \quad (3)$$

- standard deviation of time until failure

$$\sigma\{X\} = 1/r = \bar{T} \quad (4)$$

- variance of time until stability failure

$$\text{Var}\{X\} = 1/r^2 = \bar{T}^2 \quad (5)$$

The probability of at least one failure during time t can then be calculated as

$$p = 1 - e^{-rt} = 1 - e^{-t/\bar{T}} \quad (6)$$

or, for small failure rates $r \ll \bar{T}$,

$$p \approx t/\bar{T} \quad (7)$$

The estimate of the average time until stability failure \bar{T} can be found by repetition of numerical simulations N times and averaging time intervals T_i until the first stability failure from each simulation,

$$\bar{T} \approx \tilde{T} = \frac{1}{N} \sum_{i=1}^N T_i \quad (8)$$

Figure 2 compares function $g(x) \equiv -\ln[1-F(x)]$ derived from numerical simulations with the function $g(x) \equiv -\ln[1-F(x)] = x/\bar{T}$ following, for exponential distribution, from eq. (2) for $x \geq 0$. Figure 3 plots standard deviation σ of time until failure event vs. the average time until failure \bar{T} in comparison with the theoretical line for exponential distribution $\sigma = \bar{T}$, following from (4). Figures 2 and 3 confirm the validity of assuming Poisson process for stability failures and exponential

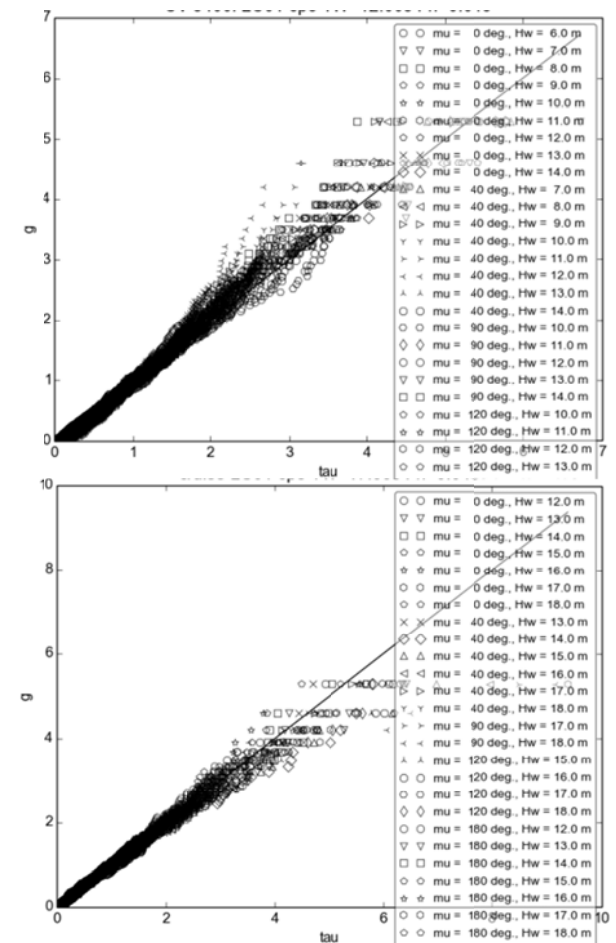


Figure 2: Function $g = -\ln(1-F)$ (y-axis) vs. non-dimensional time until stability failure $\tau = T/\bar{T}$ (x-axis) from numerical simulations (symbols) and theoretical exponential distribution (2) (line) for a container ship (top) and a cruise vessel (bottom).

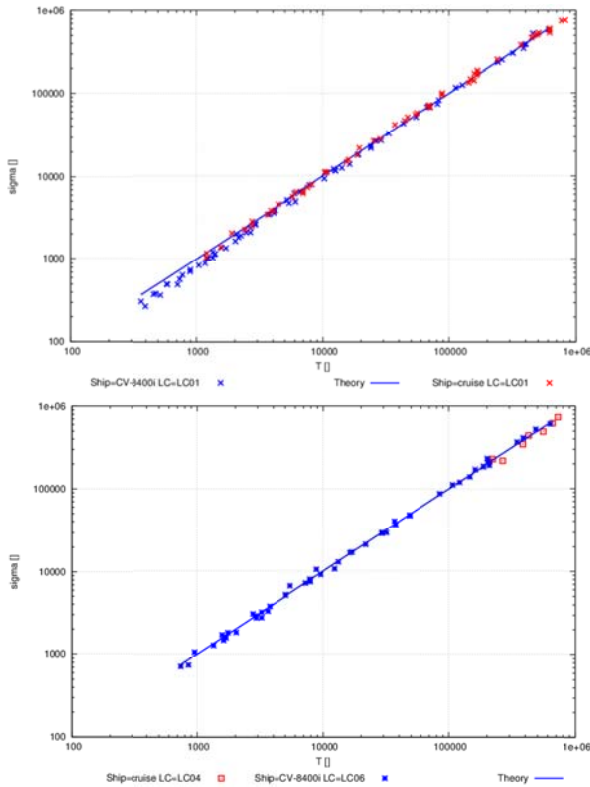


Figure 3: Standard deviation of time until stability failure (y-axis) vs. average time until stability failure \tilde{T} (x-axis) from numerical simulations (symbols) and theoretical exponential distribution (4) for exceedance of 40° roll angle (top) and 6.3 m/s^2 lateral acceleration (bottom).

distribution for time interval until stability failure, if care is taken in numerical simulations that stability failure events are independent of each other.

Although stability failure has not been defined yet within the Second Generation Intact Stability Criteria, an obvious definition is an exceedance of some roll angle or lateral acceleration threshold. In the examples considered here, exceedance of roll angle of 40° or lateral acceleration of 6.3 m/s^2 was used for illustration.

A practically relevant question is the required number of stability failure events to be encountered in simulations for an accurate enough estimate \tilde{T} of the average time until stability failure \bar{T} . The standard deviation σ_m of the mean time until stability failure \bar{T} satisfies, for large enough N , the law of large numbers

$$\sigma_m = \sigma / \sqrt{N} \quad (9)$$

where σ is the standard deviation of the time until stability failure. Using $\sigma = \bar{T}$ according to (4) for exponential distribution and requiring 95% confidence for the estimate \tilde{T} leads to the half-breadth of the 95%-confidence interval equal to

$$\Delta T = 1.96\sigma_m = 1.96\tilde{T}/\sqrt{N};$$

thus, the required number of stability failure events

$$N = 1.96^2 / (\Delta T / \tilde{T}) \quad (10)$$

Figure 4 shows the 95% confidence interval ΔT as percentage of \tilde{T} depending on the number of stability failure events N ; $N=100$ and 200 correspond to about 20 and 13% error, respectively.

3. PROBLEM OF RARITY

Using probabilistic safety measures as criteria requires some form of counting of stability failures, which means that stability failure events should be really encountered during numerical simulations. For the cases of interest in practical approval, the typical number of stability failure events per design life is very low: of the order of magnitude of less than one per design life (about 30 years), which means that the relevant average time until stability failure in simulations is more than 30 years.

Besides, accurate estimation of average time to failure from numerical simulations requires many repetitions of simulations in multiple random realisations of sea states: about 200 according to Fig. 4, if 10%-accuracy is required. This means, however, very long simulation time: for the considered 30 years and 200 realisations, 6000 years of simulation time.

Even with significantly simplified numerical simulation methods, achieving, for example, 1/1000 ratio of computation time to the simulation time, the resulting computational effort is too large. Below, two procedures are proposed that can significantly reduce computational time.

4. NUMERICAL TOOLS AND EXAMPLES

In the examples below, numerical simulations were carried out with a seakeeping simulation tool *rolls* [2], combining linear hydrodynamics with

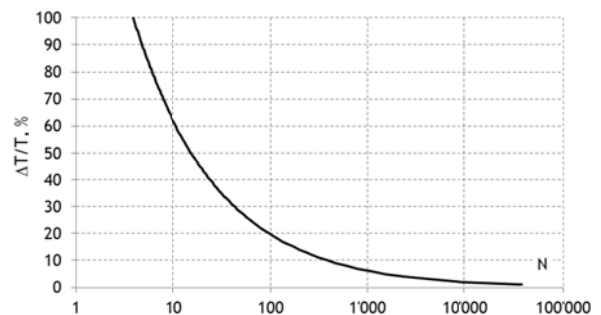


Figure 4: 95% confidence interval ΔT as percentage of \tilde{T} vs. the number of stability failure events N .

nonlinear Froude-Krylov and restoring forces, which is about 10^3 times quicker than real time for motion simulations in irregular short-crested waves.

As example ships, a cruise vessel, 1700, 8400 and 14000 TEU container ships and a RoRo ferry were used. For each vessel, three low-*GM* loading conditions were selected, for illustration of the pure loss, parametric roll and dead ship condition stability failure modes, and three high-*GM* loading conditions to illustrate excessive accelerations stability failure mode, Fig. 5.

5. EXTRAPOLATION OF FAILURE RATE OVER WAVE HEIGHT

To reduce the total simulation time required for probabilistic direct stability assessment and probabilistic operational guidance, extrapolation of

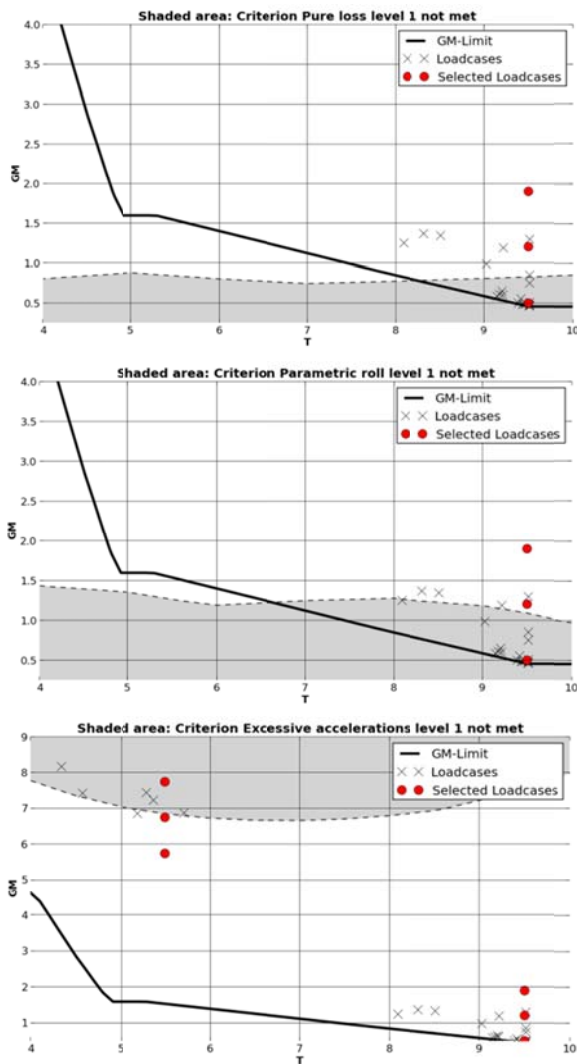


Figure 5: Loading conditions in example computations (●) for 1700 TEU container ship: draft (x-axis) vs. *GM* (y-axis), minimum *GM* according to 2008 IS Code (—), Level 1 vulnerability areas (grey) for pure loss (top), parametric roll (middle) and excessive accelerations (bottom) and loading conditions from Trim and Stability Booklet (×).

stability failure rate r or average time until stability failure $T=1/r$ over wave height (at the same wave period) can be used. This approach can be used to efficiently take into account all sea states in a scatter table, thus, if this method is applied for direct stability assessment, the results can be directly used as operational guidance.

The extrapolation method, proposed first by Tonguc and Söding [3], is applied here in the following form:

$$\ln T = A + B/h_s^2 \tag{11}$$

where T is the average time until a stability failure, h_s is the significant wave height, and A and B are constants, independent from the significant wave height but depending on wave period and direction, ship speed and loading condition.

A linear extrapolation of $\ln T$ over $1/h_s^2$ can be performed for such values of $\ln T$, for which $\ln T$ linearly depends on $1/h_s^2$, see e.g. Fig. 6. Note that linear extrapolation is also acceptable when the dependency of $\ln T$ on $1/h_s^2$ is convex, as in the example in Fig. 7; linear extrapolation in such cases leads to under-estimation of the average time until stability failure, i.e. to conservative results.

To find a value of $\ln T$, at and above which linear extrapolation over $1/h_s^2$ can be performed (in an accurate or at least conservative way), series of numerical simulations were performed for all ships and loading conditions described above at various forward speeds and seaway periods and directions. For each of these combinations, significant wave height was systematically varied. The average time until stability failure was defined from $N = 200$

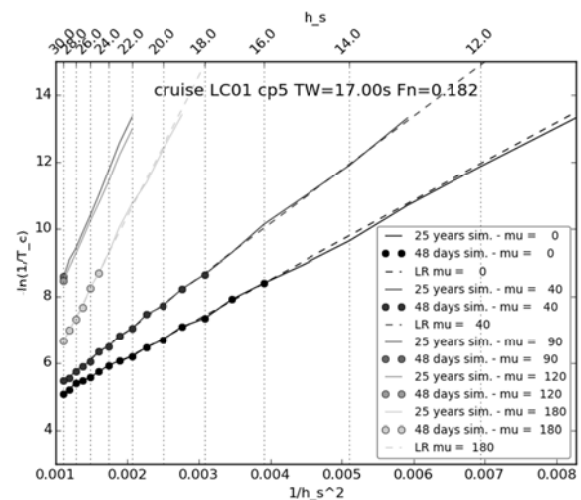


Figure 6: Examples of extrapolation approximating well results of direct simulations.

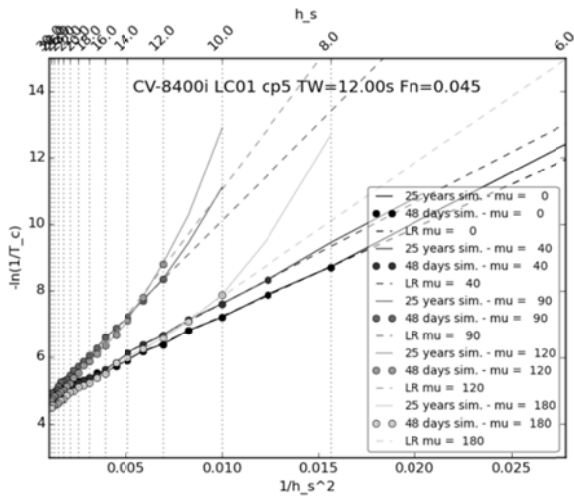


Figure 7: Examples of extrapolation leading to conservative results.

realisations of the same sea state until the first stability failure event (exceedance of 40° roll angle was used as stability failure event). The results of this study show that

- For most situations, the dependency of $\ln T$ on $1/h_s^2$ becomes linear for $\ln T > 5$, Fig. 8.

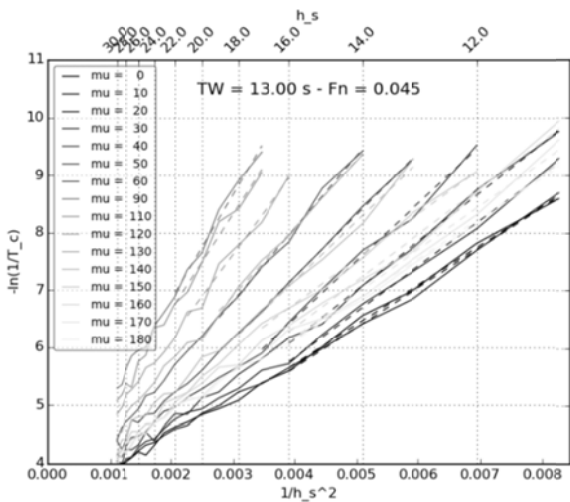


Figure 8: Examples of linear dependency of $\ln T$ on $1/h_s^2$ over complete range of wave heights.

- In many situations, the dependency of $\ln T$ on $1/h_s^2$ is slightly to moderately convex, Fig. 9 (top), in some cases strongly convex, Fig. 9 (bottom); for such cases, linear extrapolation of $\ln T$ over $1/h_s^2$ for $\ln T > 5$ would lead to conservative results, i.e. is still acceptable.
- In some situations, the dependency of $\ln T$ on $1/h_s^2$ is concave for $\ln T < 6$, Fig. 10; in such cases, extrapolation can be performed for $\ln T > 6$ to avoid non-conservative errors.

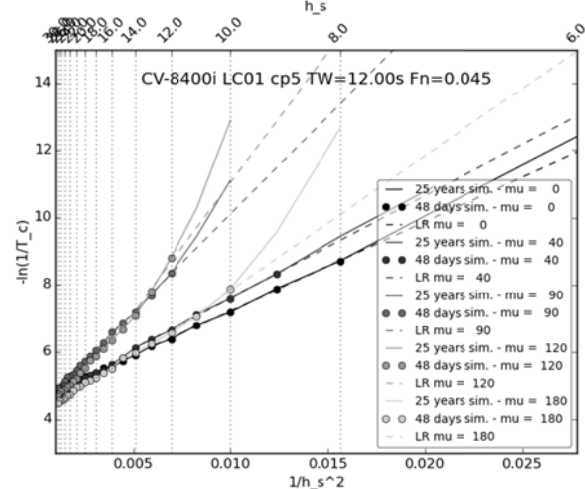
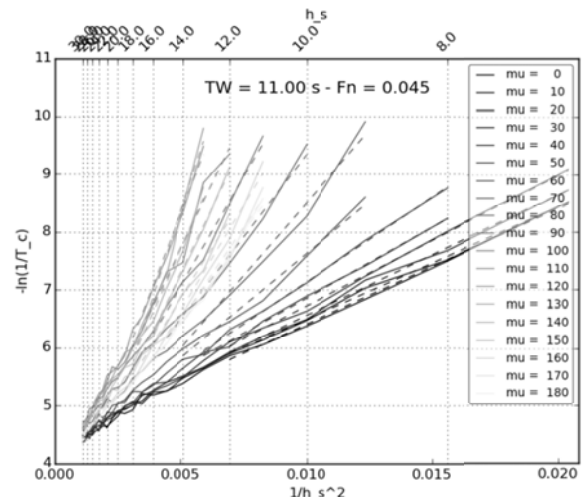


Figure 9: Examples of convex dependencies of $\ln T$ on $1/h_s^2$; linear extrapolation is conservative.

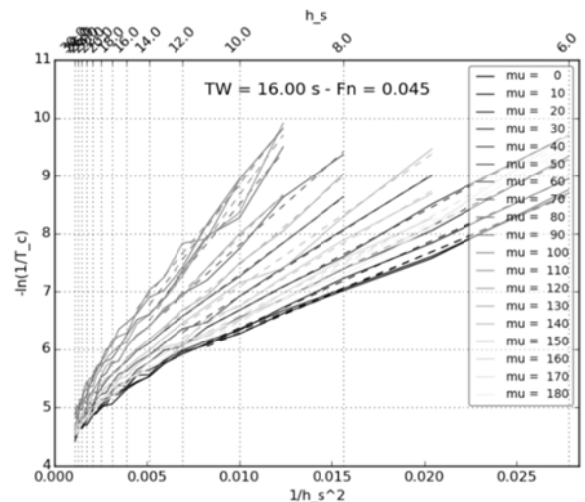


Figure 10: Concave dependencies of $\ln T$ on $1/h_s^2$ for $\ln T < 6$; linear extrapolation can be used for $\ln T > 6$.

Note that $\ln T = 6$ means about 400 s time interval until stability failure, which is feasible for modern numerical simulation methods.

If extrapolation of failure rate (or time interval until failure) over wave height is used, the required number of failure events used for averaging at each wave height can be reduced, because linear extrapolation can be simultaneously used as a smoothing linear fit to remove stochastic oscillations. Figure 11 compares dependencies of $\ln T$ on $1/h_s^2$, obtained with 200 (solid lines) and 20 (dashed lines) realisations per point. Although dashed lines show more stochastic oscillations, they can still be used for a linear fit.

For loading conditions, marginally fulfilling Level 1 parametric roll vulnerability criteria, direct simulations can cover rather large part of a scatter table in a feasible simulation time. Such sea states are highlighted green in the example (North Atlantic scatter table) in Fig. 12; sea states for which extrapolation over wave height had to be used are highlighted blue.

6. DESIGN SEA STATES

Probabilistic direct stability assessment requires summation of short-term probabilities of stability failure over all sea states in a scatter table and over all seaway directions. For example, the IACS scatter table for the North Atlantic contains 197 non-zero entries; if assessment is performed for every 10° seaway directions, the number of short-term simulations becomes 3743 (for each forward speed and for each loading condition). One possibility to reduce the required number of short-term assessments is to reduce the total space of conditions encountered during design life (wave height, period and direction and ship speed) to a small number of representative situations, assumed to be sufficient for norming: ships performing well enough in the selected situations will also perform well enough in all possible conditions (“design sea states” method).

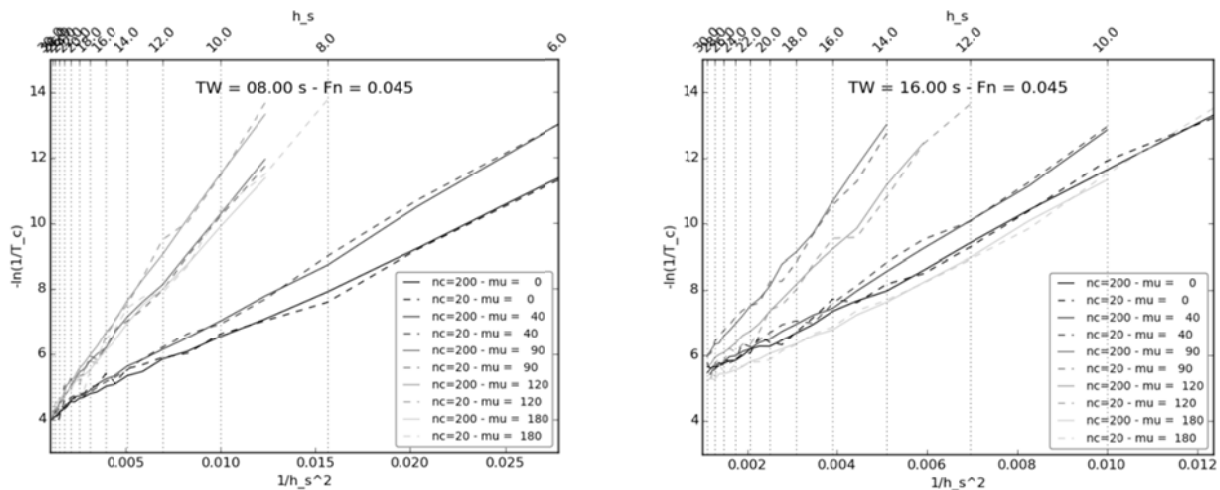


Figure 11: Examples of dependencies of $\ln T$ on $1/h_s^2$ using $N=200$ (solid lines) and 20 (dashed lines) realisations for a cruise vessel (left) and a 8400 TEU container ship (right).

HS/Tz	2	3	4	5	6	7	8	9	10	11	12	13	14	15	16	17	18
16										0.3	0.4	0.4	0.3	0.2			
15									0.5	1.0	1.3	1.2	0.7	0.3	0.2		
14								0.4	1.5	3.0	3.6	2.9	1.8	0.8	0.3		
13						0.1	1.4	4.6	8.3	9.1	6.9	3.9	1.8	0.6	0.2		
12						0.7	4.5	13.5	21.9	22.0	15.4	8.1	3.5	1.2	0.3		
11						2.3	14.0	37.4	54.3	49.9	32.1	15.7	6.2	2.0	0.6	0.2	
10					0.2	7.9	41.5	97.4	126.2	104.7	61.7	27.9	10.3	3.2	0.9	0.2	
9					2.1	26.1	116.3	237.0	271.9	202.7	108.8	45.2	15.5	4.5	1.1	0.3	
8					7.8	82.2	305.2	533.3	536.5	357.0	173.4	66.0	20.8	5.6	1.4	0.3	
7					0.3	29.0	243.2	740.5	1095.1	955.6	562.4	245.5	85.1	24.7	6.2	1.4	0.3
6					4.1	103.6	667.6	1633.6	2012.3	1503.4	774.4	301.1	94.4	25.1	5.9	1.2	0.3
5					19.0	347.4	1664.3	3193.7	3212.1	2021.5	899.0	307.9	86.4	20.8	4.5	0.8	0.1
4				0.5	88.6	1064.7	3641.5	5304.3	4240.3	2198.2	828.4	245.9	61.0	13.2	2.5	0.4	
3				9.0	386.5	2840.3	6542.8	6894.4	4207.4	1735.8	538.0	134.9	29.0	5.6	1.0	0.1	
2			0.1	72.1	1457.4	5780.8	8104.1	5669.4	2452.7	754.8	181.8	36.7	6.6	1.0	0.1		
1		1.5	291.4	1815.4	2811.2	1820.4	665.5	165.2	31.3	5.2	0.4						

Figure 12: Sea states in which failure rate was defined direct from numerical simulations (green) or extrapolated over wave height (blue); numbers correspond to frequency of occurrence of sea states in North Atlantic wave climate.

Various definitions of design sea states are possible; here design sea states cover all zero-upcrossing periods of a scatter table (with a step of 1 s), but with only one significant wave height per wave period; this wave height was defined using the wave steepness table from [3]. Three wave directions (head, beam and following) were used in each design sea state to cover parametric and synchronous roll and pure loss of stability.

For comparison, also full probabilistic direct stability assessment was performed, taking into account all zero-upcrossing seaway periods and all wave heights in the North-Atlantic scatter table and for all wave directions (assuming them uniformly distributed) with 10° step. Exceedance of 40° roll angle was used as stability failure. Note that in the full probabilistic assessment, it is not possible to separate contributions from parametric or synchronous roll or pure loss of stability in the total probability of stability failure.

The aim of this study was to compare results of full probabilistic stability assessment (full scatter table, all wave directions) with the assessment in design sea states (about 10 sea states, three wave directions). Stability failure rates in design sea states were weighted and summed; the weights were taken equal to the occurrence frequencies of zero-upcrossing periods. This assessment was performed for the same ships and loading conditions as in the previous section, separately at several forward speeds.

Using significant wave heights according to the wave steepness table [4] leads to relatively steep seaways. Still, stability failure rates could not be computed directly in some cases (particularly in short waves) because of too rare stability failure events; in such cases, extrapolation of stability failure rate over significant wave height was used. Examples in Fig. 13 illustrate this: the significant wave heights according to [3] are shown with vertical blue lines. In less steep sea states, e.g. as those suggested by Italy for Level 2 vulnerability assessment for parametric roll, stability failure events are much less rare and might require extrapolation at all wave periods. On the other hand, steeper design sea states than those according to [3] may be difficult to implement in model tests.

Figure 14 compares the dependencies of the weighted stability failure rate in design sea states

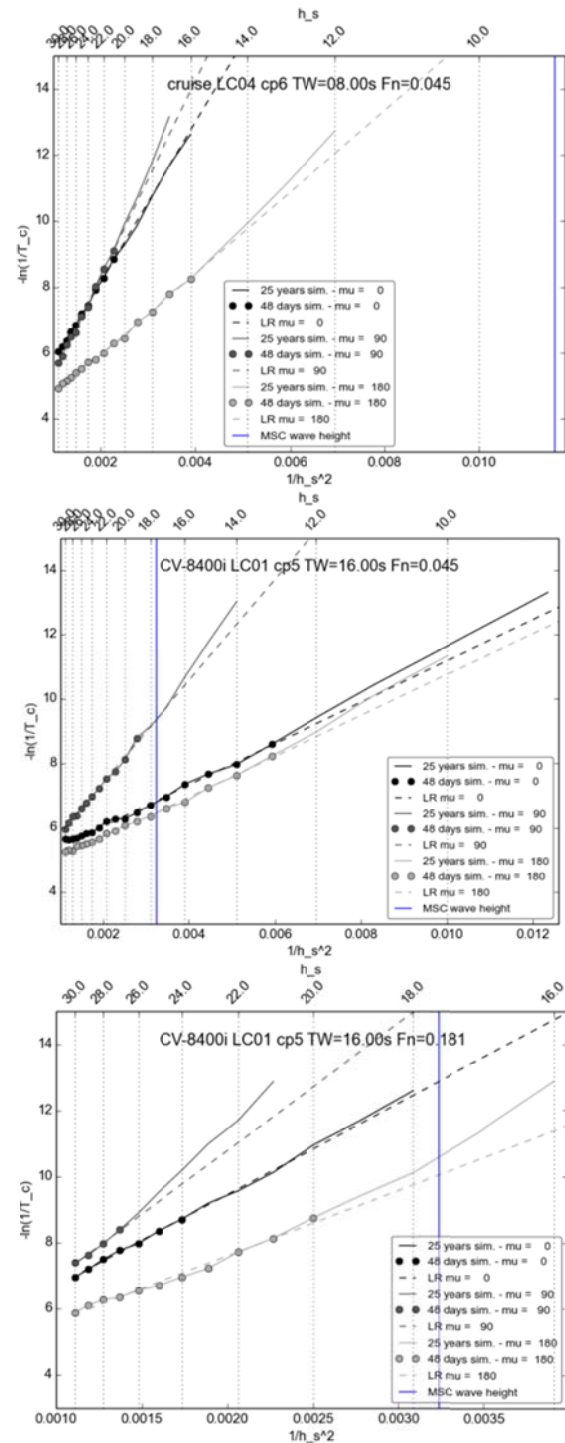


Figure 13: Examples of dependencies of $\ln T$ on $1/h_s^2$ in design sea states; vertical blue lines correspond to wave height according to seaway steepness table from [3].

(y-axis) on the long-term stability failure rate in all sea states and all wave directions (x-axis) for the four vessels between following, beam and head waves. Figure 15 shows weighted sums of stability failure rates over all design sea states (y-axis) vs. long-term stability failure rate in all sea states and all wave directions (x-axis) between the four vessels, each point corresponds to a combination of a loading condition and forward speed.

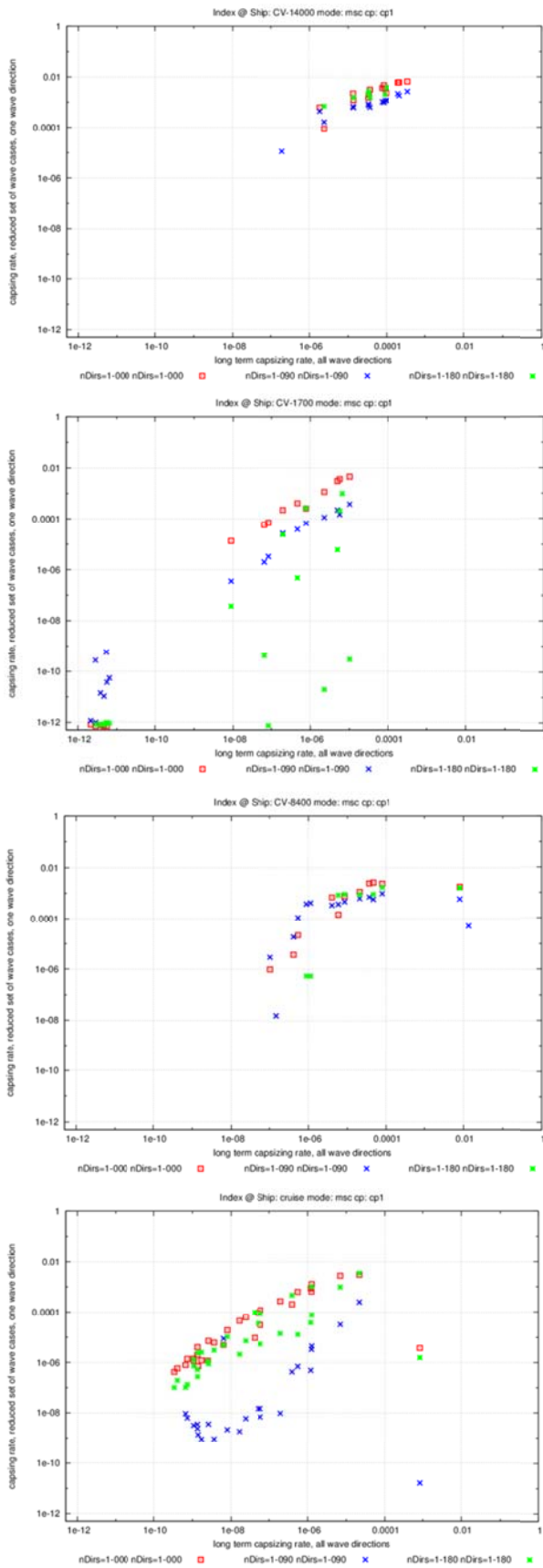


Figure 14: Stability failure rates in design sea states (y-axis) at three wave directions (different symbols) vs. long-term stability failure rate in all sea states and all wave directions (x-axis) for four vessels.

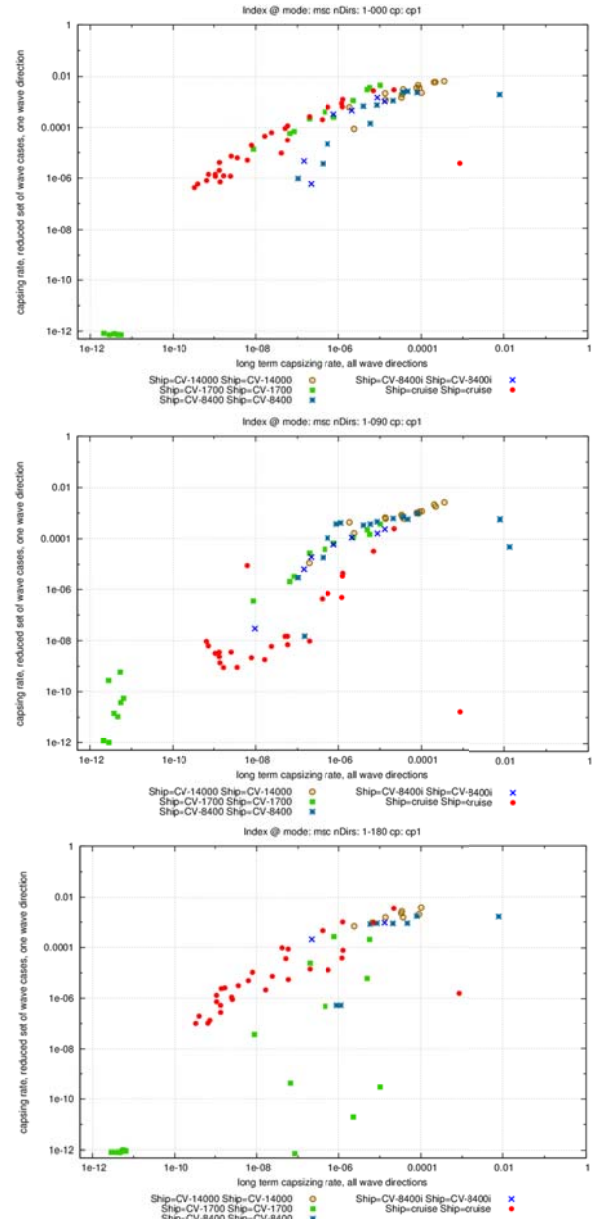


Figure 15: Stability failure rates in design sea states (y-axis) vs. long-term stability failure rate in all sea states and all wave directions (x-axis) for four vessels (different symbols) in following (top), beam (middle) and head (bottom) waves.

A similar comparison was performed for excessive accelerations stability failure mode for loading conditions with large initial GM values. The stability failure was defined as the exceedance of 6.3 m/s^2 lateral acceleration; simulations in design sea states were performed only in beam waves (long-term probabilistic assessment was still performed in all wave directions). Figure 16 shows the weighted sum of stability failure rates in design sea states in beam waves (y-axis) vs. the long-term excessive accelerations stability failure rate (x-axis) separately for each of the four vessels; Fig. 17 summarises results.

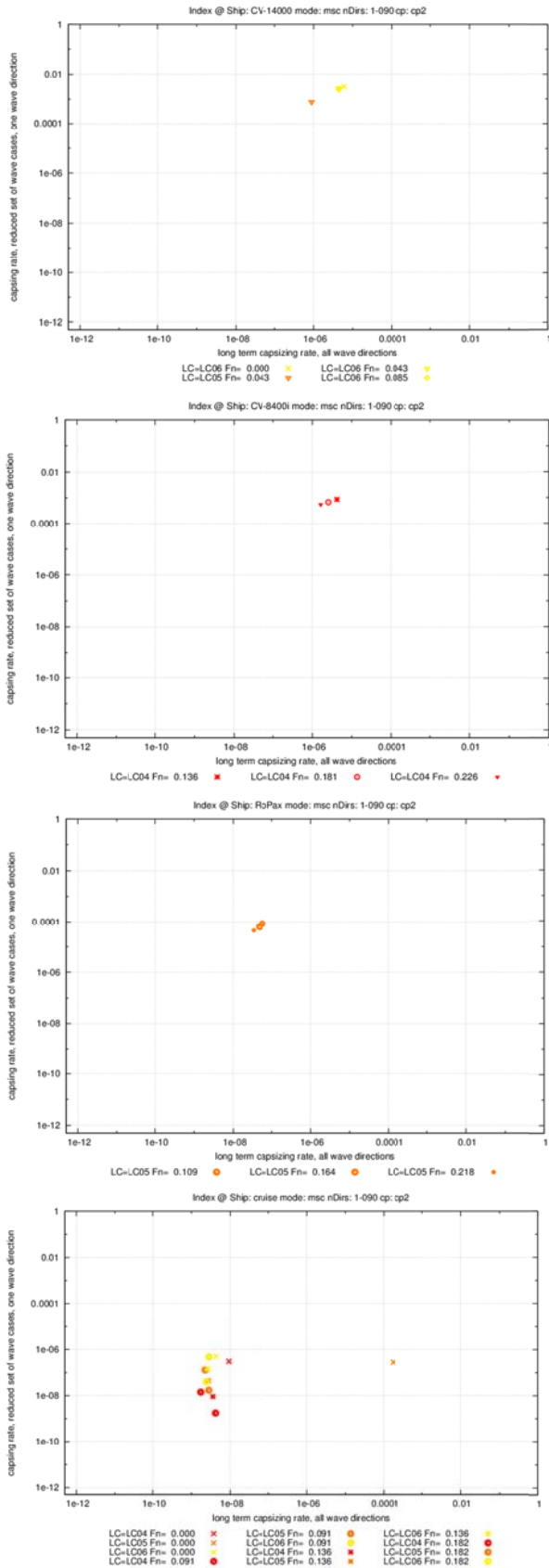


Figure 16: Excessive acceleration stability failure rate in beam design sea states (y-axis) vs. long-term stability failure rate in all sea states and all wave directions (x-axis) separately for each of four vessels.

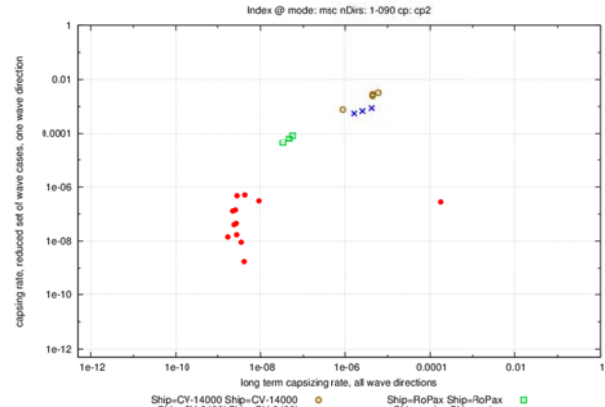


Figure 17: Excessive acceleration stability failure rate in beam design sea states (y-axis) vs. long-term stability failure rate in all sea states and all wave directions (x-axis) for four vessels (different symbols).

The concept of design sea states can be used if the dependency of the full long-term stability failure rate on the stability failure rate defined in design sea states is monotonous (i.e. ranking of different loading conditions is the same in the full long-term assessment and in the design sea states) and, besides, the same for all ships and all loading conditions. Figures 15 and 17 confirm, in principle, that this dependency is approximately monotonous, i.e. ranking of ships, loading conditions and forward speeds is correctly reproduced. However, these dependencies show significant scatter between ships and forward speeds, which means that standards, defined for the “design sea states” method will have to be selected conservatively for some ships, i.e. that this assessment is not the “true Level 3” assessment. This scatter requires further consideration, e.g. the idea of different design sea states for different stability failure modes may provide better results.

For the loading conditions on the margin of Level 1 vulnerability assessment, short-term stability failure rate in design seaways is of the order of $5 \cdot 10^{-3}$ 1/s in full scale; this corresponds to time until stability failure of about 30 s in model scale, which is feasible for model tests as well as for numerical simulations.

7. PRACTICAL CONSIDERATIONS

The preparation of the simulations has required about 2 days for 5 ships (6 loading conditions for each). Note that the required input is not part of standard approval, thus the preparation has required much manual work, which will not be required in

the future. The computation time per loading condition per forward speed was 750 h processor time for the full long-term assessment using extrapolation of failure rate over wave height. When design sea states assessment was used, the entire computational time was 68 h per loading condition per forward speed. Note that the reduction of the computational time of the design sea states method compared to the full assessment was only $750/68 \approx 11$ times, from which $19/3 \approx 6$ times due to the reduced number of wave directions; thus, the reduction of computing time due to the reduced number of wave heights (1 in the design sea states method vs. 16 in the full assessment) was only 1.7 times.

Extrapolation of stability failure rate over wave height in a probabilistic direct stability assessment can be applied to provide accurate or at least conservative results in acceptable computational time. The advantage of this approach is that the results of direct stability assessment can be directly used as operational guidance. On the other hand, design sea states approach can reduce the total computational time required for direct stability assessment by more than 10 times compared to the method based on extrapolation. Although the results of assessment in design sea states cannot be used as operational guidance, this method can be used to sort out sufficiently safe loading conditions at a lower computational cost, and then use a more comprehensive method to develop operational guidance only for those loading conditions that fail direct assessment.

Operational Guidance is defined as “*the recommendation, information or advice to an operator aimed at decreasing the likelihood of failures and/or their consequences*” [5]; it is assumed to be developed using outcomes of the direct stability assessment. Operational Guidance can be implemented, in principle, according to the following approaches: (1) pre-computation and approval of Operational Guidance at the design stage; (2) pre-computations by an on-shore provider before departure; and (3) real-time computations during operation.

Following option (1) Operational Guidance is pre-computed and approved in the design stage, which allows using most comprehensive numerical tools and statistical procedures, e.g. probabilistic assessment. However, such computations can be

performed only for assumed input parameters, most importantly, standard seaway spectra. Sensitivity of the results to the input parameters needs to be investigated. In option (2), Operational Guidance is pre-computed by an on-shore provider before departure from the port, using the most actual weather forecast available. This approach allows, in principle, using comprehensive numerical tools and statistical procedures. The drawback of this option is the possibility of unforeseen delays in the ship operator time schedule. In option (3), required computations are performed in real-time (on board or onshore) during operation, once accurate weather forecast is available, thus both numerical tools and statistical procedures have to be significantly simplified; note that the advantage of more accurate weather data may be to some degree compensated by reduced accuracy of numerical tools and statistical procedures. Note also that “real time” means here simulations well before encountering heavy weather conditions, in order to enable route changing to avoid heavy weather if operational measures are not sufficient to achieve the required safety level.

Input from all interested stakeholders is required to discuss advantages and drawbacks of options (1)-(3).

Finally, practical approval of Level 3 procedures (both direct stability assessment and operational guidance), needs quantification of the uncertainty of the proposed methods, both for the full assessment based on the extrapolation over wave height and for the design sea states method.

REFERENCES

- [1] IMO (2015) Report of the Working Group on Intact Stability SDC 2/WP.4, Annex 5
- [2] H. Söding, V. Shigunov, T. Zorn and P. Soukup (2013) Method *rolls* for simulating roll motions of ships, *Ship Technology Research – Schiffstechnik* **60**(2)
- [3] E. Tongué and H. Söding (1986) Computing capsizing frequencies of ships in seaway, *Proc. 3rd Int. Conf. on Stability of Ships and Ocean Vehicles*
- [4] IMO-MSC (2006) Interim Guidelines for alternative assessment of the Weather Criterion, MSC.1/Circ.1200
- [5] IMO (2008) Revision of the Intact Stability Code - Report of the Working Group (Part 1) SLF 51/WP.2, Annex 2

Regulatory Aspects of Implementation of IMO Second Generation Intact Stability Criteria

William S. Peters, *USCG Office of Design and Engineering Standards*

Vadim Belenky, *Naval Surface Warfare Center Carderock Division*

ABSTRACT

Development of second generation intact stability criteria at IMO began in 2005, but is based on research that has been carried out over many decades. While research can identify algorithms or processes that can successfully replicate or describe physical phenomena of ship stability failure, a regulation requires an assessment about whether or not a standard has been satisfied. Even if presented in a probabilistic format, the assessment of regulatory compliance ultimately comes to an evaluation of whether there is an acceptable likelihood of failure. The development of the second generation intact stability criteria acknowledges both the contribution of intact stability research through the use of levels of vulnerability criteria and the challenge of identifying methods of assessment that are simultaneously reliable, consistent, and robust. This challenge is further complicated by understanding that a given ship may be assessed to have both an acceptable and unacceptable likelihood of failure based upon the ship's loading condition. This paper discusses these and related aspects of the development of regulations for the second generation intact stability criteria. In particular, procedures for revision and rectification of the criteria, standards and explanatory notes are discussed. The industry already provided valuable feedback on consistency between the levels of vulnerability criteria on pure loss of stability. More feedback is expected in the next few years, so the regulator has to be ready to process and use this feedback

Keywords: *IMO, Second Generation Intact Stability Criteria, 2008 IS Code.*

1. INTRODUCTION

The development of the IMO second generation intact stability criteria has been an intense effort spanning many years. Even while the work to restructure the 1993 intact stability code was underway, the goal to address the problems against accidents related to stability which generally had not yet been solved was understood. Indeed, the preamble to the 2008 IS Code recognizes this: *"...the safety of a ship in a seaway involves complex hydrodynamic phenomena which up to now have not been fully investigated and understood. Motion of ships in a seaway should be treated as a dynamical system and relationships between ship and environmental conditions such as wave and wind excitations are recognized as extremely important elements. Based on hydrodynamic aspects and stability analysis of a ship in a seaway, stability criteria development poses complex problems that require further research."* That the work to realize this goal is coming to fruition is a testament to the

perseverance and diligence of those persons involved in the effort.

The care by which the outcomes of this work are placed into a regulatory framework is no less important than the work itself. Further, the introduction of these new criteria into a recognized international instrument such as the 2008 IS Code represents - at least for some entities in the maritime industry - added regulatory encroachment where - they believe - none is really needed. Machiavelli identified the problem: *"There is nothing more difficult to take in hand, more perilous to conduct, or more uncertain in its success, than to take the lead in the introduction of a new order of things."* That the second generation intact stability criteria regulation is an initiation of a new order of things is a view difficult to successfully oppose.

The development of the second generation stability criteria recognizes that stability failure may be caused by different physical mechanisms, and, as identified in section 1.2 of Part A of the

2008 IS Code on dynamic stability phenomena in waves, the different modes of stability failure are explicitly considered:

- Restoring arm variation problems, such as parametric excitation and pure loss of stability;
- Stability under dead ship condition, as defined by SOLAS regulation II-1/3-8;
- Maneuvering related problems in waves, such as broaching-to (initiated by surf-riding); and
- Excessive accelerations (SLF 53/19, paragraph 3.28).

As has been discussed previously, the appearance of novel hull forms renewed interest in dynamic stability, (see e.g. France, et al. 2003) and in development of methods to assess dynamic stability. The development has emphasized an adequate replication of the physics of stability failure and on making the new criteria performance-based (Belenky, et al. 2008). In other words, instead of addressing certain types of ships, the new criteria bases ship assessments on the hull geometry, the loading condition, and the physics of the stability failure.

The multi-tiered structure of new criteria addresses the potential complexity of the application of the new criteria. The first-level vulnerability check is very simple and quick, but conservative. If vulnerability to a particular stability failure mode is determined not to occur, no further assessments are needed. If not, then a more detailed, but less conservative analysis follows, which is the second-level vulnerability assessment.

2. THE CURRENT STATUS

The IMO Sub-committee on Ship Design and Construction (SDC) finalized the five elements of the criteria as Draft amendments to Part B of the 2008 IS Code for:

- Vulnerability Criteria of Levels 1 And 2 for the Pure Loss of Stability Failure Mode (Annex 1 of SDC 2/WP.4);
- Vulnerability Criteria of Levels 1 And 2 for the Parametric Rolling Failure Mode (Annex 2 of SDC 2/WP.4);
- Vulnerability Criteria of Levels 1 And 2 for the Surf-Riding / Broaching Failure Mode (Annex 3 of SDC 2/WP.4).
- Vulnerability Criteria of Levels 1 And 2 for the Dead Ship Condition Failure Mode (Annex 1 of SDC 3/WP.5).

- Vulnerability Criteria of Levels 1 And 2 for the Excessive Acceleration Failure Mode (Annex 2 of SDC 3/WP.5).

The criteria and standards for each of these five stability failure modes are addressed in the foregoing documents. The development of the explanatory notes for the second generation instability criteria is expected to ensure uniform interpretations and application of the new criteria such that two assessments of the same ship's loading condition yields a common result. The technical background of these criteria is described in Peters, *et. al.* (2011). Annexes 3 through 7 of document SDC 3/WP.5 contain the current drafts of the explanatory notes for each of the five stability failure modes.

3. GENERAL CONSISTENCY ISSUES

A critical element of the robustness of the criteria is a reliable and repeatable assessment method. Common difficulties are the implied relationships between Parts A and B in the Code that, currently, are handled as footnotes. Mandatory criteria in part A refers to loading conditions defined in Part B (Sections 3.3. and 3.4, respectively). Part A criteria regarding righting lever properties allows for alternative criteria for cases where the angle of the maximum righting lever when less than 25 degrees.

Further, the last paragraph of the section (2.3.5) on the weather criterion points out that the criterion was based on ships having certain parameters, the most significant of which is probably the beam to draft ratio (B/d) to be less than 3.5. The current requirement permits the angle of roll to be determined by model tests using the procedures in MSC.1/Circ.1200. Given the costs associated with model tests the desirability of permitting an analytical method as an alternative is clear. The challenge for this is to ensure that the alternative method provides reliably consistent outcomes for ships with loading conditions that satisfy the weather criterion and those loading conditions with parameters beyond those provided.

4. CONSISTENCY ISSUES IN PURE LOSS OF STABILITY

Large values of B/d seem to contribute to consistency issues of vulnerability criteria for pure loss of stability. Inconsistency between Levels 1

and 2 of the vulnerability criteria has been reported in Annex of SDC 3/6/2, when analyzing results for cruise ships for values of drafts and GM , i.e. maximizing B/d ratio. To explore this, a case study was performed with a notional cruise ship to determine the underlying reason for inconsistency. The geometry and principal particulars of the notional ship are presented in Figure 1 and Table 1. With the value of $B/d = 4.75$, the notional ship's characteristics are similar to other ships for which the inconsistency has been observed.

Table 1 Principal particulars of notional ship for the case study

Length BP, m	260
Length OA, m	271.7
Beam, m	38
Draft, m	8
Speed, kt	25

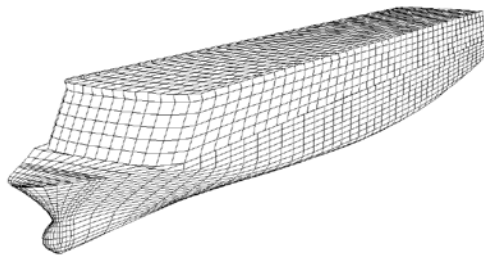


Figure 1 Geometry of notional ship for the case study

The main control parameter for the study was the Depth to the freeboard deck, which was varied from 15 to 18 m in 1 meter increments. The following steps were carried out for each value of depth:

- Step 1: Calculate the limiting KG value based on 2008 IS Code (Part A, 2.2 only – the weather criterion was not evaluated since the B/d ratio is out of applicable range).
- Step 2: Carry out the vulnerability criterion Level 1 check for the critical KG. If the case is found not to satisfy the Level 1 standard, the KG is reduced and the case is re-checked. If the case is still found not to satisfy the Level 1 standard, the KG is reduced again. This process is repeated until the Level 1 criterion is satisfied.
- Step 3: Carry out the vulnerability criterion Level 2 check for the step 2 determined KG

The results are shown in Table 2. The third column in the table identifies the limiting factor from the 2008 IS Code, A/2.2. The inconsistency between the Level 1 and 2 is observed for the values of depth of 16 and 17 m

Table 2 Vulnerability check for pure loss of stability

D, m	KG, m	Limit factor	Level 1 GM, m	Level 2 CR1	Level 2 CR2
Standard values =			> 0.05m	< 0.06	< 0.06
15	16.74	f_{max}	3.0935	0.0005	0.00039
16	19.5	f_{max}	0.33	0.089	0.036
17	19.78	GM_{min}	0.053	0.073	0.048
18	19.78	GM_{min}	0.053	0.036	0.048

The mechanism of inconsistency may be partially understood from Figure 2, which shows the GZ curves for different wave steepness, when the wave crest is near amidships. One can see that somewhere between above the steepness 0.03 (actually above 0.0334 as the Level 1 criterion is satisfied), the GZ curve becomes completely negative. Because there are a sufficient number of wave cases from the wave scatter table that are capable of causing such a deterioration of the GZ curve, the total probability exceeds the standard value of 0.06.

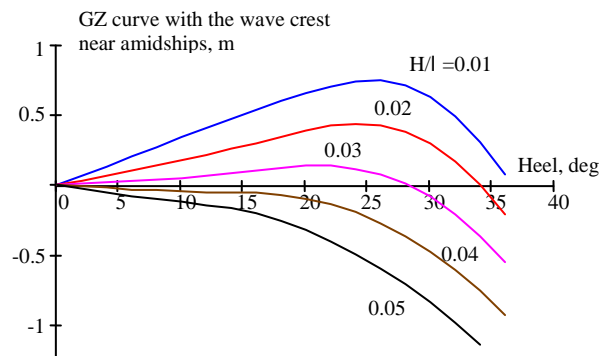


Figure 2 GZ curves in waves for different values of wave steepness, $D=17$ m

As the inconsistency has been discovered, two questions should be answered: why is the vulnerability criterion inconsistent and what can be done to insure consistency in the future?

Possible Reason for Inconsistency

The Level 1 criterion is based on the minimum GM value calculated during the wave pass. As is well-known, the GM does not characterize the stability of a ship in large heel angles. At the same time, the Level 2 criteria include stability characteristics at large angles of heel such as the minimum value of the angle of vanishing stability in waves and minimum value of the heel angle under specified heeling moment. Thus, a consistency between Levels 1 and 2 is not automatic.

Such an answer may lead to another question: more than a hundred sample ships have been tested during the development of the vulnerability criteria, but why has this inconsistency not been discovered earlier in the criteria development as the consistency between the levels was one of the items checked when testing the vulnerability criteria?

The parameters of the GZ curve are not independent values. Further, testing of the second generation intact stability criteria generally assumed that the first generation criteria are satisfied. A possible reason, therefore, why it was not discovered earlier is probably that the consistency was implicitly provided by this dependence. Thus, when the parameters of a ship to be tested were out of the usual range ($B/d = 4.75$), the “traditional” means of providing consistency was no longer available.

Resolving the Inconsistency

Once the inconsistency has been discovered and its reason understood, it must be resolved. For the multi-tiered second generation intact stability criteria, the following three-step procedure may be considered:

Step one – establish the ground truth: is a ship where the inconsistency between the levels is discovered, actually vulnerable to the stability failure of interest?

Step two –consider if refining the calculation method for cases where the inconsistency is found, solves the problem. If it does, then, the explanatory notes can be revised with the identified process, which may be considered as a new interpretation.

Step three – consider if changing a standard solves the problem. If it does, the regulation document may be updated, but there would not be a need to redo the sample calculations.

Consideration of revising the criteria should occur only if both step two and three are unsuccessful and the compelling need to resolve the inconsistency remains evident.

Step One: Ground Truth

The inconsistency between Level 1 and 2 means that Level 1 criteria indicate vulnerability, while the Level 2 criterion does not. As an approved direct stability assessment procedure is not yet available, the ground truth has to be established based on practical experience. As it is

noted in SDC 3/6/2, there are no reliable data on vulnerability of cruise ships to pure loss of stability. Three cases of stability failure attributable to pure loss of stability have occurred with passenger and ro-ro ferries, not cruise ships (Maritime New Zealand, 2007; Swedish Accident Investigation Board, 2008; Transportation Safety Board, 2011). Indeed, caution has to be exercised, but for the time being assume the notional ship is non-vulnerable to pure loss of stability.

Step Two: Refinement of Calculation Method

Inclusion of the weathertight volume as buoyant volume into the stability calculations could be an example of such refinement. Why is it a good idea?

Consider the following scenario: when a ship heels due to degradation of stability near the wave crest, superstructures will immerse and provide additional drag; speed will decrease and the wave will take over the ship. Once the wave crest passes, stability will be partially regained and a ship may return to the upright position. As a result, the duration of the immersing of the superstructure may be not sufficient for progressive flooding to occur through the closed weathertight openings. Thus, the exclusion of the weathertight volume may make the Level 2 assessment too conservative. Is this possible?

Table 3 shows results of calculations for the notional ships with the volume of superstructure included as it was assumed “weathertight.” Figure 3 shows GZ curves for different wave steepness, when the wave crest is near amidships calculated with the superstructure included. This inclusion lead to a decrease of the CR1 values in the Level 2 check as they are related to the range of stability. As expected, there is no effect on the CR2 value since this reflects stability at smaller angles. Formally, the inconsistency has been resolved because the Level 2 criterion no longer indicates vulnerability

Table 3 Vulnerability check for pure loss of stability with the weathertight volume included

D, m	KG, m	Limit factor	Level 1 GM, m	Level 2 CR1	Level 2 CR2
Standard values =			> 0.05m	< 0.06	< 0.06
15	16.74	f_{max}	-	-	-
16	19.5	f_{max}	0.33	0.0028	0.036
17	19.78	GM_{min}	0.053	0.0035	0.048
18	19.78	GM_{min}	0.053	0.0035	0.048

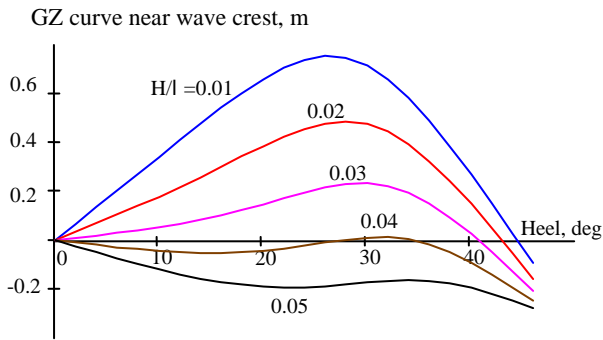


Figure 3 GZ curves in waves for different values of wave steepness, $D=17$ m with superstructure included

Step Three: Changing Standards

While in a formal sense the inconsistency has been resolved, the values in Table 3 are quite close to the standard. So, a re-consideration of the standard value may be appropriate.

The current standards are set by comparison of the criteria values for a ship with known vulnerabilities and ships known not to be vulnerable. Usually, the gap between these quantities is large enough that a change of the standard value may be allowed towards less conservative side without introducing new inconsistencies.

Alternatively, the standard may be customized for different size of ships (say, on the basis of length). The GZ curves in Figure 2 and Figure 3 computed for the wave steepness 0.05 look very dangerous with or without including the superstructure. However for a ship with length of 260 m, the wave height is 13 m for steepness of 0.05. There is a low likelihood that a ship of this size and power (and under control) would encounter a wave of this size by the stern.

The Level 2 vulnerability criterion for pure loss of stability is, in fact, a long-term probabilistic criterion. As it was shown by the simulation study (Boonstra, *et al* 2004, ter Bekke, *et al*, 2006, van Daalen, *et al* 2005) carried out in the Netherlands and summarized in SLF 49/INF.7, the long-term probabilistic assessment performed without including any (even extremely simple) operator model may lead to overconservative results. Thus, it may be meaningful to include such considerations when customizing the standard for different sizes of ships.

5. SUPPORT OF REGULATIONS

Regulations or rules define a relationship between a criterion and a standard. When a regulation comes into effect, it does so only after a normally lengthy process that includes identification of compelling need, development, testing, proposal, notice and comment, revision, approval and adoption. Each of these stages adds to the support that is necessary for the regulation application to be consistent not only for the ships that are tested but also for those that are not tested. Hence, the regulation support includes interpretations on the implementation of the regulation as well as providing for regulatory updating to reflect changes in accepted safety level and design, construction and operation practices. In this way, regulations may be conceived as similar to published software.

There is a constant opposite pull between the need for easily amendable regulations and the need for regulatory stability to aid commerce. Outside the scope of this discussion there exist international issues that are bogged down because of the difficulties of regulatory amendment. This experience, like similar others, demonstrate that regulations should include flexible amendment procedures based on the needed support.

While the support issues are not explicitly considered in the framework of IMO's second generation intact stability criteria (Annex 1 to SLF 54/3/1), the explicit separation of criteria and standards facilitates rational and transparent organization of regulation support.

The criteria reflect current understanding of physics of stability failure expressed with the different level of complexity, depending on the level. The standards reflect the operational experience and empirical safety level. Adjusting the standard allows the regulation or rule to be "tuned" as experience is gained; thus being the principal channel of support of the second generation IMO intact stability criteria.

6. SUMMARY

The paper briefly reviews the current status of implementation of the second generation of IMO intact stability criteria, recalls its main idea and refers to the most important technical publications on the topic.

The main focus is on the consistency aspects of the implementation of the new criteria. The most important one is the consistency between the mandatory and recommendation parts – *i.e.* between the parts A and B of the 2008 IS code as the implementation of the second generation criteria is expected in part B.

The other consistency aspect is how to handle new information indicating inconsistency between Level 1 and 2 of the vulnerability criteria. The paper discusses an idea of three-step procedure that may be useful for these issues. The three steps are: establishing the ground truth (what level needs adjustment), consider adjustment through calculation method and the adjustment of the standard.

Finally, the paper discusses general issues of regulation support, concluding that the structure of the second generation intact stability criteria allows robust and transparent support through adjusting the standards as application experience is gained.

7. ACKNOWLEDGEMENTS

The portion of this paper describes work performed by NSWCCD and funded by the USCG Office of Design and Engineering Standards.

Discussions of the consistency issues on the vulnerability criteria for pure loss of stability with G. Streppel (Mayer Werft), K. Spyrou's (National Technical University of Athens), N. Umeda (Osaka University) and G. Bulian (University of Trieste) were very fruitful.

Opinions expressed in this paper are those of the authors and do not necessarily express the position of the United States Government.

8. REFERENCES

Belenky, V., J. O. de Kat, Umeda, N. (2008) "Towards Performance-Based Criteria for Intact Stability". *Marine Tech.*, Vol. 45 No 2, pp:101–123.

Boonstra, H., de Jongh, M.P., Palazzi, L. (2004) "Safety Assessment of Small Container Feeders", *Proc. of PRADS 2004*, Lübeck-Travemünde, Germany.

France, W. M., Levadou, M., Treakle, T. W., Paulling, J. R., Michel, K. Moore, C. (2003) "An Investigation of Head-Sea Parametric Rolling and its Influence on Container Lashing Systems". *Marine Tech.*, Vol. 40, No 1, pp. 1–19.

IMO SDC 2/WP.4 (2015) Development of Second Generation Intact Stability Criteria. Report of the Working Group, London, UK.

IMO SDC 3/6/2 (2015) Criteria Further validation of some draft second generation intact stability criteria. Submitted by Germany

IMO SDC 3/WP.5, (2016) Development of Second Generation Intact Stability Criteria. Report of the Working Group, London, UK.

IMO SLF 49/INF.7 (2006) Containership safety, submitted by the Netherlands, London, UK.

IMO SLF 54/3/1 (2011) Report of the Working Group at SLF 53 (Part 2), Submitted by the Chairman of the Working Group, London, UK.

Maritime New Zealand (2007) Incident Report Heavy Weather/Cargo Shift Aratere 3 March 2006. Maritime New Zealand Investigation Report 06-201, vi+57 p, 2007.

Peters, W., Belenky, V., Bassler C., Spyrou, K., Umeda, N., Bulian, G., Altmayer, B. (2011) "The Second Generation of Intact Stability Criteria an Overview of Development", *SNAME Trans.* Vol. 119.

Swedish Accident Investigation Board (2008) Loss of M/S FINNBIRCH between Oland and Gotland, 1 November 2006, Report RS 2008:03e

ter Bekke, E. C. A., Willeboordse, E.J., van Dallen, E.F.G., Boonstra, H., Keizer, E.W.H. Ale, B. (2006) "Integrated safety assessment of small container ship", *Proc of 8th Intl. Conf. on Probabilistic Safety Assessment and Management*, ASME, New Orleans, Louisiana, USA.

Transportation Safety Board (2011) Heel Accident of Ferry Ariake, Marine accident investigation report MA2011-2, Tokyo, February, 2011 (in Japanese).

van Daalen, E.F.G., Boonstra, H., Blok, J.J. (2005) "Capsize probability analysis for a small container vessel" *Proc. of 6th Intl. Ship Stability Workshop*, Istanbul, Turkey.

Different Computations of Parametric Roll Level 2 Criterion

François Grinnaert, *French Naval Academy Research Institute*, francois.grinnaert@ecole-navale.fr

Jean-Yves Billard, *French Naval Academy Research Institute*, jean-yves.billard@ecole-navale.fr

Jean-Marc Laurens, *ENSTA Bretagne*, Jean-Marc.LAURENS@ensta-bretagne.fr

ABSTRACT

The second generation intact stability criteria are currently under development and validation at the IMO. These criteria are organized in 5 failure modes and 3 levels of assessment in each failure mode. The level 2 for parametric roll failure mode consists of two checks marked C1 and C2. The C2 check is based on the computation of the maximum roll angle of the ship in both head and following sea by solving the differential equation of parametric roll through a probabilistic approach. The future regulation proposes an analytical solution of the maximum roll angle. It also allows a numerical one-degree-of-freedom simulation for solving the differential equation and finding the maximum roll angle without specifying any method or parameter. During the latest International Conference on the Stability of Ships and Ocean Vehicles, experts in the field proposed a method and some parameters for this numerical solving: initial roll angle, simulation duration (in terms of number of ship's natural roll periods) and non-linear GZ. This paper deals with the influence of these parameters used to compute the C2 check on the resulting KG_{\max} curve. Results show that the simulation duration has a major influence on the KG_{\max} while the initial roll angle has a limited influence. As expected, linearizing GZ is not relevant.

Keywords: *Parametric Roll, Differential Equation, KG_{\max} curve*

1. INTRODUCTION

The second generation intact stability criteria are currently being developed and validated at the IMO. They have been presented in detail by Umeda (2013). This paper deals with their version amended in February 2015 and January 2016 by the Sub-Committee on Ship Design and Construction of the IMO (SDC 2/WP.4 and SDC 3/WP.5). These new criteria are organized in 5 failure modes: parametric roll, pure loss of stability, dead ship condition, surf-riding/broaching and excessive acceleration. In each failure mode, 3 levels of assessment are defined. The first level requires simple calculations and ensures large safety margins. The second level is based on more complex computations associated with probabilistic approaches of the phenomena. It ensures medium safety margins. The third level consists of a direct assessment using numerical simulations and ensures optimized safety margins. The second level of parametric roll considers two verifications. The

first check (C1) considers the GM variation in waves and the reference speed corresponding to the parametric resonance using a probabilistic approach based on a table of 16 weighted waves. This paper deals with the second check of parametric roll failure mode (C2). This check considers the maximum roll angle in each of the 197 non-zero-weighted waves of the IACS Wave Scatter Diagram (IACS, 2001) for 7 different ship speeds corresponding to head and following seas. Although both checks are embedded in the same criterion, C2 is considered as a separate criterion in this paper. Thus, a KG_{\max} curve can be associated with it for any ship. The maximum roll angle is calculated as the maximum absolute value of the function $\Phi(t)$ solution of the differential equation of parametric roll. The new regulation (SDC 2/WP.4 and SDC 3/WP.5) proposes to calculate the maximum roll angle from an analytical solution of the differential equation. It also allows a one-degree-of-freedom numerical simulation. During the 12th International Conference on the Stability of

Ships and Ocean Vehicles, Peters *et al.* (2015) proposed to solve this equation with a simulation time equal to 15 natural roll periods of the ship and an initial roll angle equal to 5 degrees. They also recommended considering a non-linear GZ. These proposals have been included in the explanatory notes of the new regulation (SDC 3/WP.5). The goal of this paper is to study the influence of each of these proposals on the KG_{\max} curves associated with the C2 criterion for several ships chosen for their variety of behavior with regard to parametric roll.

2. GENERAL PRINCIPLES

Differential Equation

The differential equation to be solved is established as follows:

$$J_{44}\ddot{\Phi} + B_{44}\dot{\Phi} + WGZ(\Phi, t) = 0 \quad (1)$$

J_{44} denotes the roll moment of inertia, including added inertia. B_{44} denotes the non-linear damping coefficient. In this paper, it is computed according to Kawahara *et al.* (2009) and Ikeda *et al.* (1978) for the lift component. W denotes the ship's weight. $GZ(\Phi, t)$ is the righting arm, as a function of the roll angle Φ and the time t , varying with the wave encounter frequency. In this study, GZ is computed in calm water and "modulated" by the GM in waves, as proposed by Belenky *et al.* (2011), Peters *et al.* (2015) and SDC 3/WP.5. The solving of the differential equation provides the maximum roll angle, which is used to calculate the coefficient C2. Since the number of non-zero-weighted waves is large, Grim's effective wave height concept (1961) is used to render the computation faster. The method used to compute C2 and the associated KG_{\max} is detailed by Grinnaert *et al.* (2016).

Ships

The KG_{\max} curves associated with the C2 criterion are computed for 4 different ships chosen for their different behavior with regard to parametric roll. The main particulars of all ships are listed by Grinnaert, *et al.* (2016).

The first ship is the well-known C11 container ship. She is vulnerable to parametric roll (France, *et al.* 2001).

The second ship is a 319 m container ship. An extreme-roll accident occurred on this ship (Kaufmann, 2009). She is assessed as possibly

vulnerable to parametric roll by the level 2 criterion (Grinnaert, *et al.*, 2016) although neither the test in the towing tank nor direct assessment computation have proven this yet.

The third ship is a roll-on roll-off vessel presented by Garne (1997). She is assessed as non-vulnerable to parametric roll by the level 2 criterion although parametric roll may occur in some conditions in some lightly-weighted waves (Grinnaert, *et al.*, 2016).

The last ship is a tanker. The wall-sided shape of her hull from bilge to deck makes her clearly non-vulnerable to parametric roll (Grinnaert, *et al.*, 2016).

3. INFLUENCE OF SIMULATION DURATION

Since parametric roll is a resonance phenomenon due to the repetition of the encounter of waves, attaining the steady state roll amplitude is essential to determine the vulnerability to this failure mode. Thus, the duration of the simulation is important. The KG_{\max} curves associated with the C2 criterion are computed for the four ships previously presented for 6 different simulation durations, given as a number of the ship's natural roll period. The following durations are tested: 3, 4, 6, 10, 15 and 20 natural roll periods. Peters *et al.* (2015) and SDC 3/WP.5 recommend a simulation duration equal to 15 roll periods.

Figure 1 and Figure 2 show the results for both container ships. We observe that the KG_{\max} significantly varies with the time duration, but the curves associated with 10, 15 and 20 roll periods are fully coincident for both ships. This proves that the steady state roll amplitude has been attained between 6 and 10 roll periods.

Figure 3 shows the results for the Ro-Ro vessel. We observe that all curves are close together. The KG_{\max} is slightly affected by the simulation duration. The curves associated with 10, 15 and 20 periods are fully coincident.

Figure 4 shows the results for the tanker. We observe that all curves are coincident and correspond to zero-GM. This proves that the tanker is not vulnerable to parametric roll: parametric roll never occurs, regardless of the wave and speed (the C2 coefficient is set to 1 if the average value of GM in waves is negative, see Grinnaert, *et al.* 2016).

The simulation duration has no effect on KG_{max} curves.

This first test shows that:

- 1) The more the ship is vulnerable to parametric roll, the more the simulation duration has an influence on the KG_{max} curve associated with the C2 criterion.
- 2) The relevance of the simulation duration equal to 15 natural roll periods of the ship proposed by Peters, *et al.* (2015) is confirmed.

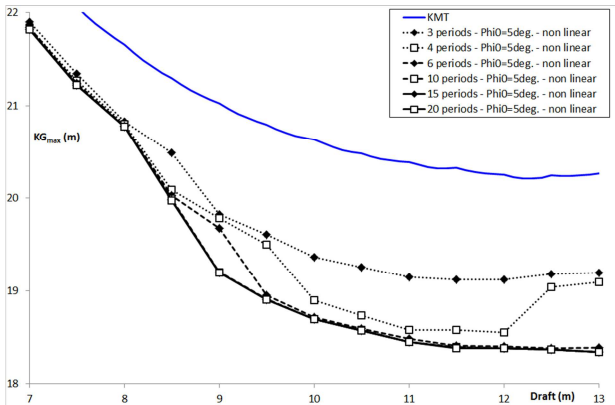


Figure 1: Influence of simulation duration on KG_{max} curves associated with the C2 criterion for the C11 container ship.

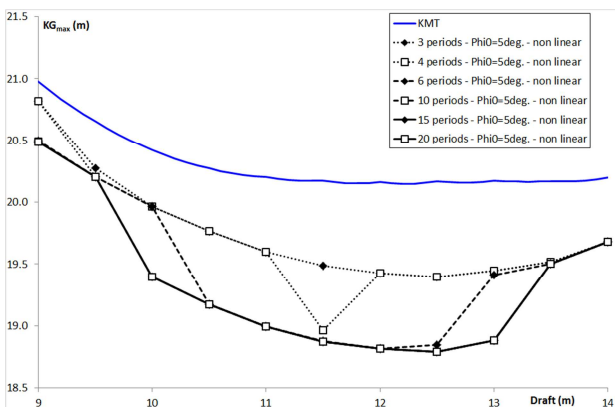


Figure 2: Influence of simulation duration on KG_{max} curves associated with the C2 criterion for the 319 m container ship.

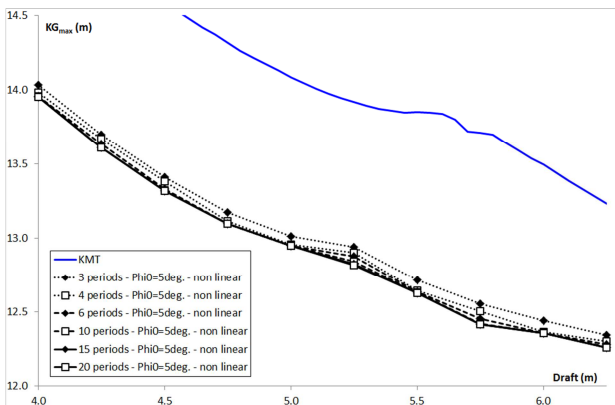


Figure 3: Influence of simulation duration on KG_{max} curves associated with the C2 criterion for the Ro-Ro vessel.

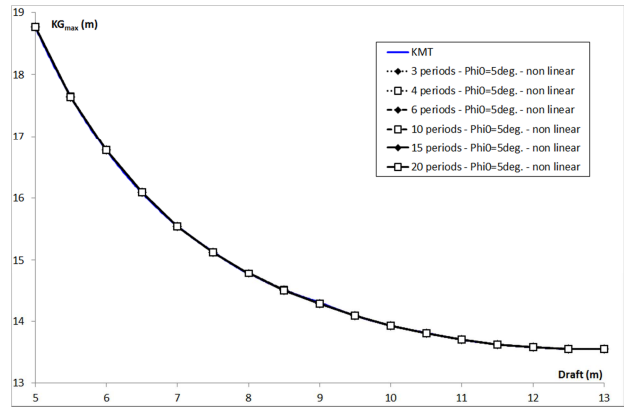


Figure 4: Influence of simulation duration on KG_{max} curves associated with the C2 criterion for the tanker (all curves are coincident).

4. INFLUENCE OF INITIAL ROLL ANGLE

The right term in equation (1) is equal to zero because there is no transverse excitation in parametric roll. The ship is assumed to sail in pure head or following seas. Thus, a non-zero initial roll angle (or a non-zero initial roll speed) must exist to initialize the numerical phenomenon during the simulation. Peters *et al.* (2015) and SDC 3/WP.5 recommend an initial roll angle equal to 5 degrees. Since the C2 coefficient increases if the maximum roll angle exceeds 25 degrees (see SDC 2/WP.4), it may be interesting to start the simulation with an initial roll angle larger than 5 degrees, in order to reduce the number of natural roll periods of the ship needed to attain the steady state roll amplitude. Computations performed with an initial roll angle equal to 10 degrees show that the steady state roll amplitude is attained between 6 and 10 roll periods, as if the initial roll angle were 5 degrees. Computations with other durations between 6 and 10 roll periods would probably prove that the initial roll angle has an influence on the duration needed to attain the steady state roll amplitude. However, the initial roll angle has no major influence on this duration.

Even if the influence of the initial roll angle on the duration needed to attain the steady state roll amplitude is limited, the initial roll angle may also have an influence on the KG_{max} . This should be limited, but not zero. KG_{max} curves are computed for the ships previously presented with initial roll angles equal to 5 and 10 degrees. The results are shown in Figure 5 to Figure 8 respectively for the C11 container ship, the 319 m container ship, the Ro-Ro vessel and the tanker. As expected, we observe that the initial roll angle has no influence

on the KG_{max} curves of the tanker since she is not vulnerable to parametric roll (Figure 8). On the three other ships, the initial roll angle has a light influence on the KG_{max} . Only one point differs significantly for the 319 m container ship (Figure 6, draft equal to 9.5 m, difference of approx. 0.5 m between both KG_{max}).

To conclude this second section, we can note the following:

1) The initial roll angle has no major influence on the duration needed to attain the steady state roll amplitude.

2) Since the initial roll angle has a limited influence on the KG_{max} associated with the C2 criterion, it is wise to clearly specify its value in the future regulation.

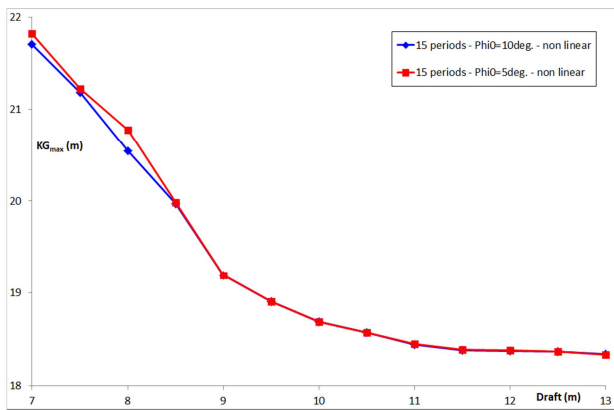


Figure 5: Influence of the initial roll angle on KG_{max} curves associated with the C2 criterion for the C11 container ship.

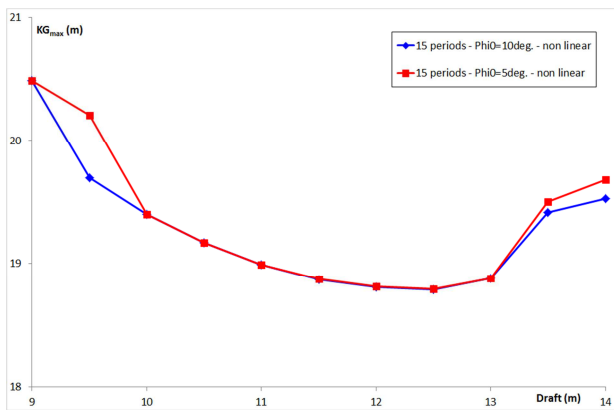


Figure 6: Influence of the initial roll angle on KG_{max} curves associated with the C2 criterion for the 319 m container ship.

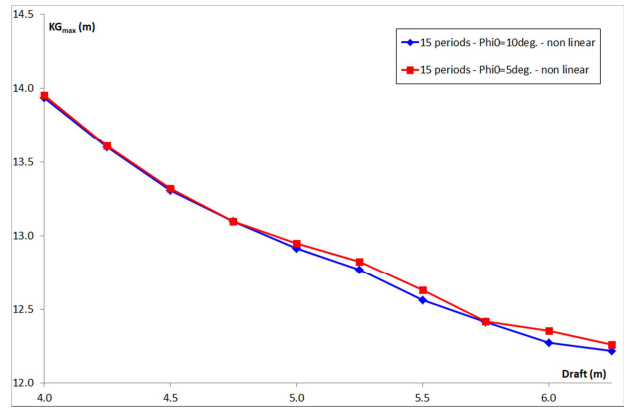


Figure 7: Influence of the initial roll angle on KG_{max} curves associated with the C2 criterion for the Ro-Ro vessel.

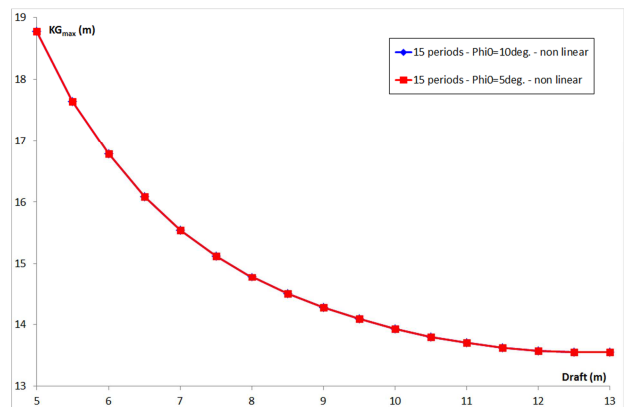


Figure 8: Influence of the initial roll angle on KG_{max} curves associated with the C2 criterion for the tanker (both curves are fully coincident).

5. INFLUENCE OF LINEARIZED GZ

Parametric roll is a failure mode that could cause capsizing. Thus, it seems logical to study it at large roll angles with a non-linear GZ which is recommended by Peters *et al.* (2015) and SDC 3/WP.5. However, the C2 coefficient increases if the maximum roll angle exceeds 25 degrees (see SDC 2/WP.4). Thus, an error on GZ at angles larger than 25 degrees has no influence on the result. Since many ships have a linear GZ up to an angle equal to 25 degrees, it is interesting to compare KG_{max} associated with the C2 criterion computed with linear and non-linear GZ. GZ curves are computed in calm water for the four ships previously presented at full load draft and KG equal to KG_{max} given by the C2 criterion (except for the tanker where the KG has been chosen for GM equal to 0.175 m since her GM_{min} associated with C2 is zero). They are shown in Figure 13 to Figure 16. All configurations of GZ versus GM are presented: the non-linear GZ is significantly larger than the linearized GZ ($GZ_{lin} = GM \times \Phi$) for both the 319 m container ship and tanker (Figure 14 and Figure

16). The non-linear GZ is lower than the linearized GZ for the Ro-Ro vessel (Figure 15) and the GZ of the C11 container ship is relatively linear (Figure 13). The non-linear GZ and linearized GZ are used to compute the KG_{max} curves associated with the C2 criterion. The results are shown in Figure 9 to Figure 12.

As expected, the linearized GZ reduces the KG_{max} of the 319 m container ship (Figure 10). This reduction is so large that considering the linearized GZ instead of the real GZ would probably be an error.

It would be logical to expect a similar result on the tanker (Figure 12) since her GZ curve has the same configuration, but the linearized GM has no influence on KG_{max} at a full load draft (11 m). However, KG_{max} is reduced by the linearized GZ at lower drafts: the tanker is assessed as vulnerable to parametric roll if her GM is lower than 50 centimeters. The “jump” of KG_{max} between drafts equal to 10 m and 10.5 m is a characteristic of the KG_{max} curves associated with the C2 criterion. These KG_{max} curves are the lower envelope of the restricted zones in the surface formed by both draft and KG (where $C2 > 0.06$, see Grinnaert, *et al.*, 2016). Lesser jumps are observed in Figure 10 and Figure 11.

The result on the Ro-Ro vessel is unexpected (Figure 11): at full load draft (5.5 m), the KG_{max} given by the linearized GZ is more conservative than that given by the real GZ although the linearized GZ is larger than the real GZ. This is due to the highly non-linear behavior of the parametric roll differential equation.

The result on the C11 container ship is as expected (Figure 9): since the non-linear GZ and linearized GZ almost overlap up to an angle of 25 degrees, linearizing the GZ has a very limited influence on the KG_{max} associated with C2.

To conclude this last section, we observe that, as expected, linearizing the GZ is not relevant, unless the real GZ is linear up to 25 degrees for all drafts scanned by the KG_{max} curve.

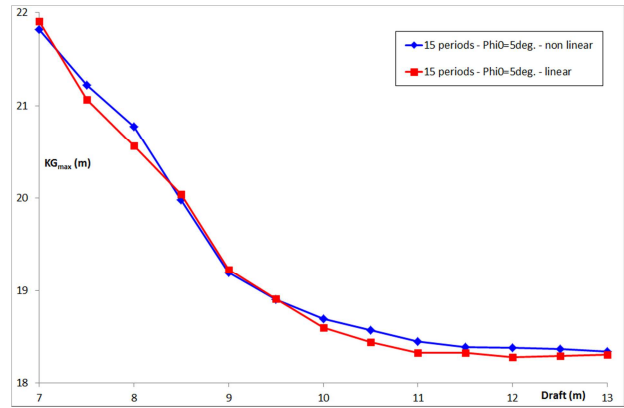


Figure 9: Influence of the GZ linearity on KG_{max} curves associated with the C2 criterion for the C11 container ship.

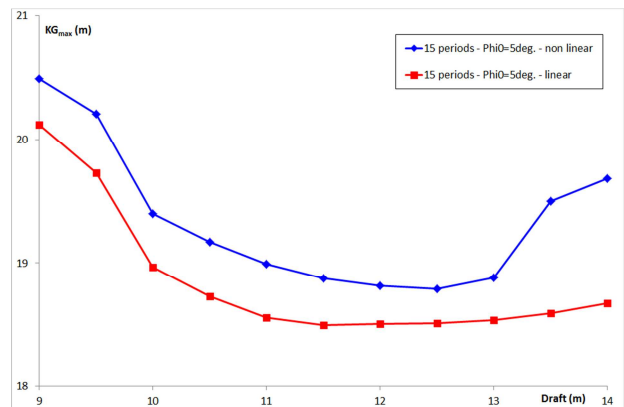


Figure 10: Influence of the GZ linearity on KG_{max} curves associated with the C2 criterion for the 319 m container ship.

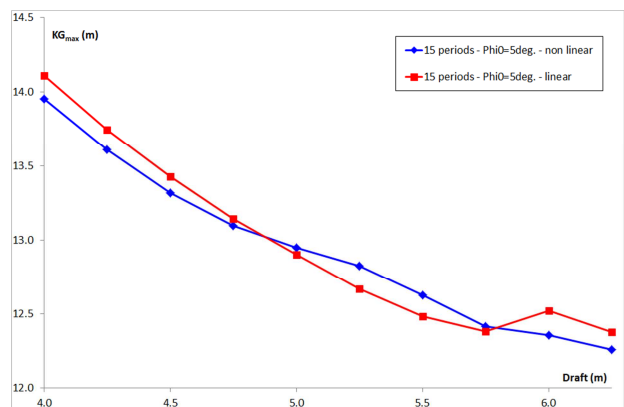


Figure 11: Influence of the GZ linearity on KG_{max} curves associated with the C2 criterion for the Ro-Ro vessel.

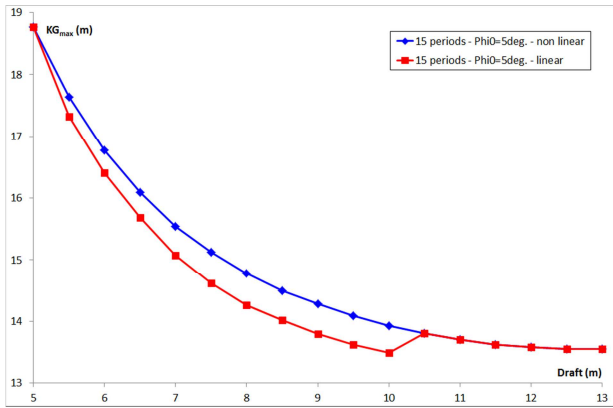


Figure 12: Influence of the GZ linearity on KG_{max} curves associated with the C2 criterion for the tanker.

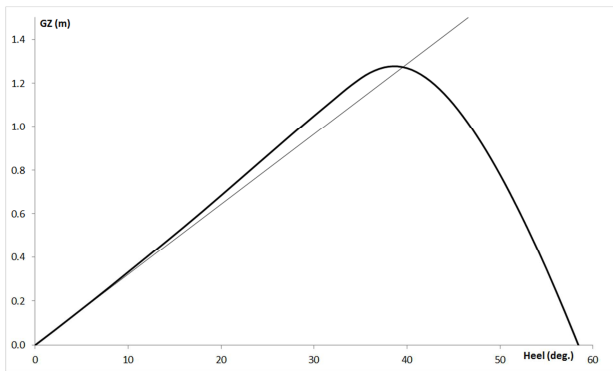


Figure 13: GZ curve of the C11 container ship.

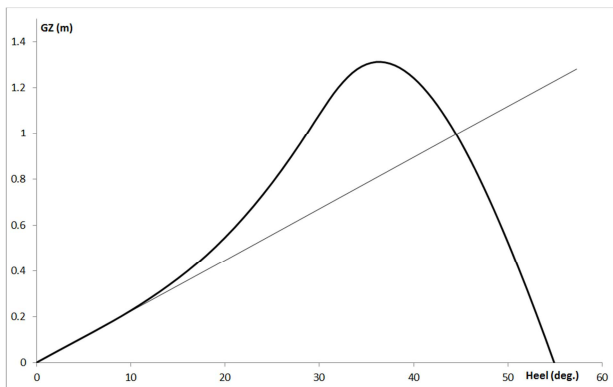


Figure 14: GZ curve of the 319 m container ship.

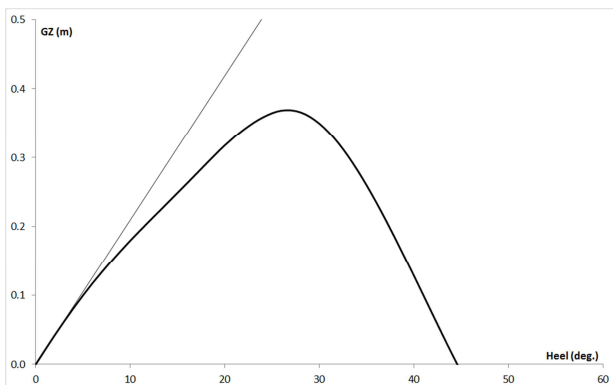


Figure 15: GZ curve of the Ro-Ro vessel.



Figure 16: GZ curve of the tanker.

6. CONCLUSION

KG_{max} curves associated with the C2 criterion have been computed for four different ships chosen for their variety of behavior with regard to parametric roll. The influence of the one-degree-of-freedom simulation duration, the initial roll angle and of linearizing the GZ has been assessed.

The results of these sensitivity tests clearly show that the more the ship is vulnerable to parametric roll, the more the simulation duration has an influence on the KG_{max} associated with the C2 criterion. A simulation duration equal to 15 natural roll periods of the ship guarantees the attainment of the steady state roll amplitude for a ship known as highly vulnerable to this failure mode. The initial roll angle has no major influence on the duration needed to attain the steady state roll amplitude, but its influence on the KG_{max} exists. In the latest amendment of the new regulation (SDC 3/WP.5), the values of both the simulation duration and initial roll angle are clearly specified in order to avoid any possible interpretation of the rule. As expected, except in special cases, linearizing the GZ is irrelevant.

7. REFERENCES

Belenky V., Bassler C., Spyrou K., 2011, “Development of Second Generation Intact Stability Criteria”, US Navy, Naval Surface Warfare Center Carderock Division, NSWCCD-50-TR-2011/065.

France W. N., Levadou M, Treacle T. W., Paulling J. R., Michel R. K., Moore C., 2001, “An Investigation of Head-Sea Parametric Rolling and its Influence on Container Lashing Systems”, SNAME Annual Meeting.

Garme K., 1997. "Model Seakeeping Experiments Presented in the Time-Domain to Facilitate Validation of Computational Tool", Kungl Tekniska Högskolan, Stockholm.

Grim O., 1961, "Beitrag zu dem Problem der Sicherheit des Schiffes im Seegang", Schiff und Hafen, Heft 6, S. 490-497.

Grinnaert F, Billard J.-Y., Laurens J.-M., 2016, "KG_{max} Curves Associated with 2nd Generation Intact Stability Criteria for Different Types of Ships", Journal of Marine Science and Application (accepted).

Ikeda Y., Himeno Y., Tanaka N., 1978, "Components of Roll Damping of Ship at Forward Speed", Department of Naval Architecture University of Osaka Prefecture, Report No 404.

IMO 2015, "Development of Second Generation Intact Stability Criteria, Development of Amendments to Part B of the 2008 IS Code on Towing and Anchor Handling Operations", SDC 2/WP.4 2nd session.

IMO 2016, "Finalization of Second Generation Intact Stability Criteria, Amendments to Part B of the 2008 IS Code on Towing, Lifting and Anchor Handling Operations", SDC 3/WP.5, 3rd session.

International Association of Classification Societies, 2001, Rec. No. 34. Standard Wave Data, Rev.1.

Kaufmann J, 2009, "Fatal Accident on Board the CMV Chicago Express During Typhoon "Hugupit" on September 24 2008 off the Coast of Hong Kong", Bundesstelle für Seeunfalluntersuchung. Investigation Report 510/08.

Kawahara Y., Maekawa K., Ikeda Y., 2009. "A Simple Prediction Formula of Roll Damping of Conventional Cargo Ships on the Basis of Ikeda's Method and Its Limitation", 10th International Conference on Stability of Ships and Ocean Vehicles, St Petersburg.

Peters W., Belenky V., Chouliaras S., Spyrou K., 2015, "Requirements for Computational Methods to be Used for the IMO Second Generation Intact Stability Criteria", 12th International Conference on the Stability of Ships and Ocean Vehicles, Glasgow.

Umeda N., 2013, "Current Status of Second Generation Intact Stability Criteria Development

and Some Recent Efforts', 13th International Ship Stability Workshop, Brest.

Validation of One Numerical Method for Parametric Roll Criteria with Experiments

Jiang Lu, *China Ship Scientific Research Center, Wuxi, China*, lujiang1980@aliyun.com

Min Gu, *China Ship Scientific Research Center, Wuxi, China* gumin702@163.com

ABSTRACT

The numerical methods for the direct stability assessment of parametric roll are currently under development at the International Maritime Organization (IMO) for the second generation intact stability criteria. For providing a numerical method for parametric roll with sufficiently simple and enough reliable, firstly, heave and pitch motions obtained by a strip theory applied to an upright hull is used to determine the simultaneous relative position of the ship to waves in time domain; secondly, the nonlinear Froude-Krylov component of roll restoring variation is calculated by integrating wave pressure up to wave surface with the heave and pitch motions; secondly, the dynamic effect which consists of radiation and diffraction components is taken into account. Finally, the proposed numerical method is validated by four ships with four experiments.

Keywords: *Parametric roll, second generation intact stability criteria, dynamic stability, stability in waves*

1. INTRODUCTION

The numerical methods for direct stability assessment of parametric roll are under development at the International Maritime Organization (IMO) for the second generation intact stability criteria (IMO SDC.3, 2016). Parametric roll in head seas is a nonlinear phenomenon involving dynamic heave and pitch motions, and it is still difficult to be predicted accurately in head seas. IMO is also calling for the validation of numerical methods or guidelines for finalization of second generation intact stability with samples.

Several successful predictions of parametric roll in following waves have been reported (Munif and Umeda, 2000) due to the fact that coupling with dynamic heave and pitch is not important while the wave induced added resistance is generally small in following waves.

Although the accurate prediction of head-sea parametric roll is difficult at this stage due to the fact that the coupling with heave and pitch is significant and the added resistance as well as the resulting speed loss cannot be simply ignored, the effect of dynamic heave and pitch motions on parametric roll has been investigated so far by many researchers and found that restoring arm variation in head waves depends on dynamic heave

and pitch motions (Taguchi, et al., 1995). The effect of surge motion, with added resistance taken into account, on parametric roll was investigated by some researchers (Umeda, et al., 2008; Umeda & Francescutto, 2008; Lu, et al., 2010, 2011, 2012), but an experimental study with and without surge was not conducted in the above investigations. The partially restrained experiments with the surge motion restrained and free running experiments with the surge motion free were conducted in the reference (Lu, et al., 2016).

In a linear seakeeping theory the roll motion of a symmetric hull has no effect on heave and pitch motions, the coupling from parametric roll to heave and pitch is not taken into account in above studies. Rodriguez et al. (2007) observed subharmonic components in heave and pitch motions when parametric roll occurs in their experiments. Neves et al. (2009) using their nonlinear heave-pitch-roll mathematical model numerically subsequently revealed an interesting bifurcation structure of heave and pitch motions together with parametric roll. Later Lu et al (2013, 2016) also observed subharmonic components in pitch motion and heave displacement together with parametric roll in their free-running model experiment and half restrained model experiment, but failed to reproduce this phenomenon with a coupled heave-

roll-pitch mathematical model based on a nonlinear strip theory (Hashimoto & Umeda, 2012).

Many prediction methods for parametric roll ignore the radiation and diffraction effects on restoring variation but some methods do not. Boroday (1990) and Umeda & Hashimoto (2006) took into account the radiation and diffraction effects using a strip theory on the restoring variation. Hashimoto et al. (2007) reported that radiation and diffraction effects on the restoring variation could result in larger parametric roll amplitude, which improves accuracy for a car carrier. The effect of radiation and diffraction forces on restoring variation for parametric rolling still remains open which requires further experimental and numerical studies with more examples as mentions in the reference (Lu, et al., 2016).

As mentioned in the reference (Lu, et al., 2016), there are several issues should be discussed to finalize the guidelines in this respect and IMO is also calling for conducting more examples to finalize the guidelines of parametric roll with sufficiently simple and enough reliable methods. Therefore, the authors carry out the first step to validate the uncoupled numerical models by conducting four free running experiments with a post Panamax C11 class containership, a pure car carrier, a passenger ship and a 4250TEU containership, respectively.

2. MATHEMATICAL MODEL

The uncoupled roll model (Hashimoto et al. 2007, Umeda, et al., 2008) which has been used for estimating parametric roll for many years is expressed as (1) and called as 1 DOF approach. Although this model is a 1 DOF of rolling model, heave and pitch motions are taken into account to estimate restoring variation. Restoring moment in waves is calculated as a sum of two components. One is the nonlinear Froude-Krylov component, which is calculated by integrating wave pressure around the instantaneously wetted hull surface with heave and pitch motion obtained by a strip theory applied to an upright hull. The other is the hydrodynamic effects which result from radiation and diffraction components that are extrapolated nonlinearly with regards to roll angle (Lu, et al., 2011, 2012).

Since the prediction accuracy of restoring moment in head seas could be improved if the dynamic component is included. The dynamic effect is calculated by applying a strip theory to different heeled hulls with regards to simultaneous roll angle while it is assumed a linear relationship with the wave height. This effect is considered as an additional effect on GZ by dividing calculated dynamic roll moment with a ship displacement.

$$\ddot{\phi} + 2\mu\dot{\phi} + \gamma\phi^3 + \frac{W}{I_{xx} + J_{xx}}GZ(t, X_G, \zeta_G, \theta, \phi) = 0 \quad (1)$$

where: ϕ : roll angle, μ : linear roll damping coefficient, γ : cubic roll damping coefficient, W : ship weight, I_{xx} : moment of inertia in roll, J_{xx} : added moment of inertia in roll, GZ : righting arm, t : time, ζ_G : heave displacement and θ : pitch angle, X_G : instantaneous ship longitudinal position.

3. SUBJECT SHIPS

The principal particulars of the post Panamax C11 class containership, the pure car carrier, the passenger ship and the 4250TEU containership used for this research are shown in Tables 1 -4 .

Table 1 Principal particulars of the C11 containership

items	ship	model
length: L_{pp}	262.0 m	4.0m
breadth: B	40.0 m	0.611m
Depth: D	24.45m	0.373m
mean draught: T	11.5 m	0.176m
block coefficient: C_b	0.560	0.560
Pitch radius of gyration: K_{yy}	$0.24L_{pp}$	$0.24L_{pp}$
metacentric height: GM	1.928 m	0.029m
natural roll period: T_ϕ	24.68 s	3.05s

Table 2 Principal particulars of the car carrier

items	model
length: L_{pp}	4.2m
breadth: B	0.624m
Depth: D	0.774m
mean draught: T	0.197m
block coefficient: C_b	0.646
Pitch radius of gyration: K_{yy}	$0.25L_{pp}$
metacentric height: GM	0.019m
natural roll period: T_ϕ	3.45s

Table3 Principal particulars of the passenger ship

items	model
length: L_{pp}	3.0m
breadth: B	0.514m
Depth: D	0.239m
mean draught: T	0.127m
block coefficient: C_b	0.515
Pitch radius of gyration: $K_{\dot{\gamma}}$	$0.24L_{pp}$
metacentric height: GM	0.023m
natural roll period: T_{ϕ}	2.865s

Table 4 Principal particulars of the 4250TEU containership

items	model
length: L_{pp}	4.0m
breadth: B	0.511m
Depth: D	0.307m
mean draught: T	0.20m
block coefficient: C_b	0.643
Pitch radius of gyration: $K_{\dot{\gamma}}$	$0.30L_{pp}$
metacentric height: GM	0.026m
natural roll period: T_{ϕ}	2.7s

4. EXPERIMENTS

The four free running experiments were conducted in the seakeeping basin (length: 69m, breadth: 46m, depth: 4m) of China Ship Scientific Research Center, which is equipped with flap wave makers at the two adjacent sides of the basin. The ship model was driven by a propeller in the free running experiment. The pitch and roll amplitudes were measured by a MEMS (Micro Electro-Mechanical System)-based gyroscope placed on the ship model and the wave elevation was measured by a servo-needle wave height sensor attached to the towing carriage.



Figure 1: The C11 containership model in the free running experiment



Figure 2: The pure car carrier model in the free running experiment.



Figure 3: The passenger ship model in the free running experiment.



Figure 4: The 4250TEU containership model in the free running experiment.

5. RESULTS AND DISCUSSIONS

5.1 The C11 Containership

The head-sea parametric roll of C11 containership in the free running experiments is recorded. Although the Froude number of the forward speed is limited to 0.15 due to the length of the seakeeping basin, the forward speed is not limited in the simulations. In the results, the minus Froude numbers mean the forward speed in following seas while the positive Froude numbers mean the forward speed in head seas. FK means only Froude-Krylov components of roll restoring variation are considered while FK+R&D means the radiation and diffraction components of roll restoring variation are also considered.

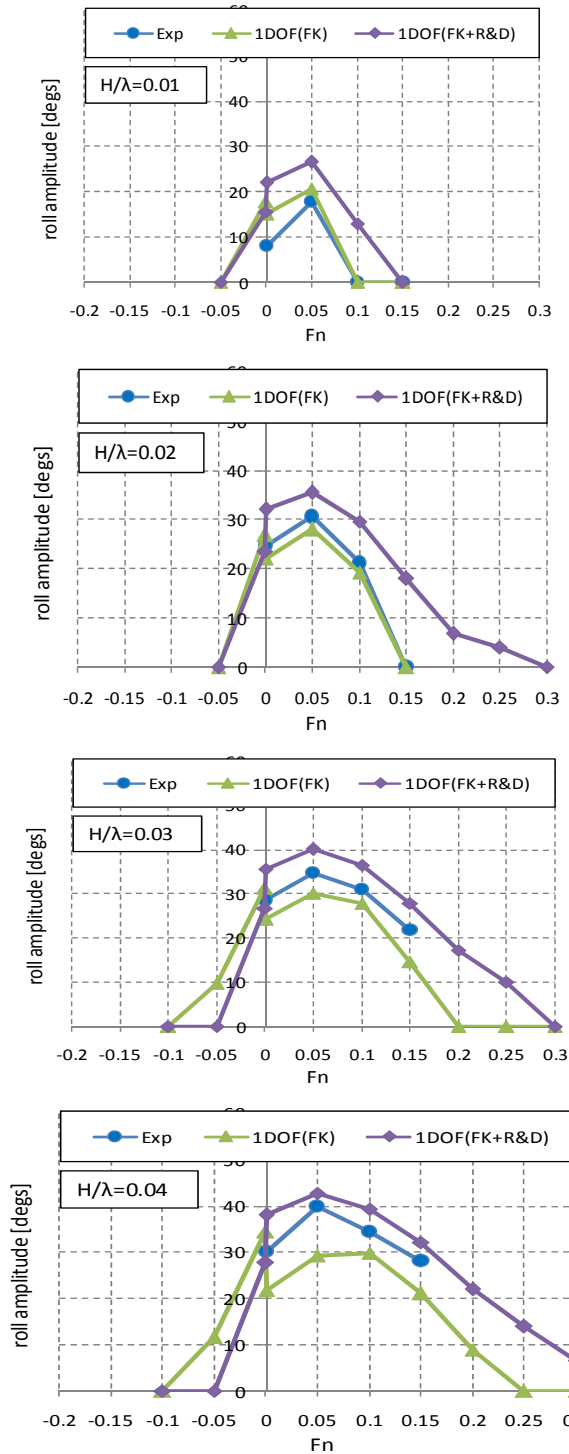
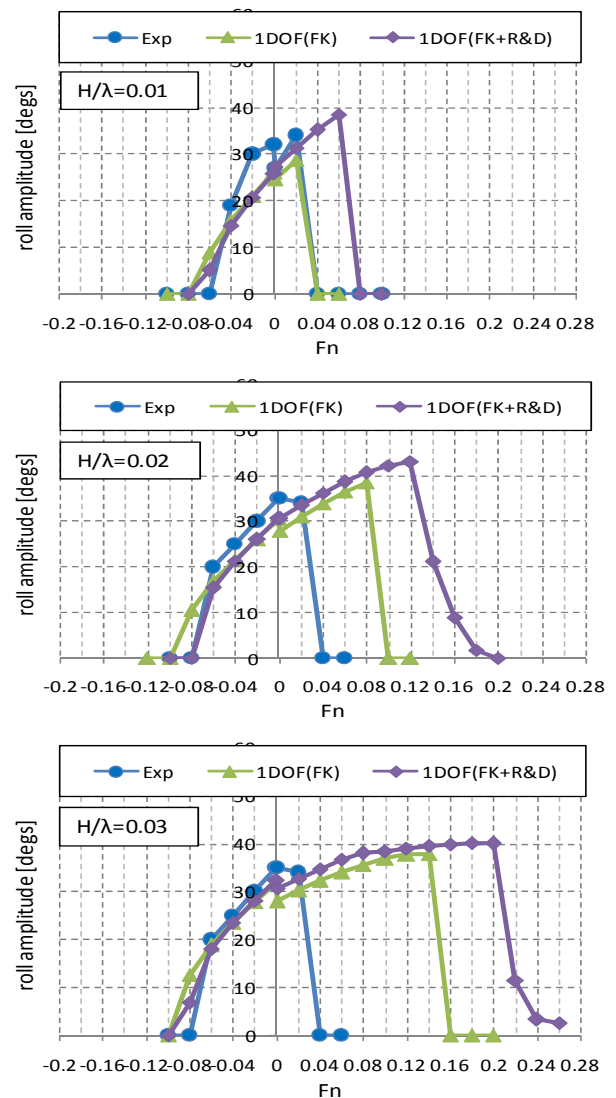


Figure 5: Comparisons of parametric roll between experiments and simulations, under the condition of $\lambda/L_{pp}=1.0$, $\chi=0^\circ$ and 180° .

The prediction of head-sea parametric roll in the 1 DOF approach with Froude-Krylov, radiation and diffraction components is generally larger than that in the experiments while the prediction of head-sea parametric roll with the Froude-Krylov on its own is generally smaller than that in the experiments except for $H/\lambda=0.01$ as shown in Fig. 5. The speed range of parametric roll with the 1 DOF (FK+R&D)

is larger than that in the experiments while the speed range of parametric roll with the 1 DOF (FK) is more close to that in the experiments in head seas. The above conclusions are not always fit for parametric roll in following seas. The difference between the simulations with the 1 DOF (FK) and the 1 DOF (FK+R&D) is not so larger and the simulations with the 1 DOF (FK) is more conservative than that with the 1 DOF (FK+R&D) in following seas, and the radiation and diffraction effects on restoring variation could be ignored in following seas.

5.2 The Pure Car Carrier



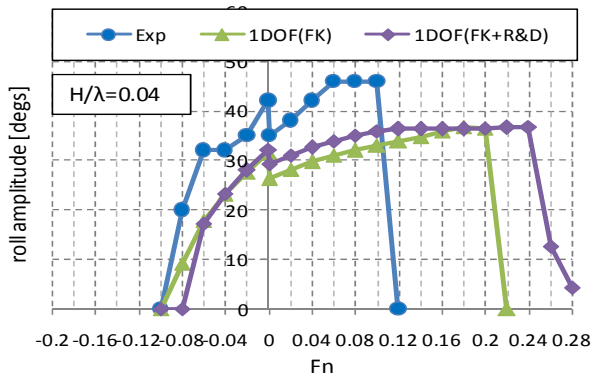


Figure 6: Comparisons of parametric roll between experiments and simulations, under the condition of $\lambda/L_{pp}=1.0$, $\chi=0^\circ$ and 180° .

The prediction of head-sea parametric roll in the 1 DOF (FK+R&D) is generally larger than that in the 1 DOF (FK) while this conclusion is not always fit for parametric roll in following seas. Both simulations overestimate the speed range of parametric roll and underestimate the maximum roll amplitude corresponding to the maximum roll in the experiments in head seas. Both simulations have a good agreement with the experiments in following seas, and the radiation and diffraction effects on restoring variation could be ignored in following seas.

5.3 The Passenger Ship

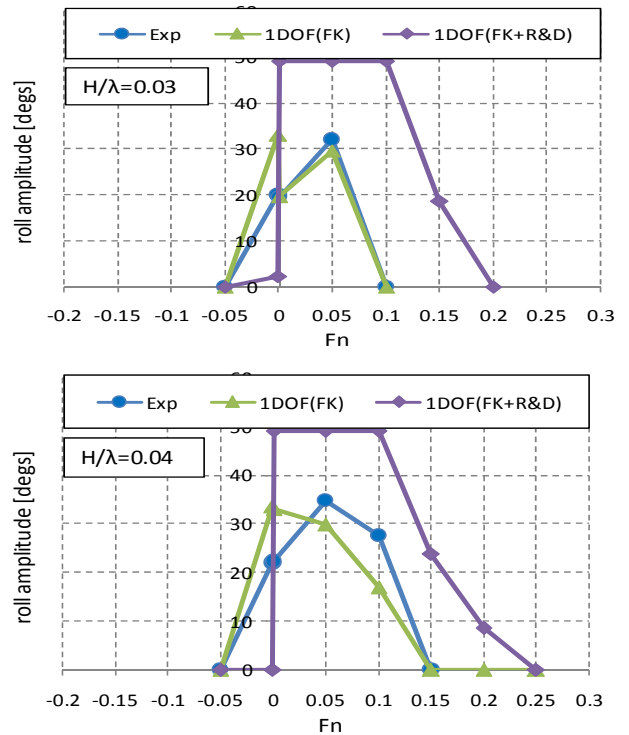
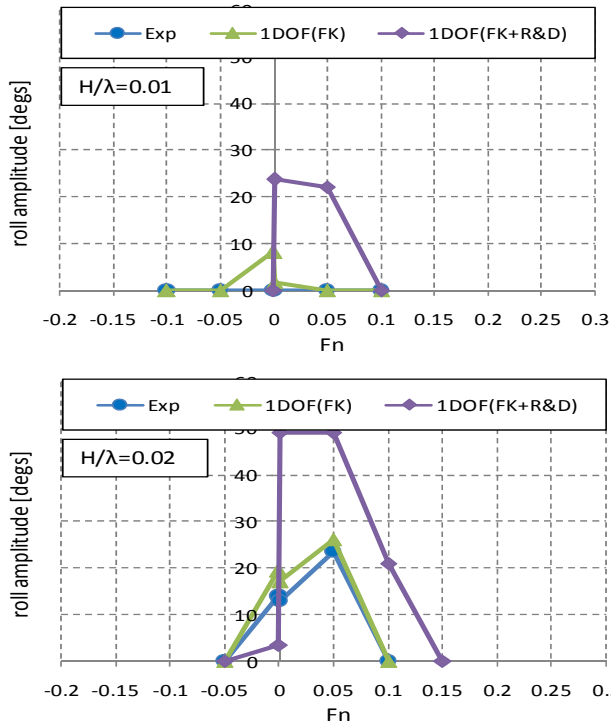
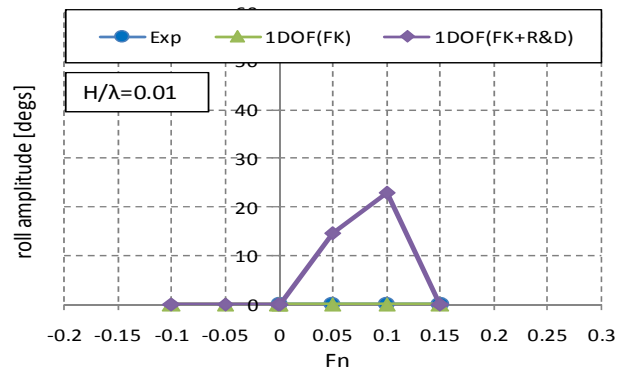


Figure 7: Comparisons of parametric roll between experiments and simulations, under the condition of $\lambda/L_{pp}=1.0$, $\chi=0^\circ$ and 180° .

The prediction of head-sea parametric roll in the 1 DOF (FK+R&D) overestimates the speed range and maximum angles of parametric roll while the prediction of following-sea parametric roll in the 1 DOF (FK+R&D) underestimates the speed range and maximum angles of parametric roll. The prediction of parametric roll with the 1 DOF (FK) is more close to experiments than that with the 1 DOF (FK+R&D). The radiation and diffraction effects on restoring variation could be ignored in following seas and that in head seas should be further studied for this kind ship.

5.4 The 4250TEU Containership



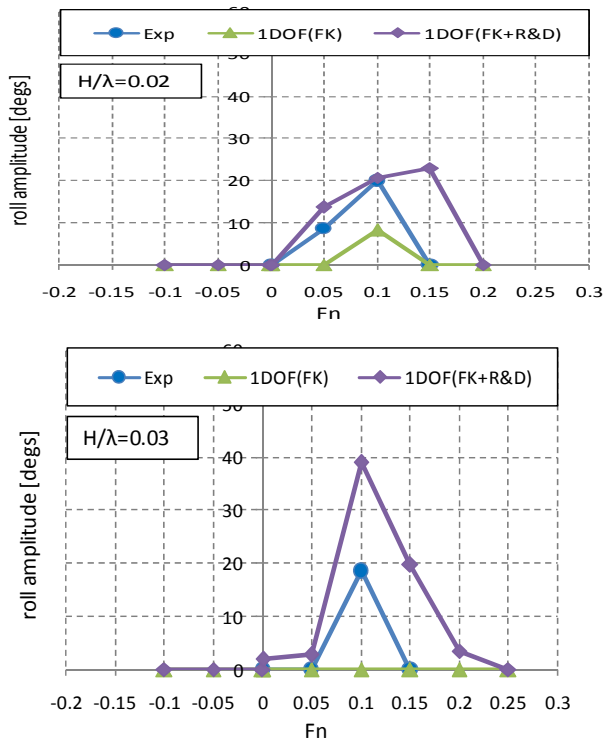


Figure 8: Comparisons of parametric roll between experiments and simulations, under the condition of $\lambda/L_{pp}=1.0$, $\chi=0^\circ$ and 180° .

The prediction of head-sea parametric roll in the 1 DOF (FK+R&D) overestimates the speed range and maximum angles of parametric roll while the 1 DOF (FK) fails to predict parametric roll at some points because the 4250 TEU containership is not vulnerable to parametric roll and parametric roll is disappeared while wave height increase. The simulations cannot accurately agree with that in the experiments, but the simulations can also prove that the 4250 TEU containership is not vulnerable to parametric roll.

Parametric roll is a nonlinear phenomenon due to the roll restoring force variation and involve dynamic heave and pitch motions in head seas. As examined by above four ships, it is still difficult to predict parametric roll accurately in head seas. However, the 1 DOF approach can predict parametric roll successfully for the post Panamax C11 class containership, and can also identify vulnerable ships of parametric roll successfully.

6. CONCLUSIONS

On the basis of validating the 1 DOF approach by conducting four free running experiments with a post Panamax C11 class containership, a pure car carrier, a passenger ship and a 4250TEU

containership, respectively, the following remarks can be made:

- 1) The effect of radiation and diffraction component on restoring variation should be taken into account in head seas if a conservative prediction of parametric roll in direct stability assessment is required.
- 2) The effect of radiation and diffraction component on restoring variation could be ignored in following seas if a simplified prediction of parametric roll is required.
- 3) One method could not be fit for all kind of ships for predicting parametric roll, and the 1 DOF approach can be recommended for parametric criteria at this stage due to its simple application.

A universal method should be found for most kind of ships for parametric roll criteria in future and this kind of ships whose parametric roll disappears with the wave height increase should be pay attention and more examples with experiments and numerical simulations should be conducted to finalize the guidelines of parametric roll criteria.

7. REFERENCES

Boroday I. K., 1990, "Ship Stability in Waves: On the Problem of Righting Moment Estimations for Ships in Oblique Waves", Proceedings of the 4th International Conference on Stability of Ships and Ocean Vehicles, pp. 441-451.

Hashimoto H. and Umeda N., 2012, "Validation of a Numerical Simulation Model for Parametric Roll Prediction using PCTC", Proceedings of the 11th International Conference on Stability of Ships and Ocean Vehicles, pp.141-149.

Hashimoto H., Umeda N. and Sakamoto G., 2007, "Head-Sea Parametric Rolling of a Car Carrier", Proceedings of Proceedings of the 9th International Ship Stability Workshop, Hamburg, 4.5.1-4.5.71.

IMO 2016, Finalization Second Generation Intact Stability Criteria, SDC 3/WP.5.

Lu J., Umeda N. and Ma K., 2010, "Modeling Parametric Roll in Regular and Irregular Head Seas with Added Resistance Taken into Account", Proceedings of the 5th Asia-Pacific Workshop on Marine Hydrodynamics, Osaka Pref Univ, pp.93-98.

Lu J., Umeda N. and Ma K., 2011, "Predicting Parametric Roll in Irregular Head Seas with Added Resistance Taken into Account", Jour. of Marine Science and Technology, Vol.16, pp.462-471.

Lu J., Min G. and Umeda N., 2012, "Numerical Approaches on Parametric Roll in Head Seas", the 10th International Hydrodynamics, Petersburg, Russia, pp. 83-88.

Lu J., Min G. and Umeda N., 2013, "A Study on the Effect of Parametric Roll on Heave and Pitch Motions in Head Seas", Proceedings of the 13th International Ship Stability Workshop, Brest, France, pp.185-191.

Lu J., Gu M. and Umeda N., 2016, "Experimental and Numerical Study on Several Crucial Elements for Predicting Parametric Roll in Regular Head Seas", Jour. of Marine Science and Technology (under reviewed).

Munif A., and Umeda N., 2000, "Modeling Extreme Roll Motions and Capsizing of a Moderate-Speed Ship in Astern Waves", Journal of the Society of Naval Architects of Japan, Vol. 187, pp. 405-40824.

Neves Ma.A.S., Vivanco J.E.M. and Rodriguez C.A., 2009, "Nonlinear Dynamics on Parametric Roll of Ship in Head Seas", Proceedings of the 10th International Conference on Stability of Ships and Ocean Vehicles, pp.509-520.

Rodriguez C. A. et al., 2007, "Validation of a Container Ship Model for Parametric roll", Proceedings of 9th International Ship Stability Workshop, Hamburg.

Taguchi H., Ishida S., Sawada H. and Minami M., 1995, "Model Experiments of Ship Capsizing in Astern Seas", Journal of the Society of Naval Architects of Japan, Vol.177, pp.207-217.

Umeda N., Hashimoto H., Stern F., Nakamura S., Sadat-Hosseini H., Matsuda A. and Carrica P., 2008, "Comparison Study on Numerical Prediction Techniques for Parametric Roll", Proceedings 27th Symposium on Naval Hydrodynamics, Seoul Nat Univ, pp. 5-10.

Umeda N., and Francescutto A., 2008, "Performance-Based Ship Operation", Proceedings 2nd International Workshop on Risk-Based Approaches in Maritime Industry, Univ. Strathclyde, 2.2.1-2.2.9.

Umeda N. and Hashimoto H., 2006, "Recent Developments of Capsizing Prediction Techniques of Intact Ships Running in Waves", Proceedings of the 26th Symposium on Naval Hydrodynamics, Rome, USB.

SESSION 2

Validation of numerical methods

Towards Accurate Computations of Active Stabiliser Fins, focusing on Dynamic Stall

Gerson Fernandes, *MARIN Academy*, gcf105@yahoo.com

Geert Kapsenberg, *MARIN*, G.K.Kapsenberg@marin.nl

Maarten Kerkvliet, *MARIN*, M.Kerkvliet@marin.nl

Frans van Walree, *MARIN*, F.v.Walree@marin.nl

ABSTRACT

Steps towards accurate and efficient characterisation of the hydrodynamic behaviour of active stabiliser fins have been conducted using computational fluid dynamics. Conditions seen at hydrodynamic testing facilities (Reynolds number = 135,000), with an angle of attack variation described as $\alpha(t) = 10^\circ + 15^\circ \sin(\omega t)$ have been modelled in two dimensions with various RANS turbulence models (k- ω SST, k- $\sqrt{\text{kl}}$, Spalart-Allmaras & LCTM) for reduced frequencies $k=0.1$ & 0.05 . Solutions were compared to experimental results and results from other calculation methods (LES) and to results from a typical sea keeping code. The results showing the hysteresis loop for C_L and C_D show that a good agreement was seen to the literature. For seakeeping applications, moderate refinement in time and space is sufficient, and that the k- ω SST turbulence model best matches the C_L and C_D curves found in the literature. The increased knowledge of stabiliser fins dynamics will be used to improve time-domain seakeeping codes and possible also the control laws for active stabilizer fins.

Keywords: *Active stabiliser fins; Dynamic stall; Computational fluid dynamics; RANS turbulence models; Roll damping*

1. INTRODUCTION

The subject of roll damping is an engineering topic with active research, and is important for a wide range of ship types, affecting not only the cargo but also the comfort and safety of the passengers and crew on board. The problem originates from the lack of inherent roll damping from a bare hull, and is compounded by the dominant importance of viscous effects (Wang et al. 2012)(Bačkalov et al. 2015). To overcome this deficiency, devices such as bilge keels, anti-roll tanks, for example, can be employed. Alternatively, stabilizer fins can also be used, where an appropriately mounted fin is used to produce a roll restoring moment. Furthermore, stabilizer fins can be passive or active; the latter consist of moving surfaces as a component of a control system. Typically, the fin operates by changing the angle of attack, and can enter the dynamic stall regime. Dynamic stall occurs when a lifting surface is subject to a sufficiently large variation of the angle of attack, (Leishman 2006). Towing tank experiments (Gaillarde 2003) have shown that the dynamic stall angle by far exceeds the static value. This result was a strong motivation for this study.

The subject of dynamic stall presents a set of challenges on its own. This was studied in the context of helicopter blades for example by (McCroskey, Carr, and McAlister 1976), with its own and distinct Reynolds (Re) and Mach number regime. Less attention has been given to the Reynolds regime of order 100,000 but comparatively recently, two investigations stand out. A study by (Lee and Gerontakos 2004), concerned low-speed wind tunnel experiments for a NACA 0012 section at Reynolds number=135,000. Secondly, (Kim and Xie 2016) conducted thorough Large Edge Simulations (LES) for the same geometry, where a good agreement was seen to the experiments and further, the influence of free-stream turbulence was assessed. Other results performed with RANS models include (Wang et al. 2012) and (Gharali and Johnson 2013), where in general the maxima and minima and overall hysteresis loop for the force coefficients agree with the experimental results. However, the force coefficients show large oscillations, particularly on the down stroke.

The work presented here will detail numerical simulations performed with computational fluid

dynamics (CFD) code for conditions seen at hydrodynamic wind/wave testing facilities of an isolated stabilizer fin section. Given the difficulties forecasted in the literature, a careful and progressive approach will be adopted. Two reduced frequencies will be tested and compared to the literature and a typical seakeeping code.

The end objective of this work is to improve the knowledge of the stall of stabiliser fins, with particular emphasis on improving current seakeeping codes, which currently model poorly the behaviour at high angles of attack and hysteresis.

2. METHODOLOGY

ReFRESCO

The numerical simulations performed with CFD code described in (ReFRESCO), a viscous-flow code that solves the incompressible Navier-Stokes equations. This finite-volume code uses a cell-centred approach and the SIMPLE pressure-correction equation for mass conservation. Time stepping is performed implicitly with a second-order backward scheme. Turbulence models are used in a segregated approach, and include the $k-\omega$ SST (Menter and Langtry 2003), $k-\sqrt{k}$ (Menter, Egorov, and Rusch 2006), Spalart-Allmaras (Aupoix and Spalart 2003) and the LCTM (Langtry and Menter 2009).

Geometry, Grid Generation & Boundary Conditions

The fin section was assumed to be a NACA 0012. This symmetrical airfoil has been the subject of several numerical and experimental investigations. The analytical equations describing this airfoil have been closed, resulting in a rounded trailing edge with a small radius (0.125% of the chord). The computational domain is discretised using the commercial software GridPro. The resulting structured mesh had a circular far field of 100 chords radius (from a domain size study), as boundary related issues were beyond the current scope. The entire boundary layer was resolved, and therefore a y^+ ,

$$y^+ = u_* y / \nu \quad (1)$$

(where u_* : friction velocity and ν : kinematic viscosity) value of < 1 was required. This is done to correctly remove the necessity of employing wall functions. Boundary conditions were such that an

inflow and outflow boundaries were present at the extremes of the domain, and a pressure condition above and below (see schematic in Figure 1). Two dimensionality was ensured using symmetry boundaries on the sides. Five geometrically similar grids, ranging from 368-56k cells were tested (see Figure 2).

Two grid motion methods have been tested, a rigid grid motion and grid deformations using a radial basis function, where no appreciable difference was seen. The target iterative convergence, an important metric when performing CFD results, was set to $1E-5$ in the L_{INF} (worst case). Typically, the RMS (L_2 norm) residual value is 1-2 orders lower.

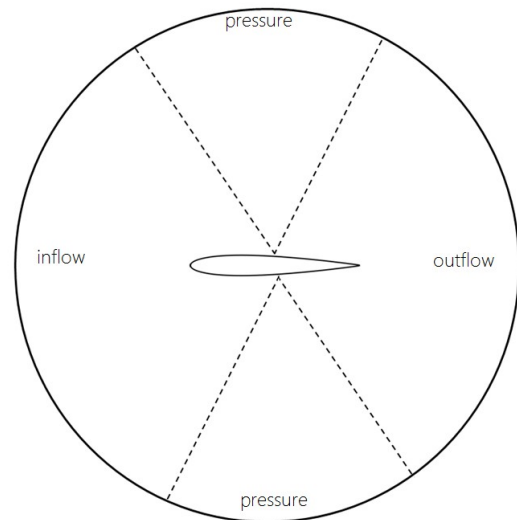


Figure 1: Boundary condition schematic

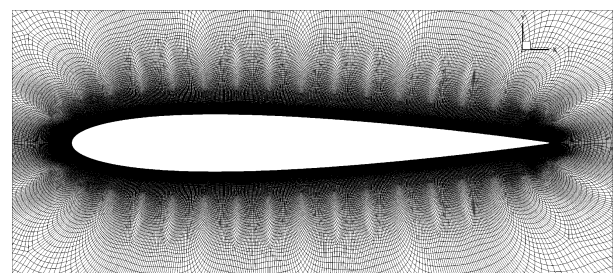


Figure 2: Mesh around the NACA 0012 section

PanShip

Results were also compared to PanShip (Walree 2002), a typical seakeeping code. PanShip is an unsteady time domain boundary element method for ships equipped with (or without) lifting surfaces for motion control. Linearised free surface effects are incorporated through the use of transient Green functions. Lifting surfaces are discretised in to quadrilateral panels with a constant source and doublet strength. Wake sheets consisting of doublet

panels emerge from the trailing edge. Viscosity effects are approximated by using empirical formulations for frictional resistance and drag due to flow separation.

Flow conditions and Fin Section Kinematics

Flow conditions typically seen in towing tanks have been modelled, and given the availability of the literature, the Reynolds number is chosen as:

$$Re = \frac{\rho U_{\infty} c}{\mu} = 135,000 \quad (2)$$

where ρ : density, U_{∞} : inlet velocity, c : chord length & μ : dynamic viscosity.

The prescribed fin motions are described as:

$$\alpha(t) = \alpha_{mean} + \alpha_{amp} \sin(\omega t) \quad (3)$$

The mean angle of attack (α_{mean}) was 10° and the amplitude of oscillation ($\alpha_{amp} = \pm 15^{\circ}$).

The frequency of oscillation is non-dimensionalised in the reduced frequency,

$$k = \frac{\omega c}{2U_{\infty}}. \quad (4)$$

Two reduced frequencies were tested, 0.1 & 0.05. The force coefficients are normalised with respect to the chord length, inlet velocity, α_{mean} and planform area.

3. RESULTS, $k=0.1$

Iterative convergence

A typical iterative convergence is shown in Figure 3, where also the C_L and angle of attack can be seen (including a starting up transient). The force signal is seen to be periodical; no signal processing has been performed of the presented force coefficient signals. The LES results are phase averaged over 3 cycles and the experiments over 100 cycles, which could explain the smoothness of the results. It is seen how part of the cycle of oscillation does not meet the target iterative convergence, and that these time steps are near the maximum incidence, where the flow is very complex and therefore numerically more difficult to solve. An effort was made to further improve the convergence, but no appreciable difference was seen in the force signal. Hence, the current shown results presented are deemed to be sufficiently converged.

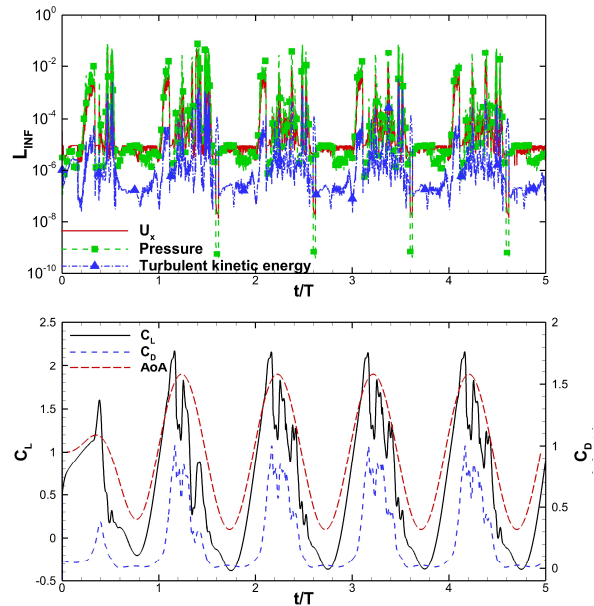


Figure 3: Typical convergence for U_x , pressure & turbulent kinetic energy equations (upper figure) and C_L signal (lower figure). Reduced frequency, $k=0.1$; turbulence model: $k-\omega$ SST; time step, $T/dt=800$.

Turbulence Model

The force coefficients for all the tested turbulence models against the AoA are shown in Figure 4-6 below for all the tested turbulence models. The upstroke has a very different behaviour compared to the down stroke, where, different to the smooth slope on the upstroke, the down stroke shows several oscillations. These oscillations correspond to the shedding of vortices, and given the inherent differences in the turbulence models, this results in a different shedding strength and location. The peak C_L values are comparable for all turbulence models and agree well with the LES, but are approximately 8% lower than the experiments. A detailed discussion and possible explanation for this mismatch is given in (Kim 2013). The LCTM model does account for laminar-turbulent boundary layer transition, but no appreciable difference is seen for this case. Given the current reduced frequency, it is likely that inertial effects dominate the viscous phenomena, such as boundary layer transition. Comparing to the LES, it appears that the $k-\omega$ SST model better captures the down stroke behaviour. When oscillations in the C_L occur, the values are also higher than predicted by the LES. This over prediction could be explained by the two-dimensional nature of the current CFD simulations. Similarly, the C_D curve shows a good agreement between all the RANS models.

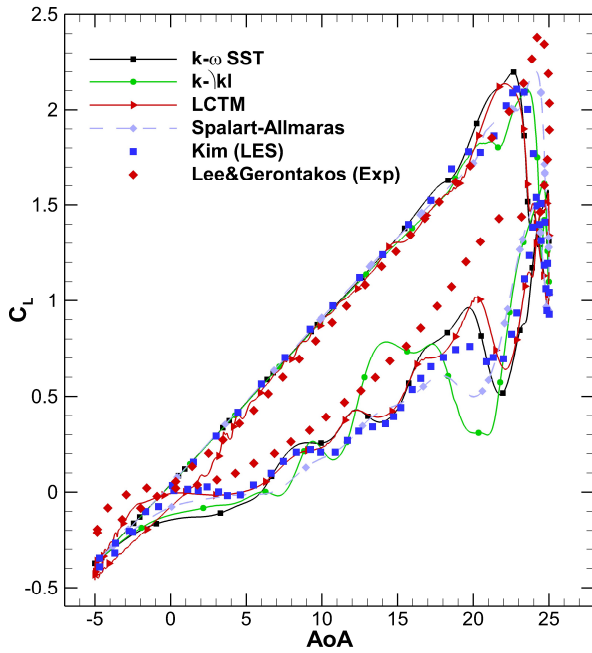


Figure 4: C_L vs AoA for the various turbulence models

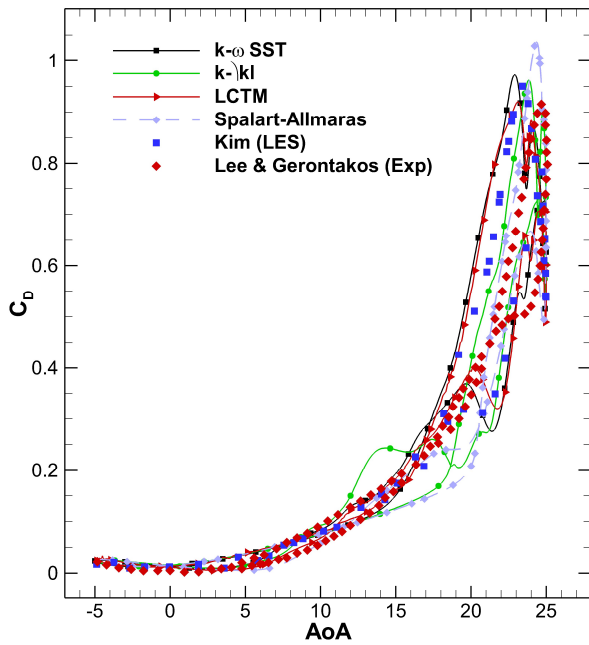


Figure 5: C_D vs AoA for the various turbulence models

Time step refinement

Given the unsteady nature of the problem, it is important to assess the sensitivity of the force coefficients on the time step. Four time steps have been tested with the $k-\sqrt{kl}$ model, and the effect on the C_L is shown in Figure 6. It can be seen that during the upstroke (-5→25 degrees), no significant influence of the time step is seen (this is also evident by the easier convergence, see Figure 3). However, during the down stroke (25→-5 degrees), relatively small differences in amplitude are seen, and are essentially identical when the incidence

returns to approximately -5 degrees. These differences are again attributed to the shedding of the vortices, but are not of primary interest for a seakeeping context and therefore a value of $T/dt = 400$ (T : period of oscillation), will suffice.

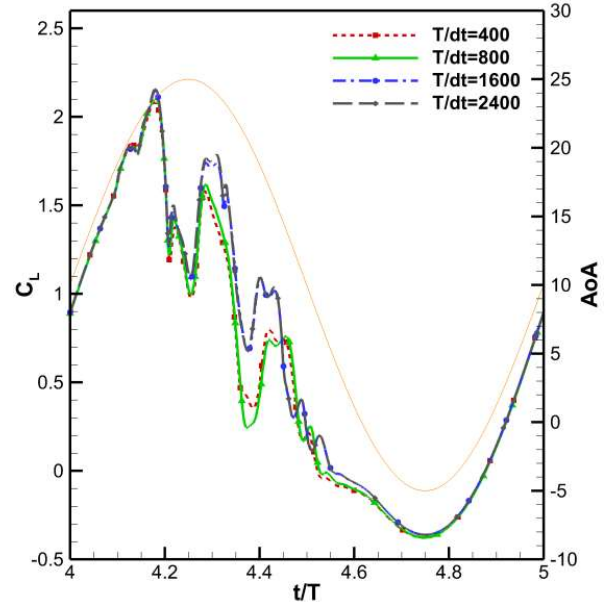


Figure 6: C_L vs t/T for various time steps ($k-\sqrt{kl}$ model, finest grid). Incidence also shown (right axis)

Grid Refinement

The five geometrically similar grids have been tested, and are shown below in Figure 7-8 (see figure caption for legend information). Some relevant grid parameters are shown in Table 1 (see caption for details). The flow can again be divided into two distinct motions, the up and down stroke. The coarsest grid loses much of the detail comparing to the other grids, showing a smoother profile. Apart from the coarsest grid, all grid densities show a good agreement of the C_L vs AoA to the LES. The peak C_L and its associated AoA are also in agreement. Again, the main differences are seen during the down stroke, where the coarsest grid loses much of the detail seen in the finer grids. The C_D is in good agreement for all grid densities.

Grid	Cells	$y^+ _{max}$	$\overline{y^+} _{max}$	Max. C_L	Max. C_D
A	368E3	0.42	0.24	2.18	1.00
C	187E3	0.57	0.35	2.16	0.941
E	104E3	0.69	0.44	2.15	0.927
G	56E3	1.0	0.6	2.26	0.952

Table 1: Summary of grid refinement study. Showing number of cells, maximum y^+ found in the cycle, the phase averaged maximum y^+ , and the maximum C_L and C_D .

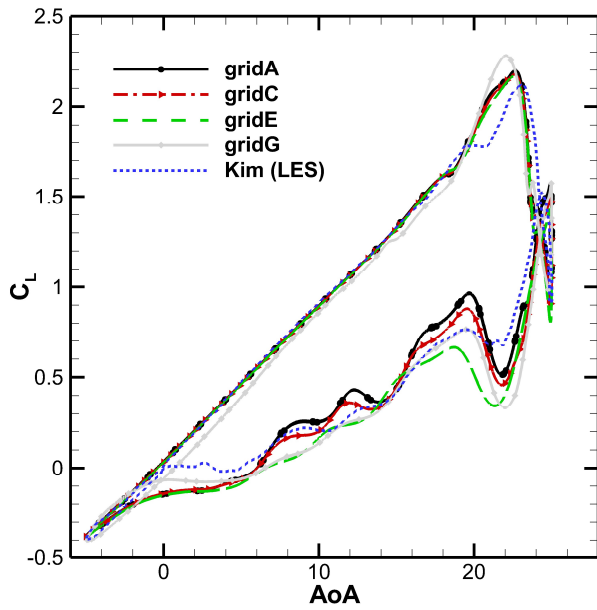


Figure 7: C_L vs AoA for different grid densities, $k-\omega$ SST turbulence model. Note grid denoted “A” is the finest (368k cells) and “G” is the coarsest (56k cells)

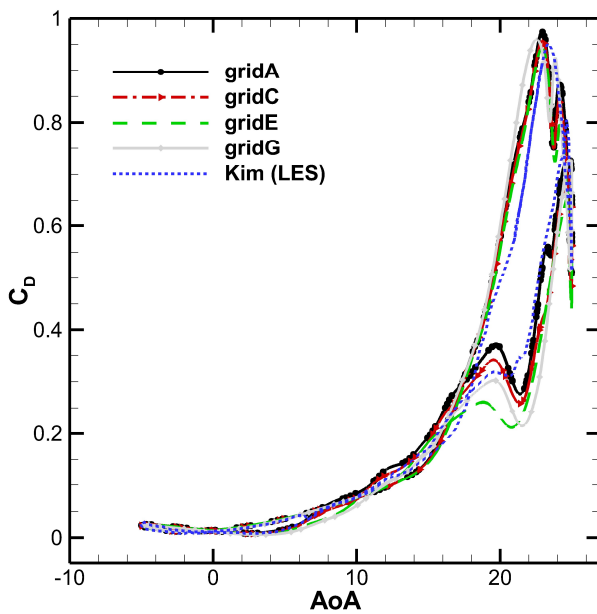


Figure 8: C_D vs AoA for different grid densities. See previous figure for legend information

Discussion & comparison with PanShip

The comparison of the ReFRESHCO results with results from literature and with PanShip results is shown in Figure 9. ReFRESHCO results show that stall is adequately captured. The sharp decrease in force (from about 2.2 to 0.5 for the C_L) between 20 degrees on the up and down stroke compares well to published data. This decrease is of practical engineering importance, indicating how quickly the fin loses a large portion of the generated lift force. It is also shown that between approximately 0 degrees on the down stroke and 0 degrees on the

upstroke, no hysteresis effect is observed. This compares to the LES, while the experiments predict a small hysteresis effect at this portion of the cycle. PanShip can predict the maximum and minimum C_L , and the upstroke behaviour, as well as some hysteresis. The largest difference is seen on the down stroke, where the complex system of vortices is inherently not accounted for. The enclosed area (a measure of the work done) between up and down strokes is also much smaller. The notable decrease in force mentioned above is also not captured.

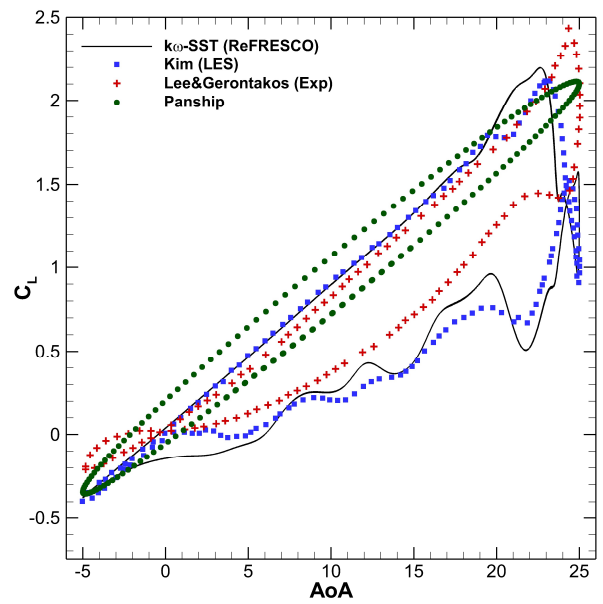


Figure 9: C_L vs AoA, comparison with PanShip

The maximum C_D shows an under prediction of close to 50% compared to all the other results, and is higher at the minimum AoA. Again, some hysteresis is present.

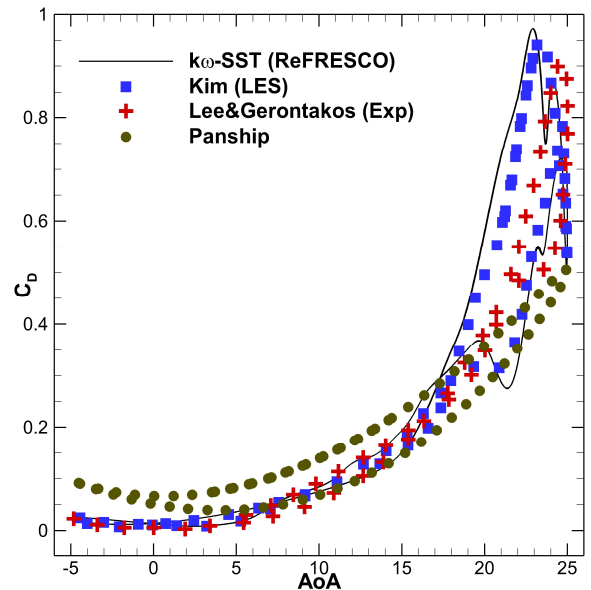


Figure 10: C_D vs AoA, comparison with PanShip

4. RESULTS, $k=0.05$

A lower reduced frequency (and therefore slower rotation velocity) has been performed for $k=0.05$. The comparison of force coefficients between ReFRESKO, literature and PanShip is shown in Figure 11 and Figure 12. The current ReFRESKO results appear to over predict the maximum C_L and C_D by 19% and 21.4% respectively (see “flow field description” below for further discussion). With exception of the peak value, a good agreement is seen for both for force coefficients. Another difference captured by the current ReFRESKO results are the oscillations seen on the down stroke, which are not present in the literature. The solution obtained is periodical, and in the figures below 4 cycles are plotted, and practically no differences are observed between the cycles.

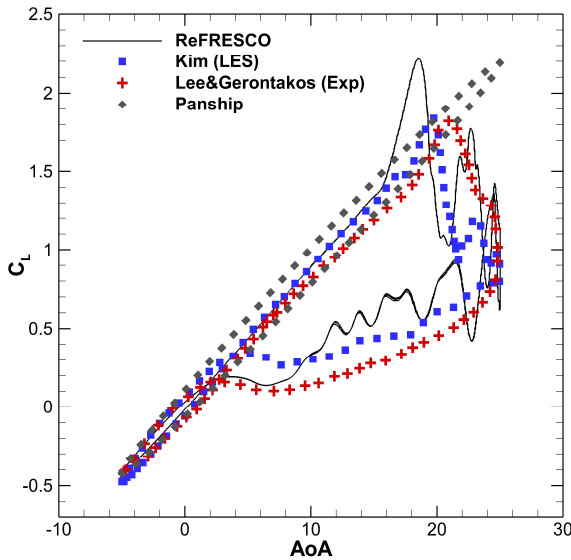


Figure 11: C_L vs AoA, $k=0.05$

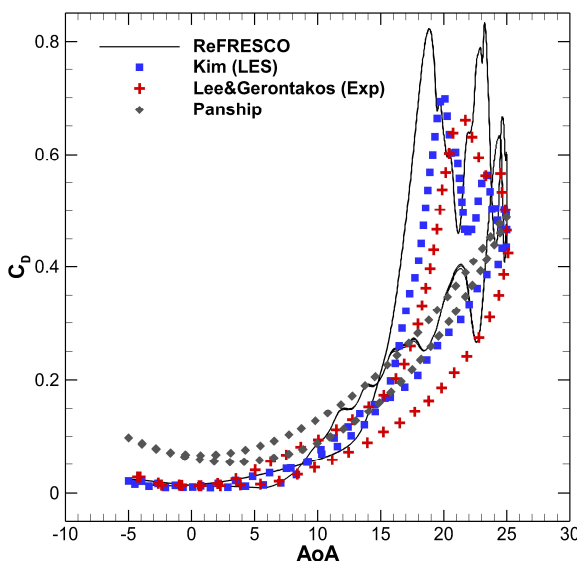


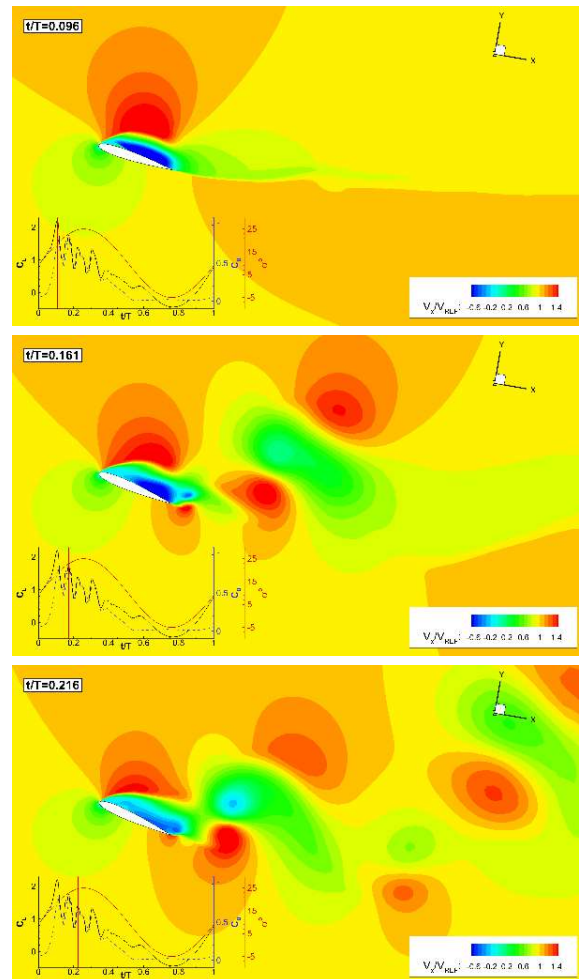
Figure 12: C_D vs AoA, $k=0.05$

Contrasting with the higher reduced frequency, it can be seen that between approximately 5 degrees on the down stroke and upstroke, no influence of the hysteresis is observed (comparing to 0 degrees for $k=0.1$).

Flow field description

The flow field is shown in Figure 13, coloured by the non-dimensional stream wise velocity (U_x/U_∞) contours (see caption for details). The calculated peak in C_L and C_D that is not seen in the other results is the result from an over prediction of the negative pressure of the suction side. Once this dominant vortex has been shed, the forces compare better to the LES results.

From the flow field it can also be seen how the oscillations in the force coefficients arise from the shedding of vortices and that the predominant vortex results from the leading edge vortex. The complex flow field also highlights the complexity of the flow, consisting of leading and trailing edge shear layers, bluff-body like shedding from the fin section and adynamic wake. For $k=0.05$, the maximum C_L occurs at $\sim 19^\circ$.



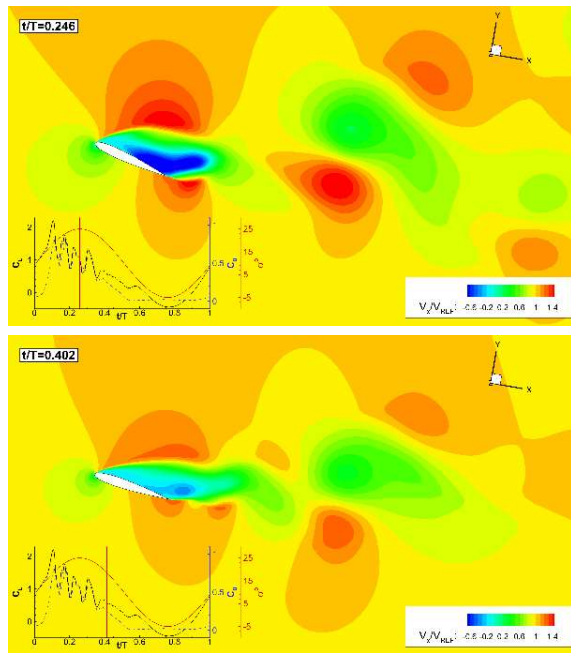


Figure 13: Flow field (stream wise/inlet velocity ratio) showing differing portions of the pitching cycle. 18.6° upstroke; 22.8° upstroke; 24.7° upstroke; maximum AoA, 25°; first down stroke oscillation, 18.7° down stroke

5. CONCLUSIONS

The flow around an stabilizer fin section performing an harmonically oscillating motion has been calculated using CFD. The sensitivity to different RANS turbulence models, time steps and grid refinements have been studied and recommendations are made for these settings assuming the current engineering context. Periodical solutions were obtained for all cases. The iterative convergence was monitored, and the boundary layer resolved at all time steps. Results were compared to literature, where overall a good agreement was found. Specifically, the maximum and minimum values for C_L and C_D (in particular for $k=0.1$) and the upstroke profile of the force coefficients compared well to published results. For $k=0.05$, peak values are over predicted by $\sim 20\%$ compared to the literature. The oscillations seen on the force coefficients of the down stroke are attributed to the complex system of vortices present, and are visualised by contour plots. Comparison to a typical seakeeping code shows the big improvement in correctly predicting the stalling behaviour of the fin section. The upstroke behaviour is comparable between the seakeeping code and the CFD, but the classical method vastly under estimates the effect of the stalling behaviour on the down stroke.

6. FURTHER WORK

Further work will be done to incorporate the obtained knowledge on the dynamic stall effect for seakeeping applications. Two methods are currently being assessed, either using a database calculated a-priori, or a robust coupling between the CFD code and the seakeeping tools.

7. ACKNOWLEDGEMENTS

The authors are grateful to Dr. Yusik Kim and the Aerodynamics and Flight Mechanics (AFM) group of the University of Southampton for their valuable comments and making their data available.

8. REFERENCES

- Aupoix, B., and P.R. Spalart. 2003. "Extensions of the Spalart–Allmaras Turbulence Model to Account for Wall Roughness." *International Journal of Heat and Fluid Flow* 24(4): 454–62.
- Bačkalov, Igor et al. 2015. "Ship Stability, Dynamics and Safety: Status and Perspectives." In *12th International Conference on the Stability of Ships and Ocean Vehicles*, Glasgow, UK.
- Gaillarde, Guilhem. 2003. "Dynamic Stall and Cavitations of Stabilizer Fins and Their Influence on the Ship Behaviour." In *FAST*, Naples.
- Gharali, Kobra, and David a. Johnson. 2013. "Dynamic Stall Simulation of a Pitching Airfoil under Unsteady Freestream Velocity." *Journal of Fluids and Structures* 42: 228–44. <http://dx.doi.org/10.1016/j.jfluidstructs.2013.05.005>.
- Kim, Yusik. 2013. "Wind Turbine Aerodynamics in Freestream Turbulence." University of Southampton.
- Kim, Yusik, and Zheng-Tong Xie. 2016. "Modelling the Effect of Freestream Turbulence on Dynamic Stall of Wind Turbine Blades." *Computers & Fluids* 129: 53–66.
- Langtry, Robin B., and Florian R. Menter. 2009. "Correlation-Based Transition Modeling for Unstructured Parallelized Computational Fluid Dynamics Codes." *AIAA Journal* 47(12): 2894–2906.
- Lee, T., and P. Gerontakos. 2004. "Investigation of Flow over an Oscillating Airfoil." *Journal of Fluid Mechanics* 512: 313–41.

-
- Leishman, J. G. 2006. Cambridge Aerospace Series *Principles of Helicopter Aerodynamics*. New York: Cambridge University Press.
- McCroskey, W. J., L. W. Carr, and K. W. McAlister. 1976. "Dynamic Stall Experiments on Oscillating Airfoils." *AIAA Journal* 14(1): 57–63.
- Menter, F. R., Y. Egorov, and D. Rusch. 2006. "Steady and Unsteady Flow Modelling Using the K-skL Model." *Proceedings of the International Symposium on Turbulence, Heat and Mass Transfer*: 403–6.
- Menter, F. R., and M. Langtry. 2003. "Ten Years of Industrial Experience with the SST Turbulence Model." In *Fourth International Symposium on Turbulence, Heat and Mass Transfer*, eds. K. Hanjalic, Y. Nagano, and M. Tummers. Ankara, Turkey.
- "ReFRESHCO." www.refresco.org.
- Walree, F Van. 2002. "Development, Validation and Application of a Time Domain Seakeeping Method for High-Speed Craft with a Ride Control System." In *24th Symposium on Naval Hydrodynamics*, Fukuoka, Japan.
- Wang, Shengyi et al. 2012. "Turbulence Modeling of Deep Dynamic Stall at Relatively Low Reynolds Number." *Journal of Fluids and Structures* 33: 191–209.

Fast time domain evaluation of Anti-Roll Tank and ship coupling using non-linear retardation functions

Nicolas F.A.J. Carette, MARIN, n.carette@marin.nl

ABSTRACT

Anti-Roll Tanks (ART) have been used for more than a century to damp the roll motion of ships. These devices exist in various configurations, passively and actively controlled. All versions rely on resonant water motions in a chamber which, by essence, is a very non-linear process. To account for these non-linearities, several approaches have been proposed, where the most recent and complete one is the direct coupling of time domain seakeeping codes with a CFD models of the ART. However, this approach comes at the price of relatively high computation effort. This is in contradiction with the need for long simulations to establish the effects of the non-linearities in the ART reaction forces on extreme events. To reduce the computation costs of a direct simulation, a new technique is proposed which uses retardation functions based on harmonic ART response data. The technique proposed here uses a family of retardation functions with a Hilbert transform method for time dependent interpolations to capture the non-linearity in the response of the tank as a function of excitation amplitude.

Keywords: *Time domain; seakeeping; Anti-roll tank; free surface tank; U-tank*

1. INTRODUCTION

In the early design phase, numerical methods provide an efficient method to predict the motions of a ship. However, it is well known that, due to its underlying resonance principle, the response of an ART is strongly non-linear. This is already known for a long time from observations on board ships (see Watts 1883; Lewison 1975) and is confirmed by numerical studies (see Chu et al. 1968; Verhagen, van Wijngaarden 1965) and experimental campaigns (see van den Bosch, Vugts 1966; Stigter 1966). Therefore, the numerical model that predicts the merits of an ART should take these non-linear effects into account.

Time domain seakeeping codes are widely used to study the behaviour of a ship in a seaway when non-linearities, in either the excitation or the reaction forces, are expected. Therefore, a method to include also the effect of an ART in such a simulation seems of great value. The most straightforward approach is to couple such seakeeping code to a CFD model of the ART (see van Daalen et al. 2001; Cercos-Pita et al. 2015). However, CFD calculations of an ART take typically in the order of several hours per hour of simulation on multi-CPU clusters, whereas time domain seakeeping codes usually runs faster than real time on a simple single-core desktop PC. Early

approaches attempted to simplify response of an ART by considering an that of an equivalent pendulum. However, this is considered too simplistic to capture the non-linearity of the response (see Abramson, Silverman 1966). Therefore, because of the absence of another analytical time domain model, both for either free surface or U-type ART, another approach is proposed here.

The approach developed here is based on the use of so-called retardation functions, or more commonly named impulse response functions, for damping and added mass of floating oscillating bodies as proposed by Cummins (see Cummins 1962; Ogilvie 1964; Journée 2001). Such an approach is very fast and light regarding computational effort, and can be used for any ART if its reaction forces (damping, restoring or added mass) are available. However, this method assumes a linear damping. This problem is addressed by means of an interpolation based on the instantaneous excitation envelope. Following earlier work (Carette 2015), the effective gravity angle (EGA), which is determined by the local transverse accelerations and the local vertical accelerations, is adopted as the measure for the excitation of the ART.

2. METHOD

ART response

The response of the ART at each time step can be written in the form of a convolution of its retardation function and history of excitation velocity $\dot{\phi}$. Because the response of a tank is easily known at zero-frequency, rather than at infinite frequency, the infinite added mass is here replaced by the zero-frequency restoring term, and leads thus to the following equation for the roll reaction moment at time t :

$$M_x(t) = \int_0^{\infty} K(\tau) \dot{\phi}(t-\tau) d\tau + C_0 \phi(t) \quad (1)$$

where K is the retardation function obtained from equation (2), and the damping b is derived from harmonic oscillation tests (see van den Bosch, Vughts 1966), CFD calculations (Kerkvliet et al. 2014) or frequency domain ART models (see Verhagen, van Wijngaarden 1965; Stigter 1966). The restoring term C_0 is of course the free surface effect of the ART, and can be easily estimated based on the tank geometry.

$$K(\tau) = \frac{2}{\pi} \int_0^{\infty} b(\omega) \cos(\omega\tau) d\omega \quad (2)$$

To cope with the non-linearity of the response due to the excitation amplitude, a linear interpolation is used. Prior to the time domain calculations, N retardation functions are computed for a range of amplitudes of the excitation ϕ_a , rather than only one like in the case of a perfectly linear damping. At each time step during the simulation, the current amplitude is estimated from the envelope of the excitation amplitude which is computed using a Hilbert transform. The history of the excitation envelope is stored along with the history of the excitation amplitude and velocity. The history of the envelope is used to obtain time dependent linear interpolation coefficients c_i for each time step in the past. The retardation function at the current time step is obtained by summation of the coefficients and the retardation functions along the amplitude axis. In this way, each motion sample will be convoluted with a retardation function obtained from linear interpolation based on the amplitude envelope at that time.

$$K(t) = \sum_{\phi_a}^N c_i(t-\tau) K_i(t-\tau) \quad (3)$$

For every step in the simulation the local envelope of the excitation amplitude is obtained through a Hilbert transform of the history of the preceding time steps. The window of the envelope has the a time span equal to the one of the retardations. However, such a transform has large deviations at the fore and aft ends of the window, thus leading to incorrect prediction of the envelope at the current time step. Various techniques have been developed to reduce those effects in signal analysis, with the easiest being a simple mirroring of the data. However, mirroring the data can introduce discontinuities that reduce its benefits. An alternative method uses motion prediction based on the current position, velocity and acceleration. The quality of this method is however limited in the case of non-linear simulations. In the present work a hybrid method is used. The method detects different cases and applies either central symmetry, axial symmetry, time shifts or motion prediction. Afterwards, to smoothen the mirroring, a slope correction of the mirrored part of the data is applied by using the instantaneous acceleration compared to the slope at the mirroring junction. The different mirroring cases are:

- Immediately before a zero crossing: a central symmetry around the zero crossing is done (Figure 1).
- Close to a peak: a y-axis symmetry around the peak is used.
- After a peak: y-axis symmetry around the back-face of the peak is done (Figure 2).
- After a zero crossing:
 - If the sample is lower than a peak in the past: a y-axis symmetry around the back face of a lower peak (Figure 3).
 - If the sample exceeds all available peaks in the past: no symmetry is used, the two next samples are predicted using the current position, speed and acceleration.

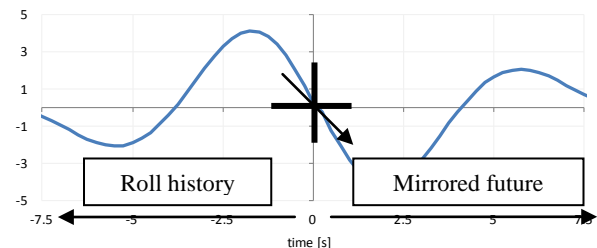


Figure 1: Central symmetry at zero crossing

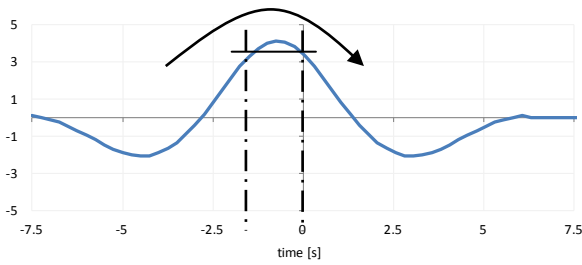


Figure 2: Back face symmetry after peak

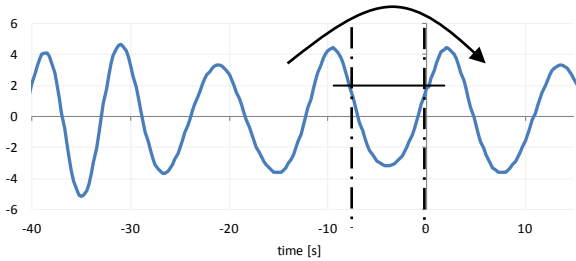


Figure 3: y-axis symmetry around a previous peak

Coupled response

The ship motions are computed using a time domain solver where the response of the tank is added as an external force computed at the beginning of each time step before the integration. The motion excitation applied to the ART is based on the EGA, rather than the roll, which is computed at the centre of the ART, and is defined as the angle to the vertical of the acceleration in the transverse plane. This angle thus includes the roll angle, but also the sway and heave accelerations at the tank location. Use of the EGA, which introduces a strong sway-roll coupling which was not accounted for in the older roll-based methods.

Initially, for verification purposes, a simple one degree of freedom solver using added mass, potential damping and wave excitation from a potential code was used. This solver uses a 5th order Runge-Kutta integrator available in the scipy library (see Hairer et al. 1993). A linear and quadratic damping can also be included. The integrated function is given in equation (4):

$$\ddot{\phi} = \frac{F_{inc} + F_{diff} + F_{ret} + F_{ART} - B_L \dot{\phi} - B_q \dot{\phi} \ddot{\phi} + C_{xx} \phi}{I_{xx} + A_{xx}} \quad (4)$$

The excitation force at each integration time step i is based on the average between the current time step and the previous time step. The retardation forces, including those of the ART, are based on the previous time step and kept constant during the integration.

The time domain, six degrees of freedom code FREDYN was used (see de Kat, Paulling 1989; de

Kat, Paulling 2001). This code uses a linear added mass, wave damping and diffraction from 2D strip theory calculations. The Froude-Krilov component in the wave excitation is non-linear, taking into account the instantaneous underwater geometry. The code includes various semi-empirical models for control surfaces and appendages. As in the 1 DoF model, the ART forces are computed at each time step from the motion history up to that step, and kept constant during the integration.

3. RESULTS

To verify the non-linear retardation function technique, a stepwise approach was used. Firstly, the use of impulse response functions to capture the damping and restoring effects of an ART was verified using forward and backward convolutions. Secondly, the envelope capturing technique was evaluated on its own by means of spectral analysis. Thirdly, the time domain response of a tank tested under irregular roll motion was computed. Finally, the computed coupled motions of a ship with an ART were compared to experiments.

Retardation function of an ART

Due to its relatively narrow peak, the damping of an ART will lead to relatively longer retardation functions than a typical wave damping operator. Moreover, for an ART, the added mass is not used, but the restoring term. The shape of the restoring coefficient of an ART is however not optimal for a Fourier transform, that is required in the derivation of the retardation function, as it has an offset between the value at zero and at infinite frequencies, due to the free surface effect. A Fourier transform works better in the case of a signal starting and finishing at the mean value.

To verify the adopted approach, the response of a reference U-tank was generated using Stigter's model (see Stigter 1966). The use of this analytical model is to ensure that the frequencies can be freely chosen to ensure the highest quality of the retardation functions. The chosen tank has a natural period of 8.3 seconds and a mass of water of about 134 tonnes. This tank has some internal damping due to limited ventilation, although it has rounded duct edges, such that its damping peak at low amplitude is relatively narrow. At larger amplitudes, the width of the peak increases rapidly. Figure 4 shows that the damping from the

analytical model is in very good agreement with experimental data, both in the frequency and in the amplitude directions. Figure 5 presents the derived retardation functions based on the damping at various excitation amplitudes. Due to the width of the damping peak at small amplitudes, the retardation function is much longer than at larger amplitudes.

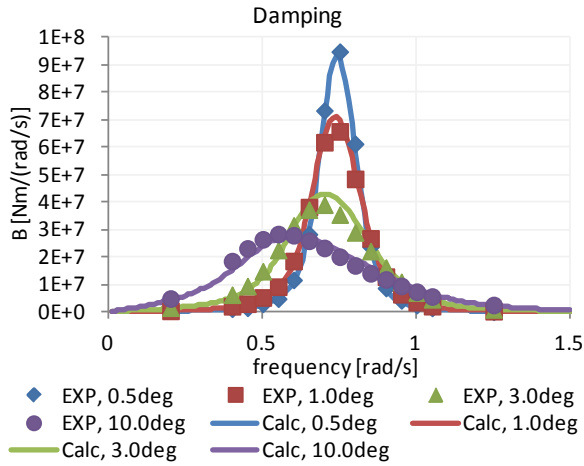


Figure 4: Damping of U-tank using Stigter's model

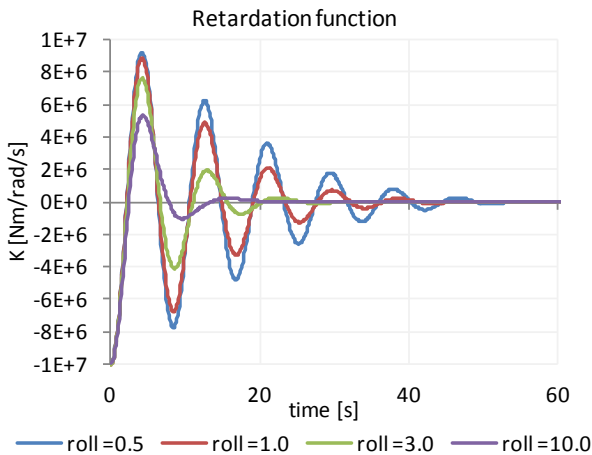


Figure 5: Retardation functions for ART

To check the representation of the restoring term, it was reconstructed from the retardation functions using the inverse convolution given in equation (5).

$$c(\omega) = \omega \int_0^t K(t) \sin(\omega t) dt \quad (5)$$

Figure 6 shows that the obtained restoring term is good at the lower frequencies and around the resonance area, but deviates from the frequency domain values for increasing frequency and roll amplitude. The deviation seems to be driven by the amplitude of the damping at very low frequencies. The error in the restoring term should not be too

important around the natural period of the tank, otherwise the resonance of the coupled ship and ART system will be affected by this method as the restoring term has a direct influence on the resonance frequency. If the resonance conditions are of importance for the ship performance study, it would be advised to correct the free surface effect C_0 such that the restoring term after convolution is zero at the natural period of the tank. The motions at low frequencies will then be affected by the artificially reduced free surface effect.

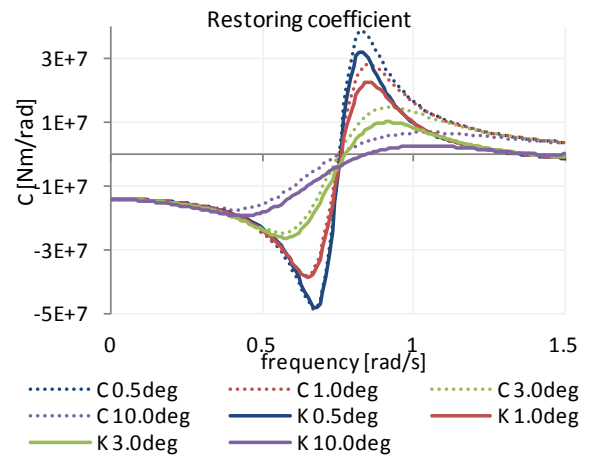


Figure 6: Restoring term of ART before and after convolution

Overall, the shape of the response of f an ART in terms of its damping and restoring moments seem well represented by the used retardation functions, although it may lead to relatively long convolution time spans in the case of small amplitudes and low internal damping.

Estimation of the excitation envelope

The linear interpolation technique between the retardation functions relies on the evaluation of the current motion amplitude. Due to the end effects of the Hilbert transform, this evaluation is subject to some error depending on the current sample being around a peak, around a zero crossing or in-between. To evaluate the quality of the hybrid mirroring technique, some tests were carried out with synthetic time traces generated from different types of spectra, and the envelope was compared with various parameters such as time span, time step, spectrum width and peak frequency of the spectrum. The time trace was generated for 1800 s. The spectrum was based on a simple Hanning window centred around the peak frequency, and with a given width.

Firstly, the effect of the time span of the window used for the envelope was studied. A time trace was generated with an irregular spectrum with a peak frequency of 1 rad/s and a width of 0.5 rad/s. The time step used was 0.1 s. A window with a given time span was then ran across the signal, and the envelope at the end of the window was compared to the envelope of the complete signal. Figure 7 shows that the length of the time span does not have much effect on the quality of the envelope using the hybrid mirroring, and is considerably better than a direct Hilbert transform of the window. The direct Hilbert transform shows strong oscillations around the true envelope at twice the peak frequency of the spectrum. The envelope with the mirrored data shows much smaller deviations, however it is somewhat discontinuous. The discontinuities are due to the discrete logic in the mirroring technique.

Figure 8 shows the spectrum of the envelope. The direct Hilbert transform of the window typically shows a peak at twice the peak frequency of the spectrum of the signal. The envelope with mirrored data has much lower deviations at those frequencies. The discontinuities due to the discrete logic introduce local peaks in the spectrum, but at frequencies way above the region of interest.

Secondly, the peak frequency of the signal spectrum was varied, keeping the width of 0.5 rad/s and the window span to 60 s. Figure 9 shows that the hybrid mirroring technique yields a very good estimate of the envelope around the peak frequency of the spectrum for a range of peak frequencies. It also clearly shows the peak in the direct Hilbert at twice the peak frequency of the spectrum. This peak could be problematic as it might affect the ART response in a frequency region where it already increases the ship motions; however, the hybrid technique solves this issue.

Finally, the width of the signal spectrum was varied from very narrow (0.25 rad/s) to very wide (2 rad/s), keeping the peak frequency at 1 rad/s. Figure 10 shows that the width of the spectrum does not have much influence on the quality of the envelope with mirroring, with a slight improvement as the width is reduced, although at the cost of peaks in the envelope spectrum at the harmonics of the incoming spectrum.

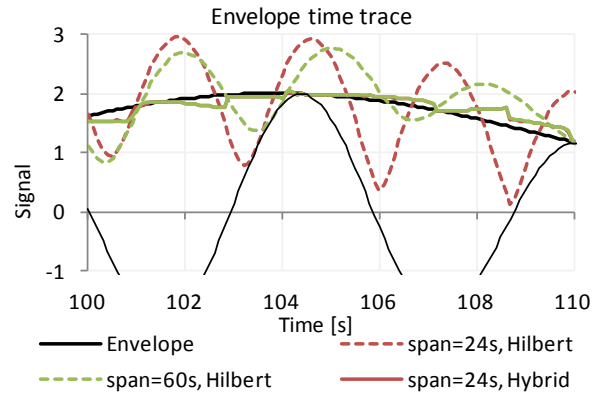


Figure 7: Envelope with various window sizes

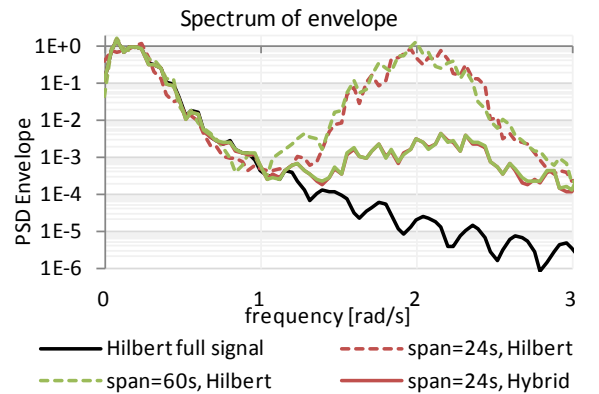


Figure 8: Spectrum of the envelope with various time spans

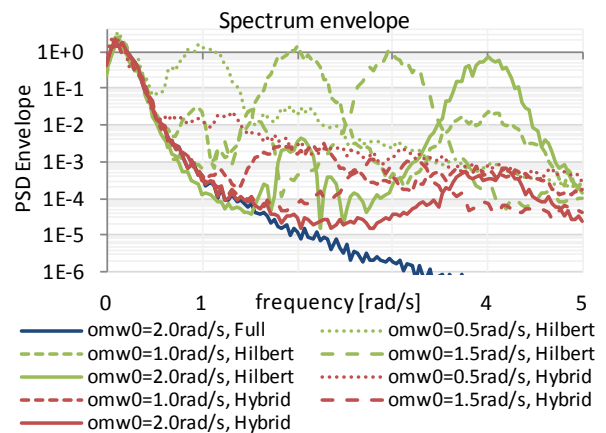


Figure 9: Spectrum envelope with various peak frequencies

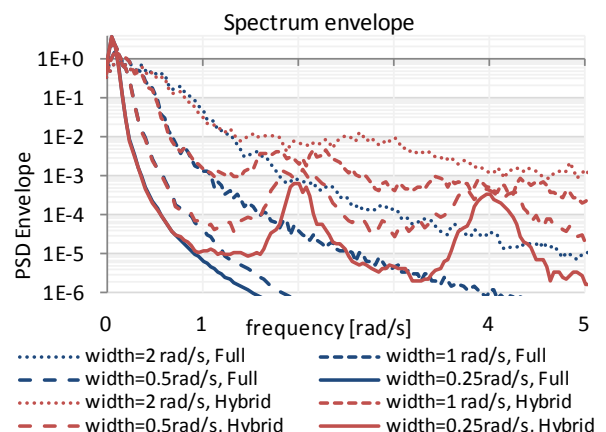


Figure 10: Spectrum of the envelope with various signal spectrum width

Non-linear retardation functions

The reference U-tank used up to now was also tested with irregular roll excitation with a significant amplitude of 2 degrees on an oscillation table. The test was carried out for 30 minutes full scale. The tank was tested with rounded and sharp duct edges to vary the internal damping. A flume type free surface tank of similar natural period and weight was also tested with the same motion time traces. In both cases, the peak of the motion spectrum was centred around the natural period of the tank. To validate the non-linear retardation functions, the response of both tanks was computed for a range of amplitudes using Stigter’s model for the U-tank and with Verhagen’s model for the free surface tank. The range of amplitudes was chosen such that it would overlap the irregular roll motions during the test. The non-linear retardation functions based on these operators were then used to reconstruct the irregular reaction forces of the tank using a time step of 0.25 s, which was sufficiently small to have no influence on the calculation. Figure 11 presents the result of the calculations compared to the experiments in the form of distributions of the amplitudes of the reaction moment. The frequency of exceedance is plotted on a Raleigh scale, on this scale the amplitude distribution of a narrow-banded perfectly linear process would show as a straight line (see Ochi, Bolton 1973). The amplitude has been divided by the RMS of the linear solution. The results show a clear improvement with the non-linear solution that now follows a non-linear distribution with a bias towards lower extremes. This distribution of the amplitudes of the response moment shows that the tank is, as expected, less efficient at large amplitudes than it is at small ones. Therefore, the response of the ship may be biased towards larger extremes if the tank is the significant source of damping.

As an example, a one degree of freedom simulation was carried out with the DDG51 equipped with the tested U-tank ART. The loading condition of the vessel was chosen to be tuned with the ART, and in such way that the ART would represent about 2% of the displacement. The calculations were performed with and without the ART for 10 h with a time step of 0.1 s. The calculations without ART were done with additional damping such that the RMS motions

would be similar to those with the ART. This was done with either a purely linear damping, or with non-linear damping. Figure 12 presents the distribution of the amplitudes of roll from the different solutions. As expected, the roll amplitude distribution with the linear damping follows the (straight-line) Rayleigh distribution. The result with the non-linear damping shows considerably lower extreme values. What was less expected is that the ship with ART presents an almost linear distribution. This means that an ART reduces typical values of the response (for instance the mean amplitude, or the RMS) much better than the extreme values.

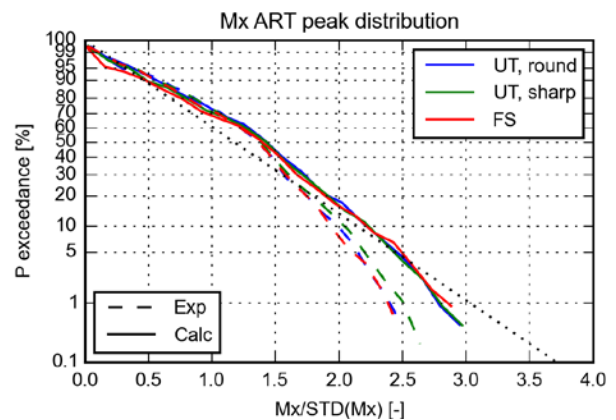


Figure 11: ART response moment distribution with irregular motions of 2 deg SSA

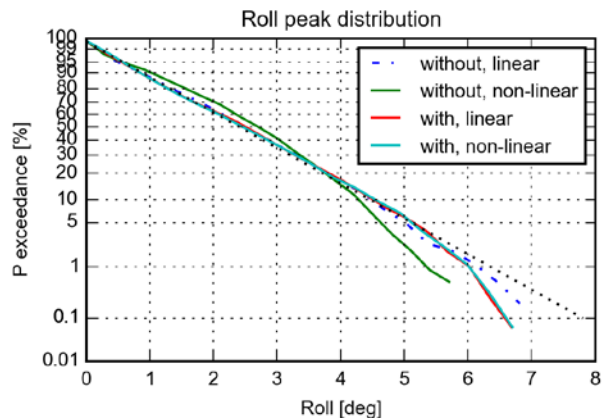


Figure 12: Roll distribution, 1DoF time domain, Hs=0.5m, Tp=8.7s, with and without ART

The fact that the roll with ART ends up more linear than one would expect based on the RAO of the tank moment is partly due to the width of the wave spectrum and tank size. Indeed, the ART response decreasing with increasing amplitude does not have the same effect at the roll resonance as at other frequencies. The ART damps the motions at resonance, but increases them at lower and higher frequencies, the non-linearities partly cancelling each other. This also explains why the solution with

the linear retardation functions gives very similar results to the one with non-linear retardation functions, in this case with the linearization around the significant roll amplitude. However, using non-linear retardation functions saves the trouble of having to find the right linearization amplitude. Moreover, in the case of tanks with larger dimensions in the longitudinal direction of the ship, the frequencies where the tank increases the motions are further apart. This, combined with a narrow wave spectrum, might even increase the larger roll amplitudes.

Coupled motions

Finally, the coupling of non-linear retardation functions for an ART with ship motions were verified by comparison with experimental data. An 18000 tonnes heavy lift vessel equipped with a 210 tonne free surface ART was tested in beam seas at zero speed. The waves were generated with a JONSWAP spectrum with a peak period equal to the ship’s natural roll period and with two different heights, 0.75 and 1.5 metres. The tests and calculations were carried out for 30 minutes full scale. The ship model was restrained in surge, sway and yaw by means of a soft spring setup with low natural frequencies to avoid interaction with the roll response. Prior to the tests, roll and sway decay tests were performed.

The calculations were carried out with FREDYN without surge, yaw and pitch motions. The sway motions were restrained with a spring coefficient corresponding to the experimental soft spring. The roll damping parameters were based on a linear and a quadratic coefficient derived from the roll decay tests. The response of the ART was derived using Verhagen’s model, and checked by means of oscillation tests for the ART. The excitation of the ART was the EGA at the tank’s location. Figure 13 shows the roll distribution with and without tank from the experiments and calculations. It shows that the calculation model captures quite well the damping due to the tank. The distribution of roll with ART appears also much more linear than with only bilge keels. Figure 14 presents the RAO of roll, where the double peaked character of the response with ART is clearly visible. The predicted RMS of roll was within 1% from the result of the experiment for the lower wave height and within 7% for the higher wave height. On a single core 2.1GHz PC the

calculations without ART were running at 15 times faster than real time, and those with ART at 3 to 7 times real time.

The use of the EGA rather than the roll is in this case quite important as the roll period of the ship is very long. In such a case, the sway motions are not small compared to the roll, especially of the damped ship, such that the EGA deviates substantially from the roll. Figure 15 presents the roll distribution with the free surface tank using either roll or EGA as excitation parameter during the calculations.

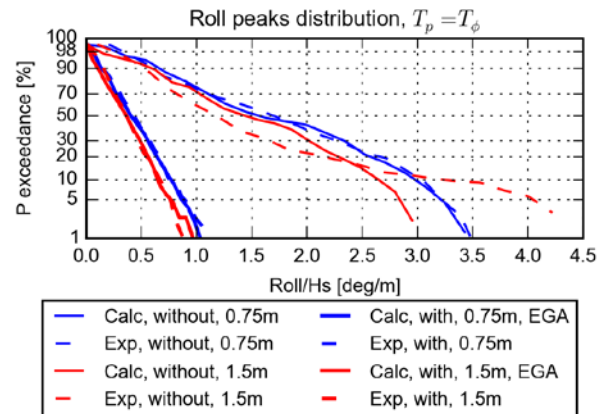


Figure 13: Roll distribution with and without free surface tank

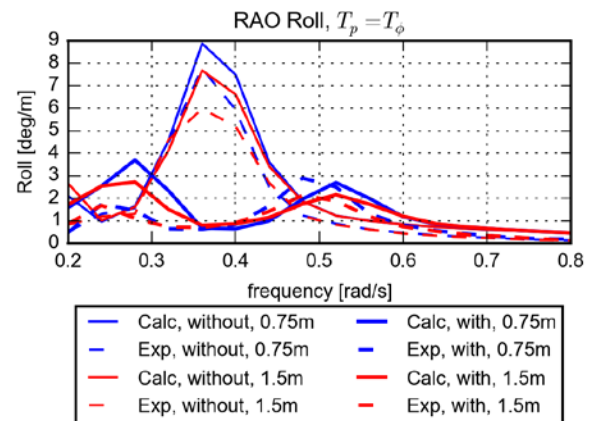


Figure 14: Roll RAO in irregular waves, with and without free surface tank

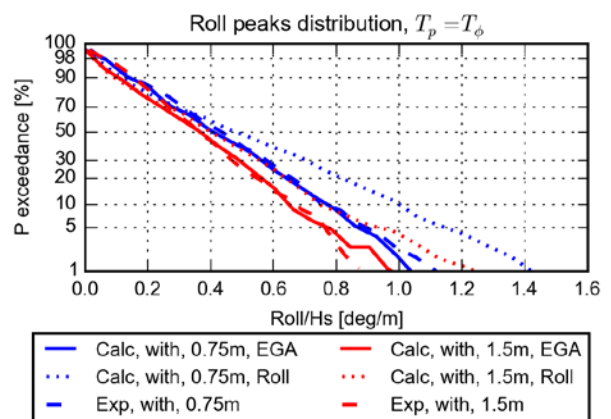


Figure 15: Roll distribution, with tank, roll vs. EGA

4. CONCLUSIONS

A new technique to include the non-linear effect of an ART in time domain calculations has been successfully developed. It uses an estimate of the envelope of the EGA and an interpolation in a set of amplitude dependent retardation functions..

The adopted use of retardation functions to capture the response of the ART as a function of excitation frequency and amplitude works with good accuracy. The use of envelope based interpolation at each time step offers a fast and efficient technique to capture the excitation amplitude dependence of the tank response.

The hybrid mirroring technique offers an accurate envelope prediction at the end of the time window. This technique greatly improves the quality of the Hilbert transform at the ends, but at the cost of small discontinuities at high frequency

Finally, the use of the EGA as excitation parameter for the tank greatly improves the prediction of the tank-ship coupling in conditions where the sway is non-negligible, which should be the case if the tank is properly designed.

5. REFERENCES

Abramson, H.N. & Silverman, S., 1966, "Dynamic Behavior of Liquids in Moving Containers" Nasa Sp-10. NASA, ed.,

van den Bosch, J. & Vugts, J., 1966, "Roll damping by free surface tanks", Delft.

Carette, N.F.A.J., 2015, "A study of the response to sway motions of free surface anti-roll tanks". In *World Maritime Technology Conference*. Providence, RI, USA.

Cercos-Pita, J.L., Bulian, G. & Souto-iglesias, A., 2015, "Time domain assessment of nonlinear coupled ship motions and sloshing in free surface tanks". In *International Conference on Ocean, Offshore and Arctic Engineering*. St John's, Newfoundland, Canada, pp. 1–11.

Chu, W., Dalzell, J. & Modisette, J., 1968, "Theoretical and experimental study of ship-roll stabilization tanks", *Journal of Ship Research*, pp.165–180.

Cummins, W.E., 1962, "The Impulse Response Function and Ship Motions", *Schiffstechnik*, 9, pp.101–109.

van Daalen, E.F.G. et al., 2001, "Anti Roll Tank Simulations with a Volume Of Fluid (VOF) based Navier-Stokes Solver". In *Symposium on Naval Hydrodynamics*.

Hairer, E., Norsett, S.P. & Wanner, G., 1993, "Solving Ordinary Differential Equations I, Nonstiff problems" 2nd ed. Springer-Verlag, ed., Springer-Verlag.

Journée, J., 2001, "Offshore Hydromechanics", de Kat, J.O. & Paulling, J.R., 2001, "Prediction of extreme motions and capsizing of ships and offshore marine vehicles". In *International Conference on Offshore Mechanics and Arctic Engineering*. Rio de Janeiro, RJ, Brazil.

de Kat, J.O. & Paulling, J.R., 1989, "The simulation of ship motions and capsizing in severe seas" SNAME, ed., *The society of naval architects and marine engineers*, 5.

Kerkvliet, M. et al., 2014, "Analysis of U-Type anti-roll tank using URANS. Sensitivity and validation.". In *International Conference on Ocean, Offshore and Arctic Engineering*. San Francisco, USA.

Lewis, G.R.G., 1975, "Optimum design of passive roll stabilizer tanks", *Royal Institution of Naval Architects*.

Ochi, M. & Bolton, W., 1973, "Statistics for prediction of ship performance in a seaway - Part 1", *International Shipbuilding Progress*, 20, pp.27–54.

Ogilvie, T., 1964, "Recent progress toward the understanding and prediction of ship motions". In *5th Symposium on naval hydrodynamics*.

Stigter, C., 1966, "The performance of U-tanks as a passive anti-rolling device", Delft.

Verhagen, J.H. & van Wijngaarden, L., 1965, "Non-linear oscillations of fluid in a container", *Journal of Fluid Mechanics*, 22(part 4), pp.737–751.

Watts, P., 1883, "On a method of reducing the rolling of ships at sea". In *Royal Institution of Naval Architects*.

Specific Intended Uses: Establishing verification, validation and accreditation objectives

Arthur M. Reed, *David Taylor Model Basin, Carderock Division, Naval Surface Warfare Center*,
arthur.reed@navy.mil

ABSTRACT

IMO's implementation of the Second Generation Intact Stability Criteria has put in place a multitiered process by which the adequacy of a vessel's stability can be assessed. The most stringent criteria is Direct Assessment where by a vessel is assessed using a physics-based simulation tool. To be applied to stability assessment, these tools should undergo a formal Verification, Validation and Accreditation (VV&A) to assure that they perform adequately. Before the VV&A can be performed, the problem for which the simulation tool is to be assessed must be defined. This use—the *objectives* of the simulation are defined by the establishment of Specific Intended Uses (SIUs). SIUs will be characterized, and the way in which they are used will be defined.

Keywords: Verification, Validation and Accreditation; VV&A; Formal VV&A, Specific Intended Uses, SIU

1 INTRODUCTION

Beginning in the early 2000's efforts were initiated to develop performance based stability criteria for commercial vessels with the re-establishment of the intact-stability working group by IMO's Subcommittee on Stability and Load Lines and on Fishing Vessels Safety (SLF) (cf. Francescutto, 2004, 2007). Over time, the terminology to describe the new intact stability criteria evolved from "performance based" to "next generation" to "2nd generation"—the terminology in use today. This entire evolution is described in the introduction to Peters, *et al.* (2011).

The SLF Working Group decided that the second-generation intact stability criteria should be performance-based and address three modes of stability failure (SLF 48/21, paragraph 4.18):

- *Restoring arm variation* problems, such as parametric roll and pure loss of stability;
- *Stability under dead ship condition*, as defined by SOLAS regulation II-1/3-8; and
- *Maneuvering related problems in waves*, such

as surf-riding and broaching-to.

Ultimately, a fourth mode of stability failure was added:

- *Excessive accelerations.*

The criteria and processes were first introduced in Belenky, *et al.* (2008). The state-of-the-art in the assessment of vulnerability is presented in detail in Peters, *et al.* (2011) and further summarized in Reed & Zuzick (2015)

The deliberations of the Working Group led to the formulation of the framework for the second generation intact stability criteria, which is described in SLF 50/4/4 and was discussed at the 50th session of SLF in May 2007. The key elements of this framework were the distinction between parametric criteria (the 2008 IS Code) and performance-based criteria, and between probabilistic and deterministic criteria. Special attention was paid to probabilistic criteria; the existence of the *problem of rarity* was recognized for the first time and a definition was offered. Also, due to the rarity of stability

failures, the evaluation of the probability of failure with numerical tools was recognized as a significant challenge.

The “Second-generation intact-stability criteria” are based on a two-tiered assessment approach: for a given ship design, each stability-failure mode is evaluated using two levels of vulnerability assessment in the first tier. A vessel that fails to comply with the first- and second-level criteria of the first tier must progress to the second tier where it is examined by means of a direct assessment procedure based on tools and methodologies corresponding to the best state-of-the-art physics-based prediction methods in the field of ship-stability failure prediction.

If decisions regarding the adequacy of a vessel stability-wise, are going to be made based on the predictions of a Modeling and Simulation (M&S) tool, there must be a reasonable assurance that the tool provides acceptably accurate results. The process by which a tool may be determined to be sufficiently accurate is known as Verification, Validation and Accreditation (VV&A).

Reed & Zuzick (2015) quoted “Verification, Validation, and Accreditation are three interrelated but distinct processes that gather and evaluate evidence to determine, based on the M&S’s intended use, the M&S’s capabilities, limitations, and performance relative to the real-world objects it simulates.” Definitions for these three terms are provided below, each followed by a practical commentary relevant to computational tools for predicting dynamic stability.

1. Verification—the process of determining that a M&S’s implementation accurately represents the developer’s conceptual description and specification, i.e., does the code accurately implement the theory that is proposed to model the problem at hand?

2. Validation—the process of determining the degree to which an M&S is an accurate representation of the real world from the perspective of the intended uses of the M&S, i.e., does the theory and the code that implements the theory accurately model the relevant physical problem of interest?

3. Accreditation—the official determination

that an M&S, . . . is acceptable for use for a specific purpose, i.e., is the theory and the code that implements it adequate for modeling the physics relevant to a specific platform? In other words, are the theory and code relevant to the type of vessel and failure mode for which it is being accredited?

In the process leading to accreditation by a Flag Administration, VV&A must be a formal process with structure that is prescribed. This structure includes the identification of an Accreditation Authority (AA) and the establishment of accreditation panels; and is described in Reed & Zuzick (2015).

The process of accreditation requires Specific Intended Uses (SIUs)—the objectives against which accreditation occurs, the subject of this paper.

2 ROLE OF SIUS IN ACCREDITATION

As just described, accreditation is the process by which a computational tool is certified as being sufficiently accurate and thus acceptable for use in a particular case for a particular vessel or class of vessels. In the IMO context, this would be a vessel of a particular size and proportions, which will have a particular mode of operation. In practice this would also be tied to a particular mode of stability failure, and would be defined as a particular SIU.

SIUs are the statements that define the scope of the problem or simulation that is to be modeled, and for which the M&S will be accredited. In the context of direct assessment under second-generation intact stability, this will need to include a definition of the type of vessel for which the M&S tool is to be accredited—accreditation for small fishing vessels may well not apply to a container carrier; as well as the mode of stability failure that is anticipated to be an issue. There can, and in fact would likely be multiple SIUs for the same VV&A activity.

2.1 Example of an SIU

As stated earlier, the SIU effectively defines the objective of the accreditation. As such, the SIU needs to answer the questions “what” and “why.” The “what” part of the answer will in the case of accreditation have two parts, one part pertaining to the

type of vessel, and the other pertaining to the mode of stability failure. An example of this would be the accreditation of a code for predicting parametric roll of a container carrier—container carrier would be the type of vessel and parametric roll would be the mode of stability failure.

The “why” question relates to the way in which the predictions from the code will be used. Will the code be used to determine whether a vessel is susceptible to parametric roll in head seas at 24 kt in a particular sea state, or will it be used to derive a speed polar plots for susceptibility to parametric roll in a series of sea states. The answer to the “why” question serves to define the scope of the effort required in the accreditation process.

To clarify, an example of an SIU is: “The XYZ simulation tool will be used to generate operator guidance polar plots for all applicable speeds and headings against pure loss of stability for RO/PAX vessels in the 11,000–13,000 t displacement range, lengths of 130–150 m, and with beam-to-draft ratios of 4.5 to 5.5. These polar plots will enable the vessel operators to avoid situations where pure loss of stability could be an intact stability issue. The information used to generate the operator guidance polar plots will be developed using numerical data generated by the XYZ simulation tool.”

In the example SIU, the answers to the “what” question are RO/PAX vessels in a particular size range with the stability failure mode being pure loss of stability. The answer to the “why” question is to generate operator guidance polar plots for all applicable speeds and headings.

2.2 Requirements Flow-Down Table

The answers to the “what” and “why” questions within the SIU are used to determine what needs to be characterized and analyzed from the perspective of the V&V process. This is accomplished by the development of a Requirements Flow-Down Table. In the Requirements Flow-Down Table, each SIU is decomposed into several high level requirements (HLRs), which characterize important aspects of the SIU. The HLRs are each further mapped into several detailed-functional requirements (DFRs). A comparison metric and an acceptance criterion are identified for each DFR.

Additional clarification is provided by the definition of the comparison metrics and their associated acceptance criteria. HLRs reflect the technical specifications provided by SME-opinion. DFRs provide additional specifications as necessary to more fully describe each HLR. Requirements Flow-Down Tables are useful tools in high-level assessment of the appropriateness of the proposed accreditation criteria as well as required components of the Accreditation Plan (DoD, 2012).

An example of a Requirements Flow-Down Table, Table 1, is provided for the example SIU given above.

3 SUMMARY

With the advent of the second-generation intact stability criteria, IMO has initiated a two-tier performance-based stability assessment process for unconventional hulls with a risk of intact stability failure. If the design fails the first and second level tests of the first tier, it then progresses to the second tier and direct assessment, which requires an accredited physics-based simulation tool.

Accreditation requires that a set of Specific Intended Uses (SIUs) defining the objectives of the accreditation be defined. These SIUs must define what the M&S is to be accredited for (type of vessel and mode of stability failure) and why (the product to be produced by the M&S).

Additionally, the Requirements Flow-Down Table which is used to define comparison metrics and acceptance criteria based on the SIUs are described, and an example is provided.

REFERENCES

- Belenky, V., J. O. de Kat & N. Umeda (2008) Towards Performance-Based Criteria for Intact Stability. *Marine Tech.*, 45(2):101–123.
- DoD (2012) Department of Defense, USD (AT&L) MIL-STD-3022 w/Change 1: Department of Defense Standard Practice: Documentation of Verification, Validation, and Accreditation (VV&A) for Models and Simulations, 55 p.
- Francescutto, A. (2004) Intact Ship Stability—The Way Ahead. *Marine Tech.*, 41:31–37.

- Francescutto, A. (2007) Intact Stability of Ships—Recent Developments and Trends. *Proc. 10th Int'l Symp. Practical Design of Ships and Other Floating Struct* (PRADS '07). Houston, TX, Vol. 1, pp. 487–496.
- IMO SLF 48/21 (2005) Report to Maritime Safety Committee, London, UK, 65 p.
- IMO SLF 50/4/4 (2007) Framework for the Development of New Generation Criteria for Intact Stability, submitted by Japan, the Netherlands and the United States, London, UK, 6 p.
- Peters, W., V. Belenky, C. Bassler, K. Spyrou, N. Umeda, G. Bulian, B. Altmayer (2011) The Second Generation Intact Stability Criteria: An Overview of Development. *Trans. SNAME*, 119:225–264.
- Reed, A. M. & A. V. Zuzick (2015) Direct Assessment Will Require Accreditation—What This Means. *Proc. 12th Int'l Conf. Stability of Ships & Ocean Vehicles* (STAB '15), Glasgow, UK, pp. 51–78.

Table 1 Example Requirements Flow-Down Table.

High Level Requirements	Detailed Functional Requirement	Comparison Metric	Acceptance Criteria
<p>HLR 1.a Simulation must demonstrate good correlation to model data for ship responses to elemental tests to suggest that underlying physics are sound.</p>	<p>DFR 1.a.1 Simulation must demonstrate the ability to successfully predict critical motion values in a large number of Quantitative Accreditation conditions for which model test data is available for comparison. DFR 1.a.2 Collective SME judgment shall ultimately decide whether or not this requirement is met (regardless of the code's ability to meet the suggested quantifiable metrics).</p>	<p>CM 1.a.1 Check-list of quantifiable metrics defining "reasonable" correlation for elemental tests used to inform SME opinion CM 1.a.2 SME opinion/judgment</p>	<p>AC 1.a ARP will vote using SME opinion informed by elemental test comparisons whether to assess subsequent acceptance criteria.</p>
<p>HLR 1.b The simulation and model-scale data must show consistently good correlation ranging from the more simple conditions to the more complex conditions. Good correlation must be demonstrated for the range of operational, environmental, and loading conditions defined in the Quantitative Accreditation scope for which comparison model data are available.</p>	<p>DFR 1.b.1 Parameters which characterize the ship's operating condition relative to the seaway, and identify the corresponding critical motion, must be assessed. DFR 1.b.2 All comparisons must take into account all known sources of uncertainty (sampling, instrument, condition, etc.). DFR 1.b.3 Parameters that are used to define Quantitative Accreditation polar plots risk values and lifetime risk calculation must be assessed. If direct validation of these quantities is not achievable, a sufficient substitute quantity shall instead be assessed. (rare motion metrics) DFR 1.b.4 Parameters that are used to evaluate the Quantitative Accreditation system health must be assessed. (non-rare motion metrics)</p>	<p>CM 1.b.1 Mean values, μ, of achieved speed and heading CM 1.b.2 90% uncertainty intervals on the each parameter (model and simulation) CM 1.b.3 The 90th percentile of peak amplitudes, A90%, of motions (in lieu of exceedance rates of physical limit thresholds which are not expected to be available for validation) CM 1.b.4 Mean standard deviation, σ, of motions</p>	<p>AC 1.b.1 Differences between mean achieved speed and mean achieved heading for each validation condition must be less than specified amounts. AC 1.b.2 The 90% confidence intervals on each parameter value (σ and A90%) for a given motion and condition must overlap in order to suggest that the underlying populations (model and simulation) may be the same.</p>

Table 1 (Cont'd) Example Requirements Flow-Down Table.

High Level Requirements	Detailed Functional Requirement	Comparison Metric	Acceptance Criteria
<p>HLR 1.c Necessary accuracy of the simulation shall be influenced by an appropriate balance between technical excellence and judiciousness</p>	<p>DFR 1.c Thoughtful engineering judgment shall be applied in the determination of permissible differences between simulation and model test results.</p>	<p>CM 1.c Margin applied to observed sample parameter values (defined in CM 1.b.2 and CM 1.b.3)</p>	<p>AC 1.c The observed values of compared sampled parameters may be deemed acceptable if the difference between the values is less than a specified amount. (margin)</p>
<p>HLR 1.d The safety of the ship and sailor must be prioritized and reflected in the criteria established for validation.</p>	<p>DFR 1.d.1 Reasonable conservatism on the part of the simulation solution should be endorsed to promote the overall safety of the sailor.</p>	<p>CM 1.d.1 Margin applied to observed sample parameter values (defined in CM 1.b.2 and CM 1.b.3)</p>	<p>AC 1.d.1 The margin allowed by AC 1.c shall be increased by 50% in the case of over-prediction on the part of the simulation to allow for additional conservatism on the part of the simulation. (additional conservative margin)</p>
	<p>DFR 1.d.2 Determination of simulation tool success must only be reached using reasonably high-fidelity validation data sets.</p>	<p>CM 1.d.2 Combined uncertainty in the comparison, calculated as a function of the 90% uncertainty intervals (CM 1.b.2) on both data sets, model and simulation</p>	<p>AC 1.d.2 Successful validation comparisons for both rare and non-rare motions (σ and A90%) may only be accepted if the combined uncertainty in both data sets is sufficiently small.</p>
<p>HLR 1.e Simulation must be deemed usable for conditions within the current scope of the Quantitative Accreditation for which comparison model test data is not available.</p>	<p>DFR 1.e.1 Simulation must demonstrate the ability to successfully produce critical motion values in a large number of Quantitative Accreditation conditions for which model test data is available for comparison.</p>	<p>CM 1.e.1 Number of conditions which successfully pass the following criteria: AC 1.b.1 through AC 1.d.</p>	<p>AC 1.e 70% of Quantitative Accreditation conditions for which model data are available for comparison must pass criteria (AC 1.a through AC 1.d) for 100% of critical motion parameter values. (rare and non-rare motion assessments calculated independently)</p>

SESSION 3

Novel approaches to ship stability

Towards a theory of surf-riding in two-frequency and multi-frequency waves

K.J. Spyrou, k.spyrou@central.ntua.gr, I. Kontolefas, ikon@central.ntua.gr, N. Themelis, nthemelis@naval.ntua.gr
School of Naval Architecture and Marine Engineering, National Technical University of Athens, Greece

ABSTRACT

Steps are taken towards extending the theory of surf-riding for multi-chromatic waves. New bifurcation phenomena are identified and classified that are intrinsic to the presence of extra frequencies in the excitation. Alternative types of surf-riding are discovered. Chaotic transients seem to be quite a common feature of ship surge motion in extreme following seas.

Keywords: ship motions, surf-riding, Lagrangian coherent structures, basin erosion, chaos

1. INTRODUCTION

The theory explaining the nonlinear surging and surf-riding of ships in steep following waves has been built upon the assumption of monochromatic waves (Spyrou 1996). Many tacitly take for granted that these phenomena endure, in almost identical form, in irregular seas too. Nevertheless, the multi-chromatic sea renders the phase space flow of the underlying dynamical system time-dependent, a fact bearing many new possibilities of dynamic behaviour. For example, a ship can appear transferring randomly, in finite time intervals, between ordinary surging and surf-riding-like behaviour. Then, the concept of surf-riding equilibrium that had been the basis for explaining involuntary high speed runs in following waves is gone [Spyrou et al. 2014, Belenky et al. 2016; Themelis et al. 2016].

It is greatly desirable all yet undocumented motions types that can be realized in irregular seas to be systematically identified, evaluated and classified. However, conventional computational techniques that had been, up to now, successfully applied for studying the effect of monochromatic seas are not sufficient and a novel set of state-of-art computational tools will be required.

Driven by these observations, the first results from an ongoing exploration into the unsteady phase space of ship surging under bi-chromatic and multi-chromatic excitation will be presented; on the one hand demonstrating the approach; and on the other, identifying and analyzing new extreme types

of ship behaviour, in relation to the frequency content and intensity of wave excitation.

2. DESCRIPTION OF APPROACH

Unidirectional wave fields are considered, created by the superposition of two or more wave components, propagating in the direction of ship motion. A standard mathematical model that can reproduce asymmetric surging and surf-riding has been employed, incorporating multi-frequency excitation (Spyrou et al. 2014). The examined ship was a tumblehome topside vessel, from the ONR series, with length $L=154$ m, beam $B=18.8$ m and mean draft $T=5.5$ m.

Our analysis is focused on the identification of system's hyperbolic *Lagrangian coherent structures* (LCS) in phase space. The analysis is not constrained by the number of frequencies in the excitation, nor by the nature of it ("regular" or "irregular"). The LCS are phase space objects of a separatrix nature that can be considered as analogous to the stable and unstable manifolds of hyperbolic fixed points of autonomous dynamical systems. Hence, they indicate basins of attraction and, in general, they expose the skeleton of the flow. The LCS concept came about from the interbreeding of nonlinear dynamics and fluid mechanics (Haller & Yuan 2000; Shadden 2011). In a physical flow, LCS appear as cores of trajectory patterns, identified as being, locally, the strongest attracting/repelling material surfaces advected with the flow. A few approaches have been proposed for their identification, which vary

in their robustness, potential for handling multi-dimensional phase space, in terms of computational cost, etc. Here we have implemented a scheme based on the calculation of the largest finite-time Lyapounov exponent (FTLE) field (Shadden et al. 2005; Kontolefas et al. 2016). Alternative approaches (not reported here) are also under evaluation.

For the bi-chromatic sea in particular, supplementary calculations were performed; specifically, a massive campaign of time-domain simulations. The goal was to capture the mean and the amplitude of the surge velocity oscillation, at steady state, in order to evaluate how these relate with characteristic reference velocities, such as the nominal speed and the celerities of the participating wave components.

3. PRINCIPAL FEATURES OF THE UNSTEADY PHASE-SPACE FLOW

Bi-chromatic waves

The ship is excited by two harmonic waves, defined as follows: the first (identified from now on as the “primary”), has fixed length λ_1 equal to the ship length L and its steepness is set at $s_1 = 0.035$. The other (“secondary”), can be regarded as a perturbation effect; nonetheless, its height will be allowed sometimes to become large. It will have a comparable frequency value, while its steepness will be varied according to the scenario.

The arrangement of system’s LCS right upon the inception of global surf-riding is revealed through the two time shots of Fig. 1. Some differences from the monochromatic case are noticed: firstly, crossings of LCS (i.e. essentially of manifolds) appear, accompanied by the usual, in these cases, stretching and folding process. Secondly, as evidenced from Fig. 2, surf-riding is oscillatory (the power spectrum of the motion is also shown). In fact, this is a universal feature of surf-riding in bichromatic waves. It will be revealed later that the celerity of the primary wave dictates the mean value of ship velocity during surf-riding. The perturbing wave on the other hand, is responsible for velocity’s oscillation around the celerity of the primary wave.

The crossing of LCS brings along the fractalisation of basin boundaries and subsequently, basin erosion. In the series of graphs of Fig. 3, the

steepness of the secondary wave is raised from a very low value, in order to observe the successive transformations of phase space, as the effect of the secondary wave is intensified. The steepness of the primary wave is set lower than previously; in such a way that, in the absence of the secondary wave, coexistence of surging and surf-riding would exist (this fact is basically confirmed by the first graph of Fig. 3).

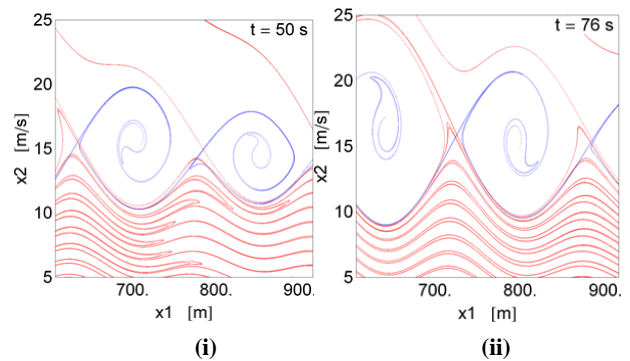


Figure 1: Phase-space portraits at different time instants, for bi-chromatic wave excitation. The attracting and repelling LCS (blue and red curves respectively) are shown. Parameters were set to the following values: $(\lambda_1, s_1, \omega_2/\omega_1, s_2/s_1, u_{nom}) = (L, 0.035, 0.9, 0.3, 12)$.

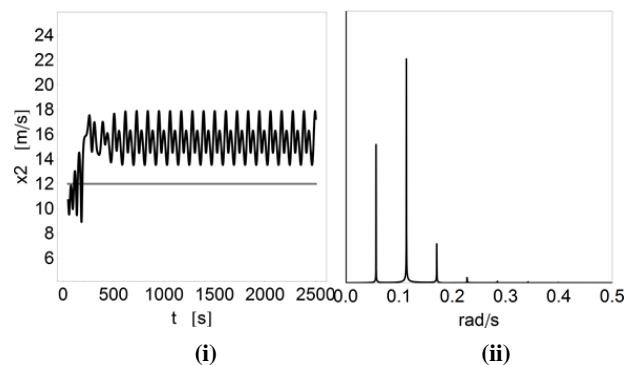


Figure 2: Character of surf-riding in bichromatic waves. (i) Time history of surge velocity (black curve) contrasted to the nominal speed (grey line). (ii) The discrete Fourier transform of the time history of surge velocity.

The fact that basin boundaries become fractal is verified by zooming successively onto a small area enclosing a basin boundary segment, revealing the well-known self-similarity pattern (see Fig. 4). The erosion of surf-riding’s basins bears an important consequence: surging becomes motion destination from areas deep into surf-riding’s domain, in a rather unpredictable manner. Two time-domain simulation examples, shown in Fig. 5, verify this behaviour. The particularly long, seemingly chaotic, transient of case 2 should be noticed.

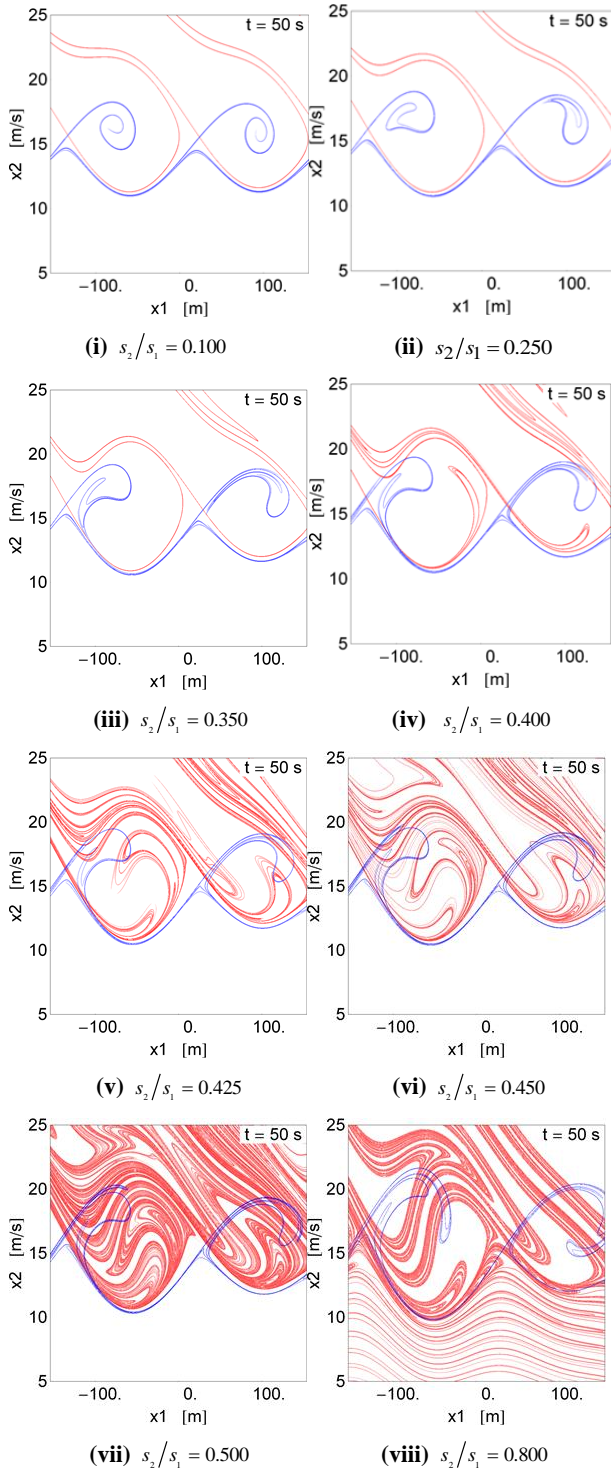


Figure 3: Transformation of the phase space as the steepness of the secondary wave is increased, due to tanglings of the attracting and the repelling LCS (blue and red curves respectively). The time shot is always at 50 s. Parameters have been assigned the following values: $(\lambda_1, s_1, \omega_2/\omega_1, u_{nom}) = (L, 0.02, 0.85, 12.5)$.

A strong hint about the arrangement of surf-riding and surging domains is offered from the graphs of Fig. 6, representing the field produced by the integration of phase-space-particles squared velocity along trajectories. The process of fractal destruction of the surf-riding domain is confirmed.

Although the ship was very close to global surf-riding when the secondary wave excitation was established, this extra forcing did not lead to global surf-riding but to the fractal erosion of the surf-riding domain.

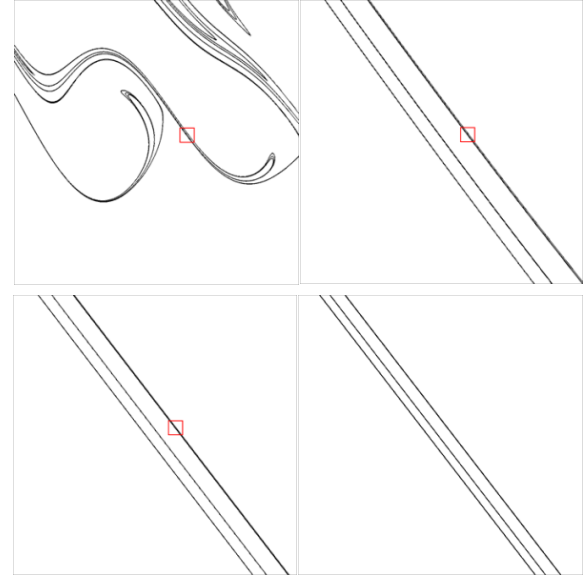


Figure 4: Self-similarity is revealed by successive enlargements of small rectangles placed on a surf-riding basin boundary [it corresponds to Fig. 3(iv)].

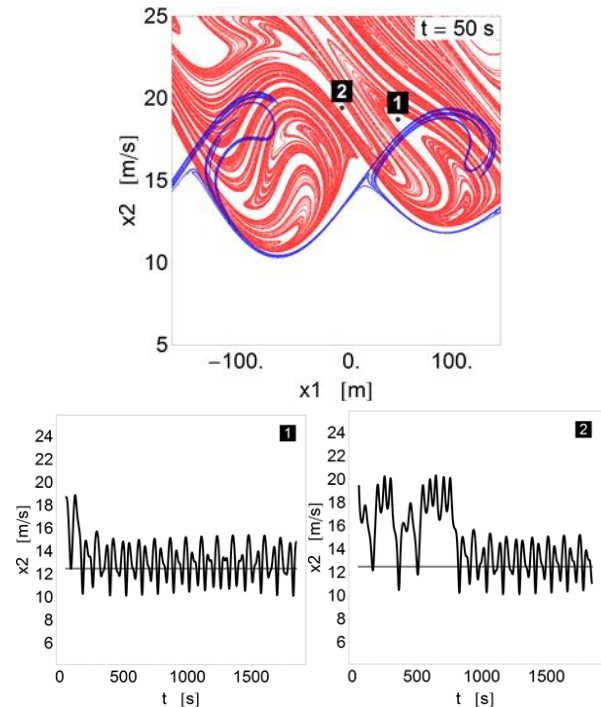


Figure 5: The erosion of surf-riding basins creates possibility of initiating surging from deep within the surf-riding area $(\lambda_1, s_1, \omega_2/\omega_1, s_2/s_1, u_{nom}) = (L, 0.02, 0.85, 0.500, 12.5)$.

Behaviour for “irregular” wave excitation

The time-changing LCS for wave excitation deriving from a JONSWAP spectrum, are shown in Fig. 7. We considered a frequency band with width $0.5\omega_p$, centred on spectrum’s peak $\omega_p=0.598$ rad/s.

The significant wave height was $H_S=5.5$ m. The spectrum was discretized through 48 components. Ship's nominal speed was 12 m/s. Substantial time variation of phase space flow can be noticed and, at first reading, the flow shows less coherence. In Fig. 7 is illustrated, in addition, the evolution of two groups of initial conditions (the green and the red) separated by a repelling LCS segment. Their initial placement is shown in the first of these graphs. The green points are found directed towards lower velocities (they should be identified as engaged in surging) compared to the red points that seem like being trapped at a higher velocity region. As a result, eventually, the green points lag behind the red points.

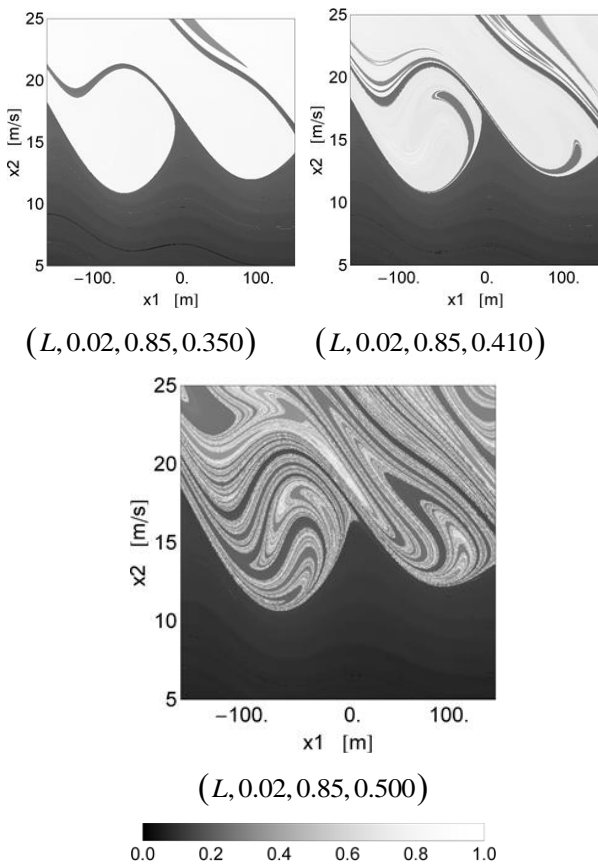


Figure 6: First row: Areas of surging (dark) and surf-riding (pale). Second row: Surging has dominated the entire phase space (pale regions indicate high-velocity transients not ending on surf-riding). The values of the parameters λ_1 , s_1 , ω_2 / ω_1 and s_2 / s_1 are indicated below the corresponding graph. Nominal speed is 12.5 m/s.

In the final investigation targeting the phase space, an irregular perturbation (calculated from a spectrum) was superimposed to a harmonic excitation, in such a way that, the wave energy content (based on the amplitudes of the participating discrete harmonics including the primary one) was maintained constant. The

excitation was computed by applying a filter that had one of its parameters working as a control knob, gradually raising the amplitudes of the perturbation harmonics while lowering primary's (see Fig. 8). The spectrum (of JONSWAP type) had $T_p=9.93$ s and $H_S=7$ m. The number of participating harmonics was $n=74$ and ship's speed was set at 12 m/s.

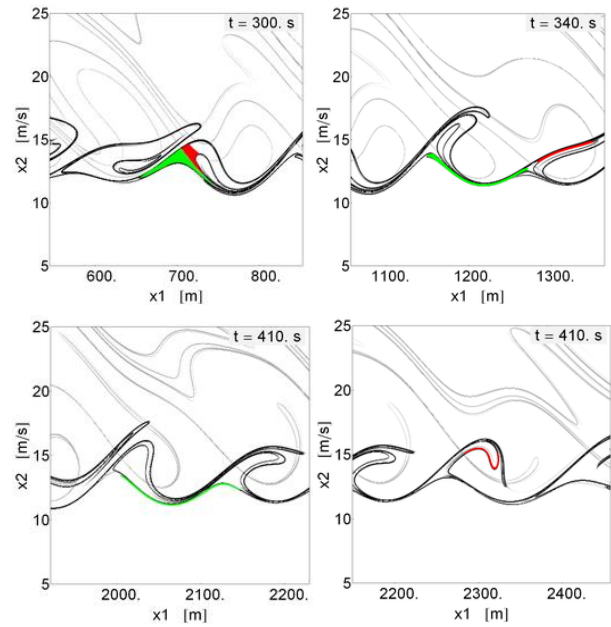


Figure 7: Portrait of phase space flow for JONSWAP spectrum. Two selected sets of initial conditions (appearing as green and red areas) evolve into different velocity ranges.

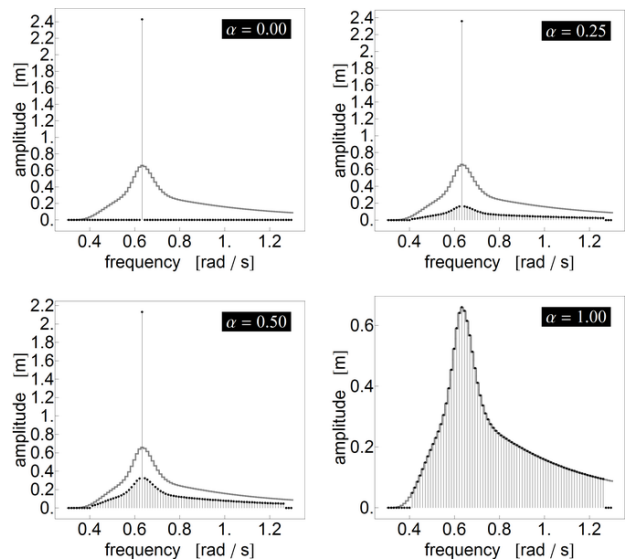


Figure 8: Wave amplitudes (black dots) obtained from a JONSWAP spectrum on the basis of energy equivalence, compared to the amplitude of the primary harmonic, as the control parameter α is gradually increased from 0 to 1. The intact spectrum (defining the energy level) is shown in grey.

In Fig. 9 are illustrated successive transformations of the phase space, which are provoked by the gradual turning of the excitation

from mainly regular to mainly irregular. We have started, again, from a condition very close to the beginning of global surf-riding. Whilst, this time, global surf-riding did truly happen, it was followed by an erosion process of the surf-riding basins, provoked by LCS tanglings corresponding to neighboring surf-riding basins.

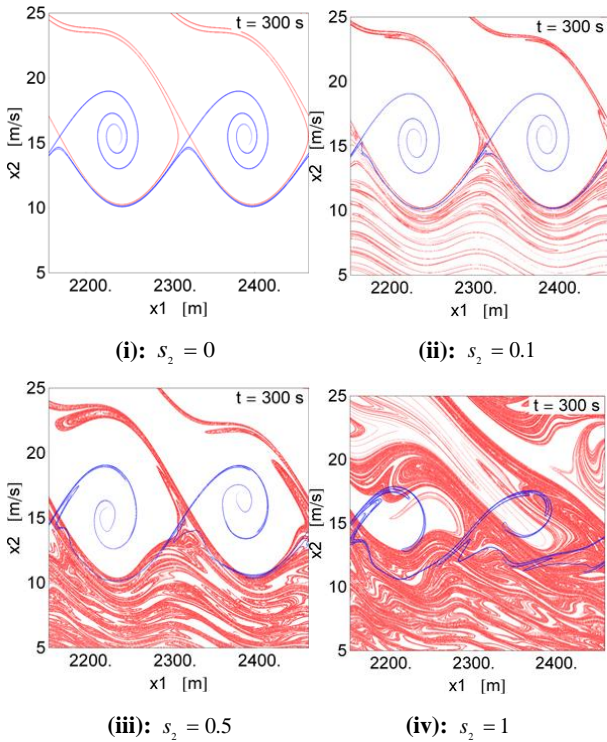


Figure 9: Transformations of phase space arrangement as one moves from a regular to an irregular excitation.

This is a new event where a surf-riding basin intrudes into another basin of the same kind. This makes uncertain the destination where the ship will settle, although surf-riding remains as the certain outcome.

It is evident therefore that, several new phenomena of behaviour become possible when one looks beyond the monochromatic sea; implying that, the probabilistic evaluation of a ship's tendency for surf-riding in irregular seas becomes an even more daring task.

4. CHARACTERIZATION OF HIGH SPEED RUNS

The final aspect considered was the characterization of the encountered types of surf-riding. Consider once more the idea of having a steep primary wave, perturbed by a secondary harmonic that is kept initially at a very low height. Naturally, one would expect to see a perturbed

version of surf-riding, ruled by the celerity of the first wave. When the two wave components start having comparable magnitudes however, the outcome becomes difficult to predict. Three examples, corresponding to frequency ratios 0.8, 0.9 and 1.05, are shown, respectively, in Figs 10, 11 and 12. For frequency ratio 0.8, and as the steepness ratio is raised, the mean surge velocity falls initially perfectly on the celerity of the primary wave. Later however there is a jump to the celerity of the secondary wave, returning shortly to intermediate values (in-between the two celerities). Further increase of the steepness leads to domination of the celerity of the secondary wave. A look into the fluctuating surge velocity reveals period doublings and chaos. Some surf-riding oscillations are extremely large, driving the ship, in repeating short spells, to very high speed values. Similar patterns are noticed for the other two frequency ratios. It should be also noticed that the reference system is moving with the wave celerity c_1 of the prime wave ($\lambda = L$), thus the horizontal axis of the figures of the the mean surge velocity corresponds to c_1 .

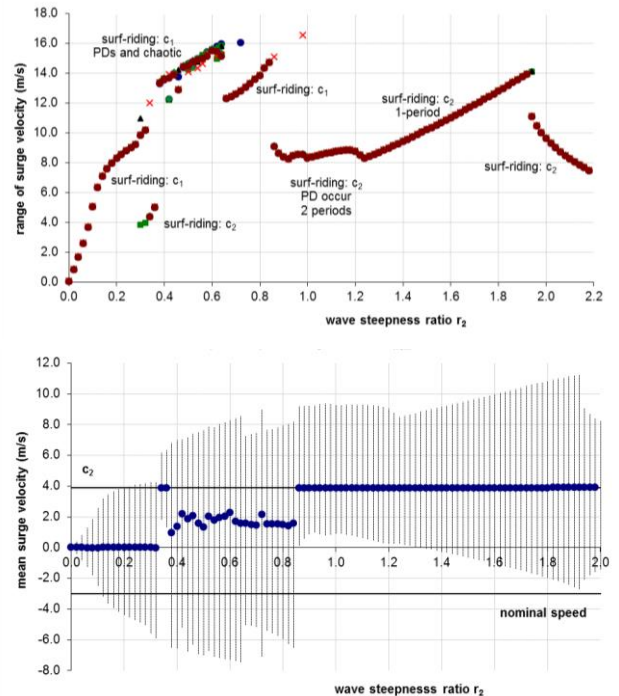


Figure 10: Range of surge velocity (upper) and mean value of surge velocity (down), for frequency ratio (of secondary to primary wave) 0.8, steepness of primary wave 1/30, nominal speed 12.5 m/s and initial surge velocity 10.5 m/s.

5. CONCLUSIONS

Several new phenomena of ship surge dynamics were observed when two or more frequencies were included in the excitation. In bi-chromatic waves, different types of oscillatory surf-riding exist, governed either by the first or by the second wave component. However, no coexistence of these two types was noticed as stable motions. Moreover, chaotic motions were identified in the intermediate range, sometimes extending to very high surge velocity values. They are preceded by homoclinic/heteroclinic tanglings of LCS found, creating fractalization of the surf-riding basin boundaries. Such phenomena were noticed in bichromatic as well as in multichromatic waves and seem to be quite common. In general, the exhibited dynamic behavior is very rich.

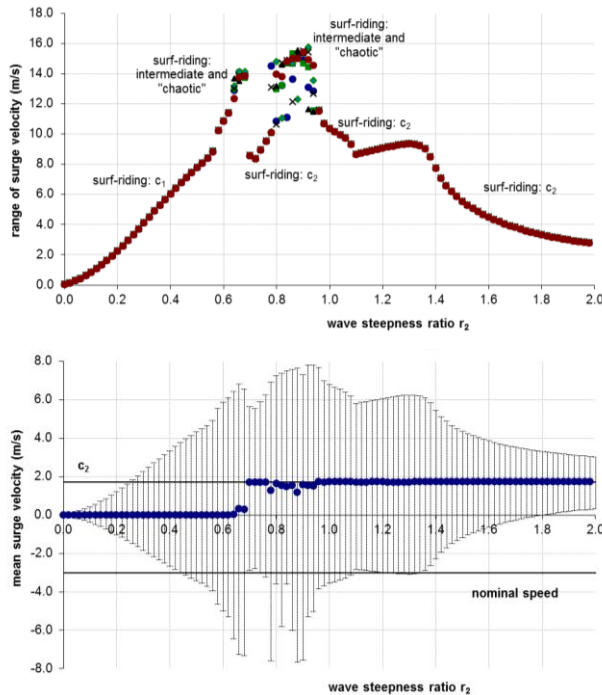


Figure 11: As Fig. 10, with frequency ratio 0.9.

6. ACKNOWLEDGEMENTS

The two following sources are acknowledged for sponsoring parts of the investigations reported in this paper:

The Greek General Secretariat of Research and Technology, in the framework of the General Program “ARISTEIA I”, with contract reference number GSRT-252.

The Office of Naval Research under Dr. Thomas Fu and the Office of Naval Research

Global under Dr. Woei-Min Lin (grant number N62909-13-1-7).

Moreover, useful discussions with Dr. Vadim Belenky and Mr. Kenneth Weems of the David Taylor Model Basin are acknowledged.

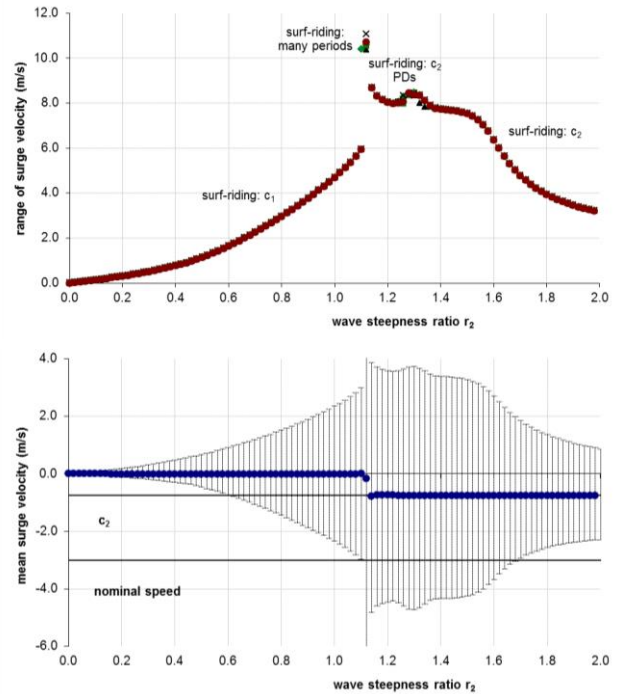


Figure 12: As Fig. 10, with frequency ratio 1.05.

7. REFERENCES

Belenky, V., Weems, K. & Spyrou, K. 2016, “On probability of surf-riding in irregular seas with a split-time formulation”, *Ocean Engineering*, DOI: 10.1016/j.oceaneng.2016.04.003.

Haller, G. and Yuan, G., 2000, “Lagrangian coherent structures and mixing in two-dimensional turbulence” *Physica D*, 147, pp.352-370.

Kontolefas, I. & Spyrou, K.J., 2016, “Coherent structures in phase space, governing the nonlinear surge motions of ships in steep waves”, *Ocean Engineering*, DOI:10.1016/j.oceaneng.2016.02.013.

Shadden, S.C., Lekien, F., Marsden, J.E., 2005, “Definition and properties of Lagrangian coherent structures from finite-time Lyapunov exponents in two-dimensional aperiodic flows”, *Physica D*, 212(3-4):271-304.

Shadden, S.C., 2011, “Lagrangian coherent structures”, *Transport and Mixing in Laminar Flows: From Microfluids to Oceanic Currents*, Roman Grigoriev (ed.), Wiley-VCH.

Spyrou, K. J., 1996, “Dynamic instability in quartering seas: The behaviour of a ship during

broaching”, Journal of Ship Research, SNAME, 40, No 1, 46-59.

Spyrou, K., Belenky, V., Themelis, N. & Weems, K., 2014, “Detection of surf-riding behavior of ships in irregular seas”, Nonlinear Dynamics, 78(1):649-647.

Themelis, N. Spyrou, K.J., & Belenky, V., 2016, ““High runs” of a ship in multi-chromatic seas”, Ocean Engineering, DOI: 10.1016/j.oceaneng.2016.04.024.

Split-time Algorithm Implementation in Advanced Hydrodynamic Codes

Kenneth Weems, *Naval Surface Warfare Center Carderock Division*

Vadim Belenky, *Naval Surface Warfare Center Carderock Division*

ABSTRACT

The paper describes the current state of numerical implementation of the split-time method for the estimation of probability of capsizing in irregular waves using an advanced numerical code – Large Amplitude Motion Program (LAMP). The split-time method resolves the probability of capsizing into two steps. The first step or “non-rare” problem is the statistical estimation of crossing rates over an intermediate threshold; the second step or “rare” problem is the calculation of the probability of capsizing after crossing. Motion perturbations are used to estimate the latter. The value of the perturbation of the roll rate at the instant of crossing which would lead to capsize is used as a metric of danger. Metric values from all crossings are extrapolated using the generalized Pareto distribution to determine a rate of capsize after crossing. The implementation is based on 3 degrees-of-freedom model (heave-roll-pitch), in which the body nonlinear formulation is used for hydrostatic and Froude-Krylov forces while all other hydrodynamic forces are modeled with empirical coefficients. The paper describes the initial testing of the algorithm, problems that were encountered and ongoing development including introduction of the hydrodynamic memory effects in the simulation of perturbed motions

Keywords: *Probability of capsizing, Numerical Simulations, split-time method, motion perturbation*

1. INTRODUCTION

The objective of the split-time method is to use the capability of advanced numerical codes for the estimation of the probability of rare event such as capsizing in waves. As capsizing in realistic conditions is too rare to be observed with a practical set of numerical simulation, the split-time method proposes the separation of the problem into “non-rare” and “rare” problems based on what is observable and non-observable in “normal” numerical simulations in random irregular seas.

The solution of the “non-rare” problem consists of computing a set of simulations in pseudo-random realizations of the irregular sea conditions and identifying crossings of an intermediate threshold roll angle. In this context, crossings consist of up-crossings of the positive threshold roll angle and down-crossings of the negative threshold roll angle. Crossings of this threshold should be observable in these “normal” numerical simulations in a statistically representative quantity. The choice of the threshold is arbitrary, but only independent crossing events can be used for the further calculations. As a result, the selection of the intermediate threshold is a mostly an issue of

calculation efficiency – too low of a threshold will result in a large number dependent crossings, many of which would need to be discarded, while too high of a threshold will result in too small a number of crossings.

The “rare” problem focuses on the estimation of the conditional probability of capsizing when crossing has occurred. A metric of the danger of capsizing is calculated at the instant of each crossing using a motion perturbation approach. A series of perturbation simulations are performed in the same waves as the non-rare simulation, starting from the crossing point but with the roll rate increased until capsizing is observed. The smallest roll rate perturbation which leads to immediate capsizing is the metric of capsizing danger as it measures how close the ship was to capsizing, even though capsizing or even an extreme roll angle may not have been observed.

Once the sufficient size of metric value sample (sufficient number of crossings) has been collected, the tail of its distribution can be modeled and used to estimate the conditional probability of capsizing at the instant of crossing, as illustrated in Figure 1.

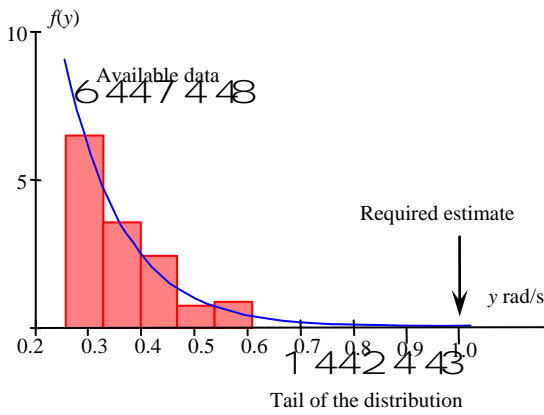


Figure 1 Calculation of the conditional probability of capsizing after crossing

In order to facilitate the modeling of the tail, the metric is calculated as:

$$y_i = 1 - \frac{\dot{\phi}_{Ui}}{\dot{\phi}_{Cri}}; \quad i = 1, \dots, N_U \quad (1)$$

where $\dot{\phi}_{Ui}$ is the value of rate roll observed at the i -th crossing, $\dot{\phi}_{Cri}$ is the value of perturbed roll rate at that crossing which lead to capsizing, and N_U is the number of crossing observed. The probability of capsizing after crossing is calculated by extrapolating this distribution to a value of 1.0.

A review of the background theory of the split-time method for the probability of capsizing in wave is available from Belenky, et al. (2016).

2. NUMERICAL CODE

The initial implementation of the split-time method is carried out using the Large Amplitude Motion Program (LAMP) as a platform. LAMP is a

mature all-purpose numerical code for ship motions and loads; its theoretical background is described by Lin and Yue (1990). Hydrostatic and Froude-Krylov forces are calculated with the full 3D body-nonlinear formulation. The diffraction and radiation forces are computed using a 3-D potential flow panel model using either a body-linear or body-nonlinear formulations. Other forces (roll damping, maneuvering forces, control systems, etc.) are included using a variety of time-domain models.

The LAMP system consists of a number of modules providing tools for the preparation and verification of input data and the post-processing of simulation results.

3. CALCULATION SCHEME

The overall sequence of calculations is illustrated in Figure 2. After setting up the LAMP model, a number of independent records, each corresponding to different realizations of the same irregular sea spectrum, are computed. A typical set of simulations contains 200 records of 30 minutes each. The 30 minute record length is long enough for the initial transition to be considered small portion of the record, but short enough to require a moderate number of wave components (usually 250-300) wave components to avoid self-repeating effect. Presenting the 100 hours sample in 200 independent records also facilitates parallel calculations, so a cluster or High Performance Computing (HPC) can be used in its full effect and mitigates potential non-ergodicity effects.

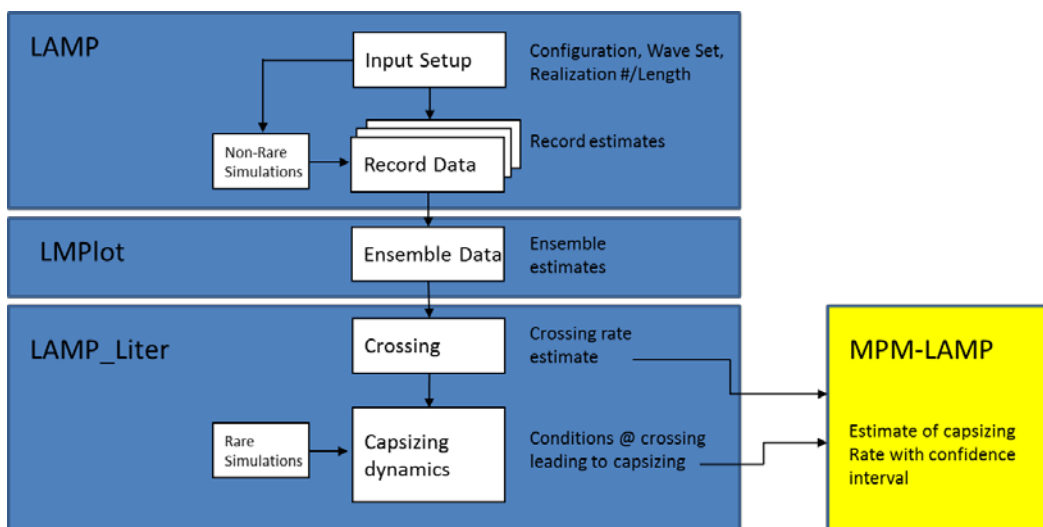


Figure 2 General scheme of split-time method implementation with LAMP

The set of the time history records computed for exactly the same set of conditions (wave spectrum, ship speed and relative wave heading) represent an ensemble. Statistical estimates of the ensemble are computed using LMPlot, which is the principal LAMP-system module for post-processing and plotting.

The LAMP_Liter module reads the non-rare simulation histories, identifies crossings of one or more specified threshold levels, calculates the estimated crossing rate and runs the perturbation simulations to find the value of the metric at each crossing. The MPM-LAMP module fits the GPD to the metric values, extrapolates to find the probability of capsizing after crossing and calculates the overall capsizing rate.

The initial implementation and testing of the split-time method in LAMP considers 3-DOF motions (heave-roll-pitch) and uses the 3-D body nonlinear formulation for hydrostatic and Froude Krylov forces, while diffraction and radiation are modeled using empirical coefficients rather than the full potential flow solution of the wave-body interaction problem. This configuration of the LAMP solver is known as LAMP-0. For these calculations, the same options are used for both the non-rare and rare simulations, though this is not required by either the theory or its implementation.

4. NON-RARE PROBLEM

The non-rare problem is solved by searching for crossings of one or more prescribed threshold roll angles. Once a crossing has been found, the value of the roll rate at the instant of crossing is determined by interpolation, see Figure 3.

The rate of crossing is estimated over the ensemble of records:

$$\hat{\mathbf{x}} = \frac{N_U}{N_T \mathbf{Dt}} \quad (2)$$

where N_U is the observed number of crossings, N_T is total number of data points in all records, and \mathbf{Dt} is the time increment (data sampling rate), which is assumed to be the same for all records. The boundaries of the confidence interval of the crossing rate are calculated with the assumption of binomial distribution (Belenky, et al. 2016).

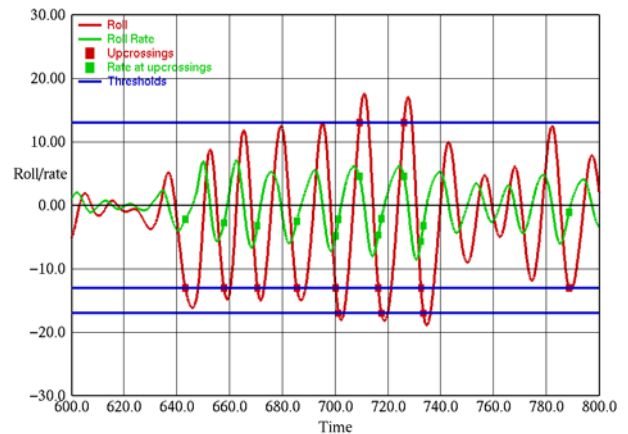


Figure 3 Non-rare problem: search for crossings and calculation of the roll rate values at the instants of crossing

5. RARE PROBLEM

The calculation of the critical roll rate is carried out using the motion perturbation method (MPM) as illustrated in Figure 4. The MPM is essentially a series of short simulations, starting from the instant of crossing, in the same waves as the non-rare simulation and with initial conditions other than roll rate set to ship's position and velocity at the crossing. The initial roll rate is systematically changed until capsizing is observed. Note that when the perturbed simulation does not capsize, the motion returns to its original time history. The critical roll rate is the smallest roll rate leading to capsizing.

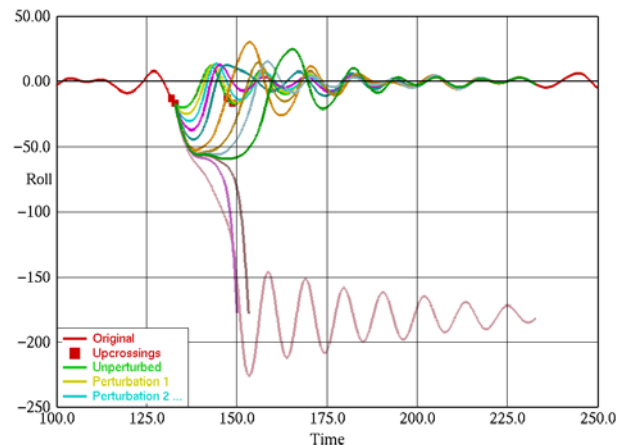


Figure 4 Calculation of critical roll rate with the motion perturbation method

As it can be seen from Figure 4, some of the time histories, while obviously bound to capsize, did not actually reach the motion about the capsized equilibrium. The reason is that LAMP calculations sometimes exhibit numerical instability when roll angle passes 90 degrees. This numerical instability is caused by the way in which the 3-DOF motion

constraints have been implemented in the LAMP's 6-DOF dynamic solver.

The split-time, however, does not require simulations to be carried so far – it is simply necessary to determine whether capsizing would occur. In fact, to reduce the computational effort, the perturbation simulations are usually truncated as soon as a roll angle of 90 degrees is reached or the motion converges to the unperturbed solution.

After the calculation of the capsizing likelihood metric (1), the results must be de-clustered, as the fitting of the GPD requires independent data points. As can be seen from Figure 3, crossings are observed in clusters and are likely to not be independent events. To produce independent data points, the metric data (1) is de-clustered. An estimate of the auto-correlation function for the roll response is calculated from the non-rare motion data and a de-correlation time is found by looking for the point where the envelope of the peaks of the auto-correlation falls below 0.05, see Figure 5.

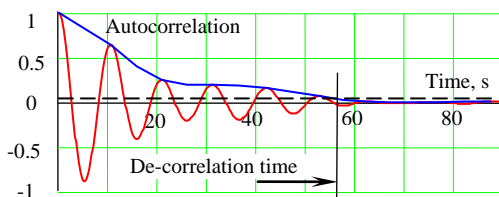


Figure 5 Calculating de-correlation time from the auto-correlation of the roll response

Crossing events which are separated by the de-correlation time are assumed to be independent while events closer than that are assumed to be part of a cluster. The largest metric value in each cluster is selected to provide only independent data for the GPD fit.

The procedure for fitting the GPD distribution to the LAMP-computed metric has been implemented following Campbell, et al. (2016).

6. INITIAL TESTING

Initial testing has been performed on a Windows workstation and on the NSWCCD SeaTech Linux cluster. On the SeaTech cluster, 5 cores on each of 10 nodes can be used to run 50 LAMP or LAMP-Lite simulations in parallel, resulting in a run time for the complete procedure of about 30 minutes per long-crested condition for a properly selected threshold.

Initial testing considered 10 conditions: two significant wave heights with five relative headings each. The fitted GPD distributions have shown smaller values of the shape parameter in comparison to the validation runs made with the volume-based numerical model (Weems, et al. 2016). A full investigation into the relationship between the GPD parameters and the characteristics of the hydrodynamic model and dynamical system remains for future work, though some first steps in this direction can be found in Belenky, et al. (2016a).

7. HYDRODYNAMIC MEMORY

A significant challenge of using motion perturbation methods with numerical seakeeping simulation tools is the consideration of the hydrodynamic memory effect. Hydrodynamic memory is an effect in which the flow field and forces of the wave-body hydrodynamic interaction problem are dependent on the short or medium-term history of the solution and cannot be completely quantified as functions of the state variables and their derivatives as in a model based on ordinary differential equations (ODE). In potential flow seakeeping models, this memory is associated with the unsteady disturbance wave field generated by the ship's unsteady motion (radiation waves), interaction with the incident wave (diffraction waves) and forward speed (Kelvin waves). In viscous flow solvers (e.g. RANS and LES), they will also be associated with the generation and evolution of vortical flow structures and the like.

Motion perturbation analysis requires simulations starting at crossing points of the non-rare simulations with variations to selected state variables, which will be the roll velocity for the present capsizing problem. It is relatively straightforward to save the complete state of the calculation, including the unsteady free surface disturbance, and then to restart the perturbation simulation from this point. However, large variations in the roll rate generally result in a significant transient behavior due to the impulsive change in velocity, which often lead to instability in the free surface potential flow solution.

The simplest solution to the problem is to use an ODE-like approximation for the disturbance wave forces in the perturbation simulations rather than attempting to solve the free surface potential

flow problem. In its most basic form, this consists of the prescribed added mass and damping coefficients of the LAMP-0 model used in the implementation and initial testing of the MPM described above and in the validation cases described in Weems, et al. (2016). As these provide an explicit calculation of the radiation and diffraction effects in terms of the state variables, they have no problem with the perturbation to the roll rate or other state variables and have the significant advantage that they result in a relatively fast calculation of the perturbation simulations. The approach is, however, approximate and the effect of the approximation will need to be quantified.

The incorporation of the regular time-domain free surface potential flow solution in the perturbation simulations comes down to introducing the perturbation of the motion while maintaining the stability and correctness of the flow solution. The most promising scheme identified to date is to begin the perturbation calculation some time, perhaps 10-20 seconds, before the crossing event, with prescribed motions during the period up to the event. The prescribed motions would be based on the motions from the non-rare simulation with the velocity perturbation feathered in over this time. An advantage of such an approach is that it could be implemented with regular check-pointing of the non-rare solution without having to identify and save crossing points during the non-rare simulations. A disadvantage of such an approach is that it will be computationally relatively expensive.

Another approach toward incorporating memory into the perturbation simulations would be to use an impulse response function (IRF) solution of the disturbance potential. The IRF-based formulation of the wave-body interaction problem uses body-linear solutions of the impulsive radiation and diffraction problems that are convoluted with the wave and motion time history to provide a very rapid approximate body-nonlinear solution. The method has long been used for constant course and speed seakeeping simulations (Weems, et al. 2000), and could be adapted to the perturbation simulations in which the ship can be assumed to have constant course and speed for the duration of the perturbation. The motion perturbation would still need to be added to the

motion history but stability and speed issues would be considerably mitigated.

It is quite likely that practical considerations will drive the implementation toward an ODE-like model of the disturbance, albeit one with non-constant coefficients derived from the motion history. However, a solution with the more complete hydrodynamic memory is necessary to quantify the effect of the memory and develop the required models.

8. SUMMARY AND CONCLUSIONS

The paper described the current state of implementation of the split-time estimation of method for probability of capsizing. The metric of likelihood of capsizing is the difference between observed and critical roll rate at the instant of crossing of an intermediate threshold. The critical roll rate (minimal perturbed roll rate leading to capsizing) is calculated with a motion perturbation method (MPM).

The split-time/MPM method has been implemented in the Large Amplitude Motion Program (LAMP). For the initial implementation and testing, the hydrodynamic forces are modeled with empirical coefficients, while hydrostatic and Froude-Krylov forces were computed with full 3D body-nonlinear formulation (LAMP-0). Motions were simulated with three degrees of freedom: heave, roll and pitch

Ongoing implementation and testing work includes the introduction of hydrodynamic memory in the perturbed motion calculations and free surge, sway and yaw motion in the non-rare and rare simulations.

9. ACKNOWLEDGEMENTS

The work described in this paper has been funded by the Office of Naval Research through the NSWCCD Independent Applied Research (IAR) program under Dr. Jack Price.

Discussions with B. Campbell of NSWCCD were very helpful. Calculations were carried out using NSWCCD's SeaTech cluster. The SeaTech team, particularly P. McCarthy, have been very helpful in setting up the code execution scheme.

10. REFERECES

Belenky, V., Weems, K., Lin, W.M. (2016) "Split-time Method for Estimation of Probability of Capsizing Caused by Pure Loss of Stability" in *Ocean Eng*, DOI: 10.1016/j.oceaneng.2016.04.011.

Belenky, V., Goltzer, D., Pipiras, V., Sapsis, T. (2016a) "On the Tail of Nonlinear Roll Motions" *Proc. 15th Intl Ship Stability Workshop*, Stockholm, Sweden

Campbell, B., Belenky, V., Pipiras, V. (2016) "Application of the Envelope Peaks over Threshold (EPOT) Method for Probabilistic Assessment of Dynamic Stability", in *Ocean Eng*. DOI:10.1016/j.oceaneng.2016.03.006.

Lin, W.M., and Yue, D.K.P. (1990) "Numerical Solutions for Large Amplitude Ship Motions in the Time-Domain," *Proc. 18th Symp. on Naval Hydrodynamics*, Ann Arbor, Michigan, USA, pp. 41–66.

Weems, K., Lin, W.M., Zhang, S, Treacle, T. (2000). "Time Domain Prediction for Motions and Loads of Ships and Marine Structures in Large Seas Using a Mixed-Singularity Formulation", *Proc. OC2000*, Osaka, Japan

Weems, K., Belenky, V., Campbell, B. (2016) "Validation of Split-time Method with Volume-Based Numerical Simulation", *Proc. 15th Intl Ship Stability Workshop*, Stockholm, Sweden.

Motion Perturbation Metric for Broaching-to

Vadim Belenky, *Naval Surface Warfare Center Carderock Division*

Kostas Spyrou, *National Technical University of Athens*

Kenneth Weems, *Naval Surface Warfare Center Carderock Division*

ABSTRACT

The paper describes the formulation and calculation of a Motion Perturbation Metric for estimating the probability of broaching-to within the framework of the split-time method. The probability estimation procedure within the split-time framework is divided into two steps or problems. The non-rare problem is focused on statistically observable events and is intended to be solved with a set of relatively high-fidelity numerical simulations in random irregular seas. It is usually related to the statistical estimation of an upcrossing of an intermediate level. The rare problem is formulated for the time instant of upcrossing and is focused on the conditional probability of broaching-to when the upcrossing of the intermediate level has occurred. It is solved by evaluating an instantaneous metric of the likelihood of broaching-to that is extrapolated to the level of broaching-to using a Generalized Pareto Distribution. The motion perturbation method calculates the metric by perturbing the dynamical system toward a dangerous state in phase space. The dangerous state is defined as a set of initial conditions leading to broaching-to, defined here as a deviation from the commanded heading exceeding a given value. The distance in phase space towards the closest dangerous state is the value of metric at the given instant of time.

Keywords: *Broaching-to, Surf-riding, Split-time method, Motion Perturbation Method, MPM*

1. INTRODUCTION

The estimation of a probability of broaching-to in irregular waves from a limited set of high-fidelity numerical simulations has been one of the objectives of the long-term ONR (the US Office of Naval Research) project “A Probabilistic Procedure for Evaluating the Dynamic Stability and Capsizing of Naval Vessels.” An overview of the general status and recent progress of the project can be found in Belenky, et al. (2016).

Broaching-to is a violent, uncontrollable turn which occurs despite maximum steering effort. It occurs in following and quartering seas and is, in general, infrequently encountered by a normally controlled ship. Broaching-to may occur in two different scenarios, the most frequent of which is the development of directional instability in yaw during surf-riding (Spyrou, 1996, 1997).

As broaching-to is a strongly nonlinear phenomenon, the split-time framework may be well-suited for its probabilistic characterization. The main idea of the split-time method is to

separate the very complex problem of the probabilistic evaluation of rare events in a complex nonlinear dynamical system into two less complex problems. An intermediate threshold for one of the state variables is introduced. The value for the threshold is chosen such that the upcrossings can be observed at a statistically significant rate with high-fidelity time-domain numerical simulation. The rate of upcrossing can then be estimated from the time series – this is the “non-rare” problem. The second part of the split-time method is the “rare” problem, which is focused on calculating a “metric” value which quantifies the risk of the rare event at the instant of each upcrossing. The “metric” must include information on physics that goes beyond what was observed within the simulation. For example, surf-riding can co-exist with periodic surging, and even if only periodic surging was observed in the “non-rare” simulations, the metric should reveal that surf-riding was possible at this time instant for different initial conditions.

The numerical value of the metric is meant to express the “distance to failure” at the instant of upcrossing. Each upcrossing yields a single

number, but as the upcrossings were observed in statistically significant quantities, the metric values may be fitted with a Generalized Pareto Distribution (GPD) to produce an extrapolated estimate for the probability of failure.

2. INITIAL DEFINITION OF METRIC

Belenky, et al. (2016) considered a metric for the likelihood of surf-riding that was defined as a distance between the current state and the state where ship would be captured into surf-riding, measured along the line between the current state and the stable surf-riding equilibrium (pseudo-equilibrium in case of excitation with more than one frequency). The practical implementation of this metric encountered difficulties due to the complexity of the phase space of surf-riding in the multi-frequency environment (Spyrou, et al. 2016).

At the same time, the deviation of heading due to broaching-to can be easily detected and measured from a relatively short numerical simulation, see Figure 1. The simulation uses a simplified 3-DOF (surge-sway-yaw) mathematical model that is described in Spyrou, et al. (2015).

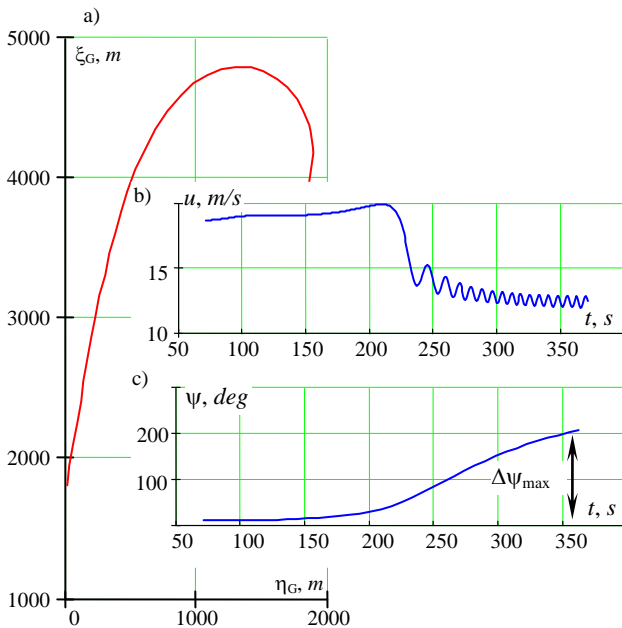


Figure 1 Broaching-to after surf-riding in regular waves: a) trajectory; b) time history of horizontal speed; c) time history of heading

Small deviations in heading, however, will be frequently encountered in oblique waves and do not represent any real danger as they can be easily corrected without adverse consequences. A minimum heading deviation corresponding to

broaching-to is therefore defined, somewhat arbitrarily, to be 10 degrees. The initial formulation of the metric is then defined as a distance, in phase space, between the initial state and a critical state leading to a deviation of 10 degrees from the commanded heading, measured along the line between the initial state and a “dangerous” point. The dangerous point leads to broaching-to with a heading deviation which significantly exceeds 10 degrees. The definition of the dangerous point includes, but is not limited to, the stable surf-riding equilibrium/pseudo-equilibrium (Spyrou, et al. 2016; Belenky, et al. 2016a).

3. MOTION PERTURBATION METHOD

The idea of the motion perturbation method (MPM) is to look into alternative variants of the behavior of the dynamical system if the current state is perturbed. It is similar to the motion stability concept: the current state is given a perturbation and the perturbed solution is followed into the future. The difference is that the perturbation is meant to be large.

The perturbations are carried out in multi-dimensional phase space, starting from the vector of initial condition X_0 toward the “dangerous” vector (or point) X_d :

$$\bar{X}_S(\varepsilon) = \bar{X}_0 - \varepsilon \cdot (\bar{X}_d - \bar{X}_0); \quad \varepsilon \in [0; 1] \quad (1)$$

A set of sample heading time histories from these perturbations is shown in Figure 2.

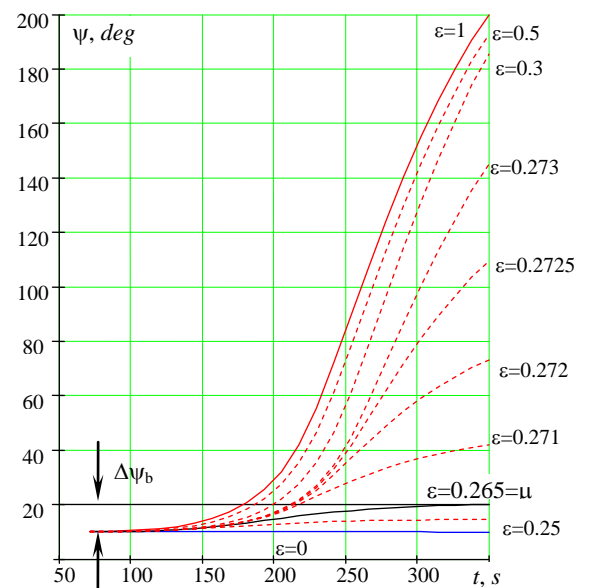


Figure 2 Heading time histories corresponding to perturbations in phase space, for the case of regular wave with a coexistence of periodic surging and surf-riding

The wave in this case is a regular wave for which both periodic surging and surf-riding can result for the same propeller rate. The heading time history which results in a maximum heading deviation of exactly 10 degrees yields the value of metric for the considered case.

4. FURTHER REFINEMENTS OF METRIC FORMULATION

The testing of the initial metric formulation is described in Belenky, et al. (2016). It includes surging/surf-riding coexistence mode in regular waves, bi-chromatic, tri-chromatic and full-band irregular waves. One conclusion was that the stable surf-riding pseudo-equilibrium is not necessarily the most dangerous point. The actual domain of broaching-to in full-band irregular waves may be shifted in comparison to the coexistence case in regular waves, see Figure 3.

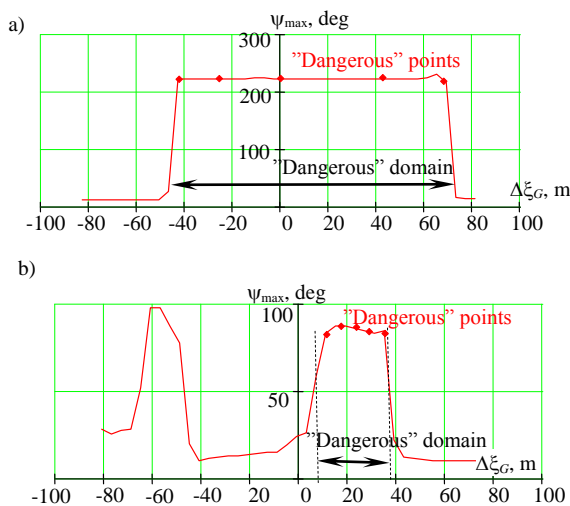


Figure 3 Maximum yaw angle as a function of the initial position of the wave relative to the position of the stable surf-riding equilibrium / pseudo-equilibrium (a) regular waves: surging / surf-riding coexistence mode (b) full-band irregular waves

As a result, an additional step has been added to the metric calculation procedure – a search for dangerous points. This information allows a refinement of the metric calculation. The value of metric actually determines a single point on the boundary of “dangerous broaching” domain in phase space. Several “dangerous” points yield several points on the boundary. The metric can therefore be reformulated as a distance to the boundary in a more strict geometric sense.

The metric also needs to be reformulated to be comparable between different upcrossings, because the critical value ε is defined in terms of relative distance.

Figure 4 shows a projection of the phase space for the coexistence case into the surging phase plane: the distance is measured in ship lengths and the surging speed is expressed in terms of Froude number. The “dangerous” domain is presented with five points. Each of them is used to get a direction for perturbations. Five values of ε corresponding to a heading deviation of 10 degrees have then been obtained.

Figure 4 shows the projection of these boundary points onto the surging phase plane. Three of these points (shown as solid circles) were used to fit the arc of a circle and find its center. It is no surprise that the line between the initial position and the center of the fitted circle comes from the stable surf-riding equilibrium.

The distance between the initial point and the fitted circle on the surge phase plane is measured on the line towards the center of the circle.

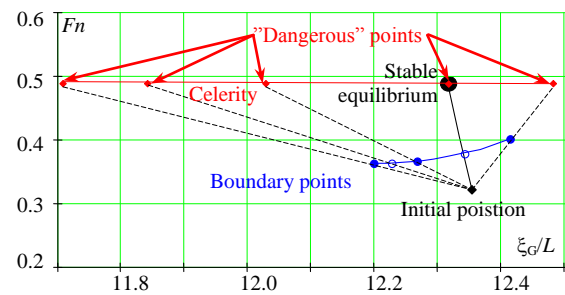


Figure 4 Projection of the phase space on the plane distance vs. surging speed: regular wave, surging / surf-riding coexistence mode

Figure 5 shows this projection for the case of full band irregular waves. This case is more complex. The line between the initial point and the center of the fitted circle does not cross the arc; as the dangerous domain is too narrow. The direction is defined then by the shortest distance shown with red line.

The updated calculation scheme of the metric assumes that the boundary of the “dangerous” domain is smooth. However, Spyrou, et al. (2016) shows that the boundary of the surf-riding domain in the bi-chromatic case can be fractal. These fractal boundaries present difficulties in getting a numerical solution efficiently, as most iteration

methods may fail. The fractal boundary has to be approached from one side only and may require development of special computational techniques. However, the considered case seems to have a smooth boundary, as it can be seen from Figure 6.

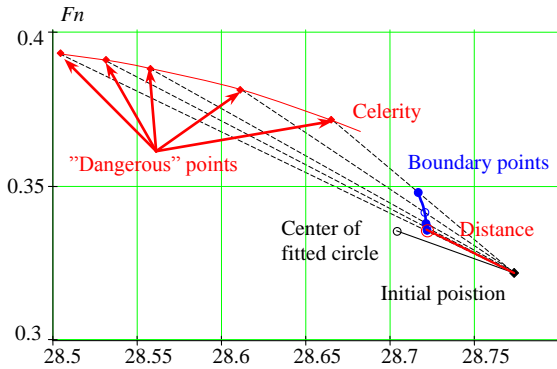


Figure 5 Projection of the phase space on the plane distance vs. surging speed: regular wave, full-band irregular waves

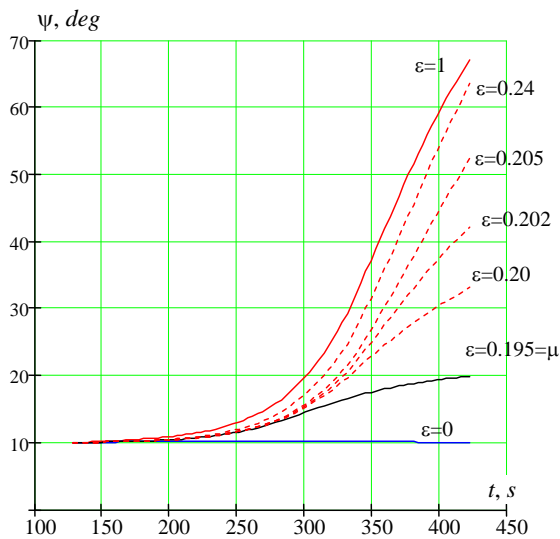


Figure 6 Heading time histories corresponding to perturbations in phase space: full-band irregular case

5. SUMMARY AND CONCLUSIONS

The paper describes the refinement of a MPM metric of likelihood of broaching-to, which is intended to be using within the split-time framework for evaluating a probability of broaching-to in irregular waves.

As the “dangerous” domain for broaching-to in irregular waves does not necessarily contain the stable surf-riding pseudo-equilibrium, a search for

dangerous points needs to be carried out. These dangerous points are used to set the direction of MPM perturbations to find points on a broaching domain boundary. These boundary points are projected on the surging phase plane and fitted with a circle; the distance to the curve is the value of the MPM metric.

6. ASKNOWLEGEMENTS

The work described in this paper has been funded by the Office of Naval Research (ONR) under Dr. Thomas Fu and by ONR Global under Dr. Woei-Min Lin.

7. REFERENCES

Belenky, V., Weems, K., and Spyrou, K. 2016, “Towards a Split-Time Method for Estimation of Probability of Surf-Riding in Irregular Seas,” *Ocean Engineering*, DOI: 10.1016/j.oceaneng.2016.04.003.

Belenky, V., Spyrou, K., and Weems, K., 2016a, “On Probabilistic Properties of Surf-riding and Broaching-to in Irregular Waves,” *Proc. of 31-st Symp. on Naval Hydrodynamics, Monterey, CA., USA* (submitted)

Spyrou, K.J., 1996, “Dynamic Instability in Quartering Seas: The Behavior of a Ship During Broaching,” *Journal of Ship Research*, Society of Naval Architects and Marine Engineers, Vol. 40, No. 1, 1996, pp. 46-59.

Spyrou, K., 1997. “Dynamic instabilities in quartering seas – part III: nonlinear effects on periodic motions”, *Journal of Ship Research*, Vol. 41, No 3, pp. 210-223.

Spyrou, K.J., Themelis, N., and Kontolefas, I., 2015, “Development of Probabilistic Models for Evaluating the Dynamic Stability and Capsizing Tendency of Naval Vessels with Respect to Broaching-to (second year), Technical Report,” ONR Grant N62909-13-1-7.

Spyrou, K., Kontolefas, I. Themelis, N., 2016 “Towards a Theory of Surf-riding in Two-frequency and Multi-frequency waves,” *Proc. of 15th Intl Ship Stability Workshop, Stockholm, Sweden* (submitted).

SESSION 4

Computational and stochastic methods

New models of irregular waves—way forward

Arthur M. Reed, *David Taylor Model Basin, Carderock Division, Naval Surface Warfare Center,*
arthur.reed@navy.mil

Alexander B. Degtyarev, *St. Petersburg State University,* deg@csa.ru

Ivan Gankevich, *St. Petersburg State University,* i.gankevich@spbu.ru

Kennith Weems, *David Taylor Model Basin, Carderock Division, Naval Surface Warfare Center,*
kennith.weems@navy.mil

ABSTRACT

In a series of papers, Degtyarev and Reed have presented the theory and provided the results from an autoregressive model for representing a seaway—at a point in space, over a line and over a plane, all as a function of time (1-D, 2-D & 3-D, respectively). In several other papers, Degtyarev and Gankevich have provided the theory for a technique for efficiently computing the velocity potential beneath a prescribed 1-D or 2-D surface, varying with time. Together this series of papers provides the information needed to compute the fully nonlinear hydrostatic and Froude-Krylov pressures under a seaway in an efficient manner without having to be concerned with the computing-time constraints imposed by the use of a Fourier series representation of a seaway imposed by the use of a Longuet-Higgins model. The next step is to apply these models in a seakeeping code so that the practical aspects of using these appealing theoretical approaches can be assessed. This paper provides a very brief description of the methods, and outlines some of the issues that must be dealt with in interpreting them.

KEYWORDS

Autoregressive modelling; Wave modelling; Sea state modelling

1 INTRODUCTION

The, Longuet-Higgins' Fourier series based model of a seaway (Longuet-Higgins, 1962) is distinguished by its clarity and the simplicity of the computational algorithm. However, it is not without some serious shortcomings inherent in models of this class:

- The Longuet-Higgins' model is only designed to represent a stationary Gaussian field. Normal distribution of the simulated process is a consequence of the central limit theorem. Its application to the analysis of

more general problems such as the evolution of ocean waves in a storm, or the study of ocean waves distorted in shallow water represents a significant challenge.

- Models of this class are periodic and need a very large number of frequencies in order to generate statistically independent non-repeating waves for long simulations (Benlenky, 2005) and the computation time increase linearly with the number of frequencies.
- In the numerical implementation of the Longuet-Higgins' model, it appears that

the rate of statistical convergence is very slow. This is seen as a distortion of the energy spectrum of the simulated process.

- The Longuet-Higgins model is not obviously appropriate when simulating complex waves that have a broad spectrum with many peaks, and in describing extreme events.

These latter three points become particularly critical in numerical simulation. In a time domain computation of the responses of a vessel in a random seaway, the repeated evaluation of the velocity at hundreds or thousands of points on the hull for thousands or tens of thousands of time steps can become a major factor determining the execution speed of the code (Beck & Reed, 2001). This becomes an even more significant issue in a nonlinear computation where the wave model is even more complex. Developing a less time intensive method for modeling the ambient ocean-wave environment has the potential for significantly speeding up the total simulation process.

2 AN AUTOREGRESSIVE MODEL OF OCEAN WAVES

The autoregressive model (ARM) of ocean waves is an alternative to the Longuet-Higgins' approach that models a stochastic moving surface as a linear transformation of white noise with memory. ARMs are commonly used in other areas of probabilistic mechanics and dynamics to model stationary ergodic Gaussian random processes with given correlation characteristics (Box, *et al.*, 2008), but they have not been extensively applied to wind waves.

2.1 One dimensional Wind-Wave Model

The formal mathematical framework of regressive wave models was developed by Spanos (1983), Gurgunidze & Trapeznikov (1988) and Rozhkov & Trapeznikov (1990). The latter built a one-dimensional model of ocean waves $\zeta(t)$, on the basis of an autoregressive-moving average (ARMA) model

In practice, it has been more common to use an autoregressive model:

$$\zeta_t = \sum_{i=1}^N \Phi_i \zeta_{t-i} + \epsilon_t, \quad (1)$$

where ζ_t is the wave elevation at time t , N is the order of the model, Φ_i are the regression coefficients, ζ_{t-i} are the N last realizations of ζ_t , [$i = 1, \dots, N$], ϵ_t is Gaussian white noise with variance σ_ϵ^2 . The equation for ζ_t can be directly related to the power spectrum of the seaway by:

$$S_\zeta(\omega) = \frac{\sigma_\epsilon^2}{2\pi} \frac{\Delta}{\left|1 + \sum_{j=1}^N \Phi_j \exp[-ij\Delta\omega]\right|^2}, \quad (2)$$

where Δ is the sampling interval of the series.

The autoregressive coefficients of (1) can be estimated from the autocovariance function (K_ζ) by solving the Yule-Walker equations:

$$K_\zeta(i) = \sum_{k=0}^N \Phi_k K_\zeta(k-i), \quad (3)$$

and the variance of the white noise σ_ϵ^2 can be calculated as:

$$\sigma_\epsilon^2 = V_\zeta - \sum_{j=0}^N \Phi_j K_\zeta(j). \quad (4)$$

where V_ζ is the variance of the waves being simulated. The derivation of these formulae can be found in Degtyarev & Reed (2011).

In theory, the number of autoregressive coefficients N tends to infinity. In practice, it has been found that remarkably few coefficients are required to recreate the wave surface and to recover the stochastic properties of the wave. As the periodicity of the wave evaluation is dependent only on the random number generator, very long wave records can be modeled without self-repeat and at very small cost.

2.2 3-D Wave Model

For application to numerical simulation in three dimensions (2-D space + 1-D temporal)

having components (x, y, t) , the expression for the wave elevation is:

$$\begin{aligned} \zeta(x, y, t) = & \sum_{ix=0}^{Nx} \sum_{iy=0}^{Ny} \sum_{it=0}^{Nt} \Phi_{(ix, iy, it)} \\ & \times \zeta(x - ix \cdot \Delta x, y - iy \cdot \Delta y, t - it \cdot \Delta t) \\ & + \sigma_\epsilon^2 \epsilon_{(ix, iy, it)} \end{aligned} \quad (5)$$

Degtyarev & Boukhanovsky (2000) present numerical procedures for estimating the parameters of the 3-D ARM for waves and the dispersion of the corresponding field of white noise, as well as the transition to a wave field with an arbitrary distribution. The procedures generally follow the one-dimensional implementation and are based on the solution of the generalized Yule-Walker equations (*cf.*, Degtyarev & Reed, 2011), though with additional computational features.

3 IMPLEMENTATION OF THE AUTOREGRESSIVE WAVE MODEL IN A SIMULATION CODE

A principal objective of the current effort is to apply the autoregressive incident wave model to time domain ship motion simulations. The issues and procedures are relevant to any hydrodynamic code; and, to a large degree, the use of autoregressive wave models in general.

In the seakeeping calculations, the following incident wave quantities must be computed:

- Incident elevation at points on the hull surface in order to determine the incident wave waterline and create a panel model of the wetted hull surface
- Incident wave pressure ($\rho \partial \Phi_0 / \partial t$) on each wetted hull panel to calculate Froude-Krylov forces
- Incident wave velocity ($\nabla \Phi_0$) at the control point of each body panel for potential flow body boundary condition
- Incident wave velocity ($\nabla \Phi_0$) for the inflow to external forces models such as appendage lift and drag.

In calculations using the standard Longuet-Higgins' model, the incident wave is defined by

a discrete set of component waves, each with a specified frequency, amplitude, heading, and phase; and these incident wave quantities are generally computed directly using Fourier series expressions.

With the autoregressive wave model, the incident wave is defined by a regression order (N_x, N_y, N_z) and increment $(\Delta x, \Delta y, \Delta z)$, a set of regression coefficients $(\Phi_{(ix, iy, it)})$, corresponding variance of white noise (σ_ϵ^2) and a set of seeds for the pseudo-random number generator. At each time step of the simulation, the incident wave model is set up by the following steps:

1. Compute the elevation field on a grid of points around the ship
2. Estimate derivatives of the elevation in time and space
3. Solve for the velocity potential field beneath this elevation grid
4. Estimate derivatives of the velocity potential in time (Froude-Krylov pressure) and space (incident wave velocity)
5. Set up interpolation functions for the elevation and potential derivatives on the local grids.

The required evaluations of the incident wave elevation, pressure, and velocity are then handled by the interpolation functions. These steps are described in more detail below.

4 INCIDENT WAVE ELEVATION FIELD

The form of the expression for the autoregressive wave elevation (5) naturally leads to the evaluation of the local wave elevation field on a grid of points with spatial increments corresponding to the Δx and Δy of the regression model:

$$\begin{aligned} x_{i_x} &= x_0 + (i_x - 1)\Delta x; & i_x &= 1, \dots, M_x \\ y_{i_y} &= y_0 + (i_y - 1)\Delta y; & i_y &= 1, \dots, M_y \\ t_{i_t} &= t_0 + (i_t - 1)\Delta t; & i_t &= 1, \dots, M_t \end{aligned}$$

$$\begin{aligned}\zeta_{(i_x, i_y, i_t)} &= \zeta(x_{i_x}, y_{i_y}, t_{i_t}) \\ &= \sum_{j_x=0}^{N_x} \sum_{j_y=0}^{N_y} \sum_{j_t=0}^{N_t} \Phi_{(j_x, j_y, j_t)} \\ &\quad \times \zeta_{(i_x-j_x, i_y-j_y, i_t-j_t)} + \sigma_\epsilon^2 \epsilon_{(i_x, i_y, i_t)}\end{aligned}\quad (6)$$

where M_x and M_y define the size of the wave elevation evaluation grid, which is dictated by the size of the domain over which elevations are required and will generally be larger, sometimes far larger, than the length of regression.

The elevation calculation is advanced in time along with the simulation itself. In the application of the autoregressive wave model, the time step of the simulation is matched to the time step of the wave autoregression function. In principle, however, different time steps could be accommodated by either interpolating the wave elevation data in time or performing multiple wave time steps for each simulation time step.

Since the elevation at each point is dependent only on the elevations at lesser or equal x , y , or t , the method is explicit and easily calculated by sweeping through the elevation grid in x and y at each time step. Calculating the elevation on a finite grid presents no major problem—the summation is simply truncated at the edge of the grid.

The required extent of the wave elevation grid will generally be the region over which incident wave data is required plus some allowance at the minimum x and y edges for a “ramp-up” region. For a 3-D potential flow calculation, this is simply the extent of the hull’s wetted surface. The issue is a bit more complicated for simulations with forward speed or a significant amount of drift. The 3-D autoregressive wave model is generally cast in a global coordinate system, so the x - and y -grid lines of the evaluation must be inherently fixed in space. Constructing a grid covering the entire range of the simulation would be impractical for a simulation of any length, so a local grid scheme is implemented.

In the local grid scheme, the grid is moved

with the ship but grid lines are maintained at integer multiples of the increment grid. In effect, grid lines are added in front of the ship and removed from behind it as the simulation progresses. The addition of grid lines forward of the ship must account for the “ramp-up” time of these added lines. Therefore, the resulting grid must be elongated in the direction of travel. For a typical seakeeping problem with a more-or-less constant speed and heading, the x extent of the grid will be:

$$x_0 = \left(\left\lfloor \frac{(x_g(t) - L/2)}{\Delta x} \right\rfloor - N_x \right) \Delta x \quad (7)$$

$$M_x = N_x + \left(\frac{L + 2UN_t\Delta t}{\Delta x} \right) \quad (8)$$

where $x_g(t)$ is the global x -coordinate of the ship’s center (mid-ships) at a given time, L is the ship length, N_x and Δx are the regression order and increment in x , N_t and Δt are the regression order and increment in time, and U is the ship speed; $\lfloor \cdot \rfloor$ is the integer floor function, used to round the grid extents to integer multiples of the grid spacing, so grid lines will be coincident from time step to time step.

For cases with large unsteady motion, including maneuvering in waves and broaching, the grid expansion must consider unsteady speed in both x and y . Figure 1 shows a notional wave evaluation grid (not every grid line is shown) at three simulation time steps for a ship in a slow-speed turn.

4.1 Random White Noise

The term $\sigma_\epsilon^2 \epsilon_{(i_x, i_y, i_t)}$ in Equation (5) represents a field of white noise. σ_ϵ^2 is the variance of the white noise model and is a scalar value calculated from the regression coefficients described above. Along with the regression coefficients, this value will be constant for stationary waves and a function of time for non-stationary (e.g. rising or falling) seas. The quantity $\epsilon_{(i_x, i_y, i_t)}$ is a random function that should have unit variance and the same distribution as the wave elevations. For a Gaussian (normal) distribution, it can be readily approx-

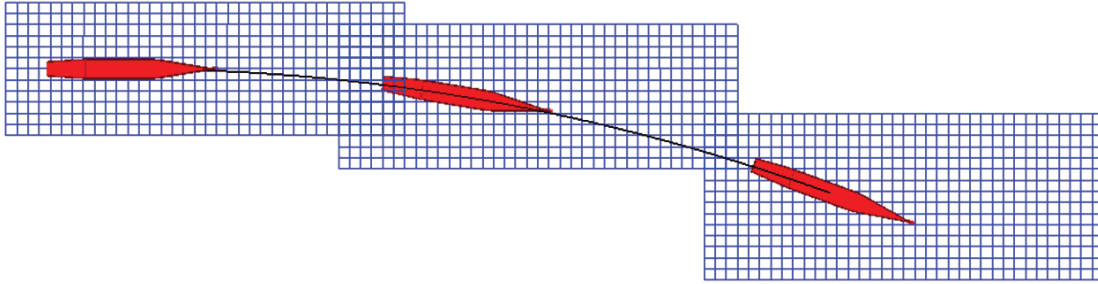


Fig. 1 Moving Elevation Grid for a Low Speed Turn

imated by the expression:

$$\epsilon = \sum_{i=1}^{12} R_i - 6 \quad (9)$$

where R_i is a random value of uniform distribution, and range $[0,1]$, which is the typical value of the intrinsic pseudo-random number function available in most math libraries.

4.2 Repeatability of the Wave Model

In the same way that the “random” phases of the wave components provide different realizations of the irregular wave field in a Longuet-Higgins model, the “randomness” of $\epsilon_{(ix,iy,it)}$ provides independent realizations of the ARM wave field. It is therefore necessary to be able to generate independent sets of these random values.

However, it is also highly desirable to be able to reproduce the identical calculation of the wave field. This is useful for visualizing the motion in waves, post-processing calculations such as relative motion and slamming, or simply repeating a simulation for a specific set of waves. To do this, it is necessary to use a pseudo-random number generator with a seed specification option and to record the size and origin of the regression grid.

4.3 Derivatives of the Elevation Field

Derivatives of the wave elevation in space and time are needed for calculation of the velocity potential field. In an initial implementation, these derivatives are computed using finite difference of the values on the wave elevation grid.

In order to allow a central difference calculation of the time derivative, the elevation calculation is run one time step ahead of the simulation. As the implementation of autoregressive continues, the calculation of these derivatives must be evaluated along with the effect and requirements of grid resolution and time step.

5 CALCULATION OF THE INCIDENT WAVE POTENTIAL FIELD

A significant challenge of using the ARM of wave for numerical simulations is that the ARM provides only the elevation field while numerical ship-motion codes generally require the pressure and velocity field beneath these waves. In panel methods, the pressure field is required in order to evaluate the Froude-Krylov forces and the velocity field is required to set up the body boundary condition for the disturbance potential boundary-value problem. In order to address this challenge, the implementation must incorporate an “inverse problem” solver which computes the incident wave velocity potential ($\phi_0(x, y, t)$) beneath the specified wavy surface. This inverse problem solution, which is described in more detail in Degtyarev & Gankevich (2012) and Gankevich & Degtyarev (2015), is summarized below.

The inviscid, incompressible potential flow beneath a free surface is described by the sys-

tem of equations:

$$\begin{aligned}\nabla^2\phi &= 0, \\ \phi_t + \frac{1}{2}|\nabla\vec{\phi}|^2 + g\zeta &= -\frac{p}{\rho} \quad \text{on } z = \zeta(x, y, t), \\ \frac{D\zeta}{Dt} &= \nabla\vec{\phi} \cdot \vec{n} \quad \text{on } z = \zeta(x, y, t),\end{aligned}\quad (10)$$

where ϕ is the incident wave potential, D/Dt is the substantial derivative and \vec{n} is the local normal vector to the free surface. The first of these equations satisfies continuity throughout the fluid domain while the second and third are the dynamic and kinematic free-surface boundary conditions, respectively. In the inverse problem, the free surface is known.

5.1 2-D Solution

For unsteady, two-dimensional (x, z, t) flow, (10) can be rewritten as:

$$\begin{aligned}\phi_{xx} + \phi_{yy} &= 0 \\ \phi_t + \frac{1}{2}(\phi_x^2 + \phi_z^2) + g\zeta &= -\frac{p}{\rho} \quad \text{on } z = \zeta(x, t) \\ \zeta_t + \zeta_x\phi_x &= \frac{\zeta_x}{\sqrt{1 + \zeta_x^2}}\phi_x + \phi_z \quad \text{on } z = \zeta(x, t).\end{aligned}\quad (11)$$

The 2-D potential at any time can be written as a Fourier transform of a function multiplied by an exponential:

$$\phi(x, z) = \int_{-\infty}^{\infty} E(\lambda)e^{\lambda(z+ix)}d\lambda. \quad (12)$$

This potential implicitly satisfies the continuity equation and can be substituted into the kinematic boundary condition to give:

$$\frac{\zeta_t}{1 - i\zeta_x - i\zeta_x/\sqrt{1 + \zeta_x^2}} = \int_{-\infty}^{\infty} \lambda E(\lambda)e^{\lambda(\zeta+ix)}d\lambda. \quad (13)$$

This expression represents a forward bilateral Laplace transform and can be inverted to yield a formula for the coefficients $E(\lambda)$:

$$\begin{aligned}E(\lambda) &= \frac{1}{2\pi i} \frac{1}{\lambda} \int_{-\infty}^{\infty} \frac{\zeta_t}{1 - i\zeta_x - i\zeta_x/\sqrt{1 + \zeta_x^2}} \\ &\times e^{-\lambda(\zeta+ix)}dx.\end{aligned}\quad (14)$$

Substituting (14) into (12) yields the final result:

$$\begin{aligned}\phi(x, z) &= \frac{1}{2\pi i} \int_{-\infty}^{\infty} \frac{1}{\lambda} \\ &\left(\int_{-\infty}^{\infty} \frac{\zeta_t}{1 - i\zeta_x - i\zeta_x/\sqrt{1 + \zeta_x^2}} e^{-\lambda(\zeta+ix')}dx' \right) \\ &\times e^{\lambda(z+ix)}d\lambda.\end{aligned}\quad (15)$$

It should be noted that while the free surface must be single valued, the slope of the wave is not assumed to be small, as has been in previous solutions of the inverse problem. Gankevich & Degtyarev (2015) provide a comparison of the previous and present methods.

In the numerical implementation of this scheme for the elevations generated via the autoregressive model, the infinite inner and outer integral limits of (15) are replaced by the corresponding wave surface size (x_0, x_1) and wave number interval (λ_0, λ_1) so that the inner integral converges.

The solution of the 3-D problem (2-D spatially + 1-D time) is similar though it, not surprisingly, involves double integrals.

5.2 Estimate and Interpolation of Potential Derivatives

The inverse velocity potential calculation provides the potential on a line of x -points or a grid of (x, y) -points corresponding to the elevation data evaluated from the ARM. Currently, there is no analogous formulae for the fluid velocities, the derivatives of the velocity potential. So derivatives must be calculated using finite difference techniques.

The lateral (x, y) resolution of the velocity potential will be dependent upon the resolution of the wave elevation field. However, in the vertical, (z) , direction, the potential can be evaluated for any z , so the resolution and range of the vertical distribution of the potential and its derivatives can be selected based on the requirements of the problem.

6 SUMMARY

Degtyarev & Reed (2011, 2012) presented the development of an autoregression model for incident random waves that is far more computationally efficient than the Fourier series like model of Longuet-Higgins. This model is amenable to modeling the synoptic and temporal processes associated to the development and evolution of ocean waves in a storm.

Degtyarev and Reed also showed that the waves produced by the autoregression model have the correct statistical characteristics spatially and temporally to represent ocean waves—the desired wave spectra can be reproduced and the distributions of physical characteristics is correct. Although the model does not explicitly contain the physics of gravity waves, by using 2- and 3-dimensional (1- or 2-dimensions in space + time) autoregression functions based on actual wave measurements, the model even captures the dispersion relation for gravity waves.

Degtyarev & Gankevich (2012) and Gankevich & Degtyarev (2015) have provided a technique for efficiently computing the velocity potential beneath a prescribed 1-D or 2-D surface, varying with time.

This paper attempts to continue that development by outlining an implementation of an auto-regressive incident wave model for use in a time-domain numerical ship-motion simulation code. Several key aspects of this implementation are described, including the efficient evaluation of the ARM on a set of moving grids for a simulation with steady or unsteady forward speed and the calculation of the incident wave velocity potential field beneath a prescribed wave surface. The latter procedure is not only a critical element of the application of the ARM, but provides a mechanism for implementing other non-traditional ocean wave models in numerical simulations. The complete details of the implementation and examples will be provided in Weems, et al (2016), to be presented later this year.

It remains to be determined whether or not

the ARM with the subsequent solution of an initial value problem for the velocity potential beneath the wave surface—the inverse problem, is computationally competitive with a Longuet-Higgins Fourier series based model. However, there certainly will be a point where it is competitive, as the Longuet-Higgins model's speed is inversely related to the number of coefficients required.

Several areas where future research is needed have been identified. One of the most critical appears to be the derivation of a direct method for computing the velocities in the fluid domain, a method similar to that used to compute the velocity potential.

ACKNOWLEDGMENTS

Professor Degtyarev's work with NSWCCD has been supported by the Office of Naval Research Global's Visiting Scientist Program. The authors are grateful to Dr. Woei-Min Lin of ONRG and Dr. Vadim Belenky of NSWCCD for their effort in arranging this effort.

REFERENCES

- Beck, R. F. & A. M. Reed (2001) Modern Computational Methods for Ships in a Seaway. *Trans. SNAME*, Vol. 109, pp. 1–51.
- Belenky, V. (2005) On Long Numerical Simulations at Extreme Seas. *Proc. 8th Int'l. Ship Stability Workshop*, Istanbul, Turkey, 7 p.
- Box, G. E. P., G. M. Jenkins & G. C. Reinsel (2008) *Time series analysis: Forecasting and control*, 4th Ed., Wiley, xx+746 p.
- Degtyarev, A. B. & A. Boukhanovsky (2000) Peculiarities of motion of ship with low buoyancy on asymmetrical random waves. *Proc. Int'l Conf. Stability of Ships and Floating Vessels*, Launceston, Tasmania, Australia, Vol. 2, pp. 665–679.
- Degtyarev, A. B. & I. Gankevich (2012) Evaluation of hydrodynamic pressures for autoregression model of irregular waves. In *Proc. 11th Int'l. Conf. Stability of Ships and Ocean Vehicles*, Athens, pages 841–852,

- 2012.
- Degtyarev, A. B. & Reed, A. M. (2011) Modeling of Incident Waves Near the Ship's Hull: Application of Autoregressive Approach to Problems of Simulation in Rough Seas. *Proc. 12th Int'l. Ship Stability Workshop*, Washington, D.C., pp. 175–187.
- Degtyarev, A. B. & Reed, A. M. (2012) Synoptic and Short-Term Modeling of Ocean Waves. *Proc. 29th Symp. Naval Hydromechanics*, Goteborg, Sweden, L. Larsson (ed.), 21 p. (Also: *Int'l. Shipbuilding Progress*, 2013, 60(1–4):523–553.)
- Gankevich, I. & Degtyarev, A.B. (2015) Computation of Pressures in Inverse Problem in Hydrodynamics of Potential Flow. *Proc. 12th Int'l. Conf. Stability of Ships and Ocean Vehicles*, Glasgow, UK, 5 p.
- Gurgenidze, A. T. & Y. A. Trapeznikov (1988) Probabilistic model of wind waves. In: *Theoretical foundations and methods of calculating wind waves*, Leningrad, Gidrometeoizdat, pp. 8–23.
- Longuet-Higgins, M. S. (1962) The Statistical Analysis of a Random, Moving Surface. *Phil. Trans. Royal Soc. London, Ser. A, Mathematical and Physical Sciences*, 249(966):321–387.
- Rozhkov, V. A. & Y. A. Trapeznikov (1990) *Probabilistic models of oceanographic processes*, Leningrad, Gidrometeoizdat.
- Spanos, P. D. (1983) ARMA Algorithms for Ocean Wave Modeling. *J. Energy Resources Technology*, Trans. ASME, Vol. 105:300–309.
- Weems, K., A. M. Reed, A. B. Degtyarev & I. Gankevich (2016) Implementation of an Autoregressive Wave Model in a Numerical Simulation Code. *Proc. 31th Symp. Naval Hydromechanics*, Monterey, CA, 12 p.

Validation of Split-time Method with Volume-Based Numerical Simulation

Kenneth Weems, *Naval Surface Warfare Center Carderock Division*

Vadim Belenky, *Naval Surface Warfare Center Carderock Division*

Bradley Campbell, *Naval Surface Warfare Center Carderock Division*

ABSTRACT

The paper describes the results of a statistical validation of the calculation of the probability of capsizing in irregular waves with the split-time method. The objective of the validation is to demonstrate that the split-time method correctly estimates probability of capsizing without necessarily observing it. Very large data sets of motion simulations were produced for severe sea conditions using a very fast but qualitatively realistic volume-based code, and a “true” rate of capsizing was determined by collecting the observed capsizes in this data. A series of small subsets of these data sets were then used with the split-time estimation, which was compared to the observed rate. In order to validate the evaluation of the confidence interval, the comparison was performed many times and the percentage of successful estimations was counted. If this percentage tends to the confidence probability, the statistical validation is successful. The paper contains results for 14 different conditions, varying significant wave height, modal period and relative heading. For the 95% confidence probability, the percentages of successes were between 80% and 100% for 50 sets; between 87% and 99% for 150 sets and finally converged to the theoretical 95% when all the sets were averaged.

Keywords: *Statistical validation, Probability of capsizing*

1. INTRODUCTION

The probabilistic assessment of capsizing in irregular waves with advanced hydrodynamic codes leads to the solution of an extrapolation problem. Capsizing is too rare to be observed in realistic sea conditions within a reasonable simulation time. The split-time method is a technique of extrapolation that is specifically intended for the estimation of capsizing probability; its development is reviewed in Belenky, et al. (2016). The cited reference reported a successful statistical validation for a single condition (significant wave height, modal period, speed and heading). The objective of the present study is to check the robustness and repeatability of that success by carrying out additional validation calculations for different conditions.

The development of extrapolation methods for probabilistic assessment of seakeeping in extreme condition (Anastopoulos, et al. 2016, Belenky, et al. 2016, Campbell, et al. 2016) poses the problem of statistical validation. The result of simulation-based extrapolation is a random number that is estimated with a confidence interval. If a true value is known,

the extrapolation can be regarded as successful if this true value falls within the confidence interval. However, due to the very same random nature, a single successful extrapolation result is hardly convincing. How would one know if this was not just a coincidence?

To ensure that the result is stable relative to the environmental conditions, Smith and Campbell (2013) and Smith, et al. (2014) introduced a multi-tier concept of statistical validation, which was originally proposed by Smith (2012) for general ship motion validation. The first tier is elemental – it is successful if the extrapolation result contains a “true” value within its confidence interval (the methodology of obtaining the true value is considered in the next section). The extrapolation procedure is then repeated several times for exactly the same condition, but using independent data sets – this is second tier. A successful validation for a given condition produces a certain percentage of successes, referred to as a “passing rate.” Smith and Campbell (2013) proposed 90% as a level for acceptance, based on practical considerations.

The third tier of statistical validation includes consideration of several conditions reflecting the expected operations. It is not yet clear how many of those conditions need be successful for an extrapolation method to pass. Examples of the application of the procedure for the EPOT (Envelope Peak over Threshold) method (Campbell, et al. 2016) are considered in Smith (2014) and Smith and Zuzick (2015).

The calculation of the confidence interval of the extrapolated estimate is a key element for the statistical calculation and should be validated separately. The Generalized Pareto distribution (GPD) was used to approximate a tail for both split-time method and EPOT, from which one can create a set of GPD distributed data and apply the calculation of confidence interval. If these calculations are correct, the passing rate must tend to the confidence probability used in those calculations, see Glotzer, et al. (2016) for details.

This paper applies this multi-tiered procedure (Smith and Zuzick, 2015) to the evaluation of the probability of capsizing in irregular waves with the split-time method.

2. EVALUATION OF “TRUE VALUE”

The extrapolation validation procedure reviewed in the previous section requires *a priori* knowledge of the probability of capsizing. Theoretical solutions for probability of capsizing are available for piecewise linear models (Belenky, et al, 2016), but while these models do describe capsizing qualitatively, i.e. as a transition between two stable equilibria, they are too simplistic to be considered as realistic ship motions. In particular they cannot describe the realistic change of stability in waves as well as the fact that the hydrostatic restoring is inseparable from wave excitation for large-amplitude ship motions.

These effects are naturally included in advanced hydrodynamic codes (Reed, et al. 2014) such as LAMP (Lin and Yu 1990). However, these high-fidelity codes are not fast enough to produce samples of sufficient size that a statistically relevant number of capsizes can be observed in relevant wave conditions, as millions of hours may be required (Campbell, et al. 2016).

The solution was proposed by Weems and Wundrow (2013). The idea is to compute

instantaneous submerged volume and calculate the inseparable hydrostatic and Froude-Krylov forces from this volume. The rest of the forces are approximated as coefficients. This approach yields reasonable results for relatively long waves, as the wave curvature is not resolved over the ship breadth but is resolved over the ship length, see Figure 1. Weems and Belenky (2015) show the qualitative adequacy of the approach by comparing shape of distributions of roll motion between the volume-based calculation and LAMP.

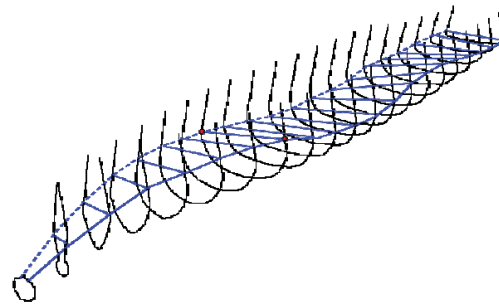


Figure 1 Station/incident wave intersection for volume based hydrostatic and Froude-Krylov forces for the ONR Tumblehome hull in stern oblique seas (Weems and Wundrow, 2013)

The use of the volume-based calculation instead of surface pressure integration for hydrostatic and Froude-Krylov forces makes the model almost as fast as models based on ordinary differential equations. Weems and Belenky (2015) reported that 10 hours data was generated in 7 seconds on a single processor of a laptop computer, allowing millions of hours of simulation data to be practically computed on a standard workstation or modest sized cluster.

3. ESSENCE OF THE SPLIT-TIME METHOD

The objective of the split-time method is to provide a means to use an advanced numerical code for estimating the probability of rare event without actually observing it in simulations. Its principal idea is to separate the estimation procedure into an observable or “non-rare” problem and a non-observable or “rare” problem. The “non-rare” problem is an estimation of the crossing rate of an intermediate threshold. It has to be low enough to observe a statistically significant number of upcrossing events in, say 100 hrs, but high enough so that most of these upcrossings can be treated as independent events.

The “rare” problem is solved for each upcrossing with a motion perturbation scheme shown in Figure 2. The roll rate is perturbed at the instant of upcrossing until capsizing is observed. The minimum value of roll rate perturbation leading to capsizing is a metric of the danger of capsizing danger at the instant of upcrossing.

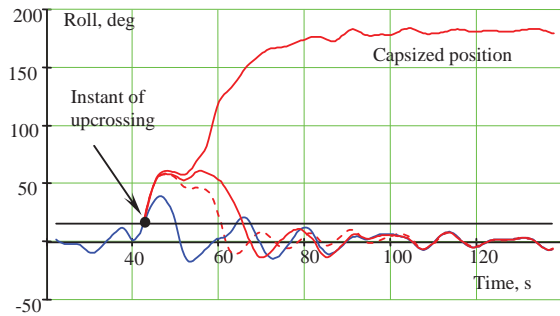


Figure 2 Illustration of motion perturbations

Given a sufficient number of upcrossings, the tail of the distribution of the metric value can be modeled with Generalized Pareto distribution (GPD), from which the estimate for the probability of capsizing can be evaluated. The most up-to-date description of the procedure can be found in Belenky, et al. (2016).

4. RESULTS

A typical example of the tier-two validation set is shown in Figure 3. A Bretschneider spectrum was used to simulated long-crested waves with a significant wave height of 9.0 m and a modal period of 14 s.

The subject ship is the ONR tumblehome topside configuration (Bishop, et al. 2005), speed

was 6 knots and heading 60 degrees relative to wave propagation. The “true” value of the capsizing rate was estimated from 176 capsizing cases observed during 200,000 hours of the volume-based simulations.

The tier-two validation data set consists of 50 independent extrapolations shown in Figure 3. Each extrapolation estimate uses 100 hours of volume-based simulations, with no capsizing cases observed during those times. The extrapolation result is presented with a confidence interval for the 0.95 confidence probability. Besides these boundaries, each extrapolation has the most probable value (x in Figure 3) and the mean value (circle in Figure 3). The calculation of the mean and most probable value is discussed in details in Belenky, et al. (2016). The tier-one validation is successful if the confidence interval contains the “true” value. The case shown in Figure 3 has 45 individual extrapolations that contain the “true” value in its confidence interval. The tier-two validation is successful when a percentage of the underlining tier-one validation successes is close to the accepted confidence level. This number is 0.90 for the considered case, which would be considered a successful “passing rate” by Smith and Campbell (2013).

The environmental conditions for the entire validation campaign described in this paper are presented in Table 1, while the results are summarized in Table 2. The tier-two validation procedure was repeated three times on independent data to check the variability of the results.

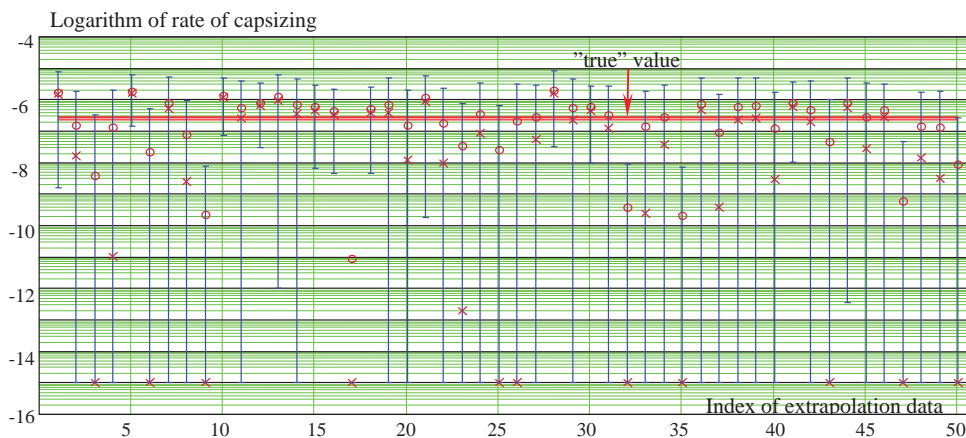


Figure 3 Example of validation tier-two case; significant wave height 9.0, modal period 14s, heading 60 deg, passing rate 0.90

Table 1 Summary validation conditions and “true” value estimates

Significant wave height, m	Modal Period, s	Heading, degrees	Exposure, hr	Number of Capsizes	Estimate of rate 1/s	Low boundary of rate	Upper boundary of rate
8.5	14	45	200,000	8	1.13E-08	4.24E-09	1.98E-08
8.5	14	60	200,000	31	4.38E-08	2.97E-08	5.93E-08
9	14	35	720,000	12	4.71E-09	2.04E-09	7.37E-09
9	14	40	200,000	12	1.70E-08	8.48E-09	2.68E-08
9	14	45	200,000	51	7.20E-08	5.37E-08	9.18E-08
9	14	50	20,000	7	9.89E-08	2.83E-08	1.84E-07
9	14	55	60,000	69	3.25E-07	2.50E-07	4.05E-07
9	14	60	200,000	176	2.49E-07	2.12E-07	2.85E-07
9	14	65	200,000	80	1.13E-07	8.90E-08	1.38E-07
9	14	70	200,000	6	8.48E-09	2.83E-09	1.55E-08
9	15	45	345,000	10	8.19E-09	3.11E-09	1.33E-08
9	15	60	300,000	11	1.04E-08	4.71E-09	1.70E-08
9.5	15	45	1,000,000	157	4.44E-08	3.74E-08	5.13E-08
9.5	15	60	1,000,000	242	6.84E-08	5.98E-08	7.70E-08

Table 2 Summary of validation results

Significant wave height, m	Modal Period, s	Heading, degrees	Subset duration, hrs	Passing rate Sample 1	Passing rate Sample 2	Passing rate Sample 3	Averaged passing rate
8.5	14	45	2,000	1.00	0.98	0.90	0.96
8.5	14	60	2,000	0.92	0.96	0.94	0.94
9	14	35	2,000	1.00	0.98	0.98	0.99
9	14	40	2,000	1.00	0.98	1.00	0.99
9	14	45	2,000	0.98	0.98	0.96	0.97
9	14	50	2,000	0.98	0.92	0.94	0.95
9	14	55	2,000	0.90	0.80	0.92	0.87
9	14	60	2,000	0.90	0.86	0.94	0.90
9	14	65	2,000	0.94	0.92	0.94	0.93
9	14	70	2,000	0.92	1.00	0.90	0.94
9	15	45	2,000	0.98	0.96	0.96	0.97
9	15	60	2,000	0.96	0.98	0.98	0.97
9.5	15	45	2,000	0.96	0.94	0.96	0.95
9.5	15	60	2,000	0.98	0.94	0.96	0.96

There were two cases when the passing rate fell below 0.9: for headings 55 and 60 degrees at 9 m waves. In general, the variability of the passing rate within the same environment condition is not small. The last column in Table 2 shows averaged passing rate per condition, which is equivalent to 150 extrapolation data sets. The averaging passing rate fell below 0.9 only once, for 55 degree heading, indicating favorable tendency with the increase of sample size.

Finally, if one averages the passing rate over all the conditions tested, the theoretical 0.95 is obtained. This is yet another indication of the statistical correctness of the split-time method.

5. CONCLUSIONS AND FUTURE WORK

The split-time method for estimating probability of capsizing caused by pure loss of stability has been subjected to statistical validation for 14 environmental conditions. The true values were obtained by a very fast volume based numerical simulation with a time of exposure of up to one million hours full-scale. The rare problem solution is based on single degree-of-freedom perturbations. The average passing rate per condition varied from 0.87 to 0.99, falling below 0.90 for a single condition. The passing rate averaged over all the tested condition was 0.95, while the confidence probability was 0.95. These results are encouraging.

At the same time, the described validation campaign shows the necessity to refine the acceptance criteria, in particular what passing rate should be expected depending on how many extrapolation data sets were used. The acceptance criteria are needed for the tier-three validation level which addresses overall acceptance.

6. ACKNOWLEDGEMENTS

The work described in this paper has been funded by the Office of Naval Research through the NSWCCD Independent Applied Research (IAR) program under Dr. Jack Price.

Discussions with Art Reed, Tim Smith (NSWCCD) and Vlasdas Pipiras (University of North Carolina) were fruitful.

7.

8. REFERENCES

Anastopoulos, P.A., Spyrou, K.J., Bassler, C.C., and Belenky, V. (2015) "Towards an Improved Critical Wave Groups Method for the Probabilistic Assessment of Large Ship Motions in Irregular Seas," *Probabilistic Engineering Mechanics*, DOI: 10.1016/j.probengmech.2015.12.009.

Belenky, V., Weems, K. and W.M. Lin (2016) "Split-time Method for Estimation of Probability of Capsizing Caused by Pure Loss of Stability" in *Ocean Engineering*, (in Press DOI: 10.1016/j.oceaneng.2016.04.011).

Bishop, R. C., W. Belknap, C. Turner, B. Simon, and J. H. Kim (2005) "Parametric Investigation on the Influence of GM, Roll damping, and Above-Water Form on the Roll Response of Model 5613." Report NSWCCD-50-TR-2005/027.

Campbell, B., Belenky, V. and V. Pipiras (2016) "Application of the Envelope Peaks over Threshold (EPOT) Method for Probabilistic Assessment of Dynamic Stability, in *Ocean Engineering* (in Press DOI: 10.1016/j.oceaneng.2016.03.006).

Glotzer, D., Pipiras, V., Belenky, V., Campbell, B., T. Smith (2016) "Confidence Interval for Exceedance Probabilities with Application to Extreme Ship Motions", *REVSTAT Statistical J.* (Accepted).

Lin, W.M., and Yue, D.K.P. (1990) "Numerical Solutions for Large Amplitude Ship Motions in the Time-Domain," *Proc. 18th Symp. on Naval Hydrodynamics*, Ann Arbor, Michigan, USA, pp. 41–66.

Reed, A., Beck, R. and Belknap, W. (2014) "Advances in Predictive Capability of Ship Dynamics in Waves," Invited Lecture at 30th *Symposium of Naval Hydrodynamics*, Hobart, Australia.

Smith, T. C. (2012) "Approaches to Ship Motion Simulation Acceptance Criteria," *Proc. of 11th Intl Conference of the Stability of Ships and Ocean Vehicles*, Athens, Greece pp 101-114.

Smith, T. C. (2014) "Example of Validation of Statistical Extrapolation," in *Proceedings of the 14th*

Intl. Ship Stability Workshop, Kuala Lumpur, Malaysia.

Smith T.C., Campbell, B.L. (2013) "On the Validation of Statistical Extrapolation for Stability Failure Rate," *Proc. 13th Intl. Ship Stability Workshop*, Brest, France.

Smith, T. C., and Zuzick, A. (2015) "Validation of Statistical Extrapolation Methods for Large Motion Prediction," *Proc. 12th Intl. Conf. on Stability of Ships and Ocean Vehicles (STAB 2015)*, Glasgow, UK.

Smith, T. C., Campbell, B. L., Zuzick, A. V., Belknap, W. F., and Reed, A. M. (2014) "Approaches to Validation of Ship Motion Predictions Tools and Extrapolation Procedures for Large Excursions of Ship Motions in Irregular

Seas," *Computational Stochastic Mechanics – Proc. of the 7th Intl. Conference (CSM-7)*, edited by G. Deodatis and P. Spanos, Santorini, Greece.

Weems, K. and Belenky, V. (2015) "Fast Time-Domain Simulation in Irregular Waves With Volume-Based Calculations for Froude-Krylov and Hydrostatic Force," *Proc. 12th Intl. Conf. on Stability of Ships and Ocean Vehicles (STAB 2015)*, Glasgow, UK.

Weems, K. and Wundrow, D. (2013) "Hybrid Models for Fast Time-Domain Simulation of Stability Failures in Irregular Waves with Volume-Based Calculations for Froude-Krylov and Hydrostatic Force," *Proc. 13th Intl. Ship Stability Workshop*, Brest, France.

On the Tail of Nonlinear Roll Motions

Vadim Belenky, *Naval Surface Warfare Center Carderock Division*

Dylan Glozter, Vlasdas Pipiras, *University of North Carolina*

Themistoklis P. Sapsis, *Massachusetts Institute of Technology*

ABSTRACT

The paper describes the qualitative study of the tails of the distribution of large-amplitude roll motions. The nonlinearity of a dynamical system is modeled with piecewise linear stiffness with stable and unstable equilibria. Closed-form formulae were derived for the peak value and its distribution. The tail of the distribution is heavy until in close proximity to the unstable equilibrium and then becomes light with the right bound at the unstable equilibrium. It is shown that the tail structure is related to the shape of the stiffness curve. Physical reasoning for such tail structure is based on the phase plane topology. The tail first becomes heavy due to stretching of the phase plane, which is a result of nonlinearity. The inflection point in the tail (when it becomes light) is related to increased capsizing probability in the vicinity of unstable equilibrium; the position of the inflection point can be evaluated, defining domain of heavy tail applicability.

Keywords: *Nonlinear Roll Motion, Distribution, Extremes*

1. INTRODUCTION

Probabilistic assessment of partial dynamic stability failure is essentially an extreme value problem for nonlinear roll motions. Some progress has been recently reported by Campbell, *et al* (2016) on applying Generalized Pareto distribution (GPD) to model the extreme values of roll peaks, above appropriate threshold (Coles, 2001). Mathematical aspects of the problem are treated in (Glotzer et al 2016). Statistical validation of this method was described by Smith and Zuzick (2015). While, in general, the method has shown satisfactory performance, its accuracy may be improved by applying one-parameter GPD instead of two-parameter GPD. It requires introducing a relation between the GPD parameters based on physical properties of the dynamical system. This relation is the main objective of this paper.

Normally, GPD has two parameters: shape and scale. If the shape parameter equals zero, GPD turns into the exponential distribution. This is the case of a normally distributed quantity; distribution of its extreme values can be approximated by the exponential distribution. If the shape parameter is positive, the tail is usually referred to as “heavy,” as its probability of extreme value is higher compared to normal/exponential case. If the shape parameter is negative, the probability of extreme value is lower compared to exponential and the tail is referred as “light.” One of the specific features of a light tail is a right bound, the upper limit of the

distribution; all values exceeding the right bound have zero-probability.

The appearance of right bound in a distribution of roll peaks has a clear physical reason. A peak implies a return after reaching a local maximum. As a ship may capsize, there is a limit for the roll peak, which should be reflected as a right bound by statistics. However, GPD fitting, reported in Campbell, *et al* (2016) resulted in positive shape parameter and no right bound.

The question this paper tries to answer formulates as follows: if a ship can capsize, the tail of roll peak distribution should be light, so why is a heavy tail observed in numerical simulations?

2. PIECEWISE LINEAR SYSTEM

A dynamical system with piecewise linear stiffness is probably the simplest model of capsizing, as it allows recreation of correct phase plane topology, see Figure 1. It also allows a closed form solution for probability of capsizing under some assumptions; see review in (Belenky, *et al* 2016). So consider a dynamical system:

$$\ddot{\phi} + 2\delta\dot{\phi} + \omega_0^2 f_L(\phi) = f_{E\phi}(t) \quad (1)$$

where δ is a linear damping coefficient and $f_{E\phi}$ is a stochastic process of roll excitation, while the roll stiffness f_L is shown in Figure 1. It is assumed that the excitation is “switched-off” once the roll angle exceeds ϕ_{m0} , reflecting absence of resonance for negative GM and limited ability to react on waves.

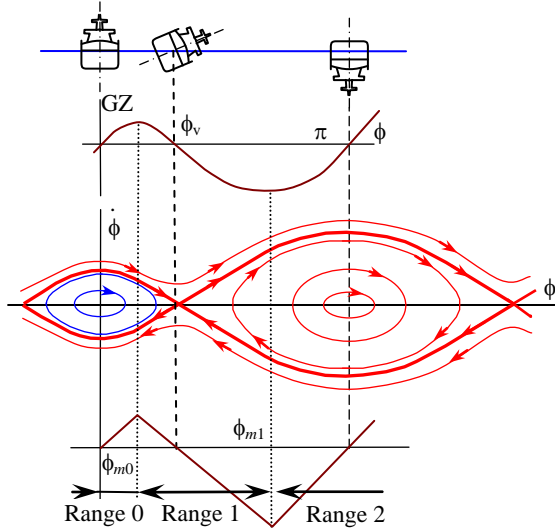


Figure 1 Phase plane topology of capsizing and piecewise linear stiffness (Belenky, et al 2016).

Here absence of damping for $\phi > \phi_{m0}$ is also assumed. While in reality roll damping is increased for large roll angles, it is not expected to cause qualitative change. In the absence of capsizing, the solution for the range 1 is expressed as:

$$\phi = H \cosh(\omega_1 t + \varepsilon) + \phi_v, \quad \phi_{m0} < \phi \leq \phi_{m1} \quad (2)$$

where: $\omega_1 = \omega_0 \sqrt{k_1}$, arbitrary constants are

$$H = -\frac{1}{\omega_1} \sqrt{\omega_1^2 (\phi_{m0} - \phi_v)^2 - \dot{\phi}_1^2} \quad (3)$$

$$\varepsilon = \tanh^{-1} \left(\frac{\dot{\phi}_1}{\omega_1 (\phi_{m0} - \phi_v)} \right) \quad (4)$$

$\dot{\phi}_1$ is a roll rate at upcrossing. The value of peak is expressed as:

$$\phi_{\max}(\dot{\phi}_1) = H + \phi_v, \quad 0 < \dot{\phi}_1 \leq \dot{\phi}_{cr} \quad (5)$$

$\dot{\phi}_{cr}$ is critical roll rate corresponding to capsizing conditions:

$$\dot{\phi}_{cr} = \omega_1 (\phi_v - \phi_{m1}) \quad (6)$$

3. DISTRIBUTION OF PEAKS

Formula for the peak (3) is a deterministic function of a single random variable. This random variable is the roll rate at the instant of upcrossing. Assuming that the upcrossings of the level ϕ_{m0} are so rare, that is the upcrossing events can be assumed independent, then the distribution of the roll rate at upcrossing follows Rayleigh (see Leadbetter, et al. 1983, Lindgren, 2013, also in Belenky, et al. 2016):

$$f_d(\dot{\phi}_1) = \frac{\dot{\phi}_1}{\sigma_d^2} \exp\left(-\frac{\dot{\phi}_1^2}{2\sigma_d^2}\right) \quad \dot{\phi}_1 > 0 \quad (7)$$

Where σ_d is a standard deviation of roll rates for range 0, i.e. without influence of crossings. To ensure that only roll peaks are considered, there is no capsizing and a normalizing constant is needed. It is equal to probability of capsizing:

$$f_d(\dot{\phi}_1) = \left(1 - \exp\left(-\frac{\dot{\phi}_{cr}^2}{2\sigma_d^2}\right)\right)^{-1} \frac{\dot{\phi}_1}{\sigma_d^2} \exp\left(-\frac{\dot{\phi}_1^2}{2\sigma_d^2}\right) \quad (8)$$

$$0 < \dot{\phi}_1 < \dot{\phi}_{cr}$$

The function (5) is monotonic; the distribution of this function is:

$$f_{\max}(\phi_{\max}) = f_d(G^{-1}(\phi_{\max})) \cdot \left| \frac{d}{d\phi_{\max}} G^{-1}(\phi_{\max}) \right| \quad (9)$$

$$\phi_{m0} < \phi_{\max} < \phi_v$$

where G^{-1} is an inverse of the function (5)

$$G^{-1}(\phi_{\max}) = \omega_1 \sqrt{(\phi_v - \phi_{m0})^2 - (\phi_v - \phi_{\max})^2} \quad (10)$$

$$\phi_{m0} < \phi_{\max} < \phi_v$$

Substitution of (10) and (8) into (9) yields the following distribution density.

$$f_{\max}(\phi_{\max}) = \frac{\phi_v - \phi_{\max}}{C} \exp\left(-\frac{\omega_1^2 (\phi_v - \phi_{\max})^2}{2\sigma_d^2}\right) \quad (11)$$

$$\phi_{m0} < \phi_{\max} < \phi_v$$

where

$$C = \frac{\sigma_d^2}{\omega_1^2} \left(\exp\left(-\frac{\omega_1^2 (\phi_v - \phi_{m0})^2}{2\sigma_d^2}\right) - 1 \right) \quad (12)$$

Distribution (11) is plotted in Figure 2.

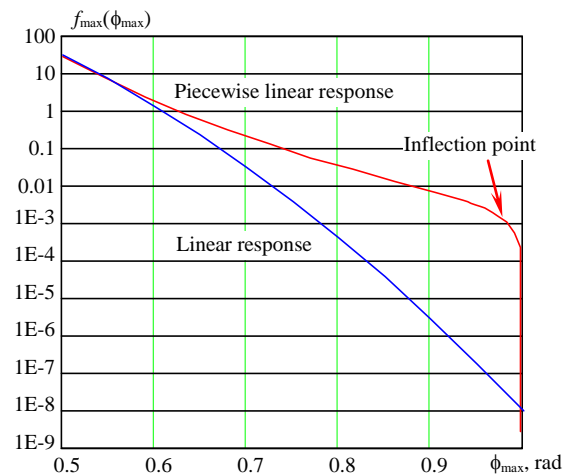


Figure 2 Distribution of peaks of piecewise linear and linear response

To see if the distribution (11) has a heavy tail, compare it to the distribution of peak of a linear system, corresponding to the range 0. Distribution of large peaks of a linear system can be approximated with truncated Rayleigh distribution (Belenky and Campbell 2012):

$$f_{L_{\max}}(\phi_{\max}) = C_L \frac{\phi_{\max}}{\sigma_x^2} \exp\left(-\frac{\phi_{\max}^2}{2\sigma_x^2}\right) \quad (13)$$

$$\phi_{\max} > \phi_{m0}$$

$$C_L = \exp\left(-\frac{\phi_{m0}^2}{2\sigma_x^2}\right)$$

The tail of Rayleigh distribution can be approximated with exponential distribution; thus equation (13) may serve as benchmark; a larger probability than (13) means heavy tail. Figure 2 shows that the piecewise linear system produces this heavy tail through practically the entire range 1. Then, it reaches an inflection point and quickly tends to zero.

Figure 2 answers the question, posed at the end of section 1. The tail actually is heavy for most of the interval and then turns light in the vicinity of unstable equilibrium.

Peaks of the response of the piecewise linear system with unstable equilibrium shows an interesting behavior. The “true” limiting distribution has a light tail, but a heavy tail can be used for approximation at least until the “inflection point.” One may say that the piecewise linear system has two tails. What are the conditions for having two tails?

4. DEPENDENCE ON THE SECOND SLOPE

Consider behavior of the distribution (11) when the slope coefficient k_1 tends to zero. Using the relation between k_1 and the position of unstable equilibrium

$$\phi_v = \phi_{m0} \frac{1+k_1}{k_1} \quad (14)$$

When k_1 reaches zero, the unstable equilibrium ceases to exist.

$$\lim_{k_1 \rightarrow 0} \phi_v = \lim_{k_1 \rightarrow 0} \left(\phi_{m0} \frac{1+k_1}{k_1} \right) = \infty \quad (15)$$

The limit transition converts equation (11) into the exponential distribution:

$$\lim_{k_1 \rightarrow 0} f_{\max}(\phi_{\max}) = \frac{\omega_1^2 \phi_{m0}}{\sigma_d^2} \times \exp\left(-\frac{\omega_1^2 \phi_{m0}}{\sigma_d^2} (\phi_{\max} - \phi_{m0})\right) \quad (16)$$

The process of this limit transition is illustrated below. The slope of the range 1 is changed systematically from -1 to 0, as plotted in Figure 3. Figure 4 shows corresponding changes in the distribution of the peaks. The heavy part of the tail becomes lighter, until it reaches the exponential distribution (16) for $k_1=0$. The “inflection point” moves to the right, until it eventually disappears when the position of unstable equilibrium goes to infinity.

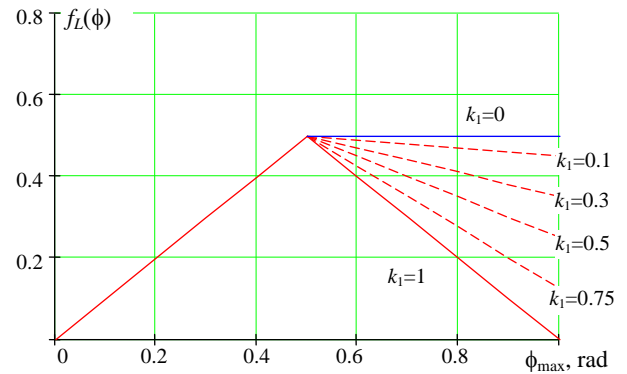


Figure 3 Variation of piecewise linear stiffness

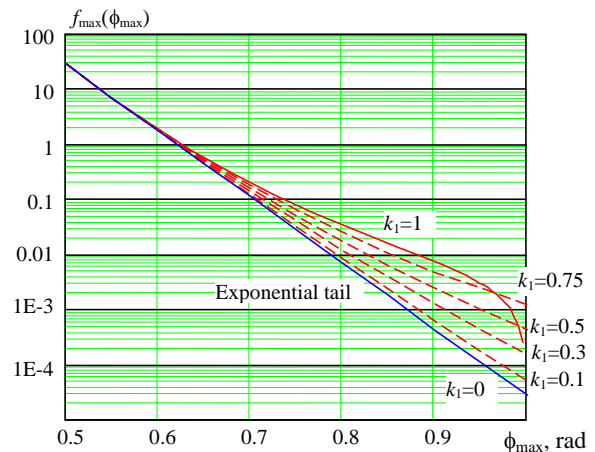


Figure 4 Distribution of peaks of piecewise linear response for different slopes of the second range

The changes in the slope coefficient for the range 1 mean changes in the shape of stiffness. Thus, shape of the stiffness after the maximum defines the shape of the tail, while the position of the unstable equilibrium defines the position of the “inflection point.” The softening nonlinearity ($k_1 > 0$) seems to be responsible for the “two-tails” structure. It disappears when k_1 becomes zero.

5. WHITE NOISE EXCITATION

The relation between “two-tails” structure, shape of stiffness and presence/absence of the unstable equilibrium points to a possible fundamental relation between the distribution and topology of the phase plane. This link may be revealed if one gets a closed-form expression for joint distribution of motions and velocities. It can be done using the Kolmogorov-Fokker-Plank equation, if white noise excitation is assumed. Indeed, it is far from reality, but the system (1) under white noise excitation may have similar relation between the distribution and phase plane.

Assuming

$$f_{E\dot{\phi}}(t) = s\dot{W}(t) \quad (17)$$

where $W(t)$ is Wiener process and s its scaling factor or intensity. The the steady-state joint distribution of the motions and velocities is expressed as (see *e.g.* Sobczyk, 1991):

$$f_{\infty}(\phi, \dot{\phi}) = C_W \exp\left(-\frac{4\delta}{s^2} H(\phi, \dot{\phi})\right) \quad (18)$$

where C_W is a normalizing constant and $H(\dots)$ is the Hamiltonian (total energy without dissipation) of the dynamical system (1)

$$H(\phi, \dot{\phi}) = \frac{1}{2} \dot{\phi}^2 + V(\phi) \quad (19)$$

Potential $V(\phi)$ is symmetrical relative to the origin and for $\phi < \phi_v$ is expressed as:

$$V(\phi) = \frac{\omega_0^2}{2} \begin{cases} \phi^2 & 0 \leq \phi < \phi_{m0} \\ \phi_{m0}^2 - k_1(\phi - \phi_{m0})^2 & \phi_{m0} \leq \phi \end{cases} \quad (20)$$

The current study is focused on the properties of the tail of large-amplitude response, so the distribution (18) needs to be limited to non-capsizing case. In terms of phase plane, it corresponds only to the area within the separatrix, see Figure 5. The Hamiltonian implicitly contains definition of the separatrix, as it is the only line going through the unstable equilibria:

$$\dot{\phi}_s(\phi) = \pm \sqrt{H(\pm\phi_v, 0) - V(\phi)} \quad (21)$$

The distribution of piecewise linear response, not leading to capsizing is expressed as:

$$f_s(\phi) = C_S \int_{-\dot{\phi}_s(\phi)}^{\dot{\phi}_s(\phi)} f_{\infty}(\phi, \dot{\phi}) d\dot{\phi} \quad (22)$$

where C_S is another normalizing constant.

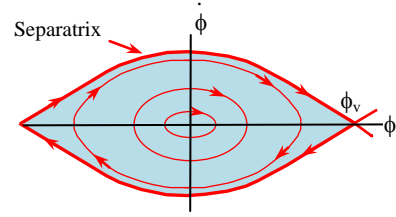


Figure 5 Separatrix and non-capsizing area

Figure 6 shows distribution of piecewise linear response under the “no-capsize” condition computed with formula (22). This distribution has three distinct regions: Gaussian core (i), heavy tail (ii) and light tail (iii). The structure of the tail is exactly the same as in the previous case in Figure 2, where excitation was correlated but switched off above the knuckle point (where damping was absent, too).

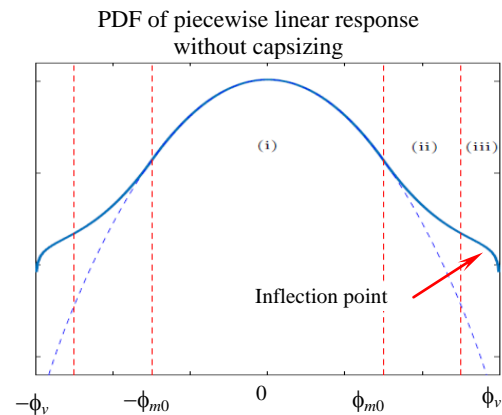


Figure 6 Distribution of piecewise linear response under no-capsize condition

The result in Figure 6, is one more argument that the structure of the tail is defined by stiffness shape. Thus, the correlation of the excitation can be neglected for this type of qualitative study. This provides a number of research tools that can only be applied for white noise excitation.

6. HEAVY TAIL STRUCTURE

Two previous sections presented some arguments that the observed tail structure is a result of the stiffness shape, and presence of the unstable equilibrium, in particular. Presence of the unstable equilibrium makes nonlinearity soft. The piecewise linear system does not differ much in that sense from a nonlinear system with smooth stiffness, as most known qualitative properties are present (Belenky, 2000).

Figure 7 compares linear and piecewise / nonlinear systems both in terms of potential and phase plane. As the linear system contains more potential energy, the potential function of the piecewise system is always below the linear one. The phase trajectories are, in fact, the level lines of the potential function. As a result the phase plane of the piecewise linear system (1) or a system with softening nonlinear stiffness is stretched compared to a linear system.

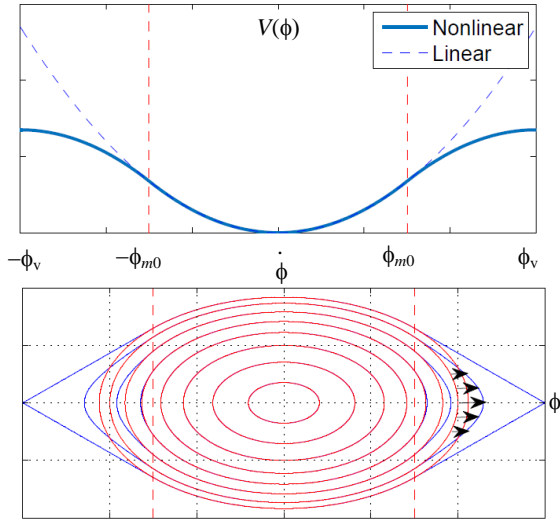


Figure 7 Stretching of the phase plane caused by soft nonlinearity of stiffness

Another way to illustrate this stretching is to compare short portions of time history of the piecewise linear system. Both responses start at the same time instant at the “knuckle” point with the same initial velocity. As it can be seen from Figure 8, the response of the piecewise linear system (2) is always above the similar linear response.

This also means that the piecewise linear system spends more time above the knuckle point than the linear system under the same initial conditions. As a result, probability of finding the piecewise linear system above the knuckle point is higher and the tail of the response is heavier than the linear one.

Also, one can see at Figure 8 that the local maximum of the piecewise linear response is larger than the linear one. Thus the tail of peaks of the nonlinear response is heavier than the linear one, as it can be seen in Figure 2.

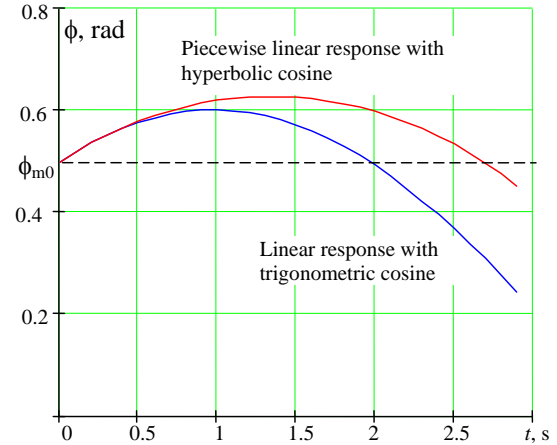


Figure 8 Piecewise linear response above the knuckle point vs. linear response

7. LIGHT TAIL STRUCTURE

Obviously, the tail of both response and its peaks becomes light because of the presence of unstable equilibrium. Consider how it is reflected in the distribution (22), by substitution formula (18) and (19):

$$f_s(\phi) = C_S C_W \exp\left(-\frac{4\delta}{s^2} V(\phi)\right) \times \int_{-\dot{\phi}_s(\phi)}^{\dot{\phi}_s(\phi)} \exp\left(-\frac{4\delta \dot{\phi}^2}{2s^2}\right) d\dot{\phi} \quad (23)$$

The integrand is in fact the normal distribution as:

$$\sigma_d^2 = \frac{s^2}{4\delta} \quad (24)$$

The integral term does not play much of a role when the motion displacement is far from the unstable equilibrium. The separatrix goes through very large velocities for most of range 2 and the integral in (23) is close to one (after being multiplied by its normalizing constant). Once the motion approaches the unstable equilibrium, the limits of integration do get close to each other. As a result the integral term in (23) decreases and forces the entire distribution down, until it reaches zero at the point of unstable equilibrium.

Understanding of this mechanism allows estimation of the position of the inflection point. It can be checked that the logarithm of the distribution (11) has the inflection point at:

$$\phi_{\text{inf}} = \phi_v - \frac{\sigma_d}{\omega_1} \quad (25)$$

Position of the inflection point defines a boundary of the heavy tail range and it should be possible to find it for a general nonlinear system.

8. CONCLUSIONS

The original motivation for this study was to answer a simple question, why the GPD fit shows a heavy tail for peaks of roll motions, when it is expected to be light because a ship can capsize and the peaks cannot exceed a certain limit. The answer was found by analyzing a dynamical system with an unstable equilibrium and piecewise linear stiffness. The distribution has “two-tails” structure: it is heavy at first, but becomes light in close vicinity of the unstable equilibrium.

This “two-tails” structure is a result of the presence of an unstable equilibrium and related softening nonlinear stiffness. The heavy tail is a result of stretching of the phase plane. The light tail appears in close vicinity to the unstable equilibrium, where most trajectories lead to capsizing so the probability of non-capsizing is very small.

The “inflection point” of the tails is the boundary between heavy and light tail. Its position can be found and used as a limit of applicability of the heavy tail assumption.

The shape of stiffness and related topology of the phase plane is the main factor defining the tail structure of the response of dynamical system. Qualitative tail structure seems to be the same for the dynamical system with correlated or white noise excitation.

Further research includes a wider variety of nonlinear dynamical systems, as well as metrics of likelihood of capsizing and broaching-to. A technique for estimation of the position of the “inflection point” should be developed for generic nonlinear systems and eventually use this information to reduce uncertainty of GPD fit.

9. ACKNOWLEDGEMENT

The work described in this paper has been funded by the Office of Naval Research under Dr. Thomas Fu and by NSWCCD Independent Applied Research (IAR) program. Participation of Prof. Pipiras and Prof. Sapsis was facilitated by the Summer Faculty Program supported by ONR and managed by NSWCCD under Dr. Jack Price,

who also managed IAR program. Participation of Mr. Glotzer was facilitated by NWCDD NREIP program managed by Ms. Rachel Luu.

10. REFERENCES

Belenky, V. L., (2000) “Piecewise linear approach to nonlinear ship dynamics”, in Contemporary Ideas on Ship Stability Vassalos, D., Hamamoto, M., Papanikolaou, A. and D. Molyneux, eds., Elsevier, pp.149-160.

Belenky, V. and Campbell, B. (2012) “Statistical Extrapolation for Direct Stability Assessment”, *Proc. 11th Intl. Conf. on Stability of Ships and Ocean Vehicles STAB 2012*, Athens, Greece, pp. 243-256

Belenky, V., Weems, K. and K. Spyrou (2016) “Towards a Split-Time Method for Estimation of Probability of Surf-Riding in Irregular Seas”, in *Ocean Engineering* (in Press DOI: 10.1016/j.oceaneng.2016.04.003).

Campbell, B., Belenky, V. and V. Pipiras (2016) “Application of the Envelope Peaks over Threshold (EPOT) Method for Probabilistic Assessment of Dynamic Stability, in Ocean Eng. (DOI: 10.1016/j.oceaneng.2016.03.006).

Coles, S., 2001 *An Introduction to Statistical Modeling of Extreme Values*. Springer, London.

Glotzer, D., Pipiras, V., Belenky, V., Campbell, B., T. Smith, (2016) "Confidence Interval for Exceedance Probabilities with Application to Extreme Ship Motions", REVSTAT Statistical J. (Accepted).

Leadbetter, M. R., Lindgren, G. & Rootzen, H. (1983), Extremes and Related Properties of Random Sequences and Processes, Springer Series in Statistics, Springer-Verlag, New York-Berlin

Lindgren, G. (2013), Stationary Stochastic Processes, Chapman & Hall/CRC Texts in Statistical Science Series, CRC Press, Boca Raton, FL. Theory and applications

Smith, T. C., and Zuzick, A., (2015) “Validation of Statistical Extrapolation Methods for Large Motion Prediction” in *Proc. 12th Intl. Conf. on Stability of Ships and Ocean Vehicles (STAB 2015)*, Glasgow, UK.

Sobczyk, K. (1991), Stochastic Differential Equations, Kluwer Academic Publishers, Dordrecht, The Netherlands.

Numerical Simulation KPI Equation

A.V. Bogdanov, *Fac. of Appl. Math, and Cont. Proc., St. Petersburg University, Russia, bogdanov@csa.ru*
 V.V. Mareev, *Fac. of Appl. Math, and Cont. Proc., St. Petersburg University, Russia, map@csa.ru*

ABSTRACT

The analysis of different numerical procedures for nonlinear equations describing strong waves evolution is carried out. We have chosen master equation, that is the generalization of Kadomtsev-Petviashvili-I Equation (KPI), that shows major part of the problems in ocean waves evolution and at the same time most difficult from the point of view of numerical algorithm stability. Some indications for choosing of correct numerical procedures are given.

Keywords: *Kadomtsev-Petviashvili-I Equation, numerical methods, solution stability*

In the numerical integration of KPI equation instead of the original equation its integral-differential analogue is considered

$$u_t + 0.5(u^2)_x + \beta u_{xxx} = \eta \int_{-\infty}^x u_{yy}(x', y, t) dx' + G(x, y) \quad (1)$$

The solution of equation (1) in the half-plane $t \geq 0$ is sought for the initial distribution $u(x, y, 0) = q(x, y)$.

Numerical simulation of the equation (1) is carried out using linearized implicit finite-difference scheme, with, in some cases, flux correction technique (FCT).

Solution of the equation (1) is performed using the approximation for the central-difference operators. The order of approximation of a difference scheme in the calculation is of the order of $O(\Delta t, \Delta x^2, \Delta y^2)$. The resulting system of difference equations is reduced to the form:

$$a_j \Delta u_{j-2,k}^{n+1} + b_j \Delta u_{j-1,k}^{n+1} + c_j \Delta u_{j,k}^{n+1} + d_j \Delta u_{j+1,k}^{n+1} + e_j \Delta u_{j+2,k}^{n+1} = f_{jk}^n \quad (2)$$

with $\Delta u_{jk}^{n+1} = u_{jk}^{n+1} - u_{jk}^n$.

The system (2) is solved by the five-point sweep (Thomas algorithm).

At the boundaries of the computational domain $[x_1, x_M] \times [y_1, y_L]$ set of difference boundary conditions is imposed. Traditionally the so-called "flow conditions" are used: $u_x = u_{xx} = 0$ along the boundary lines x_1 and x_M , and $u_y = 0$ along the lines y_1 и y_L .

As the initial distributions three surfaces were selected:

1. The parallelepiped.
2. Gaussian distribution.
3. The ellipsoid of rotation.

In our case, we want to investigate the influence of the shape of the initial distribution on the further evolution of the perturbation. To unify the choice of distribution parameters, we fix the volume and variety of shapes and parameters for ellipses that fit into the bottom of the box.

Compare the numerical calculation results with the known analytical solution of the KPI equation.

We apply the finite-difference scheme (2) for the equation, similar to (1):

$$[u_t + 3(u^2)_x + u_{xxx}]_x = 3u_{yy} \quad (3)$$

For the equation (3) there exist lump type soliton solution, i.e. in the form:

$$u(x, y, t) = 4 \frac{-(x - 3\mu^2 t)^2 + \mu^2 y^2 + 1/\mu^2}{[(x - 3\mu^2 t)^2 + \mu^2 y^2 + 1/\mu^2]^2} \quad (4)$$

On fig. 1 we compare the exact solution with the numerical solution for a single point in time when $y = 0$.

One can see the results difference is within the tolerance accepted for purely implicit difference scheme.

In KdVB equation is calculated using a difference scheme, which includes a flux correction procedure. It is interesting to examine the possibility of the use of this approach in our case.

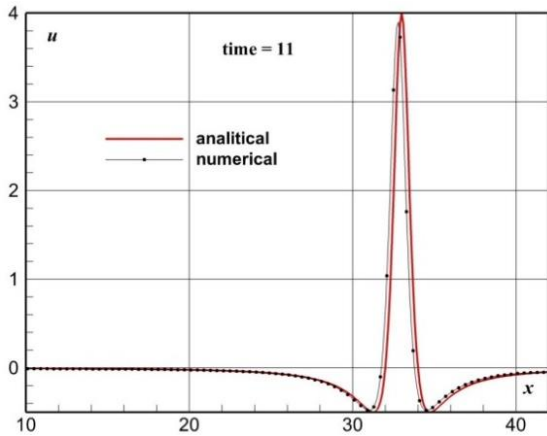


Figure 1: Comparison of exact solution (4) with numerical one for $t = 11$. Mesh being 700×500 , $\Delta x = \Delta y = 0.1$, $\Delta t = 2 \cdot 10^{-5}$, $y = 0$.

Finally, after the analysis carried out after numerical experiments, it was decided not to use, in general, anti-aliasing algorithm. The resulting numerical dispersion ripples did not significantly affect the nature of the perturbations and, most importantly, do not underestimate the amplitude and velocity of the soliton.

Let us consider the dependence of the results of the calculation on the initial distribution. To do this, some of the values of geometrical parameters are necessary to be fixed. The volume of initial perturbation is the same for all figures: $V = 120$.

Calculations were carried out without smoothing procedure up to the time $t = 8$; the number of nodes is 800×700 ; the time step $\Delta t = 5 \cdot 10^{-5}$; mesh steps $\Delta x = \Delta y = 0.1$.

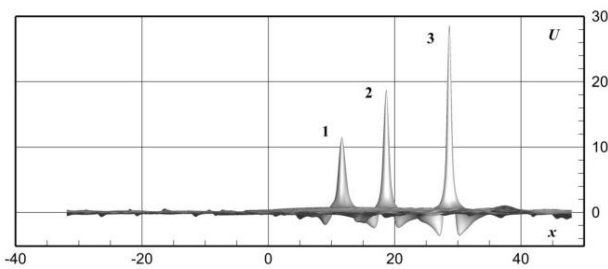


Figure 2: The formation of solitons with different initial distributions for $t = 8$, $V = 120$. Mesh 800×700 , $\Delta x = \Delta y = 0.1$, $\Delta t = 5 \cdot 10^{-5}$, $y = 0$.

As it clearly seen from fig. 2 the largest soliton is formed from the original form of the ellipsoid of revolution.

Consider the initial distribution of Gaussian type, with different volumes. All calculations were performed without anti-aliasing. With the help of numerical simulation we find the situation in which after relatively small increase in volume, compared with the previous value, sharply increases the

amplitude of the resulting soliton. The process is similar to the pressure jump (fig. 3).

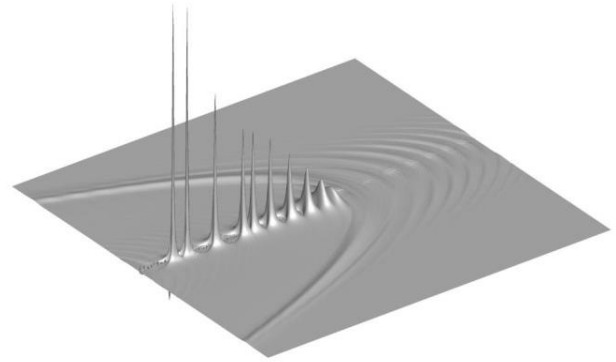


Figure 3: 3D demonstration of an abrupt increase in the soliton amplitude for the initial conditions of the Gaussian form at $t = 7$. Mesh 500×500 , $\Delta t = 10^{-4}$, $\Delta x = \Delta y = 0.2$.

Some problems may appear when the source in rhs is switched on. We have selected a source in the form of an ellipsoid of revolution, as in the case 3 of the initial distribution. Calculations of the equation (1) with a source, a natural analogue of the impact on the water surface, provide numerous options of possible situations with formation of large-amplitude solitons. The source itself generates solitons. Source intensity varies in a wide range. Field exposure source is limited by the natural conditions, but eventually forms a cluster of perturbations, out of which solitons of different amplitudes are formed. For example, we present the evolution of the perturbation without taking into account the initial distribution of any type (see Fig.4).

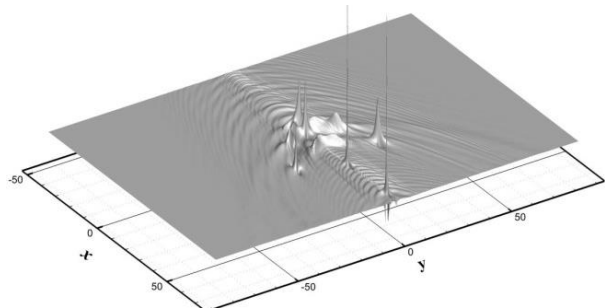


Figure 4: 3D perturbation generated by a source at $t = 15.5$. Mesh 600×850 , $\Delta t = 10^{-4}$, $\Delta x = \Delta y = 0.2$.

CONCLUSIONS

Some indications for choosing of correct numerical procedures from our study can be formulated as follows

1. The proposed scheme has a sufficient resolution for areas with large gradients.

2. Our approach effectively describes the process of soliton formation and propagation with their characteristics preservation.

3. That scheme satisfactorily calculates cases with initial distributions that are not completely integrable.

4. The time step strongly depends on the initial distribution, since the evolution of the perturbation leads to a velocity in the order of magnitude greater than is seen with a linear analog of KPI equation

5. Using of the smoothing procedure leads eventually to an underestimation of the amplitudes of the solitons. The need for a FCT procedure is not obvious.

REFERENCES

Fletcher C.A.J. Computational Techniques for Fluid Dynamics 1. 2nd edition. – Springer-Verlag, 1991. 401 p.

A. Bogdanov, V. Mareev, E. Stankova, Proceedings of the 14th International Ship Stability Workshop (ISSW), 29th September – 1st October 2014, Kuala Lumpur, Malaysia. pp. 242-245.

A. Bogdanov, V. Mareev, Numerical Simulation Perturbed KdVB Equation, EPJ Web of Conferences, Vol. 108, 02014 (2016), [MMCP 2015 Stará Lesná, Slovakia, 2015].

SESSION 5

Damage stability of passenger ships

Holistic Perspective on Damage Stability Standards for RoPax Ships

Jan Bergholtz, *Kattegatt Design AB*, jan.bergholtz@kattagattdesign.se

Tryggve Ahlman, *Swedish Shipowners' Association*, tryggve.ahlman@sweship.se

Martin Schreuder, *Chalmers University of Technology*, martin.schreuder@chalmers.se

Ronnie Hanzén, *Swedish Transport Agency*, ronnie.hanzen@transportstyrelsen.se

Per Wimby, *Stena Teknik*, per.wimby@stena.com

Sten Rosenqvist, *Rederi AB Eckerö*, sten.rosenqvist@rederiabeckero.ax

ABSTRACT

The present paper is intended to outline in brief the work and findings of a Triple-Helix project as initiated by the Swedish Shipowners' Association and concluded in mid-2015. The aim of the study has been to, in light of the ongoing IMO deliberations on revision of SOLAS Chapter II-1, review and evaluate from a holistic perspective, existing as well as proposed amendments to ro-ro passenger ship safety regulations.

Keywords: *Ro-ro passenger ship, damage stability, safety standards, holistic perspective*

1. INTRODUCTION

Ro-ro passenger ship services constitute an important part of the European maritime infrastructure, and indeed play a crucial role for Sweden in connecting seaborne transport routes to and from our neighbouring countries. Moreover, northern European countries have been leading the development of, not only the ro-ro passenger ship concept as such, but also the development of relevant safety standards for this fleet. Understandably, it is therefore crucial for the Swedish maritime sector to take part of the legislative process that covers a significant share of the Swedish maritime infrastructure.

Thus, in light of the ongoing IMO deliberations on revision of SOLAS Chapter II-1 in general and present discussions and proposals for an increased safety standard for passenger ships in particular, a Triple-Helix project has been mobilized by the Swedish Shipowners' Association, focusing on ro-ro passenger ship safety from a holistic perspective.

The aim of the study has been to review and evaluate, from holistic perspective, existing as well as proposed amendments to ro-ro passenger ship safety regulations, with the objectives to:

1. provide in-depth knowledge about and facilitate understanding of existing as well as new proposals for damage stability standards,
2. facilitate understanding of ship type specific characteristics from a safety standard aspect, and
3. if findings allow, develop comprehensive proposals for improvements resulting in a tangible safety enhancement for this ship type.

The present paper is intended to outline in brief the work and findings of the first part of this project as concluded mid-2015 [1]. Funding for a second round has recently been granted.

2. STATE OF PLAY

2.1 Background

As per the entry into force of SOLAS 2009 comprehensive amendments to SOLAS Chapter II-1 related to subdivision and damage stability requirements were introduced. Previous prescriptive concepts such as margin line, floodable length and B/5-subdivision were omitted and replaced by a probability distribution function, p_i , for a certain damage extension along the ship's subdivision length. Moreover, the deterministic assessment of single compartment and group of compartments flooding was replaced by an expression of the probability of "survival", s_i , after damage.

The rationale behind the probabilistic damage stability doctrine as applied within present SOLAS regulations, normally referred to as SOLAS 2009, is in principle based upon the assumption that the survivability of a passenger ship, defined as 50% probability to withstand capsizing for more than 30 minutes following a collision damage in a seaway signified by a critical wave height of H_{Scrit} , can be expressed as a function of the maximum value of the righting lever, GZ_{Max} , and the range of positive stability, GZ_{Range} . A limiting wave height of 4.0m has been derived by means of statistics of prevailing conditions at reported collision damages. Thus, $s_i = 1.0$ means, in principle, a 50% probability to survive (withstand capsizing) the collision damage under consideration for a time period exceeding 30 minutes in a sea state $H_s = 4.0\text{m}$.

Ro-ro passenger ships are conceptually different from other types of passenger ships. In addition to passenger accommodation and recreational areas, nowadays located above the bulkhead deck, this ship type is characterised by large vehicle decks designed for the carriage of rolling cargo which impose an increased risk, should water ingress occur resulting in large free surfaces on these decks. A number of devastating accidents related to this increased risk have occurred, the outcome of which must be regarded as intolerable.

Consequently, over the years and in particular post-ESTONIA northern European maritime administrations, ship owners and ship builders have actively participated in the development of new regulations, such as the so called Stockholm Agreement (SA), aiming at controlling and mitigating the added risk stemming from the conceptual nature of these ship types. The Stockholm Agreement requirements were initially implemented regionally as a practical instrument to attain an improved level of safety in respect of the specific characteristics of the ro-ro passenger ship concept. As of October 1st 2015 the SA requirements are mandatory for all ro-ro passenger ships trading between EU ports, [2], [3].

As per today ro-ro passenger ships are subject to some 20 ship type specific requirements, including design and operational aspects as well as annual Host State Control surveys for ships trafficking in European trades. In addition hereto, it is normal practice amongst at least northern European ship

owners to continuously work with safety related issues, in many cases beyond legislation.

Only a few ro-ro passenger ships currently in operation are designed and built to the SOLAS 2009 standards. Hence, the absolute majority of the ro-ro passenger ship fleet presently serving the European waters are built to SOLAS '90, and nowadays in compliance with the requirements of SA, a safety standard that in principle has never been deemed as insufficient. It could be mentioned that the intention of damage stability requirements as set forth in SOLAS 2009 was not to result in an enhanced safety level when compared to the previous deterministic damage stability standards, but rather to harmonize the subdivision and damage stability standards for passenger and cargo ships, and moreover to develop a modern regulatory framework that would provide an enhanced freedom for the designer to arrange the subdivision of a ship.

During the development of the probabilistic damage stability standards as outlined in SOLAS 2009 it was initially assumed that this safety standard would also accommodate for the risk of water on a vehicle deck. Nevertheless, SOLAS 2009 was questioned already before its entry into force. The criticism has primarily been related to the methodology's ability to correctly address water on deck (WOD) when assessing damage stability for ro-ro passenger ships.

2.2 Passenger Ships in General

With reference to the outcome of several research projects, such as the EMSA 1 and 2 and the GOALDS project, the WOD-issue has been extensively debated within the IMO and in particular within SLF, the former sub-committee to MSC. When now SOLAS Chpt II-1 is again subject to revision, amendments emanating from SLF 55, [8], to the calculation procedures of the survivability factor s_i for ro-ro passenger ships have been proposed, aiming at providing an equivalent safety standard when compared to the Stockholm Agreement for damage cases involving vehicle decks.

In addition, catalysed by the Costa Concordia disaster, the debate was later extended to include also the overall "safety level" for passenger ships in general, expressed by the required subdivision index R . Thus, a third research study was initiated and funded by EMSA, the so called EMSA 3, [10], the

results of which, as conveyed by the EU, [11], have constituted the basis for a proposal of the IMO MSC sub-committee SDC in terms of a new formulation of the required subdivision index R that is expected to provide an adequate raise in the “safety level” for passenger ships, [13], see Figure 1. The proposal is, at the time of writing, being discussed at the IMO MSC 96 with a view for approval at this session and adoption at MSC 97.

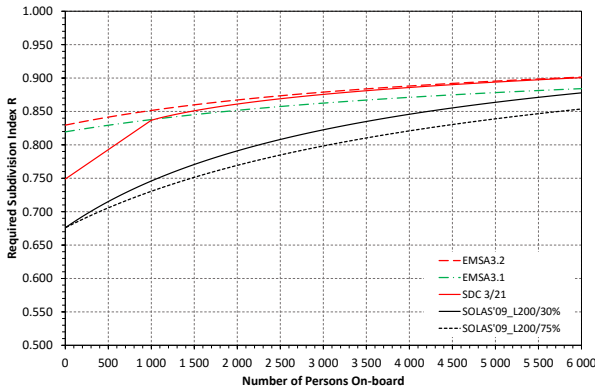


Figure 1: Graphical representation of the new formulation of Index R as proposed in SDC 3/21

The linear part of the index R line, from zero to 1 000 persons, is intended to accommodate for the fact that smaller ship were not very well represented in the EMSA 3 study. Moreover, from 1 000 to 6 000 persons on-board the proposed index R curve has been adjusted so as to fit between the EMSA 3.1 line that represents cost effective designs in respect of collision damages and the EMSA 3.2 line that represents cost effective designs in respect of both collision and grounding/raking damages.

2.3 Specific Requirements for RoPax Ships

In addition to the raise in index R for all passenger ships, also the WOD-mechanism stemming from SLF 55 for a more strict calculation procedure of the survivability factor, s_i , for ro-ro passenger ships, whenever the respective damage case under consideration involves a vehicle deck, has been incorporated into the SDC 3 proposal, [13]. Nonetheless, it has been indicated by EU COM that for ships trading between EU ports, compliance must still be demonstrated also with regard to the Stockholm Agreement as it is prescribed in Directive 2003/25/EC, [2].

2.4 Specific Requirements for SP Ships

It could be noted that a corresponding raise in safety standard to a “societal acceptance level” for Special Purpose Ships has not been deemed as necessary. Hence, for the purpose of calculating the required subdivision index for SP-ships the equation as provided in the present Regulation 6 of Chpt II-1 of SOLAS 2009 is retained, [13].

3. SURVIVABILITY FROM HOLISTIC PERSPECTIVES

In the statutory context of ships’ stability, the expression “Survivability” is normally assigned to the s-factor as defined in SOLAS II-1 Reg. 7-2, in which s_i accounts for the probability of not to capsize within 30 minutes in a specific sea state after flooding the compartment or group of compartments under consideration. Nonetheless, for the purpose of the present study the expression “Holistic Survivability” simply means the ability to control and mitigate the risk of loss of life on-board a passenger ship and entails both inherent as well as operating conditions.

Even though a significant part of the survivability of a passenger ship is composed of an adequate degree of inherent safety, e.g. a built-in capability to withstand collision or grounding without catastrophic consequences, as stipulated in the statutory requirements, the total safety of a ship from a holistic perspective is to a large extent also depending on a number of other elements, such as:

- Operational Considerations / Trading Area
- Proactive Safety Management
- Decision Support
- Emergency Safety Procedures
- Evacuation Procedures

The above listed elements are all addressed in relevant chapters of the ISM Code and play a paramount role for breaking the chain of events during the development of an incident/accident before reaching an irreversible level.

As structured way of assessing conceivable chain of events which may eventually lead to an irreversible stage when the risk of loss of lives is inevitable, is presented in Figure 2, below, in which levels for different consequences during the escalation of an accident and required corresponding control and mitigation actions are presented.

Level	Events					Action
Fatal Level	Loss of Lives and / or Ship					
Irreversible Level	Capsizing / Sinking		Uncontrolled Fire			Evacuation / Abandon Ship
Significant Level	Uncontrolled Free Surfaces ISM 8	Loss of Reserve Buoyancy ISM 8	Loss of Residual Stability ISM 8	Shift in CoG ISM 8	Unforeseen Flooding ISM 8	Mustering
Secondary Consequences	Listing / Heeling Angle ISM 8, 4	Damaged WT Integrity ISM 8, 4	Internal Flooding ISM 8, 4	Local Fire ISM 8, 4	Impact / Explosion Shock ISM 8, 4	Chain Breakers Decision Support
Primary Consequences	Structural Damage ISM 7, 4, 8	Collision ISM 7, 8, 4	Grounding Stranding ISM 7, 8, 4	Unforeseen Heeling Mom. ISM 7, 8, 4, 10	Fire Ignition ISM 7, 8, 4	Alarm / Decision Support
Incidents / Triggers	Technical Malfunction ISM 10	Navigation Error ISM 6	Lack of Training / Profession ISM 6.3	Unforeseen Environmental Conditions ISM 7	Incorrect Cargo Handling ISM 7	Awareness / Alert
Basic Functions / Qualities	Quality in Design ISM 1.2.2	Regulatory Efficiency ISM 1.2.2	Operational Quality ISM 1.2.2	Quality of Ext. Support Funct. ISM 1.2.3.7		Quality Assurance / Surveillance

Figure 2: Matrix for a Holistic Assessment of Safety Management

The matrix as was initially developed by the DESSO Project, [15], but has been expanded to also include applicable regulations of the ISM Code. Obviously the matrix can be further developed, but still in its present form, it facilitates the understanding of vulnerabilities in survivability from a holistic perspective and might further be used to illustrate what proactive safety work is needed in order to enhance the holistic survivability.

4. FINDINGS AND CONCLUSIONS

With reference to the Swedish Triple-Helix study on ro-ro passenger ship safety from a holistic perspective, [1], and to the development of the regulatory framework as outlined in the above, some findings and conclusions are presented in the below sub-sections.

4.1 Proposal for new formulation of index R

Based upon the experience of at least some of the few ro-ro passenger ships built to SOLAS 2009 it can be concluded that the methodology to take into account the effect of Water on Deck (WOD) referred to as the Stockholm Agreement (SA) normally governs the design. Hence, it seems reasonable to conclude that SA allows for some margin with regard to the requirements of SOLAS 2009 that justifies a corresponding raise of the required subdivision index R, see Figure 3.

4.2 Influence of the SLF 55 WOD-mechanism

In addition to the raise of index R the proposed amendments to SOLAS II-1 are in part also based on the WOD-mechanism as proposed by SFL 55, in which a more strict procedure for the calculation of

the survivability factor, s_i , is to be applied for ro-ro passenger ships, whenever the respective damage case under consideration involves a vehicle deck. The graph in Figure 3 illustrates the consequences for some few existing ro-ro passenger ships built to SOLAS 2009 and in compliance with SA. For one of these ships, a 600 persons RoPax built to SOLAS 2009+SA, the subdivision index margin emanating from SA has been presented. Moreover, the influence of an indicative 3% subdivision index reduction due to the SLF 55 WOD-mechanism has been plotted in the graph.

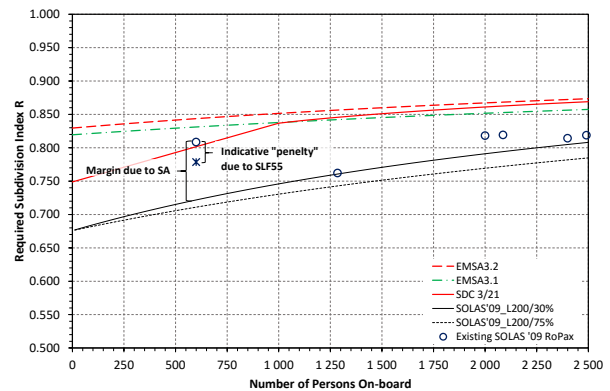


Figure 3: Graphical representation of consequences for some SOLAS '09 ro-ro passenger ships in relation to proposed new formulation of index R

In addition to a pronounced spread, e.g. 3-12% in terms of index A-reduction as reported in the Danish study, [12], in the opinion of the authors the effect of the SLF 55-proposal is rather unclear. The results of the Swedish study, [1], show that when applying the SLF 55 WOD-mechanism; for damage cases of lesser extent resulting in a limited loss of buoyancy and hence rendering a relative high residual freeboard the most effective Risk Control Option, RCO, would be an increase in G'M, see Figure 4. Whereas for damage cases of larger extent where the residual freeboard is relatively low or even negative, the most effective RCO would obviously be to increase the original freeboard, see Figure 5.

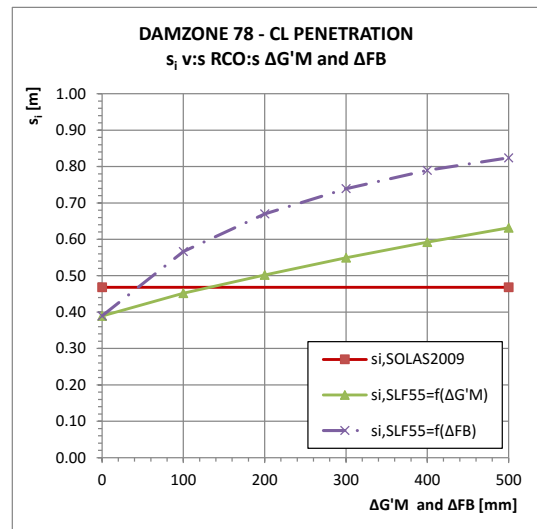
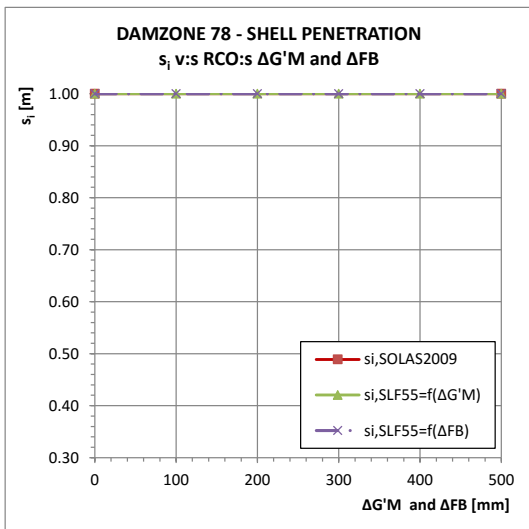
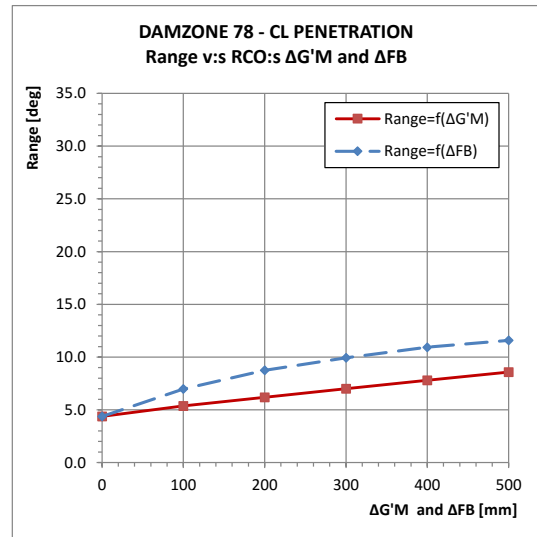
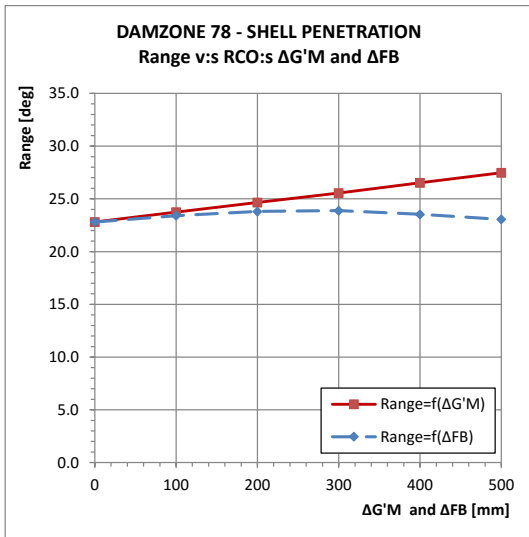
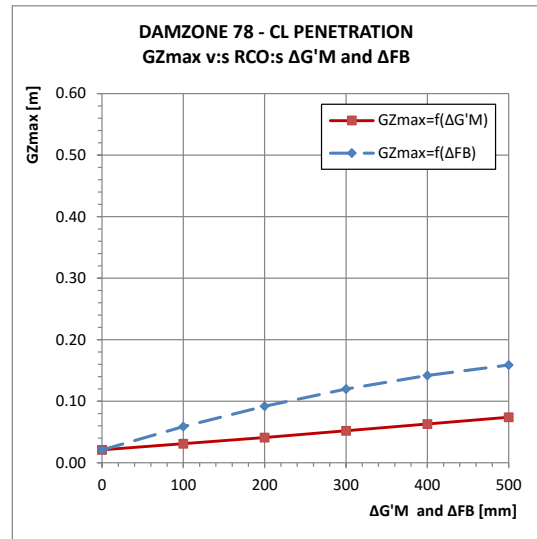
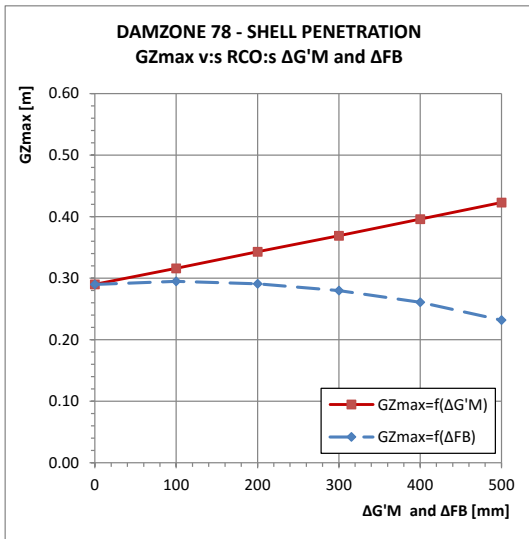


Figure 4: Evaluation of influence of the RCO:s $\Delta G'M$ and ΔFB when applying the SLF 55 WOD-mechanism – Damage Cases of lesser extent, [1]

Figure 5: Evaluation of influence of the RCO:s $\Delta G'M$ and ΔFB when applying the SLF 55 WOD-mechanism – Damage Cases of larger extent, [1]

However, as the attained subdivision index A is composed of the product sum of the probability factor, p_i , and of the survivability, s_i , for all damage cases, the respective damage extension probability distribution evidently plays some role in the overall outcome. Nonetheless, whenever the influence of the vertical probability distribution factor, v , is comparably high, it seems reasonable that the SLF 55 proposal will stimulate to some degree an increased freeboard height for new designs.

While the WOD-mechanism of the Stockholm Agreement is directly related to the residual freeboard, the SLF 55 WOD-mechanism is based on the characteristic of the GZ-curve up to 20 deg. in terms of the survivability factor s_i . Hence, in addition to the residual freeboard, the SFL 55 WOD-results are also strongly related to the metacentric height, G'M.

The EU proposal, [11] for a new formulation of index R is based upon the results of the EMSA 3 study, but also datasets from a German Study, [9], from the GOALDS project, [5], [6], [7], and from a Danish study, [12] have been considered. The later study encompasses six smaller ro-ro passenger ships for which the loading conditions have been modified, all of which resulting in increased metacentric heights, in order to attain compliance with the proposed new level of index R while applying also the SLF 55 WOD-mechanism. It could be noted that the G'M-values, as reported for some cases of this study, might render high lateral accelerations resulting in secondary problems for passengers, crew and for the securing of cargo.

Moreover, for a given set of hull lines, in particular a constant KM-value, an increase in freeboard renders a decrease in G'M due to the vertical shift of the payload on the bulkhead deck and consequently a decrease in the survivability factor s_i . Hence, for a constant "business case" it seems reasonable to assume that the proposed raise in index R together with the reduction of index A due to the SLF 55 WOD-mechanism, will impose wider beams of future ro-ro passenger ships.

In addition, it should be noted that the application of the existing Stockholm Agreement includes an operational aspect in terms of a sea state defined by the significant wave height H_s up to which the ship under consideration is intended to operate. In many cases, due to the respective trading

area, ro-ro passenger ships are designed for a significantly lesser sea state than represented by $H_{SCr} = 4.0\text{m}$ (a first quick inventory reveals that approximately 50% of the ships operating in the Baltic region are designed for $H_{SCr} < 4.0\text{m}$). This aspect is cancelled out by the implementation of the SLF 55 proposal.

It has also not been perfectly clear within the Swedish project, how the influence of Barriers on the Vehicle Decks will be taken into account within the when applying the SLF 55 WOD-mechanism. Even though obstructions on vehicle decks are normally avoided as far as practicable, the arrangement of WOD-barriers must be considered as a rather efficient RCO, and may for some cases constitute the only viable option to enhance the WOD-characteristics.

4.3 Influence of Lower Holds

It could be noted that none of the four generic ro-ro passenger ship designs constituting the basis for the EMSA 3 study were arranged with lower holds. Hence, the influence of lower hold arrangements, which when arranged normally provides for about 15% of the payload capacity, has not been considered in the proposal for a new formulation of index R. However, as indicated in Figure 3, from the attained index A for the 600 persons SOLAS 2009+SA ro-ro passenger ship which actually is arranged with a lower hold, it seems reasonable to assume that some payload capacity may be arranged in lower holds also in a future perspective, at least for the "smaller" ships. Nonetheless, for the relatively large ro-ro passenger ships arrangements of lower holds seem not to be feasible in a future perspective. Consequently, for a constant "business case" this payload needs to be carried on higher decks, yet again imposing an increased beam to compensate for the loss of G'M and/or to accommodate for the stowage of the payload. Alternatively, a reduced dwt-capacity may have to be accepted.

4.4 Inclusion of RCO:s to mitigate Collision+ Grounding Damage Scenarios

As indicated in Figure 1 in the above, the proposal for a new formulation of the index R includes investments in RCO:s to account also for grounding/raking damages, even though the EMSA 3 project itself has acknowledged that the calculation methodology for grounding damages is still not

mature enough to be implemented in a regulatory framework. The justification for adjusting the index R curve between the collision level and the collision + grounding level is based on a reasoning that for the examined cruise ships grounding/raking represents a significantly higher risk than collisions and that there is a clear trend that RCOs improving the attained index A for collision would also improve the attained index A for grounding. Nevertheless, in the opinion of the authors, it seems somewhat difficult to acknowledge the same trend for ro-ro passenger ships as these ships by necessity are arranged as to minimize asymmetries resulting in pronounced list following a damage. Thus, it is difficult to recognize that any grounding/raking damage scenario that would significantly differ from a corresponding collision damage. However, in the opinion of the authors, if such a damage case would anyhow be identified it should be adequately addressed by the existing regulation 7.5 and 7.6 in SOLAS II-1, which in principle are related to arrangement of wing tanks and vertical extent of damage assumptions while taking into consideration also damages of lesser extent.

4.5 Holistic Perspectives

Whenever new regulations are introduced it is obviously of vital importance that these regulations are compatible and coherent with relevant requirements of other instruments or codes and that necessary consequential amendments are developed. Explanatory notes and unified interpretations must to the furthest degree be present at entry into force. Even though a large amount of work has been successfully completed, it is noted that some efforts still remain, e.g. such as arrangements and control of WT doors and of essential systems.

In addition, as long as compliance is required also with the WOD-mechanism as set forth in the Stockholm Agreement, [2], which originates from a deterministic assessment of prescriptive damage assumptions, it might be difficult to utilize in full the so called freedom for the designer that has been argued to constitute one of the main objectives for implementing a goal based standard in terms of the probabilistic damage stability doctrine.

Moreover, since the probabilistic damage stability calculations are pertinent primarily to the inherent safety standard of a ship in terms subdivision and the overall result of the assessment

is presented as an attained subdivision index A, it seems reasonable that utmost efforts must be made as to provide to the crew comprehensive yet unambiguous information about the ships ability to withstand all relevant damage scenarios, for all representative loading conditions. An adequate decision support is obviously vital when immediate actions must be taken in order to break the chain of events during the escalation of an incident / accident, or in worst case if evacuation is deemed necessary.

The importance of other factors than “safety-by-design” such as operational limitations and guidance has also been recognised within the development of the second generation intact stability criteria, [14].

5. ACKNOWLEDGEMENTS

The authors would like to express their gratitude to the Swedish Maritime Administration for granting financial support to the project as outlined herein.

6. REFERENCES

- [1] Ahlman T, et al., 2015, "Damage Stability Project for: RoRo Passenger Ships – Final Report"
- [2] Directive 2003/25/EC of the European Parliament and of the Council of 14 April 2003, "on specific stability requirements for ro-ro passenger ships"
- [3] Directive 2009/45/EC of the European Parliament and of the Council of 6 April 2009, "on safety rules and standards for passenger ships"
- [4] IMO SLF 55, 2012, "Review of the Damage Stability Regulations for Ro-Ro Passenger Ships - Damage stability parameters of ro-ro passenger ships according to SOLAS 2009 amendments, including water-on-deck calculations", SLF 55/INF.6
- [5] IMO SLF 55, 2012, "Revision of the Damage Stability Regulations for Ro-Ro Passenger Ships - The GOAL based Damage Stability project (GOALDS) – Derivation of updated probability distributions of collision and grounding damage characteristics for passenger ships", SLF 55/INF.7
- [6] IMO SLF 55, 2012, "Revision of the Damage Stability Regulations for Ro-Ro Passenger Ships - The GOAL based Damage Stability project (GOALDS) – Derivation of updated probability of survival for passenger ships", SLF 55/INF.8
- [7] IMO SLF 55, 2012, "Revision of the Damage Stability Regulations for Ro-Ro Passenger Ships - The GOAL based Damage Stability project (GOALDS) – Development of a new risk-based damage stability requirement for passenger ships based on Cost-Benefit Assessment", SLF 55/INF.9
- [8] IMO SLF 55, 2012, "Revision of SOLAS Chapter II-1 Subdivision and Damage Stability Regulations - Improving the survivability of ro-ro passenger ships", SLF 55/INF.13
- [9] IMO SDC 2, 2014, "Revision of SOLAS II-1 Subdivision and Damage Stability Regulations - Proposals to improve passenger ship survivability after damage", SDC 2/INF.3
- [10] European Maritime Safety Agency, 2015, "Combined assessment of cost-effectiveness of previous parts, FSA compilation and recommendations for decision making", EMSA /OP/10/2013, Report No. 2015-0404, Rev.1 Doc. No. 18KJ9LI-60
- [11] IMO SDC 3, 2016, "Amendments to SOLAS Regulations II-1/6 and II-1/8-1 - Proposals for the required subdivision index 'R'", SDC 3/3/7
- [12] IMO SDC 3, 2016, "Amendments to SOLAS Regulations II-1/6 and II-1/8-1 – Small ro/pax ship stability study", SDC 3/INF.4
- [13] IMO SDC 3, 2016, "Report to the Maritime Safety Committee", SDC 3/21
- [14] IMO SDC 3, 2016, "Finalization of Second-Generation Intact Stability Criteria - Material relevant to operational guidance and operational limitations", SDC 3/INF.15
- [15] Björn Allenström (editor), 2006, "DESSO-Design for survival onboard", SSPA Research Report No, 132, ISBN 91-86532-45-6, ISSN 0282-5805

An alternative system for damage stability enhancement

Dracos Vassalos, *University of Strathclyde*, d.vassalos@strath.ac.uk

Evangelos Boulougouris, *University of Strathclyde*, evangelos.boulougouris@strath.ac.uk

Donald Paterson, *University of Strathclyde*, donald.paterson@strath.ac.uk

ABSTRACT

There is an ongoing and continuous initiative to improve the survivability of passenger vessels and in the past increasing safety standards have generally been catered for through the use of design(passive) measures. However, this approach is becoming saturated and any such measures to improve damage stability severely erode ship earning potential and are being resisted by industry. In a change of direction, this paper aims to explore the use of operational(active) measures for damage stability enhancement in line with IMO Circular 1455 on equivalents. An alternative system for damage stability enhancement is introduced that involves injecting highly expandable foam in the compartment(s) undergoing flooding during the initial post-accident flooding phase thus enhancing damage stability and survivability of RoPax vessels well beyond the design levels in the most cost-effective way currently available. This is a mind-set changing innovation that is likely to revolutionise design and operation of most ship types and RoPax, in particular. A case study has been performed on a large RoPax vessel with impressive results that will challenge the current established practice and open possibilities for novel and innovative design configurations.

Keywords: *Damage Stability, Passenger Ship Safety, Risk Reduction*

1. INTRODUCTION

Every time there is an accident with RoRo passenger ships, exposing their vulnerability to flooding, societal outcry follows and industry and academia “buckle up”, delving for design improvements to address the Achilles heel of this ship type, namely damage stability. However, any such improvements are targeting mainly newbuildings, which comprise a small minority of the existing fleet. Therefore, state-of-the-art knowledge on damage stability is all but wasted, scratching only the surface of the problem and leaving a high amount of ships with severe vulnerability, that is likely to lead to further (unacceptably high) loss of life. This problem is exacerbated still further, today more rapidly, as the pace of scientific and technological developments is unrelenting, raising understanding and capability to address damage stability improvements of newbuildings cost-effectively, in ways not previously considered. As a result, SOLAS is becoming progressively less relevant and unable to keep up with this pace of development. This has led to gaps and pitfalls, which not only undermine safety but inhibit progress.

However, lack of retrospectively applied legislation (supported by what is commonly known as the Grandfather Clause) is not the only reason for damage stability problems with ships. Tradition should share the blame here. In the quest for damage stability improvement, design (passive) measures have traditionally been the only means to achieve it in a measurable/auditable way (SOLAS 2009, Ch. II-1). However, in principle, the consequences from inadequate damage stability can also be reduced by operational (active) measures, which may be very effective in minimising loss of life (the residual risk). There are two reasons for this. The first relates to the traditional understanding that operational measures safeguard against erosion of the design safety envelop (possible increase of residual risk over time). The second derives from lack of measurement and verification of the risk reduction potential of any active measures. In simple terms, what is needed is the means to account for risk reduction by operational means as well as measures that may be taken during emergencies. Such risk reduction may then be considered alongside risk reduction deriving from design measures. IMO Circular 1455 on Alternatives and Equivalents offers the means for this.

This paper introduces an alternative system for damage stability enhancement that involves injecting highly expandable foam in the compartment(s) undergoing flooding during the initial post-accident flooding phase thus enhancing damage stability and survivability of RoPax vessels well beyond the design levels in the most cost-effective way currently available.

2. DAMAGE STABILITY RECOVERY SYSTEM (DSRS)

Whilst the safety of RoPax is improving, the survivability in case of a serious incident such as hull breach due to collision or grounding, resulting in water ingress, is still relatively low, particularly with most of the existing ships.

Deriving from the foregoing, the following arguments may be put forward:

- Design (passive) measures are saturated. Hence, any such measures to improve damage stability severely erode the ship earning potential and are being resisted by industry.
- Traditionally, the industry is averse to operational (active) measures and it takes perseverance and nurturing to change this norm.
- Up until recently, there was no legislative instrument to assign credit for safety improvement by active means. Only recently IMO Circular 1455 opened the door to such innovation.
- Key industry stakeholders are keen to explore this route.

Inspired by these considerations and with support from Scottish Enterprise, the University of Strathclyde is involved with R&D of a system, patent pending, that can be fitted to new or retrofitted to existing RoPax in order to reduce the likelihood of capsizing/sinking and further water ingress following a major incident / accident.

The working principle of the proposed system is simple: when a vessel is subjected to a critical damage, stability is recovered through the reduction of floodable volume within the vessel's high risk compartment(s). This is achieved by rapidly distributing fast setting, high expansion foam to the protected compartment(s), regaining lost buoyancy whilst also eliminating free surface effects and

forming a near watertight seal over unprotected openings. Moreover, with water being constrained low in the ship, it actually increases damage stability (Lower KG).

The system itself consists of a fixed supply of both foam resin and hardener agents; each stored within an individual tank and connected to a piping network for distribution. The operation of the system starts when two distribution pumps supply a flow of filtered sea water into individual resin and hardener lines. Both streams are then dosed with concentrated resin and hardener agents, before they each pass through a static mixer in order to produce a homogeneous solution of each component.

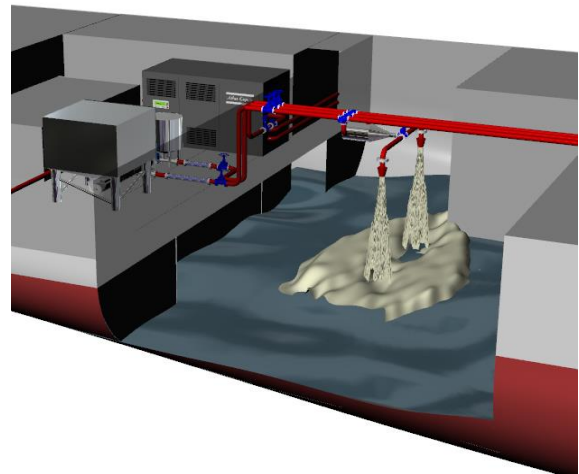


Figure 1 - System Representation

The two lines are then fed to the protected compartment where they meet and enter a foam generator. Here both streams mix and compressed air is introduced into the system for the in situ production of foam. The foam is then passed in to a branched piping network within the vulnerable compartment where both port and starboard side branches allow the foam distribution to be directed depending on the damage side.

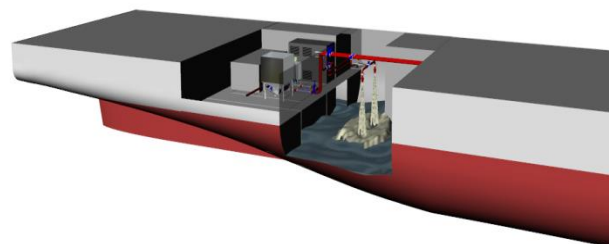


Figure 2 - System Representation

The whole process is monitored and controlled by a central system linked to vital components and sensors. The use of the system is under the full control of the crew, with a decision support system available to help the ship’s master decide where and when the system will act as well as inform all concerned of the ensuing actions.

The foam compound meets all the environmental and health criteria, it is not harmful to humans and its release does not pose any danger to the people onboard or the environment. Furthermore the foam is non-flammable and in this respect could reduce risk by other event sequences such as a fire ignited in collision. The residual clean-up post system discharge is also aided by a foam dissolving agent ensuring minimal business interruption.

3. METHODOLOGY

For the purposes of this study a large ROPAX vessel, currently operating in European waters, has been investigated with a view to assess the effectiveness of the proposed Damaged Stability Recovery System (DSRS) as a risk reduction technology. A case study has been conducted on the vessel using the probabilistic approach to damage stability (SOLAS 2009) as a means of establishing the initial level of risk associated with the design. The effects of the DSRS have then been modelled and the vessel re-examined in order to assess the risk reduction afforded by the system.

DSRS Implementation & Modelling

In order to ascertain the impact of the proposed system on vessel safety, the overall risk level associated with the vessel had to first be identified. As the attained index A represents the safety level of the vessel, the overall risk, with regards to collision damage, could be calculated according to the simple formula below.

$$Risk_{total} = 1 - A \tag{1}$$

This provided a benchmark from which to gauge any improvement on the vessel’s safety afforded by the DSRS.

In order to ensure the system was applied in the most efficient manner it was reasoned that the compartment(s) protected by the system should be those which constituted the greatest risk. As such, a risk profile of the vessel was created in order to aid in the identification of design vulnerabilities. This then provided the foundation from which a risk influenced decision could be made with regards to the compartment(s) that should be protected by the system while also highlighting the circumstances under which this protection is necessary.

The results from the probabilistic damage stability assessment afforded a straightforward way of determining the vessel’s risk profile by firstly considering the local risk associate with each damage scenario, as calculated by (Eq. 2).

$$Risk_{local} = p_i \cdot (1 - s_i) \tag{2}$$

These local risk values could then be mapped across the vessel according to damage centre in order to form the example risk profile as shown in figure 3.

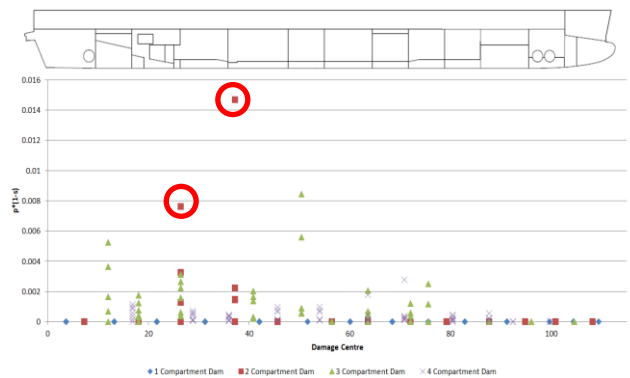


Figure 3: Example Risk Profile

In the above risk profile, risk is plotted on the vertical axis and the damage position along the horizontal. Differing lengths of damage, as measured by multiples of adjacent zones, are distinguished by marker type and colour. This enables the identification of both safety critical design spots and opportunities where safety could be improved most significantly and efficiently. Two cases in particular, circled in Fig. 3, are identified as large risk contributors. As such, it can be reasoned that the DSRS would be best applied in the protection of one if not both of the compartments which give rise to this risk.

Following this methodology for the sample vessel, the system could be applied in the most efficient and effective manner.

The analysis for the case study was conducted through modelling the vessel from the original GA and lines plans. Relevant stability documentation was used in order to ensure all unprotected and weather tight openings were taken into account. Loading condition information within the vessel’s stability booklet was used in conjunction with the damage stability GM limiting curves in order to select the SOLAS 2009 initial loading conditions.

The effects of the DSRS system were modeled through alterations to the permeability of the protected compartment(s) to account for the effect of the foam. The required volume of foam was taken as the minimum volume required to save the most demanding high risk damage scenario.

The scope of the investigation saw a one and two compartment approach to system application whereby the impact of the system was assessed when protecting the highest risk compartment and also the two highest risk compartments.

4. CASE STUDY: LARGE ROPAX

Overview

The vessel is a large ROPAX with a central cased ro-ro deck suitable for drive through operations. Further capacity is offered by a large lower hold spanning from compartments nine to fifteen. The vessel is also equipped with a hoistable car deck suitable for additional car storage. Accommodation for passengers is located within the vessel’s superstructure with cabins available for overnight journeys along with a range of public spaces including a shopping center, cinema, restaurants and bars.

The vessel was built in 1998 to a two-compartment subdivision standard according to SOLAS 90’ along with Stockholm agreement compliance with a significant wave height of 2.9m. Below the bulkhead deck the vessel is divided into a total of twenty water tight compartments and has pronounced B/5 subdivision spanning almost the entire length of the vessel and cross flooding ducts fitted to enable symmetrical flooding.

The vessel’s principal particulars and general arrangement are provided in table 1 and figure 4.

Principle Particulars	
Length o.a (m)	200.65
Length b.p (m)	185.4
Breadth (m)	25.8
Draught MLD. (m)	6.8
Displacement (t)	19468
Deadweight (t)	5830
Crew Number	200 persons
Passenger Number	1500 persons

Table 1: Principal Particulars

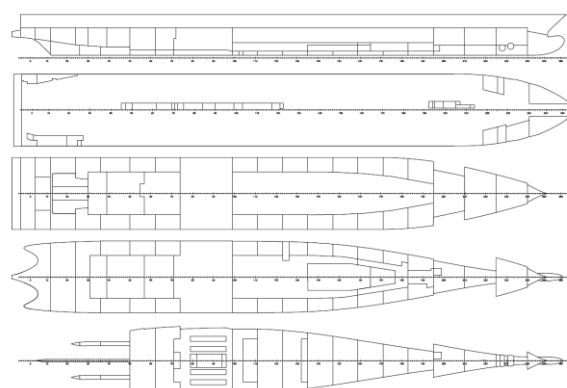


Figure 4: General Arrangement

Stability Assessment

In order to assess the damage stability performance of the vessel a total of 942 damage cases have been analysed under three loading conditions as outlined in table 2.

Table 2: Loading Conditions

	Displacement (t)	Draft(m)	GM(m)
LC1 (dl)	19468	6.8	2.226
LC2 (dp)	17412	6.4	2.003
LC3 (ds)	15087	5.733	3.191

The results of the SOLAS 2009 damage stability assessment along with the required index value calculated for this vessel can be found in table 3 below. The risk profile derived for the vessel is also provided in figure 5.

Table 3: SOLAS 2009 Results

As	0.79
Ap	0.80
AI	0.96
Attained index A	0.83
Required index R	0.795

Table 4: Re-calculated Index Values

AI	0.96
Ap	0.85
As	0.84
New Attained Index A	0.87

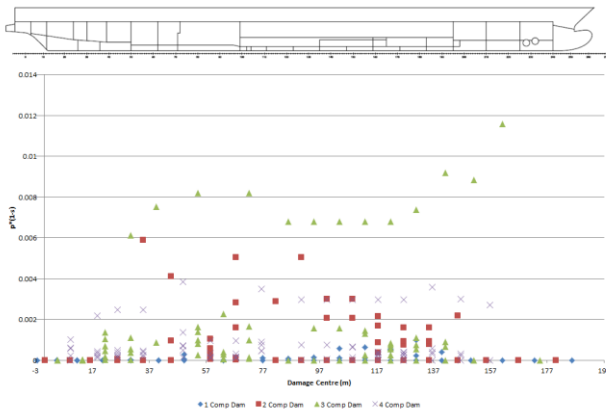


Figure 5: Risk Profile

It is noted that the required subdivision index is fulfilled with a reasonable margin in this case. However, observation of the vessels risk profile reveals several vulnerabilities existing within the vessel’s design. This risk is founded primarily by damages that penetrate beyond the B/5 longitudinal bulkhead of the lower hold. Damages involving this space were not covered by the regulations in place at the time although they do however present a significant threat to the vessel’s safety.

Damage to the lower hold gives rise to large scale flooding leading to a significant reduction in the vessel’s residual stability. Having been identified as the largest risk contributor this space was selected for application of the system.

The volume of foam required in this case was defined as that required to mitigate the risk stemming from two compartment damages involving the lower hold, equating 2000m³ expanded volume. The damage stability performance was then re-assessed following a permeability change to the lower hold to account for the effects of the foam.

The new attained index values calculated in this case can be found in table 4 along with the updated risk profile of the vessel highlighted in figure 6.

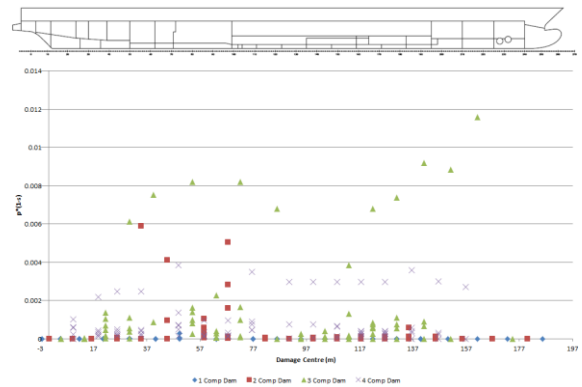


Figure 6: Updated Risk Profile

It is clear from the newly calculated results that the effects of the system have resulted in a substantial reduction of risk. This is evident in the eradication of the risk contribution made by one and two compartment damages involving the vessel’s lower hold. The risk stemming from three compartment damages to this space has also been mitigated, particularly in those damages located closer to amidships. Unfortunately there still exists a series of high risk three compartment damages towards the fore of the lower hold and mitigation of these risks would call for a larger volume of foam to be utilised. In total the system has resulted in a 130% risk reduction for a one compartment application.

Selection of the second compartment for system protection involved re-evaluation of the vessel’s risk profile. Through doing so, the vessel’s main engine room was identified as the largest of the remaining risk contributors. This particular space has a large volume coupled with a high permeability value leading to large scale flooding when damaged and serious diminishment of the vessel’s residual stability.

As the one compartment system application required an already large volume of foam the decision was made to use a constant volume of available foam in the investigation of two compartment protection. As such, the volume of foam was shared between the two protected

compartments in such cases that they were simultaneously damaged. When either of the protected compartments was damaged independently the entire volume of foam was assumed to be used for the damaged compartment in question.

The damage stability results following this process are provided in table 5 and the vessel's updated risk profile is provided in figure 7.

5. CONCLUSIONS

By combining expertise in ship damage stability and specialist knowledge in expanding foams, a non-intrusive cost effective solution to the damage stability problem of ROPAX vessels has been identified that does not interfere with the existing characteristics of the vessel, its functionality or business model, enabling the vessel to remain competitive while being above all safer.

Table 5: Re-calculated Index Values

Al	0.97
Ap	0.86
As	0.85
New Attained Index A	0.88

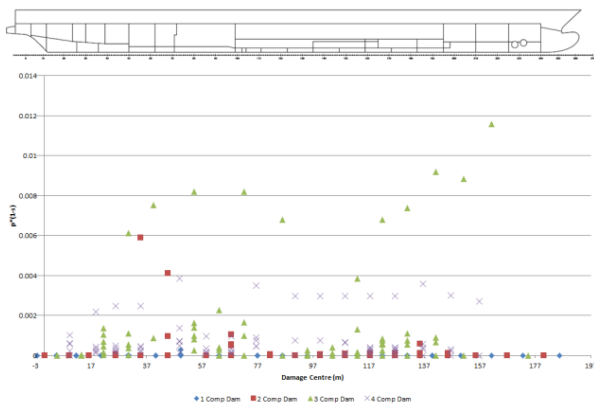


Figure 7 : Updated Risk Profile

The results in this case show that the protection of two compartments has worked to mitigate the risk stemming from damages to the main engine room but failed to eradicate these risks. In total, there has been a relative 8% additional risk reduction afforded by this further protection. In order to generate a more meaningful reduction in risk, either a larger volume of foam would be required or the range of compartments served by the system would have to be increased. The system was however able to produce an overall risk reduction of 136%.

On damaged ship survivability assessment in design and operation of passenger ships

Jakub Cichowicz, *Brookes Bell Safety at Sea*, jakub.cichowicz@brookesbell.com

Alistair Murphy, *Brookes Bell Safety at Sea*, alistair.murphy@brookesbell.com

ABSTRACT

This paper presents an alternative to SOLAS formulation for assessing damage survivability of passenger ships.

Keywords: *survivability, damage stability, SOLAS, GOALDS*

1. INTRODUCTION

In SOLAS damage stability regulations the probability of surviving (collision) damages is given in the form of s-factor - an empirical formula derived within research project HARDER (1999-2003) and subsequently adopted by IMO for the harmonised damage stability framework often referred to as SOLAS2009. Although the new framework is based on the same principle as the earlier probabilistic instrument (resolution A.265) –in principle it requires that the attained index of subdivision A (i.e. the average probability of surviving collision damage) is at least equal to the required index R - the individual building blocks of the regulations were revisited during the harmonisation process. In the case of s-factor it led to radical change in the survivability model and understandable concerns with respect to robustness and reliability of the new formulation. Given the step change to the model the recurring question was whether the new formulation preserves the safety level of deterministic approach or that of the resolution A.265. Although a definitive answer to this question could not be given the common perception was that the SOLAS 2009 overestimates survivability of RoPax ships and underestimates safety of cruise ships. In order to investigate and resolve the issue, soon after the regulations went into force, two large cooperative research were established. One study, financed by the European Maritime Safety Agency (EMSA) looked into survivability of RoPax ships whereas the other, EU-funded, project GOALDS aimed at all passenger vessels and attempted to provide the survivability measure for collision and grounding damages.

The model discussed in this paper has been derived in the project GOALDS.

2. COMMON ASSESSMENT METHODS

The process of a ship loss following hull breach and flooding to internal spaces is driven by a number of random variables with loading conditions, sea state in the moment of incident and damage extent all having great impact on chances of survival. In specific damage case loading conditions, damage extent and even sea state are all determined but the excitation and ship response are both random (stochastic) processes. This, even under assumption of stationary character of the processes, requires significant number of trials to be conducted in order to assess probability of surviving collision or grounding damages with reasonable accuracy. How accurate the assessment is depends on many factors but the most important of them is the method employed in testing.

Physical experiments

The most traditional method is based on physical experiments with a ship model positioned in a towing tank and subjected to action of beam seas. Such tests are easy to conduct and are thought to represent well the dynamics of damaged and flooded ship but they are expensive, allow for very limited and difficult control of trial parameters and suffer from poor repeatability.

On the other end of the spectrum there are CFD calculations, flexible and readily manageable and allowing for detailed modelling of flooding even in complex arrangements. This allows achieving high-accuracy predictions but comes at the expense of computational effort. This makes the CFD-based

calculations a great tool for verification or high-resolution investigations (e.g. sloshing) but renders impractical in applications requiring short calculation times.

Usually a good compromise between model tests and CFD calculations can be achieved with the help of computer codes based on linear models. Such methods allow capturing the physics of loss with reasonable accuracy - in typical applications the damaged ship is not exposed to extreme weather condition, on the contrary, the sea-state of interest does not exceed H_S of 4m.

The satisfactory in most survivability studies accuracy and relatively short computations make the numerical models a viable tool in design process, particularly when combined with techniques such as Monte Carlo sampling allowing for statistical modelling or other sampling techniques for the design space exploration.

There are however at least two applications where speed of calculations is of particular importance and for which – at present - none of the methods discussed above is practical (or at least widely utilised). These applications are regulations and decision support in emergencies, both relying extensively on empirical or semi-empirical models for their speed and ease of use.

SOLAS s-factor

Formally, SOALS s-factor is an estimate of the expected (averaged with respect to the statistical distribution of sea states in the moment of collision) probability of surviving collision damages. Its present incarnation is built around of a concept of critical significant wave height, H_{Scrit} , i.e. a sea state determining chances of survival (e.g. 50%) within a trial of specific length (e.g. 30 minutes); detailed information about the development and methodology behind the s-factor can be found in (Tagg and Tuzcu, 2002) and (Pawłowski, 2007).

If the intermediate phases and stages are neglected and only final stage of flooding is of interest, with ship already at her damage equilibrium, the s-factor is given as a product of three terms

$$s_{SOLAS} = k \cdot s_{moment} \cdot s_{final} \quad (1)$$

where k accounts for list in the final equilibrium with $k=1$ for heel angles smaller than 7 deg and diminishing gradually to zero at 15 degrees heel, s_{moment} accounts for external moments due to wind, passenger crowding or launching life-saving appliances (whichever is largest) and s_{final} being the „proper” survivability measure, linking (implicitly) the residual stability characteristics to the critical significant sea state and the distribution of sea-states in the moment of collision.

That is, in final stage of flooding the average probability of survival is given as

$$s_{final} = \left(\frac{GZ_{max}}{0.12} \cdot \frac{Range}{16} \right)^{0.25} \quad (2)$$

where $Range$ is a range of positive stability (of flooded ship) and GZ_{max} is maximum righting lever within the $Range$ with maximum contribution from both parameters set at 0.12m and 16 degrees, respectively.

The formula is simple and can be readily evaluated within all Naval Architectural packages capable of calculating righting lever (GZ) curve of a damaged ship. Unsurprisingly, the very simplicity of the expression and lack of references to notions traditionally associated with stability and safety of damaged ship, such as initial metacentric height, GM, or the residual freeboard, made Naval Architects to question whether the SOLAS s-factor actually works (Dankowski and Krüger, 2010), (Sweden and the UK, 2009), (Scott, 2010). Soon after SOLAS 2009 had come into force, it became apparent that the s-factor – as implemented by IMO, not as derived by HARDER – is a flawed and unreliable instrument.

3. ALTERNATIVE ASSESSMENT METHOD

The EU-funded project GOALDS was set up in order to examine the existing formulation (and the underlying methodology) and to propose an alternative formula(e) covering both, collision and grounding damages. The project confirmed that HARDER built the formulation on solid foundations and that the core concepts of capsized band and critical significant sea-state are indeed of great importance in assessment of the probability of survival. Furthermore, GOALDS showed that a small but important re-definition of the H_{Scrit}

practically eliminates the water on deck issue and dependency on trial's duration from the problem (Cichowicz et al, 2016). Furthermore, it was shown that at the heart of the s-factor issue lies the omission of the scaling parameters accounting for size of a ship.

In the process of re-engineering of the s-factor it was proposed to use the explicit reference to H_{Scrit} and express the probability of surviving flooding (i.e. both, collision and grounding) damages as in the following

$$s_{final} = \exp(\exp(0.16 - 1.2H_{Scrit})) \tag{3}$$

with H_{Scrit} given as

$$H_{Scrit} = \frac{A_{GZ}}{\frac{1}{2}GM \cdot Range} V_R^{\frac{1}{3}} [m] \tag{4}$$

where A_{GZ} is an area under the righting lever curve within the positive range of stability and V_R is residual watertight volume (i.e. total volume of the watertight envelope reduced by the volume of compartments “lost” in the damage).

As the below figures illustrate the GOALDS formula proved to be more accurate than its HARDER counterpart across a diversified sample of tested ships, varying in sizes and internal arrangements. In spite of this, the model has been perceived counterintuitive because of presence of GM and $Range$ in denominator, and the argument that it is the whole combination and not the individual parameters that matters failed to convince the sceptics.

Nevertheless, the argument was right and the factor within the expression has indeed strict physical significance that could not be determined directly at the time of development.

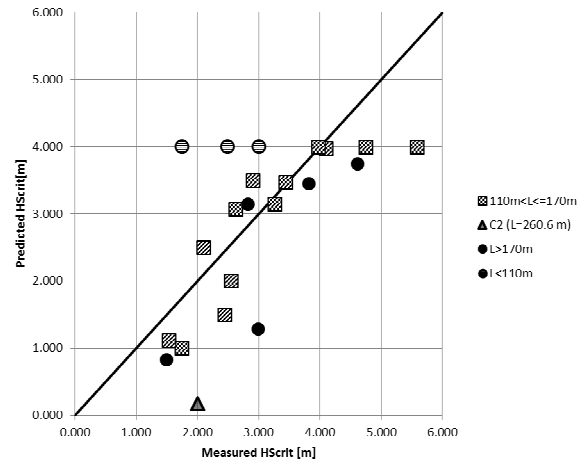


Figure 1. Comparison of measured and predicted by the HARDER model critical sea states.

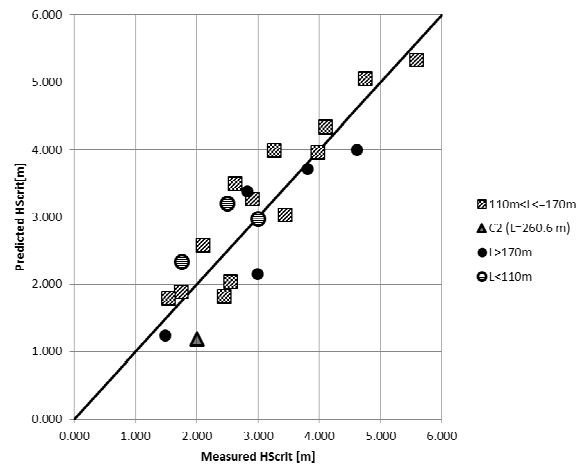


Figure 2. Comparison of measured and predicted by the GOALDS model critical sea states.

Physical significance

The key observation to be made in order to unveil the true meaning of the GOALDS formula for H_{Scrit} is that the ratio $A_{GZ} / Range$ corresponds to the average value of the righting lever within the range. It can be denoted as l_c and plotted against the GZ curve, as in the figure below.

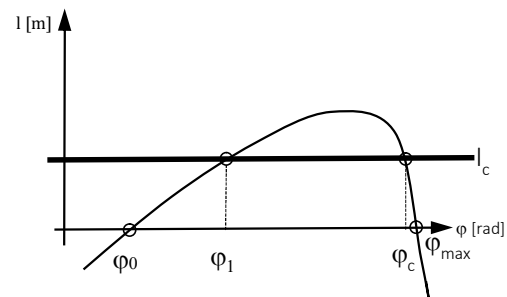


Figure 3. The average righting lever plotted against the GZ curve.

The lever l_c corresponds to external heeling moment thus the angles φ_1 and φ_c mark stable (static) and unstable equilibria. Furthermore, the tangent to GZ curve at φ_0 , i.e. GM , can be approximately given as

$$GM = \frac{l_c}{\varphi_1 - \varphi_0} \tag{5}$$

From this it follows that $\varphi_1 - \varphi_0 = \frac{l_c}{GM}$ and the H_{Scrit} formula becomes

$$H_{Scrit} = 2(\varphi_1 - \varphi_0) \sqrt[3]{V_R} \tag{6}$$

It implies that the critical significant wave height is proportional to work of the external moment equal in magnitude to average restoring moment and heeling the ship to the angle of static equilibrium.

In fact, since the lever from the external moment is known it is possible to calculate (based on the work-energy balance) a corresponding angle of dynamic heel, φ_2 , as shown in the figure below

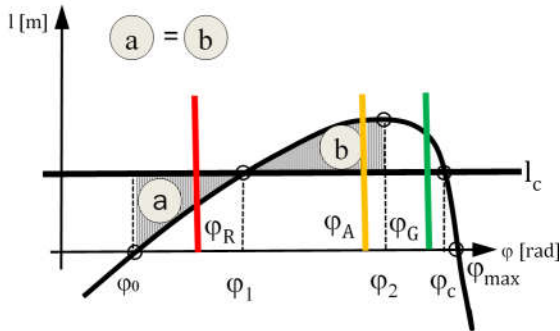


Figure 4. Dynamic heel and work-energy balance.

The red (R), amber (A) and green (G) lines are plotted in the figure above to highlight the design implications imposed by the H_{Scrit} formulation, namely that

- red (R) - no openings between φ_0 and φ_1 (except watertight); no car-deck submersion below φ_1
- amber (A) - only semi-watertight openings between φ_1 and φ_2
- green (G) - no restriction for opening type beyond φ_2 (dynamic equilibrium).

It can be readily seen from the above that the GOALDS formulation is consistent with physics of loss, rational and intuitive. For instance, the figure below shows the angle of submersion of the car-deck

edge against the angle of static equilibrium φ_1 for the all RoPax cases analysed in GOALDS.

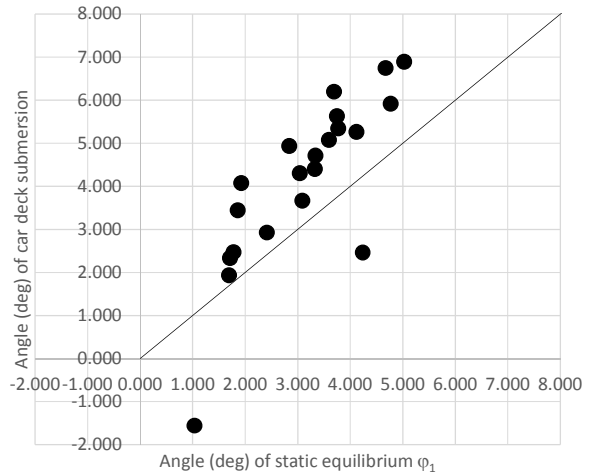


Figure 5. Car deck submersion vs static equilibrium in the GOALDS RoPax sample.

The unsurprising but having a lot of common sense observation is that apart from two cases the car-deck edge did not submerge below the angle of static equilibrium. Interestingly, both “outliers” were ships with side-casings on the car deck (furthermore one of the ships had the deck edge submerged in the equilibrium floating position). These results are in line with expectations, namely that the damaged RoPax ship will survive in sea states below which the car deck edge is not submerged (which indirectly implies that floodwater is not accumulated on the deck or that the process of accumulation is very slow). Furthermore, the results show that adding extra buoyancy distributed at the side of the car deck has positive impact on damage survivability.

Use in design of passenger ships

The GOALDS formula was derived mainly based on survivability tests of RoPax ships but, given its rational character, it can be applied to all passenger ships. This is because, in spite of obvious differences in internal arrangements and dynamics of the flooding process, both RoPax and passenger ships are lost in a consequence of uncontrolled flooding leading to diminishing stability and capsize or sinking. In case of RoPax ships this is usually because of (rapid) accumulation of floodwater in large, un-subdivided cargo spaces whereas in case of passenger ships the likely scenario involves slow progressive flooding through unprotected openings, opened semi-watertight doors or downflooding points etc. Nevertheless, the survival criterion is

same for both types of ships: there must be reserve of buoyancy and stability and the openings or design features that may lead to uncontrolled flooding should not submerge below angle of dynamic equilibrium, φ_2 . Should this cannot be achieved the critical moment, l_c , has to be lowered until the criterion is met, as shown in the sketch below

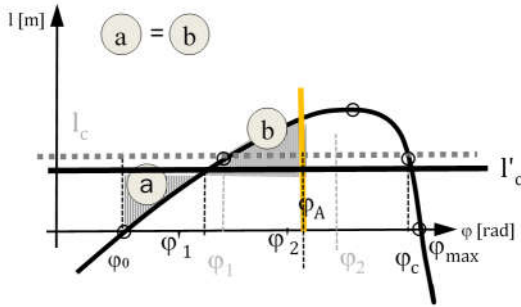


Figure 5. Lowering the survival limit to account for the design criteria.

Then for the new critical moment l'_c the critical sea state is

$$H_{Scrit} = 2(\varphi'_1 - \varphi_0) \sqrt[3]{V_R} \cong 2 \frac{l'_c}{GM} \sqrt[3]{V_R} [m] \quad (6)$$

Similar strategy can be adopted to accommodate for external moments due to wind, passenger crowding and LSA launching. They can be included by imposing a condition $l'_c = l_c - l_m$, where l_m is the healing lever due to largest of these moments, and reducing the H_{Scrit} accordingly.

As the following figure demonstrates these moments may have critical impact on survivability and the fact that they can be directly accommodated within the GOALDS formula can be considered as a clear advantage over the SOLAS approach.

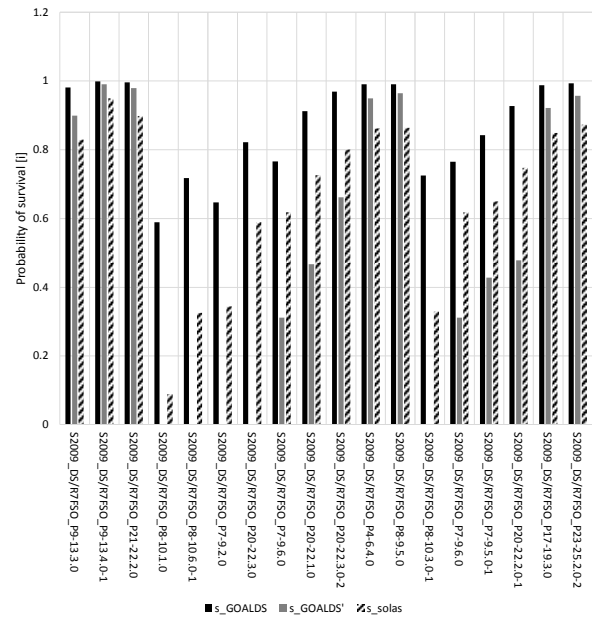


Figure 5. Probability of surviving collision damages according to SOLAS and GOALDS. SOLAS and the GOALDS series marked by apostrophe (grey bars) account for external moments

4. CONCLUDING REMARKS

The method of survivability assessment based on GOALDS formulations can be readily applied to all passenger ships irrespective of size and internal arrangement. The approach discussed in the foregoing may not capture all the fine details of the flooding and subsequent ship loss or peculiarities of a ship’s response to different sea spectra but it was never designed to do so. On the contrary, the method was intended to give a quick, yet reasonably, accurate estimate of the critical (but still safe) sea state and thus, through the probability of encountering such sea state during the collision, to determine what is the expected probability of survival, given the specific loading condition and damage case. In operation the method can be determined whether the damaged ship can survive or should be abandoned.

5. REFERENCES

HARDER (1999–2003): ‘Harmonisation of Rules and Design Rationale’, EC funded project, DG XII-BRITE, 2000–2003

GOALDS (2009-2012): ‘GOAL Based Damage Stability’. EC funded project, 233876, 2009-2012.

IMO: International Convention for the Safety of Life at Sea (SOLAS), IMO: London, UK, 1974.

IMO: Resolution A.265(VIII): Regulations on Subdivision and Stability of Passenger Ships as an Equivalent to Part B of Chapter II of the International Convention for the Safety of Life at Sea. IMO: London, UK, 1973.

TAGG, R.; TUZCU, C., 2002, "A Performance-based Assessment of the Survival of Damaged Ships—Final Outcome of the EU Research Project HARDER", In *Proceedings of the 6th International Ship Stability Workshop*; Webb Institute: New York, NY, USA.

Pawłowski, M., "Survival Criteria for Passenger Roll-On/Roll-Off Vessels and Survival Time", *Marine Technology*, 44(1), pp. 27-34.

SWEDEN and the UK. IMO SLF 52/11/1: Damage Stability Regulations for Ro-Ro Passenger Ships Report of the SDS Correspondence Group. IMO: London, UK, 2009.

DANKOWSKI, H.; KRÜGER, S., 'On the safety levels of the SOLAS 2009 damage stability rules for RoPax vessels', In *Proceedings of the 11th International Symposium on Practical Design of Ships (PRADS)*, Rio de Janeiro, Brasil, 19–24 September 2010.

SCOTT, A.L. 'Damage Stability of Ro-Pax Ships with Water-on-Deck', In *Proceedings of the 11th International Workshop on Stability of Ships and Ocean Vehicles*, Wageningen, The Netherlands, 21–23 June 2010

CICHOWICZ, J., TSAKALAKIS, N., VASSALOS, D., JASIONOWSKI, A., 'Damage Survivability of Passenger Ships—Re-Engineering the Safety Factor', *Safety* 2016, 2, 4.

Application of Vessel TRIAGE for a Damaged Passenger Ship

Petri Pennanen, *NAPA*, petri.pennanen@napa.fi

Pekka Ruponen, *NAPA*, pekka.ruponen@napa.fi

Jori Nordström, *The Finnish Lifeboat Institution*, jori.nordstrom@meripelastus.fi

Floris Goerlandt, *Aalto University, Marine Technology*, floris.goerlandt@aalto.fi

ABSTRACT

Several recent flooding emergencies on passenger ships have pointed out the need to quickly get a better assessment of the survivability onboard a damaged ship. Advanced time-domain flooding prediction methods can be used to quickly get an assessment of progressive flooding and stability of the damaged ship. This paper presents an approach for using the Vessel TRIAGE method to display the severity of the damage case on the basis of flooding prediction results. The application is demonstrated with a collision damage case of a large passenger ship.

Keywords: *damage stability, progressive flooding, decision support*

1. INTRODUCTION

Investigations of recent accidents have clearly shown that there is a need for a decision support system on board the ships, e.g. *MIT (2013)* and *MAIB (2015)*. The most important information this system should provide, is the severity of the flooding case and the probable development of it. This information must be provided in a way that is easy to understand and easy to communicate further.

The IMO has recognized this need and SOLAS currently requires all new passenger ships to be equipped with a damage stability computer for providing the master with operational information on the residual damage stability of the ship after a flooding casualty. In the recently revised guidelines, *IMO (2016a)*, however, the residual damage stability output is defined in way of presenting the residual GZ curve and floating position information. Judging the severity of the flooding case and the survivability of the people on board, based on GZ curve data, requires interpretation, and is neither instantly intuitive nor easily communicable to other involved people on the accident scene.

The first approach to a decision support based on time-domain prediction was presented by *Ruponen et al. (2012)*. Recently, also *Varela et al. (2014)* have presented a similar concept for decision support

based on progressive flooding calculation and virtual reality.

Vessel TRIAGE is a method for assessing and communicating the safety status of a vessel in distress situation, *Nordström et al. (2016)*. The concept for a decision support system, based on the Vessel TRIAGE method, for flooding emergencies was introduced by *Pennanen et al. (2015)*. The first approach for determination of the color coding was presented by *Ruponen et al. (2015)*, based on time-domain flooding prediction results. The present study reviews the applied methodology for a flooded passenger ship, and a new approach is introduced to account the flooding extent in respect to the size of the ship. Finally, a short case study with a collision damage to a large passenger ship is also presented.

2. VESSEL TRIAGE

Vessel TRIAGE is a method for assessing and communicating the safety status of vessels in maritime accidents and incidents. The method is intended for use by both vessels and maritime emergency responders to assess whether the subject vessel can provide a safe environment for the people onboard.

The method is currently under consideration for further testing its adequacy in search and rescue operations by the IMO Sub-Committee on Navigation, Communication and Search and Rescue

(IMO, 2016b). A detailed description of the method is given by Nordström et al. (2016).

The method expresses the safety status of the vessel in terms of a Vessel TRIAGE category. There are four categories: GREEN, YELLOW, RED and BLACK (see Fig. 1). However, the category BLACK is not relevant for decision support onboard the damaged ship since in that case the ship has already been lost.

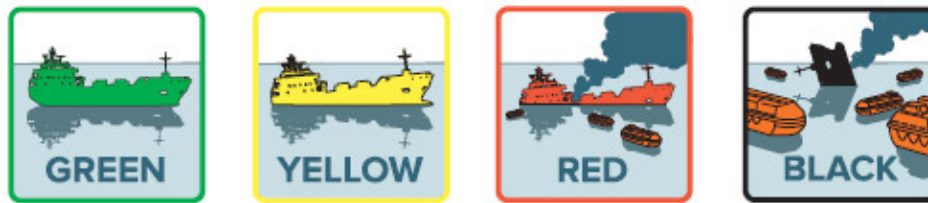
Initially it was suggested by Ruponen et al. (2015) to represent vulnerability as a real value between 0.0 and 1.0. However, based on the Vessel TRIAGE methodology, it is more simplified and

practical to consider only color codes. Thus the total survivability color code is the worst of the color codes for the separate threat factors.

3. THREAT FACTORS FOR A DAMAGED PASSENGER SHIP

Heeling and Stability

Even with a small heel angle the risk of capsizing can be significant if the stability of the ship is not good enough. Thus heeling has been a primary safety indicator since the early decision support system concepts, Lee et al. (2005).



GREEN	YELLOW	RED	BLACK
Vessel is safe and can be assumed to remain so	Vessel is currently safe, but there is a risk that the situation will get worse	Level of safety has significantly worsened or will worsen and external actions are required to ensure the safety of the people aboard	Vessel is no longer safe and has been lost
<p>GENERAL SITUATION</p> <ul style="list-style-type: none"> - The situation aboard is stable. Although the vessel may have been damaged by the accident, this damage does not threaten its seaworthiness or the people aboard. - The damage to the vessel has been assessed. It is highly unlikely that the damage will spread or get worse. - The vessel still protects the people aboard against the prevailing conditions. 	<p>GENERAL SITUATION</p> <ul style="list-style-type: none"> - Damage to the vessel might affect its seaworthiness or the full extent of the damage has not as yet been determined. - Internal damage control measures and rescue operations have not been completed. Damage control is possible with reasonable resources available to carry out the proper measures. - Damage to the vessel may pose a direct or indirect threat to the people aboard. 	<p>GENERAL SITUATION</p> <ul style="list-style-type: none"> - The vessel is significantly damaged, affecting its seaworthiness, and there is a threat to the people aboard. - A fire, leak or other damages to the vessel are not under control and escalation is highly likely. - The vessel no longer protects the people aboard against the prevailing conditions. - Major external resources are required. 	<p>GENERAL SITUATION</p> <ul style="list-style-type: none"> - The vessel is capsized, broken, sunk, burnt or otherwise damaged so badly that it no longer provides protection to the people aboard against the prevailing conditions (that is, the vessel has totally lost its seaworthiness). - Even if the vessel is still completely or partly afloat, it is no longer safe to work aboard, even to save human lives.

Figure 1: Vessel TRIAGE categories: definitions and description of general situation, Nordström et al. (2016)

The s-factor in SOLAS II-1 Part II-1 Reg. 7 is applied:

$$s_{final} = K \cdot \left(\frac{GZ_{max}}{0.12} \cdot \frac{range}{16} \right)^{\frac{1}{4}} \quad (1)$$

where GZ_{max} is limited to 0.12 m and $range$ to 16°. The effect of the heel angle ϕ is accounted with the coefficient:

$$K = \sqrt{\frac{15^\circ - \phi}{15^\circ - 7^\circ}} \quad (2)$$

when the heeling angle is between 7° and 15°. If the heeling exceeds 15° the effective s-factor is taken as zero. This is supported by the SOLAS requirement to be able to lower the lifeboats with heeling up to 15°.

The $range$ is limited to the angle, where the first unprotected opening is immersed. Only real unprotected openings above the bulkhead deck should be considered in order to avoid too conservative approach that limits the reserve buoyancy of the hull. On the other hand, if no limitation of the range is used, the results could be too optimistic.

The suggested color coding for stability of a damaged ship for Vessel TRIAGE is presented in Table 1. The change from YELLOW to RED is taken rather conservatively based on Eq. (2) so that a heel angle of 10° will result in RED. On the other hand, $GZ_{max} < 0.05$ m will trigger RED even if heeling is less than 7°. Color GREEN is possible only if heel is less than 7° and the ship has sufficient stability range and GZ_{max} .

Also alternative threshold values can be considered, but the present approach has been selected based on the current SOLAS requirements.

Table 1: Suggested Vessel TRIAGE color coding for stability

GREEN	small heeling and good stability, $s_{final} = 1.0$
YELLOW	increased risk due to heel and/or decreased stability: $0.8 \leq s_{final} < 1.0$
RED	large heeling and/or decreased stability: $s_{final} < 0.8$

Extent of Flooding

The extent of flooding can be measured as the number of WT compartments with floodwater. However, the problem is that this needs to be scaled to the size of the ship, *Ruponen et al. (2015)*. From the Vessel TRIAGE color coding point of view, the GREEN is the simplest case since the Safe Return to Port regulation forms a solid background; GREEN is possible only if flooding is limited to a single WT compartment, although e.g. *Vassalos (2007)* suggested green color and safe return to port also for more extensive damages if stability is good and all systems are available.

The criterion for a change between YELLOW and RED is more complex. A simple approach for this problem is to use floodable length curves. In order to ensure some conservativeness, constant permeability of 0.95 may be used. The curves need to be calculated for a range of draft and trim values, and linear interpolation can be used to calculate the floodable length for the actual loading condition before flooding.

The flooding extent coefficient is:

$$F_{ext} = \frac{L_{flood}}{FL(x_{flood})} \quad (3)$$

where L_{flood} is the length of flooded compartments, x_{flood} is the longitudinal center of this length and $FL(x)$ is the interpolated floodable length function at the relevant initial floating position.

The suggested Vessel TRIAGE color code for flooding extent is presented in Table 2 and illustrated in Fig. 2 for different flooding extents along with the floodable length curve. In practice the suggested threshold $F_{ext} > 1.0$ means that the color code is changed from YELLOW to RED if there is a risk of progressive flooding to undamaged compartments through flooding of the bulkhead deck.

Table 2: Suggested Vessel TRIAGE color coding for flooding extent

GREEN	flooding is limited to a single WT compartment
YELLOW	more than one WT compartment is flooded but $F_{ext} \leq 1.0$
RED	Flooding extent exceeds floodable length, $F_{ext} > 1.0$

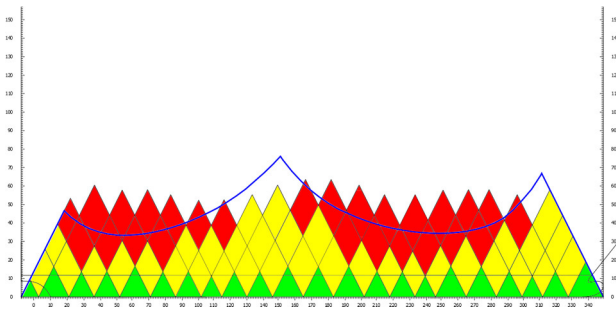


Figure 2: Example of color coding for flooding extent based on the floodable length curve.

This representation with triangles is very similar to the vulnerability analysis presented in *Jasionowski (2011)*. However, the exclusion of longitudinal and horizontal watertight subdivision may result in too conservative results, since e.g. the double bottom is not considered at all.

Evacuation

The Vessel TRIAGE methodology does not consider evacuation of the ship as a separate threat factor. However, the heeling and stability of the ship are very tightly linked with the available evacuation time, *Bles et al. (2002)*. A simplified approach for evaluating an approximate required evacuation time by using the predicted development of heel angle was presented by *Ruponen et al. (2015)*.

4. EXAMPLE OF APPLICATION

Damage Scenario

Sample calculations were done for a 125 000 GT large passenger ship design, originally developed for the EU FP7 project FLOODSTAND. The studied case is a collision damage on starboard side (SB) in the aft ship. Two WT compartments are breached, but in the aft one the breach is very small, Fig. 3. There is also an open WT door, resulting in progressive flooding to a third compartment. However, this door is successfully closed 10 min after the collision, and before water starts to flow through the door.

The reference data is first calculated with a time-domain flooding simulation, *Ruponen (2014)*. The time histories of measurement data for the flood level sensors are then generated based on the amounts of floodwater and the floating position in the reference results. This data is then used as input for automatic breach detection and prediction of progressive flooding, *Ruponen et al. (2015)*.

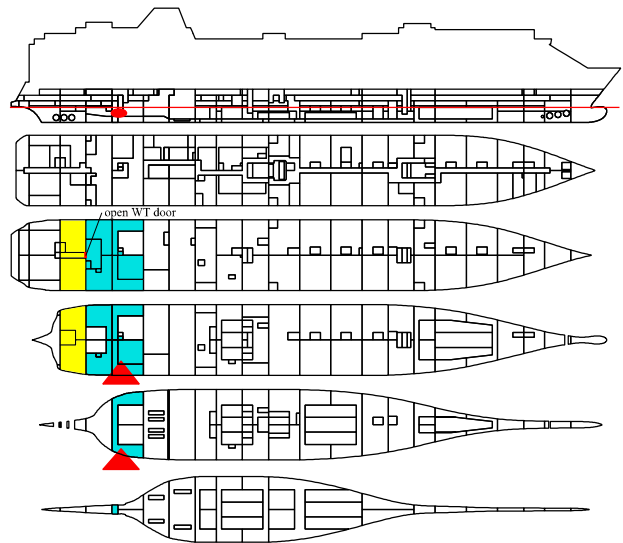


Figure 3: Damage scenario, with initially open WT door that is closed before flooding progresses to the undamaged compartment

For the analysis of the Vessel TRIAGE color coding, the worst predicted condition within the next 80 min (i.e. the required evacuation time).

Results

Initially flooding is detected only in one WT compartment since the inflow to the aft damaged compartment is very slow. Consequently the color code is GREEN since the maximum predicted heel angle is less than 7°, Fig. 4. This information is available within 5 min after the damage.

The second prediction, started 5 min after collision, accounts also flooding in the aft damaged WT compartment, where the inflow of water is much smaller. The WT door is still open, and therefore, the prediction results in progressive flooding to a third compartment. The predicted flooding extent exceeds the interpolated floodable length, and thus the color code is changed to RED, Fig. 5. The updated results are available about 8 min after damage.

The prediction that starts after the open WT door has been successfully closed, 10 min after damage, results in color code YELLOW since flooding is now limited to two compartments and heeling is predicted to be less than 7°, Fig. 6.

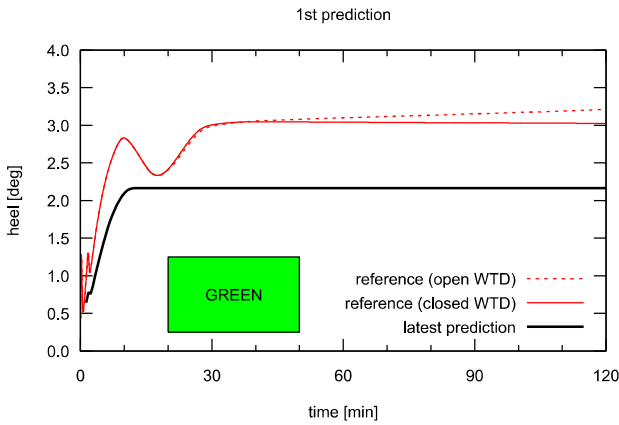


Figure 4: Results of 1st prediction flooding prediction

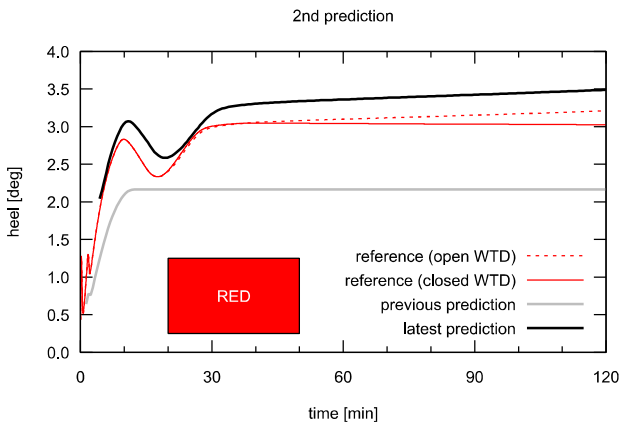


Figure 5: Results of 2nd prediction flooding prediction

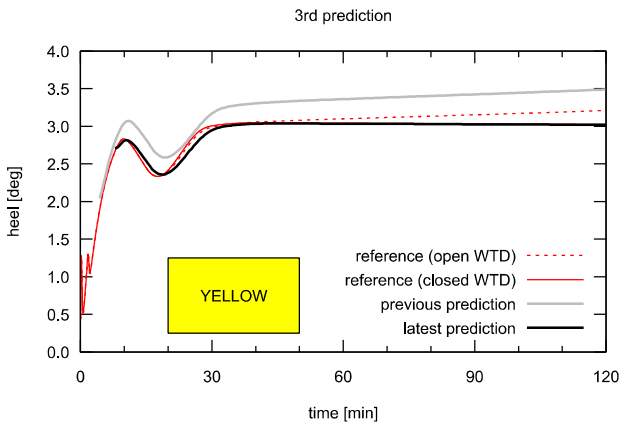


Figure 6: Results of 3rd prediction flooding prediction

5. CONCLUSIONS

Heeling angle is the most dominant component of the "s-factor" for assessing the Vessel TRIAGE color coding for damage stability. In practice this means that the color code for the threat factor stability/listing is changed from GREEN to YELLOW when heel exceeds 12°, and to RED when heel exceeds 15°. So the color YELLOW is possible only in very limited conditions. On the other hand, the proposed approach for accounting the threat factor for flooding extent, based on the pre-

calculated floodable length curves triggers the code YELLOW immediately, when flooding is detected (or predicted to spread) in two or more compartments. The result is considered to be suitably conservative, meaning that the color GREEN is only shown in cases, where the ship will certainly survive the damage, and the color RED means that evacuation and abandonment may be necessary. This is in line with the definitions for Vessel TRIAGE.

6. REFERENCES

Bles, W., Nooy, S., Boer, L.C. 2002. Influence of Ship Listing and Ship Motions on Walking Speed, Pedestrian and Evacuation Dynamics (ed. M. Schreckenberg and S.D. Sharma), Springer Verlag, pp. 437-452.

IMO 2016a. SDC 3/21, Report To The Maritime Safety Committee, Annex 3: Revised Guidelines on Operational Information for Masters of Passenger Ships for Safe Return to Port, Feb 2016.

IMO 2016b "Guidelines on Harmonized Aeronautical and Maritime Search and Rescue Procedures, Including SAR Training Matters. Amendments to the IAMSAR Manual. Revised Guidelines for Preparing Plans for Cooperation Between Search and Rescue Services and Passenger Ships (MSC/CIRC.1079) - Report of the Working Group." International Maritime Organization, Sub-Committee on Navigation, Communication and Search and Rescue 3rd Session, NCSR 3/WP.6

Jasionowski, A. 2011. Decision Support for Ship Flooding Crisis Management, Ocean Engineering, Vol. 38, pp. 1568-1581.

Lee, D., Lee, S-S., Park, B-J., Kim, S-Y. 2005. A Study on the Framework for Survivability Assessment System of Damaged Ships, Ocean Engineering, Vol. 32, pp. 1122-1132.

MAIB. 2015. Investigation of the grounding and flooding of the ro-ro ferry Commodore Clipper, Report 18/2015.

MIT. 2013. C/S Costa Concordia report on the safety technical investigation. Marine Casualties Investigative Body.

Nordström, J., Goerlandt, F., Sarsama, J., Leppänen, P., Nissilä, M., Ruponen, P., Lübcke, T., Sonninen, S. 2016. Vessel TRIAGE: a method for assessing and communicating the safety status of

vessels in maritime distress situations, Safety Science, Vol. 85, pp. 117-129.

Pennanen, P., Ruponen, P., Ramm-Schmidt, H. 2015, Integrated Decision Support System for Increased Passenger Ship Safety, Damaged Ship III, Royal Institution of Naval Architects, 25-26 March 2015, London, UK.

Ruponen, P., Larmela, M., Pennanen, P. 2012, Flooding Prediction Onboard a Damaged Ship, Proceedings of the 11th International Conference on Stability of Ships and Ocean Vehicles STAB2012, Athens, Greece, pp. 391-400.

Ruponen, P. 2014, Adaptive time step in simulation of progressive flooding, Ocean Engineering, Vol. 78, pp. 35-44.

Ruponen, P., Lindroth, D., Pennanen, P., 2015, Prediction of Survivability for Decision Support in Ship flooding Emergency, Proceedings of the 12th International Conference on the Stability of Ships and Ocean Vehicles STAB2015, 14-19 June 2015, Glasgow, UK, pp. 987-997.

Varela, J.M., Rodrigues, J.M., Guedes Soares, C. 2014. On-board Decision Support System for Ship Flooding Emergency Response, Procedia Computer Science, Vol. 29, pp. 1688-1700.

Vassalos, D. 2007. Safe Return to Port – A Framework for Passenger Ship Safety, Proceedings of the 10th International Symposium on Practical Design of Ships and Other Floating Structures, Houston, Texas, U.S.A.

Numerical Flooding Simulations- A Useful Tool For Marine Casualty Investigations

Stefan Krüger, *TU Hamburg*, krueger@tuhh.de

ABSTRACT

The recent developments in numerical tools for the prediction of the sinking process of a ship have nowadays resulted in quite reliable methods which can be applied during the design of a ship for all kinds of damage stability investigations. Such tools are most useful, too, to compute intermediate stages of flooding. Another aspect of the application of such computations is the numerical investigation of marine casualties and eventually the preparation of possible salvage operations. The paper describes some aspects and challenges of the application of such methods in the context of marine casualty investigations and discusses some principal requirements and drawbacks of such methods.

Keywords: *Sinking Simulations, Marine Casualty Investigations*

1. INTRODUCTION

Marine casualties are typically complex event chains, especially when the casualty leads to the total loss of a ship due to capsizing or sinking. Whenever such a casualty needs to be investigated, lots of computations need to be made to figure out the (most probable) event chain which has led to the final loss. During these investigations, a variety of different computational methods is applied nowadays, which extends from simple hydrostatic calculations to complex dynamic computations. The problem exists that all these methods require more or less sophisticated computational models, and they need to be validated. The validation of such methods can be performed by computing theoretical test cases, by the comparison with experiments or by full scale accidents. The validation by experiments has the advantage that all data and test conditions are well defined, which makes it quite easy to re compute these cases. Further, any deviations between experiment and computation can in most cases be reasonably explained, and such deviations often result in the refinement of the computational procedure or in the model, or both. Therefore it is a *conditio sine qua non* to validate numerical methods by experiments. However, with respect to marine casualties, experiments never reflect the full event chain as they can only focus on a small part of the problem, and they are always performed under ideal conditions. Therefore it seems plausible to also use

full scale accidents of ships for validation purposes. Besides the validation problem, investigations of full scale accidents do in fact require that the methods are applied to the real case. But the problem exists that these accidents never happen under ideal conditions where all data is exactly known. Mostly the ship has sunk and it cannot be accessed, important data are not known with sufficient accuracy and the surviving witnesses often do not clearly remember important facts. This makes the analysis of full scale accidents always challenging, and often it is not clear whether a numerical model or a computational procedure is actually suitable for the analysis. Therefore, we are running research projects where we systematically collect data of full scale capsizing or sinking events, prepare the calculation models and figure out the relevant event chains. These data are collected in a database which are used for the validation of other methods. In the framework of this paper, we have performed several root cause analyses for the German Federal Bureau of Marine Casualty Investigations (BSU). During our analyses of such accidents we always identified some technical challenges which made a further development of our methods necessary. This paper describes some of these challenges and the related methodological improvements. At first, a classification of marine casualties is presented from a methodological viewpoint.

2. SINKING CASUALTIES OF SHIPS

If a ship has a stability event or a flooding accident, it may capsize or sink. In such cases, the event chain is always quite complex, and other technical issues than stability or water tight integrity must be treated as well. This may include inter alia steering, power generation, propulsion and other related issues. Consequently, not a single method can be used for the analysis of such events. On the other hand, during such investigation time is an important factor, because the determination of the most probable root cause (or event chain) requires that many different scenarios have to be evaluated. Therefore it is very important that computational times are as low as possible. This requirement also forces a specialization of the computational methods for a clearly defined purpose. If we once accept that different methods are used for the investigation of such casualties, it makes sense to classify the casualties accordingly. This paper focusses on events where the ship has sunk due to ingress of water. From a methodological point of view, such events can be classified as follows:

- Water ingress occurs due to ship motions, and only the later accident phase may be seen as a slow sinking event. Example: The sinking of ESTONIA.
- Water ingress occurs after the ship has taken already a large heel angle due to a combination of roll motion and other heeling moments. Example: The capsizing of the SEWOL.
- Water ingress and flooding are sufficiently slow (e.g. due to a damage), and ship motions play a minor role only. Example: The sinking of the COSTA CONCORDIA.

The first and the second type of accident strongly depend on the ship motions and the water ingress due to the ship motions (at least during the first accident phase), or due to a permanently increasing heel, and this requires seakeeping analyses including dynamic treatment of the free surfaces. But these methods have limitations when the heel angle is large, and then classical sinking analyses

are used to investigate the later phase of these accidents.

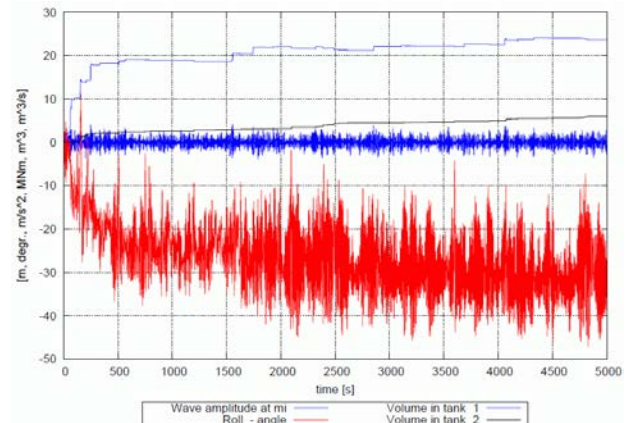


Figure 1: Time plot of roll angle, wave elevation and floodwater ingress into two compartment during the sinking of the ORTEGAL UNO (BSU 14/10), see also Fig. 4, right.

One example of such calculations for the first accident type is shown in Fig. 1 for the sinking of FK ORTEGAL UNO (BSU 14/10). The vessel was fishing in rough weather, and during the roll motion, water entered through a side opening into the fish hold. As the water tight door between fish hold and the accommodation was open, water entered into the accommodation, too. The numerical investigation of the accident showed clearly that if that door would have been closed, that ship would not have sunk. The first phase of this accident ended with a more or less steady equilibrium at abt. 35 Degree heel (see Fig. 6, right). Water then slowly entered the ship through non secured openings, and it then slowly sank. The sinking phase could then be investigated with quasi- static sinking methods.

The third type of accident is a classical sinking event and it can be analyzed with analysis tools where only the inflow fluxes need to be computed in time domain, but the momentary equilibrium floating condition can in most cases be obtained from hydrostatic calculations.

This may be demonstrated by the sinking computations we have performed for the COSTA CONCORDIA accident (Russel, BSU 310/12). Fig. 2 shows the time development of the heeling angle, and one can see that besides the relatively quick initial list to portside (negative heel), the heel angle develops quite slowly in time. The full lines in Fig.

2 stop when the ship has reached the floating position shown in Fig. 6, left.

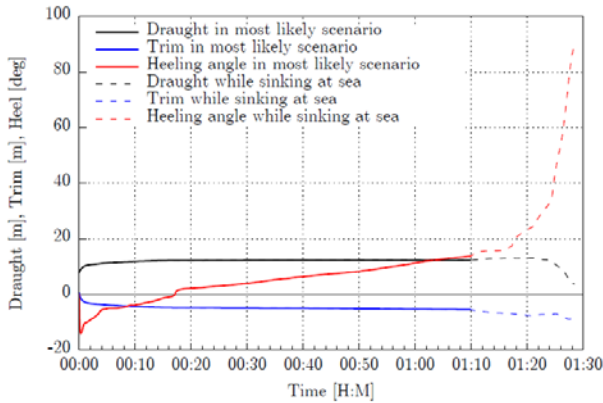


Figure 2: Computed time plot of heel angle, draft and trim for the sinking of COSTA CONCORDIA. At 1.10, the floating position shown in Fig. 4 is reached.

It must in this context also be noted that different ship types may have a completely different failure mode (as also the calculation in Figs. 1 and 2 indicate): Due to their specific subdivision, conventional passenger vessels tend to a slow and stable sinking in case of an accident with the ship more or less in an upright position (COSTA CONCORDIA, SEA DIMAOND, EXPLORER), whereas RoRo- Passenger vessels often capsize due to the massive accumulation of water on vehicle decks (HERAKLION, ESTONIA, SEWOL) or through submerged openings (VINCA GORTHON, FINNBIRCH). From a technical point of view, a capsizing during the flooding process is much more challenging compared to a slow sinking. This may be illustrated by the following casualty (BSU 266/14):

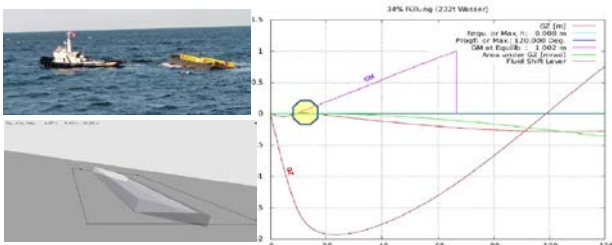


Figure 3: Capsizing of a pontoon due to slow water ingress. (BSU 266/14). Left: Situation immediately before the capsize, right: Righting levers in that situation, free movement of the floodwater. Source: BSU

Fig. 3 shows the capsizing event of a pontoon due the slow ingress of water. The pontoon suffered from a very small damage some days before the

accident, and the water tight doors of all three compartments were left open. Prior to the capsizing, there was practically no stability left (see Fig., 3, right), and when then critical amount of floodwater was reached, this resulted in a quick turn and a strong alteration of the fluxes through the opening. Due to the pontoon shape of the floating body, the hydrostatic stiffness matrix varies strongly during that phase, and it was numerically challenging to obtain both stable fluxes and a stable time development of heel during the capsizing.

It should also be noted that ships with large weathertight superstructures may stay afloat for a long time even at larger heel angles (COUGAR ACE), but they might be vulnerable with respect to sinking when water ingresses through an opening that is not secured or not water tight.

Further it should be noted that the water ingress into the ship may not only occur due to hull damage, but also due to heeling by external moments (SEWOL) or due to firefighting (LISCO GLORIA, NORMAN ATLANTIC).

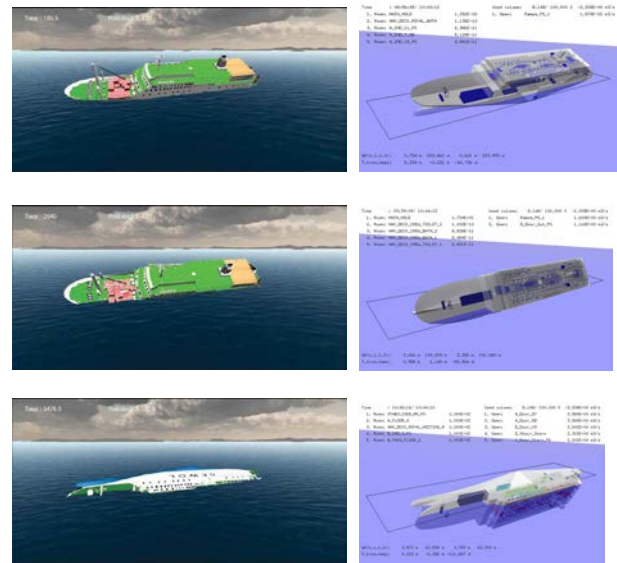


Figure 4: Capsizing the ferry SEWOL due to water ingress through the stern ramp into the ship. Left: Results of Lee (2015), right: Bley and Weltzin (2016).

This may be illustrated by the capsizing event of the SEWOL, see Fig. 4. The ship suffered from insufficient intact stability, and during a turn the cargo shifted, which lead to a steady heel which allowed water to enter the vehicle deck. When the floodwater spread within the ship through several openings, she took a large heel and sank finally.

Other than the casualty shown in Fig. 3, the stability remained positive during the capsizing and the alterations of the hydrostatic stiffness matrix were much smoother. Consequently, the computational challenges were less severe for this case, because from the methodological point of view, this particular accident may still be characterized as a slow sinking event (although the capsizing from a practical point of view was too fast to evacuate most of the passengers).

Some accidents are characterized by the fact that during some intermediate stage of flooding, progressive flooding of compartments took place which would not have been flooded in the final stage (EUROPEAN GATEWAY). These intermediate stages often occurred due to inflow obstructions, and they require adequate modelling. As a consequence it was found that the sinking simulations cannot be based on the ship data model which is usually used for statutory purposes, but a much finer model is required.

It was also found during our analyses that the status of the watertight doors is an important boundary condition for the flooding event. Either, they were open from the very beginning of the accident, or they were opened during the sinking. This was the case for the accidents shown in Figs. 1-3.

For the sake of completeness we would like to mention that there were some accidents which took place due to large free surfaces (intact ship) and a heeling moment during a turn (WALDHOF).

3. CHALLENGE OF MARINE CASUALTIES

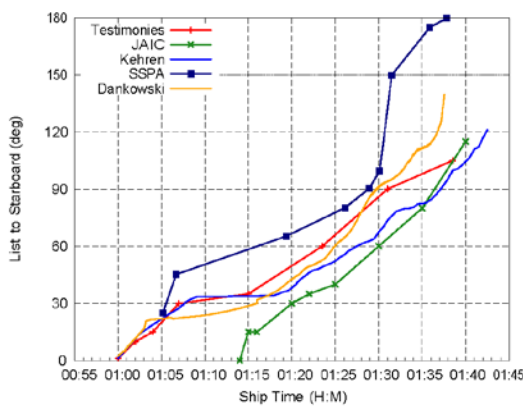


Figure 5: Development of heel angle versus time for the sinking of MV ESTONIA according to different authors. Source: Dankowski(2014)/Valanto(2008)

The main challenge of complex marine casualties is the fact that many important data are not known

with sufficient accuracy. This holds for the loading condition, for the status of opening and the possible flux through these openings as well as for other boundary conditions like cargo shift or the actual weather conditions. Consequently, as the results are sensitive to these input parameters, they show significant scatter. This is reflected by Fig. 5, which shows the development of the heeling angle over time for the ESTONIA- accident according to different authors (Dankowski (2014) and Valanto(2008)). Although the general trend is reflected well by all computations, there are significant differences. Due to this fact it has been put forward by many researchers that marine casualties are not suitable for the validation of computational methods due to these uncertainties.

But the authors disagree with this opinion for the following reason: The most important result of a marine casualty investigation is the root cause and the most probable event chain. And despite the uncertainties mentioned, after a computational sensitivity analysis there remains only one event chain which fits to all boundary conditions, and that is typically the result of the investigation. Despite the fact that the authors of Fig. 5 computed a different time series, there was no doubt on the root cause of this casualty.



Figure 6: Two examples of photogrammetric determination of the floating position. Source: BSU 330/12 (left) and 14/10 (right).

What makes the situation easier today is the fact that due to the massive presence of information technology, the documentation of marine casualties has significantly improved. In most cases, photos of the accident exist (see Fig. 6) which allow with modern photogrammetric techniques a quite precise analysis of the equilibrium floating condition during a given time stamp. Such information is much more precise compared to testimonies, and during the re calculation of the accident it is then the boundary condition that the ship in the computation must take exactly the same equilibrium floating position as documented by the photogrammetric investigation. For the cases shown in Fig. 6 it could for example clearly be

demonstrated by the computations that the documented floating positions at the given time stamps were only possible due to open water tight doors (see also Fig 1 - 3).

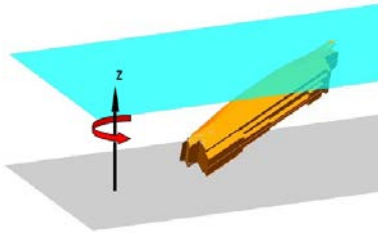


Figure 7: Computed ground contact of MV ESTONIA during the HSV/A/TUHH accident investigations (Source: Valanto).

If the ship has finally sunk or grounded, the position of the wreck is most often well documented. This information is extremely useful for the numerical investigation of the accident, because each computation must then lead exactly to this position in the final stage (see Fig. 7). On the other hand, this computation demands to compute also the very final stage of the accident, where many compartments are flooded and the equilibrium becomes unstable in all three degree of freedom. This final stage is often combined with large fluctuations of the hydrostatic stiffness matrix (including floodwater), which leads to significant oscillations of the fluxes.

Therefore, the boundary condition to compute also the very final stage of the flooding poses severe requirements to any computational method with respect to computation time and numerical stability.

4. NUMERICAL METHODS

From the above mentioned findings, we can formulate some basic requirements for numerical tools for the analysis of such casualties: First, it seems reasonable to provide a special set of methods for those accidents which are dominated by ship motions and to combine such methods with the dynamic treatment of water ingress and the motions of the floodwater in the compartments of interest. In these cases, special attention must be paid to the roll motion, and this degree of freedom must definitively be treated non-linearly. For this purpose, we use the time-domain seakeeping code E4ROLLS which was originally developed by Kröger, Petey and Söding. A good and complete

description of the underlying concept of this method is given by Söding, Shigunov, Zorn and Soukup. The motions of the free surface are obtained from the solution of the shallow water equations according to Glim (1965) and Dillingham (1981). These equations are combined with the motion prediction of E4ROLLS. Dankowski has alternatively implemented the Kurganov method (2007) for this problem. Although these methods give reasonable results for both ship motions and the water ingress, they have significant numerical problems when the heel angle takes large values (or when the ship capsizes). Most of these problems have their source in numerical instabilities when the water hits the top of the flooded compartment. Further, this dynamic analysis is very time consuming if many flooded compartments are involved, and this makes this set of methods not applicable for the analysis of the complete sinking process of a ship which typically includes many damaged compartments. During the application of these methods on full scale accidents in rough weather it eventually happened that numerical instabilities of the fluid motions occurred, which then lead immediately to unrealistic ship motions (and inflow fluxes, consequently). In all cases, these problems could be (iteratively) healed by adjusting the time steps. However, one must conclude that these methods are not yet stable enough to allow the application by unexperienced users due to these reasons.

For the analysis of the sinking process, Dankowski (2012) has developed a quasi-static method for the (slow) sinking of ships with many flooded compartments. Essentials of this method are the direct computation of the pressure propagation through full compartments by a predictor-corrector-scheme, the direct numerical computation of the hydrostatic stiffness matrix including fluid shifting moments and the automatic detection of flooding paths by a directed graph. A full description of the method may be taken from Dankowski (2012). The method is quite fast and appeared to be robust when the experimental reference cases of Ruponen (2007) were analyzed. However, the application of this method to some full scale accidents showed the following problems which needed to be solved:

- When the ship capsized during the sinking (HERAKLION, EUROPEAN GATEWAY), the quasi-static

determination of the equilibrium needed to be replaced by the solving of a differential equation with small time steps.

- The flux computation had to be stabilized in these cases when large inflow fluxes through large openings were combined with substantial ship motions
- When large compartments are filled quickly and an up flooding takes place through small openings (e. g. escalators), the flux oscillates significantly and requires numerical stabilization (COSTA CONCORDIA).
- When box-shaped objects were flooded and capsizing took place, the equilibrium determination became unstable which required numerical healing of the equilibrium determination and of the inflow- flux computation (BSU 266/14).
- Experiments with a test body having a RoRo-like subdivision showed that there can be a significant influence of the initial roll motion on the inflow flux, which made it generally necessary to replace the quasi-static equilibrium computation by the solving of differential equations. This posed new challenges on the stability of the method for box-shaped objects.
- Manderbacka and Ruponen (2015) have found out that during the initial phase of the flooding, the motion of the ingressing fluid may have a significant influence on the sinking process.
- Additional features like heeling moments, water tight door operations and pump elements needed to be included in the method to account for the individual accident circumstances.

For the sake of completeness we wish to add that during some model experiments there occurred the problem of entrapped air and its consequence on the sinking process. Although we have analyzed this phenomenon during our model tests, too (ref. Krüger, Dankowski, Kluwe et al.) we have come to the conclusion that entrapped air plays a minor role during full scale sinking only. This appears to be a problem during model tests where it may not be

possible to sufficiently ventilate the compartments due to model restrictions.

It further turned out that the sinking process is very sensitive with respect to details of the subdivision, which requires a fine model. Our computational model for the COSTA CONCORDIA included 1536 spaces, 642 compartments and 1587 openings to accurately re compute the sinking process. The computations then could be performed slightly faster than real time, but this is of course far too slow if the computations shall serve as potential decision making tools. Unfortunately from our present experience it seems not possible to obtain correct results for the sinking computations if the compartment model is too raw.

Consequently, we must conclude that these methods are useful tools on the one hand, but on the other hand we must admit that the application of such methods still requires a qualified user, which may impede the broad use of methods.

Therefore, the future goal is to stabilize the computations from a numerical point of view and to increase the computational speed significantly. This is important in view of the fact that such kind of calculations shall be performed on board as decision design tools.

5. CONCLUSIONS

The paper has shown that numerical sinking computations can successfully assist the investigation of marine casualties. As the documentation of these casualties has significantly improved, it is today well possible to clearly identify the root cause of such events by computations. Despite the fact that some information on accident data is uncertain, marine casualties are a useful validation basis. As sinking events are very complex, there must exist different computational methods to cope with the individual requirements of each accident. Although these computations are extremely useful, these methods are still not stable enough to be widely used, especially by non-experienced users. Consequently, future efforts shall be put into the problem to increase stability and computational time.

6. REFERENCES

Bley, M., Weltzien, C.: "Numerische Untersuchungen zum Untergang der Fähre SEWOL

(Numerical Investigations into the Sinking of the Ferry SEWOL”. Proc. JSTG, The German Society of Naval Architects, 2016.

Dillingham, J.: “Motion Studies of a Vessel with Water on Deck”. Marine Technology, 1981

Glimm, J.: “Solutions in the large for nonlinear hyperbolic systems of equations”. Communications on Pure and Applied Mathematics, 1965 18(4) pp. 697-715

Dankowski, H., Krüger, S.: “A Fast, Direct Approach for the Simulation of Damage Scenarios in Time Domain.” 11th Proc. IMDC, Glasgow, 2012

Dankowski, H., Krüger, S., Russel, P.: „New Insights into the Flooding Sequence of the Costa Concordia Accident”. Proc. OMAE 2014, San Francisco, Ca, USA

Federal Bureau of Marine Casualty Investigation (BSU): Report No. 14/10, Hamburg, Germany. www.bsu-bund.de

Federal Bureau of Marine Casualty Investigation (BSU): Report No. 330/10, Hamburg, Germany (unpublished, investigation cancelled, see BSU press release 18/15). www.bsu-bund.de

Federal Bureau of Marine Casualty Investigation (BSU): Report No. 266/14, Hamburg, Germany. www.bu-bund.de

Krüger, S., Dankowski, H., Hatecke, H., Kluwe, F., Lorkowski, O.: „Abschlussbericht LESSEO – Untersuchung der Lecksicherheit von Schiffen unter besonderer Berücksichtigung des zeitabhängigen Sinkverhaltens und dynamischer Einflüsse aus großen, freien Oberflächen.“ ISBN 978-3-89220-682-8.

Krüger, S., Dankowski, H., Teuscher, C.: Numerical Investigations of the Capzing Sequence of SS HERAKLION“. Proc. STAB 2012, Athens

Kurganov, A., Guergana, P.: A Second Order Well-Balanced Positively Preserving Central-Upwind Scheme for the Saint-Venant System. Communications in Mathematical Sciences, 5(1), March 2007. Pp 133-160.

Lee, G. J.: “Flow Model for Flooding Simulation of a Damaged Ship.” Proc. 12th STAB, 2015, Glasgow, UK

Manderbacka, T., Ruponen, P.: “The Impact of the Inflow Momentum on the Transient Roll

Response of a Damaged Ship ”. Proc. Stab 2015, Glasgow, UK

Ruponen, P.: “Model Tests for the Progressive Flooding of a Box-Shaped Barge”. Technical Report, Helsinki University of Technology, 2007.

Söding, H., Shigunov, V., Zorn, T., Soukup, P.: “Method rolls for Simulating Roll Motions of Ships”. Ship Techn. Research, 60, (2), pp 70-84

Valanto, P.: Research Study on the Sinking Sequence of the M/V ESTONIA. HSVA report 1663, The Hamburg Model Basin, 2008.

SESSION 6
Roll damping

Estimation of force coefficients for normal forces on bilge keels and skin friction roll damping of ships by CFD simulations

Sven Wassermann*, *Hamburg University of Technology*, sven.wassermann@tuhh.de

Gregor Krambs, *Hamburg University of Technology*, gregor.krambs@tuhh.de

Moustafa Abdel-Maksoud, *Hamburg University of Technology*, m.abdel-maksoud@tuhh.de

ABSTRACT

A finite-volume method (FVM) is used to simulate the roll motion of an ellipsoid equipped with wall-bounded flat plates with and without forward speed. Due to the circular form and a fixed roll axis of the simulated ellipsoid, only normal forces act on the plates. The normal force component in phase with the roll velocity over a harmonic roll period is estimated. The roll period, amplitude and the plate dimension are varied. The simulation results are compared with results of different model test techniques. The focus is set on modeling a simple definition for the normal force coefficient based on the Keulegan-Carpenter number (KC). Compared to Ikeda's method, an improved definition which considers a larger range of KC numbers is formulated.

To transfer roll damping results from model scale into full scale, the frictional roll damping component of different ships is investigated. FVM simulations of the roll motion with various scales are carried out. A simple extrapolation procedure based on Kato's approach is developed.

Keywords: roll damping, force coefficient method, Ikeda's method, bilge keels, skin friction roll damping, scale effects

*corresponding author, name at birth: Sven Handschel

1. INTRODUCTION

Normal Forces on Bilge Keels

The roll motion of ships in waves is weakly damped by wave radiation. Simple roll damping devices such as bilge keels (BK) have the advantage to damp ships with and without forward speed in all weather conditions. Bilge keel constructions of a width up to 450mm with shipbuilding profiles were the industry practice in the last decades. In the mean time, the ship beam grew which led to large ratio of roll radius (r_{BK}) to bilge keel width (b_{BK}), see Table 1.

The authors have found two different common techniques which are used to measure normal

KC	Examples	r_{BK}/b_{BK}	φ_a [deg]
200	plate in a tank	121.5	30
100	BK on ULCC	72.75	25
25	BK on RoPax	45.5	10
2	keel on lifeboat	7.4	5
0.3	plate at a buoy	1.2	5

Table 1: Examples of wall bounded flat plates, e.g. bilge keels, for low and high KC -numbers (r_{BK} -roll radius, b_{BK} -plate width, φ_a -roll amplitude).

forces on wall bounded plates: (A) measurement of ellipsoid models in towing tanks and (B) force measurements in U-Tanks, see Figure 1. Ikeda et al. (1976) and Fujino et al. (1979) used an ellipsoid, respectively a spindle-like body to determine the drag force coefficient c_E . Sarpkaya and O'Keefe (1996) measured the force coefficient c_E for different plate dimensions in a U-Tank. The force coefficients for different KC numbers estimated by the mentioned experimental techniques are compared in Figure 2. Additionally the approximation function which is used in Ikeda's method and Ikeda's given range of validity,

$$c_{E,Ikeda} = \frac{22.5}{KC} + 2.4 \quad \text{for } 4 < KC < 20 \quad (1)$$

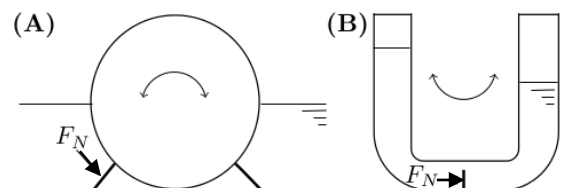


Figure 1: Techniques to measure the normal force on flat plates F_N : (A) - periodical rolling ellipsoid body in towing tank, (B) U-Tank with periodical flow.

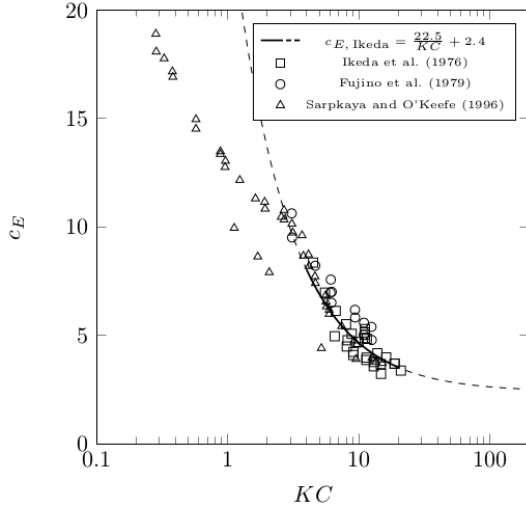


Figure 2: Force coefficients of normal forces on BK - Comparison of experimental measurement values and Eq. 1 (Ikeda's Method)

with

$$KC = \pi \frac{r_{BK} \varphi_a}{b_{BK}}, \quad (2)$$

is plotted in this Figure. It can be clearly seen that

1. no experiences exist for $KC > 20$ and
2. Eq. (1) does not fit for $KC < 3$.

The paper presents a FVM simulation approach to estimate force coefficients c_E for KC -values between 0.5 and 100. Eq. (1) will be improved.

Skin Friction Roll Damping

The skin friction roll damping is the smallest damping component and is mainly influenced by flow phenomena which depend on Reynolds number. Nevertheless, if Froude similarity is used to extrapolate the damping moment to full scale, a large scale factor can overestimate the total roll damping significantly. An extrapolation error of 5% and more is typical for large scale factors, see ITTC (2011). Figure 3 shows the influence of skin friction damping on total roll damping for the benchmarking Duisburg Test Case (DTC, el Moctar et al., 2012) container ship. The result given in Figure 3 is based on the later presented new approach.

The skin friction roll damping moment $M_F(\dot{\varphi})$ was focused on in previous studies. Especially the estimation approach of Ikeda (1978), based on results of Kato (1958) for M_{F0e} and Tamiya (1972) for forward speed correction, became common practice and is recommended by the ITTC (2011).

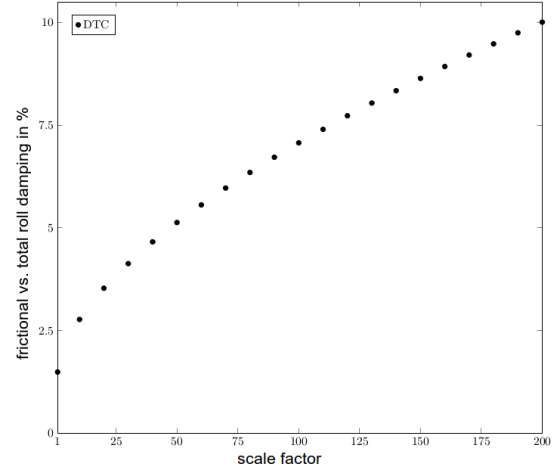


Figure 3: Influence of skin friction damping on total roll damping for Duisburg Test Case (DTC)

For a harmonic full roll cycle, it will be assumed that the roll damping moment can be approximated by a linear coefficient: $M_F(\dot{\varphi}) = M_{Fe} \dot{\varphi}$. The approach is based on the forward velocity U of the ship, the ship length L_{WL} at waterline, the roll frequency ω , the kinetic viscosity ν and the wetted surface of the ship S :

$$\frac{M_{Fe, Ikeda}}{M_{F0e}} = 1 + 0.653KC_L = 1 + 4.1 \frac{U}{\omega L_{WL}}, \quad (3)$$

$$M_{F0e} = 0.787 \rho S \bar{r}^2 \sqrt{\omega \nu} \left[1 + 0.00814 \left(\frac{\bar{r}^2 \varphi_a^2 \omega}{\nu} \right)^{0.386} \right]. \quad (4)$$

To estimate an equivalent roll radius \bar{r} , Kato (1958) used the following empirical method (\overline{OG} -distance from origin at waterline to center of gravity, coordinate system positive downwards):

$$\bar{r} = \frac{1}{\pi} \left([0.887 + 0.145C_B] \frac{S}{L_{WL}} - 2\overline{OG} \right). \quad (5)$$

Based on FVM simulations of 39 test cases of three modern monohull ship forms, a database of skin friction coefficients was generated. A comparison with Ikeda's method shows an averaged deviation of the maximum frictional moment $M_{F,max}$ formulated as mean squared error (MSE) of 1.75. Based on Kato's approach from 1958, a new extrapolation method based on the results of the database was developed. The mean squared error was reduced to 0.51.

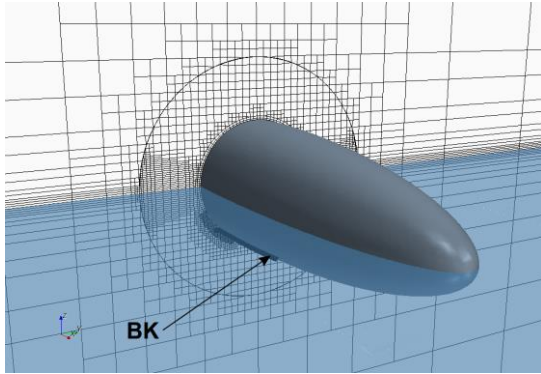


Figure 4: Simulation domain discretization for an ellipsoid body with free surface

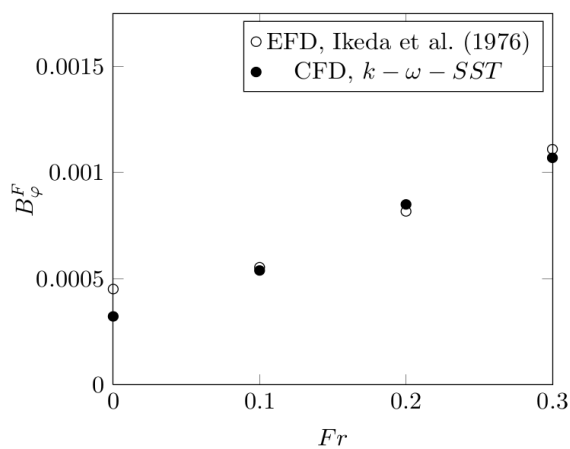


Figure 5: Frictional roll damping - comparison of experimental (Ikeda et al., 1976) and numerical results - rolling ellipsoid for various Froude numbers, grid resolution 1.3 Mio. cells, time step $\Delta t = \pi/100\omega$

2. FVM SIMULATIONS

The simulation procedure is described in detail in Handschel et al. (2012, 2014). The solver STAR-CCM+ is used to simulate the incompressible flow around the rolling ship. The FVM solves the governing equations in integral form for mass and momentum, as well as for the volume fraction of water and air and equations for the turbulence modeling. The segregated iterative solution method is based on the SIMPLE-algorithm.

The computational domain is divided into two regions, see Figure 4. An inner cylinder (rotor) is rolling around a fixed roll axis. A sliding interface boundary condition is applied between the stationary (stator) and the rotating part of the grid. The grid is unstructured and trimmed hexahedral. A prism layer on the wall region exists. Local refinements are applied near the hull, the appendages and the free water surface. A volume of fluid (VOF) method is used to calculate the free

water surface flow. In all RANSE computations, the turbulence model $k - \omega - SST$ is used. The dimensionless wall distance y^+ for the first layer reaches values between 30 and 90.

Simulation results were compared with experimental results of an ellipsoid body, see Figure 4, measured by Ikeda (1976, Figure 5) and with results of the container ship Duisburg Test Case (DTC), see Handschel et al. (2014). The CFD results are in good agreement with the experiments.

To reduce simulation time, calculations with the ellipsoid body to estimate the normal forces on bilge keels were optimized. Instead of the previous described domain discretization, an ellipsoid with only one bilge keel is simulated. The rotor-stator motion model is replaced by complete mesh motion. The multi-phase flow is reduced to a single-flow simulation. For $KC = 11.2$ a comparison was carried out. A deviation of 2% was achieved. The simulation time was further reduced by a splitting of the ellipsoid. Only half of the ellipsoid with the bilge keel was discretized. Results of the optimized CFD discretization have a good comparability to experimental results, see Figure 6.

3. NORMAL FORCES ON BILGE KEELS

To estimate normal forces on bilges keels, the moment M_{BK} around the longitudinal axis of the ellipsoid is determined by pressure integration. The moment can be formulated as Fourier polynomial:

$$M_{BK} = \sum_{j=1}^{\infty} [C_{A,j} \sin(j\omega t) + C_{B,j} \cos(j\omega t)]. \quad (6)$$

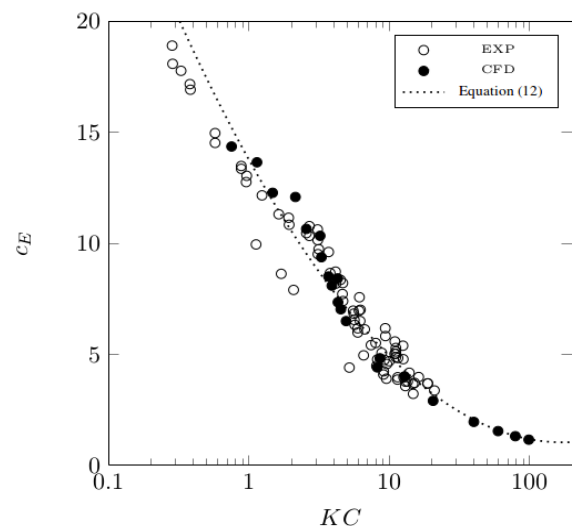


Figure 6: Force coefficients of normal forces on BK - Comparison of experimental values and CFD.

$C_{A,j}$ are coefficients in phase with the roll angle, $C_{B,j}$ coefficients in phase with the roll velocity. Assuming harmonic roll motion behavior,

$$\varphi = \varphi_a \cdot \sin(\omega t), \quad (7)$$

the equivalent damping energy E_{BKe} can be expressed by the conservation of energy approach:

$$E_{BKe} = \pi \varphi_a C_{B,1}. \quad (8)$$

Details of this approach can be found in Wassermann et al. (2016). The moment M_{BK} can also be approximated by a force coefficient c_E approach with

$$M_{BK} = \frac{\rho}{2} c_E \omega^2 \varphi_a^2 \cos^2(\omega t) \int b_{BK} r_{BK}^3 dl \quad (9)$$

which leads to the energy over a roll cycle of

$$E_{BK} = \frac{4}{3} \rho c_E \omega^2 \varphi_a^3 \int b_{BK} r_{BK}^3 dl. \quad (10)$$

The relation $E_{BKe} = E_{BK}$ results into an estimation approach for the force coefficient c_E of one bilge keel:

$$c_E = \frac{3\pi C_{B,1}}{4\rho\omega^2\varphi_a^2 \int b_{BK} r_{BK}^3 dl}. \quad (11)$$

The Fourier coefficient $C_{B,1}$ is determined with a Fast Fourier Transformation (FFT) algorithm. All other parameters are simulation inputs.

In Figure 6, results of CFD simulations and the presented experiments of Figure 2 are compared. Simulation and experimental results are in very good agreement. The experimental and the simulation results can be approximated by:

$$c_E = 0.47 \cdot \ln(KC)^2 - 4.94 \cdot \ln(KC) + 13.75 \quad (12)$$

for $0.3 < KC < 100$.

Compared to Equation (1), the range of validity is significantly extended by Equation (12). Nevertheless, Equation (12) should be applied with care because a detailed validation study for the range of KC -numbers larger 20 is still missing. Simulations to estimate results for large KC -numbers are very sensitive to small changes in

simulation setups. As a precaution, it was decided to choose simulation setups for the approximation which achieve the smallest force coefficients.

4. SKIN FRICTION ROLL DAMPING

Roll simulations with different roll setups for two ships in full scale, a RoPax (*m1413z006*, Handschel et al., 2012b) and a Pax (*m1399z001*) vessel, and simulations in model scale for the containership DTC (*m1398s001*, Handschel et al., 2014) were carried out to study skin friction roll damping. The main dimensions of the ship are listed in Table 2. The results were compared to Ikeda's method. The following differences could be observed:

1. The skin friction roll moment is not completely in phase with roll velocity. Based on measured phase angles ε_F , an averaged phase shift was determined:

$$\varepsilon_F = (-0.206 - \varepsilon_{F,BK}) \exp\left(\frac{U}{\sqrt{gL_{WL}}}\right) [rad]. \quad (13)$$

$\varepsilon_{F,BK} = 0$ for ships without, $\varepsilon_{F,BK} = 0.18$ for ships with bilge keels.

2. The influence of forward speed on the skin friction roll moment is modeled by the ratio to the zero speed skin friction roll moment, see Equation (3). A comparison of this approach to simulation results is presented in Figure 7 (upper Figure). In the lower Figure, it can be clearly seen that the forward speed effect can be described more exactly by a formulation based on the ratio KC_L/φ_a . A correction of Tamiya's equation (3) to

$$\frac{M_{Fe}}{M_{F0e}} = 1 + 0.79 \frac{KC_L}{\varphi_a} - 0.022 \left(\frac{KC_L}{\varphi_a}\right)^2 \quad (14)$$

is recommended.

3. Kato used Hughes skin friction line as formulation for the skin friction force

Dim.	m1398s001	m1399z001	m1413z006
L/B	6.979	8.176	6.525
B/D	4.246	4.456	4.304
L/D	29.631	36.433	28.087
C_B	0.632	0.647	0.542

Table 2: Main dimensions of the ships, L -ship length, B -ship breadth, D -ship draft, C_B -block coefficient

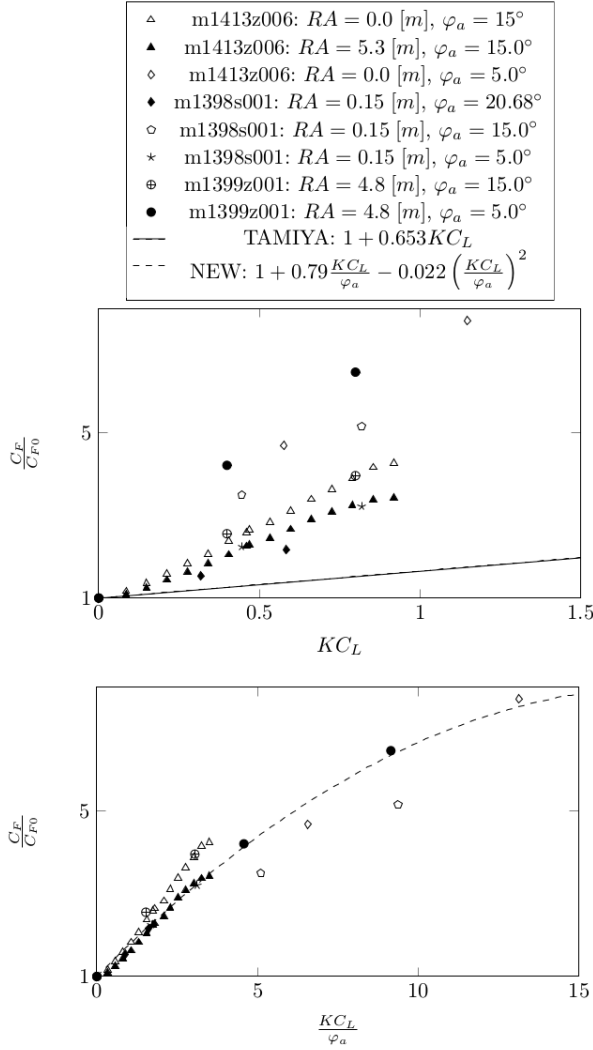


Figure 7: Skin friction forward speed correction – Comparison Tamiya’s Equation (3) and new Equation (14) – RA - different roll axis heights

coefficient. To consider the oscillating roll motion, the Reynolds number definition is modified. Based on experiments with small rolling cylinders, Kato estimated a correction factor $k = 0.51$. Although this factor could be confirmed for simulations in full scale, a factor of $k = 2.5$ is recommended to consider the correct skin friction moment in model scale, see Table 3 of the Appendix. In Figure 8, it can be clearly seen that deviations of factor k have less influence on total roll damping for ships in full scale as for ships in model scale.

In the Appendix, Table 3 shows a comparison between simulations and the improved method as well as the original Ikeda method. The comparison is presented in two columns as a ratio of the maximum friction moment $M_{F,max}$ for simulation

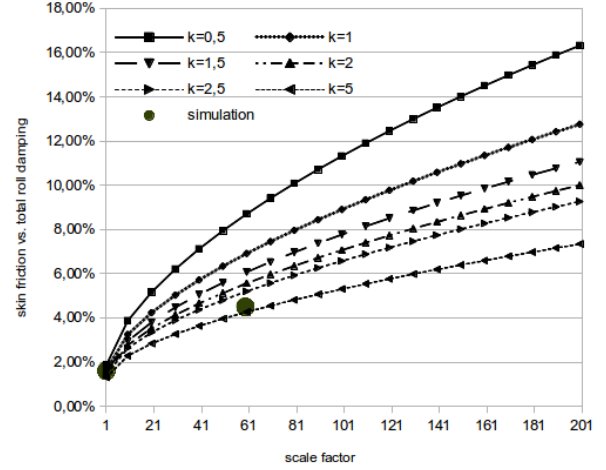


Figure 8: Ratio of skin friction to total roll damping moment over λ for different correction factors k

results to the results of the new method, column (1), and Ikeda’s method, column (2):

$$\frac{M_{F,max,simulation}}{M_{F,max,methods}} \quad (15)$$

The new approach improves the mean squared error of Ikeda’s method from 1.75 to 0.51.

For a best-practice conversion approach of total roll damping, $M(\dot{\phi}) = M_e \dot{\phi}$, from model (m) to full scale (FS) with scale factor λ , the method can be applied as follows:

$$M_{e,FS} = \frac{\rho_{FS}}{\rho_m} M_{e,m} \lambda^2 - \quad (16)$$

$$\left[\frac{1}{3\pi} \bar{r}_m^3 \varphi_a \omega_m S_m \lambda^2 (\rho_m C_{F,m} - \rho_{FS} C_{F,FS}) \cdot (-2 \sin(2\varepsilon_F) + \cos(2\varepsilon_F) + 3) \right]$$

$$C_F = C_{F0} \left[1 + 0.79 \frac{KC_L}{\varphi_a} - 0.022 \left(\frac{KC_L}{\varphi_a} \right)^2 \right] \quad (17)$$

$$KC_L = 2\pi \frac{U}{\omega_{LWL}} \quad for \quad 0 < \frac{KC_L}{\varphi_a} < 20 \quad (18)$$

$$C_{F0} = 1.328 Re_{F,x}^{-0.5} + 0.016 Re_{F,x}^{-0.114} \quad (19)$$

$$Re_{F,m} = k \frac{\bar{r}_m^2 \varphi_a^2 \omega_m}{\nu_m} \quad and \quad Re_{F,FS} = k \frac{\bar{r}_{FS}^2 \varphi_a^2 \omega_{FS}}{\nu_{FS}} \quad (20)$$

with $k = 2.5$

5. CONCLUSION

The investigation shows that the calculation of force coefficients based on Ikeda's method for normal forces on bilge keels and skin friction damping is not sufficient for today's application. Based on finite-volume method simulation results, an improved formulation for force coefficients of normal forces on bilge keels over a wider range of KC numbers could be determined, see Equation (12). To transfer the of the Reynolds number depending skin friction roll damping from model scale into full scale, an extrapolation method based on Kato's approach was developed. Especially for model tests with large scale factors, the best-practice conversion approach, Eq. (16-20), is advantageous. Nevertheless, a database with 39 simulations does not represent all types of ship forms and roll setups. To improve this approach, the database should be extended. Furthermore it should be noted that the presented simple parameter methods do not replace experiments or more exact simulation methods which should be preferred if possible.

6. ACKNOWLEDGEMENTS

The presented approximation methods were developed based on simulations which were carried out as part of a project which was funded by the German Federal Ministry of Economics and Technology under the aegis of the BMWi-project "Best-Rolldämpfung" within the framework program "Schiffahrt und Meerestechnik für das 21. Jahrhundert". The authors would like to thank the cooperation partners in the project: University Duisburg-Essen, SVA Potsdam and the DNV-GL.

7. REFERENCES

26th ITTC, Specialist Committee on Stability in Waves, 2011, "Recommended Procedures – Numerical Estimation of Roll Damping", International Towing Tank Conference, URL April 2016: <http://itcc.info>.

El Moctar, B., Shigunov, V. and Zorn, T., 2012, "Duisburg Test Case: Post-Panamax Containership for Benchmarking", Ship Technology Research / Schiffstechnik, Vol. 59/3.

Fujino, M., Ida, T., Maeto, T., Numata, T., 1979, "A consideration on the hydrodynamic

normal forces acting on bilge keel" (in Japanese), Jour. of KANSAI SNA, Vol. 144.

Handschele, S., Köllisch, N., Soproni, J.P., Abdel-Maksoud, M., 2012a, "A numerical method for estimation of ship roll damping for large amplitudes", 29th Symposium on Naval Hydrodynamics, Gothenburg, Sweden.

Handschele, S., Köllisch, N., Abdel-Maksoud, M., 2012b, "Roll Damping of Twin-Screw Vessels: Comparison of RANSE with Established Methods", Proceedings of the 11th International Conference on the Stability of Ships and Ocean Vehicles, Athens, Greece.

Handschele, S., Fröhlich, M., Abdel-Maksoud, M., 2014, "Experimental and Numerical Investigation of Ship Roll Damping by Applying the Harmonic Forced Roll Motion Technique", 30th Symposium on Naval Hydrodynamics, Hobart, Tasmania, Australia.

Ikeda, Y., Himeno, Y., Tanaka, N., 1976, "Ship roll damping – frictional component and normal pressure on bilge keel" (in Japanese), Jour. of KANSAI SNA, Vol. 161.

Ikeda, Y., Himeno, Y., Tanaka, N., 1978, "A Prediction Method for Ship Roll Damping", Report of the Department of Naval Architecture, University of Osaka Prefecture, No. 00405.

Kato, H., 1958, "On the frictional resistance to the rolling ships" (in Japanese), Jour. of KANSAI SNA, Vol. 102.

Komura, T. and Tamiya, S., 1972, "Topics on ship rolling characteristics with advance speed" (in Japanese), Jour. of KANSAI SNA, Vol. 132.

Sarpkaya, T., O'Keefe, J.L., 1996, "Oscillating flow about two and three-dimensional bilge keels", Jour. of Offshore Mechanics and Artic, Vol. 1.

Wassermann, S., Feder, D.-F., Abdel-Maksoud, M., 2016, "Estimation of Ship Roll Damping – a Comparison of the Decay and the Harmonic Excited Roll Motion Technique", Ocean Engineering Journal – Special Issues dedicated to Stability and Safety of Ships and Ocean Vehicles.

8. APPENDIX

ship	λ	BK	φ_a [°]	T [s]	RA [m]	U [m/s]	k	\bar{r} [m]	S [m ²]	(1)	(2)
m1399z001	1.0	x	5.0	9.5	4.8	5.40	0.51	12.40	9473.8	1.45	2.49
m1399z001	1.0	x	15.0	9.5	4.8	5.40	0.64	12.40	9473.8	1.27	1.47
m1399z001	1.0	x	25.0	9.5	4.8	5.40	2.67	12.40	9473.8	1.00	1.03
m1399z001	1.0	x	5.0	19.0	4.8	5.40	0.45	12.40	9473.8	1.55	3.53
m1399z001	1.0		5.0	19.0	4.8	5.40	0.23	12.34	9343.6	1.89	4.29
m1399z001	1.0	x	15.0	19.0	4.8	5.40	0.42	12.40	9473.8	1.41	1.91
m1399z001	1.0		15.0	19.0	4.8	5.40	0.12	12.34	9343.6	1.89	2.56
m1399z001	1.0	x	25.0	19.0	4.8	5.40	0.60	12.40	9473.8	1.26	1.44
m1399z001	1.0		25.0	19.0	4.8	5.40	0.11	12.34	9343.6	1.78	2.00
m1399z001	1.0	x	5.0	38.0	4.8	5.40	0.36	12.40	9473.8	1.74	4.88
m1399z001	1.0		5.0	38.0	4.8	5.40	0.26	12.34	9343.6	1.94	5.44
m1399z001	1.0	x	15.0	38.0	4.8	5.40	0.34	12.40	9473.8	1.53	2.47
m1399z001	1.0		15.0	38.0	4.8	5.40	0.13	12.34	9343.6	1.97	3.18
m1399z001	1.0	x	25.0	38.0	4.8	5.40	0.34	12.40	9473.8	1.46	1.85
m1399z001	1.0		25.0	38.0	4.8	5.40	0.09	12.34	9343.6	1.99	2.51
m1399z001	1.0	x	5.0	9.5	0.0	5.40	0.72	9.67	9473.8	1.35	2.24
m1399z001	1.0	x	15.0	9.5	0.0	5.40	0.71	9.67	9473.8	1.26	1.42
m1399z001	1.0	x	25.0	9.5	0.0	5.40	4.00	9.67	9473.8	0.93	0.94
m1399z001	1.0	x	5.0	19.0	0.0	5.40	0.75	9.67	9473.8	1.38	3.01
m1399z001	1.0	x	15.0	19.0	0.0	5.40	0.83	9.67	9473.8	1.24	1.64
m1399z001	1.0	x	25.0	19.0	0.0	5.40	1.09	9.67	9473.8	1.15	1.28
m1399z001	1.0	x	5.0	38.0	0.0	5.40	0.50	9.67	9473.8	1.62	4.37
m1399z001	1.0	x	15.0	38.0	0.0	5.40	0.46	9.67	9473.8	1.46	2.29
m1399z001	1.0	x	25.0	38.0	0.0	5.40	0.45	9.67	9473.8	1.40	1.73
m1398s001	59.5	x	4.9	2.49	0.15	1.47	5.85	0.352	5.585	0.71	1.44
m1398s001	59.5	x	12.8	2.49	0.15	1.47	2.44	0.352	5.585	1.01	1.22
m1398s001	59.5	x	4.9	3.49	0.15	0.0	3.27	0.352	5.585	0.89	0.46
m1398s001	59.5	x	19.6	3.49	0.15	0.0	1.98	0.352	5.585	1.08	0.64
m1398s001	59.5	x	4.9	2.22	0.15	0.0	2.82	0.352	5.585	0.95	0.50
m1398s001	59.5	x	14.8	2.22	0.15	0.0	1.84	0.352	5.585	1.11	0.65
m1413z006	1.0	x	5.0	14.6	5.3	0.0	0.43	10.38	4678.0	1.57	1.12
m1413z006	1.0	x	15.0	14.6	5.3	0.0	0.64	10.38	4678.0	1.29	1.05
m1413z006	1.0	x	25.0	14.6	5.3	0.0	0.45	10.38	4678.0	1.34	1.14
m1413z006	1.0	x	5.0	14.6	5.3	5.53	0.45	10.38	4678.0	1.56	3.81
m1413z006	1.0	x	15.0	14.6	5.3	5.53	0.46	10.38	4678.0	1.38	1.98
m1413z006	1.0	x	25.0	14.6	5.3	5.53	0.73	10.38	4678.0	1.22	1.43
m1413z006	1.0	x	5.0	14.6	5.3	11.06	0.44	10.38	4678.0	1.57	4.78
m1413z006	1.0	x	15.0	14.6	5.3	11.06	0.29	10.38	4678.0	1.53	2.70
m1413z006	1.0	x	25.0	14.6	5.3	11.06	0.26	10.38	4678.0	1.48	2.00

Table 3: Skin friction roll damping moment – Comparison new method (1) and Ikeda’s method (2)

Validation of CFD Simulation for Ship Roll Damping using one Pure Car Carrier and one Standard Model

Min Gu, *China Ship Scientific Research Center, Wuxi, China*, gumin702@163.com

Shuxia Bu, *China Ship Scientific Research Center, Wuxi, China*, bushuxia8@163.com

Gengyao Qiu, *China Ship Scientific Research Center, Wuxi, China*, xiaogeng502@163.com

Ke Zeng, *China Ship Scientific Research Center, Wuxi, China*, 398638829@qq.com

Chengsheng Wu, *China Ship Scientific Research Center, Wuxi, China*, cswu@163.com

Jiang Lu, *China Ship Scientific Research Center, Wuxi, China*, lujiang1980@aliyun.com

ABSTRACT

Ship roll damping is a key factor for predicting large amplitude roll motions, such as parametric roll and stability under dead ship condition. In this paper, the free roll motions of one pure car carrier and one international standard model ship 2792 for dead ship are simulated based on the unsteady RANS equations in calm water by two types of mesh, the sliding mesh and the overset mesh. The free roll decay curves of numerical simulations are compared with experimental results, and the roll damping coefficients are also compared with that from Ikeda's simplified formula. The calculated free decay curves agree quite well with the free decay curves from the experiments, and the errors of roll damping coefficient calculated by CFD are smaller than that from Ikeda's simplified formula, which validate that the unsteady RANS equations can be used to predict roll damping.

Keywords: *Roll damping, RANS, free rolling, commercial CFD codes*

1. INTRODUCTION

The large roll motions such as parametric roll and dead ship stability are one of critical risks for the safety when the ship sails in the seas, and the roll damping is essential to accurately predict these large roll motions. However, the accurate prediction of ship roll damping is very difficult, except for high cost experiments. Therefore, a numerical method to predict the large roll damping with high accuracy is desirable.

In general, most of the calculation methods are based on the potential theory, and the most common method is Ikeda's method (Ikeda, Y., 1977, 1978, 1979, 2000, 2004). These formulas can be used quite well for the conventional ships, but the prediction results are sometimes conservative or underestimated for unconventional ships (Japan, 2011a; Japan, 2011b; Sweden, 2011). This is because the large roll damping is strongly nonlinear, which has relationships with fluid viscosity and flow characteristics, such as the flow separation and vortex shedding. So the experience or semi-experience formulas can't take the full

consideration of different characteristics for different objects. Currently, the vulnerability criteria for parametric roll and dead ship stability are under development by International Maritime Organization (IMO) at second generation intact stability criteria, in which the roll damping coefficients were proposed using Ikeda's simplified method. Most of the calculated results of traditional ships by Ikeda's simplified method can fit experimental data quite well at the same order magnitude. However, if the size is outside the application range of Ikeda's method, or for the large amplitude motions in some phenomena, the accuracy will be low, which limit the application scope of Ikeda's method.

Except for Ikeda's simplified method, the Correspondence Group on Intact Stability regarding second generation intact stability criteria also proposed that the roll damping could be calculated by roll decay/forced roll test or CFD simulation (United States & Japan, 2014). Although the model tests can predict roll damping very well, but it is costly and time-consuming and most of experimental data are limited to a certain frequency

range and particular geometry, which is impossible for the large-scale expansion of the application (Bass & Haddara, 1988; Blok & Aalbers, 1991).

For the accurate calculation of roll damping, the influence of viscosity must be considered. The CFD numerical simulation can consider different objects and its characteristic, which can also reduce the cost. With the development of CFD technology, the turbulent models have been improved, such as RANS equation, discrete vortex method. In addition, the fine structure of the flow field can also be analyzed by CFD, so CFD could be widely used to predict roll damping. Forced roll method and free roll decay method are two main methods for the calculation of the roll damping.

In our previous studies (Min Gu, et al, 2015), the forced roll motions of one 2D ship section based on the methods of orthogonal design and variance analysis were carried out, in which different calculation parameters for the roll damping are analyzed, and the free motions of one 3D containership were also carried out.

The aim of this paper is to study the feasibility of CFD for the prediction of roll damping. The roll damping of one pure car carrier and ship 2792 which is provided by an IMO’s intersessional corresponding group as one of standard ships for developing the second generation intact stability criteria are simulated based on the unsteady RANS equations in calm water, and two methods are used during numerical simulations, one is sliding interface method and another is dynamic overset grid method.

In the sliding interface technique, two cell zones are used, and they are contacted by a “mesh interface”. The inner zone which is close to the bodies is moving with bodies, and the outer zone translates with bodies, which leads to the relative rotation between the outer zone and the inner zone. Overset meshes, also known as overlapping meshes, are used to discretize a computational domain with several different meshes that overlap each other in an arbitrary manner. Overset mesh has a background region enclosing the entire solution domain and one or more smaller regions containing the bodies within the domain. Both methods are most useful in problems dealing with moving bodies.

In this paper, the free roll decay curves as well as the roll damping coefficients calculated by both methods are compared with experimental results. Considering that the Ikeda’s simplified method is recommended for the evaluation of roll damping coefficient in the latest drafts for parametric roll at second generation intact stability (Correspondence Group on Intact Stability, 2015), the results of roll damping coefficients are also compared with that from Ikeda’s simplified formula.

2. SHIP GEOMETRY

The pure car carrier and the international standard model ship 2792 for dead ship stability with scale of 65.0 are adopted for the CFD computations. Main particulars of the pure car carrier and the standard model 2792 are given in Table 1 and Table 2. The body plans of the ship 2792 are shown in Fig.1, and the hull geometries of two models are shown in Fig.2 and Fig.3, respectively.

Table 1: Principal particulars of the pure car carrier.

Items	Model
Length: L_{pp}	3.5m
Mean draught: T	0.145m
Breadth: B	0.521 m
Depth: D	0.445m
GM	0.064 m
Displ.: W	169.23kg

Table 2: Principal particulars of ship 2792.

Items	Ship	Model
Length: L_{pp}	205.7m	3.165m
Mean draught: T	6.6m	0.102m
Breadth: B	32.0m	0.492m
Depth: D	20.2m	0.311m
GM	1.989m	0.0306m
Displ.: W	23986ton	87.34kg

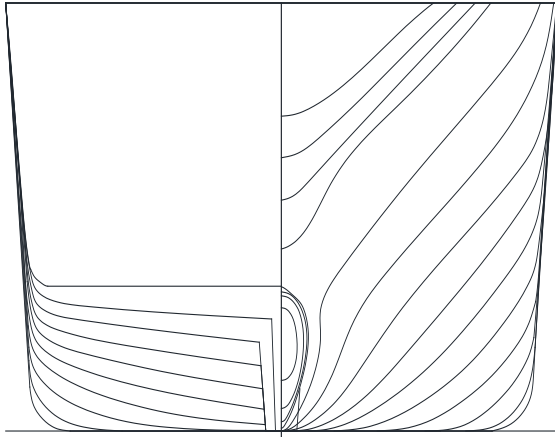


Figure 1: Lines of ship 2792.



Figure 2: Hull geometry of the pure car carrier.



Figure 3: Hull geometry of ship 2792.

3. EXPERIMENTAL

Typical models used to study roll decay are usually with bilge keels which take account of the contribution of bilge keels to roll damping. However, for simply and basically, models without bilge keels in calm water are used in this paper. The free roll decay experiments for the pure car carrier are performed at the seakeeping basin (length: 69m, breadth: 46m, height: 4m) of CSSRC (China Ship Scientific Research Center), as shown in Fig.4, and the free roll decay experiments for ship 2792 are carried out at the towing tank of Wuhan University of Technology, as shown in Fig.5. The roll decay curves are measured by a MEMS (Micro Electro-Mechanical System)-based gyroscope placed on the ship model, and the initial roll angles are 10°, 20° and 25°, respectively.



Figure 4: Free roll decay tests of the pure car carrier.

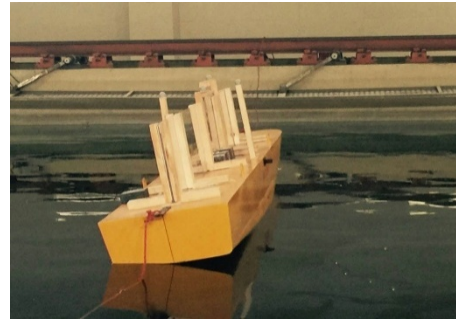


Figure 5: Free roll decay tests of ship 2792.

4. COMPUTATION METHOD

Mathematical model and numerical method

All computations are performed by solving unsteady RANS equations. RNG k-ε two-equation model is employed for the enclosure of the governing equations. The VOF method is adopted for the treatment of nonlinear free surface. The pressure-correction algorithm of SIMPLE type is used for the pressure-velocity coupling. Two methods are used during simulations, one is the sliding mesh, and another is the overset mesh. The enhanced wall function is adopted based on the previous studies (Min Gu, et al, 2015).

In simulations, the modes of roll, sway and heave are free and other modes are constrained. The solution domains are shown in Figs.6 and 7, and the types of body meshes are shown in Fig.8 and Fig.9, respectively. The boundary of the computational domain is composed of inlet boundary, outlet boundary, wall boundary (hull surface), and outlet boundary.

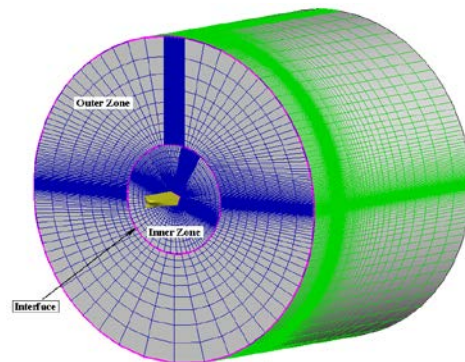


Figure 6: Computational domains and meshes with the sliding mesh method.

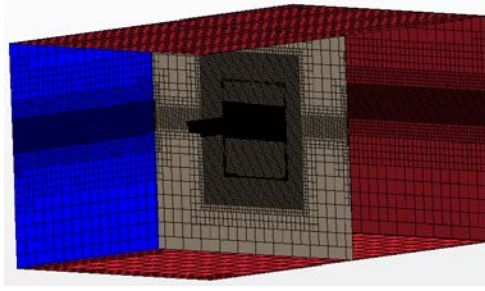


Figure 7: Computational domains and meshes with the overset mesh method.

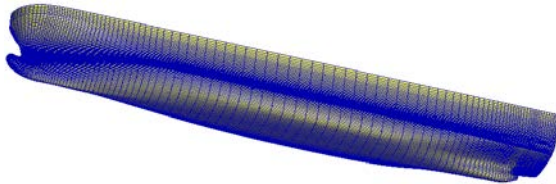


Figure 8: Hull meshes of the pure car carrier.



Figure 9: Hull meshes of ship 2792.

Analysis methods

According to the latest drafts for the vulnerability criteria of parametric roll (Correspondence Group on Intact Stability, 2015), if we introduce the equivalent linear damping coefficient $B_{44}(\phi_a)$, the roll motion in calm water can be modelled as:

$$(I_{xx} + J_{xx})\ddot{\phi} + B_{44}(\phi_a)\dot{\phi} + WGM\phi = 0 \quad (1)$$

Where, $I_{xx} + J_{xx}$: virtual moment of inertia in roll, W : ship weight, GM : initial metacentric height. Then:

$$\ddot{\phi} + 2\alpha\dot{\phi} + \omega_\phi^2\phi = 0 \quad (2)$$

$$\text{Where, } 2\alpha = \frac{B_{44}(\phi_a)}{I_{xx} + J_{xx}}, \omega_\phi = \sqrt{\frac{WGM}{I_{xx} + J_{xx}}}$$

In Ikeda's simplified formula, B_{44} is normalized as follow:

$$\hat{B}_{44} = \frac{B_{44}}{\rho \nabla B^2} \sqrt{\frac{B}{2g}} \quad (3)$$

Where, B : ship breadth, ∇ : ship displacement volume and ρ : water density.

In order to compare the results of roll damping coefficients between CFD and Ikeda's simplified formula, the extinction curve should be expressed

as the linear formula (4), which is the essential component of roll damping.

$$\phi = A\phi_m \quad (4)$$

Where, $\Delta\phi$:decrement of roll decay curve and ϕ_m :mean swing angle of roll decay curve.

The linear fitting coefficient A can also be calculated as formula (5), for the conservation of energy.

$$A = \frac{T_\phi}{4(I_{xx} + J_{xx})} B_{44}(\phi_a) \quad (5)$$

Thus,

$$2\alpha = \frac{4A}{T_\phi} \quad (6)$$

The results of 2α are compared for different methods, which can analyze the combined error of roll amplitude and roll period. The natural roll periods measured in model tests are used in the Ikeda's simplified formula, taking into consideration that only the equivalent roll damping coefficient can be calculated by Ikeda's simplified formula.

5. THE CALCULATION RESULTS AND ANALYSIS

The grid analysis

Based on our previous studies, a simple grid analysis is given out before the numerical simulation for the dynamic overset grid method.

Taking the pure car carrier as an example, the profile of the computational domain is shown in Fig.10. The computational domain is separated into two main regions, background region and overset region, and each region is further divided into several small zones. The meshes in overlap region are refined to guarantee the data exchange between overset region and background region. The waterline plane region is also refined to capture the free surface.

Generally, the size for the background region and the overset region should be large enough to simulate actual situation. However, the size of the overset region should be as small as possible to reduce computation cost in the actual simulations. In this paper, two different widths of overset region are analyzed, one is 4B(S1) and another is 5B(S2). This is because the width is the main influential size when simulating free roll motion in calm water.

The comparison results shown in Fig.11 show that the two curves are almost the same, which meaning that the width 4B is enough for the simulations.

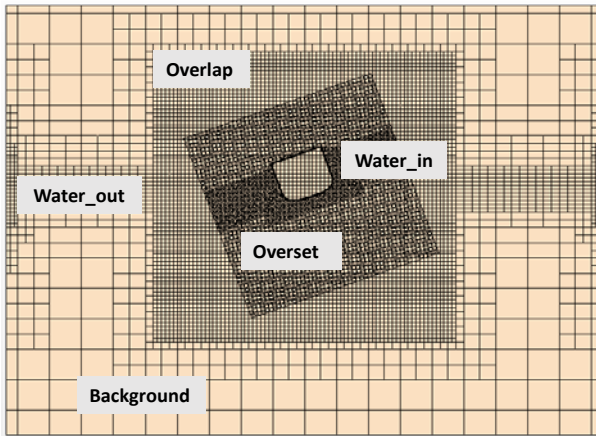


Figure 10: The profile of computational domain for the overset grid method.

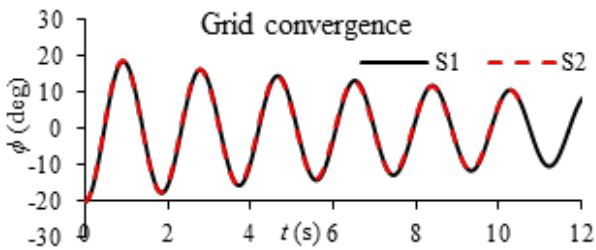


Figure 11: Comparisons between different widths of overset region.

Three cases for the grid convergence are also carried out to confirm grid density. In the first case shown as V1 in Fig.12, the base size for the background domain is equal to 0.08 and the base size for the overset domain is equal to 0.04. In the second case shown as V2, the base size is decreased to 0.07 for the background domain and 0.035 for the overset domain. In the third case shown as V3, the base size is kept for the background domain and the base size for the overset domain is decreased to 0.03. The results show that the base size in the first case is small enough for the numerical simulations.

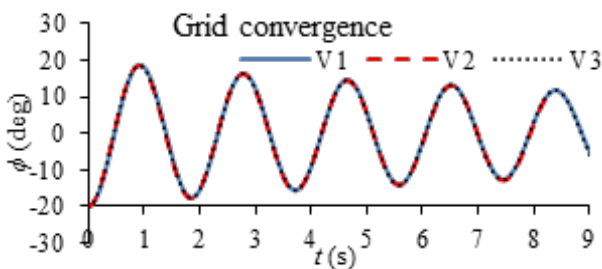


Figure 12: Comparisons between different base sizes.

The results of pure car carrier

For the free roll decay motions of the pure car carrier, the comparisons between numerical simulation results and experimental results are presented from Fig.13 to Fig.18. The results of coefficient 2α in formula (2) and (6) calculated by different methods are compared in Table 3.

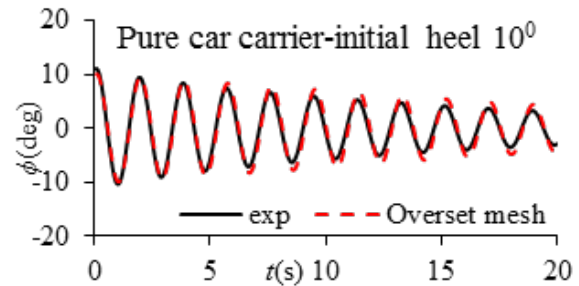


Figure 13: Free decay curves for the pure car carrier with initial heel 10°(exp, overset mesh).

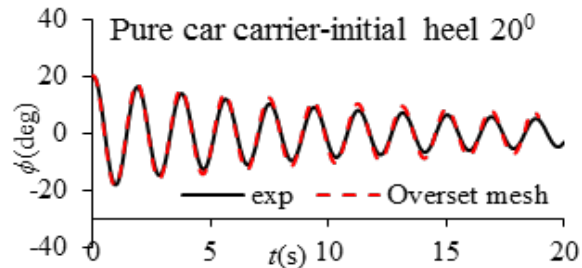


Figure 14: Free decay curves for the pure car carrier with initial heel 20°(exp, overset mesh).

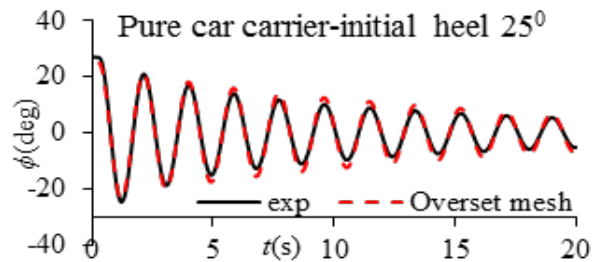


Figure 15: Free decay curves for the pure car carrier with initial heel 25° (exp, overset mesh).

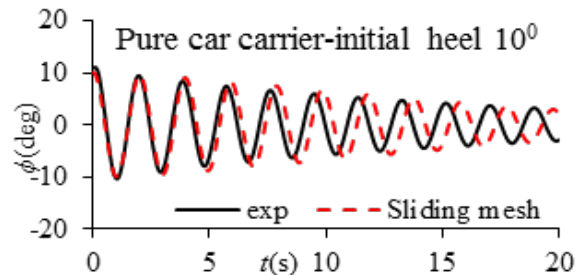


Figure 16: Free decay curves for the pure car carrier with initial heel 10°(exp, sliding mesh).

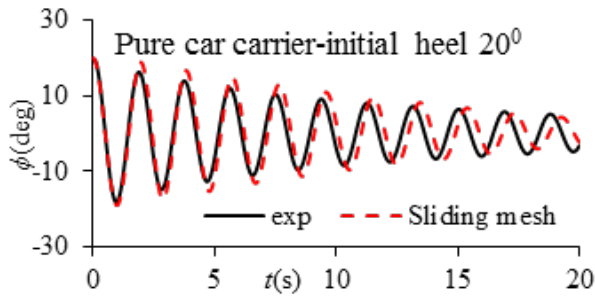


Figure 17: Free decay curves for the pure car carrier with initial heel 20° (exp, sliding mesh).

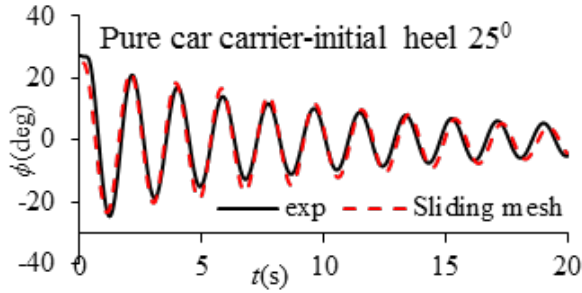


Figure 18: Free decay curves for the pure car carrier with initial heel 25° (exp, sliding mesh).

As can be seen from these figures, the roll periods calculated by the overset grid method agree better with the experimental data than that by the sliding mesh method, but the roll amplitudes calculated by the sliding mesh method are better than that by the overset grid method. Although the roll damping coefficients calculated by CFD are better than that in Ikeda's simplified formula, the errors of the pure car carrier are larger than the ship 2792 (Table 4), so the feasibility for different types of ship and different conditions should be further verified.

Table 3: Results of 2α calculated by different methods for the pure car carrier.

Initial heel	Exp	Overset mesh		Sliding mesh		Ikeda	
	Value	Value	Error	Value	Error	Value	Error
10°	0.0082	0.0050	39.02%	0.0060	26.83%	0.0046	43.90%
20°	0.0103	0.0082	20.39%	0.0089	13.59%	0.0072	30.10%
25°	0.0119	0.0092	22.69%	0.0100	15.97%	0.0085	28.57%

The results of standard model 2792

For the free roll decay motions of ship 2792, the initial roll angles 10°, 20° and 25° are simulated respectively by two methods, as shown from Fig.19 to Fig.24, and the results of coefficient 2α are shown in Table 4.

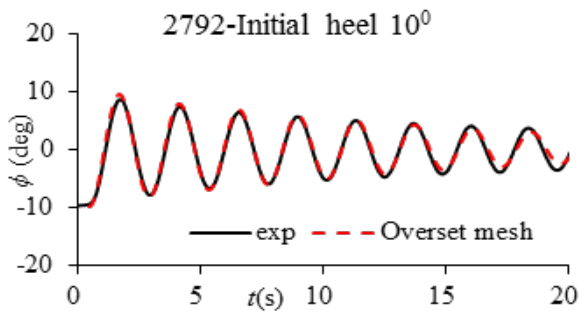


Figure 19: Free decay curves for ship 2792- initial heel 10° (exp, overset mesh).

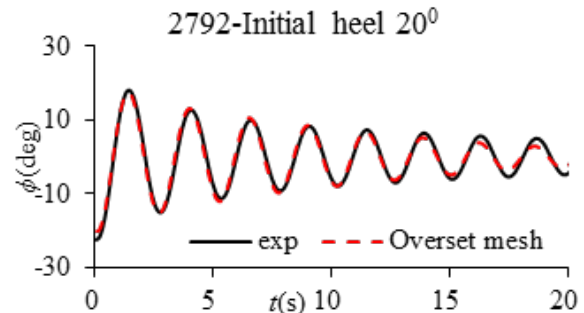


Figure 20: Free decay curves for ship 2792- initial heel 20° (exp, overset mesh).

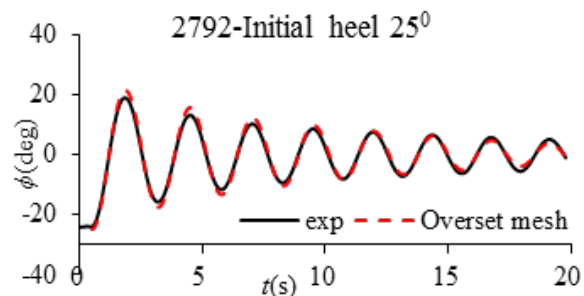


Figure 21: Free decay curves for ship 2792- initial heel 25° (exp, overset mesh).

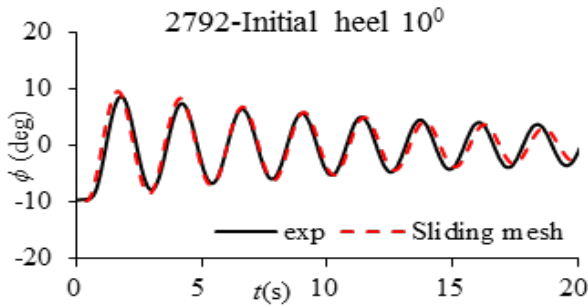


Figure 22: Free decay curves for ship 2792- initial heel 10° (exp, sliding mesh).

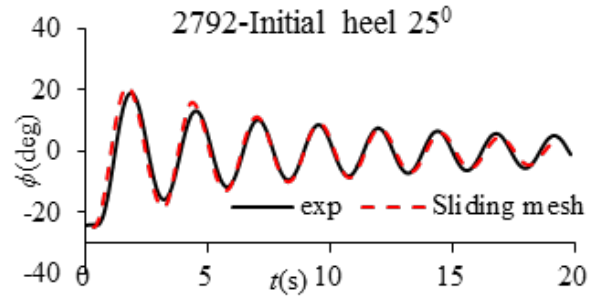


Figure 24: Free decay curves for ship 2792- initial heel 25° (exp, sliding mesh).

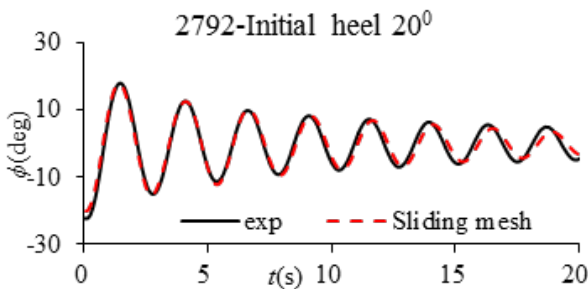


Figure 23: Free decay curves for ship 2792- initial heel 20° (exp, sliding mesh).

The curves show that the periods and amplitudes calculated by the overset grid method agree better with the experimental data than that by the sliding mesh method. The results of roll damping coefficient 2α also show that the accuracy of CFD is higher than Ikeda's simplified formula.

Table 4 Results of 2α calculated by different methods for ship 2792

Initial heel	Exp	Overset mesh		Sliding mesh		Ikeda	
	Value	Value	Error	Value	Error	Value	Error
10°	0.0076	0.0084	10.53%	0.0079	3.95%	0.0088	15.79%
20°	0.0122	0.0127	4.10%	0.0110	9.84%	0.0156	27.87%
25°	0.0157	0.0156	0.64%	0.0137	12.74%	0.0192	22.29%

6. CONCLUSIONS

As the comparisons for the free rolling motions of one standard model and one pure car carrier among two numerical simulation methods, Ikeda's simplified method and experiments, the following remarks are noted:

1) For the method of dynamic overset grid, the natural roll periods agree quite well with experimental results, but the roll amplitudes are slightly larger than experimental results. For the method of sliding interface grid, both the natural roll period and the roll amplitude are slightly larger than experimental results.

2) The roll damping coefficients calculated by CFD are better than that calculated by Ikeda's simplified formula, which indicate that CFD based on unsteady RANS equations has the ability to predict roll damping, at least for large roll amplitudes.

3) Based on our current studies, the following combination of calculation parameters are recommended when simulating free roll decay motion, unsteady RANS equations combined with RNG $k-\epsilon$ / SST $k-\omega$ two-equation turbulent model to solve flow field, VOF method to capture free surface, sliding interface technique or dynamic overset mesh technique to compute bodies motions, enhanced wall function to treat near-wall boundary layer.

In our simulations, neither of the two ships has bilge keels. However, the bilge keel damping contributes a large portion to the total damping (Bassler & Reed, 1999), so more works should be carried out in future to validate the feasibility of CFD for roll damping, and to improve the accuracy, especially for the unconventional ship with bilge keels.

7. ACKNOWLEDGEMENTS

This research is supported by Ministry of Industry and Information Technology of China (No. [2012] 533 , No. [2016] 26) and China researchfund (No.B2420132001). The authors sincerely thank the above organization

8. REFERENCES

- Blok, J.J., & Aalbers, A.B., 1991, "Roll Damping Due to Lift Effects on High Speed Monohulls", FAST'91, Vol. 2, pp. 1331-1349.
- Bassler C.C., Reed A.M., 2009, "An Analysis of the Bilge Keel Roll Damping Component Model", 10th STAB, St. Petersburg, Russia. pp:369-386.
- Min Gu, Jiang Lu, Shuxia Bu, Chengsheng Wu, Gengyao Qiu, 2015, "Numerical Simulation of the Ship Roll Damping", 12th STAB, Glasgow UK, pp:341-348.
- Ikeda, Y., Himeno, Y., & Tanaka, N., 1977a, "On Eddy Making Component of Roll Damping Force on Naked Hull", Journal of the society of Naval Architects of Japan. Vol. 162, pp. 59-69.
- Ikeda, Y., Komatsu, K., Himeno, Y., & Tanaka, N., 1977b, "On Roll Damping Force of Ship-Effect of Hull Surface Pressure Created by Bilge Keels", Journal of the society of Naval Architects of Japan, Vol. 165, pp. 31-40
- Ikeda, Y., Himeno, Y., & Tanaka, N., 1978, "Components of Roll Damping of Ship at Forward Speed", Journal of the society of Naval Architects of Japan, Vol. 143, pp. 113-125.
- Ikeda, Y., & Katayama, T., 2000, "Roll Damping Prediction Method for a High-Speed Planning Craft", Proceedings of the 7th International Conference of Ships and Ocean Vehicles (STAB'2000), Vol. 2, PP. 532-541.
- Ikeda, Y., 2004, "Prediction Methods of Roll Damping of Ships and Their Application to Determine Optimum Stabilization Devices", Marine Technology. Vol.41(2) , pp. 89-93.
- ISCG (the Correspondence Group on Intact Stability), 2015, "Draft Explanatory Notes on the Vulnerability of Ships to the Parametric Roll Stability Failure Mode", IMOSDC3/INF.10, Annex 17.
- Japan, 2011a, "Interim Verification and Validation Report on Simplified Roll Damping", IMO SLF 54/INF 12, Annex 7.
- Japan, 2011b, "Additional Validation Data on Simplified Roll Damping Estimation for Vulnerability Criteria on Parametric Rolling", IMO SLF 54/INF 12, Annex 11.
- Sweden, 2011, "Evaluation of Ikeda's simplified method for prediction of roll damping", IMO SLF 54/3/6.
- United States & Japan, 2014, "Draft Guidelines of Direct Stability Assessment Procedures as a Part of the Second Generation Intact Stability Criteria, IMO SDC1/INF.8, Annex 2.

Effect of Vortex Shedding and Free Surface Interaction on Roll Damping Due to Large Amplitude Roll Motion

Burak Yıldız, *Yildiz Technical University*, buraky@yildiz.edu.tr

Ahmet Yurtseven, *Yildiz Technical University*, ahmety@yildiz.edu.tr

Toru Katayama, *Osaka Prefecture University*, katayama@marine.osakafu-u.ac.jp

ABSTRACT

Among all ship motions, roll motion is the most important response of a ship to calculate, because large amplitude roll motions may lead to capsize, cargo shift, loss of deck cargo and other undesirable consequences. However, the accuracy of the calculated results by using linear potential flow theory, such as strip method, for roll motion lag behind the other degrees of freedom. This is because; viscosity plays an important role in roll, especially near resonance. Computational methods based on potential flow theory do not capture these viscous effects such as effective creation of vortices in the boundary layer, flow separation at appendages and vortex shedding. The vortex shedding is the main physical phenomena involved in the viscous damping of the roll motion and it affects the flow velocity around the body that may lead to pressure increase or decrease. In this study, roll damping of a forced rolling hull with bilge keel for large amplitude roll motion with free surface is calculated by using Unsteady Reynolds-averaged Navier–Stokes (URANS) solver. The generated vorticity contours around the hull and bilge keel is observed and it is showed that vortices shed from the bilge keel are proportional to amplitude of roll motion. In the case of large roll amplitude motion, the vortex shedding from the bilge keel interacts with free surface and this interaction leads to decrease on the roll damping. The results are compared with Ikeda's estimation method.

Keywords: *Roll damping, bilge keel, large amplitude, URANS, Ikeda's method, vortex shedding, free surface*

1. INTRODUCTION

Roll motion of ships is an important issue in safety and habitability of ships because it limits ship operability, affects crew performance and dynamic stability and it can lead to ship capsize. Therefore, roll motion is the most critical response of a ship in waves. For a better evaluation of roll motion, the roll damping should be calculated correctly which has a nonlinear character for large amplitudes roll motion in a seaway. The roll damping depends on not only radiated waves but also viscous effects. The roll damping from radiated waves can be computed by using linear potential theory but the viscous damping cannot be computed. The bilge

keel provides a vortex generation around the body which increases the viscous effect contribution of total damping. The generated vortices by bilge keels mitigate the roll motion by transferring energy from the ship to the surrounding fluid. Many researchers have studied the viscous roll damping prediction, e.g. Ikeda et al. [1-3], Himeno [4], and they offered some empirical methods for roll damping estimation based on model tests. Since the 1970s, Ikeda's estimation method based on the component analysis model has been used to predict roll damping. In this method, the equivalent linear damping coefficient in the roll equation, B_e , is divided into five damping components as friction,

eddy, wave, lift and bilge keel. Most modern potential flow ship motions simulation tools use this method to predict the roll motion. However, Ikeda's method is typically only valid for smaller roll motions which were only performed for roll amplitudes up to 10 degrees, and later extended to 15 degrees, where linearization is applicable. Although these limitations were acknowledged in the development of the models, the method has a few weaknesses and overestimates the results at larger roll amplitudes. The developments in CFD and experimental flow measurements have been beneficial to study these weaknesses and limitations.

Since the roll damping is dominated by vorticity, CFD based Unsteady RANS solvers have the potential to produce superior roll damping predictions compared to existing methods since the effects due to viscosity, creation of vorticity in the boundary layer, vortex shedding, and turbulence are naturally included in the calculations. The advantages, such as low cost and fast computational time compared to experiments, lead researchers to use CFD for the estimation of roll damping.

Yeung & Ananthkrishnan [5] were perhaps the first to attempt to capture the flow attributes through the application of URANS techniques, and their efforts have set the direction for further studies in this area. URANS-equation methods have been used to study the flow around two-dimensional oscillating cylinders (Korpus&Falzarano, [6]; Yeung, et al., [7]; Sarkar&Vassalos, [8]). Bassler [9] investigated the hydrodynamics of large amplitude ship roll motion as components of the added inertia and damping based on the results of forced roll test and CFD. It was shown that the effects of the hull geometry, bilge keel geometry, deck edge and the free surface all affect the hydrodynamic components during large amplitude roll motions. Avalos, et al. [10] developed a 2D,

incompressible Navier-Stokes solver to simulate free roll decay of FPSO with and without bilge keels. The simulations were compared with the experiments carried out by Oliviera and Fernandes [11]. It was observed that the vortex size and hence roll damping depends on the amplitude on roll motion and the width of bilge keel. Van Kampen [12] showed a practical method to evaluate the roll damping and motions of an FPSO with aberrant bilge keels and/or riser balconies in waves by using a commercial CFD code and the numerical results were used to modify traditional Ikeda's method. Irkal, et al., [13] carried out numerical simulations using the RANSE solver FLOW-3D to obtain the best configuration of the bilge keel for use in reducing the roll motion. The velocity and vorticity patterns around the bilge keel obtained from numerical simulations and validated with PIV measurements. Yıldız, et al., [14] showed the shallow draft effect on roll damping by using URANS method and validated the results with experiments. They also showed why Ikeda's estimation method overestimates the roll damping values at shallow draft.

Although there have been many studies on roll damping estimation by using experiments or CFD methods, there is still a critical need for development of methods for predicting large amplitude roll damping of ships with appendages. In this study, the effect of large amplitude roll motion on roll damping is investigated by using a commercial CFD code. Also the roll damping coefficients are calculated by using Ikeda's estimation method. The vorticity generation around the hull is visualized by using numerical solver. The effect of vortex shedding and free surface interaction is investigated at different roll amplitudes. It is observed that the roll damping is decreased when the bilge keel interacts with the free surface. Ikeda's method does not consider the

freesurface interaction so that the roll damping results are overestimated at large roll amplitudes.

2. ROLL DAMPING ANALYSIS

As many numerical simulations that indicate a body motion, a gradual start of the motion is needed in order to avoid strong transient flows at the earlier time-steps of the calculation. It can take considerable number of iterations to get rid of those initial peaks. The final motion of the hull will be a pure sine:

$$\phi(t) = \phi_0 \sin \omega t \quad (1)$$

A start-up function is defined that slowly increases the amplitude from zero to the final value for the first 4 periods, the frequency will be constant during the whole computation. The start-up function $f(t)$ is defined by

$$f(t) = \begin{cases} \frac{1}{2} \sin\left(\frac{1}{4} \cdot \frac{\pi}{T} \cdot t - \frac{1}{2}\pi\right) + \frac{1}{2}, & t < 4T \\ 1, & t > 4T \end{cases} \quad (2)$$

The roll angle $\phi(t)$ is now defined by

$$\phi(t) = f(t)\phi_0 \sin \omega t \quad (3)$$

The uncoupled equation of motion to describe the forced roll motion may be written as

$$(I_{\phi\phi} + a_{\phi\phi})\phi'' + B(\phi, \phi') + C(\phi) = M_E(t) \quad (4)$$

where $a_{\phi\phi}$ is the added mass for roll motion, $B(\phi, \phi')$ is the damping moment, $C(\phi)$ is the restoring moment and $M_E(t)$ is the time history of the computed moments and it is fitted with $M_E(t) = M_0 \sin(\omega t + \varepsilon)$ (5)

by applying the Fourier analysis, M_0 is the amplitude of the roll moment and ε indicates the phase angle between the prescribed roll angle and the roll moment. Time history of the computed moments is acquired via CFD simulations, then M_0 and ε can be calculated with Fourier analysis between timehistory of moments and roll angle. The final step is calculation of roll damping coefficient which can be expressed as follow:

$$B_{44} = \frac{M_0 \sin(\varepsilon)}{\phi_0 \omega} \quad (6)$$

Dimension analyses give the following dimensionless representations of the damping coefficient.

$$\hat{B}_{44} = \frac{B_{44}}{\rho \nabla B_{WL}^2} \sqrt{\frac{B_{WL}}{2g}} \quad (7)$$

3. IKEDA'S ESTIMATION METHOD

Ship roll damping may be computed using Ikeda's estimation analysis method. In this method, the equivalent linear damping coefficient in the roll equation, B_{44} , can be obtained using a linear combination of physical components, each as a function of roll amplitude, roll frequency, and forward speed.

The prediction method, which is now called Ikeda's estimation method, divides the roll damping into the frictional (B_F), the wave (B_W), the eddy (B_E) and the bilge keel (B_{BK}) components at zero forward speed, and at forward speed, the lift (B_L) is added. The roll damping coefficient, B_{44} , can be expressed as follows.

$$B_{44} = B_F + B_W + B_E + B_L + B_{BK} \quad (8)$$

Ikeda's method is developed for conventional cargo ships and it has been improved to apply many kinds of ships. However, Ikeda's method has problems to calculate roll damping when draft is shallow where the bilge keel comes closer to the sea surface during roll motion.

URANS method is a practical way to check the accuracy of the Ikeda's estimation method for such cases, and it can help us to develop more accurate models to describe and predict roll motion. The main disadvantage of URANS code at this moment is the results of these computations cannot be taken for granted. Therefore, URANS results have to be validated by comparing with experimental results.

4. NUMERICAL SETTINGS

The turbulent flow with a constant density can be described by a set of non-linear coupled partial differential equations which are derived from conservation of mass and momentum. These equations are known as Reynolds-averaged Navier-Stokes equations and conservation of mass that cannot be solved analytically for turbulent flows;

$$\left(\frac{\partial \bar{u}_i}{\partial t} + \bar{u}_j \frac{\partial \bar{u}_i}{\partial x_j}\right) = -\frac{\partial \bar{p}}{\partial x_i} + \mu \frac{\partial^2 \bar{u}_i}{\partial x_j^2} - \frac{\partial \overline{u'_i u'_j}}{\partial x_j} \quad (9)$$

$$\frac{\partial u_i}{\partial x_i} = 0 \quad \text{for } i, j = 1, 2, 3 \quad (10)$$

p defines the pressure and u shows the velocities at the each direction where i,j=1,2,3 refer to the x,y,z direction. In the present study, these equations are solved numerically by using a finite volume method based RANS solver for the flow around a forced rolling hull. A hull midsection with bilge keel is used for calculations. Table 1 shows the main dimensions of the selected model. The selected model is forced to sinusoidal roll motion at different roll amplitudes.

Table 1: Principle particulars of the model

length: L	0.80m
breadth: B	0.237m
depth: D	0.14465m
block coefficient: C _B	0.8
bilge radius	0.035m
breadth X length (BK)	0.01m x 0.80m

The selected RANS solver discretizes the transport equations before solving the equations. After the discretization step, the location of the free surface is determined by using the Volume of Fluid (VOF). The computational model has to be defined to start this step. Fig. 1 shows the computational model used in this study. There are two cell zones, the moving fluid zone and the remaining stationary zone. The cylindrical fluid zone is rotated with the

hull around the roll axis in order not to disturb the region around the body. There is an interface between stationary zone and rigid moving zone which avoids cell-deforming issue. The hull is surrounded by a circular rotating zone (inner region) and rectangular boundary (outer region). Rectangular boundary is located far enough from the body so that the velocity and pressure field generated by the oscillating body is not affected by the outer boundary. The generated mesh around the bilge keel is refined to visualize the vortices better. Fig. 2 shows the midsection of the model and the generated mesh around the hull and bilge keels.

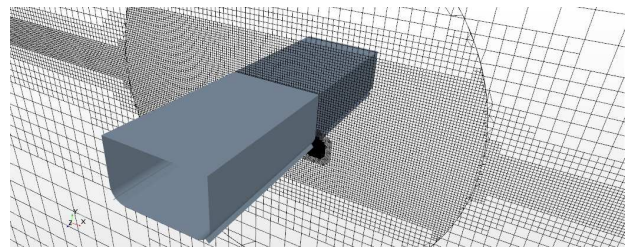


Figure 1: The geometry and computational mesh

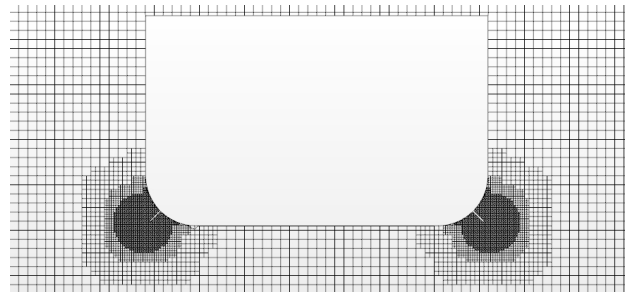


Figure 2: The generated mesh around the hull and bilge keels

5. RESULTS AND DISCUSSION

CFD computations have been carried out for the hull at different five roll amplitude values and results have been compared with Ikeda's estimation method. The moments acting on the hull and bilge keels are computed separately when the hull is forced to the roll motion. Fig. 3 and 4 show the total (hull + bilge keel) moments and bilge keel moments at different roll amplitudes. As it is shown on the Fig.3 the total moment increases when the roll

amplitude increases. However, the bilge keel moment decreases at the point where the bilge keel interacts with the free surface. This effect cannot be seen on the total moment figure because the bilge keel moment is a small portion of total moment. The effect of free surface interaction can be shown on Fig. 4. The bilge keel moment increases until 20 deg. and it decreases at 27.27 deg. where bilge keels come closer to the free surface.

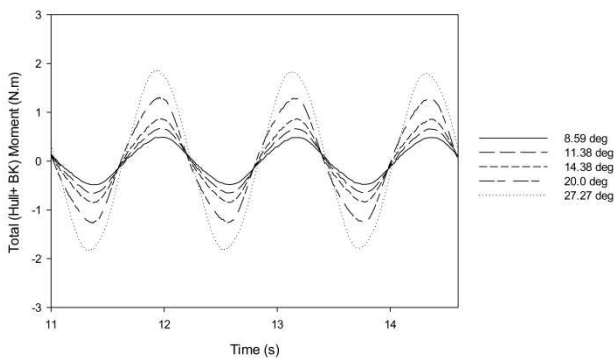


Figure 3: Time history of total (Hull + BK) moment for different roll amplitudes

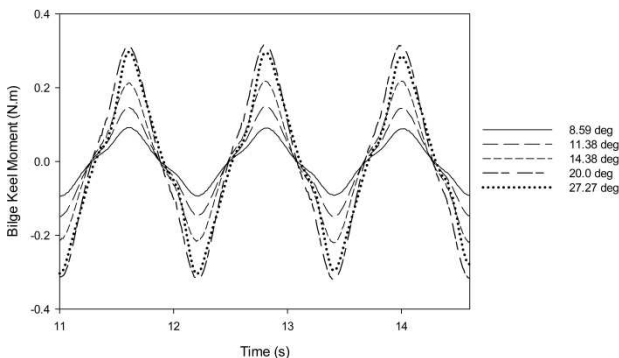


Figure 4: Time history of bilge-keel moment for different roll amplitudes

The roll damping coefficients are calculated numerically by using moments acting on the hull and bilge keels. Fig. 5 shows the numerical results and Ikeda’s method results obtained in the present study with bilge keels. The non-dimensional roll damping coefficients of the hull with bilge keels are shown for various roll amplitudes. The agreement between numerical results and Ikeda’s method for

small to moderate roll amplitudes can be observed. However, Ikeda’s assumption overestimates the values when the roll amplitude increases. This is due to free surface effect and vortex shedding from the bilge keels which are not considered in Ikeda’s method. The bilge keels interact with the free surface when the roll amplitude increases and this interaction affects the generation of the vorticity around the bilge keels. The generated vortices and vortex shedding affect the force acting on the bilge keels and the bilge keel roll damping.

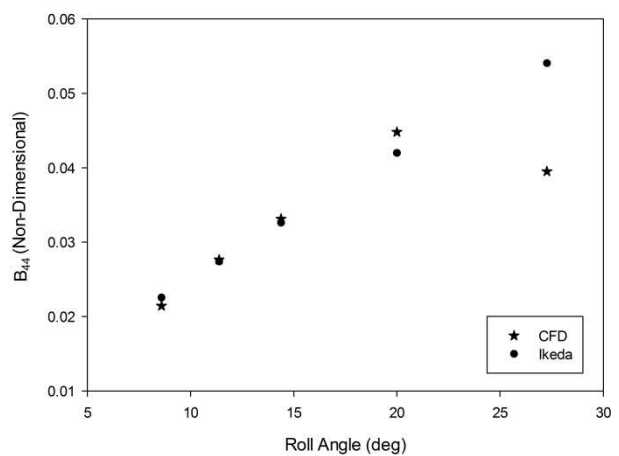


Figure 5: Roll damping coefficients at different roll angles

6. FLOW VISUALIZATION by CFD

The vorticity generation from the bilge keel corresponds to changes in the bilge keel force and the roll damping. The vortex shedding is the main physical phenomena involved in the viscous damping of the roll motion and it affects the flow velocity around the body that may lead to pressure change. To investigate the effect of the roll amplitude on the roll damping, the vorticity evolution near the bilge-keels are simulated and compared for different roll amplitudes. The blue color in the figures denotes negative (clockwise) vorticity, while the red color denotes positive (counter-clockwise) vorticity. And the vorticity (1/s) scale is same for each figure, from -50 to 50. Fig. 6 shows the generated vortices around the hull

and bilge keels at 8.59 deg. and 20.0 deg. As it is shown, the size and core of the vortices increase with the increasing roll amplitude. This explains how the roll damping increases when the roll amplitude increases. However, the roll damping decreases when the roll amplitude is 27.27 deg. At this point the bilge keel interacts with free surface as it is mentioned before. The vorticity generations around the hull are compared for different roll amplitudes to investigate the vortex shedding and free surface interaction on roll damping.

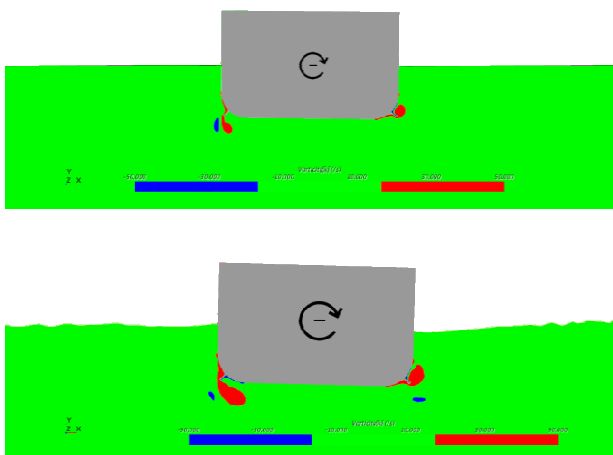


Figure 6: Vorticity contours around the hull at maximum roll speed (top=8.59 deg, bottom=20.0 deg)

Fig. 7 shows the vorticity contours around the bilge keels for 20 deg. roll amplitude, Fig. 8 is for 27.27 deg. The vortices are shown for the half oscillation period for both conditions. As it can be seen in the Fig. 7, the body is at maximum roll speed where the vortices are too strong. The generated positive vortices start to shed while the body is rolling. At the maximum roll amplitude where the roll speed is zero, the positive shed vortices start to dissipate after the hull reaches the maximum roll amplitude. At this point roll direction changes, negative vortex starts to occur from the tip of the bilge keels and rolls up gradually with increasing strength and core size. The previously generated positive vortex interacts with the newly

generated positive vortex and dissipates into the surrounding fluid while the body reaches the maximum roll velocity. The more intense negative vortex is dragging the positive vortex that is less intense, as it is also shown in Avalos et al [10]. As the body rolls to maximum amplitude, the newly generated negative vortex starts to shed from the bilge keel. When the hull reverses its direction, a new positive vortex will start to occur from the tip of the bilge keels. As the roll motion progresses in time, a new vortices will be generated every half of an oscillation and a new cycle of vortex shedding will start.

Fig. 8 shows the vorticity contours around the bilge keels for 27.27 deg. where the bilge keel interacts with the free surface. As it is shown on the figure, the vortices start to shed earlier. After the hull reaches at the maximum roll amplitude, the negative vortex starts to occur as same as 20 deg. However, the free surface affects the generation of vortices and the vortex starts to shed just after the maximum roll amplitude. This interaction with the free surface does not allow the vortices to grow up. It can be seen that the size of the vortex for 20.0 deg. condition is bigger than the large roll amplitude condition. This explains the decrease of bilge keel moment at large roll amplitude. The damping from the bilge keel decreases when the vortices become weaker.

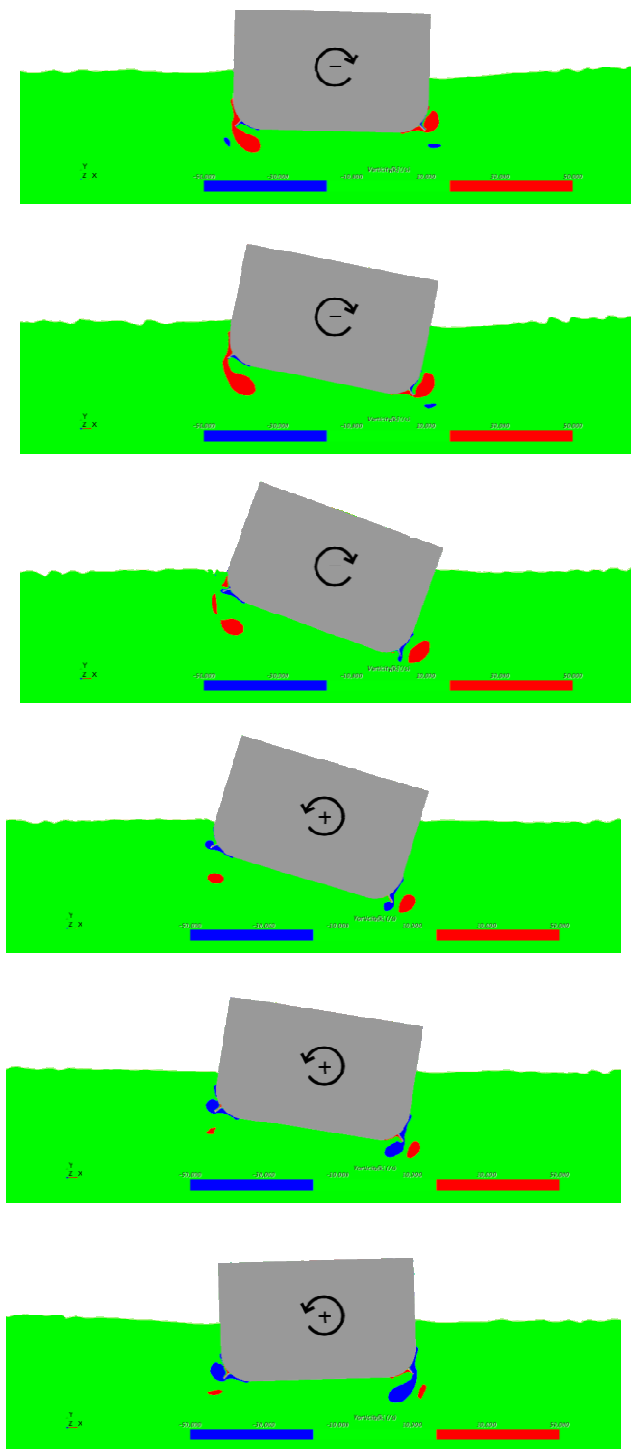


Figure 7: Vorticity contours and vortex shedding around the hull for 20.0 deg. roll amplitude

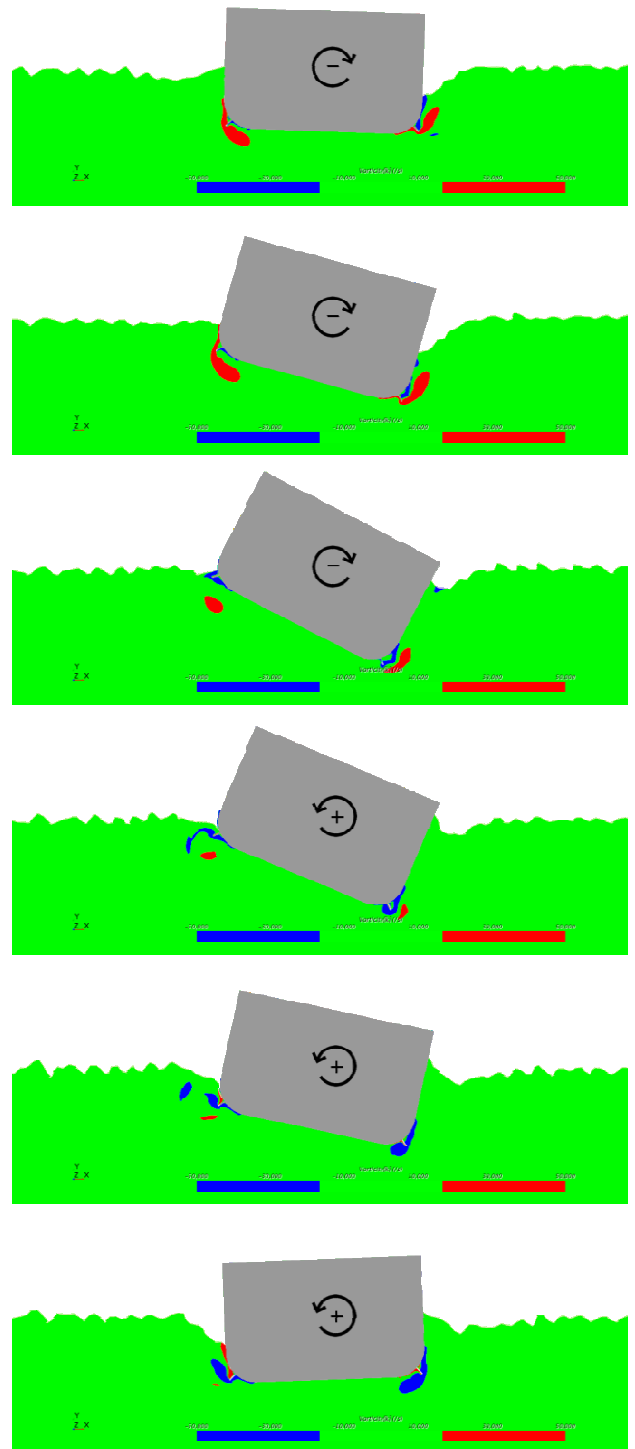


Figure 8: Vorticity contours and vortex shedding around the hull for 27.27 deg. roll amplitude

It is also observed that the free surface disturbance is stronger for 27.27 deg. as Himeno [4] cautions that the bilge keel wave-making component cannot be neglected where bilge keel interacts with free surface. It might be said the wave-making damping increases when the bilge-keel component decreases at large roll amplitudes. Wave-making damping can be calculated by using the radiated wave amplitudes but it will be studied as a future work because the mesh around the free surface needs high quality to measure wave heights.

7. CONCLUSIONS

In this paper URANS numerical solver has been used for the estimation of the effect of large amplitude roll motion on the roll damping. The unsteady flow around a forced rolling hull with bilge keels is computed. Numerical simulations are carried out and the viscous-damping coefficient is computed for various roll amplitudes. The numerical results are compared with Ikeda's estimation method.

Ikeda's estimation method shows good accuracy for small to moderate angles where linearization is applicable and the numerical results shows good agreement with Ikeda's method until 20.0 deg. However, Ikeda's method overestimates the results for large roll amplitude where the bilge keel interacts with the free surface. Ikeda's method does not consider the free surface effect and vortex shedding so that it overestimates the results. Numerical solver is used to capture the effect of vortex shedding and free surface interaction on roll damping due to large roll amplitudes. The flow around the hull with bilge keels is visualized and the generation of vortices is shown for different roll amplitudes and it is showed that vortices shed from the bilge keel are proportional to amplitude of roll motion. It is observed that the strength and the core of the

vortices grow until where the free surface interaction is not effective. This leads to increase of roll damping. The roll damping coefficient starts to decrease when the bilge keel come closer to the free surface because the free surface affects the generation of vortices and vortex shedding.

Results show that the numerical calculation is a practical and fast way to estimate the roll damping and it can be used to modify the existing method especially where the method is not applicable, like large roll amplitudes.

8. REFERENCES

- [1] Ikeda Y, Komatsu K, Himeno Y, Tanaka N. On roll damping force of ship-effect of hull surface pressure created by bilge keels. *J Kansai Soc Naval Architect Japan* 1977:165.
- [2] Ikeda Y, Himeno Y, Tanaka N. On eddy making component of roll damping force on naked hull. *J Kansai Soc Naval Architect Japan* 1977:142.
- [3] Ikeda Y, Himeno Y, Tanaka N. Component of roll damping of ship at forward speed. *J Kansai Soc Naval Architect Japan* 1978:143.
- [4] Himeno Y. Prediction of ship roll damping – state of art. Department of Naval Architecture and Marine Engineering. University of Michigan, USA, Report No, 239; 1981.
- [5] Yeung R, Ananthakrishnan P. Oscillation of a floating body in a viscous fluid. *J. Engin. Math.*, 26:211-230, 1992.
- [6] Korpus R, Falzarano J. Prediction of viscous roll damping by unsteady Navier-Stokes techniques. *J. Offshore Mech. And Arctic Engin.*, 119:108-113, 1997.
- [7] Yeung R, Liao W, Roddier D. On roll hydrodynamics for rectangular cylinders. *Proc. 8th Int. Offshore and Polar Engin. Conf.*, Montreal, Canada, Vol. 3. pp. 445-53, 1998.
- [8] Sarkar T, Vassalos D. A RANS based technique for simulation of the flow near a rolling cylinder at the free surface. *Mar. Sci. Technol.*, 5:66-77, 2000.

-
- [9] Bassler C.C. Analysis and Modeling of Hydrodynamic Components for Ship Roll Motion in Heavy Weather, Ph.D. Thesis, Virginia Polytechnic Institute and State University, 2013.
- [10] Avalos G.O.G, Wanderley J.B.V, Fernandes A.C. Roll damping decay of a FPSO with bilge keel. Proc. in ASME 32nd Int. Conf. of Offshore Mech. And Arctic Eng., 2013.
- [11] Oliveira A.C, Fernandes A.C. The nonlinear roll damping of a FPSO hull. J. Offshore Mech. Arct. Eng., 136(1):1-10, 2014.
- [12] Van Kampen M.J. Bilge Keel Roll Damping Combining CFD and local velocities, Delft Uni. Of Technology, Master of Science Thesis, 2015.
- [13] Irkal M.A.R, Nallayarasu S, Bhattacharyya S.K. CFD approach to roll damping of ship with bilge keel with experimental validation. Applied Ocean Research, Vol. 55. pp 1-17, 2016.
- [14] Yıldız B, Çakıcı F, Katayama T, Yılmaz H. URANS prediction of roll damping for a ship hull section at shallow draft. J. Marine Science and Technology, Vol. 21, Issue 1. pp. 48-56, 2016.

A framework for holistic roll damping prediction

Carl-Johan Söder, Wallenius Marine AB / KTH Royal Institute of Technology, cjsoder@kth.se

Anders Rosén, KTH Royal Institute of Technology, aro@kth.se

ABSTRACT

In this paper a framework for holistic multi-tier roll damping prediction is presented. The approach provides a platform for best possible prediction given the different stages in the ship design process. Starting from the earliest design stage a semi-empirical model gives the foundation for a complete model that is applicable for all possible loading conditions and operational conditions. The components in the model are continuously updated with input from CFD calculations and model tests when available, and finally prior to delivery of the ship the model is assessed and tuned based on full scale trials. The approach is well suited to be used as roll damping input in operational guidance systems as well as to provide feedback to the design process in a systematic manner.

Keywords: *Roll damping, Roll decay, Ikeda's method, Full-scale, Model-scale, Holistic, Extrapolation, Operational guidance*

1. INTRODUCTION

Accurate roll damping modeling is crucial to assess and control vulnerability to critical roll responses both in the design stage and in the operation. Yet, the roll damping is rarely given sufficient attention (if any) in the design process when it comes to hydrodynamic optimization.

In a typical design process the vast majority of the hydrodynamic focus is put on predicting and minimizing the power requirement of the vessel. In most cases these efforts are concentrated to one single design point, reflecting the speed and loading condition that is stipulated in the new building contract. Semi-empirical methods are normally used for the first power predictions in the conceptual stage. This may involve established methods such as Holtrop Mennen (1982) or in house methods based on reference hulls. The second stage of the process normally involves hull line optimization using Computational Fluid Dynamics (CFD) and in the third stage the most promising hull shapes are evaluated using model tests. Typically one or two hull form alternatives and several propeller and rudder configurations are tested in the towing tank. Based on these tests full scale predictions are updated using well established transparent extrapolation procedures such as ITTC (1999). Prior to the delivery the vessel is taken out on sea trial where a speed trial is conducted. For

practical reasons the speed trial is normally performed in ballast draught and evaluated for the contractual condition using procedures such as ITTC (2014) where weather effects and load case effects are eliminated. Throughout this process a power performance model is continuously updated and ultimately finalized after the sea trial, prior to the delivery of the ship. For design houses and ship yards the speed trial is a key event as contractual figures are assessed and feedback is given to the design process. A schematic picture of the different stages of the design process is given in figure 1.

If the roll damping has been given any attention in the design process this has likely been done in the model test stage by carrying out roll decay tests. At this stage the hull lines are more or less set and it is normally too late to make any drastic changes. For practical reasons the roll decay tests are likely carried out in the design condition only and the non-dimensional roll damping is evaluated from the decays and assumed to be valid for the full scale vessel, typically regardless of condition. However, the design condition does not necessarily have to be a realistic service condition and normally describes the vessels' performance in calm weather. For many ship types, ocean going vessels in particular, the loading condition and speed can be different for every voyage. Furthermore, the operation is certainly not limited to calm weather.

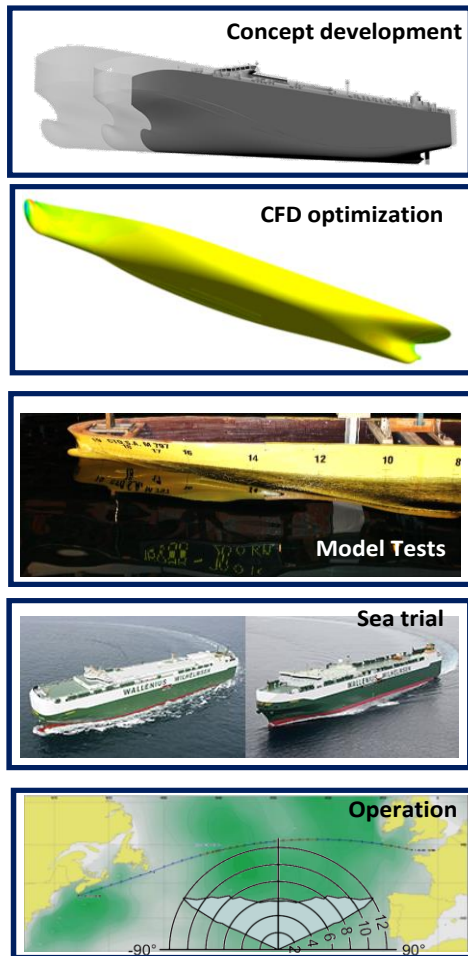


Figure 1: Illustrating the different stages in the design process

This paper presents a framework for a holistic multi-tier roll damping prediction approach where a roll damping model, that is applicable to all possible operational conditions, is developed and improved throughout the design and building process. The model is established in the earliest concept development stage and continuously improved all the way to sea trial and the delivery of the ship and is suitable to be used as input for operational guidance. The roll damping is treated on component basis and the extrapolation and tuning of these components is inspired by the well-established power prediction extrapolation procedures, such as ITTC (1999). The idea with this approach is, besides providing a platform for best possible prediction given the different stages in the design process and for the vessel in service, also to provide feedback to the design process in a systematic manner.

2. THE HOLLISTIC APPROACH

For the concept development stage the only feasible approach for estimating the roll damping is semi-empirical methods. Ikeda's method is the most established semi-empirical method and the damping is estimated as the sum of the following components:

hull lift	$\zeta_{Lift}(V)$,
bilge keel	$\zeta_{bk}(\omega_E, \varphi_a, V)$,
hull friction	$\zeta_{friction}(\omega_E, \varphi_a, V)$,
eddy making	$\zeta_{eddy}(\omega_E, \varphi_a, V)$,
wave damping	$\zeta_{wave}(\omega_E, V)$.

Besides the hull main parameters for the considered floating condition these components are also dependent on ω_E, φ_a and V which is the natural roll frequency, roll amplitude and forward speed. As load case specific components are considered the model is useful to identify operational conditions that may require particular attention and provides a good foundation for the holistic roll damping model.

2.1 Updated Lift and Aerodynamic damping

Ikeda's original method (1978) as described in Himeno (1981) and ITTC (2011) gives physically relevant estimates but quantitatively not satisfying levels for unconventional designs such as modern volume carriers. However, the method can be significantly improved with small modifications of the hull lift component. Figure 2 shows a comparison for a modern Pure Car and Truck Carrier between model tests and Ikeda's bare hull damping where the hull lift coefficient has been estimated with non-viscous CFD and applied together with Yomuru's original expressions for the levers of the lift force and the effective angle of attack. As seen, satisfying agreement with model tests is obtained. As practically the same calculation model that is used for the power predictions can be used to obtain the lift coefficient of the hull the additional work to provide required input for this estimate is fairly limited.

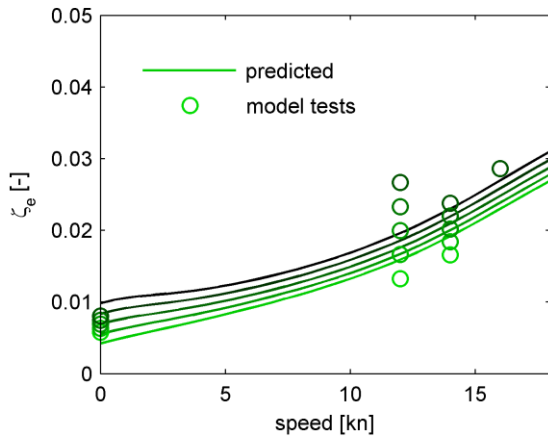


Figure 2: Predicted damping for the bare hull of a Pure Car and Truck Carrier in model scale using Ikeda's method with the lift damping component is estimated with hull lift coefficient from non-viscous CFD together with Yomuru's original expressions for the levers of the lift force and the effective angle of attack, compared with model tests for roll amplitudes of 2 to 10°.

In Söder et al (2015) it was demonstrated that aerodynamic damping not always is neglectable relative to hydrodynamic damping and therefore preferably shall be considered. The estimation of this component however requires input on the aerodynamic lift coefficient of the hull. This coefficient can either be estimated at an early stage from reference hulls or from CFD. Thus ζ_{lift} and ζ_{aero} can be replaced by $\zeta_{liftCFD}$ and $\zeta_{aeroCFD}$. An updated roll damping model can thus be given by

$$\zeta = \zeta_{liftCFD} + \zeta_{bk} + \zeta_{friction_S} + \zeta_{eddy} + \zeta_{wave} + \zeta_{aeroCFD}. \quad (1)$$

In Ikeda's model only the frictional component has a scale dependence and sub-index S here denotes full scale.

2.2 Extrapolation of model tests

Free roll decay model tests can be performed in the towing tank with the same model as used for the power predictions. Model tests at speed are typically performed with the same *Froude* number as the full scale vessel so the wave pattern shall be the same in the two scales. Currently there are no established scaling procedures for roll damping model tests. According to IMO (2006) scale models with bilge keels shall have a minimum length of 2m, the bilge keel height shall exceed 7mm and the scale factor shall not be larger than 1:75 to avoid viscous scale effects. As typical models at the established towing tanks often measures some 6 to 7m these requirements are normally fulfilled.

However, as the Reynolds numbers are different neglecting viscous scale effects is questionable, especially when the damping is low and the bilge keels are small. Worth noting here is also that model tests intended for power predictions are normally performed without bilge keels due to the uncertainties related to the viscous scale effects. An attempt is therefore made here on proposing an extrapolation procedure for model tests. The bare hull damping and the bilge keel component is treated separately and model test with and without bilge keels are required.

2.2.1 Bare hull extrapolation

To evaluate the bare hull damping a similar procedure as used in the ITTC (1999) power prediction extrapolation procedure is suggested. In those procedures the wave component, which is considered scale independent, is basically derived by deducting a semi-analytical expression for the viscous (and form) components. In a similar manner it is proposed to evaluate the wave damping component according to

$$\zeta_{wave_m} = \zeta_{bh_m} - (\zeta_{liftCFD} + \zeta_{friction_m} + \zeta_{eddy}) \quad (2)$$

where ζ_{bh_m} is the evaluated damping of the bare hull from the model tests and $\zeta_{friction_m}$ is the frictional component in model scale. In Ikeda's method the eddy component is not dependent on the Reynolds number which could be questioned. However, for simplicity the same assumption is made here.

Based on the result for the model tested load case a tuning function $k_{wave}(V)$ is used to tune the expression for the linear potential damping that was used in the earlier stage for best match with the evaluated wave damping for the tested case. The tuning function is obtained by minimizing the difference between the evaluated wave damping and the product of the tuning function and the linear potential damping $\zeta_{wave}(\omega_E, V)$ according to

$$\min_{k_{wave}(V)} \overline{\zeta_{wave_m} - k_{wave}(V) \cdot \zeta_{wave}(\omega_E, V)} \quad (3)$$

The full scale wave damping component can then be estimated as

$$\zeta_{wave_S} = k_{wave}(V) \cdot \zeta_{wave}(\omega_E, V). \quad (4)$$

The tuning function derived for the tested load case is thereafter held constant for other load cases.

2.2.2 Bilge keel extrapolation

To investigate how the bilge keels are subjected to viscous scale effects the boundary layer thickness at the bilges are studied for an actual hull shape. CFD calculations are performed in ANSYS with a 230m Pure Car and Truck Carrier in model scale 1:30 and full scale. The calculations are performed with a boundary layer mesh corresponding to $y^+ \sim 1$ in model scale and $y^+ \sim 100$ in full scale and with standard wall functions. Due to simplifications introduced with the wall functions in full scale in particular the results need to be considered with care. The boundary layers are shown in figure 3, as seen the differences in boundary layer thickness are remarkable. When considering that a typical bilge keel height of this kind of vessel is some 0.4 to 0.8m deep in full scale (or 1 to 3% of the breadth) it appears that scale effects needs to be considered even if IMO's guidance is met.

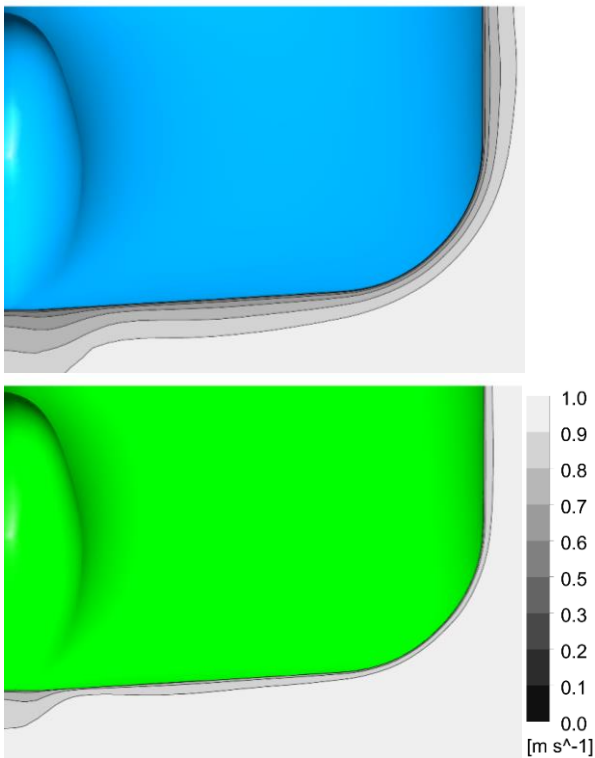


Figure 3: Comparing the boundary layer thickness in model scale at the top and full scale at the bottom for a 230m PCTC. Results are normalized and corresponds to Reynolds number that give the same Froude number, full scale speed 10kn.

In a greatly simplified manner it is investigated how the bilge keels could be affected by the different conditions by evaluating how the 2D drag of a 0.4m high flat plate perpendicular to a wall is dependent on the boundary layer thickness.

Conditions are set to represent typical local Reynolds number Re_x of full scale and model scale bilge keels given a scale factor of 1:30. The velocity fields are shown in figure 4 where also a third case without boundary layer is added.

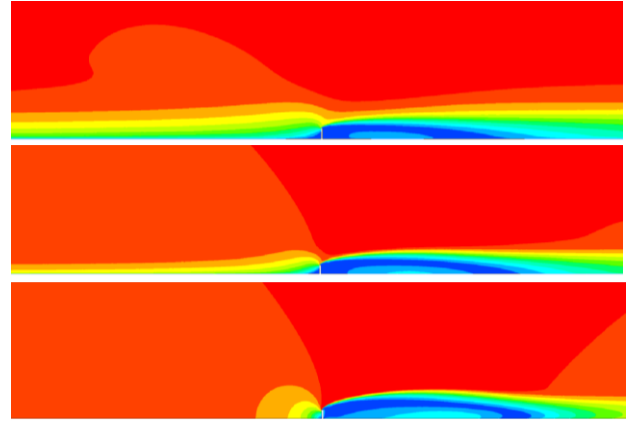


Figure 4: Comparing the boundary layer thickness over a wall where a 0.4m high flat plate is located perpendicular to the flow. Conditions are set to represent typical local Reynolds number in way of bilge keels in model scale (1:30), in full scale and without boundary layer (symmetry boundary condition).

For this specific case the calculations suggests that the drag coefficients of the plate in full scale is some 50% higher than in model scale. In addition, without any boundary layer (symmetry b.c.) the drag increases with additionally 70% relative full scale. In view of these results it is proposed to consider the scale effect of the bilge keel damping when extrapolating model tests. The following procedure is proposed.

The damping of the bilge keel component in model scale ζ_{bk_m} can be estimated as

$$\zeta_{bk_m} = \zeta_{tot_m} - \zeta_{bh_m} \quad (5)$$

where ζ_{tot_m} is the damping of the hull fitted with bilge keels in model scale. With a similar procedure as for the wave component a tuning function $k_{bk}(V)$ is estimated as

$$\zeta_{bk_m} = k_{bk}(V) \cdot \zeta_{bk}(\omega_E, \varphi_a, V) \quad (6)$$

The scale correction is estimated as the ratio between the mean dynamic pressure over the full scale bilge keel and the model scale keel according to

$$S_{bk} = \int_0^{\delta_s} \left(\frac{u(z)}{U_\infty} \right)^2 dz_s / \int_0^{\delta_m} \left(\frac{u(z)}{U_\infty} \right)^2 dz_m. \quad (7)$$

The velocity profile and the boundary layer thickness δ at the bilge keels can either be estimated using CFD or in a simplified manner

based on Prandtl's (1/7)th power law together with the local Reynolds number Re_x at a longitudinal position x according to

$$\frac{u_z}{U_\infty} = \sqrt[7]{\frac{z}{\delta}} \quad (8)$$

and

$$\delta \approx 0.385 x / \sqrt[5]{Re_x}. \quad (9)$$

The bilge keel damping in full scale can then be estimated according to

$$\zeta_{bk_S} = k_{bk}(V) \cdot \zeta_{bk}(\omega_E, \varphi_a, V) \cdot S_{bk} \quad (10)$$

2.3 Full scale assessment

The roll damping model for the full scale vessel is now given by

$$\zeta = (\zeta_{LiftCFD} + \zeta_{bk_S} + \zeta_{friction_S} + \zeta_{eddy} + \zeta_{waves_S} + \zeta_{aeroCFD}) k_{corr}. \quad (11)$$

where k_{corr} is an overall tuning coefficient or correction factor.

To assess the model and establish k_{corr} full scale trials needs to be performed. In Söder et al. (2012) full scale roll-decay tests were performed by inducing roll motion using controlled rudder impulses. This approach is suitable to use here and a sample roll decay test is illustrated in figure 5.

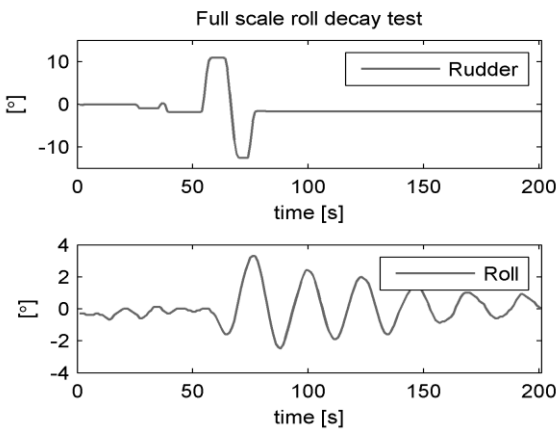


Figure 5: Time series of rudder angle and roll angle during a full scale roll decay test onboard a Pure Car and Truck Carrier.

The tests could preferably be carried out prior to delivery during the ordinary sea trail, for instance during the speed tests after completion of each speed measurement during the speed runs. This is particularly suitable as double runs typically are carried out with and against the wind direction so uncertainties related to the wind damping can be minimized.

3. EVALUATION

In figure 6 the roll damping for a Pure Car and Truck Carrier, as given by the complete model is illustrated together with model test and full scale results. In this case the model tests and full scale tests were carried out at virtually the same load case. The weather condition during the full scale trials was calm so the aerodynamic damping was negligible. The results from the complete model are given without overall correction factor as well as with correction factor. As seen there is a fairly large gap between these two curves which requires further attention. Scale effects not properly accounted for or biases in the test setup are likely causes which need to be investigated thoroughly.

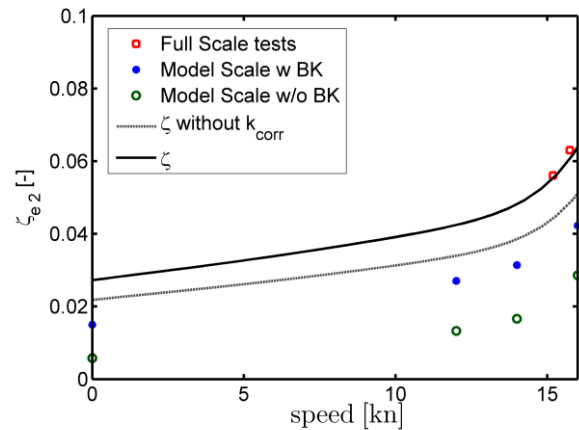


Figure 6: Damping as evaluated from model tests, full scale tests and the complete model. All three methodologies with virtually the same load case. The linear equivalent damping at 2° is given for all cases.

To demonstrate application of the holistic model it is used to estimate the damping for two “off design” conditions for the same vessel, a partial loading condition and a scantling condition. The linear equivalent damping for 2, 4 and 6° are given in figure 7 and as seen the difference in damping is large for these two cases.

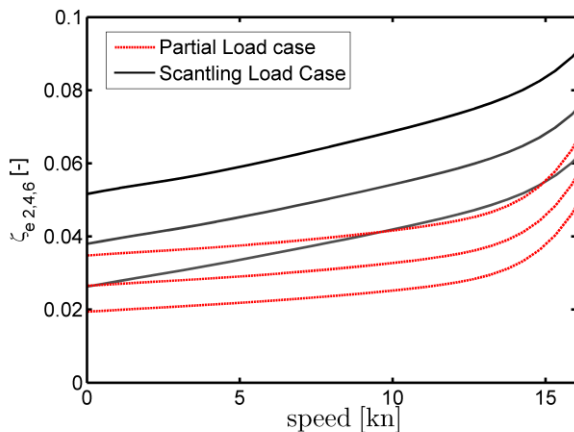


Figure 7: Damping as evaluated from the holistic model for a partial load case and a scantling case for a Pure Car and Truck Carrier. The linear equivalent damping at 2,4 and 6° are given, counted upwards.

4. DISCUSSION

Roll damping can be estimated using semi-empirical methods, computational fluid dynamics (CFD) calculations, model tests or full scale tests. None of these methods may alone be sufficient to capture the full roll damping behavior of a given ship in any given condition. However, they can all provide a valuable contribution in the different stages of the design process and in service.

The roll damping is rarely given sufficient attention (if any) in the design process when it comes to hydrodynamic optimization. Yet, with insufficient damping a new design may need to be operated with restrictions (more conservative routing) or loaded with restrictions (less cargo or more ballast water) to get an adequate dynamic behavior in certain conditions. Therefore, assessing the dynamic behavior of the vessel in different service conditions at an early stage is crucial when optimizing the design to identify if any operational conditions require particular attention.

For operational guidance systems providing in-situ ship-specific decision support, such as Ovegård et al (2012), a proper consideration of damping in the actual condition is crucial to provide relevant guidance and thus improve the safety level and avoid unnecessary deviations. With irrelevant information in onboard decision support systems guidance will be too rough which will lead to reduced safety level or unnecessarily conservative operation.

Scale effects related to roll damping requires more attention. The CFD calculations in this paper

indicate that the scale effects, especially related to the bilge keels can be significant. Further work is required and the here presented holistic approach is a way forward for addressing the problem.

5. CONCLUSIONS

In this paper a framework for holistic multi-tier roll damping prediction has been presented. The approach provides a platform for best possible roll damping prediction given the different stages in the design process and for operation.

Starting from the earliest design stage Ikeda's semi-empirical model complemented with an aerodynamic component gives the foundation for a complete model that is applicable for all possible loading conditions and operational conditions. As the hull lines evolves the model can be updated with input from CFD calculations providing the hull specific lift coefficient and a more precise lift damping component. In the next stage of the design process updated input is provided from model tests. The bare hull damping and the bilge keel damping is treated separately and model test with and without bilge keels are required to establish these components.

To evaluate the bare hull damping semi-analytical expressions for the viscous components and lift components are deducted from the total damping and the remaining part is considered to be the *Froude number* dependent potential damping. A tuning function is used to match the evaluated potential damping for the tested case with the model for linear potential damping that typically is calculated using strip theory. The method incorporates a simplified scaling procedure for the bilge keel component reflecting the different viscous effects and in the model scale relative to full scale. The scaling procedure is based on the differences in dynamic pressure over the bilge keels due to the different boundary layer and results demonstrate that these effects can be considerable. Finally prior to delivery of the ship the model is assessed and tuned based on full scale trials. In this stage the final model that can be used as input for operational guidance is assessed and feedback to the design process can be given in a systematic manner.

Further work is needed on assessing tuning functions that are robust for different load cases for the potential damping. Model tests in different load

cases and speeds are needed together with linear potential calculations for the corresponding conditions. Assessment of the full scale correlation factor also requires further attention. The accuracy of full scale trials need to be investigated and guidelines for successful tests established.

6. ACKNOWLEDGEMENTS

This research has been financially supported by the Swedish Mercantile Marine Foundation (Stiftelsen Sveriges Sjömanshus) and the Swedish Maritime Administration (Sjöfartsverket) which are both gratefully acknowledged.

7. REFERENCES

Holtrop J. & Mennen G.G.J., 1982, "An Approximate Power Prediction Method", International Shipbuilding Progress, no 29 (335), 166-170

Himeno Y., 1981, "Prediction of Ship Roll Damping- State of the Art", The University of Michigan College of Engineering, No.239.

Ikeda Y., Himeno Y. & Tanaka N., 1978, "Components of roll damping of ship at forward speed", Journal of the Society of Naval Architects of Japan, Vol. 143.

IMO, 2006, "Interim Guidelines for Alternative Assessment of the Weather Criterion", MSC.1/Circ.1200.

ITTC, 1999, "1978 ITTC Performance Prediction Method", International Towing Tank Conference, Report 7.5 – 02-03 – 01.4.

ITTC, 2011, "ITTC Recommended Procedures Numerical Estimation of Roll Damping", International Towing Tank Conference, Report 7.5-02-07-04.5

ITTC, 2014, "Speed and Power Trials", International Towing Tank Conference, Report 7.5-04-01-01.1/ 7.5-04-01-01.2

Ovegård E., Rosén A., Palmquist M., Huss M., 2012, "Operational Guidance with Respect to Pure Loss of Stability and Parametric Rolling", 11th Intl Conf on the Stability of Ships and Ocean Vehicles (STAB 2012), Greece.

Söder C-J., Rosén A., Werner S., Huss M. & Kutenkeuler J., 2012, "Assessment of Ship Roll Damping Through Full Scale and Model Scale Experiments and Semi-Empirical Methods", 11th

Intl Conf on the Stability of Ships and Ocean Vehicles (STAB 2012), Greece.

Söder C-J., Ovegård E., Rosén A., 2015, "On Aerodynamic Roll Damping", 12th Intl Conf on the Stability of Ships and Ocean Vehicles (STAB 2015), UK.

SESSION 7

Operational aspects of ship stability

Operational stability beyond rule compliance

Mikael Huss, *Senior Advisor, Wallenius Marine AB*, mikael.huss@walleniusmarine.com

ABSTRACT

This paper summarises operational experience and stability management activities within a shipping company in order to maintain safe and efficient shipping with car carriers. It is recognised that this type of ships has developed to become more sensitive to stability variations in waves and that the existing requirements in the Intact Stability Code and other IMO regulations and guidelines so far give very limited operational guidance. Stability management activities discussed include design measures, decision support systems on board, training and monitoring. It is believed that all these areas should be addressed in the future for ships that are found vulnerable under the second generation intact stability criteria presently under development within IMO.

Keywords: *Stability in waves, Parametric rolling, Car carriers, Second generation intact stability criteria*

1. INTRODUCTION

Although stability criteria in the Intact Stability Code have been applied by most national administrations for a long time, they became internationally mandatory as late as 2010 through amendments to the SOLAS and Load Line Conventions. The general criteria provide *GZ* requirements that aim to cope with various events causing large heeling moments to an intact ship. Together with other design requirements on freeboard, water and weather tightness and damage stability, a reasonable level of stability robustness is in general achieved for ships of any kind. Still, the main contribution to safety can probably be found in proactive operational measures to avoid the critical events to occur; e.g. lashing to avoid cargo shift, route planning to avoid extreme wind and waves and navigational procedures and systems to avoid collisions. Many of these measures are reflected by other requirements in other chapters of the conventions.

For ships designed to carry large volumes and high centre of gravity, such as car carriers, container vessels or cruise ships, stability is one of the major design constraints. The vulnerability to stability variations in waves, which is not explicitly covered by today's rules, becomes much more critical for these ships. The ongoing development of additional intact stability requirements with regard to phenomena such as parametric excitation and loss of stability in waves is certainly well motivated and

will also open up for additional proactive actions, including both design and operational measures.

For Wallenius Shipping with a large number of car carriers operating around the world and a continuous program with new vessel designs, stability management has been identified as a key area of interest with regard to safety, quality and efficiency objectives. This presentation gives some examples of how these three objectives have been targeted by activities in design, decision support systems, training and monitoring. It intends to open up for a discussion on what is needed to further improve safe and efficient operation in the future.

2. EVOLUTION OF CAR CARRIERS

The evolution of dedicated ships for transportation of cars and trucks can be traced back to the 1950s. Following the reconstruction after the war, the demand for new cars increased on both sides of the North Atlantic. In 1956, the Swedish ship owner Olof Wallenius who had been engaged mainly with tankers and bulkers but also with two small car carriers for the Great Lakes, received a long-term contract with Volkswagen for transport of cars to the US. At that time cars had mostly been carried in general cargo ships but were now started to be carried on larger scale in combination or alternation with other cargo on bulk carriers on demountable decks or in reefers. During the following years different concepts for handling cars were developed and tested including side ramps, bow ports and ele-

vators but the vast majority of cars were still lifted on/off in traditional cargo holds.

The RoRo concept that initially emerged for short sea transportation during the early 1960s was adopted for ocean transport in the highly innovative first and second generation combined Ro-Ro/Container vessels for Atlantic Container Line that started on Wallenius' initiative. This concept led further to the first two dedicated Pure Car Carriers (PCC) delivered in 1975-1976 with a length of 200 m, a breadth of 28.2 m and a capacity of 4900 cars. They were followed by the two first Pure Car and Truck Carriers (PCTC) in 1977 with length 190 m, Panamax breadth 32.2 m and a capacity of 5500 cars. At that time Wallenius had become a main tonnage provider for the rapidly expanding Japanese export of cars around the world (Wallenius-Kleberg, 1984)

The 200/32 m PCC or PCTC have been standard concepts for world wide car transport since then, mainly driven by the restrictions in Japanese ports and by the Panama Canal. It has been joined by the larger LCTC with a length of about 230 m and lately by 200 m vessels with a breadth beyond the present Panama restrictions, both types with a typical capacity of about 8000 cars. The world fleet consisted in the mid 2015 of about 470 car carriers with a capacity of 5000 cars or more with additionally about 60 ships in order (Fearnsearch, 2015).

Although the main dimensions of typical PCTCs have been maintained for more than three decades, the development towards more efficient ships has continued within those restrictions. Table 1 compares the capacity of three generations of PCTC. The increase in car deck capacity of about 20% is dramatic and has also resulted in significantly higher centre of gravity for the cargo, compensated for by increased form stability and increased ballasting.

Table 1: Comparison of capacity of three generation PCTC, all with length over all 200 m, breadth 32.3 m and design draught 9.5 m.

Date of delivery	Capacity car units	Deck area [m ²]	VCG of load on car decks [m]	KM at design draught [m]
1985	5300	47300	19.4	14.8
1995	5850	52400	20.4	15.7
2006	6700	56400	21.9	16.4

PCTCs may seem just as floating garages by sight but indeed their underwater hull have very sophisticated forms to obtain the lowest possible fuel consumption under variable service conditions and to obtain the the highest possible initial stability to carry large volumes of cargo with high centre of gravity. To raise the metacentre with 1.6 m as shown in Table 1, within the main dimension constraints without increasing resistance is indeed a significant achievement for increased transport efficiency.

From 1983, the intact stability criteria required by the Swedish Administration have been the same as the general criteria in the Intact Stability Code, i.e. they have remained unchanged through the development of the standard PCTC. Due to the large superstructure, the criteria are not decisive in general, only at light draft may the weather criterion require rather high GM , but that will anyway be at hand for the ballast conditions. For normal service conditions including margins for manoeuvres, wind and waves, a GM below 0.8 m has in general not been considered feasible as an operational seagoing condition. This is significantly above the GM limits given by the Code, which typically could be around 0.3 m. When the first probabilistic damage stability requirements for dry cargo ships became effective from 1992, this led to some changes in the watertight subdivision, but the GM -limit could still be maintained at about the same level as had been used in practice as minimum before. Even the significantly stricter damage stability requirements from 2009 could be handled by additional horizontal subdivision with a GM minimum at loaded condition marginally raised to about 0.9 m.

3. OPERATIONAL EXPERIENCE

The development of stability optimised hull forms has naturally also led to more stability sensitive vessels. Wallenius had an early awareness of the potential problems with stability variations in waves for this type of ships. Early in the 1990s the company supported a research project at KTH (Huss and Olander, 1994) which eventually resulted in the Seaware EnRoute Live on-board decision support system for seakeeping that also included a motion sensor with live motion recording in six degrees of freedom. This system enabled one of the first high frequency full motion recordings ever of parametric roll in head sea with the PCTC "Aida"

in 2003. Although this case was not the first and not the most severe the company had experienced at that time, the motion records made it possible to analyse and understand the phenomenon in much more detail. A report of the incident was presented to IMO in a Swedish submission to the IMO SLF sub-committee's work with review of the intact stability code (IMO 2004). After the incident, rough criteria for parametric roll were included in the live on-board guidance on all Wallenius ships in accordance with the early guidance from IMO in MSC.1/Circ.128 (IMO 2007).

Following the introduction of a new generation PCTC and LCTC in the mid 2000s with significantly more stability optimised hulls than previous generations, parametric rolling and pure loss of stability came even more in focus. In 2008, one of the new LCTC experienced heavy parametric rolling with a maximum amplitude over 30° in moderate following seas with a significant wave height of just slightly more than 4 m. Eventually, the vessel got out of resonance by changing course and speed, see Figure 1.

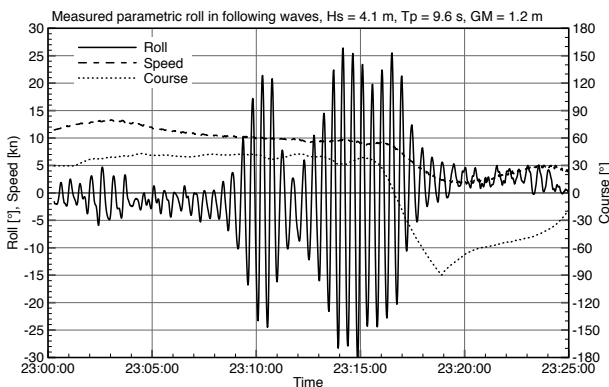


Figure 1: Measured parametric roll in following waves with a LCTC 2008.

At that time, the live warning system was not active, but would anyhow most likely not have identified the situation as critical due to the rather low wave height. This case together with two other measured parametric roll excitation in head and quartering seas with the same vessel generation have been publically reported (Rosén et al., 2012). A few more cases with parametric roll or other stability related incidents have been captured by our monitoring systems and analysed in detail and together they have indicated the need for, as well as made it possible to, develop a more thorough stability management within the shipping company.

4. DESIGN MEASURES

The first step towards achieving better control was to map the characteristics of the existing fleet and identify the trends and changes inherent in the development of more efficient vessels. In lack of suitable standard methods at that time, we developed in-house benchmarking procedures that would capture the influence from differences in hull form, damping and load conditions and provide a qualitative measure of the sensibility. We also started a regular research cooperation with KTH and Seaware in order to further develop knowledge, methods and tools in this area.

Firstly, the vessels quasi-static stability in regular waves of different length and height was analysed and compared. Figure 2 shows an example comparing the three PCTC generations listed in Table 1.

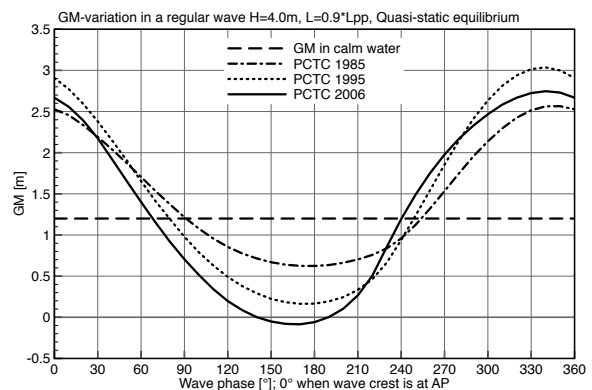


Figure 2: Comparison of three generation PCTC quasi static GM variation in regular waves. Wave height 4m, wave length 90% of Lpp.

Secondly, the roll damping at speed was estimated based on a combination of semi-empirical calculations, model tests and full scale verification (Söder et al., 2012).

Thirdly, given each vessels estimated stability variation and damping, parametric excitation in following irregular seas was simulated using a simple one degree of freedom equation with irregular GM variation obtained from linear superposition of response in regular waves. The change of average GM was roughly accounted for by adjusting the calm water GM with an addition taken from the average variation in regular waves with the same wave height as the significant wave height used in the simulations. These simulations were performed for typical critical conditions experienced under real service, like the one in Figure 1.

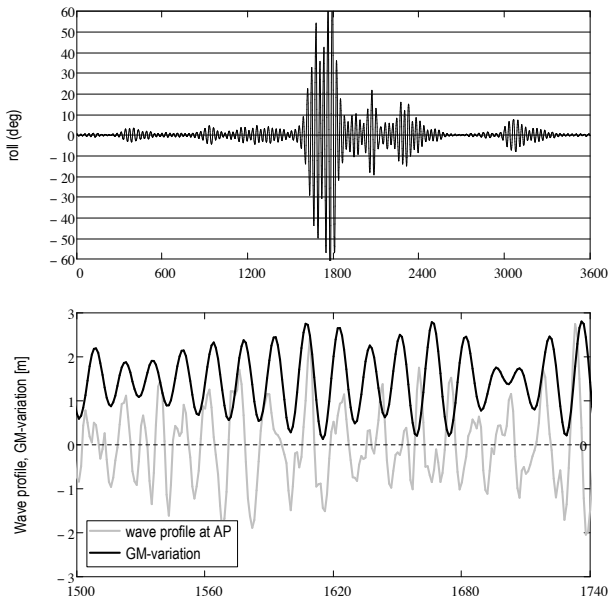


Figure 3: Example of results from a simplified 1-dof simulation of parametric rolling in following irregular sea. The upper graph shows a 1h roll sequence with typical parametric rolling. The lower graph shows a small sequence of four minutes with wave profile and GM variation during the development of large amplitude rolling.

All simulations were performed for different wave mean periods at constant significant wave height. The same sequence of waves (generated from 300 components with fixed steps in periods) was used for simulations with different ship characteristics so that the roll sequences could be compared directly with each other. The results were combined in an *ad hoc* “severity index” that incorporated both the relative frequency of roll angles above $\pm 10^\circ$ and the maximum amplitudes in accordance with Equation (1).

$$pr_{comb} = \sqrt{pr_{max}pr_{>10^\circ}}$$

where

$$pr_{max} = \min\left(\frac{\phi_{max} - \phi_{min}}{2 \cdot 60^\circ}, 1\right) \quad (1)$$

$$pr_{>10^\circ} = 1 - F_\phi(10^\circ) + F_\phi(-10^\circ)$$

F_ϕ is the cumulative distribution of roll

For the example sequence in Figure 3, $pr_{comb} = 0.29$ with $pr_{max} = 1.0$, $pr_{>10^\circ} = 0.09$.

This “severity index” distribution over periods provided a very clear qualitative differentiation between the vessel generations sensibility to parametric rolling. See one example in Figure 4 where the sequence in Figure 3 is illustrated by the dot.

As a result of this mapping it was also decided to retrofit the most sensitive existing ships with larger bilge keels in order to increase their damping and robustness with regard to stability in waves.

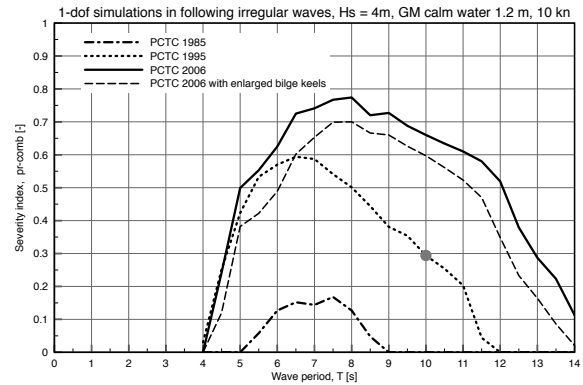


Figure 4: Qualitative comparison of different PCTC generations with regard to parametric roll. Results from 1-dof simulations in following waves with H_s 4m and varying wave periods. The effect of enlarged bilge keels on the most sensitive ship type is also included. The dot represents the simulated sequence in Figure 3 and the condition is similar to the real case shown in Figure 1.

Another aspect of highly stability optimised hull forms is that the KM is strongly varying with the trim. Due to very wide aft sections and more vertical forward sections around the water line, the waterplane area and initial stability will increase significantly with aft trim. At the same time also the resistance will increase significantly. Adding ballast in order to increase GM for a given cargo condition will also increase the resistance and fuel consumption. For the most optimised ships, typically 0.1 m increase of GM will result in about 0.5% increase in fuel consumption for the very best combination of trim and ballast and may result in significantly higher consumption rates for less optimal combinations. In order to be able to optimise stability and efficiency together all vessel types have been model tested in a wide range of combinations of draught, trim and speed. The results have then been incorporated with the loading computer as one of the decision support systems described in the following section.

All these studies of stability characteristics of the existing fleet have also resulted in an enhanced understanding of important design parameters and enabled more thorough owner’s requirements on stability and efficiency for new projects which go far beyond statutory minimum requirements.

5. OPERATIONAL DECISION SUPPORT

The Master has the unique authority and responsibility to keep the ship seaworthy in all conditions. This includes the choice of route as well as the load condition and stability. Taken into account the highly optimised ships and their complex individual characteristics and differences, we find it important to supply the Master on board with decision support to enable this authority and responsibility. With the increased knowledge obtained from simulations, monitoring and analysis, we have also realised that the support systems must reflect the individual ship rather than being generic if they are to be fully effective. This has led to a close cooperation with the system suppliers so that we can maintain control over the ship models used in their systems.

Standard support systems on board related to stability include today the following:

- Loading computer with intact and damage stability assessment including statutory limits but also with possibility to modify e.g. hold permeability to better simulate reality in the actual loading condition.
- Ballast optimisation in order to obtain target stability for a given cargo and tank configuration with lowest possible fuel consumption for a given speed.
- Route planning and route optimisation with ship and loading condition specific models for performance in wind and waves and with continuous updated weather forecasts. The objective is to find the most cost efficient route in terms of both track and speed for a given target time of arrival, while at the same time avoiding any critical condition with regard stability and ship motions in waves.
- Live warnings for critical conditions and advice on heavy weather manoeuvring to avoid critical combinations of speed and course based on real time motion measurements and analysis of the prevailing wave spectrum.

In the development of all these systems, Wallenius Shipping has been active both in drafting the detailed system specification and in developing and/or testing new methods and models. One example is the implementation of simplified models to identify risk boundaries for avoiding parametric

rolling and pure loss of stability based on linearised *GM* variation (Dunwoody, 1989; Bulian, 2010), which have been adapted and fine-tuned with operational experience and measurements from real incidents within our fleet (Ovegård et al., 2012). These models are since 2011 incorporated in the on-board system for both route planning and live warning so that the specific conditions can be accounted for as precise as possible. This includes the actual sea state and load condition as well as the general stability and damping characteristics of the individual vessel.

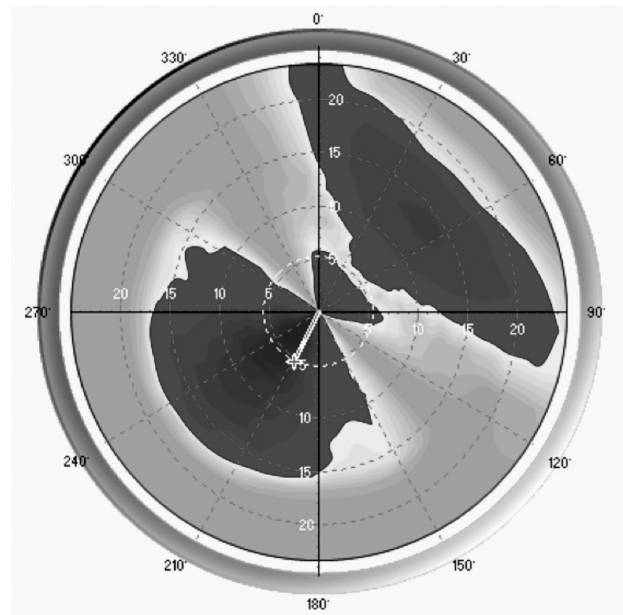


Figure 5: Example of heavy weather manoeuvring advice with regard to stability in waves in the on-board decision support system Seaware EnRoute Live.

In addition to decision support, we are also looking into the possibility to use more active supporting systems that would mitigate critical situations directly without operators' actions. Although it is still not implemented on our ships in service, it is well within reach to mitigate parametric roll using rudder control (Söder et al., 2013). This would be in line with what we see in cars today with active brake assistance systems. One of the crucial components in such systems will be the early detection of critical events that could put rudder control systems into an alert mode ready for active roll mitigation. Promising results from tests with signal based detection have recently been reported (Galeazzi et al., 2015).

6. TRAINING

Like any management strategy, stability management needs to address physical conditions (hardware), systems (software) and people. Operational stability is in the end in the hands of the crew on the ships, and their knowledge, skills and routines are decisive for the outcome. In parallel with the mapping of ship characteristics and the development of operational support, we have been running three-days stability training courses with all senior officers. The courses have been divided on the following three subjects including also hands-on training or demonstration of support systems:

- General Intact stability (Rules; Documentation; Loading computer assumptions and features; Heeling from wind and manoeuvres; Ballast optimization; Ways of assessing the stability during operation; Potential effect of cargo shift; Service experience/statistics)
- Damage stability (Subdivision and damage stability basics; Rules (pre and post SOLAS 2009); Documentation; Emergency awareness on board; Procedures for damage stability assessment on board; Shore based emergency response services; Review of public information from flooding accidents)
- Heavy weather stability (Stability variation in waves; Critical phenomena; Assessment methods and limitations; Comparison between vessel generations; Review of incidents with parametric excitation and loss of stability; Route speed and course optimization; Support system usage; Communication with ship management and ship operation)

The course discussions have mainly been targeting a common understanding that the answer to what is optimum stability is not a specific *GM* but rather an active on board stability management adjusted to the circumstances of each vessel, condition and voyage. From the office we try to support this on board management with technical systems, monitoring, analysis and recommendations.

My experience from these courses is that they have opened up for further discussion and exchange of knowledge/experience between vessels and office, they have widened the view from prescriptive to functional and they have also closed down some

myths that still prevailed both at shore and at sea within the organisation.

7. MONITORING

Within just a decade, vessel monitoring has developed from the traditional noon reports sent ashore to high frequency measurements from various systems on board feeding a number of automatic and on-demand analyses and reports for different stakeholders. Among those measurements we have today access to 6-dof rigid body motions recorded with 10 Hz resolution by a dedicated motion sensor on almost all ships. In addition, we have roll, pitch and heave together with speed, position, heading, rudder motions, wind, etcetera, recorded from the navigational systems as well as detailed data from the engine control system with 1 Hz resolution. Because of limitations in the satellite communication, these high frequency measurements are today stored on board and only aggregated statistical properties (in general mean, standard deviation, minimum, maximum and period per 10 min interval) are sent ashore and combined with weather and other route data. However, the high frequency data is still stored on board and can be retrieved on line from the ships when needed. Within short we foresee that also the full high-frequency records will be pushed ashore on a daily basis.

This means that we nowadays have the technical basis for following the dynamic behaviour of each individual ship for each individual voyage and loading condition, literally every second, always. Based on these motion measurements we can also calculate the time series of wave and wind induced (rigid-body) accelerations on any car at any position during the transport. Both for further research and for transport quality this opens up completely new perspectives and we are just in the beginning of exploring the opportunities for getting knowledge and value out of this information. Here are just a few examples included as illustration of the data.

Figure 6 shows an example of results from a study of aggregated roll statistics between June 2014 and September 2015 from 14 vessels. The data set includes in total 593000 records of 10 min data from seagoing conditions.

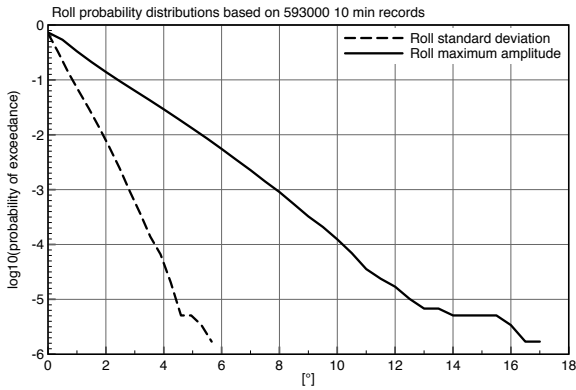


Figure 6: Long term distribution of roll standard deviation and maximum amplitudes within 10 min records from service data between June 2014 and September 2015.

If we consider the roll amplitudes in irregular seas being Rayleigh distributed (narrow banded linear response assumption), the frequency distribution of extreme amplitudes within each 10 min record set will follow:

$$f_{extr}(\phi, N) = \frac{\phi N}{\sigma_\phi^2} \left(1 - e^{-\frac{\phi^2}{2\sigma_\phi^2}}\right)^{N-1} e^{-\frac{\phi^2}{2\sigma_\phi^2}} \quad (2)$$

where σ_ϕ is the standard deviation and N is the number of amplitudes within the set.

Figure 7 shows a comparison between theoretical extreme value distribution assuming linear roll response (2) and the real distribution of maximum amplitudes to any direction measured for the same period. There is a small bias in the measured distribution compared to the theoretical that well could be the effect of non-linear damping, but in general the fit is surprisingly good.

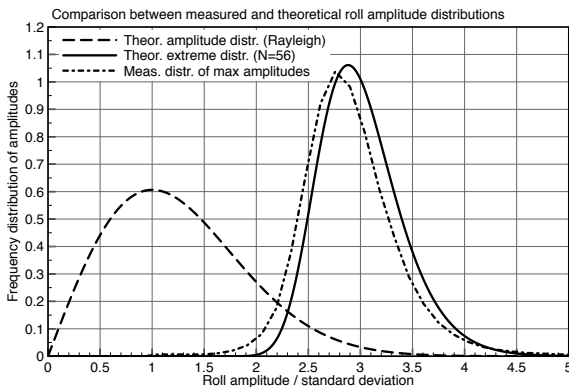


Figure 7: Distribution of roll amplitude extremes within 10 min records. N=56 corresponds to the average number of amplitudes to any direction within all records.

Within this study, limited to 14 vessels and 16 months, the statistics shows in general very moderate rolling. Only 211 10 min records were found where the maximum roll amplitude to any direction had exceeded 10° and 109 of these showed differences between maximum and minimum roll amplitudes that exceeded 18°. Most of these higher roll records could be summarised under 14 different cases/conditions of which half were identified as typically synchronous roll in stern quartering waves and the other half were likely parametrically excited roll from stability variations in waves. Of these were two in head to bow seas and five in following seas. Most of the conditions have been reported to have a GM of 2.0 m or more, so they do not in general represent low stability cases.

The two most severe records with amplitudes of 17° were from the same condition in heavy weather with following waves with a significant height of about 7 m. An extract from the records is shown in Figure 8 which include both some aggregated 10 min data and the high frequency roll records. The live warning system on board did show alert during this passage. However, there were no manoeuvring options considered feasible to fully avoid critical conditions at that time so the Master decided to keep high awareness and make necessary manoeuvres to get out of resonance whenever rolling started to develop. The amplitudes could also be kept well below critical levels.

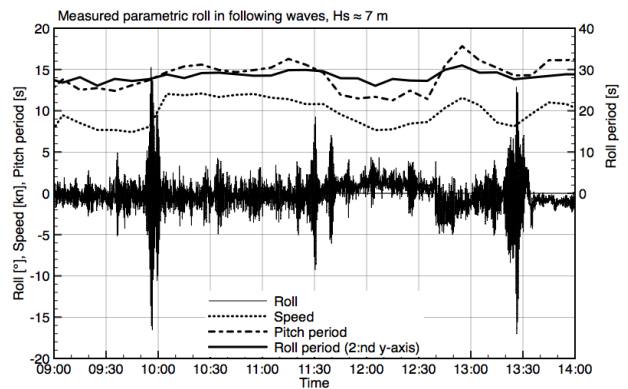


Figure 8: Sequence with the highest roll amplitudes during the studied 16-month period combined with 10 min average data for speed, pitch period and roll period. The periods have been plotted with different scales to better illustrate the excitation of large amplitudes when there is a perfect 2:1 relation between roll periods and pitch periods.

8. FUTURE REGULATORY ACTIVITIES

The IMO work with development of second generation intact stability criteria under the SDC Sub-Committee is expected to, as a first step, result in a MSC Circular to encourage Member States to apply the new interim criteria. The idea is to gain experience before the new requirements are completed and made mandatory as an amendment to the IS Code (IMO 2016). We welcome this development and think it will enhance safety and support a more proactive approach. However, there is of course also a risk that ships found vulnerable under these criteria will be considered as less safe *per se*. In our opinion and based on our experience, this need not be the case, they may just have to be operated with more active management, support and care. As in every other area, the balance between efficiency and safety is not a fixed point in time but is relying on available knowledge and technology.

This presentation aims to show that we have started on the journey towards functional stability management, but it has no intention to say that we have arrived. More research, system development and operational experience is needed to carry us further along this route.

9. REFERENCES

- Bulian G., 2010, "Checking Vulnerability to Pure Loss of Stability in Long Crested Following Waves: A Probabilistic Approach", *Ocean Engineering*, 37, pp. 1007-1026.
- Dunwoody A.B., 1989, "Roll of a Ship in Astern Seas – Response to GM Fluctuations", *Jour. of Ship Research*, 33(4), pp. 284-290.
- Fearnsearch, 2015, "World PCC Fleet", July 1 2015, published by Fernleys.
- Galeazzi R., Blanke M., Falkenberg T., Poulsen N.K., Violaris N., Storhaug G., Huss M., 2015. "Parametric roll resonance monitoring using signal-based detection", *Ocean Engineering* 109, pp.355–371.
- Huss M., Olander A., 1994 "Theoretical Sea-keeping Predictions On-Board Ships – A System for Operational Guidance and Real Time Surveillance." Report ISRN KTH/FKT/SKP/FR-94/50-SE, KTH, Sweden.
- IMO 2004, "Review of the Intact Stability Code – Recordings of head sea Parametric Rolling on a PCTC", SLF 47/INF.5 submitted by Sweden.
- IMO 2007, "Revised guidance to the Master for avoiding dangerous situations in adverse weather and sea conditions", MSC.1/Circ.128
- IMO 2016, "Finalization of the second generation intact stability criteria", SDC 3/WP.3
- Ovegård E., Rosén A., Palmquist M., Huss M., 2012, "Operational guidance with respect to pure loss of stability and parametric rolling", 11th Intl Conf on the Stability of Ships and Ocean Vehicles (STAB 2012), Greece.
- Rosén A., Huss M., Palmquist M., 2012, "Experience from Parametric Rolling of Ships", chapter in Fossen T.I., Nijmeijer H., *Parametric Resonance in Dynamical Systems*, Springer.
- Söder C.-J., Rosén A., Werner S., Huss M., Kutteneuler J., 2012, "Assessment of Ship Roll Damping Through Full Scale and Model Scale Experiments and Semi- Empirical Methods", 11th Intl Conf on the Stability of Ships and Ocean Vehicles (STAB 2012), Greece.
- Söder C.-J., Rosén A., Ovegård E., Kutteneuler J., Huss M., 2013, "Parametric Roll Mitigation Using Rudder Control", *Journal of Marine Science and Technology*, Vol.18, No.3, pp.395–403.
- Wallenius-Kleberg M. (Editor), 1984, "Walleniusrederierna 1934-1984", Memorial Book published by Rederi AB Soya and KREAB, ISBN 91-7810-129-8

Real-Time Stability Assessment in Mid-Sized Fishing Vessels

Marcos Míguez González, *Integrated Group for Engineering Research, University of A Coruña*
A Coruña, Spain, mmiguez@udc.es

Vicente Díaz Casás, *Integrated Group for Engineering Research, University of A Coruña*
A Coruña, Spain, vdiaz@udc.es

Lucía Santiago Caamaño, *Integrated Group for Engineering Research, University of A Coruña*
A Coruña, Spain, lucia.santiago.caamano@udc.es

ABSTRACT

Fishing is one of the most dangerous occupations worldwide. Most of the accidents involving mid-sized fishing vessels are due to static and dynamic stability failures, and one of the main reasons is the crew lack of training on these matters. If stability guidance systems want to be used onboard this type of vessels, they have to fulfil three main requirements: they have to be based on simplicity, they have to be very easy to use and to interact with and their installation and maintenance have to be inexpensive. Within this framework, the authors proposed their own alternative, consisting on an onboard stability guidance computer system.

In this paper, some alternatives for overcoming the main drawback of this system, which is the manual interaction with the crew, are presented. A methodology based on the frequency analysis of the ship roll motion, together with an estimation of roll inertia applying a breakdown method is proposed for determining the vessel intact stability levels in an automatic and unattended way. The performance of this methodology has been verified using data from a towing test campaign of a mid-sized stern trawler, showing accurate results.

Keywords: *Onboard stability guidance, Fishing vessels stability, Stability monitoring*

1. INTRODUCTION

Fishing is well known for being one of the most dangerous industrial sectors in many countries, such as the U.S., the U.K. or Spain, and accounts, according to ILO, for more than 24.000 casualties a year (Petursdottir et al., 2001).

Most of the accidents involving fishing vessels affect the medium-small range of the fleet, and are mainly due to stability issues, both static and dynamic, including large heel and capsizing, pure loss of stability or broaching. Several authors and studies coincide in that one of the main reasons for this large stability-related accident rate is the crew lack of training in stability matters (Míguez-González et al., 2012a).

Fishing vessel masters usually rely in their experience to determine the stability level of their vessels, and this subjective analysis is usually a not good approximation. The only element available

onboard which provides some information regarding stability to them is the stability booklet, but this is only present in the larger vessels of some countries, taking into account that under 24 m fishing vessel regulations are country-dependent. But in addition, and even in the largest vessels, crew training is not enough to let them understand the information within the booklet.

The issue of stability/operational guidance is a deeply studied topic, and its regulatory framework (including SGISC) and its application onboard large commercial vessels are attracting a lot of attention in the last years. However, when it comes to small fishing vessels, its application, due to the difference in level of training of the crews, is not so straightforward.

Regulators and administrations are aware of these facts, and some programs and publications focused on increasing the training of the masters/crewmembers of these type of vessels have

been ran worldwide (MAIB, 2008; Gudmundsson, 2009). However, and although these training programs are of paramount importance, onboard guidance provides masters with even more information to complement their knowledge and to carry out an objective analysis of the risk level of their ships in real time.

Within this last group, there are two main approximations. One is to provide masters with weather guidance, including updated information regarding sea state, which is transformed into a safety of navigation index based on ship dynamic stability curve, obtained for the design loading conditions. This methodology was implemented by the Icelandic Maritime Administration, and together with a compulsory inclining test program, it proved to drastically reduce the number of accidents involving the Icelandic fleet (Viggosson, 2009). The second alternative consists on providing the crews with an approximation of the stability level of their ship in real time, based on measurements or on a group of possible alternatives where to choose from, i.e. real time stability guidance, together or not with some input regarding sea state.

Up to date, just a few authors have dealt with the topic of developing fishing vessel oriented stability guidance systems, which have some differences to those installed onboard larger vessels: they have to be based on simplicity; they have to be very easy to use and to interact with; and their installation and maintenance has to be inexpensive. Some examples are the well-known stability matrix, the stability posters, and some others (Womack, 2002; Deakin, 2005), which provide the risk level of the ship according to the loading condition, that in some cases include the influence of the sea state and which show the obtained results using a static interface (a poster placed on the navigation bridge).

Following this premises, the authors (within the Integrated Group of Engineering Research) have proposed their own alternative, consisting on an onboard stability guidance computer system. It provides the minimum essential information related to the stability of the vessel in the current loading condition, in a very clear and understandable way, even for users with no specific training in the use of computer software (Míguez-González et al., 2012a). However, this system, which is the

prototype phase, has one major drawback, which is a common issue to all the aforementioned fishing vessel stability guidance systems: in order to determine the stability characteristics of the vessel (metacentric height and righting lever curve), it relies on the information that the crew manually introduces in the system (weight items and their positions and tank filling levels). Although the interface is very simple and it is designed to account for inaccuracies, it requires the crew interaction, which is not always guaranteed.

This paper will present one alternative for trying to overcome these major drawback, which consists on a methodology based on the frequency analysis of the ship roll motion, together with an estimation of roll inertia, for determining the vessel intact stability levels in an automatic and unattended way. The objective of this proposal is to minimize the need of external data and to maximize the accuracy of the obtained risk level.

2. METHODOLOGY

The aforementioned guidance system is composed of a naval architecture software that, from the hull form, hydrostatic data and weight distribution, and from a sea state estimation, computes a stability index based on IMO Intact Stability criteria and maximum wave to capsize (Deakin, 2005). From this data, both weight distribution and approximate sea state have to be manually introduced by the crew. In order to automate this system, it would be a great improvement to be able to monitor dynamic stability, so that basic initial stability parameters (transverse metacentric height) could be determined.

Considering the uncoupled linear equation of roll motion of the ship,

$$(I_{xx} + A_{44})\ddot{\phi} + B_{44}\dot{\phi} + g\Delta GM\phi = M_{ox} \quad (1)$$

where M_{ox} is the external excitation, I_{xx} is the ship transverse mass moment of inertia, A_{44} is the added mass in roll, B_{44} is the damping coefficient, Δ is the ship displacement and GM is the transversal metacentric height, the roll natural frequency for the case of small amplitude linear oscillations could be estimated by:

$$\omega_N^2 = \frac{g\Delta GM}{I_{xx} + A_{44}} \quad (2)$$

And rewriting the previous formula, the metacentric height would be:

$$GM = \frac{\omega_N^2(I_{xx} + A_{44})}{g\Delta} \quad (3)$$

If the Weiss formula based in the roll gyradius of the vessel (k_{xx}) is applied to obtain the transverse mass moment of inertia, the GM estimation is reduced to (Krüger and Kluwe, 2008):

$$GM = \frac{k_{xx}^2 \omega_N^2}{g} \quad (4)$$

Considering the ship as a rigid body oscillating in just one degree of freedom (roll), the problem of real time estimation of the initial stability is reduced to determining the parameters involved in this motion: natural roll frequency, transverse moment of inertia (both dry and added inertia) and vessel displacement.

Ship displacement is obtained by means of the guidance system from the weight data introduced by the crew, although this value could be also obtained in real time by means of a draft monitoring system or draft marks observation by the crew. Transverse moment of inertia is obtained using the proposed estimation of the lightship weight inertia and the data introduced by the crew in the stability guidance software. This value could be also estimated using the aforementioned Weiss formula. Added inertia in roll is precomputed for different drafts by using a strip theory code, and then the needed data is interpolated for the actual draft of the vessel. Natural roll frequency is obtained by analyzing ship roll motion, following the methodology described in the corresponding section. Once all the variables have been obtained, the estimated initial stability of the ship could be computed by means of equations (3) or (4).

The employed methodology is summarized in Figure 1.

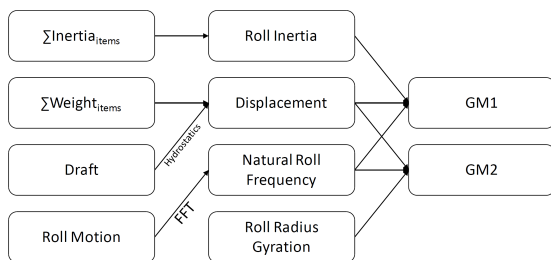


Figure 1: Applied methodology.

Roll natural frequency

In order to estimate the roll natural frequency, the vessel roll motion is analysed. The spectrum of roll motion has a peak around the roll natural frequency, which is more acute if a resonance phenomenon is taking place (Enshaei, 2013; Terada, 2014). Regarding the sampling frequency, the time series length has to be such that it contains enough information to be able to determine the position of this peak with certain accuracy. This procedure is similar to that applied in wave buoys to obtain wave height and direction; in this cases, 20 minutes intervals are usually applied, that is the minimum time window in which the sea is considered stationary (Nielsen, 2007). However, this time window is too large for the case under analysis. In 20 minutes, the ship condition could be significantly modified, even leading to a dangerous situation. In the case of stability guidance, the results are considered in real time when data are obtained at least every 3 minutes (Pascoal et al., 2007; Tannuri et al., 2003). In addition, the sampling frequency should also satisfy the Nyquist theorem (Medina, 2010).

The power spectrum of a signal shows how its energy or power is distributed throughout each component of the frequency and consequently, it permits to identify the natural frequency of the system under analysis. In order to be able to compute it, it is necessary that the signal is represented in the frequency domain. There are several tools that permit the time-frequency analysis, but to be implemented in the onboard stability guidance system is an indispensable condition that the calculation algorithm would be able to obtain the results easily in what we have considered real time. For this reason and because it is the most common way of generating a power spectrum, the Fast Fourier Transform (FFT) was chosen (Medina, 2010). In our case, an approximation of the power spectrum $S(\omega)$, where no normalization or averaging has been done, is obtained by multiplying the FFT results ($g(\omega)$) by their complex conjugate. Although the obtained results are not the real power spectrum, this has not an effect on the frequency distribution and so, on the peak frequencies of the system.

Therefore, the applied calculation procedure will be the following:

$$g(\omega) = fft(x) \tag{5}$$

$$S(\omega) = |g(\omega)|^2 \tag{6}$$

As a consequence of the discrete sampling of the signal, the “spectral leakage” may appear. The spectral leakage is no more than energy dispersion. It is usually related to the discontinuities that exist at the beginning and the end of the signal, and that could degrade the signal-noise ratio and mask other smaller signals at different frequencies. The effects of spectral leakage can be reduced decreasing the discontinuities at the edges of the signal. A possible solution is to apply a window function. The process consists of multiplying the signal by a function that reduces the signal to zero at the edges and that it is known as windowing.

Windows generally cause a reduction in the accuracy of the measured peak amplitude of the signal and also introduce damping. However, this is not a problem given the fact that the main objective is to determine the natural frequency of the system, and not to compute the exact amplitude of the spectrum peaks.

There are numerous window functions, of which we will focus only on those that offer more accuracy and, therefore, better results. These are Hanning, Blackman and Blackman-Harris windows (Boashash, 1992; Harris, 1978; Oppenheim et al., 1999).

Transverse mass moment of inertia and displacement

The transverse mass moment of inertia calculation by direct integration is a complex and time consuming process given the fact that the shape of the vessel and its density varies from one point to another. For this reason, the process is usually simplified by considering the ship as a single object with known shape and uniform density or by breaking it down into its most relevant components and approximating them to known shapes with constant density (Aasen and Hays, 2010). In this study, the lightweight mass moment of inertia has been obtained by integrating the midships structure along the length of the vessel and weighting it using the curve of areas, and also considering the weight, position and shape of the most representative lightweight elements (such as winches, main engine, diesel generators, etc.). Tanks and other cargo elements which have to be considered in the loading conditions of the vessel,

have also been taken into account using their weights, location and approximate shape.

For the sake of comparison, the Weiss formula approach (Krüger and Kluwe, 2008) has been also considered:

$$I = k_{xx}^2 \Delta \tag{7}$$

Where k_{xx} is the roll gyradius, usually taken as a percentage of the vessel’s beam.

In addition, the added mass in roll, which may be expressed as an increase in percentage over the total value, must be kept in mind. In this case, the added mass was computed by using a strip theory code.

Finally, the ship displacement can be obtained by the sum of the load items considered in the calculation of the inertia or by the vessel hydrostatics if the draft is known. This fact makes necessary the interaction with the crew in both cases. Although introducing the vessel draft in the application after checking the draft marks seems to be easier than defining all the load items, the use of draft sensing could help solving this issue and avoiding any interaction, although this alternative seems to be out of range due to cost of installation.

3. RESULTS

In order to check the proposed methodology, results from a towing test campaign of a mid-sized stern trawler had been used. These tests include regular and irregular head waves of different frequencies and heights. In some of the cases, parametric roll resonance took place. Their detailed description can be found in (Míguez-González et al., 2012b).

Table 1: Test vessel main characteristics.

Overall Length	34.50 m
Beam	8.00 m
Depth	3.65 m
Draft	3.340 m
Displacement	450 t
Metacentric Height (GM)	0.350 m
Natural Roll Frequency (ω_ϕ)	0.563 rad/s

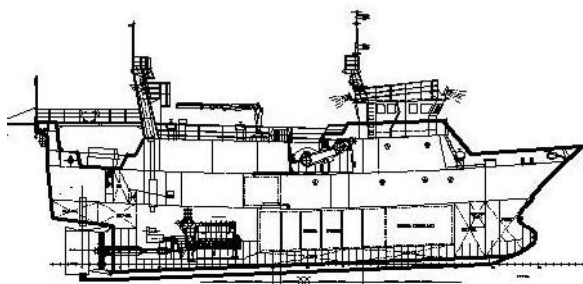


Figure 2: Test vessel.

The tested model is a 1/18.75 scale trawler; roll decay tests at different speeds and an inclining test were carried out to determine the vessel metacentric height, displacement and natural roll frequency, together with roll moment of inertia. The vessel main characteristics are shown in Table 1.

Transverse mass moment of inertia

From the data above, and applying a strip theory code to determine the vessel roll added mass, the roll dry mass moment of inertia and the roll gyradius were determined. Results are shown in Table 2.

Table 2: Test vessel mass distribution. Towing tank tests.

Load condition	Δ (t)	I_{xx} ($t \cdot m^2$)	k_{xx}/B	A_{44} ($t \cdot m^2$)
Towing Tank Tests	448	4383.60	0.391	469.26

These values were compared to those calculated by using the previously described breakdown methodology, corresponding to the four mandatory loading conditions of the vessel, taking into account the tank filling levels, the positions of the different load items and the cargo stowage in the hold of the vessel. These data would be computed by the onboard system based on the actual loading condition introduced by the crew. These results are shown in Table 3.

Table 3: Test vessel mass distribution. Breakdown method.

Load condition	Δ (t)	I_{xx} ($t \cdot m^2$)	k_{xx}/B
Fully loaded departure. No cargo	492	4450.88	0.376
Ground departure, 35% consumables, 100% catch	489	4102.09	0.362
Arrival at port, 10% consumables, 100% catch	465	3734.43	0.354
Arrival at port, 10% consumables, 20% catch	411	3545.94	0.367

The values of the roll radius of gyration obtained following this procedure are slightly smaller than those measured in the towing tank tests, and also than the reference value for this type of vessel (0.4 (Krüger and Kluwe, 2008)); roll decay and inclining tests should be carried out to verify the accuracy of the method.

However, as is indicated in Figure 1, two alternatives for the computation of the metacentric height will be considered in the onboard system. On one hand, that based on the inertia obtained using the direct calculation method including crew inputs. And on the other hand, that based on the reference value of 0.4 for the roll gyradius. These will allow us to choose the less favourable alternative.

Roll natural frequency

In this section the results obtained after applying the proposed estimation method to the roll time series in four different test runs are presented, including results using Hanning, Blackman and Blackman-Harris windows. In Table 4, the values of the obtained natural frequencies and the corresponding GM values for the four test cases are shown.

In Figure 3, the results from a test run in regular waves and where parametric resonance takes place are presented in real scale. On the top, a record of the roll motion and the application of the window functions are presented. As it was expected, the signal is reduced to zero at the edges due to windowing and its amplitude is damped. This effect is more or less pronounced depending on the type of window used. On the bottom, the results of applying the FFT to the different time series are displayed. It can be seen that most of the energy of the spectrum is concentrated in the natural frequency of the vessel. Nonetheless, there is a little scattering around it, likely produced by the discontinuities in the edges, which is reduced with the use of window functions.

In Figure 4, results from a regular wave case with no parametric rolling are presented. In contrast to the previous case, due to the absence of the resonance phenomenon there is a greater dispersion of energy, and more than one peak have been identified, although of lower intensity than the one corresponding to the natural frequency. However, the quality of the estimation of the natural frequency remains satisfactory.

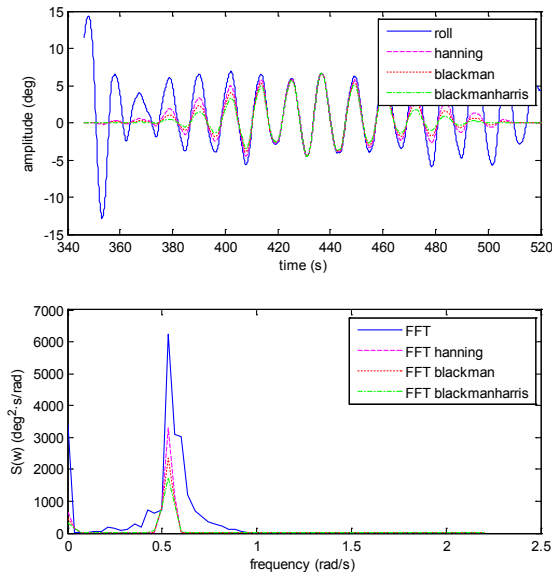


Figure 3. Test 1. Regular waves. Fn 0.1. Parametric roll occurs.

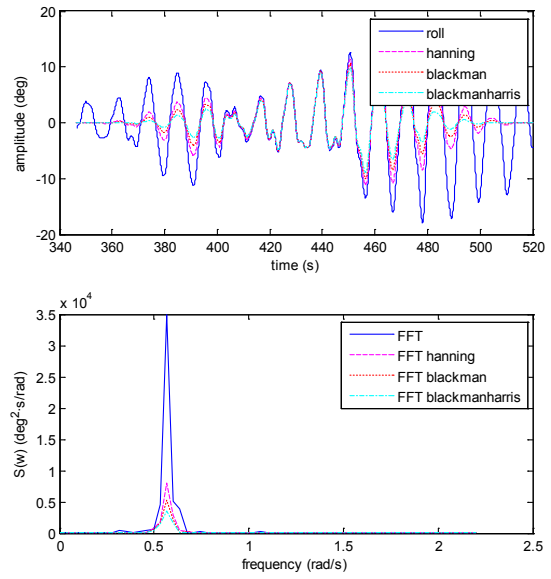


Figure 5. Test 3. Irregular waves Fn 0. Parametric roll occurs.

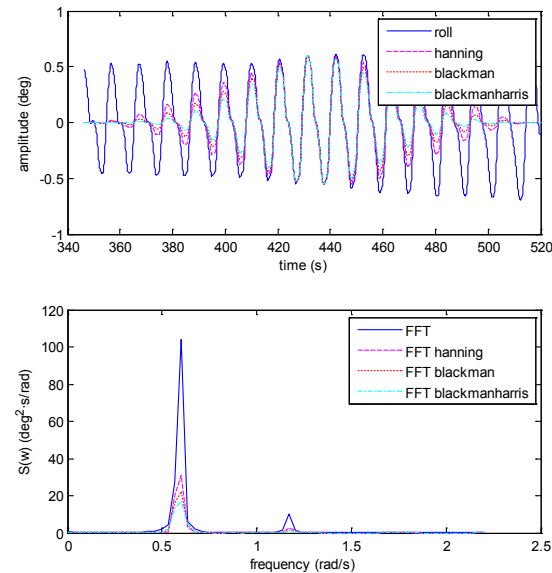


Figure 4. Test 2. Regular waves. Fn 0. No parametric roll.

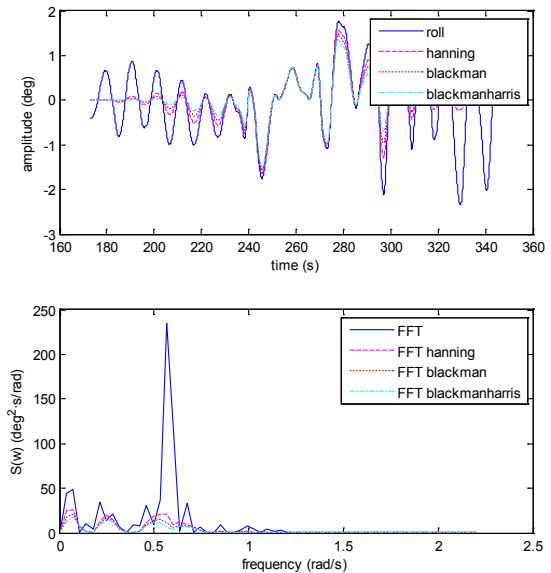


Figure 6. Test 4. Irregular waves. Fn 0.1. No parametric roll.

In the case of irregular waves, the results are similar to those obtained for regular waves. When the resonance phenomenon takes place (Figure 5) there is no energy dispersion of the spectrum and a clear single peak appears in the solution.

If no resonance occurs (Figure 6), the degree of dispersion is increased, and results obtained applying the windowed time series are not satisfactory. However, the frequency of the system can still be identified using the not windowed solution.

The values obtained in all the tests are very close to the actual value of natural frequency ($\omega_n = 0.563$ rad/s).

The relative error does not exceed 8% and in the irregular wave cases, the most realistic ones, is below 1%. The application of window functions showed no improvement in the obtained results.

Metacentric Height

The *GM* values corresponding to the natural frequencies obtained from the time series analysis, which are shown in Table 4, have been calculated by using the real value of the mass moment of inertia which was determined in the towing tank tests of the vessel.

Although the obtained relative error is small (less than a 15 % in all cases), to evaluate the

quality of the results obtained for the *GM* it is necessary to focus not only on the final value, but also on the percentage of induced error.

Table 4: Natural frequency results.

	Regular Waves		Irregular Waves	
	Test 1	Test 2	Test 3	Test 4
Fn	0.1	0	0	0.1
Parametric resonance?	Yes	No	Yes	No
ω_n no windowing (rad/s)	0.531	0.602	0.567	0.567
ω_n hanning (rad/s)	0.531	0.602	0.567	0.071
ω_n blackman (rad/s)	0.531	0.602	0.567	0.071
ω_n blackman harris (rad/s)	0.531	0.602	0.567	0.071
Resulting <i>GM</i> (no windowing)	0.311	0.400	0.355	0.355

As the results are values obtained from the combination of other variables, which have uncertainty themselves, it will be necessary to carry out an error propagation analysis that will let us know which are the variables that have more influence on the correctness of the solution (vessel displacement, mass moment of inertia or natural roll frequency).

4. DISCUSSION

The results of roll natural frequency have been validated for head seas, so the effectiveness of the proposed method is only demonstrated for this case. If the wave direction changes, the forces acting on the vessel are modified and the accuracy of the results may be affected. For this reason, it would be necessary to carry out another test campaign in which more wave incidence angles were considered, including not only head waves, but also stern and oblique ones, to analyze how the performance of the method changes with wave incidence.

Another point of concern is how the transversal moment of inertia is determined. If the breakdown method is applied, the crew have to input the load items in the system, and therefore it would carry on depending on manual data. A possible solution would be to install a remote sounding system, but the problem will be the same regarding hold stowage and individual load items (such as nets, etc.). A possible solution would be the one stated in the text that is to also apply the Weiss formula, to approximate the roll gyradius and to choose the worst situation from both alternatives. Of course, this would lead to a level of uncertainty in the

computation of *GM* that has to be evaluated by carrying out an error propagation analysis.

Finally, the last parameter to be considered is ship displacement. The case of the displacement is similar to that of the mass moment of inertia, as both of them have to rely on the interaction with the crew. Regarding the displacement, it could be determined by considering the loading condition defined by the crew, or by the input of the draft in the guidance system, which seems to be a less bothering alternative. In any case, the aforementioned uncertainty analysis will be needed to quantify the influence of the estimation of ship displacement in the calculation of *GM*.

5. CONCLUSIONS

In this paper a real time onboard estimation method of ship's initial stability, intended to be used in small and medium sized fishing vessels has been presented. The main objective of the proposed methodology was to overcome some of the drawbacks of these type of systems and to try to minimize the need for crew interaction.

In order to obtain the vessel *GM*, the natural roll frequency has been estimated by applying windowed FFT to a group of roll motion time series from a towing tank test campaign, including both regular and irregular head waves. The results show a good agreement with the real values in all the tested cases; the performance of the estimation has not been increased by the use of three different windows, Blackman, Hanning, and Blackman – Harris. However, it is necessary to complement the obtained results with those from a broader towing tank test campaign, including also stern, beam and oblique waves.

For the estimation of roll mass moment of inertia, a breakdown method is proposed based on the different load items which compose the vessel loading condition. However, this approximation still relies in manual data introduced by the crew; the use of the Weiss formula and the estimation of the vessel roll gyradius to determine the inertia implies a simplification in the calculation, although results in both cases have been very similar.

Considering that two of the premises of this system are simplicity and low cost of installation, the use of draft sensing and tank sounding for determining the vessel displacement is not a

feasible option; draft manual input seems to be the best alternative.

Finally, the need for an uncertainty analysis has been also stated in the paper. Due to the fact that the values of both roll mass moment of inertia and vessel displacement rely up to some extent on data introduced by the crew, it is necessary to determine which is their contribution to the obtained solution and the influence of the uncertainty of these data in the computation of *GM*.

6. REFERENCES

Aasen R., Hays B., 2010, "Method for Finding Min and Max Values of Error Range for Calculation of Momento of Inertia", Proc. 69th Annual Conference of Society of Allied Weight Engineers, Virginia.

Boashash B., 1992, "Estimating and Interpreting the Instantaneous Frequency of a Signal – Part 2: Algorithms and Applications", Proceedings of the IEEE, 80(4), pp. 520-538.

Deakin B., 2005, "Development of simplified stability and loading information for fishermen", Proc. RINA Conference on Fishing Vessels, Fishing Technology & Fisheries, Newcastle, UK.

Enshaei H., 2013, Prevention of Extreme Roll Motion Through Measurements of Ship's Motion Responses, PhD Thesis, School of Marine Science and Technology, Faculty of Science. Newcastle University.

Gudmundsson A., 2009, Safety practices related to small fishing vessel stability, Food and Agriculture Organization of the United Nations, Rome.

Harris J., 1978, "On the Use of Windows for Harmonic Analysis with the Discrete Fourier Transform", Proceedings of the IEEE, 66(1), pp. 51-83.

Krüger S., Kluwe, F., 2008, "A simplified Method for the Estimation of the Natural Roll Frequency of Ships in Heavy Weather", HANSA International Maritime Journal, 9, pp. 161-168.

MAIB, 2008, Analysis of UK Fishing Vessel Safety. 1992 to 2006, Marine Accident Investigation Branch, Southampton, UK.

Medina J., 2010, Análisis de Fourier para el Tratamiento de Señales, Proc. XII Encuentro de

Matemáticas y sus Aplicaciones, EPN-Quito, Ecuador.

Míguez-González M., Caamaño-Sobrinó P., Tedín-Álvarez R., Díaz-Casás V., Martínez-López A., López-Peña F., 2012a, "Fishing vessel stability assessment system", Ocean Engineering, 41, pp. 67-78.

Míguez-González M., Díaz-Casás V., Lopez-Peña F., Pérez-Rojas L., 2012b, "Experimental parametric roll resonance characterization of a stern trawler in head seas", Proceedings of the 11th International Conference on the Stability of Ships and Ocean Vehicles, Athens.

Nielsen U.D., 2007, "Response-based estimation of sea state parameters – influence of filtering", Ocean Engineering, 34(13), pp. 1797-1810.

Oppenheim A.B., Schaffer R.W., Buck J.R., 1999, Discrete Time-Signal Processing, Prentice-Hall, Inc, New Jersey.

Pascoal R., Guedes Soares C., Sørensen A.J., 2007, "Ocean wave spectral estimation using vessel wave frequency motions", Journal of Offshore Mechanics and Artic Engineering, 129(2), pp. 90-96.

Petursdottir G., Hannibalsson O., Turner J.M.M., 2001, Safety at sea as an integral part of fisheries management, Food and Agriculture Organization of the United Nations, Rome.

Tannuri E.A., Sparano J.V., Simos A.N., Da Cruz J.J., 2003, "Estimating directional wave spectrum based on stationary ship motion measurements", Applied Ocean Research, 25(5), pp. 243-261.

Terada D., 2014, "Onboard Evaluation of the Transverse Stability for Officers Based on Nonlinear Time Series Modeling", Journal of Maritime Researches, 4, pp. 31-42.

Viggosson G., 2009, "The Icelandic Information System on Weather and Sea State", Proc. Seminar on Fishing Vessels' Crews and Stability, World Fishing Exhibition, Vigo.

Womack J, 2002 "Small Commercial Fishing Vessel Stability Analysis. Where are we now? Where are we Going?", Proc. 6th International Ship Stability Workshop, New York.

Estimation of the metacentric height by using onboard monitoring roll data based on time series analysis

Daisuke Terada, *Japan Fisheries Research and Education Agency*, dterada@affrc.go.jp

Masahiro Tamashima, *FLUID TECHNO Co., Ltd.*, mtamashima@fluidtechno.com

Ikuo Nakao, *FLUID TECHNO Co., Ltd.*, inakao@fluidtechno.com

Akihiko Matsuda, *Japan Fisheries Research and Education Agency*, amatsuda@affrc.go.jp

ABSTRACT

In this paper, a novel procedure to estimate the metacentric height (GM) is proposed based on an autoregressive modeling procedure and a general state space modeling as to an onboard monitoring roll data. Firstly, the autoregressive modeling procedure is applied to estimate a natural frequency on the roll motion. After that, the general state space modeling procedure is applied to estimate the GM by using the estimated natural frequency. In order to verify the proposed procedure, model and onboard experiments were carried out. From these results, it can be confirmed that the proposed procedure can achieve the good estimation in which the estimated results are good agreement with the given one in model experiments and the derived one from stability manual corresponding to the ship condition in onboard experiments.

Keywords: *General state space modeling procedure, Monte Carlo Filter, Nonlinear observation*

1. INTRODUCTION

It is very important for a captain, officers and crews of a ship to understand the value of metacentric height (GM) under navigation. On the other hand, technique of onboard measurement on ship motions, vibration and so on has been improved in recent years. From this background, the onboard monitoring data concerning ship motions can be used to develop a safe navigation support system for heavy weather operation. In the fact, Bradley and Macfarlane (1986), Brown and Witz (1996), Ohtsu (2008) and so on had developed the system to estimate the GM. And also, Iseki et al. (2013) and Hirayama (2015) have developed the navigation support system to remain the safe navigation in heavy weather operation.

In these research, as to the way to estimate the GM dynamically, there are Brown and Witz (1996) and Ohtsu (2008). These methods use the natural frequency on the roll motion. However, it seems that the way to estimate the natural frequency has some problems. That is, in these methods an autoregressive model is used to estimate the natural frequency. In Brown and Witz (1996) the model order of the autoregressive model is fixed with 2nd order. And also in Ohtsu (2008) the natural frequency is approximated by a peak frequency of a

spectrum on the roll motion, although the model order of the autoregressive model can be automatically determined by Akaike Information Criterion (AIC) [Akaike, 1973]. As the pointed out by Yamanouchi (1956), in general the roll motion cannot be approximated by 2nd order autoregressive model, since the roll motion in waves is driven by a colored noise sequence. And the natural frequency cannot be approximated by the peak frequency of the spectrum, since the peak frequency on the roll motion slightly varies with an encounter angle relationship between the ship and waves. Therefore, to estimate the natural frequency needs to use the way like Yamanouchi (1956). In this paper we focused on the way of Yamanouchi (1956) from the viewpoint of the convenience of calculation algorithm, although as such way there are Ohtsu and Kitagawa (1989), Iseki and Ohtsu (1999), Terada and Kitagawa (2009) and Terada et al. (2016).

On the other hand, even if we can estimate the natural frequency, we must also estimate a radius of gyration (k). This is big problem with respect to accurate estimation of the GM. In order to treat this problem, in general an empirical formula is used. However, according to knowledge of recent statistical science, we can also estimate the k with the GM. That is, we can apply the way called a

general state space modeling procedure [Kitagawa, 1996] which is a class of time series analysis. This way is especially effective to solve the nonlinear problem in time series analysis, since these is the powerful tool to achieve the state estimation of the state space model which is called the Particle Filter (Monte Carlo Filter).

From these background, in this paper, we introduce a novel procedure to estimate the GM based on time series analysis concerning the onboard monitoring roll data. This procedure is constructed by the combination of two different statistical methods. First one is an estimation of the natural frequency of roll motion based on the way of Yamanouchi (1956), and other one is an estimation of the GM by using the estimated natural frequency at the previous step based on the general state space modeling procedure. In the second step, as mentioned before, the k is also estimated with the GM at same time. In this case, the influence of the estimation error of the natural frequency can be absorbed in the process of the general state space modeling procedure. This point is the most different point from other method to estimate the GM, and is novelty. In order to verify the accuracy of the proposed procedure, model and onboard experiments were carried out. From there results, we can confirm that the proposed procedure can achieve the good estimation in which the estimated results are good agreement with the given one in model experiments and the derived one from stability manual corresponding to the ship condition in onboard experiments. Obtained findings are reported in detail.

2. ESTIMATION OF THE NATURAL ROLL FREQUENCY

As the amplitude of the roll motion is enough small, consider the following roll motion equation:

$$\ddot{x}(t) + 2\alpha\dot{x}(t) + \omega^2x(t) = u(t) \quad (1)$$

where, $x(t)$ is a roll angle of the ship, α is a damping coefficient, $\omega (=2\pi f)$ is a natural angular frequency, f is a natural frequency and $u(t)$ is an external disturbance, respectively. Here, as mentioned before, $u(t)$ is treated as the stochastic process and does not satisfy the assumption of the white noise sequence, since the characteristics of the roll motion change with the frequency

characteristic of the external disturbances such as waves and winds.

According to Yamanouchi (1956), Equation 1 can be approximated by the following 2nd order autoregressive model.

$$x(n) + a_1x(n-1) + a_2x(n-2) = u(n) \quad (2)$$

Where,

$$\begin{cases} \alpha = -\frac{1}{2} \log a_1 \\ f = \cos^{-1} \left(-\frac{a_1}{2\sqrt{a_2}} \right) \end{cases} \quad (3)$$

On the other hand, $u(n)$ can be also approximated by the following M -th order autoregressive process.

$$u(n) = \sum_{i=1}^M b_i u(n-i) + v(n) \quad (4)$$

Where $v(n)$ is the Gaussian white noise sequence with mean 0 and variance σ^2 . By substituting Equation 2 into Equation 4, then the following autoregressive model can be obtained.

$$x(n) = \sum_{i=1}^{M+2} c_i x(n-i) + v(n) \quad (5)$$

Here, for example, if $M = 2$, then the relationship between coefficients c_* and a_* , b_* can be written as follows:

$$\begin{cases} c_1 = a_1 + b_1 \\ c_2 = a_2 + a_1 b_1 + b_2 \\ c_3 = a_2 b_1 + a_1 b_2 \\ c_4 = a_2 b_2 \end{cases} \quad (6)$$

Therefore, to estimate the natural frequency, we firstly perform the determination of the best autoregressive model based on the minimum AIC estimation method [Akaike, 1973]. And then, the coefficients a_1 and a_2 can be obtained by solving the algebraic equation like Equation 6. And finally, the natural frequency can be calculated by using the relation of Equation 3. It should be noted that the solution of Equation 6 can be calculated by using the Newton-Raphson method.

3. ESTIMATION OF THE METACENTRIC HEIGHT (GM)

To estimate the GM and the k , consider the following equation:

$$f = \frac{\sqrt{g GM}}{2\pi k} \quad (7)$$

where g is the gravitational acceleration. Furthermore, allow that the f , the GM and the k in Equation 7 gradually change with the time n . Then, Equation 7 can be expressed as follows:

$$f(n) = \frac{\sqrt{g GM(n)}}{2\pi k(n)} \quad (8)$$

In this case, we add an observation noise in Equation 8, and consider that model the observation model in the general state space model. Moreover, we replace the $f(n)$ with the $y(n)$ according to the general expression of the state space modeling procedure and we consider that the $y(n)$ ($= f(n)$) is given as the observation data. As a results, Equation 8 can be written as follows:

$$y(n) = h(GM(n), k(n)) + \varepsilon(n) \quad (9)$$

where $h(*)$ is the nonlinear mapping function corresponding to Equation 8 and $\varepsilon(n)$ is the observation noise according to the Gaussian white noise sequence with mean 0 and variance τ^2 .

Now, we introduce the following vector:

$$\mathbf{x}(n) = [GM(n), k(n)]^T. \quad (10)$$

Where, the notation T means the transpose of the vector. And, suppose that the time evolution of the GM(n) and the $k(n)$ can be achieved by a random walk model shown in Equation 11.

$$\mathbf{x}(n) = \mathbf{x}(n-1) + \mathbf{w}(n), \quad (11)$$

where $\mathbf{w}(n)$ is the 2-dimensional Gaussian white noise sequence with mean vector $\mathbf{0}$ and variance-covariance matrix Σ . Here, we consider Equation 11 the system model in the general state space model.

By simultaneously considering the Equation 9 and 11, we can obtain the following general state space modeling procedure.

$$\begin{cases} \mathbf{x}(n) = \mathbf{x}(n-1) + \mathbf{w}(n) \\ y(n) = h(\mathbf{x}(n)) + \varepsilon(n) \end{cases} \quad (12)$$

Note that $h(\mathbf{x}(n))$ in Equation 12 is same with $h(GM(n), k(n))$ in Equation 9.

To implement the state estimation of Equation 12, we apply the Monte Carlo Filter (MCF), which is a type of the particle filter, proposed by Kitagawa (1996). The MCF is powerful tool for the nonlinear and non-Gaussian state space modeling such as the

general state space modeling, and can be expected as the way to estimates the Eq. 12, since we use the nonlinear observation model shown in Eq. 9. Concretely, the estimation of the probability distribution can be done by the repeat of the one-ahead prediction and the filtering based on an idea of sequential Bayesian inference. This significant merit is that the estimates gradually converge the true value. It should be noted that we show the detail of the MCF in APPENDIX-I.

Note that this procedure is called ‘‘A Self-organizing state space modeling procedure’’ [Kitagawa, 1998], since the procedure includes the completely unknown parameter $k(n)$.

4. RESULTS AND DISCUSSIONS

Model experiments

In order to verify the proposed procedure, we firstly carried out the free running model experiments concerning a container ship at the marine dynamics basin belonging to Japan Fisheries Research and Education Agency. The principal particulars and the photo are shown in Table 1 and Fig. 1, respectively.

Table 1: Principal particulars of the sample ship.

L_{pp}	85.0 m	GM	0.828 m
B	14.0 m	T_ϕ	13.3 sec
d_m	3.54 m	k'_{yy}	0.264
W	2993.21ton		

Note: Scale ratio = 1/33



Figure 1: Photo of the sample ship.

We show the one of the results of the model experiments. The conditions are as follows:

- The model ship speed is corresponding to 10[knots] in actual ship.
- The encounter angle relationship between the ship course and the wave direction is 0[degrees], that is, the model ship ran under the following seas.
- The measurement device is the Fiber Optic Gyro (FOG) sensor made by Tamagawa seiki Co., Ltd., and its sampling rate is 20[Hz].
- The waves are the long-crested irregular waves, are reproduced by the conditions in which the significant wave height $h_{1/3}$ is 1[m] and the mean period T_{01} is 6[sec].
- Note that the results of the model scale have been transformed in to the value of the actual ship.

As preparation of the GM estimation, as shown in Fig. 2 we made the 100 data set from one record of the measured time series data such that the number of analysis data always becomes 300 samples, because the measurement time in the model experiment has the constraint. It should be noted that to use 300 samples is decided by the viewpoint of the calculation time.

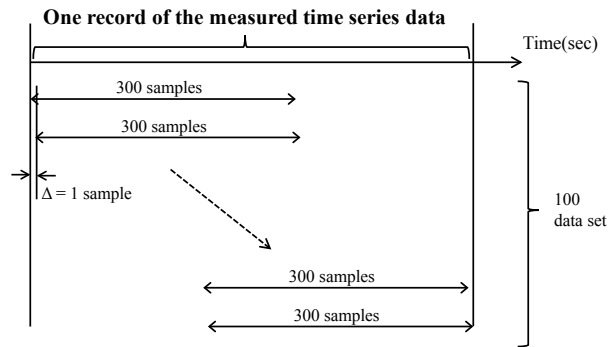


Figure 2: Schematic diagram concerning the contraction of the data set.

The estimation of the GM was performed against these data. Fig. 3 and Fig. 4 show the results of the natural frequency and the GM, respectively. In these figures, the horizon axis indicates the number of the data set. In Fig. 4, the vertical axis indicates the expectation of the filter distribution estimated by the MCF. As mentioned above, the estimated GM depends on the accuracy of the estimated natural frequency, since the GM is calculated by using the estimated natural frequency. From these figures, it can be seen that the estimated GM is bigger than the given one, when the estimated natural frequency is bigger than the given one. However, it can be seen that the estimated GM gradually coincides with the given one, when the estimated natural frequency approaches to the given one. Therefore, it can be considered that the proposed procedure is the powerful tool concerning the GM estimation.

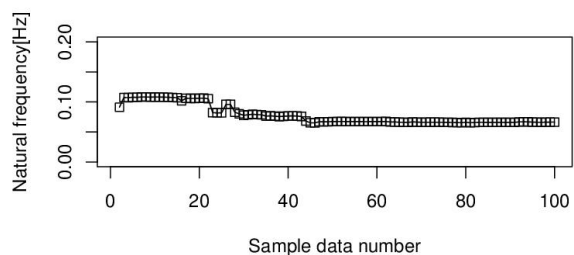


Figure 3: Results of the estimated natural frequency.

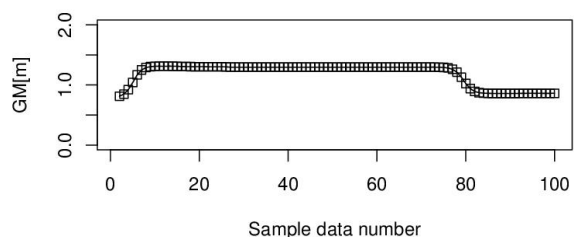


Figure 4: Results of the estimated GM.

Onboard experiments

Secondly, we carried out the onboard experiments concerning the container ship shown in Table 1 and Fig. 1 in order to verify the proposed procedure. In this case, we used the data measured under the navigation from Tokyo to Sendai in Feb. 23, 2015. This was a voyage of one and a half days. The GM recorded in the abstract log of the sample ship at that time is 2.23[m]. This value was calculated by a loading calculator based on stability manual. The measurement of the roll motion was done by the satellite compass “SC-30” made by FURUNO ELECTRIC CO., LTD. The stationary time series without the influence of an altering course and a speed change were used in order to evaluate the estimated GM. Fig. 5 and Fig. 6 show the results of the natural frequency and the GM, respectively. In these figures, the horizon axis indicates the number of the data set. In Fig. 6, the vertical axis indicates the expectation of the filter distribution estimated by the MCF. From Fig. 5, it can be seen that the results of the natural frequency of each data set have large dispersion comparison with the results of the model experiments. As to this, it may be considered that there is the limitation of the way of Yamanouchi (1956), since the actual seas confirmed by the weather map at that time was quite complex. Under the influence of this result, as shown in Fig. 6, it can be seen that the results of the GM of each data set have slight dispersion. However, the average of these is 2.04[m], we consider that the estimated GM can be competently canceled the influence of the fluctuation of the natural frequency. This fact is most important point, and is the evidence that modeling succeeds. Therefore, as well as the discussion of the model experiments, it can be considered that the proposed procedure is the powerful tool concerning the GM estimation, even if the case of actual seas.

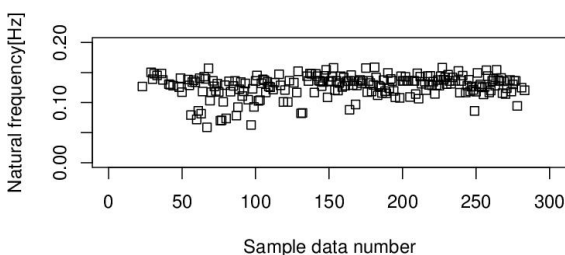


Figure 5: Results of the estimated natural frequency.

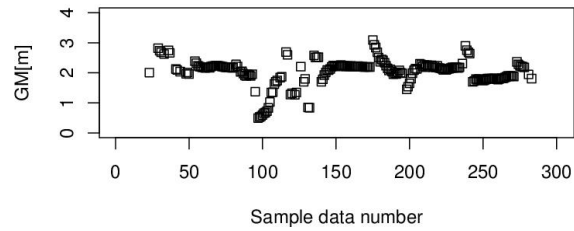


Figure 6: Results of the estimated GM.

5. CONCLUSIONS

In this paper, we introduce the novel procedure to estimate the metacentric height (GM) based on time series analysis concerning the onboard monitoring roll data. This procedure is constructed by the combination of two different statistical methods. First one is an estimation of the natural frequency of roll motion based on the way of Yamanouchi (1956), and other one is the simultaneous estimation of the GM and the radius of gyration by using the estimated natural frequency at the previous step based on the general state space modeling procedure. And this procedure also has the characteristics in which the influence of the estimation error of the natural frequency can be absorbed. This point is the most different point from other method to estimate the GM, and is novelty. In order to verify the accuracy of the proposed procedure, model and onboard experiments were carried out. The main conclusions are summarized as follows.

- I. From the free running model experiments, we can confirm that the proposed procedure can achieve the good estimation in which the estimated results are good agreement with the given one in model experiments.
- II. From the onboard experiments, we can confirm that the proposed procedure can achieve the good estimation in which the estimated results are good agreement with the derived one from stability manual corresponding to the ship condition in onboard experiments, even if the case of actual seas.

Therefore, we can conclude that the proposed procedure for the GM estimation is the powerful tool to remain the safe navigation, because the GM estimation can achieve with only the time series data of roll motion.

6. ACKNOWLEDGEMENTS

This work was supported by Nagasaki Prefectural Industrial Promotion Foundation. Authors would like to thank all affiliated parties.

7. REFERENCES

Akaike H., 1973, "Information theory and an extension of the maximum likelihood principle", Proc. of the 2nd International Symposium on Information Theory, Petrov, B. N., and Caski, F. (eds.), Akadimiai Kiado, Budapest: pp.267-281.

Bradley M. S. and Macfarlane C. J., 1986, "The In-service Measurement of Hydrostatic Stability", Offshore Technology congress, Paper 5345.

Brown T. D. and Witz J. A., 1996, "Estimation of Vessel Stability at Sea Using Roll Motion Records", Trans. of the Royal Institution of Naval Architects, Vol. 130, pp.130-146.

Hirayama T., 2015, "Historical Review on the Development of Measurement Technologies for Actual Ships -Mainly on the Ship Research Association of Japan (in Japanese)", Text of the Marine Dynamics Symposium "Ship Performance Monitoring in Actual Seas", pp.39-73.

Iseki T. and Ohtsu K., 1999, "On-line Identification of the Ship Motion Parameters (in Japanese)", Journal of the SNAJ, No. 186, pp.107-113.

Iseki T., Baba M. and Hirayama K., 2013, "Hybrid Bayesian Wave Estimation for Actual Merchant Vessels", Marine Navigation and Safety of Sea Transportation (Edited by Tomasz Neumann), pp.293-298.

Kitagawa G., 1996, "Monte Carlo Filter and Smoother for non-Gaussian nonlinear state space model", Journal of Computational and Graphical Statistics, Vol.5, No.1, pp.1-25

Kitagawa, G., 1998, "A Self-organizing state space model", Journal of the American Statistical Association, Vol.93, No.443, pp.1203-1215

Ohtsu K. and Kitagawa G., 1989, "Full Scale Data Depended Statistical Estimate of the Parameters in the Equation of Ship's Oscillation Application of a Continuous Auto Regressive Model (in Japanese)", Journal of the SNAJ, No. 165, pp.181-191.

Ohtsu K., 2008, "Statistical Analysis and Control of Ship's Motion -Review and Prospect of

the Studies for 40 Years (in Japanese)", Journal of the Tokyo University of Marine Science and Technology, Vol. 4, pp. 37-48.

Terada D. and Kitagawa G., 2009, "Direct Estimation Method for the Ship Motion Parameters based on Time Series Analysis -Verification based on one degree of free model (in Japanese)", Journal of the JASNAOE, Vol. 9, pp.127-137.

Terada D., Hashimoto H. and Matsuda A., 2016, "Estimation of Parameters in the Linear Stochastic Dynamical System Driven by Colored Noise Sequence", Proc. of 47th ISCIE International Symposium on Stochastic Systems Theory and Its Applications 2015, (in Press).

Yamanouchi Y., 1956, "On the Analysis of ships, Oscillations as a Time Series (in Japanese)", Journal of zosen kyokai, vol. 99, pp.47-64.

8. APPENDIX-I

Here, as mentioned before, we show the detail of the Monte Carlo Filter (MCF).

Here, it should be noted that in this part, the symbol (n) that is a meaning of variable for the time used in Eq. (12) is expressed by subscript symbol, for simple expression of equations. In this method, each probability density function that is the predictor $p(\mathbf{x}_n|\mathbf{Y}_{n-1})$ and the filter $p(\mathbf{x}_n|\mathbf{Y}_n)$; where \mathbf{Y}_n is the set of observations (y_1, \dots, y_N) , is approximated by J particles, which can be regarded as independent realizations from that distribution. According to Kitagawa (1996), it can be shown that these particles can be recursively given by the following Monte Carlo Filter algorithm:

[Step 1]

Generate the 2 dimensional random number $\mathbf{f}^{(j)}_0 \sim p_0(\mathbf{x})$ for $j = 1 \sim J$.

Here, the $\mathbf{f}^{(j)}_0$ are the initial values of the state variables for the j -th which are sampled from the initial filter distribution $p_0(\mathbf{x})$ of the state variables. It should be noted that the assumption in which the radius of gyration (k) exists within from $0.3B$ to $0.5B$ was used, and the realizations were sampled from a uniform distribution $U[0.3B, 0.5B]$. On the other hand, as to the metacentric height (GM), the realizations were sampled from a normal (Gaussian) distribution $N(\mu, (\mu/4)^2)$. Where, μ was given by the following equation:

$$\mu = (0.8Bf)^2 \quad (\text{A-1})$$

[Step 2]

Repeat the following steps for $n = 1 \sim N$.

1. Generate the 2 dimensional random number $\mathbf{w}^{(j)}_n \sim q(\mathbf{w})$ for $j=1 \sim J$.

Here, the $\mathbf{w}^{(j)}_n$ are the realizations of the system noise for the j -th which are sampled from the given system noise distribution $q(\mathbf{w}) \sim N(0, \Sigma)$.

2. Compute the following equation:

$$\mathbf{p}^{(j)}_n = \mathbf{f}^{(j)}_{n-1} + \mathbf{w}^{(j)}_n \quad (\text{A-2})$$

Here, the $\mathbf{p}^{(j)}_n$ are the realizations of the predictive distribution, and this equation correspond with the random walk model for the one ahead prediction shown in Eq. 11.

3. Compute the likelihood function $\alpha^{(j)}_n$ as follows:

$$\alpha^{(j)}_n = \frac{1}{\sqrt{2\pi\tau^2}} \times \exp\left(-\frac{1}{2\tau^2} g(y_n, \mathbf{p}^{(j)}_n)^2\right) \quad (\text{A-3})$$

Note that $g(*,*)$ is the following inverse function concerning the observation noise $\varepsilon(n)$.

$$g(y_n, \mathbf{x}_n) = y_n - \frac{\sqrt{g \text{GM}_n}}{2\pi k_n} \quad (\text{A-4})$$

Here, the likelihood function $\alpha^{(j)}_n$ expresses the good fit to the data of the realizations concerning the predictive distribution of the state variables, and have a role of a weight function. The realizations for the GM and the k have infinite combination in this stage. Therefore, the following sampling with replacement can be done in order to obtain the filter distribution of the state variables.

4. Generate $\mathbf{f}^{(j)}_n$ according the following probability for $j=1 \sim J$ by the resampling of $\mathbf{p}^{(1)}_n \sim \mathbf{p}^{(j)}_n$.

$$\Pr(\mathbf{f}^{(j)}_n = \mathbf{p}^{(j)}_n) = \frac{\alpha^{(j)}_n}{\alpha^{(1)}_n + \dots + \alpha^{(j)}_n} \quad (\text{A-5})$$

In this stage, as to the realizations of the GM and the k sampled from the predictive distribution, the realizations in which the fit to the data is wrong are disappeared and the realizations in which the fit to the data is good are copied.

As mentioned above, the separation of the GM and the k can be achieved appropriately by the repeat of the one ahead prediction process (1. and 2.) shown in the [Step 2] and the filtering process (3. and 4.) shown in the [Step 2]. Anyway, it is very important point to use the assumption in which the GM and the k vary with the time, and the separation of them can be achieved appropriately by this effect.

Note that in this study the number of particles is 1,000,000 from the view point of the calculation time. The accuracy of the state estimation, namely the estimation of the GM and the k , depends on the number of realizations.

Maneuverability in Adverse Conditions: Assessment Framework and Examples

Vladimir Shigunov, *DNVGL, Hamburg, Germany*, vladimir.shigunov@dnvgl.com

Apostolos Papanikolaou, *NTUA-SDL, Athens, Greece*, papa@deslab.ntua.gr

Dionysia Chroni, *NTUA-SDL, Athens, Greece*, dchroni@central.ntua.gr

ABSTRACT

Maneuverability of ships is presently regulated by the IMO Standards for Ship Maneuverability, which do not address ship maneuverability in adverse conditions. The importance of norming maneuverability in adverse conditions increased after the introduction of EEDI, which led to concerns that fulfilling EEDI by simply reducing ship's installed power may lead to insufficient maneuverability in adverse conditions. Responding to the need for norming the maneuverability in adverse conditions, *Shigunov and Papanikolaou (2013)* presented additional criteria and an assessment procedure ("Comprehensive Assessment"), which is based on a relatively simple mathematical model and allows using alternative methods (model tests, numerical simulations or empirical formulae, depending on designer's needs) for different components of the environmental forces and responses (waves, wind, maneuvering forces, rudder forces). This procedure is especially suitable for ships with innovative propulsion and steering solutions, but may be impracticable if it is to be applied to all ships. Therefore, two additional procedures were developed, namely the "Simplified Assessment", which has the complexity of a spreadsheet calculation but takes all relevant physics and ship particulars into account, and even a much simpler "check", which is based on empirical formulae (of the complexity of a pocket calculator), determining the required installed power as a function of ship's deadweight, windage area, rudder area, propeller characteristics and engine type. This paper outlines the rationale and status of these developments.

Keywords: *Manoeuvrability in Waves; Numerical Assessment Methods; Simplified Assessment*

INTRODUCTION

The implementation of the Energy Efficiency Design Index (EEDI) has raised justified concerns that some ship designers might choose to simply lower the installed power to achieve EEDI requirements, which can lead to insufficient manoeuvrability of ships under adverse weather conditions. A requirement was added to the Reg. 21, Ch. 4 of MARPOL Annex VI to verify that the installed propulsion power is sufficient to maintain manoeuvrability under adverse conditions. The first such verification procedure, provided in the *2012 Interim Guidelines*, issued in 2012 [1], was based on three levels of assessment (Level 3, Comprehensive Assessment, Level 2, Simplified Assessment and Level 1, Minimum Power Lines). In the revised, *2013 Interim Guidelines* [2], Level 3 was removed as too complex; in Level 2, numerical methods were replaced with model tests, which is too complex for this assessment level; besides, a

formulation of Level 1 was accepted, that does not relate to propulsion or steering characteristics of ships. In 2014, these were extended into Phase 1 of EEDI implementation (until December 31, 2019). Although *2013 Interim Guidelines* is an effective provision to prevent new built ships from underpowering, the mentioned elements can be improved. To address this, several research initiatives have started in EU (project SHOPERA [3], *Energy Efficient Safe Ship Operation*), Japan, Germany, The Netherlands, Korea and China.

Manoeuvrability of ships is presently addressed by IMO *Standards for Ship Manoeuvrability*, adopted in 2002 [4], which norm turning, initial turning, yaw-checking, course-keeping and emergence stopping abilities of ships, which are evaluated in simple manoeuvres in calm water. These Standards have been often criticized for not addressing ship manoeuvring characteristics at limited speed, in restricted areas and in adverse

weather conditions. Two questions arise: first, whether the acceptance limits of the existing criteria are strict enough to ensure sufficient manoeuvrability also at low speed and in adverse conditions, and second, whether all relevant ship characteristics are covered by the existing criteria or additional criteria are required. Whereas existing experience and knowledge do not provide clear answer to the first question, the answer to the second question is obvious when we note that one of tasks of steering is withstanding environmental forces; because different ships experience different environmental forces, the ship-specific assessment of ship's steering and propulsion abilities to withstand these forces appears a necessary part of minimum manoeuvrability requirements.

Based on the analysis of accident statistics, detailed accident reports, interviews of ship masters and existing proposals for manoeuvrability criteria in adverse conditions, work [5] proposed to consider three scenarios (manoeuvring in the open sea, manoeuvring in coastal areas and manoeuvring at limited speed in restricted areas); for each of these scenarios, the following practical criteria were proposed:

- In the open sea: (C1) *the ship should be able to keep heading in head to bow-quartering seaway up to 60° off-bow*;
- In coastal areas: *the ship should be able, in waves and wind from any direction, to keep (C2) a prescribed course and (C3) a prescribed advance speed*;
- At limited speed in restricted areas: *course-keeping at a specified low speed in strong wind in (C4) shallow water, (C5) shallow water near a bank and (C6) shallow water during overtaking by a quicker ship*.

ASSESSMENT FRAMEWORK

Whereas *IMO Manoeuvrability Standards* [4] are evaluated in full-scale trials, this is impossible in adverse weather conditions; model tests and numerical computations are possible alternatives. In principle, criteria C1-C6 can be directly evaluated in transient model experiments with self-propelled ship models in simulated irregular waves and wind, for all required combinations of wave direction and wave period. However, such an approach is impracticable at the present state of technology: First, reliable statistical predictions

require repeating tests in multiple long realisations of each seaway, which is too expensive. Second, only few suitable facilities exist world-wide, which makes such tests impractical for routine design and approval. Finally, verification of such tests by the Administration is impossible, especially in marginal cases (which are of interest in approval), where results strongly depend on steering time history. Alternatives to such model tests – direct numerical simulations of transient manoeuvres in irregular waves – are not mature enough yet for routine design and approval [6].

The alternative procedure proposed in SHOPERA (referred further to as Comprehensive Assessment) is based on separate simple model tests, numerical simulations or empirical formulae to account for different effects (wave forces, wind forces, manoeuvrability coefficients, rudder forces), which are combined in a relatively simple numerical model for ship motions. The procedure is based on neglecting oscillatory forces and moments due to waves and thus considering only time-average forces, moments and other variables, assuming that the time scale of their oscillations is shorter than the time scale of manoeuvring motions.

This reduces the evaluation of criteria C1-C6 to a solution of coupled equations of motion in the horizontal plane under the action of time-average wave-induced forces and moments (index *d*), wind forces and moments (*w*), calm-water forces and moments (*s*), including interaction effects, rudder forces (*R*) and propeller thrust (*T*). Projecting forces on the *x*- and *y*-axes and moments on the *z*-axis of the ship-fixed coordinate system, Fig. 1, leads to a system of equations, converging to a steady state described by the following system (note that achieving a converged solution can be realised in different ways, including time-domain simulation):

$$X_s + X_w + X_d + X_R + T(1-t) = 0 \quad (1)$$

$$Y_s + Y_w + Y_d + Y_R = 0 \quad (2)$$

$$N_s + N_w + N_d - Y_R I_R = 0 ; \quad (3)$$

I_R is the lever of the yaw moment due to rudder, which in general differs from $L_{pp}/2$ due to the pressure redistribution on the ship stern due to rudder influence.

Figure 1 shows the coordinate system: origin *O* in the main section at the water plane; *x*-, *y*- and

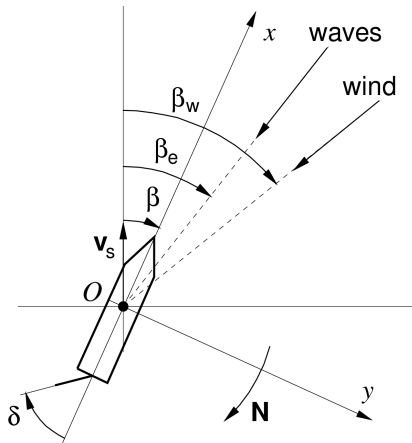


Figure 1. Coordinate system and definitions

z -axes point towards bow, starboard and downward, respectively (positive rotations and moments with respect to z -axis are clockwise when seen from above). For simplicity of description and without loss of generality, the ship is assumed to sail in the north direction with the speed v_s ; its heading deviates from the course by the drift angle β (positive clockwise when seen from above). The main wave and wind directions are described by angles β_e and β_w , respectively (0, 90 and 180° for waves and wind from the north, east and south, respectively); rudder angle δ is positive to port.

The converged solution, described by the equation system (1)-(3), provides the required propeller thrust T (from which, the advance ratio J , rotation speed n of the propeller, and required P_D and available P_D^{av} delivered power are found), drift angle β and rudder angle δ .

Any contribution in the system (1)-(3) can be defined individually, with the most suitable methods (empirical, numerical or experimental), depending on the designer needs and available technology. Innovative propulsion and steering solutions can be directly leveraged when necessary, by using high-fidelity results for the corresponding components. If, in the future, better numerical or experimental methods or empirical formulae are developed, they can be accommodated by the procedure without the need to revise Guidelines. The procedure is also easily verifiable in approval, because each of the contributions can be easily verified or updated, if necessary.

Note that a methodologically similar approach is used for the different problem of ship capsizing in

dead ship condition [7], [8]: even though seakeeping tests in beam seaway at zero forward speed are much easier to carry out and to evaluate than transient manoeuvres in seaway, still a simpler method is used, which is more accurate and more efficient. It is based on series of separate simple tests in well-controlled conditions (steady drift in beam wind, roll decay in calm water and roll in regular beam waves) which are used to define separately different elements (heel angle, roll damping and effective wave slope), which are put together in a simple analytical model.

Figure 2 shows examples of converged solutions described (1)-(3), corresponding to the application of the manoeuvring criteria in coastal areas C2 and C3 in polar coordinates *ship speed* (radial coordinate) – *seaway direction* (circumferential coordinate, head waves and wind come from the top). Along the line A, the required delivered power P_D is equal to the available delivered power P_D^{av} , along line B the speed is equal to the required minimum advance speed (here 4.0 knots), and line C limits the highlighted area in which the required rudder angle for course-keeping exceeds the maximum rudder angle (assumed here 25° as an example).

The left plot corresponds to a seaway in which the installed power is sufficient to fulfil both criteria C2 and C3 (line A does not cross lines B and C). Further to the right, the following combinations of wave height and period are shown: installed power is marginally sufficient to provide 4.0 knots advance speed in head seaway (line A crosses line B in head seaway); installed power is marginally sufficient to provide 4.0 knots advance speed in bow-quartering seaway (line A crosses line B in bow-quartering seaway); and installed power is marginally sufficient for course-keeping in nearly beam seaway (line A crosses line C).

An important question is how the accuracy of each of the components of system (1)-(3) influences the final result. To investigate this, each of the coefficients of forces and moments in the system (1)-(3) was disturbed by $\pm 10\%$ in turn, and the maximum ratio P_D/P_D^{av} was evaluated at the significant wave height 5.5 m and zero-upcrossing wave periods from 7 to 15 s along the lines 4.0 knots (criterion C2) and rudder angle 25° (criterion C3).

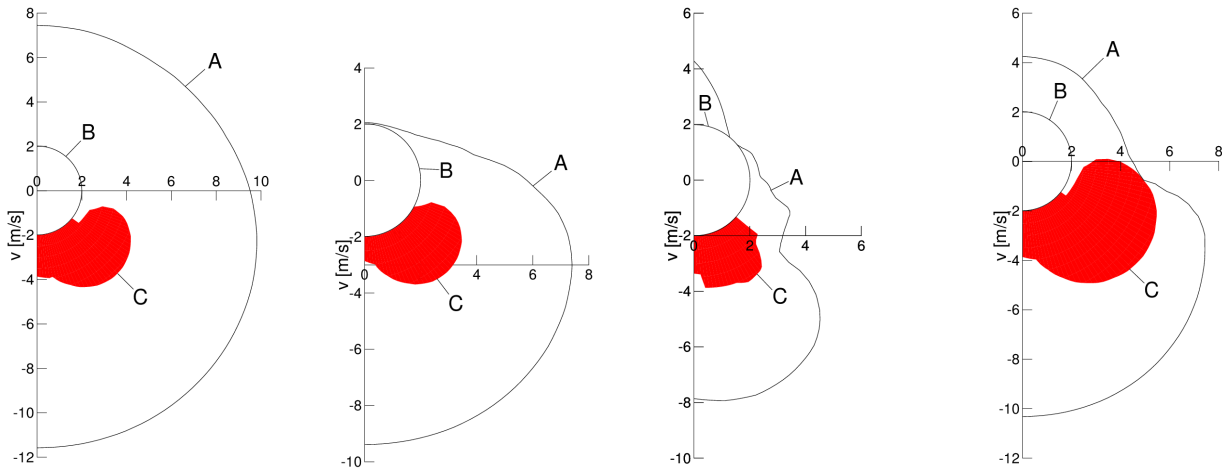


Figure 2. Examples of assessment results in polar coordinates *ship speed* (radial coordinate) – *seaway direction* (circumferential coordinate, head waves and wind come from the top): line “required power equal to available power” (line A), line “advance speed 4.0 knots” (line B) and line “rudder angle 25°” (line C)

The results, shown in Table 2 as percentage of the change of the ratio P_D/P_D^{av} due to change of each force or moment coefficient by 10%, indicate that the most important contribution is the time-average wave x -force (added resistance), followed by calm-water z -moment, calm-water y -force, time-average wave y -force and x -force on the rudder.

Table 2. Change of ratio of required to available delivered power in percent due to 10%-change of different components of forces and moments

Contributions	x -force	y -force	z -moment
Calm-water	0.7	1.7	1.8
Wind	1.4	0.6	0.4
Waves	3.5	1.7	0.3
Rudder	1.7	0.0	

If empirical formulae are used for all contributions, this assessment (*Comprehensive Assessment*) is not expensive; still it requires the solution of a nonlinear system of 3 equations for many cases (combinations of forward speeds and seaway headings). Whereas acceptable for a designer, consultancy or Class, this may be still too complex for Administrations to verify. Therefore, it is suggested that even simpler alternative assessment procedures are disposed. The Comprehensive Assessment will be anyway required for cases with large uncertainties, such as innovative propulsion and steering design solutions;

for the majority of conventional vessels, however, simple checks should be sufficient. In particular, it is foreseen to develop two simpler assessment procedures: a *Simplified Assessment* procedure, which is based on significant simplifications, such as reduced number of assessment cases and reduced complexity of the motion equations, but still takes into account all relevant physics for propulsion and steering (similar in complexity to the existing Level 2 assessment in the *2013 Interim Guidelines*); and another, simplest assessment procedure, based on the definition of the required minimum installed power as an empirical function of main ship parameters (similar in complexity to the existing Level 1 assessment in the *2013 Interim Guidelines*, but taking into account *propulsion* and *steering* characteristics of vessels).

SIMPLIFIED ASSESSMENT PROCEDURES

Principles

The aim of the simplification is to reduce the number of solution cases, as well as, if possible, the number of terms in motion equations (1) to (3). However, the procedure should still remain a first-principles assessment, keeping all relevant physics from the Comprehensive Assessment. In particular, this procedure evaluates the same criteria (C1-C6) as those enforced in the Comprehensive Assessment. In this paper, such Simplified Assessment procedures are presented concerning the following two criteria: propulsion ability (advance speed at least 4.0 knots in all seaway directions) and steering ability (course keeping in all seaway directions).

Propulsion Ability

The starting point is the system of equations (1)-(3), which has to be solved for all relevant forward speeds and all possible seaway directions to demonstrate that the ship is able to keep forward speed of at least 4.0 knots in seaway from any direction. Noting that bow seaways are most critical for required power at a given speed (Fig. 2, second and third plots from left), it is enough to consider only seaways from 0 to about 60° off-bow in the assessment. Further, neglecting the influence of drift on the required thrust and required power allows omitting equations (2) and (3). Thus only eq. (1) needs to be considered in head waves:

$$X_s + X_w + X_d + X_R + T(1 - t_H) = 0 \quad (4)$$

However, it is important to keep in mind that the time-average longitudinal force due to waves X_d in eq. (4) should be taken as the maximum force in mean wave directions between 0 and 60° off-bow.

The contributions X_s , X_w , X_d , X_R and thrust T in eq. (4) can be found using any method from the Comprehensive Assessment (empirical, numerical or experimental). However, it seems logical to allow using also simpler approximations for these terms in the Simplified Assessment.

For example, using semi-empirical models for the rudder resistance X_R , e.g. [9], [10], will lead to an implicit dependence of X_R on the propeller thrust T , requiring an iterative solution of eq. (4). To allow a simpler, non-iterative solution, assume $X_R = -t_R T$, where t_R is an empirical constant. In bow-quartering waves, a significant rudder angle may be required for steering, which leads to $t_R = 0.2$ (based on Comprehensive Assessment for 15 vessels). This results in a simple non-iterative equation for the required thrust T :

$$T = -\frac{X_s + X_w + X_d}{1 - t_H - t_R}, \quad (5)$$

where t_H is the thrust deduction on the ship hull.

At 4.0 knots advance speed, the influence of forward speed on propeller can be neglected, i.e. using the bollard pull assumption (K_T and K_Q at zero advance ratio $J=0$) instead of full open-water propeller curves provides accurate enough results, Fig. 3.

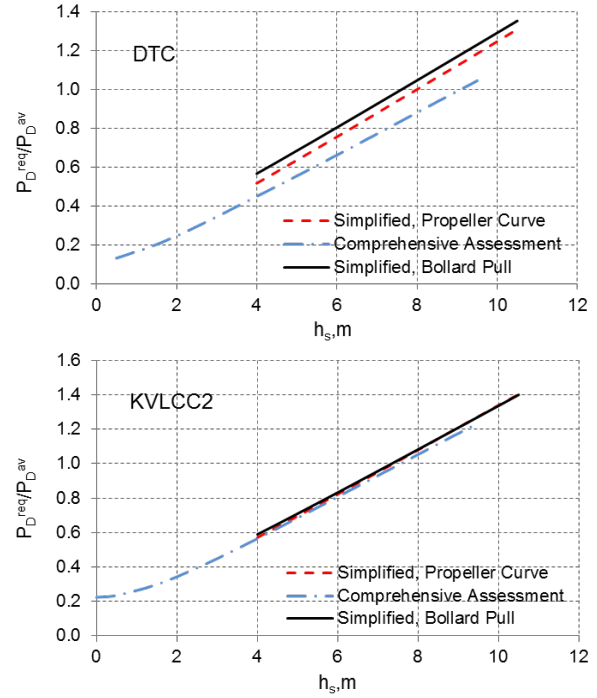


Figure 3: P_D/P_D^{av} vs. h_s according to Comprehensive and Simplified Assessments; the latter using propeller curves and bollard pull assumption

To define the calm-water resistance X_s at 4.0 knots advance speed, the ITTC regression line is accurate enough:

$$X_s = -C_F(1+k)0.5\rho v_s^2 A_0, \quad (6)$$

where $C_F = 0.075(\log_{10} Re - 2)^{-2}$ is the friction coefficient, $Re = v_s L_{pp}/\nu$ is the Reynolds number, k is the form-factor, v_s is ship speed, and A_0 is the wetted surface of the hull.

Wind resistance $X_w = -0.5X'_w \rho_a (v_s + v_w)^2 A_F$ can be defined using the air density ρ_a , wind speed v_w , frontal windage area A_F , and head wind resistance coefficient X'_w , which can be assumed conservatively as 1.0 in the Simplified Assessment.

The most challenging term in eq. (5) is the time-average longitudinal force in short-crested irregular waves (“added resistance”) X_d , taken as the maximum over the wave directions 0 to 60° off bow. In the 2013 *Interim Guidelines*, it can be defined only using model tests. According to the SHOPERA approach, it can be defined using any method from Comprehensive Assessment (empirical, numerical or experimental) to define quadratic transfer functions of X_d in regular waves, combined with a spectral integration. Again, using

alternative simpler approximations seems to be appropriate in the Simplified Assessment; here, an empirical expression is proposed, based on computations with the software *GL Rankine* [11], a spectral integration using JONSWAP spectrum with $\gamma = 3.3$ and \cos^2 -wave energy spreading and taken as maximum over mean wave directions 0 to 60° off-bow and peak wave periods from 7.0 to 15.0 s:

$$X_d = -83L_{pp}C_B^{1.5} \left(1 + \sqrt{Fr}\right) h_s^2; \quad (7)$$

$Fr = v_s(gL_{pp})^{-1/2}$ is the Froude number. Figure 4 shows results of eq. (7), y-axis, vs. numerical computation, x-axis, for 14 bulk carriers (BC), tankers (TA) and container vessels (CV).

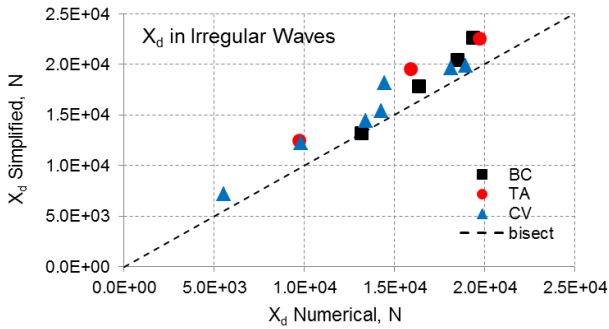


Figure 4: X_d in irregular short-crested waves according to eq. (7) vs. numerical computations.

Figure 5 compares results of the proposed simplified propulsion ability assessment procedure with the Comprehensive Assessment for 4 bulk

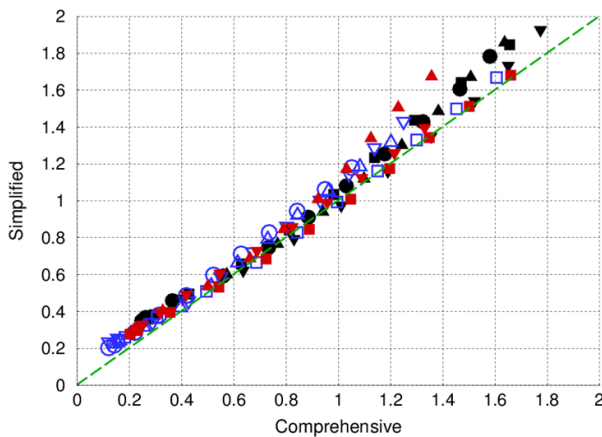


Figure 5: Ratio of required to available delivered power according to Simplified (y-axis) vs. Comprehensive (x-axis) Propulsion Ability Assessment for 4 bulk carriers (■, ▲, ▼, ●), 3 tankers (■, ▲, ▼) and 4 container ships (□, △, ▽, ○) in waves of significant wave heights from 0.0 to 9.5 m.

carriers, 3 tankers and 4 container ships at $h_s = 0$ to 9.5 m. The plot shows the ratio of the required to available delivered power $P_D/P_D^{av} > 1$ according to the Simplified (y-axis) vs. Comprehensive (x-axis) Assessment. The proposed Simplified Assessment procedure is sufficiently accurate to slightly conservative, especially for $P_D/P_D^{av} > 1$ (which is not relevant anyway). This procedure was implemented in MS Excel for practical use.

Steering Ability

The starting point is the system (1)-(3), which is being solved for all relevant forward speeds and all seaway directions to check that *the ship is able to keep course in seaway from any direction*. Note that for the steering ability, both the steering system and propulsion (which influences steering ability) are required and should be integral parts of the assessment: e.g. ships with powerful propulsion may have a smaller rudder, whereas ships with weaker propulsion may compensate this with larger or more effective steering devices.

The first simplification stems from an observation, which based on the results of Comprehensive Assessment for about 15 ships, that the steering ability is challenged to the largest degree in seaway directions close to beam (Fig. 2, right), i.e. the point with the maximum ratio of the required to available delivered power along the line of maximum rudder angle (further referred to as *critical conditions for steering* for brevity) is close to beam seaway. This allows reducing the simplified steering ability assessment to beam seaways only (from the norming point of view: ships with better steering ability in beam seaway will also have better steering ability in all seaway directions). Thus the system (1)-(3) results in the following system:

$$X_s + X_w^{90} + X_d^{90} + X_R + T(1 - t_H) = 0 \quad (8)$$

$$Y_s + Y_w^{90} + Y_d^{90} + Y_R = 0 \quad (9)$$

$$N_s + N_w^{90} + N_d^{90} - Y_R I_R = 0 \quad (10)$$

solved only in beam seaways; superscript 90 at the time-average wave and wind forces means that their evaluation is required only in beam waves and transverse winds, respectively.

To validate the simplification (8)-(10), the ratio of the required to available delivered power P_D/P_D^{av} computed using this simplification was compared

with the comprehensive steering ability assessment using system (1)-(3) for 15 vessels; results for a 14000 TEU container ship (DTC, top) and a very large crude oil carrier (KVLCC2, bottom) in Fig. 6 show that the simplification (8)-(10) is sufficiently accurate.

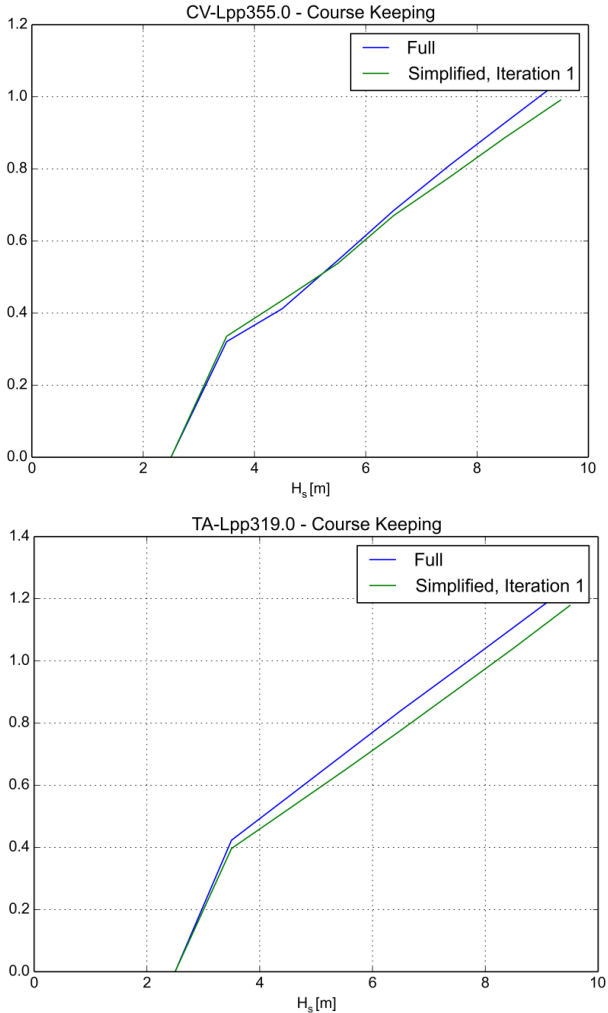


Figure 6: Ratio of required to available delivered power vs. significant wave height according to comprehensive steering ability assessment (blue line) and simplified system (8)-(10) (red line) for DTC (top) and KVLCC2 (bottom) in full load.

The analysis of the terms of system (1)-(3) using Comprehensive Assessment shows that none of terms is negligible compared to the other terms, thus none of the terms can be simply omitted. To identify possible simplifications, introduce the levers of yaw moments as follows:

$$l_s \equiv N_s/Y_s, \quad l_w \equiv N_w/Y_w, \quad l_d \equiv N_d/Y_d, \quad (11)$$

and rewrite eq. (10) using these definitions as

$$l_s Y_s + l_w Y_w^{90} + l_d Y_d^{90} - Y_R l_R = 0 \quad (12)$$

Express Y_s from eq. (9) as

$$Y_s = -Y_w^{90} - Y_d^{90} - Y_R \quad (13)$$

Introducing eq. (13) into eq. (12) leads to the following combination of equations (9) and (10):

$$Y_w^{90} (l_w - l_s) + Y_d^{90} (l_d - l_s) = Y_R (l_s + l_R) \quad (14)$$

Analysis of the terms of converged solutions of the system (1)-(3) in the critical conditions for steering ability (i.e. forward speeds and seaway directions, for which P_D/P_D^{av} is maximum along the line $\delta = \delta_{max}$, see Fig. 2, right) shows that

$$l_s \sim L_{pp}/2, \quad l_w \ll l_s, \quad l_d \ll l_s, \quad (15)$$

Fig. 7, thus eq. (14) can be simplified as

$$Y_w^{90} (0 - l_s) + Y_d^{90} (0 - l_s) = Y_R (l_s + l_R)$$

or

$$Y_R = -b(Y_w^{90} + Y_d^{90}) \quad (16)$$

where

$$b = l_s / (l_s + l_R) \quad (17)$$

As a result, the system of equations (8)-(10) reduces to one equation

$$X_s + X_w^{90} + X_d^{90} + X_R + T(1 - t_H) = 0 \quad (18)$$

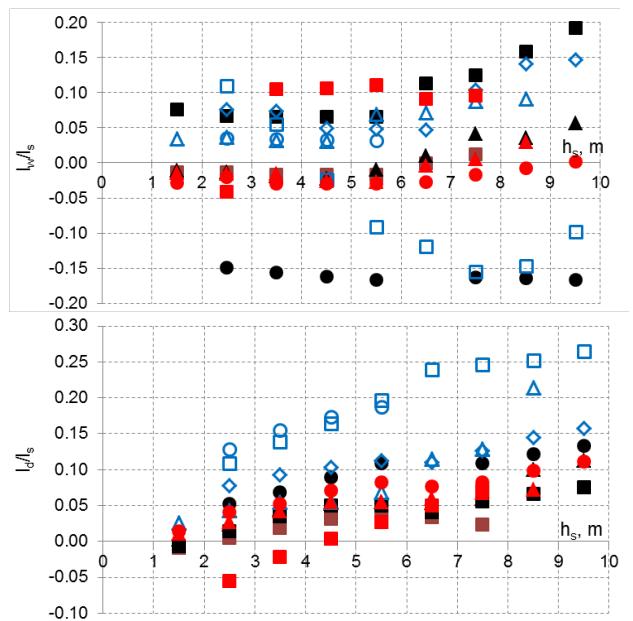


Figure 7: Ratios of levers l_w/l_s (top) and l_d/l_s (bottom) in the critical conditions for steering ability (combinations of forward speeds and seaway directions, for which P_D/P_D^{av} is maximum along the line $\delta = \delta_{max}$)

This equation is solved only for beam seaway; its solution (the maximum attainable speed and corresponding propeller rotation speed and thrust) defines the maximum available lateral steering force on the rudder Y_R^{av} . This steering force should not be less than the required lateral steering force defined by eq. (16), $Y_R^{req} = -b(Y_w^{90} + Y_d^{90})$.

As an approximation, assume $l_R \approx 0.5L_{pp}$, then definition (17) simplifies to

$$b = -l_s / (l_s + 0.5L_{pp}), \quad (19)$$

which can also be written as

$$b = \frac{Y_s l_s}{Y_s l_s + Y_s 0.5L_{pp}} = \frac{N_s}{N_s + 0.5Y_s L_{pp}} = \frac{N'_s}{N'_s + 0.5Y'_s} \quad (20)$$

where $Y'_s = Y_s / (0.5\rho L_{pp} T_m v_s^2)$, $N'_s = N_s / (0.5\rho L_{pp}^2 T_m v_s^2)$ are the coefficients of calm-water side force and yaw moment, respectively; note that they depend only on drift angle β .

To validate these approximations, Fig. 8 compares the ratio of the required to available delivered power according to approximations (16), (18) and (20) with the same ratio from the Comprehensive Assessment for the 15 sample ships. In the Simplified Assessment, the value of b is taken from the Comprehensive Assessment, as the exact value $b = N_s / (N_s + 0.5Y_s L_{pp})$ in critical conditions for steering ability; the approximation provides accurate to slightly conservative results.

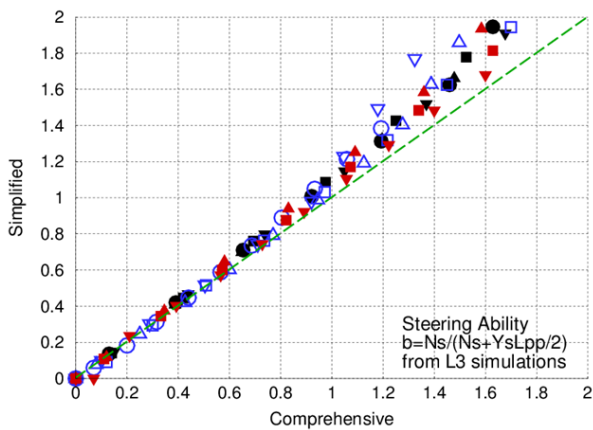


Figure 8: Ratio of required to available delivered power according to Simplified Assessment (16),(18),(20) with exact value of $b = N_s / (N_s + 0.5Y_s L_{pp})$ taken from Comprehensive Assessment (1)-(3) (y axis) vs. the same ratio from Comprehensive Assessment (x axis) for 4 bulk carriers (■,▲,▼,●), 3 tankers (■,▲,▼) and 4 container ships (□,△,▽,○) in waves of h_s from 0.0 to 9.5 m.

Obviously, the value of b depends on drift angle β in critical conditions for steering ability (b is a decreasing function of β), which depends on ship size and geometry, installed power and wave height and period. To provide a conservative recommendation for the value of b , it was evaluated in critical conditions for the steering ability using the Comprehensive Assessment and compared with its values at various drift angles for 11 ships (4 bulk carriers, 4 container ships, 3 tankers). This comparison shows that using the value of b at drift angle of $\beta = 5^\circ$ leads to a maximum conservative error (overestimation) for b of up to 16%, and to acceptable accuracy results of the Simplified Assessment, Fig. 9.

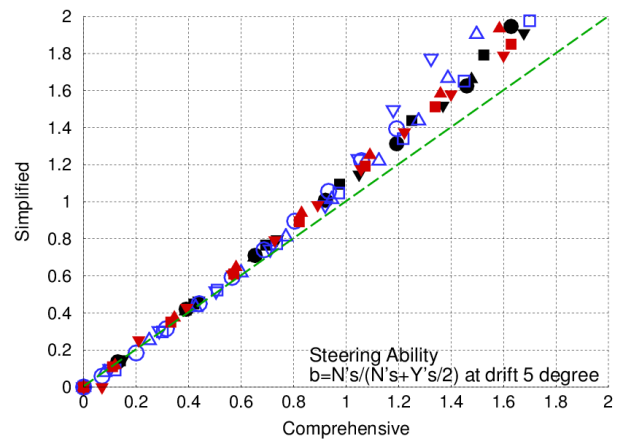


Figure 9: Ratio of required to available delivered power according to Simplified Assessment (16),(18),(20) using value of $b = N'_s / (N'_s + Y'_s / 2)$ at drift angle $\beta = 5^\circ$ (y axis) vs. the same ratio according to Comprehensive Assessment (x axis) for 4 bulk carriers (■,▲,▼,●), 3 tankers (■,▲,▼) and 4 container ships (□,△,▽,○) at h_s from 0.0 to 9.5 m.

If even calm-water manoeuvring derivatives Y'_s and N'_s are not available, it is useful to have a conservative assumption for b . It proves that a maximum value of $b = 0.4$ could be used based on the results for the 11 sample ships, Fig. 10 (here, even a more conservative assumption $b = 0.5$ was used). This assumption actually leads to very conservative results for container ships (for DTC, RANSE-computed value of b at drift angle 5° is 0.25). An empirical formula for b at $\beta = 5^\circ$ as a function of main ship particulars is required and needs to be developed.

To define the other terms in equations (16), (18), in addition to Comprehensive Assessment

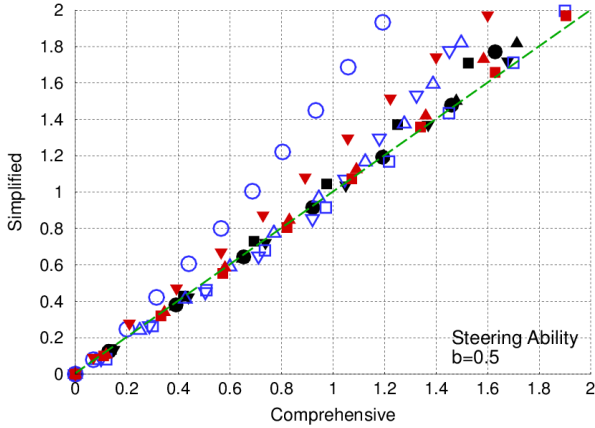


Figure 10: Ratio of required to available delivered power according to Simplified Assessment (16),(18) employing value of $b=0.5$ (y axis) vs. the same ratio according to Comprehensive Assessment (x axis) for 4 bulk carriers (■,▲,▼,●), 3 tankers (■,▲,▼) and 4 container ships (□,△,▽,○) in waves of h_s from 0.0 to 9.5 m.

methods (empirical, numerical and experimental), it is logical to introduce simplified approximations, consistent with the complexity of the Simplified Assessment, which are considered below.

The increase in rudder resistance X_R is significant in critical conditions for steering, because both rudder angle and the ratio P_D/P_D^{av} are maximal. Because X_R implicitly depends on thrust, which is itself part of solution, a simple assumption $X_R = -t_R T$ is used to avoid iterative solution of eq. (18). According to Comprehensive Assessment results for 15 vessels, $t_R = 0.3$ is recommended.

To calculate the available lateral force on rudder Y_R , model by Söding [9] was used with $\delta_{max} = 25^\circ$ as a conservative assumption.

The lateral force due to beam wind is calculated as $Y_w^{90} = -0.5Y_w^{90} \rho_a A_L v_w^2$; where $Y_w^{90} = 1$ can be used as a conservative assumption for the lateral wind force coefficient. The longitudinal component of the wind resistance in beam seaway X_w^{90} can be neglected, thus $X_w^{90} = -0.5X_w^{90} \rho_a A_F v_s^2$.

Approximation of the calm-water resistance in eq. (18) is more difficult than in eq. (5): the ITTC regression line cannot be used, because it would under-estimate resistance at the (rather high) forward speeds relevant in critical conditions for steering. If the resistance curve is available e.g. from model tests, it can be directly used; alternatively, resistance curve should be approximated in such a way as to fit those

parameters that are used in approval and are available to Administration, e.g. the maximum continuous rating (MCR) of the engine, corresponding propeller rotation speed n_{MCR} and ship speed at MCR v_{MCR} . In this case, the calm-water resistance curve can be „calibrated“ as

$$X_s = -C_F(1+k)0.5\rho v_s^2 A_0 \left(1 + c_{MCR} v_s^2 / v_{MCR}^2\right) \quad (21)$$

where parameter c_{MCR} is adjusted in such a way that $P_B = MCR$ when $n = n_{MCR}$ and $v_s = v_{MCR}$.

For the time-average longitudinal wave force in irregular short-crested beam waves X_d^{90} , a simple empirical formula is proposed, obtained from numerical computations with *GL Rankine* and spectral integration for JONSWAP spectrum with $\gamma = 3.3$ with \cos^2 -spreading, as a maximum over peak wave periods from 7.0 to 15.0 s:

$$X_d^{90} = -380L_{pp} C_B^{1.5} (0.1 + Fr) h_s^2 \quad (22)$$

Comparison of results of eq. (22) with numerical computations is shown in Fig. 11 at the forward speed of 4.0 m/s.

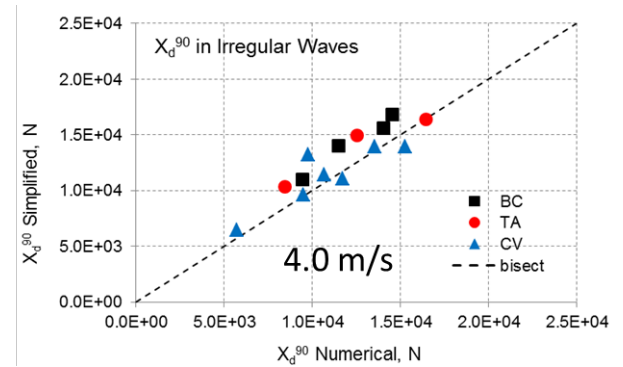


Figure 11: X_d^{90} in irregular short-crested beam seaway according to eq. (22) (y-axis) vs. numerical method (x-axis) for 4 bulk carriers (BC), 3 tankers (TA) and 7 container ships (CV).

Similarly, a simple empirical formula for the time-average lateral wave force Y_d^{90} in irregular short-crested beam seaway, obtained for JONSWAP spectrum with $\gamma = 3.3$ and \cos^2 -spreading, is proposed as the following function of peak wave period:

$$Y_d^{90} = -\frac{540L_{pp} h_s^2}{1 + T_p^5 / (C_B L_{pp}^{0.5})^5}; \quad (23)$$

Fig. 12 compares results of eq. (23) with numerical computations with *GL Rankine* followed by spectral integration.

This procedure was implemented in a MS Excel for practical use.

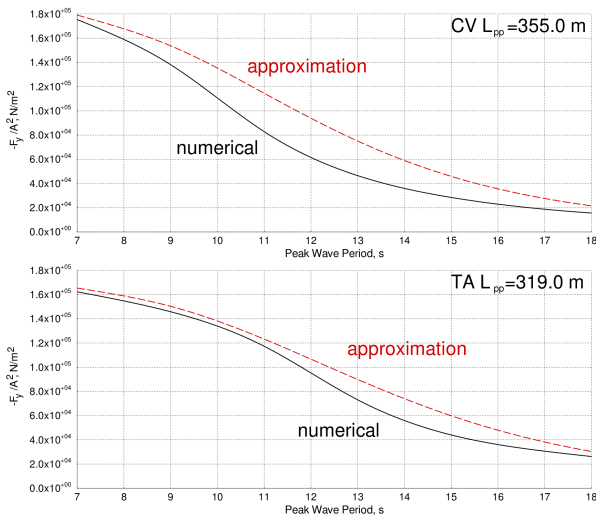


Figure 12: Y_d^{90} at significant wave height of 1.0 m according to eq. (23) (dashed red line) and numerical method (solid black line) vs. peak wave period for DTC (top) and KVLCC2 (bottom).

OUTLOOK

The herein outlined Simplified Assessment procedure for the maneuverability of ships in adverse weather conditions is currently under finalization and validation in the project SHOPERA; it requires, however, the following developments: First, the extension on ships with unconventional steering and propulsion arrangements (twin propellers, twin rudders, controlled-pitch propellers, diesel-electric and turbine propulsion and ships with pod drives). Second, the development of the Simplified Procedure for weather-vaning ability (criterion C1) and maneuverability at limited speed in restricted areas (criteria C4-C6). Third, the finalization of “simplified” empirical methods, consistent with the Simplified Assessment, for the time-average wave forces in irregular short-crested waves: X_d in bow and in beam waves and Y_d in beam waves, in addition to the numerical and empirical methods required for the Comprehensive Assessment. Finally, the development of an empirical formula for b , as a function of main ship particulars.

The next level of simplification, namely a simple empirical formula, is currently being developed in the project SHOPERA based on results of the Comprehensive Assessment for a large number of sample vessels, see e.g. the approach used in [12].

ACKNOWLEDGMENTS

This paper was partly supported by the Collaborative Project SHOPERA (Energy Efficient Safe Ship OPERATION) funded by DG Research of EC (Grant Agreement number 605221); the views expressed in this paper are those of the authors and do not necessarily reflect the views of EC.

REFERENCES

- [1] IMO (2012) Interim Guidelines for Determining Minimum Propulsion Power to Maintain the Manoeuvrability of Ships in Adverse Conditions, MSC-MEPC.2/Circ.11
- [2] IMO (2013) Interim guidelines for determining minimum propulsion power to maintain the Manoeuvrability in adverse conditions, IMO Res. MEPC.232(65)
- [3] Papanikolaou, A., Zaraphonitis, G., Bitner-Gregersen, E., Shigunov, V., El Moctar, O., Guedes Soares, C., Devalapalli, R., Sprenger, F. (2015) Energy Efficient Safe Ship Operation (SHOPERA), Proc. 4th World Maritime Technology Conference (WMTTC 2015)
- [4] IMO (2002) Standards for ship manoeuvrability, Res. MSC.137(76)
- [5] V. Shigunov and A. Papanikolaou (2014) Criteria for minimum powering and maneuverability in adverse weather conditions, 14th Int. Ship Stability Workshop (ISSW 2014), Kuala Lumpur, Malaysia
- [6] Manoeuvring Committee (2008) Final report and recommendations to 25th ITTC, Proc. 25th ITTC, Vol. I
- [7] IMO (2006) Interim Guidelines for Alternative Assessment of the Weather Criterion, MSC.1/Circ.1200
- [8] IMO (2007) Explanatory Notes to the Interim Guidelines for Alternative Assessment of the Weather Criterion, MSC.1/Circ.1227
- [9] Brix, J. E. (1993) Manoeuvring Technical Manual. – Seehafen Verlag, Hamburg
- [10] H. Söding (1998) Limits of potential theory in rudder flow predictions, Proc. Symp. Naval Hydrodynamics, Washington
- [11] H. Söding and V. Shigunov (2015) Added resistance of ships in waves, Ship Technology Research - Schiffstechnik **62**(1) 2-13
- [12] MEPC 62/INF.21 (2011) Reduction of GHG emissions from ships - Consideration of the Energy Efficiency Design Index for New Ships. Minimum propulsion power to ensure safe manoeuvring in adverse conditions, Submitted by IACS, BIMCO, CESA, INTERCARGO, INTERTANKO, WSC

Correlations of GZ Curve Parameters

Douglas Perrault, *Defence Research and Development Canada – Atlantic Research Centre,*
Doug.Perrault@DRDC-RDDC.GC.Ca

ABSTRACT

Over the decades of the last few centuries the stability of ships has moved from the art of the shipbuilder and master to the realm of regulatory agencies. In that time several concepts for assessing stability have emerged, all rooted in the *GZ* curve; the curve that defines the relationship between the angle of heel and the moment arm of the righting couple that would return the ship to the angle of static equilibrium, which is usually 0° . Within each concept there are usually several parameters suggested as stability criteria including righting arms, areas under the curve and moments of areas under the curve. Criteria were developed out of expert knowledge and have been supported by good service, but the basis is not clearly documented. Many of these criteria have been observed to be correlated so as to fail to provide additional information or, conversely, to give a different perspective on the same information. This study looks at the correlations between the parameters in the standards used by many navies, including those based on the seminal work by Sarchin and Goldberg and those used by the German and Dutch navies (among others). The study looks not only within each set, but looks for correlations between the parameter sets as well. The intent is to gain insight into the parameters and the phenomena they represent, and to identify the optimal parameter set for regression against probabilistic results of simulations.

Keywords: *GZ curve, Correlation of Stability Indicators.*

1. INTRODUCTION

The Cooperative Research Navies (CRNav) Dynamic Stability Project has developed tools for assessing dynamic stability of intact ships. The Naval Stability Standards Working Group (NSSWG) has overseen the use of the tools to investigate the relationship between risk of capsizing and various geometry and stability parameters. The risk of capsizing was characterized by the probability of exceeding a critical roll angle (PECRA), although the “critical roll angle” could also take on a number of other important connotations, such as machinery or weapon limits.

The probability of exceeding a critical roll angle (PECRA) is determined by running multiple, time-domain simulations of a ship in a specific loading condition at a set speed and heading (the operating point of the vessel) in waves of a given significant height and modal period (the environmental condition). The time series of roll responses are used to determine the PECRA. The probability outcomes are later used as the regressands (response variables) in analysis

investigating relationships with parameters associated with ship stability.

A former paper [1] describes the study of how the PECRA vary with the input control variables of ship speed (V), ship heading relative to the wave system (β), significant wave height (H), and modal wave period (τ). The study looked into the variations between ships and between loading conditions, and investigated the issue of the range and resolution of the sets of input control variables that will fully characterize the total probability of exceeding a critical roll angle (TPECRA) across all input variables for each load condition of each ship.

The objective of the present study is to look at those *GZ* parameters that may be indicators of risk. While the PECRA in the former study are the regressands, the parameters in focus here are regressors. The set of regressors starts with a selection of parameters that form criteria in many naval standards, broadening the selection of parameters, essentially by using each of the parameters across all of the methods. The study then seeks to reduce the number of parameters to those that are not linearly correlated, and should, therefore, provide additional information. The goal

of the work is first to find the smallest set of parameters that can still represent the likely set of regressors, and second to identify the groups of parameters that are linearly correlated.

The next section will discuss the choice of parameters. Following that will be a brief description of how the data was validated prior to correlation analysis. The section after that will discuss the reduction of the parameter set based on the correlation analysis. Finally conclusions will be presented.

2. SELECTION OF PARAMETERS AS REGRESSORS

Although work is on-going to improve capabilities for assessing stability in real environments, many of the current criteria in both merchant and military standards are based on the GZ curve. In particular, many naval stability standards are based on work by Sarchin and Goldberg [2], and by Wendel [3] and influenced by the work of Rahola [4]. The principal tool has been the GZ curve, a locus of righting arms as the ship is inclined to various angles of heel. Various naval standards use very similar criteria but often have differences too. The seminal paper by Sarchin and Goldberg [2] formed the basis or greatly influenced the standards of the US and its allies, while the foundational work of Wendel [3] provided the basis for the German and Dutch naval standards (as well as other nations). The former work was based on US experience during World War 2, including the tragic (intact) loss of several vessels during a typhoon in 1944. It works with the Calm-Water (Still-Water) GZ Curve and heeling levers corresponding to winds of up to 100 knots. The latter work also applied the concept of balancing the ship on a wave.

A set of parameters were selected to represent the majority of those used to evaluate stability performance in the various naval standards.

Basic Parameters

Some of these parameters significantly pre-date Sarchin and Goldberg [2]. As such they have been applied by some naval organizations for a very significant period of time and are the framework upon which such standards as NES109 [5] were built (see Figure 1 and Table 1).

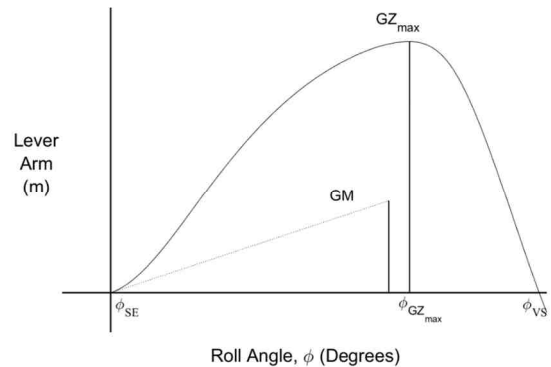


Figure 1: Basic Righting Arm Parameters - Fully Static Angles and Lever Arms.

Sarchin and Goldberg

Other measures were derived from an energy balance approach. These assess the relationship between the shape and area characteristics of the calm water righting curve against an assumed environmentally induced heeling curve. The energy balance assessment parameters selected are given in Figure 2 and Figure 3. These measures were proposed by Sarchin and Goldberg [2] and form the core of many of the current naval stability standards (e.g., [5][6][7][8]).

Table 1: Basic Righting Arm Parameters - Fully Static Angles and Lever Arms.

Parameter	Description	Source
GM	The metacentric height (fluid) for the ship at the given loading condition. Assessed for $n000$, $c000$, $t000$, and $s000$ only.	Bouguer
ϕ_{SE} (ϕ_{SE})	The angle of <u>S</u> tatic <u>E</u> quilibrium for the ship at the given loading condition, in a particular <i>balance state</i> . This angle is typically, but not necessarily, 0° for a ship with no heeling lever (e.g. wind). When a beam wind is applied, it is the angle at which the wind heeling lever arm curve first intersects the <i>balance state</i> GZ curve.	RN c. 1900 S & G [2]
ϕ_{VS} (ϕ_{VS})	The angle of <u>V</u> anishing <u>S</u> tability for the ship at the given loading condition, in a particular <i>balance state</i> . When a beam wind is applied, it is still the angle of vanishing stability, but it may occur at the angle where the wind heeling lever arm curve intersects the <i>balance state</i> GZ curve a second time, if the intersection is above the $GZ = 0$ axis.	
RPS $RRPS$	Range of positive stability for the ship at the given loading condition, in a particular <i>balance state</i> . If there is no down-flooding or other influences, this will be $\phi_{VS} - \phi_{SE}$. The residual range of positive stability for the ship at the given loading condition, in a particular <i>balance state</i> , with a beam wind applied. (See also ϕ_{VS})	RN c. 1900 vH [10] BV [9]
ϕ_{GZmax} (ϕ_{GZmax})	The angle at which the maximum righting lever arm occurs for the ship at the given loading condition, in a particular <i>balance state</i> . The angle at which the maximum residual righting lever arm occurs for the ship at the given loading condition, in a particular <i>balance state</i> , with a beam wind applied. The residual righting lever is the righting lever remaining above the wind lever curve.	RN c. 1900
$GZmax$ ($GZmax$)	The maximum righting lever arm of the ship at the given loading condition, in a particular <i>balance state</i> . The maximum residual righting lever arm of the ship at the given loading condition, in a particular <i>balance state</i> , with a beam wind applied.	RN c. 1900 vH [10]
ϕ_{REF} (ϕ_{REF})	The reference angle for the ship at the given loading condition, in a particular <i>balance state</i> , with a beam: $\phi_{REF} = \begin{cases} 35^\circ & \text{if } \phi_{SE} \leq 15^\circ \\ 5^\circ + 2 \times \phi_{SE} & \text{otherwise} \end{cases}$	vH [10] BV [9]
$GZ\phi_{REF}$ (GZ'_{REF})	The residual righting lever arm at ϕ_{REF} for the ship at the given loading condition, in a particular <i>balance state</i> , with a beam wind.	BV [9]
A_{ratio}	The ratio of areas A_1 / A_2 for the ship at the given loading condition, in a particular <i>balance state</i> , with a beam wind. A_1 The area under the <i>balance state</i> GZ curve, above the $GZ = 0$ axis and the wind heeling lever arm curve, between ϕ_{SE} and ϕ_{VS} ($A_{\phi_{SE}-\phi_{VS}}$ assuming no down-flooding). A_2 The area above the <i>balance state</i> GZ curve, and under the wind heeling lever arm curve, between ϕ_{SE} and the <i>roll-back</i> angle, ϕ_{RB} , where the difference, $\phi_{SE} - \phi_{RB}$, is typically 25° .	S & G [2]

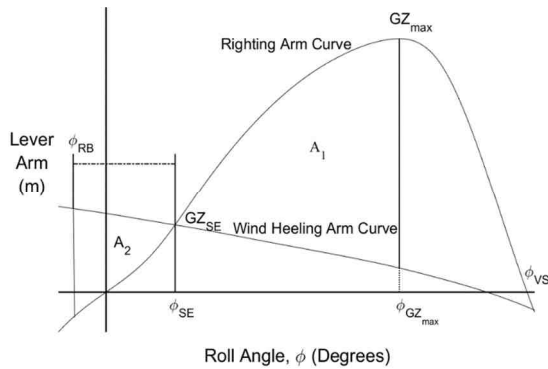


Figure 2: Illustration of the Sarchin and Goldberg [2] Criteria.

In the original Sarchin and Goldberg [2] criteria and therefore the US Navy standard, DDS 079 1 [5], these parameters are related to the application of a beam wind heeling arm as detailed in Table 2.

Wendel

A different approach is achieved by employing righting curves that have been determined with the vessel being balanced on a crest or in a trough of a wave of an assumed proportion to the vessel. Figure 3 and Table 1 illustrate the wave adjusted GZ assessment parameters selected from those embodied in van Harpen [10] (the RNLN navy standard) based on BV1030-1 [9], the German Federal Navy standard, which originates in the work of Wendel [3].

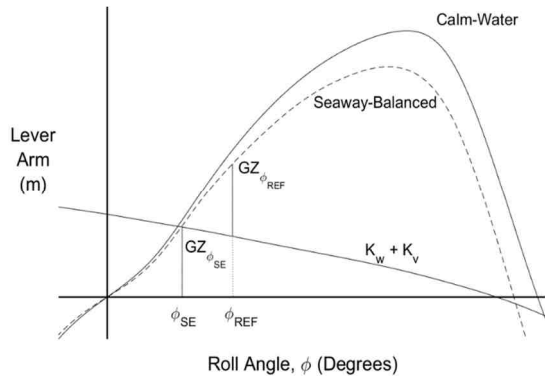


Figure 3: Illustration of the van Harpen [10] (Wendel, see [3]) Criteria.

These measures take the effect of waves on the transverse stability into account by calculating the righting arms with the vessel balanced on a sinusoidal wave of a height H (m) which is determined according to:

$$H = \frac{\lambda}{10 + 0.05\lambda} \quad (1)$$

where the wavelength, λ is set equivalent to the design waterline length of the vessel.

The wave-balanced GZ curves are determined for the cases where the vessel is balanced with the crest amidships and with the trough amidships and also for what is termed the seaway-balanced righting arm which is the mean of the former curves:

$$GZ_{seaway} = \frac{GZ_{trough} + GZ_{crest}}{2} \quad (2)$$

As part of the van Harpen criteria, an additional GZ parameter, the residual righting arm, GZ'_{REF} , is determined at a reference angle, ϕ_{REF} (see [10]).

As applied in van Harpen [10] and BV1030-1 [9], these measures are related to the application of a heeling arm that is a combination of the beam wind heeling and a free surface heeling arms, $K_w + K_v$, as detailed in Table 2. Note that the beam wind heeling arm, K_w , differs from that used for the Sarchin and Goldberg criteria, in that the former employs a $\cos^3(\cdot)$ relationship and the latter a $\cos^2(\cdot)$. Because the question of how to model the wind is not settled, for the sake of simplicity only the Sarchin and Goldberg beam heeling arm is considered in this investigation.

All standards suggest the use of various wind speeds for different vessels and operational environments. The full set of wind speeds examined herein is: 50, 60, 70, 80, 90, and 100 knots.

Form Parameters

In order to aid the subsequent analysis and allow some degree of discrimination between traditional and more modern hull forms a number of form parameters have also been selected for analysis. These are listed in Table 4.

3. EXPANSION OF PARAMETER SET

The parameters that are normally used only with a particular GZ curve and wind lever curve were extended for use with all four wave balance curves and all wind conditions, except for GM which was only evaluated for the curves without wind heeling levers applied.

Areas between major angles (see Table 3) were included in the parameter set. Note that the areas at higher angles do not attempt to account for down-flooding as this would make comparing results between ships more difficult. Also included is the determination of the 1st moment of area of the

righting arms again with, and without, the application of the various heeling arms.

Each parameter is prefixed by a code (*bwwww*) which defines the wave balance and the wind speed used. The first letter designates the wave balance condition and the following three digits define the wind speed applied:

$b \in \{n, c, t, s\}$ corresponding to the balance state $\in \{\text{'calm-water' (no wave), 'crest-balanced', 'trough-balanced', 'seaway-balanced'}\}$

$www \in \{050, 060, 070, 080, 090, 100\}$ corresponding to the wind speed $\in \{50, 60, 70, 80, 90, 100\}$ knots.

MATLAB functions were used to investigate the calm water *GZ* curve and the wave adjusted curves with and without a wind lever applied. This results in 28 cases altogether for each loading condition of each ship (see Figure 4).

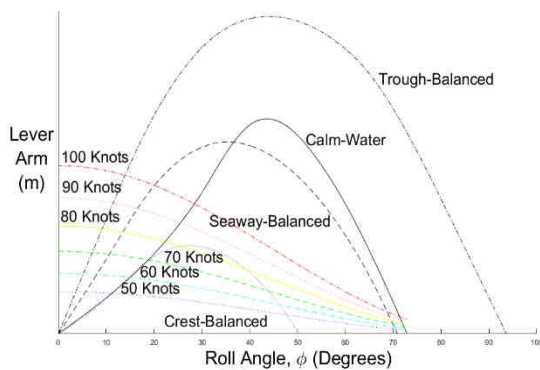


Figure 4: Range of Righting Arm and Wind Heeling Arm Curves.

4. SHIPS

Eight frigate-type ships were used in this study, with volume displacements from 2400 to 5060 cubic meters and *GM* values between 0.267 and 1.645. The ships were defined as watertight up to and including the weatherdeck. No account was taken of the presence of superstructure for buoyancy, but the lateral and frontal areas of the superstructure were used to calculate the wind heeling curves. All load conditions were at zero trim.

It is important to note that:

- Some of the loading conditions may not reflect practice as they were originally chosen to accomplish a study different from the current one.

- Most of the ships in this study were not designed against the wave-balance methodology.
- The methodologies – whether based on Sarchin and Goldberg or on Wendel – do not apply the wind speeds as indiscriminately as they are applied in this study.

Tqble 2: Heeling Terms for Energy Balance and Wave Adjusted Analysis.

Parameter	Definition	Origin	Naval Standard
l_w	<p>The wind heeling arm</p> $l_w = \frac{0.0195V^2 A_w h \cos^2 \phi}{\Delta \times 1000}$ <p>V = nominal wind speed (kts) A_w = lateral sail area (m²) h = height of center of area above half draft (m) Δ = displacement (tonnes)</p>	S & G [2]	DDS079 [5] CFTO [7] RAN [8] NES109 [6]
K_w	<p>The wind heeling arm</p> $K_w = \frac{p_w A_w h}{\Delta} \times (0.25 + 0.75 \cos^3 \phi)$ <p>A_w = lateral sail area (m²) h = height of center of area above half draft (m) Δ = displacement (tonnes)</p> $p_w = C_w \frac{\rho_a V_a^2}{2}$ <p>C_w = lateral windage coefficient (s²·m⁻¹) ρ_a = air density (tonnes·m⁻³) V_a = wind speed (m·s⁻¹)</p>	BV [9]	vH [10]
KL_v	<p>he free surface heeling arm</p> $K_v = \frac{\sum_{j=1}^n \rho_j i_j}{\Delta} \sin \phi$ <p>ρ_j = density of contents of each slack tank (tonnes·m⁻³) i_j = moment of inertia of each free surface (m⁴) Δ = displacement (tonnes)</p>	BV [9]	vH [10]

Tqble 3: Stability Assessment Parameters from GZ Curve – Areas under the GZ Curve.

$A_{\phi 1 \phi 2}$	The area under the <i>balance state</i> GZ curve between two specific roll angles. The residual area under the <i>balance state</i> GZ curve between two specific roll angles, above the $GZ = 0$ axis and the wind heeling lever arm curve.	
$M1x A_{\phi 1 \phi 2}$	The 1 st moment (about the $GZ = 0$ axis) of the area under the <i>balance state</i> GZ curve between two specific roll angles. The 1 st moment (about the $GZ = 0$ axis) of the residual area under the <i>balance state</i> GZ curve between two specific roll angles, above the $GZ = 0$ axis and the wind heeling lever arm curve.	
$M1y A_{\phi 1 \phi 2}$	The 1 st moment (about the $\phi = 0$ axis) of the area under the <i>balance state</i> GZ curve between two specific roll angles. The 1 st moment (about the $\phi = 0$ axis) of the residual area under the <i>balance state</i> GZ curve between two specific roll angles, above the $GZ = 0$ axis and the wind heeling lever arm curve.	
Case 1:	$\phi 1 = \phi iSE$	$\phi 2 = \phi iVS$
Case 2:	$\phi 1 = \phi iSE$	$\phi 2 = \phi iGZmax$
Case 3:	$\phi 1 = \phi iGZmax$	$\phi 2 = \phi iVS$
Case 4:	$\phi 1 = \phi iSE$	$\phi 2 = \phi iREF$
Case 5:	$\phi 1 = \phi iREF$	$\phi 2 = \phi iVS$
		CRN [1] (<i>calm water areas</i>) BV1030-1 [9] (<i>wave balance areas</i>)

Table 3: Form Assessment Parameters.

Parameter	Description
L	Length on waterline (m)
L_{aft}	Length on waterline aft of midship (m)
L_{fwd}	Length on waterline forward of midship (m)
B	Breadth on waterline (m)
T_{Mean}	Mean draft (m)
F_{Mean}	Mean freeboard (m)
A_{MS}	Midship area (m ²)
A_{WP}	Waterplane area (m ²)
A_{WPaft}	Waterplane area aft of midship (m ²)
A_{WPfwd}	Waterplane area forward of midship (m ²)
∇	Volume of displacement in loading condition (m ³)
∇_{aft}	Volume of displacement aft of midship (m ³)
∇_{fwd}	Volume of displacement forward of midship (m ³)
RoB	Reserve of Buoyancy (m ³)
VCB	Vertical Center of Buoyancy (m)
LCG	Longitudinal Center of Gravity (m)
KG	Vertical centre of gravity (fluid) (m)
A_{RR}	Relative rudder area (%)

5. GZ CURVE AND FORM PARAMETER DATA VALIDITY

As can be seen in Figure 4, sometimes the wind heeling curve passes over top of the righting arm curve. This happens mostly with the crest-balanced curve, but in a few instances with the seaway-balanced curve.

The MATLAB code used in this study will return “NaN” for the *GZ* parameters associated with these load conditions. When, for a given ship, the number of loading conditions with valid data drops to 2 the correlation function will also return “NaN”, avoiding the false linear correlation based on only 2 data points (linear by default).

In addition to checking for those cases where data is not available due to the wind curve exceeding the *GZ* curve, the values of the parameters as read/calculated from the *GZ* curves were checked to be sure that they were real numbers and that they varied with the load conditions; i.e., were not constant. Additionally, the robustness of the data was checked by counting how many of the ships had valid data. This was intended to give some confidence that the results are more widely applicable, at least within the set of frigate-like hull forms.

The data was confirmed to be valid over all 8 ships with 2 groups of exceptions. The first group includes all the *GZ* parameters for c080, c090, c100, and s100, which are each reduced by the number of load conditions where the wind curve exceeds the *GZ* curve as mentioned above. The second group is made up of the areas and moments of areas under the *GZ* curve associated with *phiREF* at higher wind speeds and/or lower *GZ* curves; i.e., for n080, n090, n100, c050, c060, c070, c080, c090, c100, t070, t100, s080, and s090. The two groups overlap for c080, c090, and c100, but not for s100, or any *GZ* parameters not associated with *phiREF*. The only other data that was valid for less than all 8 ships was the *IMO AIA2* ratio for the crest-balanced curve, which could be related to the low *GZ* curve.

6. REDUCTION OF PARAMETER SET

Within the large set of parameters several parameters are correlated. This would cause problems for the multi-parameter regression.

If the correlated parameters were grouped together, a single representative could be chosen for the regression analysis. The question becomes: Which parameter is the optimal representative of the group? Two options are immediately apparent. The first option is to “let the data decide”; the parameter that is most strongly correlated with the others is the best representative; this would seem to indicate it is in a sense “central” in the group. The second option is to choose a parameter based on additional, user-supplied requirements. For example, ease of calculation could be an additional criterion. Alternatively, the most physically meaningful parameter the selection condition. This suggests that there is a ranking of the parameters based on computational ease or other considerations, and that the ranking could be used to choose the “optimal” representative of the group. Analysis was performed with several ranking schemes, but the groupings based on linear correlation were quite consistent for all of them.

Correlation results

The valid data for the candidate parameters were checked for linear correlation using the built-in function in MATLAB. The correlation results were also filtered such that only correlation coefficients with a p-value less than 0.05 were kept. This means that there is less than 5% risk that the correlation coefficient is in error in predicting the linear correlation between the parameters.

Correlation analysis can be thought of as analogous to finding the relative projection of a vector on a plane, where the percent of the vector that falls in the plane is a function of the angle the vector makes out of the plane. Indeed, the correlation coefficient is analogous to the cosine squared of that angle. The cosine squared of 45° is 0.5 and represents a vector that is as much in-plane as out-of-plane. At 30° (0.75), the vector is more aligned with the plane, and at 15° (0.933), the vector is strongly aligned with the plane.

The correlation coefficients were evaluated to give a pass-fail matrix for each of the three thresholds. The sum of the matrices was taken across all 8 ships as a measure of robust correlation. The sums for each threshold were compared to investigate the strength of the correlations. The difference in the number of correlations exceeding 0.5 and the number exceeding 0.75 was only 0.25% of the total possible correlations, while the difference in the number exceeding 0.933 and the number exceeding 0.75 was 12.3% of the total possible (0.933 vs. 0.5 was 12.45%). It is clear that

most of the change in robustness occurs between the 0.75 and 0.933 thresholds, meaning that most of the linear correlations found are reasonably strong and robust across the ship set, and 87.7% of the correlations are very strong and robust.

Partitions

The correlation results for all three thresholds showed a clear partitioning of the parameters into groups as follows:

The relative rudder area, A_{RR} , is robustly correlated with the mean freeboard and the reserve of buoyancy in all wave balances and wind conditions. The relation between the latter 2 variables is understandable, as they are both measures of the hull form above the water. The link to the relative rudder area may be due to design “rules of thumb”. The consistency across wave and wind states is to be expected, since these parameters are associated with ship form and are independent of the environmental conditions for any given waterline.

In a similar manner, the other form parameters are robustly correlated; i.e., the vertical center of buoyancy with the mean draft, the midship cross-sectional area, the waterplane area as a whole and split into fore and aft areas, as well as the volume displacement as a whole and in fore and aft volumes. The after waterplane area can be less robustly correlated to the others at the highest threshold. All these measures are related to the immersed hull geometry, and all are independent of environmental conditions for a specified waterline.

The longitudinal center of gravity is correlated to itself across all wind speeds and wave balances, as expected. It is also correlated to the A_{RR} – freeboard – reserve of buoyancy group for half of the ships. One might have expected it to be more related to underwater form than above-water form.

The vertical center of gravity, KG , is correlated strongly with ϕ_{iSE} and ϕ_{iREF} up to the 0.75 threshold, but separates at the 0.933 threshold.

The areas and moments related to the GZ curve between ϕ_{iSE} and ϕ_{iREF} do not show robust correlations. This would indicate they should be independent regressors.

The remaining GZ parameters, $AIA2$, GM , ϕ_{iVS} , ϕ_{iGZmax} , RPS , $GZmax$, $GZ\phi_{iREF}$, and the areas and moments between ϕ_{iSE} and ϕ_{iVS} ,

ϕ_{iSE} and ϕ_{iGZmax} , ϕ_{iGZmax} and ϕ_{iVS} , and ϕ_{iREF} and ϕ_{iVS} , are correlated for all ships at some wind-wave states, and for fewer ships at others.

The groups above are independent of each other for most ships and wind-wave cases examined, and therefore represent a partitioning of the parameters into an above-water-geometry group that could be represented by the reserve of buoyancy or mean freeboard; a below-water-geometry group that could be represented by the mean draft; the LCG ; a small group of GZ parameters that are correlated to KG ; a larger set of GZ parameters that are correlated to $GZmax$, and, finally, a number of independent parameters that are either related to the area between ϕ_{iSE} and ϕ_{iREF} or are less robustly correlated to $GZmax$ at certain wave balances and wind speeds.

7. CONCLUSIONS

Very few of the parameters investigated resulted in invalid data. In only one case was the data unavailable over all load conditions. Only a few cases were found where the data was constant over the load conditions and therefore the parameters could not be used as regressors.

Form parameters were consistently partitioned into an above-water set and an underwater set. $GZmax$ and many other GZ parameters showed strong correlations robustly over the set of ships. Parameters associated with the REF angle from the German and Dutch standards showed mixed correlation results; i.e., not robust over the ship set for all wind-wave cases. They were, however, not always available for all wind-wave cases.

The following groups of regressors are suggested:

Independent of wave balance or wind speed:

- Mean freeboard – representative of the group including relative rudder area and reserve of buoyancy.
- Mean draft – representing the group containing VCB, AMS, AWP, AWPaft, AWPfwd, VolDisp, VolDispft, and VolDispfd.
- KG .

Wind and wave influenced:

- GZ_{max} – representing most of the other GZ parameters.

Independent regressors:

- Parameters associated with the REF angle from the German and Dutch standards. With these it is clear that the wave balance and wind speeds influence the data.

8. FUTURE WORK

Future work could include non-dimensional ratios of parameters.

Linearity in correlations can also be described as linearity in the coefficients; that is, the data itself could be acted upon by a function such as $\sin(x)$ or $\exp(x)$, or it could be raised to a power (e.g., x^2). These functions could be used to reduce the parameter set further if “linear” correlations can be found.

9. REFERENCES

- [1] Perrault, D. E., ‘*Exploration of the Probabilities of Extreme Roll of Naval Vessels*’, Twelfth International Conference on Stability of Ships and Ocean Vehicles, STAB ’15, Glasgow, Scotland, UK, June 2015.
- [2] Sarchin, T. H., and Goldberg, L. L., ‘*Stability and Buoyancy Criteria for U.S. Naval Surface Ships*’, SNAME Transactions, New York, Vol. 70, 1962.
- [3] Arndt, B., Brandl, H., Vogt, K., ‘*20 Years of Experience: Stability Regulations of the West-German Navy*’, Second International Conference on Stability of Ships and Ocean Vehicles, STAB ’82, Tokyo, Japan, Oct. 1982.
- [4] Rahola, ‘*The Judging of the Stability of Ships and the Determination of the Minimum Amount of Stability Especially Considering the Vessel Navigating Finish Waters*’, PhD Thesis, Technical University of Finland, Helsinki, 1939.
- [5] Naval Ship Engineering Center, Design Data Sheet - Stability and Buoyancy of U.S. Naval Surface Ships, DDS 079-1, U.S. Navy, Naval Sea Systems Command, Washington DC, 1 August 1975.
- [6] DEFSTAN 02-109, Issue 1, Naval Engineering Standard N.E.S. 109 Part 1 Issue 4, 1999, Stability Standards for Surface Ships Part 1, Conventional Ships. U.K. Ministry of Defence.
- [7] C-03-001-024/MS-002, ‘Stability and Buoyancy requirements Canadian Armed Forces Surface Ships’, 1979.
- [8] Navy (Aust) Standard A016534, Material Requirements for RAN Ships, Submarines and Systems, ‘*Naval Architecture Requirements - Stability of RAN Ships and Boat*’, 1999.
- [9] BV1030-1, Construction Regulations for German Naval Vessels: Stability of Surface Combatants. Federal Office of Defence Technology and Procurement, Koblenz, Dec 2001.
- [10] van Harpen, N.T., ‘Eisen te stellen aan de stabiliteit en het reservedrijfvermogen van bovenwaterschepen der Koninklijke Marine en het Loodswezen’, April 1970.

Application of 2nd Generation Intact Stability Criteria on Naval Ships

François Grinnaert, *French Naval Academy Research Institute*, francois.grinnaert@ecole-navale.fr

Paola Gualeni, *University of Genoa*, paola.gualeni@unige.it

Jean-Yves Billard, *French Naval Academy Research Institute*, jean-yves.billard@ecole-navale.fr

Jean-Marc Laurens, *ENSTA Bretagne*, Jean-Marc.LAURENS@ensta-bretagne.fr

Nicola Petacco, *University of Genoa*, nicola.petacco@edu.unige.it

ABSTRACT

The second generation intact stability criteria are currently under finalization and validation at the IMO. These criteria are organized in five stability failure modes and three levels of vulnerability assessment in each failure mode. Although this new regulation will not apply to naval ships, it is interesting to investigate the behavior of this vessel typology as well, due to their geometry and typical Froude number. This paper deals with of the pure loss of stability and parametric roll phenomena. Level one and level two vulnerability criteria for three naval ships of different size (helicopter carrier, destroyer, offshore patrol vessel) are applied. Results show an overall satisfactory behavior of the three ships investigated by the new regulation, for both failure stability modes.

Keywords: *Parametric Roll, Pure Loss of Stability, 2nd Generation Intact Stability Criteria, Naval Ship*

1. INTRODUCTION

The second generation intact stability criteria are currently being finalized and validated at the IMO. These new criteria are organized in five stability failure modes: parametric roll, pure loss of stability, dead ship condition, surf-riding/broaching and excessive acceleration. In each failure mode, three levels of assessment are defined. The first vulnerability level criterion is set in order to require simple and approximate evaluations and entailing therefore a larger “safety margin”. The second level in general is based on more accurate computations associated with a statistical averaging of the phenomena. Safety margins are accordingly tuned. The third level should consist of a direct assessment using robust and comprehensive numerical simulations and presumably allowing more awareness about safety margins. This paper deals with the criteria version for Pure Loss (PL) of stability and Parametric Roll (PR) defined during the second and third sessions of Sub-Committee on Ship Design and Construction of the IMO (SDC 2/WP.4 and SDC 3/WP.5). These new criteria

assess in particular the wave profile effect of ship stability. Wave cases to be considered are based on a wave scatter diagram. For unrestricted sailing area, the new regulation imposes the one included in the IACS Recommendation No 34 (2001) corresponding to the Northern Atlantic. The new regulation allows the use of another wave scatter table if the ship is sailing in a restricted area.

Accidents caused by these failure modes may be fatal (Kaufmann, 2009) or may cause significant financial loss (France, *et al.* 2001) but they are fortunately rare. The number of naval ships in service is significantly smaller than the number of merchant vessels (and their time at sea is smaller too), therefore, from the risk point of view, it could be less interesting to address such kind of problems. However it cannot be excluded in principle that naval ships are not vulnerable to such stability failures. Although the new regulations are not intended for naval ships, it seems interesting to assess the outcome of their applications. In fact the hull geometry and the speed of naval ship typology are in principle a remarkable combination worthy of attention.

The goal of this study is to determine the vulnerability of three representative naval ships to the pure loss of stability and parametric roll failure modes as assessed by the new level one and level two vulnerability assessment criteria. The ships are chosen for their variety of typology and size: a helicopter carrier, a destroyer and an offshore patrol vessel. The principle consists in comparing the KG_{\max} curves and the relevant GM_{\min} associated with the new criteria to those associated with the current IMO criteria (IS Code 2.2 and 2.3, IMO, 2009) and French military criteria (DGA, 1999). Methods used to compute the new criteria and the associated KG_{\max} curves are described by Grinnaert, *et al.* (2016).

2. PRESENTATION OF SHIPS

The main particulars of the three naval ships are listed in Table 1.

The first ship is the well-known former French Helicopter Carrier *Jeanne d'Arc*. She is known as non-vulnerable to heavy seas after serving for over 45 years as trainee ship on all seas around the World. Her data have been provided by the French Historic Service of Defense (SHD, 1957). Her numerical model is shown in Figure 1.

The second ship is the David Taylor Model Basin hull number 5415. She is presented by Moelgaard (2000). Imaginary superstructures inspired by those of the DDG-51 *Arleigh Burke* are added to her model to allow the computation of weather criteria of current IMO and military regulations. The data of this ship are available on the www.simman2008.dk website. Her hull is shown in Figure 2

The third ship is representative of a 1500-ton (full load) Offshore Patrol Vessel. Her hull is shown in Figure 3.

		Jeanne d'Arc	DTMB 5415	OPV
Length BP	L_{pp} m	172	142	80.6
Breadth	B m	24	19.06	9.6
Draft	d m	6.5	6.15	3.37
Displacement	Δ t	11768	8634	1250
Froude number	F_n -	0.338	0.413	0.457
Bilge keels length	L_{bk} m	55.7	35.7	24.0
Bilge keels breadth	B_{bk} m	1.2	0.55	0.30
Metacentric height	GM m	1.5	1.5	1.15

Table 1: Main particulars of ships

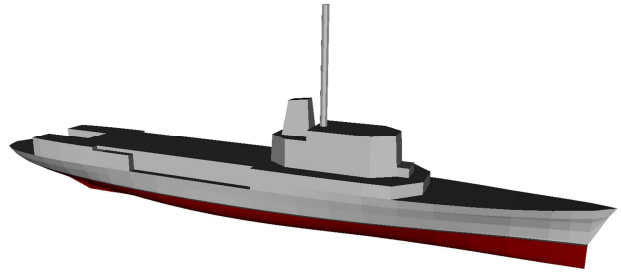


Figure 1: Numerical model of the Helicopter Carrier *Jeanne d'Arc*.



Figure 2: Hull of the DTMB-5415.



Figure 3: Hull of the Offshore Patrol Vessel.

3. PURE LOSS OF STABILITY

Physical Background

When a ship is sailing in head or following waves, the immersed volume distribution changes due to the wave profile. This causes variations of restoring moment which may be significant if the wave length is comparable to the ship length and if the wave steepness is high. In turn this might imply large heel angle or capsize if GZ curve weakness lasts for a long time. Thus, ships sailing at high speed in following waves may be vulnerable to this failure mode.

Presentation of Criteria

The pure loss of stability criteria apply to the ships having a Froude number larger than 0.24. All the three naval ships studied in this paper are well over this threshold.

The level one criterion requires that the minimum metacentric height in waves is larger than 0.05 m. Two methods are proposed to calculate its value. The first method considers a parallel waterplane at lower draft. It may be implemented with the hydrostatic table. The second method considers the minimum GM for 10 positions of wave crest along the ship; the wavelength λ is the ship's length and wave height is 0.0334λ . The level two criterion consists of a statistical approach

aimed to weight each wave scenario on the basis of a wave scatter table. For each wave derived from the table, the criterion considers the angle of vanishing stability and the angle of stable equilibrium under a steady heeling lever which value depends on both the wave and ship speed. In all these calculations the wave length is assumed equal to the ship length.

For more details, please refer to the new regulation (SDC 2/WP.4 and SDC 3/WP.5).

Results

The KG_{max} curves associated with level one and level two criteria of pure loss of stability for the three naval ships are shown in Figure 4 to Figure 6. The curves associated with the level one criterion are drawn in blue (first method) and red (second method). The curves associated with the second level are drawn in green. The grey curves indicate the KG_{max} associated with the current IMO IS Code regulation (dot line) and the current DGA French military regulation (dash line). The light blue curves give the height of the transverse metacenter and can be interpreted as zero-GM curves. We can observe following facts:

1) The two possible versions of level one give significantly different results for all ships. This point is also observed on merchant ships (Grinnaert, *et al.*, 2016).

2) The first method of level one is extremely conservative and require a large metacentric height which may conflict with the excessive acceleration criteria. The end-of-life loading condition of the FS *Jeanne d’Arc* (12,000 tons, GM=1.5m) and the representative loading condition of the Offshore Patrol Vessel do not fulfill the condition.

3) The level two is more conservative than the second method of level one. This point, which is unexpected and undesirable in the regulation, is observed also for some merchant ships (Grinnaert, *et al.*, 2016).

4) Since the level one curve (red curve, level one-second method) associated with pure loss of stability criteria is located above the curve associated with the military regulation, all the assessed ships can be deemed in principle as non-vulnerable to this stability failure mode by the new regulation. In case of the Destroyer and the Patrol

Vessel this is true also with a rather considerable margin.

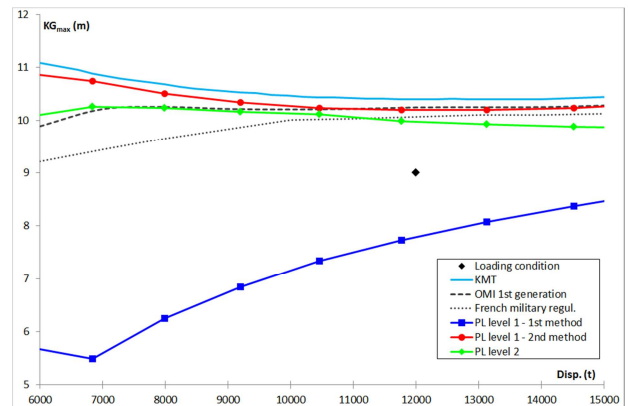


Figure 4: KG_{max} curves associated with the pure loss of stability criteria for the Helicopter Carrier *Jeanne d’Arc*.

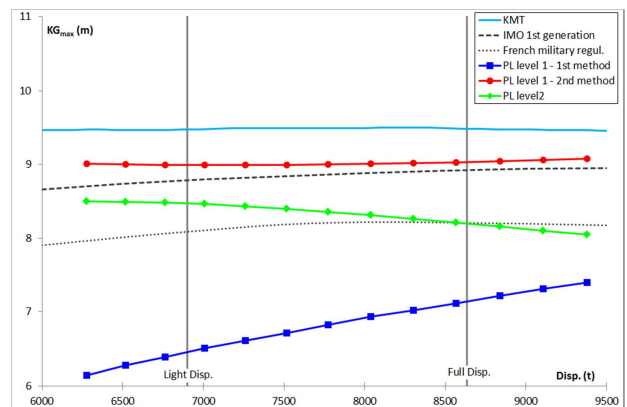


Figure 5: KG_{max} curves associated with the pure loss of stability criteria for the DTMB-5415.

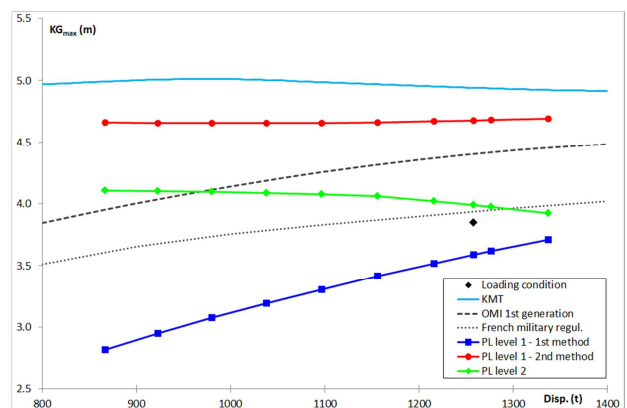


Figure 6: KG_{max} curves associated with the pure loss of stability criteria for the Offshore Patrol Vessel.

4. PARAMETRIC ROLL

Physical Background

Parametric roll is due to the repetition in time of variation of ship restoring moment in waves. It occurs when the wave encounter frequency is approximately twice the ship’s roll natural

frequency. This failure mode is mostly observed on container ships (France, et al., 2001) because the classical hull shape of these ships may generate a large restoring moment variation. Increasing roll damping by providing large bilge keels is an efficient way to prevent parametric roll.

Presentation of Criteria

The level one criterion requires that the non-dimensional GM variation in waves ($\Delta GM/GM$) is lower than a coefficient R_{PR} with value is between 0.17 and 1.87, largely depending on bilge keels area. Two methods are proposed to calculate the value of ΔGM . The first method considers parallel waterplanes at higher and lower drafts. The second method considers 10 positions of wave crest along the ship, the wavelength λ is the ship's length and wave height is 0.0167λ . ΔGM is half the difference between the maximum and the minimum metacentric heights.

The level two criterion is made of two checks. The first check (C1) considers the GM variation in waves and the reference speed corresponding to the parametric resonance using a weighted average approach based on a table of 16 waves defined in terms of length, height and weight. The second check (C2) considers the maximum roll angle in waves and each wave scenario is weighted from the Wave Scatter Diagram; the final result is a combination for 7 different ship speeds corresponding to head and following seas. The maximum roll angle is computed by solving the one-degree-of-freedom differential equation of parametric roll.

For more details, please refer to the new regulation (SDC 2/WP.4 and SDC 3/WP.5).

Results

The KG_{max} curves associated with level one and level two criteria of parametric roll for the three naval ships are shown in Figure 7 to Figure 9. The curves associated with the level one criterion are drawn in blue (first method) and red (second method). The curves associated with the second level are drawn in green (C1 in plain line, C2 in dash line). The grey curves indicate the KG_{max} associated with the current OMI regulation (dot line) and French military regulation (dash line). The light blue curves give the KMT or zero-GM. We can observe following facts, some of which are similar to those observed in pure loss of stability:

1) The two possible versions of level one yields significantly different results for all ships.

2) The first method of level one is extremely conservative and requires a large metacentric height which may conflict with the excessive acceleration criteria. The end-of-life loading condition of the FS *Jeanne d'Arc* does not fulfill the condition. The representative loading condition for the Patrol Vessel is compliant but practically positioned on the curve.

3) The KG_{max} curves associated with the second level of vulnerability assessment, in the C2 check version, is coincident with the KMT curve for the Helicopter Carrier. This means that parametric roll never occurred during the one-DOF simulation.

4) The curves associated with the level one second method and both checks of level two are located above the curve associated with the current military regulation. Thus, all assessed ships can be deemed as non-vulnerable to the parametric roll by the new regulation.

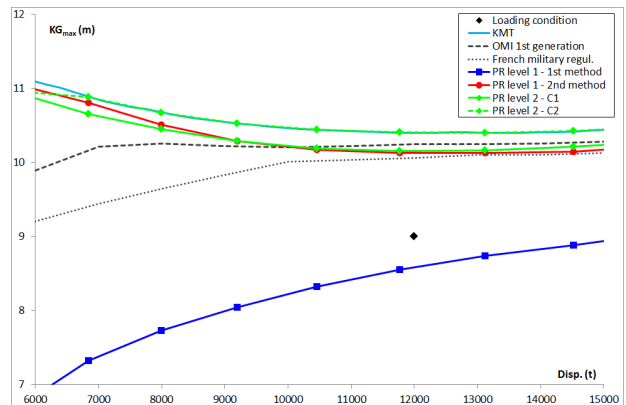


Figure 7: KG_{max} curves associated with the parametric roll criteria for the Helicopter Carrier *Jeanne d'Arc*.

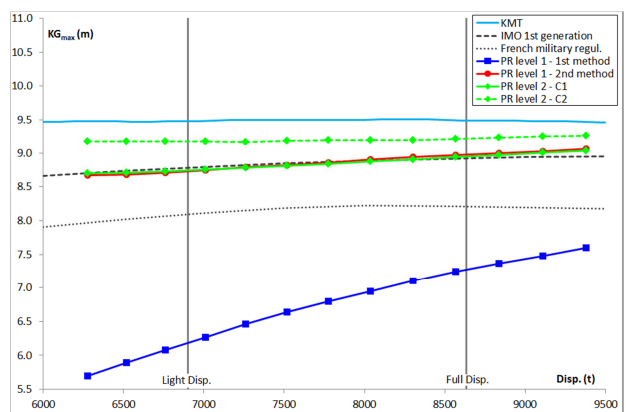


Figure 8: KG_{max} curves associated with the parametric roll criteria for the DTMB-5415.

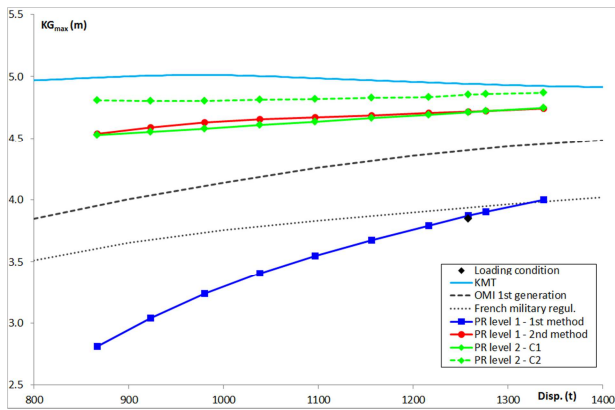


Figure 9: KG_{max} curves associated with the parametric roll criteria for the Offshore Patrol Vessel.

5. CONCLUSION

The computation of KG_{max} curves associated with level one and level two criteria of pure loss of stability and parametric roll for three different naval ships shows that these ships are not vulnerable to these failure modes according to the new regulation. Thus, the application of this regulation during the design of these vessels should not have improved their safety during sailing in waves. It also shows what has been already evidenced for merchant ships i.e. that the first method of level one (which considers parallel waterplanes) implies extremely large metacentric height which may conflict with the future excessive acceleration criteria.

It has been interesting to practically quantify for each ship the different level of safety provided by the IS code and the military set of rules: as expected, the navy rules are more severe and in the investigated cases it seems exactly of the appropriate amount in order to avoid ships appear vulnerable to the pure loss and parametric roll failures.

The three ships chosen in this study have relatively classical “military hull shape”. Thus, it is logical to find similar results. However, some other military vessels have significantly different hull shape (aircraft carrier, amphibious and assault vessels, military tankers, scientific vessels ...) and may be worthy of assessment.

6. REFERENCES

Direction Générale de l’Armement, 1999, Stabilité des bâtiments de surface de la marine nationale, Instruction générale n° 6018 A (restricted diffusion, in French).

France W. N., Levadou M, Treacle T. W., Paulling J. R., Michel R. K., Moore C., 2001, “An Investigation of Head-Sea Parametric Rolling and its Influence on Container Lashing Systems”, SNAME Annual Meeting.

Grinnaert F, Billard J.-Y., Laurens J.-M., 2016, “ KG_{max} Curves Associated with 2nd Generation Intact Stability Criteria for Different Types of Ships”, Journal of Marine Science and Application (accepted).

IMO, 2009, International Code of Intact Stability 2008, London.

IMO, 2015, “Development of Second Generation Intact Stability Criteria, Development of Amendments to Part B of the 2008 IS Code on Towing and Anchor Handling Operations”, SDC 2/WP.4 2nd session.

IMO, 2016, “Finalization of Second Generation Intact Stability Criteria, Amendments to Part B of the 2008 IS Code on Towing, Lifting and Anchor Handling Operations”, SDC 3/WP.5, 3rd session.

International Association of Classification Societies, 2001, Rec. No. 34. Standard Wave Data, Rev.1.

Kaufmann J., 2009, Fatal Accident on Board the CMV Chicago Express During Typhoon "Hugupit" on September 24 2008 off the Coast of Hong Kong, Bundesstelle für Seeunfalluntersuchung. Investigation Report 510/08.

Moelgaard, A., 2000, PMM-tests with a model of a frigate class DDG-51. Danish Maritime Institute 2000071, Report No. 1.

Service Historique de la Défense, 1957, CAAPC, Jeanne d'Arc 1961, Plan des formes, Plan n° 6174.

Conduction of a wind tunnel experiment to investigate the ship stability weather criterion

Arman Ariffin, *ENSTA Bretagne, LBMS EA 4325, Brest, France*

arman.ariffin@ensta-bretagne.org

Shuhaimi Mansor, *Faculty of Mechanical Engineering, Universiti Teknologi Malaysia, Malaysia*

shuhaimi@mail.fkm.utm.my

Jean-Marc Laurens, *ENSTA Bretagne, LBMS EA 4325, Brest, France*

jean-marc.laurens@ensta-bretagne.fr

ABSTRACT

A wind tunnel experiment has been set up to examine several assumptions regarding the weather criterion of the intact stability code. The experimental trials are conducted in the Low-Speed Wind Tunnel of the Aeronautics Laboratory at the Universiti Teknologi Malaysia. Two models are tested. The first model is an academic model that allows comparisons to be made with analytical models. The second model is the DTMB 5415 to present a military realistic case. The models are properly weighted to present the correct hydrostatic characteristics. A water tank is installed in the wind tunnel test section; the models are free to roll around the longitudinal axis passing through the buoyancy centre owing to a frictionless rod. The experimental results are then compared with the results of the stability code using the IMO weather criterion and the military criteria. Finally, in the experimental trials, many configurations are tested to assess the effects of various geometrical parameters.

Keywords: *Second generation intact stability criteria, wind tunnel, roll angle*

1. INTRODUCTION

Intact stability is a basic requirement to minimise the capsize risk for vessels. It is a guideline for the ship designer, the ship operator and the classification society to design, build and commission the ship before it starts its service life at sea. A comprehensive background study of intact stability development was written by Kuo & Welaya (Welaya & Kuo, 1981). Their paper "A review of intact stability research and criteria", stated that the first righting arm curve was proposed by Reed in 1868, but that the application was presented by Denny in 1887. In addition, in 1935, Pierrottet tried to rationally establish the forces which tend to capsize a ship and proposed a limiting angle at which the dynamic level of the ship must be equal to or greater than the sum of energy exerted by the inclining moments. However, Pierrottet's proposal was too restrictive for the design process and it was not accepted.

Kuo and Welaya also mentioned the famous doctoral thesis written by Jaakko Rahola in 1939. Rohola's thesis evoked widespread interest throughout the world at that time because it was the first comprehensive study and proposed method to evaluate intact stability which did not require complex calculations (Rohala, 1939).

The Sub-Committee on Stability and Load Lines and on Fishing Vessels Safety 48th Session (IMO, 2005) emphasized the requirement of revising the current IS Code. The importance of the comprehensive review of the current IS Code 2008 would significantly affect the design and ultimately enhance the safety of ships (Mata-Álvarez-Santullano & Souto-Iglesias, 2014).

Intact Stability is a crucial criterion that concerns most naval architects at the design stage. The current Intact Stability (IS) Code 2008 is in force. Except for the weather criterion, the IS Code 2008 only applies to the hydrostatics of the ship. It

does not cover the seakeeping behaviour of the ship and first and foremost, it always considers a ship with a negligible trim angle. In head seas, the ship can present a significant angle of trim which may affect the righting arm. Van Santen also presented an example of a vessel capsizing due to of the small angle of trim (Van Santen, 2009).

For the enhancement and improvement of intact stability criteria, the International Maritime Organisation (IMO) introduced the new generation intact stability criteria in 2008 (Francescutto, 2007). Figure 1 presents the procedure to apply to the second generation intact stability rule. Once the basic criteria have been satisfied, each failure mode is verified to satisfaction at the most conservative level.

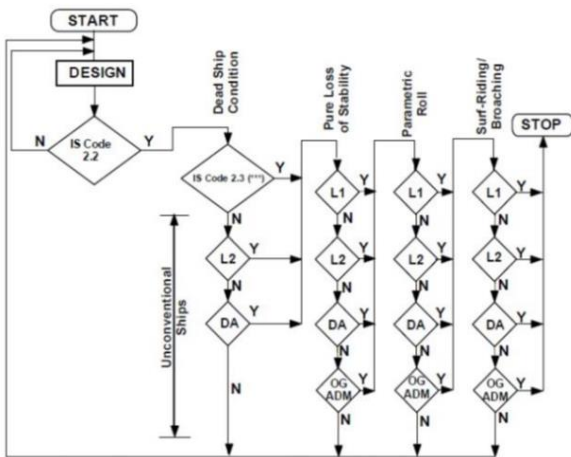


Figure 1: Structure of Second Generation Intact Stability Criteria

2. DEVELOPMENT OF SECOND GENERATION INTACT STABILITY CRITERIA

The last Sub-committee on Ship Design and Construction meeting at IMO recalled that SDC 2 had agreed, in principle, to the draft amendments of the 2008 IS Code regarding vulnerability criteria and the standards (levels 1 and 2) related to parametric roll, pure loss of stability and surf-riding /broaching (SDC 2/WP.4, annexes 1 to 3). For this purpose, SDC 2 had invited member governments and international organisations to bring the criteria to the attention of ship designers, shipyard operators, ship owners and other interested parties, and to observe and test the application of the finalised vulnerability criteria, in order to gain experience with regard to their use.

The draft amendment of the IS Code regarding vulnerability criteria and the standards (levels 1 and 2) related to dead ship condition and excessive acceleration are contained in SDC 3/INF.10 Annex 1 and 2. The level 1 check for dead ship condition is basically the same method used for current IS Code 2.3 which is weather criteria. If it failed, the design should process to level 2 check and the direct assessment. Direct assessment procedures for stability failure are intended to employ the most advanced state-of-the art technology available either by numerical analysis or experimental work for quantitative validation as stated in SDC 1/INF.8 Annex 27 (IMO, 2013).

3. THE WEATHER CRITERION

The IS Code 2008 Part A 2.3 contains the weather criterion. The ship must be able to withstand the combined effects of beam wind and rolling. The conditions are:

- the ship is subjected to a steady wind pressure acting perpendicular to the ship's centreline which results in a steadywind heeling lever (lw_1).*
- from the resultant angle of equilibrium (φ_0), the ship is assumed to present an angle of roll (φ_1) to windward due to wave action. The angle of heel under action of steady wind (φ_0) should not exceed 16° or 80% of the angle of deck edge immersion, whichever is less.*
- the ship is then subjected to a gust wind pressure which results in a gust wind heeling lever (lw_2); and under these circumstances, area b shall be equal to or greater than area a, as indicated in Figure 2.*

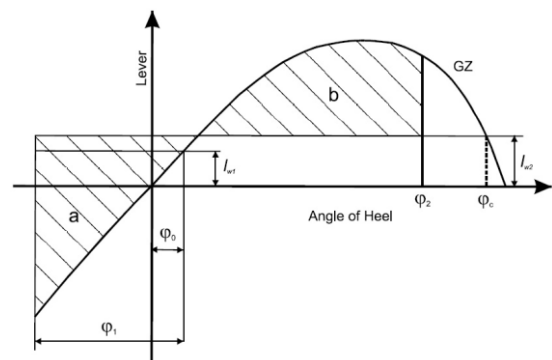


Figure 2: Severe wind and rolling

The heeling lever shall be calculated using formula:

$$l_{w1} = \frac{P \cdot A \cdot Z}{1000 \cdot g \cdot \Delta} \quad (1)$$

$$l_{w2} = 1.5 l_{w1} \quad (2)$$

where l_{w1} = steady wind heeling angle, l_{w2} = gust wind heeling lever, P = wind pressure of 504 Pa, A = projected lateral area (m^2), Z = vertical distance from the centre of A to the centre of the underwater lateral area or approximately to a point at one half of the mean draught (m), Δ = displacement (t) and g = gravitational acceleration). In Figure 1, a Direct Assessment (DA) can be used to verify the weather criterion for unconventional ships. The DA can be experimental. The present study shows how such an experimental DA can be conducted for two models, a civilian ship and a military ship.

In the weather criterion, two main rules are commonly used. For commercial ship, it uses the IMO weather criterion and for naval ship, it uses the Naval Rules. The IMO Weather criterion is shown in Figure 2 and the weather criterion for naval ship is shown in Figure 3. The significant different between IMO and Naval Rules are presented in the Table 1.

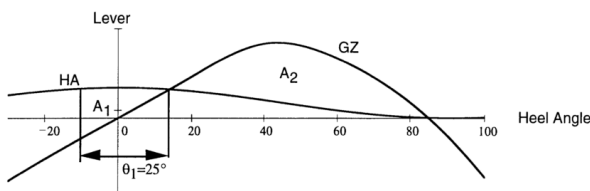


Figure 3: Weather Criteria for Naval Ships

Table 1 Comparison IMO and naval rules for weather criterion

Criterion	IMO	Naval Rules
Wind velocity	26 m/s	100 knots
Roll back angle	various*	25°
WHA	constant	$\cos^2\theta$
Ratio A_2/A_1	≥ 1	≥ 1.4
Gust	Yes	No

* roll back angle (ϕ_1) calculated based on IS Code 2008

WHA – wind heeling arm, A_2 - restoring energy, A_1 – capsizing energy

4. SHIP MODEL

Two models were used for the experimental work. The first model is an academic container ship geometry referred as “ASL shape” in the rest of the paper. The second model is a research ship model, the well know DTMB 5415 (Molgaard, 2000). The

5415 DTMB model is widely used for the research study in seakeeping (Begovic, Day, & Incecik, 2011; Jones & Clarke, 2010; Yoon et al., 2015). The basic geometry is presented in Table 2. The body plan and perspective view for “ASL shape” is shown in Figure 4. The body plan and perspective view for “5415 shape” is shown in Figure 5.

Table 2 Basic ship model geometry

Ship model	ASL shape	5415 shape
LOA, (m)	140	153.3
BOA, (m)	20	20.54
Draft, (m)	12	6.15
Displacement, (tonnes)	26,994	8,635
VCG, (m)	10	7.555
LCG, (m)	70.037	70.137
KM, (m)	10.206	9.493
GM, (m)	0.206	1.938

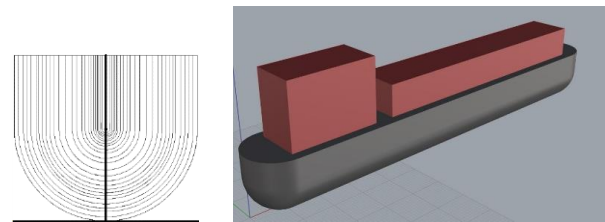


Figure 4: Body plan (left) and perspective view (right) of the ASL shape

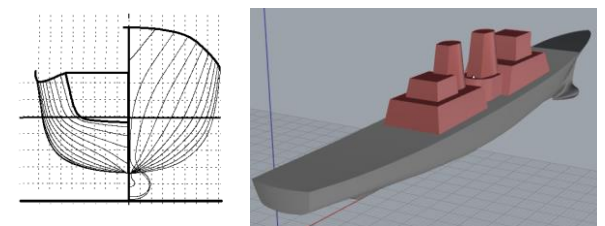


Figure 5: Body plan (left) and perspective view (right) of the 5415 shape

5. EXPERIMENTAL INVESTIGATION

A wind tunnel test was conducted at the low speed wind tunnel facility at Univerisiti Teknologi Malaysia. This wind tunnel has a test section of 2m (width) x 1.5m (height) x 5.8m (length). The maximum test velocity is 80m/s (160 knots). The wind tunnel has a flow uniformity of less than 0.15%, a temperature uniformity of less than 0.2°C, a flow angularity uniformity of less than 0.15° and a turbulence level of less than 0.06% (Ariffin, Mansor, & Laurens, 2015).

Ship model

Two ship models were tested as described in Paragraph 4. Both models were constructed at ENSTA Bretagne, France using the Computer Numerical Control (CNC) machine. The material used was polystyrene. Both models were designed in 3D drawing and imported to CNC machine program for fabrication process. The hulls were divided into six parts for the cutting process. Then, all parts were glued and laminated with a fiberglass. The superstructure used the synthetic glass. The completed ship models are shown in Figure 6.



(a)



(b)

Figure 6: Complete build ship models (a) ASL shape (b) 5415 DTMB shape

Inclining test

To determine the correct centre of gravity, inclining tests were performed. The inclining test is a procedure which involves moving a series of known weights, normally in transverse direction, and measuring the resulting change in the equilibrium heel angle of the ship. By using this information and applying basic naval architecture principles, the ships’ vertical centre of gravity is determined from the GM. We also verified that the natural roll period is as expected. Two devices were used for the data recording, first is the Ardu Flyer device and smartphone (Djebli, Hamoudi, Imine, & Adjlout, 2016).

Wind tunnel setup

The models were allowed to heave and roll freely. It was not allowed to yaw because the model must be hold at the longitudinal axis to avoid the model bump to water tank side. The models were fixed with a rod both at bow and stern (Figure 7). It is passing through the point of longitudinal centre of buoyancy. Both rods at bow and stern were aligned using laser light to confirm the shafts positioned at same axis. The arrangement of rod used in this experiment is frictionless therefore, minimum interaction between the rod and rod stand can be obtained.

To allow the model to float in the wind tunnel, a water tank fabricated with glass of 8mm thickness was installed. Since the wind tunnel is not water tight, to avoid any leak of water during the experiment, a dummy pool was placed underneath the platform. The dummy pool is capable to cope the total volume of water if the glass water tank gets damaged. The arrangement in the test section is shown in Figure 8.

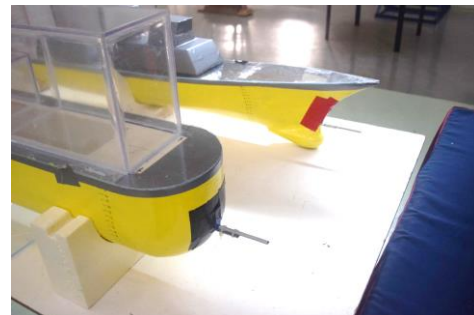


Figure 7: Rods fixed at ship models



Figure 8: Arrangement in the test section.

The experiment started with the model placed in the water tank with the correct draft (Figure 9). A laser light is used to ensure the vessel is upright. The test started with measurement of the stable heel. The wind tunnel velocity was increased

slowly while the heel angle was recorded using the Ardu Flyer device. The Ardu Flyer is a complete open source autopilot system designed for 3D robotics. This experiment involved three models configuration as stated below:

- a. ASL shape.
- b. 5415 shape.
- c. ASL with bilge keel shape.

A roll back angle (ϕ_2^*) measure was performed for all the models. The definitions of (ϕ_1) and (ϕ_2^*) are shown in Figure 10. The test steps are as follow:

- a. Model placed in water tank.
- b. Wind applied and the wind velocity and heel angle recorded.
- c. Roll back angle (ϕ_1) applied at the model.
- d. Then model is suddenly released.
- e. The maximum counter roll back angle (ϕ_2^*) recorded.



(a)



(b)

Figure 9: Ship models ready to be tested in wind tunnel test section (a) ASL shape (b) 5415 DTMB shape

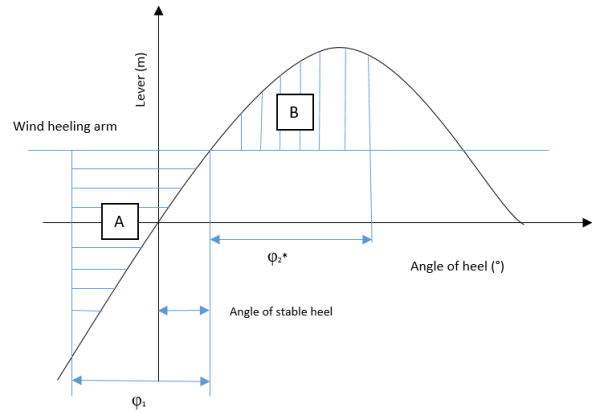


Figure 10: Definitions used in this experiment

Scaling criteria

The models used in the experiment were scale down to 1:100. It is the same scale used by (Begovic et al., 2011) for the ship motion experiment using DTMB 5415 model. For the GZ curve, the model and full scale ship has a same curve shape but values for the model are divided by 10^2 . For weight calculation, values used for the model are divided by 10^6 . For the wind velocity, the value used for the model is divided by 10.

Boundary layer

When the air flow over the ocean surface from any direction, a natural boundary layer is formed. This means that the wind velocity at the surface is zero and increase with higher altitude. The boundary layer thickness in the test section for this experiment is about 35mm and the velocity profile is shown in Figure 11.

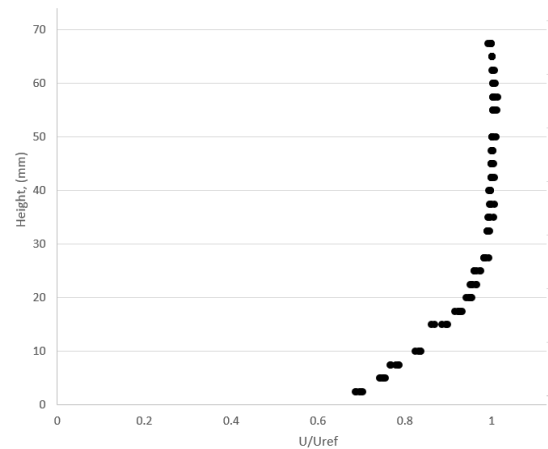


Figure 11: The velocity profile curve

To compute the weather criterion, the General Hydro Static software (GHS) was used. The GHS uses a strip method and it is widely used in the

marine industry (Ariffin, Laurens, & Mansor, 2016). In GHS, there are 2 methods to specify the wind either by wind velocity or wind pressure. Specifying a wind velocity, V_{wind} , in GHS gives a standard velocity profile with V_{wind} at 10 metres from the ground (Yalla, 2001). When specifying a velocity pressure, a constant value is given. The calculation in this paper for GHS results were obtained using the wind pressure input.

6. RESULTS

Angle of stable heel (ϕ_0) vs wind velocity

Figure 12 shows the graph for angle of stable heel, ϕ_0 versus wind velocity for the two models and two methods; IMO and experimental. The 5415 curves are following a parabolic shape since as we can see in Figure 13, the GZ curve of 5415 shape follows a linear curve up to 30 degrees. Furthermore, the experimental curve is below the IMO curve which indicates that the drag coefficient C_D , of the ship silhouette is smaller than 1, the value assumed in the IMO formula (Figure 12). The ASL curves present different shapes and behaviour. At first, they do not present the parabolic shape because as we can see in Figure 13, the GZ curve is only linear up to 5 degrees. Furthermore, the experimental curve for this case is above the IMO curve (Figure 12). That is explained by the fact that the drag coefficient C_D , for the box shape of the ASL is bigger than 1. This can be confirmed by the many references that exist giving the drag coefficients of basic shapes, see for example (Scott, 2005).

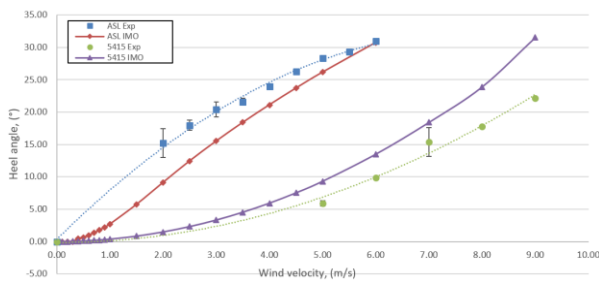


Figure 12: Graph of wind velocity and angle of stable heel for ASL shape and 5415 shape on the experimental results and GHS calculation

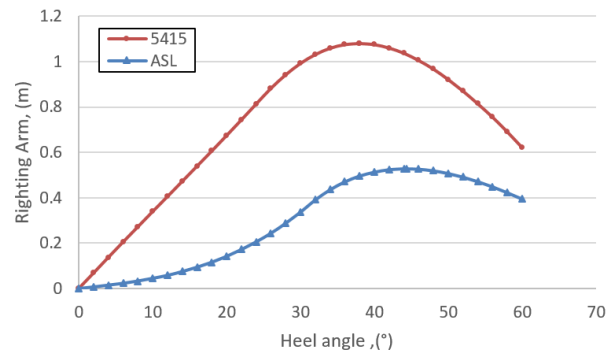


Figure 13: The GZ curves for ASL shape and 5415 shape

Roll back angle (ϕ_2^*) versus roll to windward (ϕ_1)

Figure 14 shows the roll back angle (ϕ_2^*) versus roll to windward (ϕ_1) for ASL shape for wind velocity range of 2 m/s to 4 m/s. Figure 15 shows the roll back angle (ϕ_2^*) versus roll to windward (ϕ_1) for 5415 shape. In the absence of damping the results should be like a swing where ϕ_2^* follows ϕ_1 . The results suggest a far more complex behaviour where the hydrostatic force shape is playing an important role.

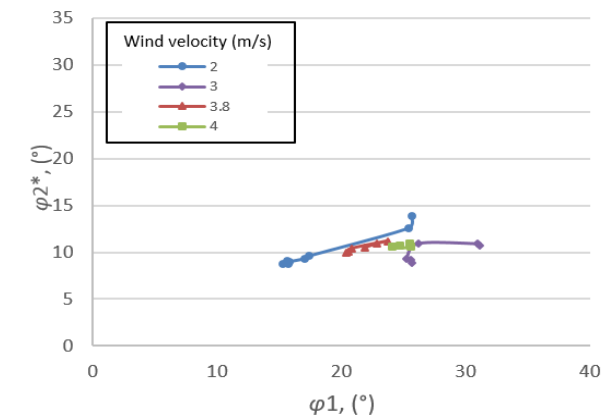


Figure 14: Roll back angle (ϕ_2^*) vs roll to windward (ϕ_1) for ASL shape

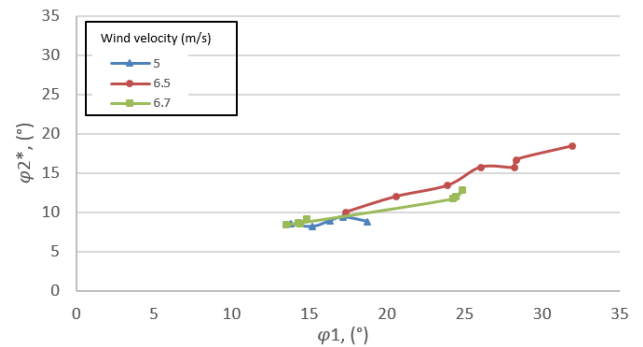


Figure 15: Roll back angle (ϕ_2^*) vs roll to windward (ϕ_1) for 5415 shape.

Ratio ϕ_2^* and ϕ_1 with bilge keel

Figure 16 shows the ratio (ϕ_2^*/ϕ_1) for the ASL shape and the ASL with a bilge keel. Both models were tested at wind velocity 2m/s. For the bare ASL, the average ratio is 0.55 and for the ASL with bilge keel, the average ratio is 0.43. As expected, the configuration with bilge keel contributes to more roll damping than configuration without bilge keel.

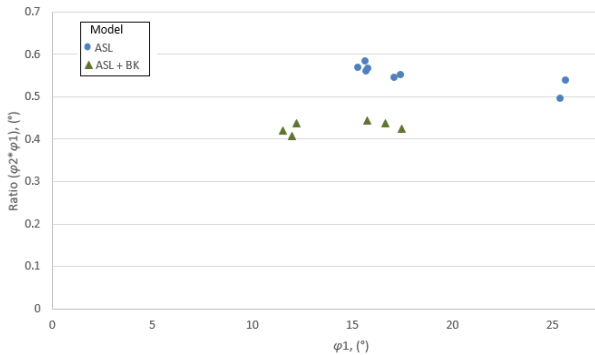


Figure 16: Roll back angle (ϕ_2^*) vs roll to windward (ϕ_1) for ASL shape, 5415 shape and ASL with bilge keel configuration

Yaw angle effect on stable heel

Figure 17 shows the angle of stable heel for the ASL and the 5415 both with the wind direction from star board 75° and port 105°. For the ASL, the values of ϕ_0 are smaller for the beam wind than those obtained with the yaw angles. In other words the assumption of the beam wind in the IMO code is not necessarily conservative. This phenomenon also appears for the 5415.

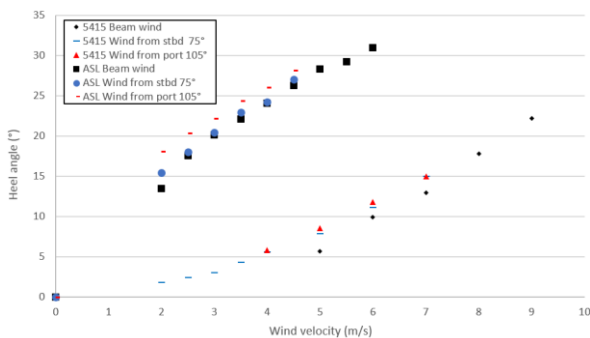


Figure 17: Angle of stable heel for wind from starboard 75° and port 105°

Effect of roll to windward (ϕ_1) and roll back angle (ϕ_2^*) with yaw angle

Figure 18 shows the result for ϕ_1 and ϕ_2^* for the ASL and the 5415 with beam wind and wind from starboard 75°. For the ASL, the beam wind

has higher ϕ_2^* than wind from starboard 75° and for the 5415, the beam wind has smaller ϕ_2^* than wind from starboard 75°. The two models have a different response to the yaw angle. The behaviour is a combination of the superstructure geometry, the GZ curve and the damping.

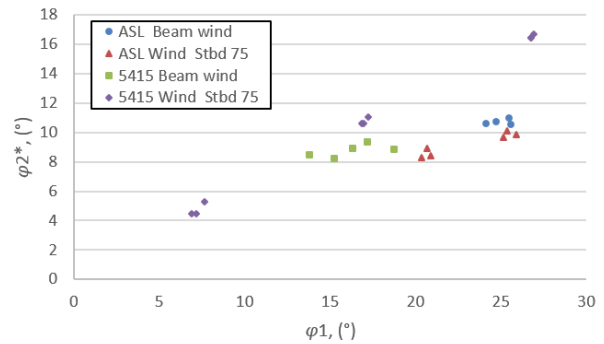


Figure 18: Roll back angle (ϕ_2^*) vs roll to windward (ϕ_1) for 5415 shape with wind from port 105

Comparison IMO GHS and experimental result

Figure 19 shows the comparison results between IMO and experimental results. For the ASL, the counter roll back angle (ϕ_2^*) obtained from experimental results is 24.07°, lower than IMO which is 29.638°. Therefore, IMO result is more conservative. For the 5415, the counter roll back angle (ϕ_2^*) obtains from experimental results is 16.31°, lower than Naval Rules which is 33.82° for ratio capsizing and restoring energy 1.0 and 39.45° for ratio capsizing and restoring energy 1.4. Therefore, the IMO and Naval rules are always more conservative.

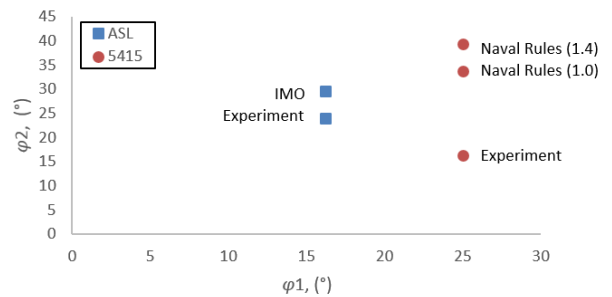


Figure 19: Comparison result for IMO rules and Naval Rules

7. CONCLUSION

In this paper the authors presented an experimental Direct Assessment (DA) of the weather criterion for two different models; a civilian ship with a simple geometry and a military ship, the well-known DTMB 5415. To conduct the

experiments, the low speed wind tunnel of UTM was used. Both models were placed in a water tank in the wind tunnel. Both models were free to roll so the heel angle could be measured and compared with the IMO and Navy Rules.

Although the assumptions taken by the rules are not always conservative, the final results always show that the experimental values are lower than the values given by the rules.

8. ACKNOWLEDGEMENT

The authors would like to acknowledge the support of the Government of Malaysia, the Government of the French Republic and the Direction des Constructions Navales (DCNS).

9. REFERENCES

- Ariffin, A., Laurens, J. M., & Mansor, S. (2016). Real-time Evaluation of Second Generation Intact Stability Criteria. In *Smart Ship Technology* (pp. 26–27).
- Ariffin, A., Mansor, S., & Laurens, J.-M. (2015). A Numerical Study for Level 1 Second Generation Intact Stability Criteria. In *International Conference on Stability of Ships and Ocean Vehicles* (pp. 183–193).
- Begovic, E., Day, a. H., & Incecik, a. (2011). Experimental Ship Motion and Load Measurements in Head and Beam Seas. *Proceeding of The 9th Symposium on High Speed Marine Vehicles*, 1–8.
- Djebli, M. A., Hamoudi, B., Imine, O., & Adjlout, L. (2016). The application of smartphone in ship stability experiment The Application of Smartphone in Ship Stability Experiment, (January). <http://doi.org/10.1007/s11804-015-1331-9>
- Francescutto, A. (2007). The Intact Ship Stability Code: Present Status and Future. In *Proceedings of the 2nd International Conference on Marine Research and Transportation, Naples, Italy, Session A* (pp. 199–208).
- IMO. (2005). *SLF 48/21 Report to the Maritime Safety Committee*.
- IMO. (2013). *SDC 1/INF.8 - Development of Second Generation Intact Stability Criteria*.
- Jones, D. a., & Clarke, D. B. (2010). *Fluent Code Simulation of Flow around a Naval Hull: the DTMB 5415*.
- Mata-Álvarez-Santullano, F., & Souto-Iglesias, A. (2014). Stability, safety and operability of small fishing vessels. *Ocean Engineering*, 79, 81–91. <http://doi.org/10.1016/j.oceaneng.2014.01.011>
- Molgaard, A. (2000). *PMM-test with a model of a frigate class DDG-51*.
- Rohala, J. (1939). *The Judging of the Stability of Ships and the Determination of the Minimum Amount of Stability*.
- Scott, J. A. (2005). Drag of Cylinders & Cones. Retrieved from <http://www.aerospaceweb.org/question/aerodynamics/q0231.shtml>
- Van Santen, J. (2009). The Use of Energy Build Up to Identify the Most Critical Heeling Axis Direction for Stability Calculation for Flooding Offshore Structures. In *10th International Conference on Stability of Ship and Ocean Vehicles* (pp. 65–76).
- Welaya, Y., & Kuo, C. (1981). A Review of Intact Ship Stability Research and Criteria. *Ocean Engineering*, 8, 65–84.
- Yalla, S. K. (2001). *Liquid Dampers for Mitigation of Structural Response: Theoretical Development and Experimental Validation*.
- Yoon, H., Simonsen, C. D., Benedetti, L., Longo, J., Toda, Y., & Stern, F. (2015). Benchmark CFD validation data for surface combatant 5415 in PMM maneuvers – Part I: Force/moment/motion measurements. *Ocean Engineering*, 1–30. <http://doi.org/10.1016/j.oceaneng.2015.04.087>

USN's Recently Defined Standard Practice for the Construction of a Composite Allowable KG_A Curve for Single Load Point Evaluation using the Load Shift Method

Vytenis A. Senuta, *Naval Surface Warfare Center Carderock Division*

Lauren E. Moraski, *Naval Surface Warfare Center Carderock Division*

ABSTRACT

USN ships are required to satisfy stability criteria in accordance with T9070-AF-DPC-010/079-1 “Design Practices and Criteria for U.S. Navy Surface Ships Stability and Reserve Buoyancy” dated 19 January 2016. These criteria address the hazards at sea and expected loading conditions throughout the service life of a ship. Allowable KG (KG_A) is the highest vertical center of gravity that satisfies a stability criterion. Typically, ships are required to satisfy multiple intact and damage criteria, so multiple KG_A 's are calculated. This paper and the recent update of USN T9070-AF-DPC-010/079-1 is intended to inform the commercial community of the USN practice of the load shift method for damage KG_A calculations.

Keywords: Allowable KG , Load shift method ...

1. INTRODUCTION

USN ships are required to satisfy stability criteria in accordance with T9070-AF-DPC-010/079-1 “Design Practices and Criteria for U.S. Navy Surface Ships Stability and Reserve Buoyancy” dated 19 January 2016. These criteria address the hazards at sea and expected loading conditions throughout the service life of a ship. Allowable KG values are calculated for intact and damage stability.

In the USN, the vertical center of gravity (G) is measured from the bottom of the keel (K), and the distance is referred to as KG . Allowable KG (KG_A) is the highest vertical center of gravity that satisfies a stability criterion. Typically, ships are required to satisfy multiple intact and damage criteria, so multiple KG_A 's are calculated. The lowest of these KG_A is the governing KG_A . Often the governing KG_A represents a combination of criteria at various displacements. This is often referred to as Composite KG_A , or, just simply, KG_A . When assessing ship stability, a ship's KG (typically from a weight report or inclining experiment) is compared to (plotted against) its KG_A . If KG is below the KG_A , the ship satisfies all stability criteria. If KG is above, then it fails at least one

stability criterion and corrective measures must be taken – either lower KG or raise KG_A .

For the USN, all KG_A values reference the Full Load Departure Condition. The lowest of the calculated KG_A values at a particular displacement becomes governing for that displacement; these lowest values are then connected to create a KG_A curve over a specified displacement range.

Typically, intact KG_A is calculated for the following hazards as applicable to the design: beam wind, high speed turn, icing, topline pull, crowding of personnel, and lifting of heavy weights. Damage KG_A is calculated for side damage and raking. Intact KG_A calculation is sufficiently applicable for the operating displacement range of a ship since all hazards are applied to the hull externally. However, since damage impacts the hull internally, it is highly dependent on loading (e.g. tank volumetric emptiness) and therefore KG_A necessitates the use of the Load Shift Method. This method projects damage KG_A values calculated for other load conditions to its Full Load Departure condition equivalent.

USN ship design was traditionally performed by the USN technical community up through contract design. The load shift method was

commonly known and formal documentation was not deemed necessary. However, with changing times, commercial design agents and shipyards are increasingly involved in USN ship design. Without proper documentation, guidance and design requirements, commercial entities could not be expected to properly implement the load shift concept. This paper and the recent update of USN T9070-AF-DPC-010/079-1 is intended to inform the commercial community of the USN practice of the load shift method for damage KG_A calculations.

2. ALLOWABLE KG

USN Allowable KG (KG_A) references the Full Load Condition. It is a singular curve, that represents the most conservative or limiting intact and damage stability capability that satisfies all design applicable USN stability criteria. It is calculated during the ship design phase. It is meant to satisfy all foreseeable loading conditions throughout the operating range (Min Op to Full Load) and throughout the expected or projected service life (typically 30 years). Once calculated during the design phase, there is no need to recalculate, unless the hull form, watertight bulkhead configuration, or ship mission changes which affects liquid amount or location, or space load densities. A singular KG_A curve also simplifies stability limits to the Sailor. A singular Allowable KG curve contributes to commonality as crews change throughout the service life. Also, once a singular KG_A curve is calculated, it does not need to be recalculated for unique loading conditions. It is a relatively conservative limit, but it is an efficient, all-inclusive limit that is relatively simple to understand for the non-naval architect, ship design management, and ship's force who must assure ship safety.

3. OPERATING RANGE AND LOADING

The design operating range of a USN surface combatant is from the Minimum Operating Condition (Min Op) to the Full Load Departure Condition (Full Load), unless otherwise specified. Min Op is basically 1/3 of Full Load loads, with exceptions. The Load Shift Method is used to calculate the damage KG_A curve based on the expected limiting case loading condition of the operating range yielding the highest KG . It assumes that, if the ship design can satisfy USN

stability criteria for the worst loading condition with the highest KG , then the ship is safe in the entire range of operating conditions.

Stability is calculated for the worst loading condition to meet USN criteria. The result is an allowable KG , but for that worst loading condition only. The worst case loading condition can be any loading combination between Min Op and Full Load, per DDS 079-1. Traditionally, the worst operating loading condition has been a modified Min Op. This is a loading scenario, where loads located below KG are depleted, but loads above KG are preserved. This is a very likely scenario, e.g. a ship returns from deployment with fuel and other liquids depleted, but with ammunition and other stores still onboard. In this case, the modified Min Op yields a higher KG than traditional Min Op. Therefore, it will be used in the example below.

4. LOAD SHIFT

USN KG_A curves reference the Full Load Condition. The delta between the worst loading condition loads and the Full Load Condition loads must be calculated. This delta will serve as the load shift. The load shift consists of a weight (Full Load Condition loads weight minus the "worst" loading condition loads weight) and vertical moment (Full Load Condition loads vertical moment minus the "worst" loading condition loads vertical moment). The load shift will be added to the calculated damage allowable KG values of the worst loading condition to produce Full Load Equivalent Damage KG_A values. The load shift can be applied to the worst loading condition damage KG_A 's at a range of displacements to produce Full Load Equivalent Condition damage KG_A 's at a range of displacements. This is the Full Load Equivalent Damage KG_A curve. The Full Load Equivalent Damage KG_A values are then compared against the calculated Full Load Damage KG_A values and the lesser of the two values at each calculated displacement is used in the Composite Damage KG_A curve.

5. METHODOLOGY

The weight (LS_{WT}) and vertical moment (LS_{MOM}) components of a load shift from Full Load of any other condition are defined as:

$$LS_{WT} = WT_{WL} - WT_{MO} \quad (1)$$

$$LS_{MOM} = WT_{FL} \cdot KG_{FL} - WT_{MO}KG_{MO} \quad (2)$$

where:

WT_{FL} full load displacement

WT_{MO} minimum operating displacement

KG_{FL} full load vertical center of gravity KG

KG_{MO} minimum operating vertical center of gravity KG

Accordingly the Minimum Operating Allowable KG, KGA_{MO} , can be load shifted back to the Full Load range of displacements as follows:

$$KGA_{LS} = \frac{KGA_{MO}WT_{MO} + LS_{MOM}}{WT_{MO} + LS_{WT}} \quad (3)$$

KGA_{MO} - minimum operating allowable KG

KGA_{LS} - Load shifted minimum operating Allowable KG

Example

The chart in Figure 1 shows the positions of Full Load and Min Op displacement and KG. These are typically attained from a design weight estimate. The Full Load displacement and KG are 7400 tonnes and 20.278 meters, respectively. The Min Op condition is 6400 tonnes and 22.000 meters, respectively. A load shift is calculated below:

$$LS_{WT} = WT_{FL} - WT_{MO} \quad (4)$$

$$= 7400 - 6400 = 800 \text{ tonnes}$$

$$LS_{MOM} = WT_{FL}KG_{FL} - WT_{MO}KG_{MO} \quad (5)$$

$$= 7200 \cdot 20.278 - 6400 \cdot 22.000$$

$$= 51983 \text{ tonne-meters}$$

A damage allowable KG (KG_A) is then determined via typical stability analysis methods for the appropriate stability criteria for a Min Op Loading Condition:

Condition	Displacement (tonnes)	Allowable KG (meters)	Moment (tonne-meters)
Min Op	5500.0	23.500	129250.0

The load shift is applied to the above modified Min Op Condition KG_A to produce a Full Load Equivalent Damage Allowable KG (the MinOp KG_A is “load shifted” to the Full Load Condition displacement range):

Condition	Displacement (tonnes)	Allowable KG (meters)	Moment (tonne-meters)
Min Op	5500.0	23.500	129250.0
+ Load shift	800.0		5198.3
Full Load	6300.0	21.341	134448.3

The load shift application is repeated for a range of Min Op Condition displacements and corresponding damage allowable KG’s to produce a range of Full Load Equivalent Condition displacements and damage allowable KG’s, see data in Table 1. With the damage Full Load Equivalent Allowable KG’s now calculated, a curve can be plotted, see Figure 2 . When compared to a sample family of calculated intact and damage Allowable KG curves, the chart may appear as shown in Figure 3. The lowest of all allowable KG points will be used to produce the final, composite, and singular Full Load Allowable KG, shown in Figure 4.

In the example above, the ship’s Full Load displacement and KG is plotted and compared with the Allowable KG and Displacement Limit. Fortunately for this ship, it is currently below the Allowable KG and less than the Displacement Limit. Therefore, it is safe in not only the Full Load condition, but in all operating conditions that contributed to the composite KG_A curve. However, the ship’s weight/KG growth may change over time and will require monitoring.

This curve will serve all foreseeable loading scenarios within the design operating range during the service life of the ship. It will not need to be recalculated, unless there is a change in hull form and appendages, watertight boundaries, significant load change or change in ship mission which affects liquid amount or location, or space load densities.

Incorporating LCG/Trim Shift

When discussing standard USN load shift practice, shifting the weight and KG were discussed previously; however, shifting the LCG between the two loading conditions is not typically considered. Historically, LCG shifts and trim ranges are not considered for combatant type ships since typical combatants operate with close to zero trim. For amphibious type ships with an expected operating trim range, a range of potential trims are examined for each displacement of interest. Based on the

curves for the analyzed trim range at each displacement, the expected design operating trim range can then be located on those curves and the lower KG from one end of the range is then used as the limiting KG for that displacement in order to cover the entire operating trim range. The Figure 5 shows Allowable KG (KG_A) values at a particular displacement for which an example ship has been

analyzed in a trim range between -2.0m and 2.0m, though the ship is only expected to operate between a -1.5m and 1.5m trim. The KG_A value at the -1.5m trim condition is less than the KG_A value at the 1.5m trim condition and thus the -1.5m trim KG_A value becomes the governing KG_A limit for this particular displacement.

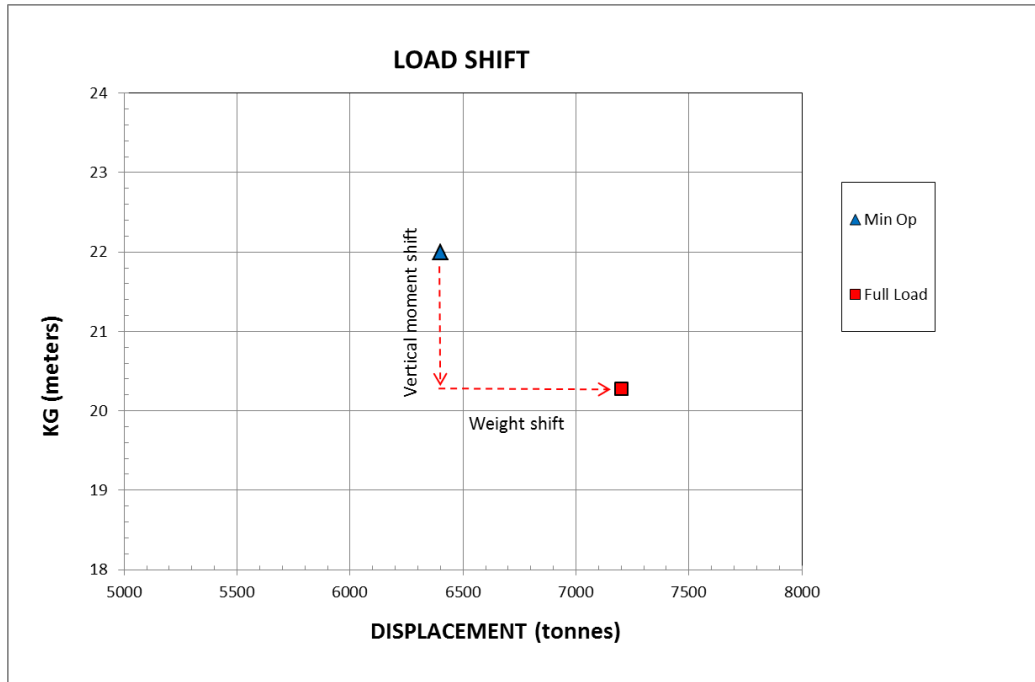


Figure 1 Example of load shift

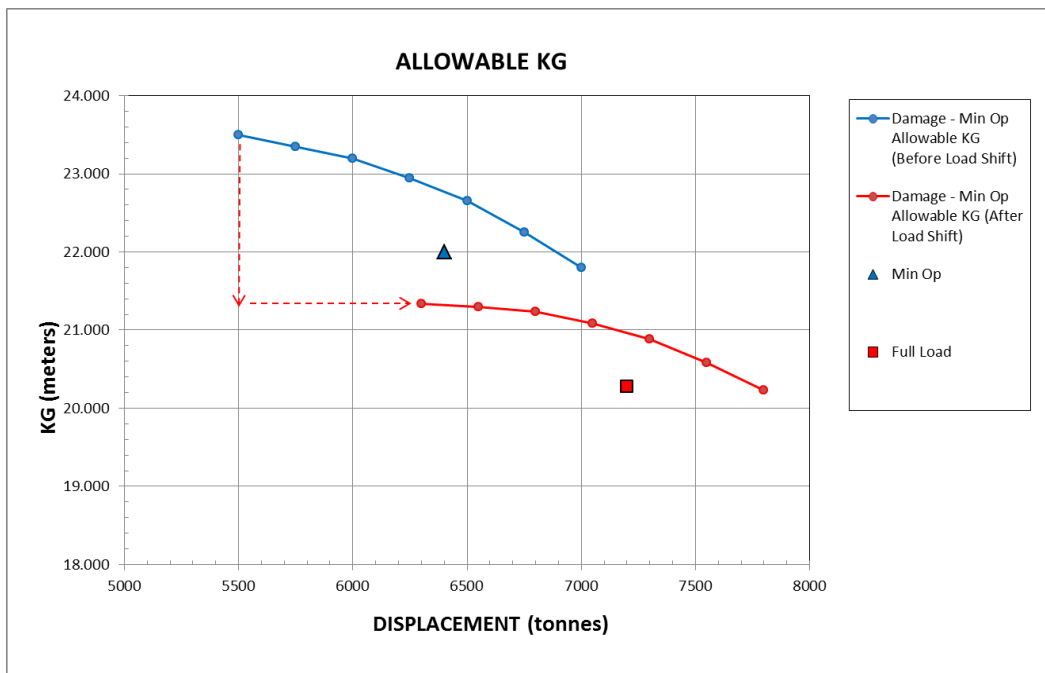


Figure 2: Load shifted allowable KG curves

Table 1 Example of load shift

BEFORE LOAD SHIFT			LOAD SHIFT		AFTER LOAD SHIFT		
Minimum Operating Condition					Full Load Condition		
Disp	Allowable KG	Moment	Weight	Moment	Disp	Allowable KG	Moment
(tonnes)	(meters)	(tonne-meters)	(tonnes)	(tonne-meters)	(tonnes)	(meters)	(tonne-meters)
5500	23.500	129250.0	800	5198.3	6300	21.341	134448.3
5750	23.350	134262.5	800	5198.3	6550	21.292	139460.8
6000	23.200	139200.0	800	5198.3	6800	21.235	144398.3
6250	22.950	143437.5	800	5198.3	7050	21.083	148635.8
6500	22.650	147225.0	800	5198.3	7300	20.880	152423.3
6750	22.250	150187.5	800	5198.3	7550	20.581	155385.8
7000	21.800	152600.0	800	5198.3	7800	20.231	157798.3

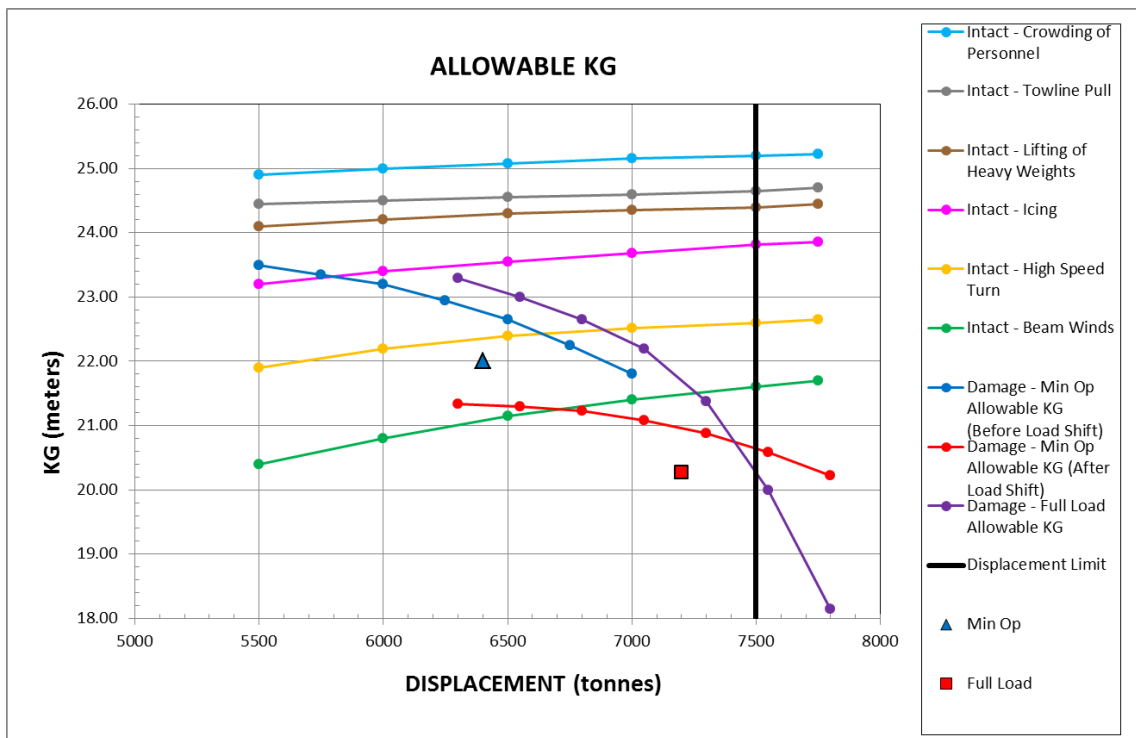


Figure 3: Family of Allowable KG curves

As mentioned earlier though, an inverse approach to addressing an operating trim range is to have a family of trim-based KG_A curves. A differentiation was made above between ship types with regard to design operating trim ranges. When considering a ship's anticipated operating trim range, another differentiation that should be considered is the variability in loading conditions. The family of trim-based KG_A curves approach would not be recommended for amphibious ships requiring a ballast polygon, for example. The family of trim-based KG_A curves approach should

only be considered when a single composite KG_A curve can be used to evaluate the current status of a ship's stability and the ship's hullform type also exhibits trim sensitivity (such as SWATHs, Off Shore Supply Vessels, etc).

To develop a family of trim-based KG_A curves, a range of displacements are examined at specified trims of interest. This is again because certain hullforms can display significantly different characteristics with regard to hydrostatics and stability when considering trim. This may be a

result of drastically changing waterplane area, LCF, LCB, or location of available reserve buoyancy over a range of trims, for instance. In contrast to the approach previously described, in cases where a family of curves is provided for guidance and those curves see significant variation depending on trim, unique consideration must be given to account for the change in LCG between loading conditions as well. Since the reason a ship would need multiple KG_A curves at multiple trim conditions is the result of significant changes to the ship's hydrostatic properties due to hullform, while a shift in LCG between loading conditions can be calculated in a manner similar to the shift in KG , it cannot be applied using the same approach. However, the same assumption applies that by using a fixed LCG shift when applying the load shift between loading conditions during design, the majority of displacement changes over the ship's service life are assumed to be lightship changes and not a result of changes to the loads. The previous load shift example has been updated to account for a trim shift and is shown below.

Full Load Condition (table to be populated with calculated LCG values at corresponding displacement/trim combinations using hydrostatic properties, see Table 2). Calculation the LCG Load Shift is done in Table 3.

MinOp Condition (calculated MinOp LCGs for each MinOp displacement based on applying LCG shift to Full Load LCGs, see Table 4.

The above calculated MinOp LCGs can then be used to calculate corresponding trim values. These are the trim values that should then be used to perform a damage stability analysis in the MinOp Loading Condition and are then considered equivalent to the Full Load trim values when load shifting the MinOp results back to Full Load for comparison.

By shifting the LCG in addition to the displacement and KG , an equitable comparison can be made between liquid loading conditions, such as MinOp and Full Load, at a given displacement and trim to determine the limiting KG in a family of allowable curves, see Figure 6. By not shifting the trim along with the displacement and KG , the damage stability analysis would not be performed at an approximately equivalent LCG in the alternate loading condition and would contradict the intent of performing the load shift in the first place, which is to create an equitable comparison of conditions. This also means that by not shifting the trim between liquid loading conditions for ships that are trim sensitive, the final KG_A curves for multiple, different trims provide an inaccurate representation of the safe operating range for the ship's KG

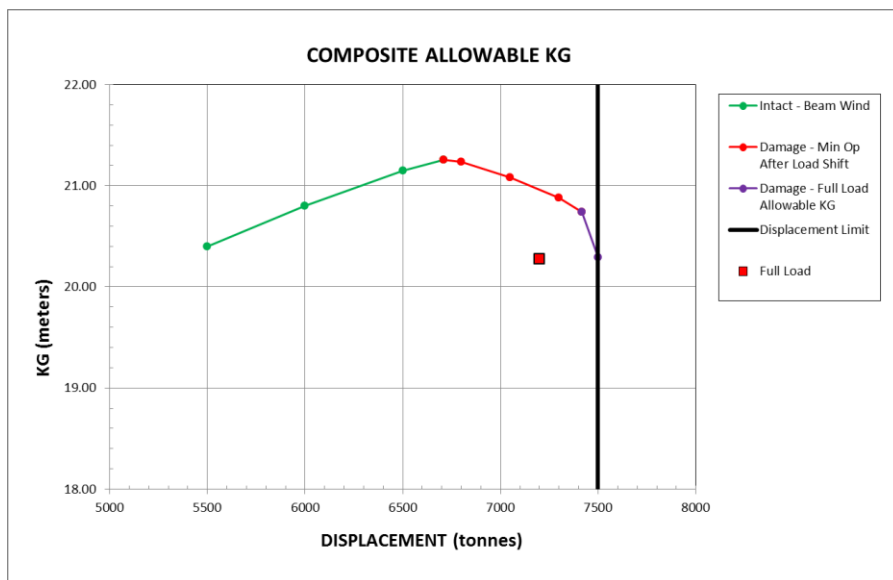


Figure 4: Full Load condition composite Allowable KG curve

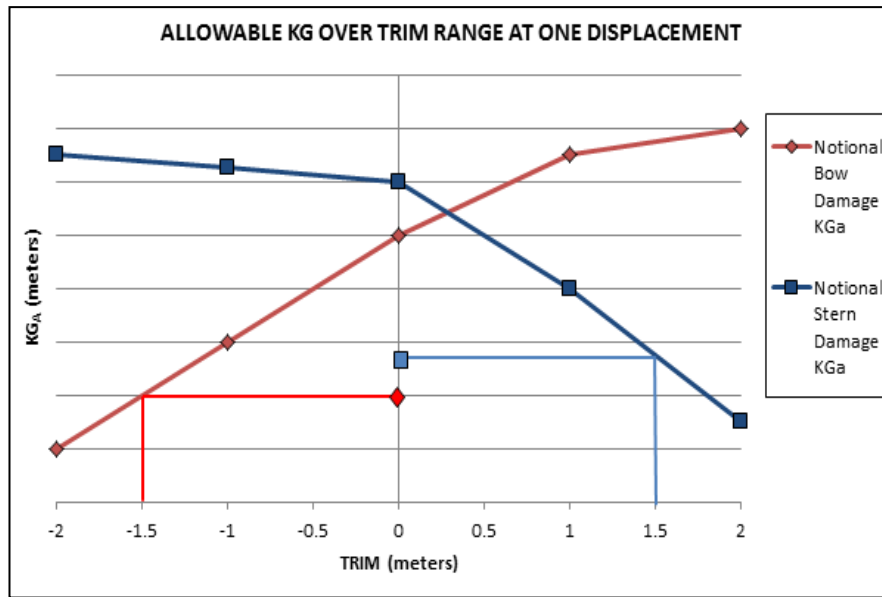


Figure 5: Allowable KG over trim range at one displacement

Table 2 LCG Trim Shift

Displacement [mt]	+0.5m trim	0.0m trim	-0.5m trim
6300	LCG _(6300,+0.5)	LCG _(6300,0.0)	LCG _(6300,-0.5)
6550	LCG _(6550,+0.5)	LCG _(6550,0.0)	LCG _(6550,-0.5)
6800	LCG _(6800,+0.5)	LCG _(6800,0.0)	LCG _(6800,-0.5)
7050	LCG _(7050,+0.5)	LCG _(7050,0.0)	LCG _(7050,-0.5)
7300	LCG _(7300,+0.5)	LCG _(7300,0.0)	LCG _(7300,-0.5)
7550	LCG _(7550,+0.5)	LCG _(7550,0.0)	LCG _(7550,-0.5)
7800	LCG _(7800,+0.5)	LCG _(7800,0.0)	LCG _(7800,-0.5)

Table 3 Calculation the LCG Load Shift:

Condition	Weight [MT]	LCG [m AFP]	L-Mom [m-MT]
Total Full Load Condition	7400	55.00	407000
Total Min Op Condition	6400	56.50	361600
Load shift	800		45400

Table 4 Calculated Min Op LCGs

Displacement [mt]			
5500	$\frac{[6300*LCG(6300,+0.5)]-45400}{5500}$	$\frac{[6300*LCG(6300,0.0)]-45400}{5500}$	$\frac{[6300*LCG(6300,-0.5)]-45400}{5500}$
5750	$\frac{[6550*LCG(6550,+0.5)]-45400}{5750}$	$\frac{[6550*LCG(6550,0.0)]-45400}{5750}$	$\frac{[6550*LCG(6550,-0.5)]-45400}{5750}$
6000	$\frac{[6800*LCG(6800,+0.5)]-45400}{6000}$	$\frac{[6800*LCG(6800,0.0)]-45400}{6000}$	$\frac{[6800*LCG(6800,-0.5)]-45400}{6000}$
6250	$\frac{[7050*LCG(7050,+0.5)]-45400}{6250}$	$\frac{[7050*LCG(7050,0.0)]-45400}{6250}$	$\frac{[7050*LCG(7050,-0.5)]-45400}{6250}$
6500	$\frac{[7300*LCG(7300,+0.5)]-45400}{6500}$	$\frac{[7300*LCG(7300,0.0)]-45400}{6500}$	$\frac{[7300*LCG(7300,-0.5)]-45400}{6500}$
6750	$\frac{[7550*LCG(7550,+0.5)]-45400}{6750}$	$\frac{[7550*LCG(7550,0.0)]-45400}{6750}$	$\frac{[7550*LCG(7550,-0.5)]-45400}{6750}$
7000	$\frac{[7800*LCG(7800,+0.5)]-45400}{7000}$	$\frac{[7800*LCG(7800,0.0)]-45400}{7000}$	$\frac{[7800*LCG(7800,-0.5)]-45400}{7000}$

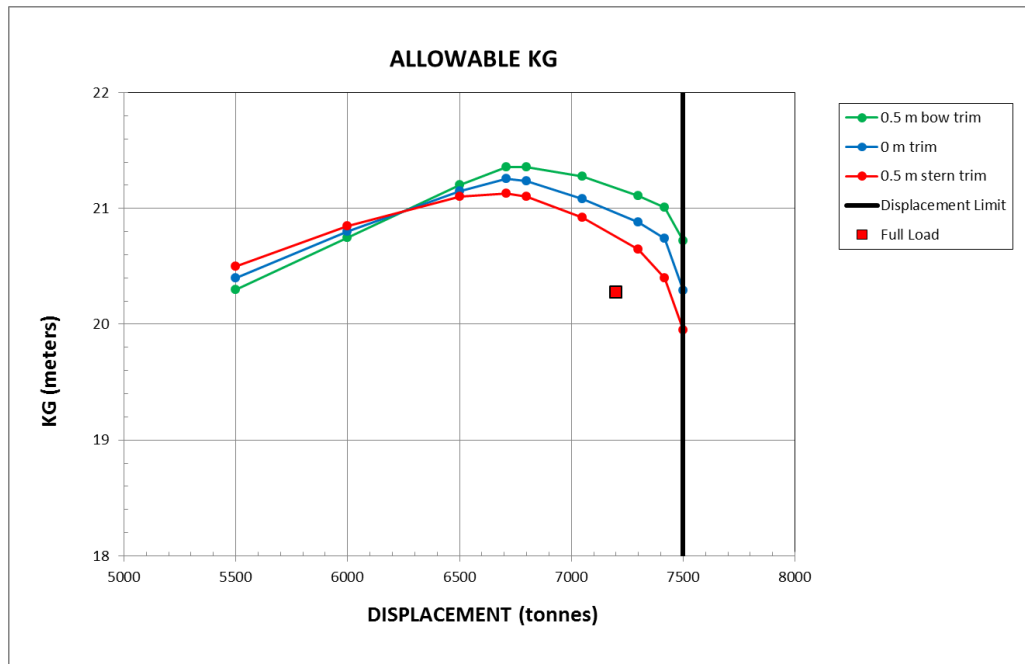


Figure 6: Allowable KG for various trims

Conclusion

The Load Shift Method is used to calculate the damage KG_A curve based on the expected limiting case loading condition of the operating range yielding the highest KG. The family of trim-based KG_A curves approach should only be considered when a single composite KG_A curve can be used to evaluate the current status of a ship’s stability and the ship’s hullform type also exhibits trim sensitivity (such as SWATHs, Off Shore Supply Vessels, etc). By shifting the LCG in addition to the displacement and KG, an equitable comparison can be made between liquid loading conditions, such as MinOp and Full Load, at a given displacement and trim to determine the limiting KG in a family of allowable curves.

By not shifting the trim along with the displacement and KG, the damage stability analysis would not be performed at an approximately equivalent LCG in the alternate loading condition and would contradict the intent of performing the load shift in the first place, which is to create an

equitable comparison of conditions. This also means that by not shifting the trim between liquid loading conditions for ships that are trim sensitive, the final KG_A curves for multiple, different trims provide an inaccurate representation of the safe operating range for the ship’s KG.

Acknowledgements

The authors would like to thank those who contributed to updating T9070-AF-DPC-010/079-1 as well as those who provided feedback on this paper. Specifically, John Rosborough of NSWCCD, and Chris Filiopoulos and Tapan Mazumdar of NAVSEA.

6. REFERENCES

Naval Sea Systems Command. (2016). *DESIGN PRACTICES AND CRITERIA FOR U.S. NAVY SURFACE SHIP STABILITY AND RESERVE BUOYANCY*. T9070-AF-DPC-010/079-1 (Approved for public release).

